

The Interstellar Medium in External Galaxies: Summaries of Contributed Papers

*Proceedings of the Second Wyoming Conference
held at Grand Teton National Park, Wyoming
July 3-7, 1989*

NASA



NASA Conference Publication 3084

The Interstellar Medium in External Galaxies: Summaries of Contributed Papers

Edited by
D. J. Hollenbach
Ames Research Center
Moffett Field, California

Harley A. Thronson, Jr.
University of Wyoming
Laramie, Wyoming

Proceedings of the Second Wyoming
Conference sponsored by the University
of Wyoming, Laramie, Wyoming, and supported
by the University of Wyoming, the National
Aeronautics and Space Administration, and
the National Science Foundation, and held at
Grand Teton National Park, Wyoming
July 3–7, 1989



National Aeronautics and
Space Administration

Office of Management

Scientific and Technical
Information Division

1990

Astronomy Library

2 QB

8 856

. W96

1989

Suppl.

Preface

This volume contains summaries of the contributed papers given at the Second Wyoming Conference, entitled "The Interstellar Medium in External Galaxies," which took place on July 3-7, 1989, in Grand Teton National Park, Wyoming. A separate publication from Kluwer Publishing contains the invited papers given at this meeting; the program of these invited papers appears on the following pages.

The purpose of the conference was to present a summary of the current understanding of the interstellar medium in external galaxies and to discuss the basic physical processes which underlie interstellar phenomena. The Second Wyoming Conference carried much of the philosophy of the First Wyoming Conference, which was entitled "Summer School on Interstellar Processes" and which focused on the interstellar medium in our own Milky Way Galaxy. We were especially interested to attract an audience of graduate students and younger astronomers and to expose them to the wide variety of interesting processes operating in the interstellar medium. Like the First Wyoming Conference, the invited talks had a "summer school" review tone; whereas the contributed papers in this volume are appropriate to typical symposia: they are generally reports on current research activities. We have, for the most part, organized the papers in this volume much as they were organized at the conference, but numerous changes have been made to improve the placement of papers in the right category. For the convenience of the reader, there is an author index and a galaxy index at the back of the volume.

Approximately 230 astronomers attended the conference and most of their names appear as authors on the contributed papers in this volume. We would like to acknowledge their contributions, and the work of the Scientific Organizing Committee (J. Bally, J. Dickey, B. Elmegreen, F. Israel, F. Schweizer, N. Scoville, J.M. Shull, C. Telesco, J. Van Gorkom, and J. Young). We are also grateful to the Local Organizing Committee (D. Barnaby, C. Wilton, and M. Shea) and to the Staff Members of the Department of Physics and Astronomy at the University of Wyoming (E. Haskell, M. Mitchum, and K. Anderson) for attending to all the details which made the conference possible and which made the stay at Jackson Lake Lodge so enjoyable for the participants and their families. We would like to thank the

University of Wyoming for sponsoring the conference, and for the financial support provided by R. de Vries (Vice President for Research), W. Eggers (Dean of Arts and Sciences), and G. Rebka (Chairman of the Department of Physics and Astronomy). We wish to thank the National Science Foundation (especially J. Wright) for financial support which enabled graduate students and other young scientists to attend the meeting, and the National Aeronautics and Space Administration (especially F. Gillett and L. Caroff) for financial support through the University of Wyoming.

The Interstellar Medium in External Galaxies

Schedule of Invited Talks

Day 1: Monday, July 3

- 8:30a - 8:45a Welcome/Announcements [H. Thronson (*Wyoming*)]
8:45a - 9:30a Overview and Background [G. R. Knapp (*Princeton*)]

I. The Cool Phase of the ISM in Galaxies

- 9:30a - 10:30a Atomic Gas [E. Brinks (*RGO*)]
10:30a - 11:30a Molecular Gas [J. Young (*Massachusetts*)]
2:00p - 2:45p Dust [M. Rowan-Robinson (*Queen Mary College*)]
2:45p - 3:30p Effects of Environment [J. Kenney (*OVRO*)]

Day 2: Tuesday, July 4

II. The Hot Phase of the ISM

- 3:30a - 9:15a Energy Input into the ISM:
 Supershells, Fountains, etc. [D. Cox (*Wisconsin*)]
9:15a - 10:00 Cooling Flows & X-Ray Emission [C. Sarazin (*Virginia*)]
10:15a - 11:00 AGNs & the ISM in the Cores of Galaxies [J. Krolik
 (*Johns Hopkins*)]
1:15p - 2:15p HII Regions & Abundances [H. Dinerstein (*Texas*)]

Day 3: Wednesday, July 5

III. Dynamics and Evolution

- 9:00a - 9:45a Models of Phases of the ISM in Galaxies [M. Begelman (*Colorado*)]
- 9:45a - 10:45a Large-Scale Dynamic Structure: Density Waves
 Propagating Star Formation, Etc. [S. Balbus (*Virginia*)]
- 10:45a - 11:30a Gas During Mergers/Collisions [M. Noguchi (*Nation. Astr. Obs.*)]
- 1:45p - 2:30p Magnetic Fields [R. Wielebinski (*MPIfR*)]

Evening Panel Discussion: **Starbursts and the ISM**
Moderated by R. McCray (*Colorado*)

Day 4: Thursday, July 6

IV. Early Evolution and Star Formation

- 8:30a - 9:15a Early ISM and Galaxy Formation [S. White (*Arizona*)]
- 9:15a - 10:00a QSO Absorption Lines, Abundances
 and the Early Halo [A. Wolfe (*Pittsburgh/UCSD*)]
- 10:00a - 11:00a Large-Scale Star Formation & the ISM [R. Kennicutt (*Arizona*)]
- 1:15p - 2:15p The Star-Gas Cycle [M. Dopita (*Mt. Stromlo/ANU*)]

Day 5: Friday, July 7

- 11:00a - 11:30a Conference Summary [J. Ostriker (*Princeton*)/
 J.M. Shull (*Colorado*)]

Additional Short Papers to Appear in Conference Proceedings:

Mass Determinations from 21 cm HI Observations [J. Dickey (*Minnesota/Leiden*)]
Mass Determinations from Millimeter-Wave CO Observations [P. Maloney (*Leiden*)]
Mass Determinations from X-Ray Observations [R. Mushotzky (*NASA Goddard*)]
Mass Determinations from Dust Observations [B. Draine (*Princeton*)]

CONTRIBUTED PAPERS

CONTENTS

Subject, Title, Authors	Page
 I. THE COOL ISM	
A. HI, Atomic Gas, Photodissociation Regions, Depletion	
"The Extragalactic Radiation Field and Sharp Edges to HI Disks in Galaxies", P. Maloney	1
"A Comparison of UV Surface Brightnesses and HI Surface Densities for Spiral Galaxies", S.R. Federman, C. Strom	4
"NGC 1058: Gas Motions in an Extended, Quiescent Spiral Disk", M.M. hansen, J.M. Dickey, G. Helou	6
"Neutral Hydrogen in the Starburst Galaxy NGC 3690/IC 694", E. Tolstoy, J.M. Dickey, F.P. Israel	8
"High Velocity Gas in External Galaxies", J. Kamphuis, J.M. van der Hulst, R. Sancisi	12
"A Scaling Law of Radial Gas Distribution in Disk Galaxies", Z. Wang	15
"Radial Profiles of Gas in Late-Type Disk Galaxies", C. Struck-Marcell	18
"Disk Mass Densities in Edge-On Spiral Galaxies", M.P. Rupen	21
"A Survey of the Properties of Early-Type Galaxies", J.N. Bregman, M.S. Roberts, D.E. Hogg	23
"Intergalactic HI in the NGC 5018 Group", P. Guhathakurta, G.R. Knapp, J.H. van Gorkom, D. -W. Kim	26
"HI and FIR Emission from SO Galaxies", P.B. Eskridge, R.W. Pogge	29
"Distribution, Kinematics, and Origin of HI Gas in SO and SO/a Galaxies", H. van Woerden, W. van Driel	32
"The Hot and Cold Interstellar Matter of Early Type Galaxies and Their Radio Emission", D. -W. Kim, G. Fabbiano	33
"Physical Conditions in Photodissociation Regions: Application to Galactic Nuclei", M.G. Wolfire, A.G.G.M. Tielens, D. Hollenbach	37
"Far-Infrared Spectroscopy of NGC 6946, IC 342, and Arp 299:", S.D. Lord, D.J. Hollenbach, S.W.J. Colgan, M.R. Haas, R.H. Rubin, E.F. Erickson	40

Subject, Title, Authors	Page
"Neutral Atomic Absorption Lines and Far-UV Extinction: Possible Implications for Depletions and Grain Parameters", D.E. Welty	42
"Empirical Relationships Between Gas Abundances and UV Selective Extinction", C.L. Joseph	45
B. H ₂ , CO and Molecular Gas	
"The FCRAO Extragalactic CO Survey: Global Properties of Galaxies", J.S. young, M. Claussen, N. Devereux, Y. Huang, J.D. Kenney, P. Knezek, L. Taccini, L. Tacconi-Garman, F.S. Schloerb, P. Viscuso S. Xie	47
"A Survey of Galaxies in CO", T. Elfhag	50
"The Ratio of Molecular to Atomic Gas in Spiral Galaxies as a Function of Morphological Type", P.M. Knezek, J.S. Young	53
"Circumstellar Molecular Gas in Starburst and Seyfert Galaxies", Y. Taniguchi, O. Kamega, N. Nakai	56
"High Resolution CO Images of Seyfert Galaxies", M. Meixner, P. Puchalsky, L. Blitz, M. Wright	59
"Aperture Synthesis CO Observations of the Inner Disk of NGC 1068", P. Planesas, N.Z. Scoville, S.T. Myers	62
"CO Aperture Synthesis of NGC 4038.9 (Arp 244)", S. A. Stanford, D.B. Sanders, A.I. Sargent, N.Z. Scoville	65
"Observations of CO in the Magellanic Irregular Galaxy NGC 55", A. Heithausen, R. -J. DeHmar	68
"Observations of CO Isotopic Emission and the Far-Infrared Continuum of Centarus A", A. Eckart, M. Cameron, H. Rothermal, W. Wild, H. Zinnecker, M. Olberg, G. Rydbeck, T. Wiklind	71
" ¹² CO and ¹³ CO J=2-1 and J=1-0 Observations of Hot and Cold Galaxies", S. Xie, P. Schloerb, J. young	72
"The Molecular Cloud Content of Early Type Galaxies", T. Wiklind, C. Henkel	75
"CS J=2-1 Emission Toward the Central Region of M82", C.E. Walker, C.K. Walker, J.E. Carlstrom, R.N. Martin	78

Subject, Title, Authors	Page
C. Interstellar Dust	
"High Resolution Sub-Millimeter Mapping of Starburst Galaxies: Comparison with CO Emission", P.A. Smith, P.W.J.L. Brand, P.J. Huxley, C.M. Mountain, N. Nakai	81
"High Spatial Resolution 100 μm Observations of the M83 Bar", B.J. Smith, D.F. Lester, P.M. Harvey	84
"Far-Infrared Observations of Circinus and NGC 4945 Galaxies", R.S. Bisht, S.K. Ghosh, K.V.K. Iyengar, T.N. Rengarajan, S.N. Tandon, R.P. Verma	86
"The 3 μm Spectrum of NGC 4565", A.J. Adamson, D.C.B. Whittet	89
"The Gas/Dust Ratio in Spiral Galaxies", N.A. Devereux, J.S. Young	92
"Spatial Analysis of IRAS Observations of Nearby Spirals", R. Ball, K.Y. Lo	95
"Contribution of Cool Dust to the FIR Brightness Distribution of NGC 6946 Sc(s) II", G. Engardiola, D.A. Harper	97
"Far-Infrared Luminosity Functions of Normal Galaxies", T. Isobe, E.D. Feigelson	100
"Evidence Against a Simple Two-Component Model for the Far-Infrared Emission from Galaxies", S.A. Eales, N.A. Devereux	103
"Emission from Small Dust Particles in Diffuse and Molecular Cloud Medium", J.P. Bernard, X. Desert	105
"Very Small Grains in the Milky Way and External Galaxies", L. Luan, M.W. Werner, C. Heils, K. Sellgren	108
"A Model for the Infrared Emission from an OB Star Cluster Environment", D. Leisautz	111
"IRAS Observations of the ISM in the α Cas Reflection Nebula", R.H. Buss, M.W. Werner	113
"Peering Beyond IRAS: The 100-350 μm Dust Emission from Galaxies", H.A. Thronson, D.A. Hunter, S. Caseg, G. Engargiola, D.A. Harper	116
"Far-Infrared Emission from Dusty Ellipticals", D. Walsh, J. Knapp	120
"Observations of the Galactic Plane by the Zodiacal Infrared Project", L. J. Rickard, S.W. Stemwedel, S.D. Price	123
"The Infrared Continuum Spectrum of X-Ray Illuminated Molecular Gas", G.M. Voit	126

Subject, Title, Authors	Page
D. The Cool ISM and the Non-Thermal Radio Continuum	
"A Comparison of the Radial Distribution of Molecular Gas and Non-Thermal Radio Continuum in Spiral Disks", N.A. Devereux, J.S. Young	127
"A Relationship Between the Integrated CO Intensity and the Radio Continuum Emission Spiral Galaxies", D.S. Adler, R.J. Allen, K.Y. Lo	130
"Radio Continuum and Far-Infrared Emission of Spiral Galaxies: Implications of Correlations", T.N. Rengarajan, K.V.K. Iyengar	133
II. HII REGIONS, HALO AND HOT GAS, COOLING FLOWS	
A. HII Regions	
"Circumstellar Ionized Gas in Starburst Nuclei", Y. Taniguchi	137
"Imaging Spectrophotometry of the Nuclear Outflow of NCG 1068", G. Cecil	140
"Large Scale Excitation of the ISM in NGC 1068", J. Sokolowski, J. Bland, G.N. Cecil, R.B. Tully	143
"Multiband Observations of Cygnus A: A Study of Pressure Balance in the Core of a Powerful Radio Galaxy", C. Carilli, S. Conner, J. Dreher, R. Perley	146
"Ionized Interstellar Froth in Irregular Galaxies", D.A. Hunter, J.S. Gallagher	149
"Ar/S", M.L. McCall, C. Stevenson, D.L. Welch	151
"Spatially Resolved Optical and Near Infrared Spectroscopy of I Zw 18", E.D. Skillman, R.C. Kennicutt	154
"Optical and Near-IR Study of LMC HII Region NIIAB", M.G. Lee	157
"HII Regions in Dwarf Irregular Galaxies of the Local Group", P. Hodge, M.G. Lee	160
"HII Regions in IC 1613: The ISM in a Nearby Dwarf Irregular Galaxy", J.S. Price, S.F. Mason, G.A. Gullixson	163
"Differences in the Size-Internal Velocity Relation of Galactic and Extragalactic HII Regions", C.R. O'Dell	166
"A Study of HII Regions in Spiral Galaxies Using Multiobject Spectroscopy", D. Zaritsky, R. Elston, J.M. Hill	169

Subject, Title, Authors	Page
"The Diffuse Ionized Interstellar Medium Perpendicular to the Plane of NGC 891", R. -J. Dettmar, J. Keppel, M.S. Roberts, J.S. Gallagher	172
B. Halo and Hot Gas	
"Hot Interstellar Gas and Ionization of Embedded Clouds", K.P. Chang, F., Bruhweiler	175
"Radiative Thermal Conduction Fronts", K.J. Korkowski, S.A. Balbus, C.C. Frstrom	177
"Energy Input and HI Spin Temperatures in Low Pressure Regions", E. Corbelli, E.E. Salpeter	180
"The Interstellar Halo of Spiral Galaxies: NGC 891", S.R. Kulkani, R.J. Rand, J.J. Hester	182
"The Onset of Galactic Winds in Early-Type Galaxies", W. Forman, C. Jones, W. Tucker, L. Daird	185
"The Environments of Double Radiogalaxies", S. Rawlings	188
C. Cooling Flows	
"Origin and Dynamics of Emission Line Clouds in Cooling Flow Environments", M. Loewenstein	191
"Narrow Band Images of Suspected Cooling Flow Galaxies", S. Deustra, G. Bothun	193
"Optical Emission from Cooling Flows in Distant X-Ray Clusters of Galaxies", M. Donahue, J.T. Stocke, G.M. Voit, I. Gioia	196
"Gas Flows in Elliptical Galaxies", L.P. David, W. Forman, C. Jones	198
"Stripping of Gas and Dust from the Elliptical Galaxy M86", D.A. White, A.C. Fabian, W. Forman, C. Jones, C. Stern	201
"ISM Stripping from Cluster Galaxies and Inhomogeneities in Cooling Flows", N. Soker, J.N. Bregman, C.L. Sarazin	203
"Accounting for the Dispersion in the X-Ray Properties of Early-type Galaxies", R.E. White, C.L. Sarazin	304
"Search for Cold Gas in Clusters With and Without Cooling Flows", D.A. Grabelsky, M.P. Ulmer	206

Subject, Title, Authors	Page
III. GAS DYNAMICS, HEATING, INTERACTIONS	
A. Gas Dynamics and Magnetic Fields in Galaxies	
"An Infrared Jet in Centarus A (NGC 5128): Evidence for Interaction Between the Active Nucleus and the Interstellar Medium", M. Joy, P.M. Harvey, E.V. Tollestrup, P.J. McGregor, A.R. Hyland	211
"NGC 4438: Ram Pressure Sweeping of a Tidally Disrupted Galaxy", J.E. Hibbard, J.H. van Gorkom	214
"NGC 3312: A Victim of Ram Pressure Sweeping?", P.M. McMahon, O. -G. Richter, J.H. van Gorkom, H.C. Ferguson	217
"The Violent ISM in M31", E. Brinks, R. Braun, S.W. Unger	221
"Supernova Remnants and Diffuse Ionized Gas in M31", R. Waterbos, R. Braum	224
"Evolution of a Superbubble Blastwave in a Magnetized Medium", K.M. Ferriere, E.G. Zweibel, M.-M. MacLow	227
"Infrared Analysis of LMC Superbubbles", F. Verter, E. Dwek	229
"Magnetic Collimation of Protostellar Winds into Bipolar Flows", M.L. Norman, J.M. Stone	232
"MHD Shocks in the ISM", D.F. Chernoff, D.J. Hollenbach, C.F. McKee	235
"What Sort of Standard Candle is Orion for Studying Molecular Hydrogen Line Emission in Galaxies?", M. Burton, P. Duxley	238
H2 Line Emission in Three Seyfert Nuclei: Evidence Against UV-Excitation", T.R. Geballe	241
"Lyman Alpha Radiation in External Galaxies", D.A. Neufeld, C.F. McKee	243
"Observations of Extended and Counterrotating Disks of Ionized Gas in SO Galaxies", R. -J. Dettmar, M. Jullien-Dettmar, A. Barteldrees	246
"The Gravitational Wakefield of a Molecular Cloud in a Disk Galaxy", M. Tagger, R. Pellat, J.F. Sygnet	249
"The Effect of Suspended Particles on Jean's Criterion for Gravitational Instability", D.J. Wollkind, K.R. Yates	250
"Virial Theorem Analysis of the Structure and Stability of Magnetized Clouds", E.G. Zweibel	252

Subject, Title, Authors	Page
"Evolution of Magnetized, Rotating, Isothermal Clouds", K. Tomisaka	255
"Infrared Polarimetry and the Magnetic Field in External Galaxies"; T.J. Jones	258
"Polarization in the Lagoon Nebula", M. L. McCall, M.G. Richer, N. Visvanathan	260
"Granularity in the Magnetic Field Structure of M83", R.J. Allen, S. Sukumar	263
B. Heating of the ISM	
"Thermal Instabilities in Protogalactic Clouds", S.D. Murray, D.N.C. Lin	267
"High Brightness Neutral Hydrogen in M31: A New Probe of Interstellar Pressure?", R. Braun, R. Walterbos	269
C. Interacting Galaxies	
"CO Observations of Southern Mergers", F. Casoli, C. Dupraz, F. Combes	273
"Star Formation on the Leading Edge of a Ring-Like Density Wave in Arp 143", P.N. Applegate	276
"A Multi-Wavelength Study of the Peculiar Galaxy NGC 2976", L.J. Tacconi, J.M. van der Hulst, P.R. Wesselius	279
"The Morphology-Density Relation for Dwarf Galaxies", H.C. Ferguson, A. Sandage	281
IV. M33 AND M51	
"Unbound Molecular Complexes in M33", C.D. Wilson	285
"Deep Narrow Band Imagery of the Diffuse ISM in M33", J.J. Hester	288
"A High Resolution CO Map of M51", D.S. Adler, K.Y. Lo, R.J. Allen	291
"M51: Molecular Spiral Arms, GMAs and Superclouds", R.J. Rand, S.R. Kulkarni	293
"Dissociation and Ionization of Molecular Gas in the Spiral Arms of M51", J.F. Kees, K.Y. Lo.	296

Subject, Title, Authors	Page
"Spiral Structure of M51: Streaming Motions Across the Spiral Arms", R.P.J. Tilanus, R.J. Allen	298
"High Spatial-Resolution IRAS Images of M51", R. Canterna, J.A. Hackwell, G.L. Grasdalen	301
V. STAR FORMATION IN GALAXIES	
"Are Bars Essential for Starbursts in Non-Interacting Galaxies?", S.M. Pompea, G.H. Rieke	305
"Aspects of the Interstellar Medium in Starburst Galaxies", M.N. Fanelli	307
"Gravitational Star Formation Thresholds and Gas Density in Three Galaxies", M.S. Oey, R.C. Kennicutt	309
"One-Dimensional Cloud Fluid Model for Propagating Star Formation", T.N. Titus, C. Struck-Marcell	312
"Star Formation in Proto Dwarf Galaxies", A. Noriega-Crespo, P. Bodemheimer, D.N.C. Lin, G. Tenorio-Tagle	314
"Infrared Spectroscopy of the Dwarf Starburst Galaxy Henize 2-10", P.R. Blanco, P.J. Puxley	317
"Small-Scale Star Formation at Low Metallicity", M. L. McCall, R. Hill, J. English	318
"Global and Radial Variations in the Efficiency of Massive Star Formation Among Galaxies", L.E. Allen, J.S. Young	321
"Molecular Gas and Star Formation in the Centers of Virgo Spirals", B. Canzian	325
"Near-Infrared Mapping of Spiral Barred Galaxies", P. Gallais, D. Rouan, F. Lacombe	329
"High Mass Star Formation in Southern Disk Galaxies", M.A. Dopita, J.R. Forster, L. Ferrario	331
"Starburst Outflows from Nearby Galaxies", W.H. Waller	334
"Dense Gas and HII Regions in the Starburst Galaxy NGC 253", J.E. Carlstrom, J. Jackson, P.T.P. Ho, J.L. Turner	337
"A Near Infrared Spectroscopic Study of the Interstellar Gas in the Starburst Core of M82", D. Lester, N. Gaffney, J. Carr, M. Joy	340
"Clues to Galaxy Activity from Rich Cluster Simulations", A.E. Evrard	343

Subject, Title, Authors	Page
"Central Star Formation in SO Galaxies", L.L. Dressel, R.W. O'Connell, C.M. Telesco	346
"Current Star Formation in SO Galaxies: NGC 4710", J.M. Wrobel	349
VI. ABSORPTION LINE SYSTEMS	
"Interpreting the Convergency of Lyman Series Absorption Lines", E.B.Jenkins	353
"Radio Continuum Observations of the Quasar-Galaxy Pair 3C232-NGC 3067", E. Haxthausen, C. Carilli, J. van Gorkom	356
"Probing the Interstellar Medium of External Galaxies Using Quasar Absorption Lines: The 3C232/NGC 3067 System", J.T. Stocke, J. Case, M. Donahue, J.M. Shull, T.P. Snow	359
"Search for CaII Absorption in Galactic Halos", D. Bowen	360
"Detection of a $Z=0.0515$, 0.0522 Absorption System in the QSO S4 0248+430 Due to an Intervening Galaxy", D.S. Wanble, V.T. Junkkarinan, R.D. Cohen, E.M. Burbidge	362
VII. RESULTS FROM NEW INSTRUMENTS AND TECHNIQUES	
"High Spatial Resolution Studies of Galaxies in the Far IR: Observations with the KAO, and the Promise of SOFIA", D.F. Lester, P.M. Harvey	365
High Angular Resolution mm- and Submm- Observations of Dense Molecular Gas in M82", W. Wild, A. Eckart, R. Genzel, A.I. Harris, J.M. Jackson, D.T. Jaffe, J.B. Lugten, J. Stutzki	368
"The Molecular Spiral Arms of NGC 6946", F. Casoli, F. Clausset, F. Viallefind, F. Combes, F. Boulanger	371
"The Molecular Spiral Arms of NGC 6946", L.J. Tacconi, S. Xie	373
"CO Mapping of the Nuclear Region of NGC 6946 and IC 342 with the Nobeyama Millimeter Array", S. Ishizuki, R. Kawabe, S.K. Okumura, K. -I.Morita, M. Ishiguro	375
"CO Excitation in Four IR Luminous Galaxies", S.J.E. Radford, P.M. Solomon, D.Downes	378
"CS in Nearby Galaxies: Distribution, Kinematics, and Multilevel Studies", R. Mauersberger, C. Henkel	381

Subject, Title, Authors	Page
"Spatial Variation of the Physical Conditions of Molecular Gas in Galaxies", J.M. Jackson, A. Eckart, W. Wild, R. Genzel, A.I. Harris, D. Downes, D.T. Jaffe, D.T.P. Ho	384
"Detection of CO Emission in Hydra I Cluster Galaxies", W.K. Huchtmeier	386
"Non-Stellar Light from High-Redshift Radiogalaxies?", S. Rawlings	389
"CO Distributions in Southern SO Galaxies", H. van Woerden, L. Tacconi	392
"The Hawaii Imaging Fabry-Perot Interferometer", J. Bland, G. Cecil, B. Tully	395
VIII AUTHOR INDEX AND GALAXY INDEX	397

I - THE COOL ISM

A - HI, ATOMIC GAS, PHOTODISSOCIATION REGIONS, DEPLETION

The Extragalactic Radiation Field and Sharp Edges to HI Disks in Galaxies

Phil Maloney, Sterrewacht Leiden

Observations of neutral hydrogen are widely used as a probe of the interstellar medium in galaxies and of galactic kinematics and dynamics. The 21-cm line can be used to determine galactic rotation curves far beyond the optical disk, and is one of the prime sources of evidence for the existence of dark haloes in spiral galaxies. However, a recent attempt to measure the 21-cm emission from NGC 3198 to very low column densities ($N_H \approx 5 \times 10^{18}$) found that the HI disk is very sharply truncated at a column density of a few times 10^{19} (Sancisi 1989, private communication). This discovery reinforces the earlier suggestion (Briggs *et al.* 1980) that extended, low-column density envelopes of neutral hydrogen are not common around galaxies. Here I suggest that the sharp edge seen to the HI disk in NGC 3198 is consistent with a model in which a self-gravitating neutral HI disk is photoionized by the extragalactic radiation field. The possibility that the extragalactic background would produce sharp edges to HI disks was first suggested by Silk and Sunyaev (1976).

The Model: The outer HI disk of a galaxy is modeled in plane parallel geometry. The extragalactic radiation field is assumed to be isotropic and is incident on the HI gas layer. The soft x-ray background shows a power-law distribution of photons with energy; because of absorption by Galactic HI, the far-UV flux is unobservable. In the presence of such a power-law spectrum the usual Strömgen approximation won't hold: since the soft x-ray photons penetrate to much greater optical depths than photons not far above the Lyman limit, the transition from highly ionized to neutral hydrogen will not be sharp. The presence of helium also becomes very important, because He and He^+ can be ionized by photons with energies $E > 24.6$ eV and $E > 54.4$ eV, respectively, where the hydrogen cross-section for photoionization is negligible, while He and He^+ recombination radiation can ionize H. Thus helium acts to degrade soft x-ray, He-ionizing photons into UV, H-ionizing photons.

The extragalactic radiation field is assumed to have a power-law spectrum between 1.5 KeV and 13.6 eV, with the actual intensity at the Lyman limit a free parameter, normalized to the $Z = 0$ value estimated by Sargent *et al.* (1979). The spectral index is then given by $\alpha = 1.45 + 0.490 \log(I_{Ly})$, where I_{Ly} is the intensity at the Lyman limit normalized to $4.0 \times 10^{-23} \text{ ergs cm}^{-2} \text{ s}^{-1} \text{ Hz}^{-1} \text{ sr}^{-1}$.

The gas is taken to have an isothermal ($\rho(z) = \rho_0 \text{sech}^2(z/z_0)$) z -distribution, where the scale-height z_0 is either specified or calculated for a self-gravitating layer with a given velocity dispersion. The gas disk is divided into a series of zones, each of which is assumed to be uniform. The calculation begins at the exterior (z -boundary) of the disk and proceeds inwards, the ionization structure in each zone being used to calculate the incremental optical depth to ionizing radiation. An iterative scheme is used to calculate the ionization, including the effects of the diffuse ionizing recombination radiation (Williams 1967).

Results: Figure 1 shows the results for 3 models with fixed z_0 and $I_{Ly} = 1$. The total and neutral hydrogen column densities are plotted against radius for an assumed exponential decrease in total HI surface density. There is a pronounced break in the slope of N_H vs. R at a column density of $\approx 3 \times 10^{19}$. The neutral column density drops by a factor of ≈ 10 in a distance of 1 scale-length. Although the column density at which the slope change occurs is in agreement with the the NGC 3198 data, the constant scale-height models cannot explain the sharpness of the edge of the HI disk

in NGC 3198: the scale-length for the HI distribution in the outer disk of NGC 3198 is about 9 kpc, whereas the VLA observations of this galaxy show that the column density drops from 5×10^{19} to 5×10^{18} on a scale of about 3 kpc. This suggests that flaring of the HI disk at large R plays an important role.

At the large galactocentric distances to which HI is observed in NGC 3198, the surface density of gas exceeds that of the stars by \approx two orders of magnitude (assuming a constant mass-to-light ratio stellar disk), so that the HI can be accurately treated as a self-gravitating thin disk; a halo component will not affect the z -structure within a few kpc of the disk midplane. For a self-gravitating thin disk, the scale-height z_0 is

$$z_0 = \frac{\sigma_z^2}{\pi G \Sigma(R)} = 8.12 \times 10^{-2} \frac{\sigma_z^2}{N_{H\text{tot}}} \text{ kpc} \quad (1)$$

where σ_z is the z -velocity dispersion of the disk and $\Sigma(R)$ is the mass surface density, and the right-hand side is for σ_z in km s^{-1} and the total hydrogen column density in units of 10^{20} cm^{-2} .

The scale-height of a self-gravitating HI disk is thus inversely proportional to column density. This flaring of the disk increases the ionization fraction of the HI by lowering the recombination rate.

Figure 2 shows the results for a series of self-gravitating models, for $I_{Ly} = 1$ and several values of σ_z . Comparison with Figure 1 shows that the decline in neutral column density occurs much more rapidly beyond the threshold column density than in the constant scale-height models, with the column density dropping by an order of magnitude in 1/3 of a scale-length.

The main conclusions can be summarized as follows:

- 1) Photoionization of neutral gas by the extragalactic radiation field can explain the sharp truncation of the HI disk seen in NGC 3198.
- 2) The HI layer must be self-gravitating, so that the z -thickness increases as the total gas column density declines.
- 3) HI in the outer disk of NGC 3198 is not in the form of clouds, but is smoothly distributed.
- 4) If the outer disk of NGC 3198 is typical, the temperature of the neutral gas cannot be greatly in excess of ≈ 3000 K, or else HI disks would have much greater z -thicknesses than are observed.
- 5) More detailed observations and careful modelling of the edges of HI disks in galaxies will allow an accurate determination of the intensity of the extragalactic radiation field near the Lyman limit; there may be interesting implications for the cosmological evolution of neutral disks and absorption-line systems.

References

- Briggs, F.H., Wolfe, A.M., Krumm, N., and Salpeter, E.E. (1980) *Ap. J.*, **238**, 510
Sargent, W.L.W., Young, P.J., Boksenberg, A., Carswell, R.F., and Whelan, J.A.J. (1979) *Ap. J.*, **230**, 49
Silk, J., and Sunyaev, R.A. (1976) *Nature*, **260**, 508
Williams, R.E. (1967) *Ap. J.*, **147**, 556

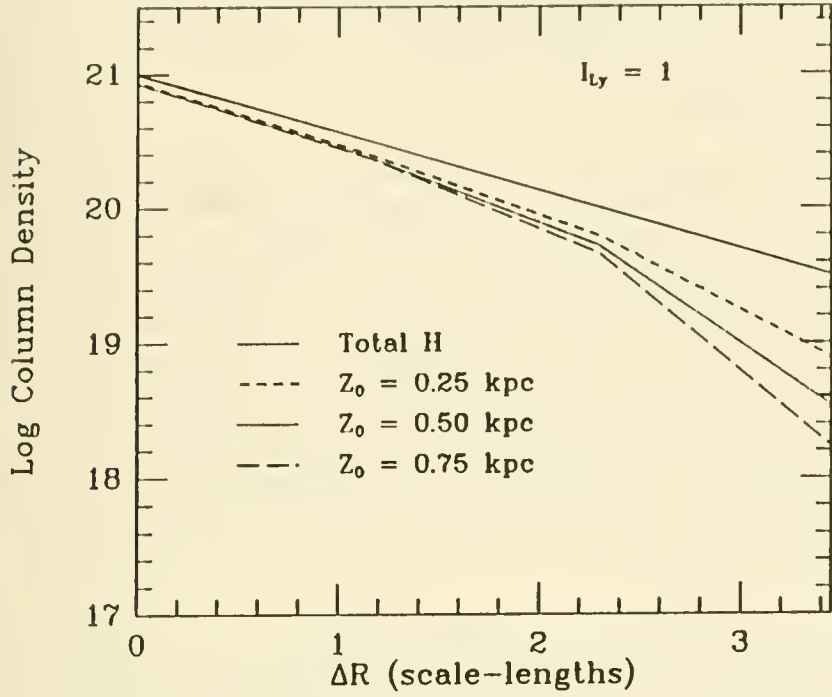


Figure 1. Total and neutral hydrogen column densities for fixed scale-height isothermal models. I_{Ly} is 1 for all models. Each model is labelled with the value of z_0 .

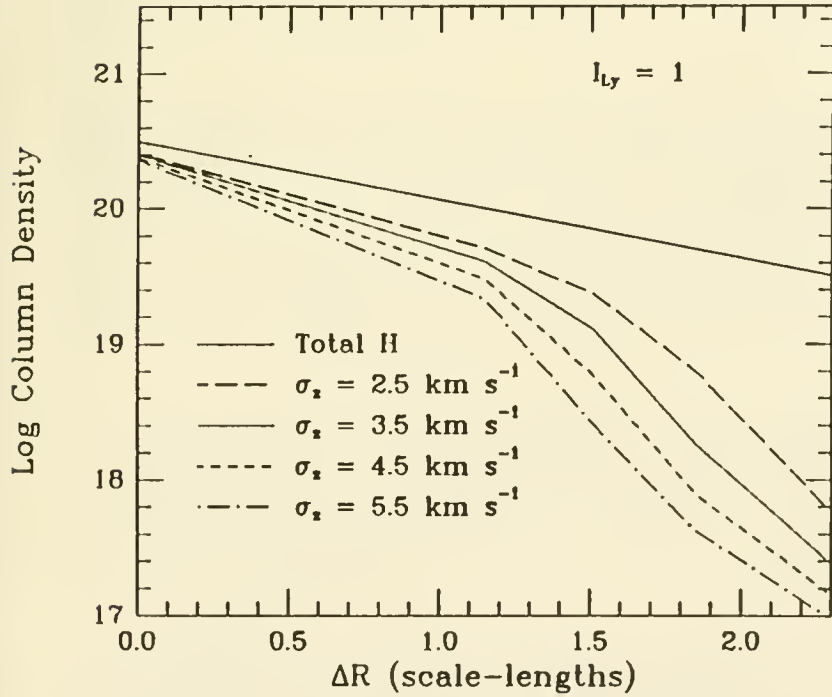


Figure 2. Total and neutral hydrogen column densities for self-gravitating isothermal models. I_{Ly} is 1 for all models. Each model is labelled with the value of σ_z .

A COMPARISON OF UV SURFACE BRIGHTNESSES AND H I SURFACE DENSITIES FOR SPIRAL GALAXIES

S.R. Federman and C. Strom
Department of Physics and Astronomy
The University of Toledo

Shaya and Federman (1987) suggested that the ambient ultraviolet flux at 1000 Å permeating a spiral galaxy controls the H I surface density in the galaxy. They found that the atomic envelopes surrounding small molecular clouds, because of their great number, provide the major contribution to the H I surface density over the stellar disk. The increase in H I surface density with later Hubble types was ascribed to the stronger UV fields from more high-mass stars in later Hubble types. These hypotheses are based on the observations of nearby diffuse interstellar clouds, which show a sharp atomic-to-molecular transition (Savage *et al.* 1977), and on the theoretical framework introduced by Federman, Glassgold, and Kwan (1979). Atomic envelopes around interstellar clouds in the solar neighborhood arise when a steady state is reached between photodissociation of H₂ and the formation of H₂ on grains. The photodissociation process involves photons with wavelengths between 912 Å and 1108 Å.

Shaya and Federman used H-α flux as an approximate measure for the far UV flux and made their comparisons based on averages over Hubble type. Here, we compare, on an *individual* basis, UV data obtained with space-borne and balloon-borne instruments for galaxies with measurements of H I surface density (Warmels 1988a, b). Our comparisons substantiate the conclusion of Shaya and Federman that the far UV field controls the H I content of spiral galaxies.

The UV data come from measurements made with the OAO-2 satellite (Code and Welch 1982), the ANS satellite (Wesselius *et al.* 1982), a rocket flight (Smith and Cornett 1982), and the balloon payload SCAP 2000 (Donas *et al.* 1987). The primary wavelength bins are those at 1500 Å, 2000 Å, and 2500 Å. The ANS data at 1800 Å and 2200 Å are averaged to estimate the measured flux at 2000 Å. The UV data are corrected for inclination and aperture. No correction for internal extinction is applied to these data, because most of the galaxies in the sample are nearly face-on and because we are interested in the ambient flux.

For the largest galaxies in our sample, the satellite observations require a correction for the aperture. The OAO-2 data were acquired with a circular aperture of 10' diameter, and the ANS data were acquired with a 2.5' x 2.5' aperture. Our correction involves the ratio of D₂₅ to the aperture. A linear correspondence, with little dispersion, between different measurements exists, indicating that even the smallest aperture is larger than the scale length in surface brightness.

Comparisons with the ANS data are stressed because more galaxies with H I data are common to this set and because these comparisons are based on a homogeneous sample. Plots of H I surface density versus UV surface brightness will be presented. The correlation between these two parameters improves as shorter wavelengths are considered. With the assumption of a linear relationship, the correlation coefficients are $r(2500) \sim 0.32$, $r(2000) \sim 0.39$, $r(1500)$

≥ 0.46 . Since H_2 is destroyed by photons with $\lambda \sim 1000 \text{ \AA}$, the improved correlation with the shortest measurable wavelengths strengthens the conclusions of Shaya and Federman (1987). These results also show that the association between interstellar material and young stars in spiral galaxies is most discernible at ultraviolet wavelengths.

REFERENCES

- Code, A.D. and Welch, G.A. 1982, Ap. J., 256, 1.
Donas, J., Deharveng, J.M., Laget, M., Milliard, B., and Huguenin, D. 1987, Astron. Ap., 180, 12.
Federman, S.R., Glassgold, A.E., and Kwan, J. 1979, Ap. J., 227, 466.
Savage, B.D., Bohlin, R.C., Drake, J.F., and Budich, W. 1977, Ap. J., 216, 291.
Shaya, E.J. and Federman, S.R. 1987, Ap. J., 319, 76.
Smith, A.M. and Cornett, R.H. 1982, Ap. J., 261, 1.
Warmels, R.H. 1988a, Astron. Ap. Suppl., 72, 427.
1988b, Astron. Ap. Suppl., 73, 453.
Wesselius, P.R., van Duinen, R.J., de Jonge, A.R.W., Aadlers, J.W.G., Luinge, W., and Wildeman, K.J. 1982, Astron. Ap. Suppl., 49, 427.

NGC 1058: Gas Motions in an Extended, Quiescent Spiral Disk

Margaret Murray Hanson
Dept. of Astrophysics, Planetary and Atmospheric Science
University of Colorado

John M. Dickey
Department of Astronomy
University of Minnesota
and
Sterrewacht Leiden

and

George Helou
Infrared Processing and Analysis Center
Caltech

We investigate in detail the motion of gas in the galaxy NGC 1058 using the VLA to map the emission in the 21-cm line. This galaxy is so nearly face-on that the contribution to the line width due to the variation of the rotational velocity across the D-array beam is small compared with the random z-motion of the gas. We confirm results of earlier studies (Lewis 1987, A. & A. Suppl., 63, 515; van der Kruit and Shostak 1984, A. & A., 134, 258) of the galaxy's total HI and kinematics, including the fact that the rotation curve drops faster than Keplerian at the outer edge of the disk, which is interpreted as a fortuitous twist of the plane of rotation in the outer disk. However, our very high velocity resolution (2.58 km s^{-1} after Hanning smoothing) coupled with good spatial resolution, allows us to measure more accurately the line width, and even to some extent its shape, throughout the disk.

One of the most interesting results of this study is the remarkable constancy of the line width in the outer disk. From radius $90''$ to $210''$ the Gaussian velocity dispersion (σ_v) of the 21-cm line has a mean value of 5.7 km s^{-1} (after correcting for the spectral resolution) with a dispersion of less than 0.9 km s^{-1} (see Figure 1). Translating this directly into a kinetic temperature ("Doppler temperature"):

$$T_{\text{Dopp}} = 121 \text{ K} (\sigma_v^2 / [\text{km s}^{-1}]^2)$$

gives 4000 K, with a dispersion of less than 1500 K over the outer disk. This constancy is observed even when comparing the spiral arms versus inter-arm regions (see Figure 2), which in the radius range from $100''$ to $150''$ the surface density modulates (defined as the ratio $N_{\text{peak}} - N_{\text{trough}} / N_{\text{peak}} + N_{\text{trough}}$) from 0.5 to 0.25 in the range $150''$ to $200''$.

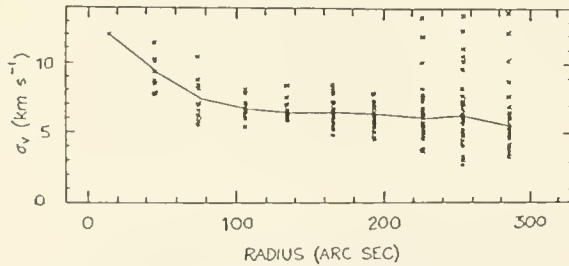


Figure 1. Radial Dependence of Line Width. Beyond $200''$ the low column densities lead to poorly determined Gaussian parameters.

One simple model to explain the constancy is that the pressure is low enough that all the neutral atomic hydrogen is in the warm phase, with little in cool, diffuse clouds. The constancy of σ_v would then be a natural consequence of the universality of the cooling

function, which determines the equilibrium temperature of the warm phase, and hence the line width. However, for solar neighborhood conditions a Doppler temperature of 4000 K would be uncomfortably low, since at least some of the line width must be contributed by macroscopic gas motions. The true kinetic temperature of the gas must then be even lower than 4000 K, a value which is already lower than most estimates for the warm phase temperature.

Another simple model would be to assume some or all of the gas is in cool clouds, whose kinetic temperature is much less than T_{Dopp} . At least some cool clouds must be present in the outer disk, as two supernovae (1961v and 1969l) have been observed there. In this case the line widths would be determined by the velocity distribution function of the clouds themselves. For instance, in the solar neighborhood, the (one dimensional) random velocity distribution for clouds has a half width of about 6 km s^{-1} . With our beam size, which corresponds to between 1 and 3 kpc depending on distance, it is reasonable to expect that many clouds contribute to each observed spectrum. This could possibly explain the smoothness of the Gaussian profiles. If we assume the individual clouds to have thermal line widths of order 1 km s^{-1} , then to find a smooth dispersion of 5.7 km s^{-1} , at least 25 clouds should contribute to each spectrum. In light of this model, the constancy of σ_v is still curious since it implies a remarkably uniform random velocity distribution for the clouds.

A second interesting result of this study is the shape of the residuals after subtracting the best fitting Gaussian from the spectrum. Higher sensitivity is needed to detect deviations from individual pixel spectra, but we can study averages of the residuals to look for widespread deviations from Gaussian-shaped line profiles. We have found that in the inner region corresponding to the optical disk ($r < 90''$) the mean residuals show a characteristic shape suggestive of two superimposed components: a broad, low level feature ($\sigma_v > 10 \text{ km s}^{-1}$) and a narrow feature ($\sigma_v < 8 \text{ km s}^{-1}$). The best-fit Gaussian will overestimate the width of the strong, narrow central line in order to reduce the residuals (data minus fit) in the wings and then underestimate the fitted line peak (see Figure 3). The source of the broad feature could be due to observing intermediate velocity clouds, like those seen in the Galaxy. It is difficult to understand the feature being due to thermal motions since it corresponds to a temperature greater than 10,000 K, where neutral hydrogen becomes collisionally ionized. Our detection is very provisional. Better measurement of this low level broad component, and confirmation of its very existence, would be best obtained from a more sensitive observation with more spectral channels. (The present VLA system could provide that with roughly the same integration time as that used here.)

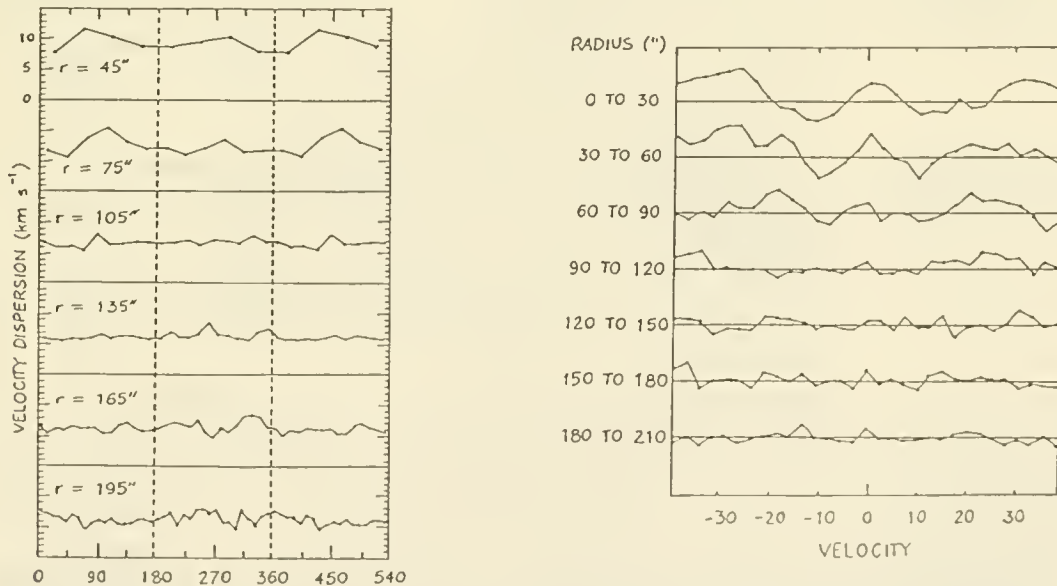


Figure 2. Azimuthal Dependence of Line Width. The spiral arms occur at 180° and 360° .
Figure 3. Data minus Gaussian fit line widths (residuals) as a function of radius.

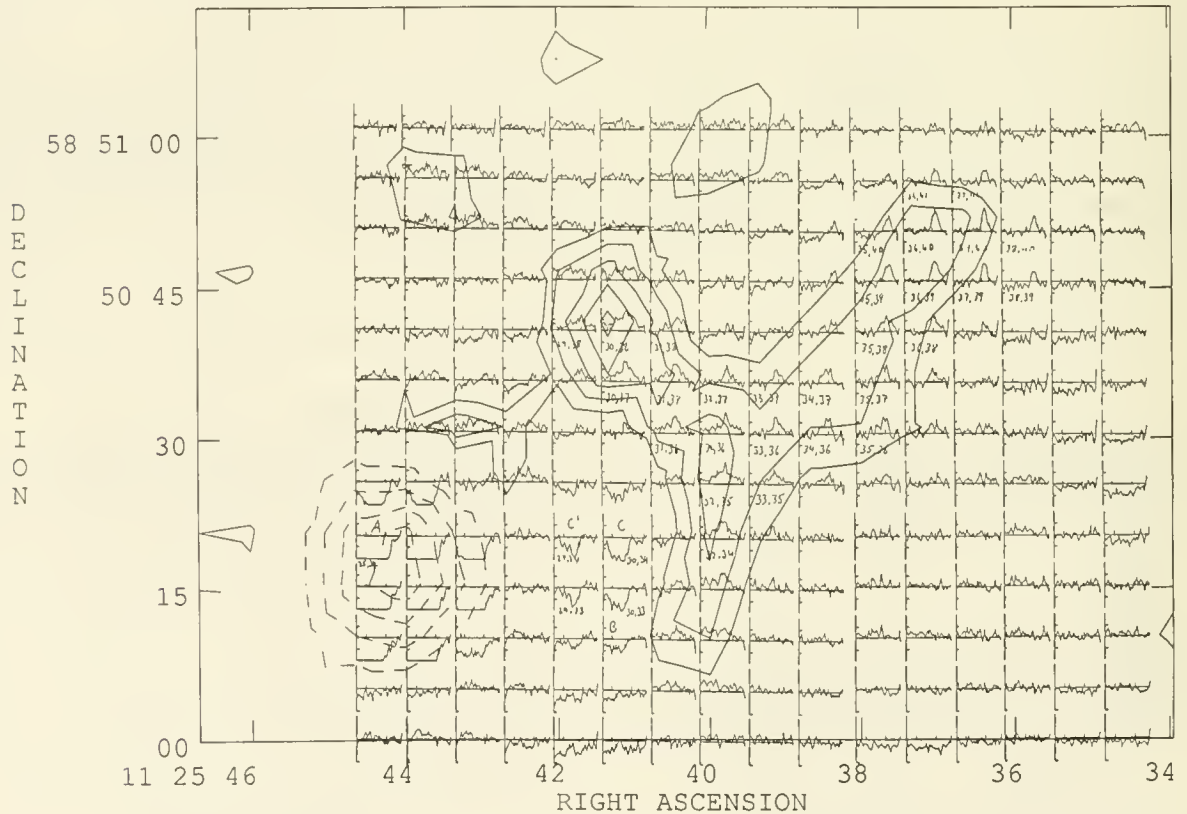
Neutral Hydrogen in the Starburst Galaxy NGC3690/IC694

E. Tolstoy, J.M. Dickey, and F.P. Israel

Sterrewacht Leiden, The Netherlands

Abstract:

We have made observations of the neutral hydrogen (HI) emission structure surrounding the very deep absorption peak [observed earlier by Dickey (1986)] in the galaxy pair NGC3690/IC694. This galaxy pair is highly luminous in the far infrared, and known to exhibit extensive star formation as well as nuclear activity. Knowledge of the spatial distribution and velocity structure of the HI emission is of great importance to the understanding of the dynamics of the interaction and the resulting environmental effects on the galaxies.



Observations:

We observed the system for 12 hours with the Westerbork Synthesis Radio Telescope (WRST), obtaining 64 maps with spatial resolution of $13'' \times 14''$ spaced by 8.2 km s^{-1} in velocity (512 km s^{-1} bandwidth). We reduced the data at Leiden and Minnesota using the AIPS package. We obtained a spectral line cube with $5.2''$ pixels, where each pixel has a velocity spectrum for its position. Thus, the three dimensions of the cube are right ascension, declination and velocity (or frequency). The velocity range of each spectrum is from 2950 km s^{-1} to 3350 km s^{-1} .

The first step in displaying the emission present in the cube is to search through the channel maps and decide which ones contain emission, and add these together into a single map (see Fig. 1). In Fig. 1, to try to get a feeling for what the cube contains, the velocity spectra for each pixel are also displayed.

Another way to study the spatial and velocity distribution of the H I emission is to fit a gaussian to the spectrum of each pixel and then map the resulting fitted parameters. We use the AIPS task XGAUS to find the integral (zeroth moment) and velocity center (first moment) of the best fit gaussian at each point. Values of the line integral, expressed in units of column density, range from $2 \times 10^{21} \text{ cm}^{-2}$ to $8 \times 10^{21} \text{ cm}^{-2}$ across the emission region.

The central velocity varies from 3080 km s^{-1} to 3256 km s^{-1} across the emission region. The northwest plume is moving with velocities consistently greater than the systemic (3196 km s^{-1}), and with a velocity gradient of about $20 \text{ km s}^{-1} \text{ kpc}^{-1}$.

We also made l-v diagrams, or position-velocity maps for several cuts through the cube at constant declination. These are shown in Fig.2. Looking through the series it seems that there is more than one velocity component present in the emission region. The two components are well separated in the north; as the slices go to lower declination these components appear to merge. It may be that these are two separate structures, or two extensions leading off from a central gas cloud.

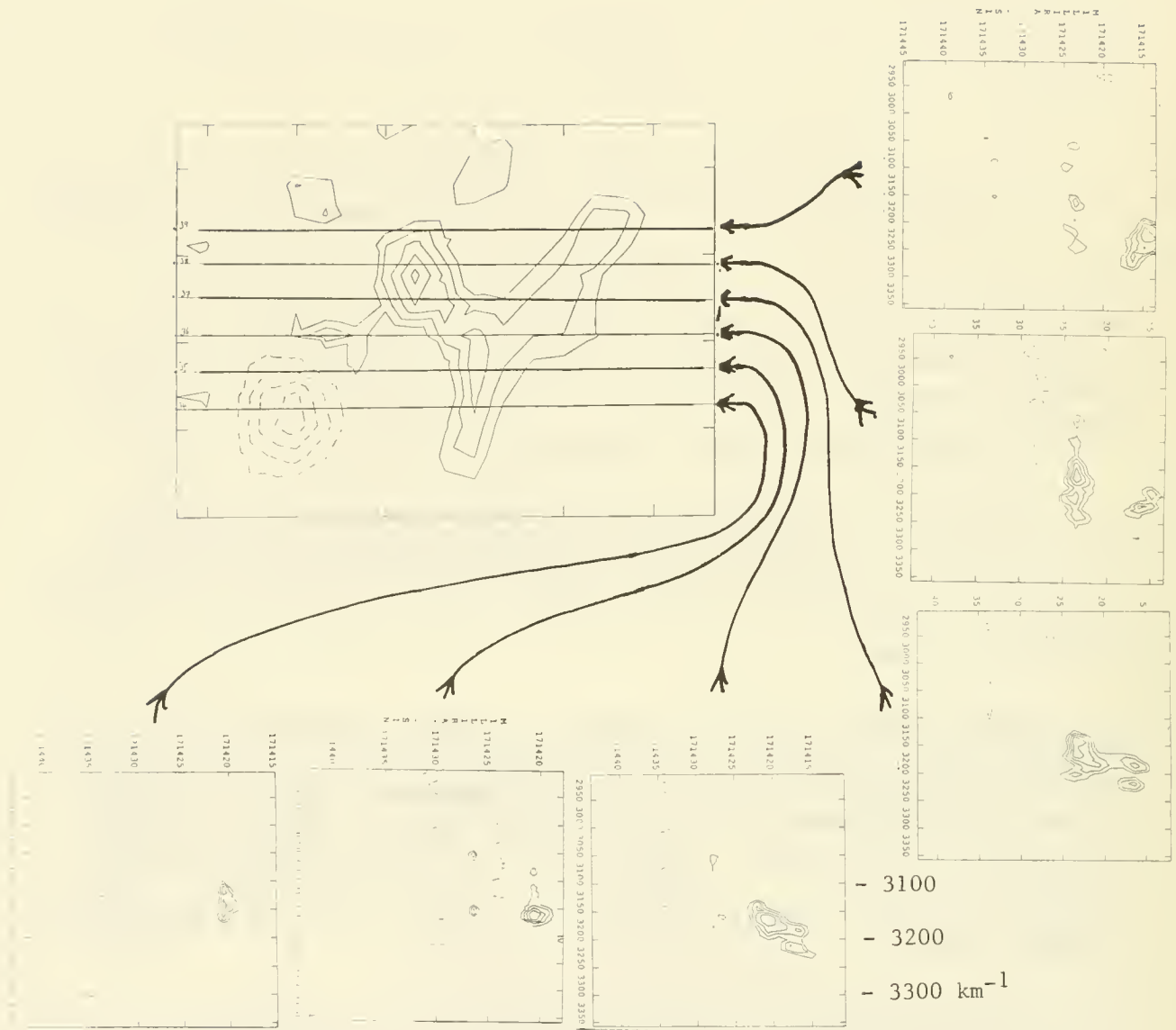


FIG. 2 : Here we have a selection of position velocity cuts through the cube, sliced along lines of constant declination spaced by 6 " as shown on the map.

Results :

We conclude that NGC 3690 + IC 694 is a very complex system, the HI dynamics of which still need some careful work.

At 6 cm and 20 cm Gehrz et al. found four compact radio continuum sources A, B, C, and C'. These seem to coincide with peaks of emission at

10 microns (Gehrz et al.) and the peaks are also discernable in the 2.2 micron map (Telesco et al. 1985). The CO $\int T dv$ map (Sargent et al. 1987) shows high column density concentrations of CO around A and C,C', but nothing is seen at B.

The arm extending 6 kpc to the north-west of NGC 3690 appears to be moving at speeds greater than the central velocity, and could well be the arm of a spiral galaxy aligned skew to our line of sight as suggested by Stanford and Wood (1989). The infra-red polarimetry of Jones (1989) seems to agree with the general alignment of our plume and also the extension seen by Stanford and Wood to the south-east, again giving the impression of a disk-like structure. However, the nuclear core of such a spiral [?] galaxy would appear to be severely misaligned with the spiral arm structure, as seen in the infra-red data (Telesco et al.). From optical and uv spectroscopy Augarde and Lequeux (1985) deduce that NGC 3690 (B,C) and IC 694 (A) are two bodies rotating in opposite senses. They assume the two galaxies are Sb or early Sc type, but conclude that their optical images are too perturbed to be certain. This fits in, in general terms, with what we find. We have yet to confirm the south-west extended structure found by Stanford and Wood, but we should be able to reach their limit with further tapering. Our velocity resolution is considerably finer, so that a clearer idea of the dynamics of the HI can be obtained.

References :

- Augarde, R., and Lequeux, J. (1985) *Astron. Astrophys.*, 147, 273.
- Dickey J.M. (1986) *Ap.J.* 300, 190.
- Gehrz, R.D., Sramek, R.A., and Weedman, D.W. (1983) *Ap.J.* 267, 551.
- Jones, T.J. (1989) submitted to *Ap.J.*
- Sargent, A.I., Sanders, D.B., Scoville, N.Z. and Soifer, B.T. (1987) *Ap.J(Lett)* 312, L35.
- Stanford, S.A. and Wood, D.O.S. (1989) Preprint.
- Telesco, C.M., Decher, R., and Gatley, I. (1985) *Ap.J.* 299, 896.

High velocity gas in external galaxies

J. Kamphuis, J. M. van der Hulst and R. Sancisi

Kapteyn Astronomical Institute
Postbus 800
NL-9700 AV Groningen
The Netherlands

Abstract

Two nearby, nearly face-on spiral galaxies, M 101 and NGC 6946, observed in the HI with the WSRT as part of a program to search for high velocity gas in other galaxies, are used to illustrate the range of properties of high velocity gas in other galaxies found thusfar.

Introduction

The origin of the high velocity clouds in our Galaxy is still not well established. A fundamental problem with these high velocity clouds is the uncertainty in distance which makes it difficult to estimate the cloud masses and their spatial distribution. If the equivalent of the high velocity clouds can be found in other galaxies one would hope to acquire better insight into the origin of high velocity gas in galaxies, including our own. We therefore began a program of sensitive observations of four nearby spiral galaxies, using the Westerbork Synthesis Radio Telescope (WSRT) in search of high velocity gas features.

The first galaxy to be observed was M 101, where a large complex of high velocity gas was found (Van der Hulst and Sancisi, 1988), with velocities of up to 160 km/sec in excess of the rotation of the gas in the local disk and with a projected size of over 10 kpc. This gas is most likely moving in a direction perpendicular to the plane, coming out of the plane rather than falling in. The HI mass of this complex is about $2 \times 10^8 M_{\odot}$. The high velocity gas is connected with the gas in the disk and possibly related to large scale HI structures in the disk such as kinks in the spiral structure and holes in the HI distribution. Because of the one-sidedness and the large velocities involved it appears unlikely that stellar winds or supernova explosions could have driven this gas out of the disk. A more plausible explanation

seems that the high velocity gas is the result of infall of gas into the disk of M 101 as described by Tenorio-Tagle and Bodenheimer (1988).

Besides this HI with very high velocity with respect to the disk we also find several regions in M 101 with HI at intermediate velocities deviating by about 50 km/sec with respect to the rotation in the local gas layer, illustrating that the gas disk of M 101 is not very quiescent. These intermediate features have velocities that are either blue- or redshifted with respect to the rotation.

In contrast to the very high velocity gas discovered in M101 there are the now well known bubbles and shells in M 31 (e.g. Brinks and Bajaja, 1986), M 33 (Deul, 1988), LMC (e.g. Meaburn, 1980) and our galaxy (e.g. Heiles 1984). Their properties are at least two orders of magnitude lower than the properties of the high velocity gas in M 101. The involving energies and sizes of these phenomena are respectively about 10^{51} - 10^{52} ergs and 0.1-1 kpc. The corresponding expansion velocities are of the order of 5-10 km/sec and hardly exceed 20 km/sec.

The first preliminary results on the second of our four survey galaxies, NGC 6946 have become available and show high velocity gas and hole/shell features which are intermediate between the HI shells in our Galaxy, M 33, M 31 and the LMC on the one hand and the M 101 complex on the other hand. Here we briefly discuss some of the new features found in NGC 6946.

Results

From the WSRT observations we obtained maps at resolutions of $15''$ ($= 0.7$ kpc for a distance of 10 Mpc), $30''$ and $60''$. The full resolution map shows no obvious velocity deviations. We did, however, find faint HI having excess velocities with respect to the gas in the disk in the $60''$ data, but the precise connection with the disk is smeared out at this resolution. Therefore we used the $30''$ data as a compromise between spatial resolution and sensitivity.

In NGC 6946 we found about 10 regions with velocities deviating by 50 to 80 km/sec from normal rotation. Most of these regions are spread throughout the disk and have either blueshifted or redshifted velocities with respect to the local rotation in the disk, but never show both. We discuss the two most striking features found at the north-western side in more detail below.

The first, in the northern inter-arm region, shows peculiar, redshifted velocities of about 50 km/sec with respect to the local disk. The redshifted velocity gas is located where the spiral arm bifurcates. Confusion with galactic foreground HI makes

it impossible to trace this gas further out to the east. The correspondence of features in the disk and the location of the redshifted gas suggests a causal relation, which could be similar to the high velocity gas of complex A in M 101 (Van der Hulst and Sancisi, 1988).

The other interesting region with peculiar velocities is associated with two HI holes. The innermost hole has a length of 5.5 kpc and an axial ratio of 3. The outer hole has a round shape and a diameter of 2 kpc.

The velocities at the edges of the inner elongated hole are blueshifted up to 60 km/sec with the highest velocities seen towards the hole centre, suggesting an expanding shell structure. The velocity deviations at the edges of the round hole are up to 100 km/sec but here no gas is detected towards the hole centre. The HI mass in this complex is about $1.2 \times 10^7 M_{\odot}$, not enough to fill the hole. The associated kinetic energy is of the order of 10^{53} ergs.

The gas complexes with the velocity deviations are not obviously associated with star forming regions such as giant HII regions or OB associations. Therefore, and because of the large kinetic energies required for producing these phenomena, it is difficult to produce these peculiar velocities with stellar winds or supernova explosions. An alternative explanation involves the infall of gas into the disk of NGC 6946 which drives a subsequent outflow of HI.

With only two galaxies studied in some detail it is not yet possible to make general statements about the presence of high velocity gas in other galaxies. Three more systems are being studied using the WSRT and the VLA. The phenomena observed in NGC 6946 and M 101 do suggest, however, the possible existence of a population of intermediate velocity structures in galaxies with quite a range of properties.

references

- Brinks, E, Bajaja, E., 1986, *Astron. Astrophys.*, **169**, 14
Deul, E., 1988, Ph.D. Thesis Leiden
Heiles C., 1979, *Astrophys. J. Suppl.*, **55**, 585
Meaburn, J., 1980, *Monthly Notices Roy. Astron. Soc.*, **192**, 365
Tenorio-Tagle, Guillermo, Bodenheimer, Peter, 1988, *Ann. Rev. Astron. Astrophys.*, **26**, 145
Van der Hulst, Thijs and Sancisi, Renzo, 1988, *Astron. J.*, **95**, 1354

A SCALING LAW OF RADIAL GAS DISTRIBUTION IN DISK GALAXIES

Zhong Wang
Astronomy Department
California Institute of Technology

Based on the idea that local conditions within a galactic disk largely determine the region's evolution time scale, we built a theoretical model to take into account molecular cloud and star formations in the disk evolution process. Despite some variations that may be caused by spiral arms and central bulge masses, we find that many late-type galaxies show consistency with the model in their radial atomic and molecular gas profiles. In particular, we propose that a scaling law be used to generalize the gas distribution characteristics. This scaling law may be useful in helping to understand the observed gas contents in many galaxies.

Our model assumes an exponential mass distribution with disk radius. Most of the mass are in atomic gas state at the beginning of the evolution. Molecular clouds form through a modified Schmidt Law which takes into account gravitational instabilities in a possible three-phase structure of diffuse interstellar medium (McKee and Ostriker, 1977; Balbus and Cowie, 1985); whereas star formation proceeds presumably unaffected by the environmental conditions outside of molecular clouds (Young, 1987). In such a model both atomic and molecular gas profiles in a typical galactic disk (as a result of the evolution) can be fitted simultaneously by adjusting the efficiency constants. Galaxies of different sizes and masses, on the other hand, can be compared with the model by simply scaling their characteristic length scales and shifting their radial ranges to match the assumed disk total mass profile $\sigma_{tot}(r)$.

The idea and an example of applying the scaling law are as follows. Suppose the disk's radial mass distribution is approximately exponential, then our evolution model generally results in atomic and molecular gas profiles shown as shadowed regions in Figure 1 and 2, respectively. For a galaxy with measured disk mass profile $\sigma_{tot}(r)$, these model results can be applied by first figuring out the position of the galactic center on radius axis, and then scaling the axis to determine its actual unit depending on the scale length of $\sigma_{tot}(r)$. For example, the Milky Way Galaxy would fit in if we put the Galactic Center at position GC (of the vertical dot-dashed line), and just ignore part of the figure to the left of that line. A galaxy of smaller mass would correspond to a shift further to the right, while a more massive one to the left. If the disk scale length of our Galaxy is about 2.9 kpc (as in the model of Caldwell and Ostriker, 1981) then the interval between small tickmarks of the horizontal axes in Figure 1 and 2 correspond to 1 kpc in radius. For comparison, we plot the observationally determined surface mass densities $\sigma_{HI}(r)$ and $\sigma_{H_2}(r)$ of our Galaxy as histograms in the two figures. The galactocentric distance of the Sun is corrected to be 9.1 kpc in both cases.

Given the fact that some variations in a number of model parameters (such as the spiral arm pattern and arm-to-interarm density contrast) do not seriously change the general outcome of our calculation, the shadowed regions of the two figures then approximate the



Figure 1. A schematic illustration of the scaling law for HI gas. The three histograms represent measured HI profiles of the Milky Way Galaxy by Burton and Gordon (1978), Kulkarni, Blitz, and Heiles (1982), and Henderson, Jackson, and Kerr (1982). The thin σ_{tot} curve is the Galaxy's disk mass model of Caldwell and Ostriker (1981). See text for details.

HI and H₂ profiles of a typical galaxy, or a galaxy “templet”. Tests show that many nearby late-type galaxies with well-sampled HI and CO maps roughly agree with such a model prediction (assuming that CO gas is a proportionality tracer of H₂). Furthermore, the scaling law provides explanation for some observational facts that have received attention only fairly recently. For example, the tendency of dwarf galaxies to have little or no molecular gas in their disks is easily understood from Figure 2, in view of the rapid decrease of $\sigma_{H_2}(r)$ with radius in the templet galaxy.

Some observational data show significant deviations from the general model results of both atomic and molecular gas. The Milky Way Galaxy, for instance, shows pronounced central depression in H₂, and perhaps in HI profile as well. These features can not, as our model work indicates, be simply accounted for without adopting new mechanisms in addition to the azimuthally averaged “one-zone” calculation. Possible causes of these features, which are found to be common among Sa and some Sb type galaxies, include radial gas flows due

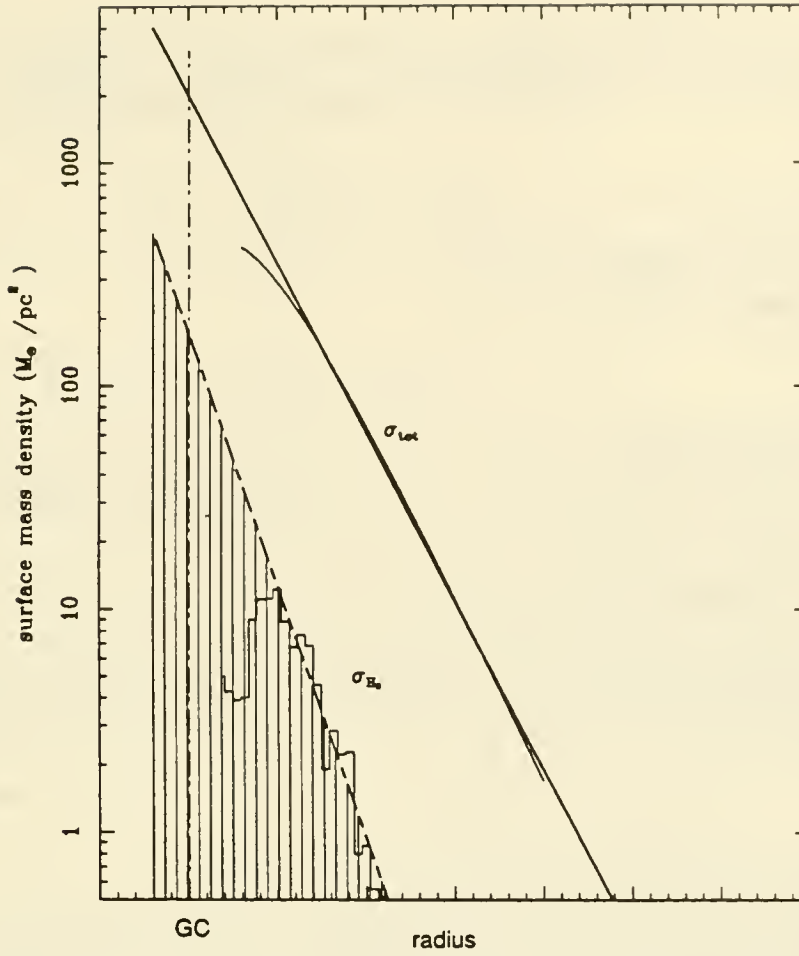


Figure 2. Same as Figure 1, but for H_2 gas. The histogram is from observations of Burton and Gordon (1978) and Clemens, Sanders, and Scoville (1988).

to the effect of the massive central bulge component in these galaxies (Wyse and Silk, 1989; Wang, 1989).

- Balbus, S. A. and Cowie, L. L. 1985, *Ap. J.*, **297**, 61.
 Burton, W. B. and Gordon, M. A. 1978, *Astr. Ap.*, **63**, 7.
 Caldwell, J. A. R. and Ostriker, J. P. 1981 *Ap. J.*, **251**, 61.
 Clemens, D. P., Sanders, D. B., and Scoville, N. Z. 1988, *Ap. J.*, **327**, 139.
 Henderson, A. P., Jackson, P. D., and Kerr, F. J. 1982, *Ap. J.*, **263**, 116.
 Kulkarni, S. R., Blitz, L., and Heiles, C. 1982, *Ap. J. (Letters)*, **259**, L63.
 McKee, C. F. and Ostriker, J. P. 1977, *Ap. J.*, **218**, 148.
 Wang, Z. 1989, Ph.D. thesis, Boston University.
 Wyse, R. F. G. and Silk, J. 1989, *Ap. J.*, **339**, 700.
 Young, J. S. 1987, in *Star Forming Regions*, IAU Symposium 115, ed. M. Peimbert and J. Jugaku, p557.

Radial Profiles of Gas in Late-Type Disk Galaxies

Curtis Struck-Marcell, Iowa State University

I. Review of Published Data

The azimuthally averaged HI distribution, and the total gas density distribution derived from HI and CO observations (and assuming $N_{H_2} = 2.8 \times 10^{20} I_{CO}$) as a function of radius in several nearby, early-type disks are examined in this study.

A. $\Sigma \propto 1/r$ where the Rotation Curve is Flat

First pointed out by Quirk (1972), and recently discussed by Kennicutt (1989) this conclusion is evident in the gas distributions considered here, and in the data of Wevers' (1984) thesis. For example, the figure shows the deviation of the azimuthally averaged HI surface density profiles from a best-fit $1/r$ profile in Wevers' galaxies. Only data from positions with circular velocities within 5% of the average value in the flat part of the rotation curve are plotted, only those galaxies with more than 3 such points were included. The curve for NGC 628 also includes the molecular gas observed by Adler and Lizst (1989). For the other sample galaxies the molecular gas either lies interior to the flat part of the rotation curve or a CO distribution has not been published. It is apparent that most of the data fall within about 25% of the mean $1/r$ profile, except in the outermost parts of some galaxies. The larger surface density deviations in these outer regions frequently correlate with deviations from flatness in the rotation curve.

B. The Gas Distribution in the Inner Disk is More Complex

The available data for the inner regions of the disks are more sparse and their interpretation is more problematic. We can only make a few tentative generalizations:

1. When the central gas surface density is high (e.g. $\Sigma > 30$ solar masses/pc²) the $1/r$ profile continues from the outer regions to deep into the central regions (e.g. IC 342, NGC 5055, NGC 6946).
2. In the other galaxies there is still a central peak in $\Sigma(r)$. In the cases considered here, this peak is clearest in M33 and NGC 2403, where it lies within the region with $v_\theta < 60$ km/s.
3. If the central peak is well interior to the $\Sigma \propto 1/r$ region, then there is a flat, $\Sigma \propto \text{constant}$, transition region (M33, NGC 2403). In NGC 628 the center may be primarily of this flat form, since the central rise is very modest.

II. Theoretical Considerations and Constraints

A. Azimuthally Averaged Hydrostatic Equilibrium (for a continuum gas)

We have *accretion* disk equations like those in the review of Pringle (1981).

1. Mass Continuity, implies $\partial \Sigma / \partial t = 0$, radial velocity $v_r = 0$, and self-diffusion term $\partial^2(r\Sigma) / \partial r^2 = 0$, which yields $\Sigma = a/r + b$, with $a, b = \text{constant}$.
2. Equation of State: Isothermal cloud gas, with sound speed $c = \text{constant}$, may be an adequate approximation.
3. Momentum Transport:
 - a) Radial Force Balance (in a potential dominated by collisionless matter). The azimuthally averaged pressure gradient force is

$$\frac{1}{r\Sigma} \frac{d}{dr}(rP) = \frac{1}{r\Sigma} \frac{d}{dr}(r\Sigma c^2)$$

Case i) $\Sigma \propto 1/r$. The pressure gradient force is zero, and centrifugal force balances gravity, just as for the stars.

Case ii) $\Sigma = \text{constant}$. The averaged pressure gradient force goes as $1/r$. In the flat rotation curve region, $v_\theta = \text{constant} \gg c$, and both gravity and centrifugal force also go as $1/r$, so pressure is negligible throughout the region. In a solid body region, $v_\theta \propto r$, so as r decreases the pressure increases relative to the centrifugal force.

b) Azimuthal Force Balance The only force is viscosity, so in equilibrium it must be zero, then,

$$v \Sigma r^3 \frac{\partial}{\partial r} \left(\frac{v_\theta}{r} \right) = \text{constant},$$

which gives a relation between Σ and v_θ . E.g.,

if $v_\theta = \text{constant}$, then $v \Sigma r = \text{constant}$ (or $\Sigma \propto 1/r$ for $v = \text{constant}$).

if $v_\theta \propto r$, then $\partial(v_\theta/r)/\partial r = 0$, and Σ is unrestricted.

if $\Sigma = \text{constant}$, then either $v_\theta \propto r$ or $v_\theta \propto 1/r$ (unphysical).

The role of (spiral) waves in transporting angular momentum, and thus influencing radial structure is not clear, and will not be considered here.

B. Local Gravitational Stability (Toomre Q)

Larson (1988) and Kennicutt (1989) have recently summarized the theoretical indications and observational evidence, respectively, showing that Toomre's (1964) gravitational stability parameter $Q = c\kappa/\pi G \Sigma$ is of order unity throughout the star-forming part of a galaxy disk. In the isothermal, $v_\theta = \text{constant}$ part of a disk this also implies $\Sigma \propto 1/r$, consistent with the other constraints, but also setting the value of Σ .

C. Secular Kinetic Equilibrium

Large clouds may have long mean free paths ($\lambda \approx 1$ kpc.) in galaxy disks, so kinetic (random walk) effects must be considered. Diffusive mass fluxes between adjacent annuli of width λ must balance, so $\Sigma r c = \text{constant}$. (For practical purposes this is equivalent to zero self-diffusion.) Momentum Flux balance between adjacent annuli implies, $\Sigma r c v_\theta = \text{constant}$. This condition is not equivalent to minimizing hydrodynamic viscous shear. E. g. the latter is zero when $v_\theta \propto r$, and $\Sigma \propto 1/r$, but the present condition is not satisfied!

III. Conclusions

- Both the available data and theoretical considerations suggest that the unique equilibrium surface density profile in the flat-rotation-curve region of the disk is $\Sigma \propto 1/r$. If this profile is also stable to non-axisymmetric disturbances, then this region may be regarded as a gas reservoir for the galaxy.
- The existence of equilibrium or quasi-steady profiles in the inner disk, where v_θ increases with r is more problematic. If $v_\theta \propto r$ in this region, then there are two hydrodynamic equilibrium forms: $\Sigma \propto 1/r$ or $\Sigma = \text{constant}$. There are examples of both forms in the observations. However, neither is a kinetic equilibrium form, so we can expect diffusive processes to funnel material from the reservoir region inwards. At the same time, the critical density for local gravitational instability is constant in regions where $v_\theta \propto r$, so if $\Sigma \approx \Sigma_{\text{crit}}$, star formation processes may oppose the kinetic ones. We do not yet understand the outcome of this interplay of forces.

Adler, D. S., and Lizst, H. S. 1989, Ap. J., **339**, 836.

Kennicutt, R. C. 1989, Ap. J. in press.

Larson, R. B. 1988, in *Galactic and Extragalactic Star Formation*, eds. R. E. Pudritz and M. Fich (Kluwer) p. 459.

Pringle, J.E. 1981, Ann. Rev. Astr. Ap. **19**, 137.

Toomre, A. 1964, Ap. J., **139**, 1217.

Wevers, B. M. H. R. 1984, thesis, Groningen.

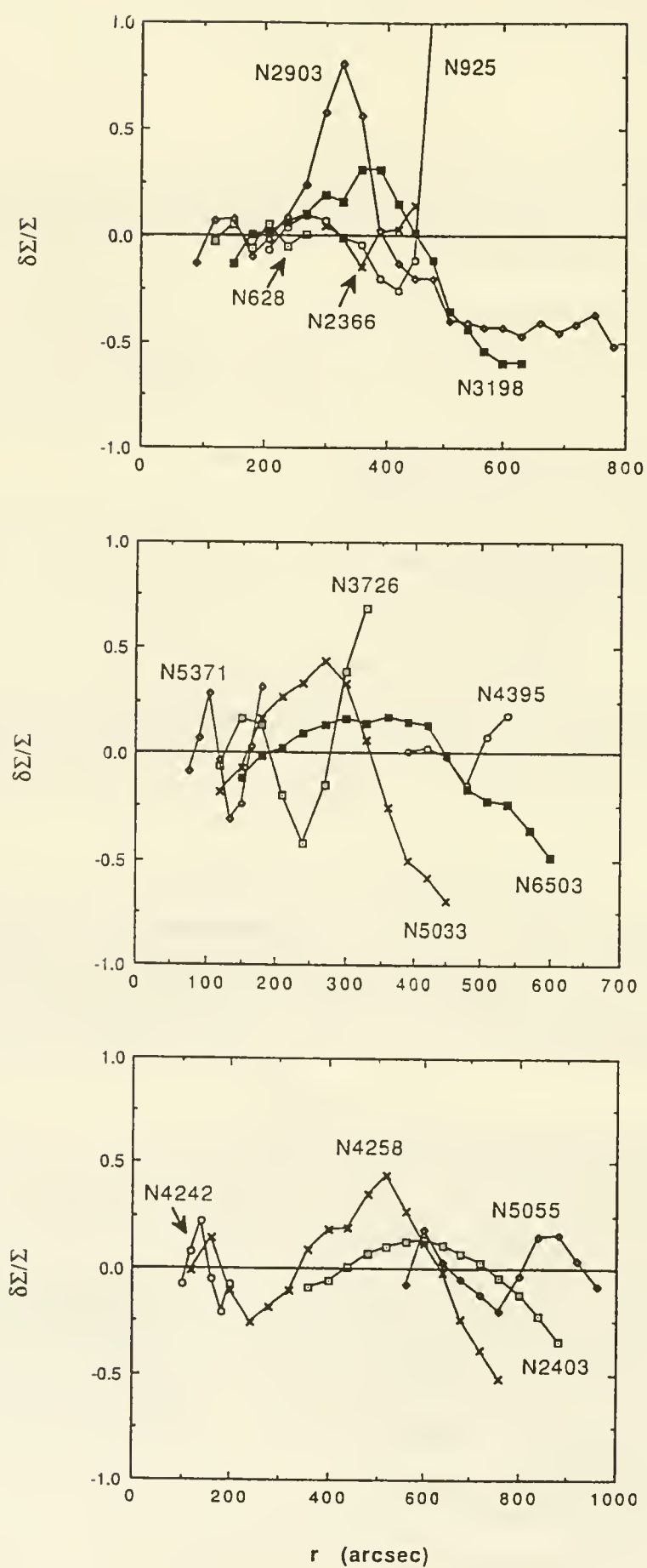


Figure 1a-c. Shows the deviation of the azimuthally averaged gas surface density profiles from a best-fit $1/r$ profile using the data from Wevers (1984) as described in the text.

Disk Mass Densities in Edge-on Spiral Galaxies

Michael P. Rupen

Center for Astrophysics

VLA observations of the neutral hydrogen gas in two nearby edge-on spirals (NGC 4565 and NGC 891) successfully resolve the thickness of the gas layers in both disks over a wide range in radii. The combination of ‘B,’ ‘C,’ and ‘D’ array data produces a 4 arcsec (~ 200 pc) beam and 21 km s^{-1} velocity resolution, combined with sensitivity to structures as large as 18 arcmin (~ 54 kpc). These observations directly constrain the mid-plane disk mass densities, under the assumption of an equilibrium between the thermal pressure of the gas and the gravitational attraction of the disk. The results of a preliminary analysis are as follows:

1. If the z -velocity dispersion of the gas is $10\sigma_{10} \text{ km s}^{-1}$, the mass densities in NGC 4565 fall from 0.11 to $0.009\sigma_{10}^2 M_{\odot}/\text{pc}^3$ between 0.7 and 3.5 optical disk scale-lengths; the decline is exponential in radius, consistent with a constant mass-to-light ratio for the disk. In NGC 891, although the mass densities also fall off with radius (from 0.09 to $0.02h\sigma_{10}^2 M_{\odot}/\text{pc}^3$ between 0.8 and 2.8 scale-lengths), there are abrupt local oscillations in the observed thickness that are difficult to model in terms of a simple hydrostatic equilibrium. Non-thermal pressures may account for these ‘wiggles,’ but the general trend of thickening with radius implies that the large-scale behavior of the thickness is determined by the balance of gravitation and thermal pressure.
2. If the disk mass distribution above the plane follows that of the old disk starlight, the mass-to-light ratio of the disk in NGC 4565 is $3_{-1}^{+3}\sigma_{10}^2 M_{\odot}/L_{\odot,B}$, and the disk mass is about $15\sigma_{10}^2\%$ of the total. The halo is probably dynamically important at all radii; the disk is not ‘maximal,’ unless the gas velocity dispersion is extremely high. If one assumes purely thermal pressures in NGC 891, its mass-to-light ratio increases with radius from 3 ± 1 to $5 \pm 2h\sigma_{10}^2 M_{\odot}/L_{\odot,B}$; again, the disk constitutes a small fraction of the mass.
3. In both galaxies, the atomic gas is an important dynamical component well before the edge of the disk, while the molecular gas may contribute a substantial fraction of the mid-plane mass density nearer the bulge.

These data also allow a detailed study of the HI in these galaxies; in general their brightness temperature distributions seem similar to that in the Milky Way. Both galaxies show asymmetric HI extensions beyond the optical disk. In NGC 4565 the extension is a surprisingly abrupt warp, which may bend back to parallel the galactic plane; the velocity structure implies the warp is continuous around the disk.

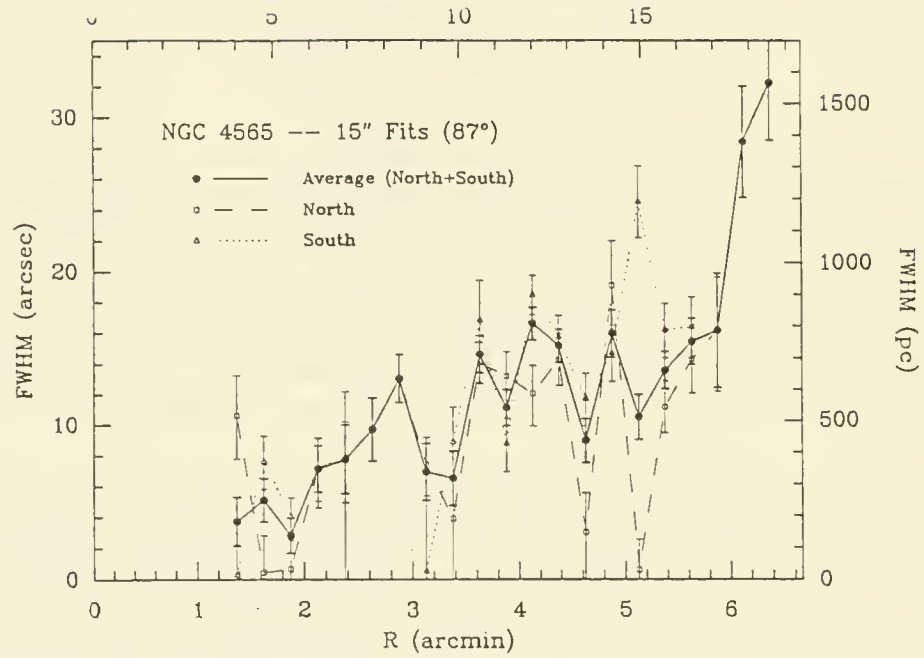


Fig. 1: Thickness of HI layer (FWHM). Inclination effects have been removed. Error bars are formal 1σ errors of the fits. Note the consistency of the (independent) fits on opposite sides of the nucleus.

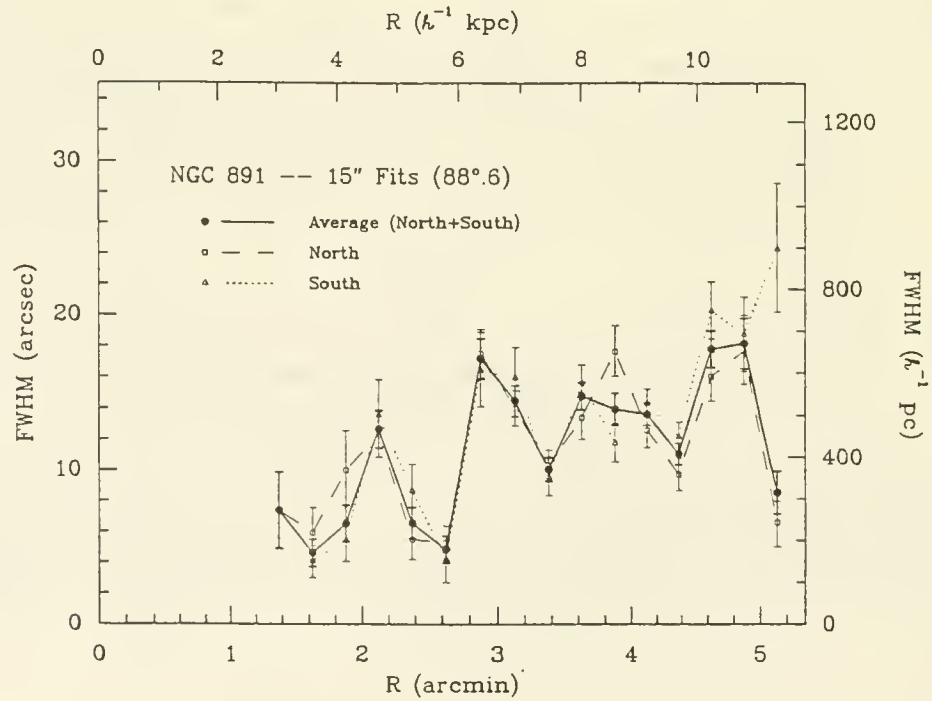


Fig. 2: Thickness of HI layer (FWHM). Inclination effects have been removed. Error bars are formal 1σ errors of the fits. Note the abrupt "jumps" in the thicknesses.

A Survey of the Properties of Early-Type Galaxies

J. N. Bregman, M. S. Roberts, and D. E. Hogg
National Radio Astronomy Observatory¹

A compilation of the properties of elliptical and early disk galaxies has been completed. In addition to material from the literature, such as IRAS fluxes, the compilation includes recent measurements of HI and CO, as well as a review of the x-ray properties by Forman and Jones. The data are used to evaluate the gas content of early systems and to search for correlations with x-ray emission.

The interstellar medium in early-type galaxies is generally dominated by hot interstellar gas ($T \sim 10^7$ K; c.f. the review by Fabbiano 1989 and references therein). In addition, a significant fraction of these galaxies show infrared emission (Knapp, et al., 1989), optical emission lines, and visible dust. Sensitive studies in HI and CO of a number of these galaxies have been completed recently, resulting in several detections, particularly of the later types. We wish to understand the connection among these different forms of the interstellar medium, and to examine the theoretical picture of the fate of the hot gas. To do so, we have compiled observations of several forms of interstellar matter for a well-defined sample of early-type galaxies. Here we present a statistical analysis of this data base and discuss the implications of the results.

The sample we have chosen is a group of 467 galaxies from the Revised Shapley-Ames Catalog that were classified there as E, SO, SBO, Sa, or peculiars of those types. We include IRAS observations, x-ray properties, and radio data on HI, CO, and continuum emission, as well as the usual optical properties. Information from the literature has been supplemented by unpublished data on HI, CO, and x-rays.

As expected the later types -- the Sa's and peculiar Sa's -- commonly have observable quantities of interstellar material. More than 90 percent of the objects that have been searched with high sensitivity have emission at both 100 microns and in HI or CO. The early disk systems, the SO's, also are frequently found in the IRAS survey, and almost half of the objects surveyed with high sensitivity at radio wavelengths are found to have either HI or CO. However, it continues to be difficult to find observational evidence for significant amounts of cold matter in elliptical galaxies. Fewer than half are known to be 100 micron sources, and very few of the ellipticals surveyed with high sensitivity are detected in HI. This is in marked contrast to the hot component of interstellar gas; more than two-thirds of the ellipticals that have been searched at x-ray wavelengths were detected.

The HI detection rate for E's and for SO's is illustrated in Fig. 1 as a histogram of the HI mass normalized by blue luminosity. Both the value of this ratio and the frequency of detection is significantly different between these two galaxy types. Capture alone, which seems to be the case for the ellipticals, cannot account for the HI in (most) SO's unless a rather complex time and depletion mechanism is invoked. A census of the

¹Operated by Associated Universities, Inc., under cooperative agreement with the National Science Foundation

interstellar content of E's and S0's is displayed in Fig. 2. Note that only detections are shown; upper limits, often very stringent, are not included in this display. In this sample the x-ray, HI, and H₂ masses are typically in the range 10⁸-10^{10.5} M_⊙ while those for dust (from 100 microns) and emission line gas are 10³-10⁷ M_⊙ (H₀=50).

The data set offers the possibility of studying the correlation between various properties of early-type galaxies. For example, in a commonly-discussed model, the source of the x-ray emitting gas in ellipticals is stellar mass loss. Ejecta from one star colliding with ejecta from another star initially heats the gas, and infall deeper into the potential well causes additional heating. When other sources of heat are unimportant, the steady-state x-ray luminosity should be the product of the total mass loss rate and the square of the velocity dispersion (Sarazin and White 1988). Since the total mass loss rate is proportional to L_{opt} , one expects $L_x \propto L_{\text{opt}} \sigma^2$. The velocity dispersion is related to L_{opt} , which leads to the prediction $L_x \propto L_{\text{opt}}^{1.7}$. Using the 48 elliptical galaxies for which improved optical data are available, (Faber *et al.*, 1989), and which have information about their x-ray emission, we find that $L_x \propto L_{\text{opt}}^{2.3}$, with an uncertainty in the exponent of 0.2. The discrepancy does not arise because of our use of the Faber-Jackson relationship. The quantities $L_x/L_{\text{opt}} \sigma^2$ and L_{opt} are correlated, demonstrating that a modification of the theoretical model is required.

REFERENCES

- Fabbiano, G. 1989, *Ann. Rev. Astr. Ap.*, **27**, in press.
 Faber, S. M. *et al.* 1989 *Ap. J. Suppl.*, **69**, 763.
 Knapp, G. R., Guhathakurta, P., Kim, D. W., and Jura, M. 1989, *Ap. J. Suppl.*, **70**, 329.
 Sarazin, C. L., and White R. E., III 1988, *Ap. J.*, **331**, 102.

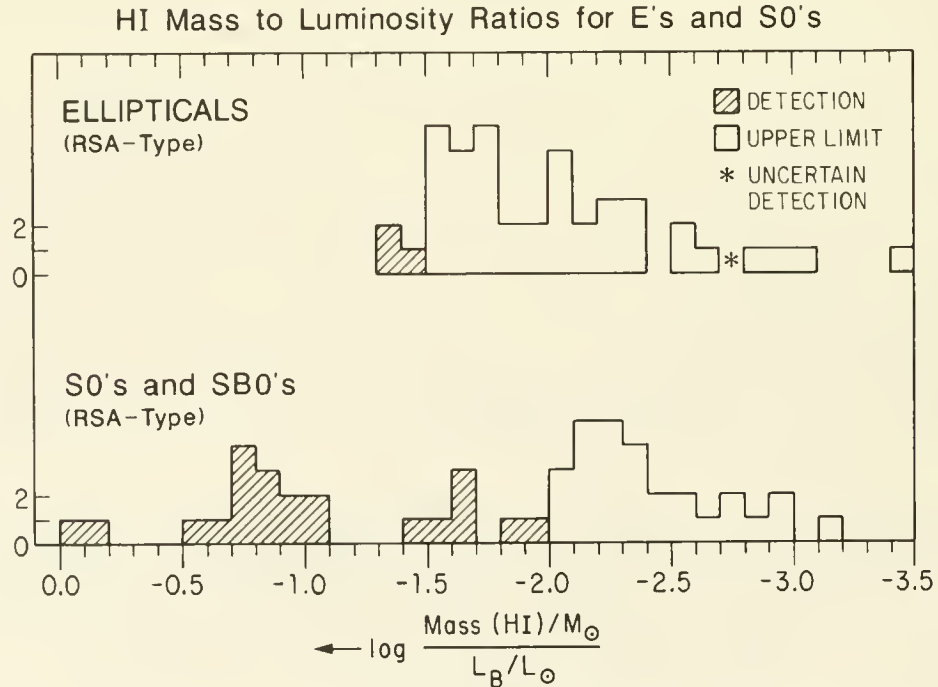


Fig. 1. Histograms of the ratios: $\log(\text{HI mass}/\text{blue luminosity})$ for E's and S0's. Detections are cross-hatched, upper limits are shown as open blocks. Only upper limits less than the lowest detections are shown. Note: Revised Shapley-Ames classifications only are used.

Masses of Interstellar Material in Early-Type Galaxies

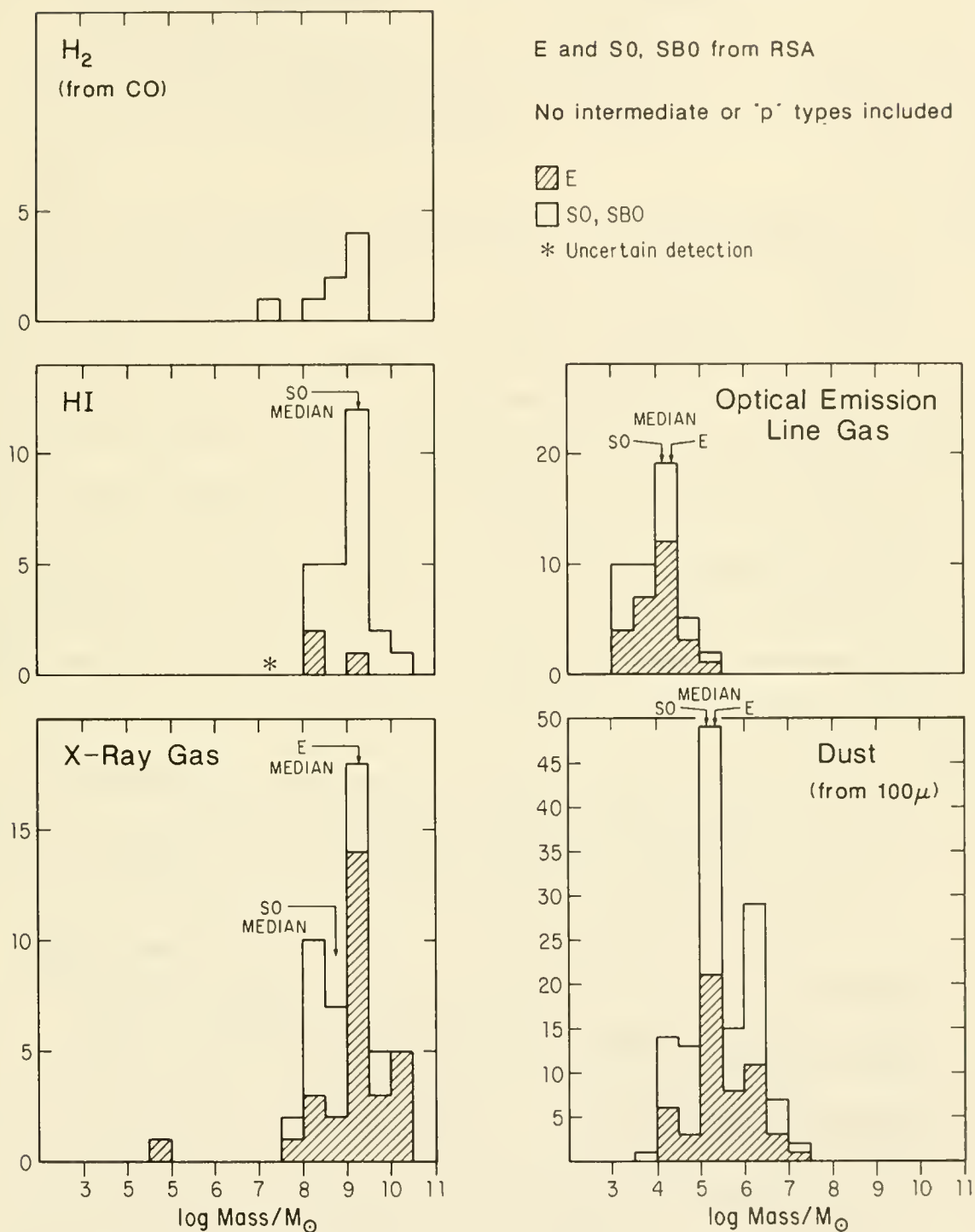


Fig. 2. A census of the amount of various forms of interstellar material in E, S0, and SB0 galaxies in the Revised Shapley-Ames Catalog, a magnitude-limited sample. Upper limits, often very stringent, are not illustrated.

INTERGALACTIC HI IN THE NGC5018 GROUP

P. Guhathakurta and G.R. Knapp, Princeton U.

J.H. van Gorkom, NRAO & Columbia U.

D.-W. Kim, CfA

This paper describes the cold interstellar and intergalactic medium in the small group of galaxies whose brightest member is the elliptical galaxy NGC5018. Our attention was first drawn to this galaxy as possibly containing cold interstellar gas by the detection by the IRAS satellite of emission at $\lambda 60\mu\text{m}$ and $\lambda 100\mu\text{m}$ at an intensity of about 1 Jy (Knapp *et al.* 1989), which is relatively strong for an elliptical (Jura *et al.* 1987). These data showed that the temperature of the infrared emission is $< 30\text{K}$ and that its likely source is therefore interstellar dust. A preliminary search for HI emission from this galaxy using the VLA showed that there appears to be HI flowing between NGC5018 and the nearby Sc galaxy NGC5022 (Kim *et al.* 1988). Since NGC5018 has a well-developed system of optical shells (cf. Malin and Carter 1983; Schweizer 1987) this observation suggests that NGC5018 may be in the process of forming its shell system by the merger of a cold stellar system with the elliptical, as suggested by Quinn (1984).

We describe follow-up HI observations of improved sensitivity and spatial resolution, and confirm that HI is flowing between NGC5022 and NGC5018, and around NGC5018. The data show, however, that the HI bridge actually connects NGC5022 and another spiral in the group, MCG03-34-013, both spatially and in radial velocity, and that in doing so it flows through and around NGC5018, which lies between the spiral galaxies. This is shown by the total HI map in Fig 1, with the optical positions of the above three galaxies labelled. The box shows the area covered by the optical image in Fig 2. The bridge seems to bifurcate at the approximate position and radial velocity of NGC5018. While the northern part continues unbroken, the southern portion disappears near the elliptical. At the distance of the group (31.4 Mpc) the projected linear extent of the northern plume is 165 kpc. The HI plume does not extend beyond either of the two spirals it joins suggesting that the galaxies are on the outbound parts of their orbits and that the interaction that produced the plume was a relatively recent one ($\sim 6 \times 10^8$ yrs), only slightly less than a crossing time ago (inferred to be about 10^9 yrs for the spirals). The merging of a cold

system with NGC5018 appears to be at least a three-body encounter.

HI is detected in eight locations in the NGC5018 group: from four late-type galaxies (including the two that are connected by the bridge), from the two tidal tails, and from two low surface brightness dwarf irregulars with very small HI line widths. Since we have acquired reasonably accurate redshifts for several group members, we are able to estimate the total mass of the group. The virial mass for the group is $\sim 7 \times 10^{12} M_{\odot}$ giving a mass-to-light ratio (M_T/L_B) $\sim 75 M_{\odot}/L_{\odot}$ indicating that the NGC5018 group contains a substantial amount of dark matter.

Multiband optical imaging and photometry of NGC5018 using the 4m at CTIO reveals the presence of a spectacular shell system, along with two prominent wisps and a pair of dust lanes (Fig 2). The greyscale image shown in Fig 2 is obtained by subtracting off a smooth elliptical fit from the galaxy. While all of the above mentioned features are signs of recent interaction, none coincide in position with the HI bridge. The colors of the shells and optical wisps appear to be similar to that of the parent elliptical ($B - R \sim 1.0$). If NGC5018 is assumed to have a flat rotation curve, the central velocity dispersion of 223 km s^{-1} (Davies *et al.* 1987) implies a circular velocity of $\sim 380 \text{ km s}^{-1}$, giving an orbital time for the outermost shell (radius = 16 kpc) of about 3×10^8 yrs, which is about a third of the age of the age of the HI plume. We believe that our HI and optical data on the NGC5018 group provides the first direct observational evidence for the formation of a shell system as an elliptical galaxy merges with a cold disk system, with this merger probably leading to the complete destruction of one of the group members.

REFERENCES

- Davies, R.L., Burstein, D., Dressler, A., Faber, S.M., Lynden-Bell, D., Terlevich, R.J., and Wegner, G. 1987, *Ap.J. (Suppl.)* **64**, 581.
- Jura, M., Kim, D.-W., Knapp, G.R., and Guhathakurta, P. 1987, *Ap.J. (Letters)* **312**, L11.
- Kim, D.-W., Guhathakurta, P., van Gorkom, J.H., Jura, M., and Knapp, G.R. 1988, *Ap.J.* **330**, 684.
- Knapp, G.R., Guhathakurta, P., Kim, D.-W., and Jura, M. 1989, *Ap.J. (Suppl.)* (in press).
- Malin, D.F., and Carter, D. 1983, *Ap.J.* **274**, 534.
- Quinn, P.J. 1984, *Ap.J.* **279**, 596.

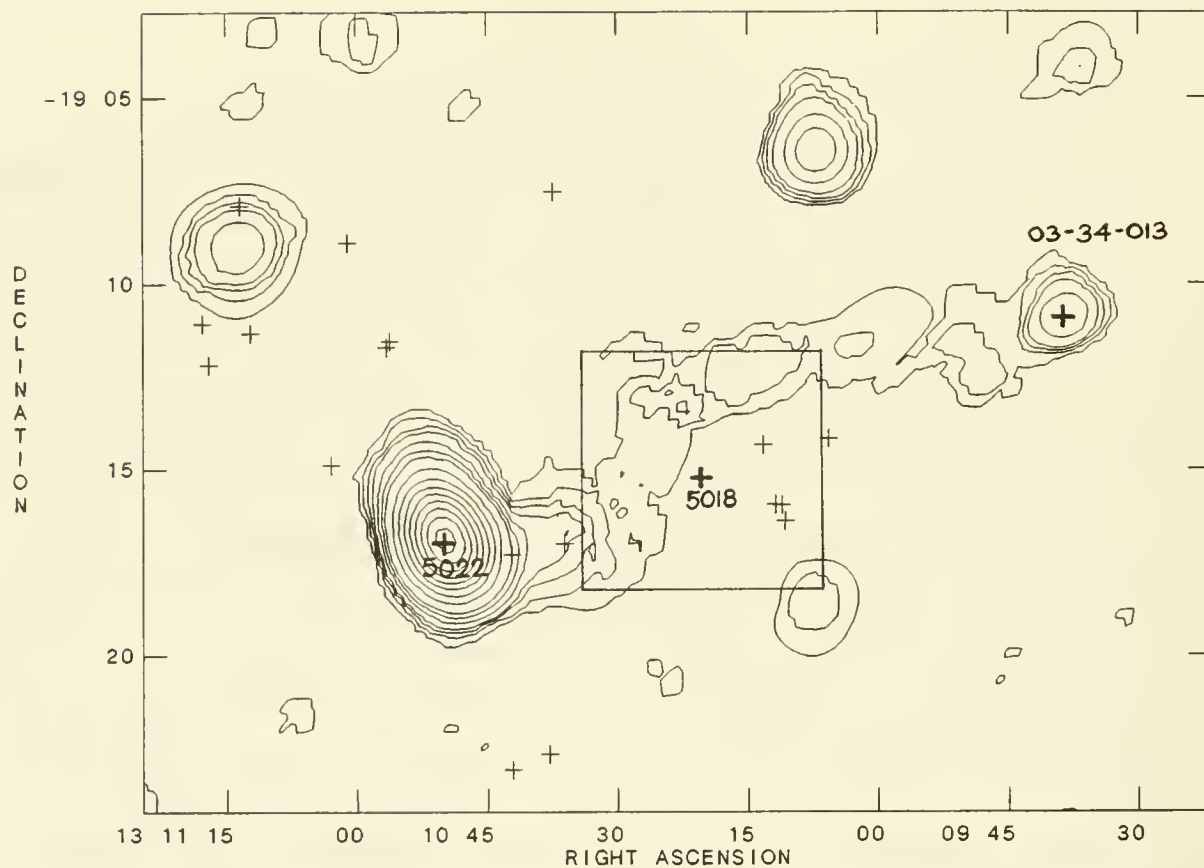


FIG 1

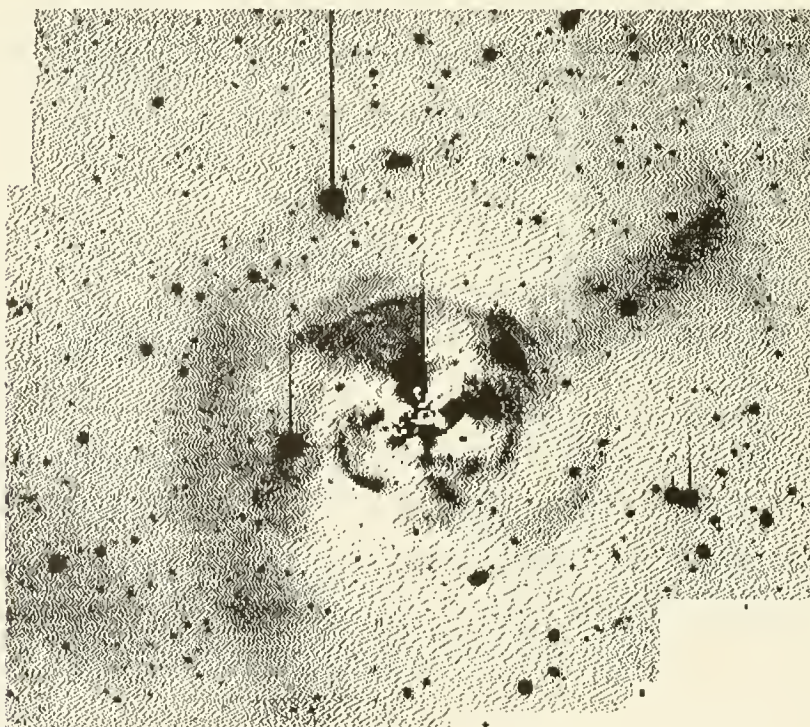


FIG 2

HI And FIR Emission From S0 Galaxies

Paul B. Eskridge

Department of Astronomy, University of Illinois

and

Richard W. Pogge

McDonald Observatory, University of Texas at Austin

A large body of work has accumulated in recent years which throws into disarray the traditional assumption that S0 systems are inert, non-starforming galaxies with uniform, old stellar populations. The copious 21cm data have been recently reviewed and assessed by Wardle and Knapp (1986). This work showed that roughly a third of the several hundred observed S0's contain detectable amounts of HI. More recently, Pogge and Eskridge (1987) have shown that a significant fraction of HI-rich systems also exhibit $H\alpha$ emission. Thronson *et al.* (1989) report detection of CO line emission from two thirds of the S0's in their sample. Both of these last papers, however, report on fairly small data sets (~ 20 objects each). From co-added IRAS data, Knapp *et al.* (1989) report that roughly two thirds of a sample of several hundred S0's are detected at 60μ and 100μ . Work by Bally and Thronson (1989) and Walsh *et al.* (1989) has shown that, while a large number of S0's follow a relation between radio continuum and FIR emission similar to that found for spirals, significant numbers of both radio-bright, and FIR-bright S0's exist. Clearly, a large number of factors are involved in determining the state of the ISM in S0 galaxies. The class is probably heterogeneous, suggesting that large data samples are required to sort out various sorts of objects. The 21cm and FIR samples are the two largest currently available. It is therefore of interest to compare the two and see where this leads.

The 21cm data were drawn largely from Wardle and Knapp (1986), with some additional sources. The most significant of these being Chamaraux *et al.* (1986). The FIR data were determined from 60μ and 100μ flux densities in Knapp *et al.* (1989), using the relationship given in Lonsdale *et al.* (1985). The intersection of these samples is a set of 254 objects. Rather than making a series of assumptions as to the distances of these objects, we decided to simply scale all the quoted observational data by the true apparent blue flux of each object. Thus, what we examine is the relative brightness of the 21cm line emission or FIR emission to the blue optical emission for each galaxy. Obviously, an optical band which is less seriously effected by internal absorption, such as the *H*-band, would have been preferable. Such data are, however, not generally available.

An examination of the full data set indicates that a limit analysis of the sort discussed by, e.g., Walsh *et al.* (1989) would be most appropriate. However, we have initially limited ourselves to an analysis of the detections only. The double detections appear to be roughly fit by a power-law, with significant populations of both 21cm-excess and FIR-excess galaxies. An iterative least-squares power-law fit was made to the double detections. Galaxies

which deviated from this fit by more than $3\sigma_i$ were removed from the sample, and the fit was repeated. The fit was essentially unaltered by this second pass. Figure 1 shows those double detections which survive the 3σ rejection, along with the power-law fit.

As mentioned above, the 3σ rejection yields sets of galaxies which are either significantly HI- or FIR-bright, relative to the fit. In addition, examining the two single-limit data sets provides a number of systems which are also clearly inconsistent with the fit. Figure 2 shows all these points, again with the fit line drawn in.

In a Universe in which there were a smooth, consistent relationship between the amounts of gas in the neutral atomic and molecular phases, the rate and efficiency of star-formation, the IMF, and the gas-to-dust ratio, and in which there were no other significant processes contributing to the FIR emission (ambient heating of grains, nuclear emission ...), one would expect a tight correlation between the total HI content and the total FIR emission in a given galaxy. The obvious interpretation is that the power-law galaxies basically fit this picture: they are normal star-forming systems, which are able to process their neutral gas into stars in a fairly typical manner for disk galaxies. (Note that this does NOT mean they are “typical SO’s”, whatever that means).

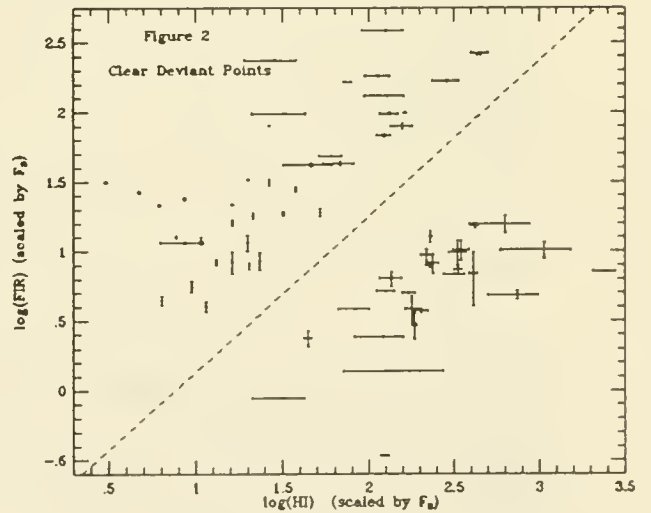
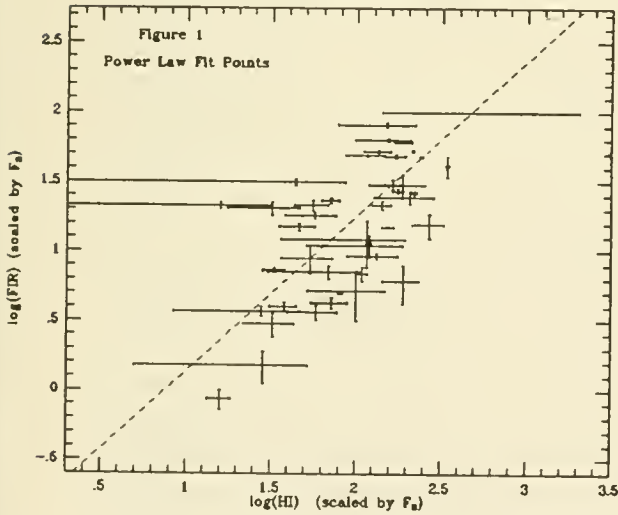
Those galaxies which are HI-bright, relative to their FIR emission (or limit) are clear candidates for systems which have accreted their gas. In fact, the extreme systems in this category for which HI maps have been published (van Driel 1987 and references therein, Schweizer *et al.* 1989) all appear, on the basis of those maps, to have accreted their gas. It is also likely that a number of these systems have not accreted their gas, but the total amount and concentration of what gas they do have is simply insufficient to trigger star-formation at this time. This pertains mainly to those systems which have small ratios of HI to blue flux, but essentially no sign of FIR emission to quite low levels.

Those galaxies which are FIR-bright for their HI emission (or limit) do not have so simple an explanation. Three physical processes appear to be at work: enhanced star-formation (as in NGC 694, Balzano 1983); ram-pressure stripping, especially for the Virgo SO’s, which may lead to both reduced HI and enhanced FIR, due to compressionally induced star-formation; FIR emission from grains heated by the ambient radiation field of a basically gas-poor galaxy. In general, those systems with both FIR and HI detections are more FIR-bright than those with FIR detections but HI limits. This suggests the first and second processes are important in the double detected galaxies in this sample. More observational work, specifically CO and H α studies are needed to sort out these various possible effects.

While further consideration of these data are clearly warranted, including a statistical assessment of the limit points, the following results are already clear: HI and FIR flux data can be used to isolate strong candidates for systems which have gained their HI gas via accretion; a rough power-law relationship exists for galaxies which are undergoing relatively normal star-forming activity; a heterogeneous class of galaxies with strong FIR emission compared to their HI emission exists. Further work is required to determine the various physical processes responsible for this last class.

REFERENCES

- Bally, J., and Thronson H.A., Jr. (1989). *Astron. J.* **97**, 69.
- Balzano V.A. (1983). *Astrophys. J.* **268**, 602.
- Chamaraux, P., Balkowski, C., and Fontanelli, P. (1986). *Astron. Astrophys.* **165**, 15.
- Knapp, G.R., Guhathakurta, P., Kim, D.-W., and Jura, M. (1989). *Astrophys. J. Suppl.* **70**, 329.
- Lonsdale, C.J., Helou, G., Good, J.C., and Rice, W. (1985). Cataloged Galaxies and Quasars in the IRAS Survey. (Jet Propulsion Laboratory, D-1932).
- Pogge, R.W., and Eskridge, P.B. (1987). *Astron. J.* **93**, 291.
- Schweizer, F., van Gorkom, J.H., and Seitzer, P. (1989). *Astrophys. J.* **338**, 770.
- Thronson, H.A., Jr., Tacconi, L., Kenney, J., Greenhouse, M.A., Margulis, M., Tacconi-Garman, L., and Young, J.S. (1989). *Astrophys. J.* In press.
- van Driel, W. (1987). PhD. Dissertation, Groningen University.
- Walsh D.E.P., Knapp, G.R., Wrobel, J.M., and Kim, D.-W. (1989). *Astrophys. J.* **337**, 209.
- Wardle M., and Knapp, G.R. (1986). *Astron. J.* **91**, 23.



Distribution, Kinematics, and Origin of HI Gas in S0 and S0/a Galaxies

H. van Woerden and W. van Driel
Kapteyn Astronomical Institute

A minority of S0 and S0/a galaxies are known to be enriched in HI gas. Their HI content does not appear to correlate with optical properties of the galaxies.

We have mapped the HI distribution and motion in about 20 gas-rich S0 and S0/a galaxies using Westerbork and the VLA. Most gas-rich S0 galaxies show outer rings of HI, often with radii of about $2R_{25}$. Several show inner rings and some have both inner and outer rings. The outer rings are often strongly inclined. Almost all objects have large central holes in their HI distribution. Non-barred S0/a galaxies show filled HI disks, like the early-type spirals. Barred S0/a galaxies show large central HI holes.

In most cases, the HI appears to be in well-ordered rotation. A few objects with large outer HI rings show very high M/L ratios, suggesting massive dark halos. The Tully-Fisher relation for gas-rich lenticulars is similar to that of the spirals.

We discuss possible evolutionary scenarios for these objects.

THE HOT AND COLD INTERSTELLAR MATTER OF EARLY TYPE GALAXIES AND THEIR RADIO EMISSION

Dong-Woo Kim and Giuseppina Fabbiano
Harvard-Smithsonian Center for Astrophysics

Over the last few years, the knowledge of the interstellar matter (ISM) of early type galaxies has increased dramatically. Many early type galaxies are now known to have ISM in three different phases: cold (HI, dust and molecular material), warm (ionized) and hot (X-ray emitting) gas. Early type galaxies have smaller masses of cold ISM ($10^7 - 10^8 M_\odot$; Jura *et al.* 1987) than later type spiral galaxies, while they have far more hot gas ($10^9 - 10^{10} M_\odot$; Forman *et al.* 1985, Canizares *et al.* 1987). In order to understand the relationship between the different phases of the ISM and the role of the ISM in fueling radio continuum sources and star formation, we have compared observational data from a wide range of wavelengths.

The Cold and Hot Interstellar Matter

The far infrared luminosity and mass of HI gas are correlated, although with considerable scatter, suggesting that the far infrared emission is due to dust in the ISM, and not to nuclear activity (see Jura 1986 and Kim 1988). The observational uncertainties are sometimes quite significant, particularly for the HI observations. There are also a few *intrinsic* reasons for the observed scatter: The dust temperature varies with the distance from the center and also varies from one galaxy to another because of different radiation sources; In some galaxies, a large fraction of the cold ISM may be in the form of molecular material; Also there may be an environmental dependence of the amount of HI gas. Nevertheless, a correlation between these two quantities is suggested by the enhanced far infrared detection rate in the HI sample (see Table 1). This result is confirmed using the method of Schmitt (1985) which uses the information in the upper limits (see Fabbiano *et al.* 1989 for applications of this method). The use of this test insures us against a distance bias in our results. The test showed that the HI masses and far infrared luminosities are correlated (the correlation coefficient is $0.76^{+0.05}_{-0.04}$, where the uncertainties are at 1σ). The dust lanes seen in optical imaging observations are a direct evidence of the presence of dust, and indeed the far infrared detection rate in the dust lane galaxies are as high as those in the HI sample (Table 1, see also Veron-Cetty and Veron 1988).

The next question is: Is there a correlation between cold and hot gas? Figure 1 shows a plot of far infrared luminosities against X-ray luminosities. No correlation (or anticorrelation) is found by the Schmitt analysis. For the less luminous galaxies the far infrared luminosity does appear to increase as the X-ray luminosity increases. However, for the X-ray bright galaxies the far infrared luminosity does not increase correspondingly. These are believed to contain hot gas because of the excess X-ray emission over what is expected by stellar X-ray sources (see Canizares *et al.* 1987; Fabbiano 1989).

If the cold and hot gas have the same origin, namely from mass losses of late type evolved stars, one would expect a correlation between the two different phases of ISM. If the cold gas results from cooling flows in the X-ray emitting hot gas, one would also expect a correlation. On the other hand, if the infrared emitting dust was destroyed by interacting with the hot gas, one may expect an anti-correlation. In our sample, there is

neither a correlation nor an anti-correlation. A possible explanation is an external origin of cold ISM. This idea is supported by the decoupled gas and stellar kinematics in many well studied galaxies like NGC 1052 (van Gorkom *et al.* 1985). However, one can not exclude an internal origin, because some isolated early type galaxies, for which therefore no apparent nearby source of cold gas exists, have fairly regular gas kinematics (e.g., Kim *et al.* 1988).

Star formation, Nuclear Activity and Radio emission

Walsh *et al.* (1989) compared the far infrared and the non-thermal radio continuum emission. They showed that about half of the SO galaxies have infrared and radio continuum fluxes consistent with the relationship between these two quantities found in spiral galaxies (e.g., Wunderlich *et al.* 1987), suggesting that at least some SO galaxies are currently forming stars. They also found that the ellipticals with significant far infrared emission are more likely to have intense radio emission possible connected with nuclear activity than those without and that therefore cold gas is responsible for fueling the radio source. More recently, Fabbiano *et al.* (1989) showed that X-ray and radio luminosities are correlated. This suggests a connection between the hot gas and nuclear radio sources perhaps through accreting cooling flows fueling a central black hole. Because far infrared and X-ray emission are not correlated, as discussed above, the conclusion of these two studies are in apparent contradiction. To address this problem, we have re-examined the far infrared, X-ray and radio continuum correlations.

Recent VLA surveys by Wrobel and Heeschen (1989) and Fabbiano *et al.* (1989) are used for radio continuum data. These high sensitivity surveys (detection limit ~ 0.1 mJy) made it possible to study radio faint sources which may not be dominated by the nuclear radio emission. As an example of traditional single dish surveys, Dressel and Condon's (1977) Arecibo surveys are also used. Figure 2 shows the comparison between far infrared and radio emission (a: luminosity vs luminosity, b: flux vs flux). Three lines are drawn in the figures to illustrate the location of spiral galaxies in this plane (see Walsh *et al.* 1989). These are not the best fit to the data of spiral galaxies but just lines with a unit slope.

There seem to be three different populations of early type galaxies (see also Walsh *et al.* 1989; Bally and Thronson 1989). About 1/3 of galaxies (mostly S0) are within the line boundaries, hence are consistent with the relationship followed by spirals. This relationship is most likely due to star formation although the star formation rates in these galaxies are smaller than those in spirals. Another half of galaxies (mostly E) are above the lines with excess radio emission for a given far infrared emission. The excess radio continuum emission is related to nuclear activity (for example, active radio galaxies such as M87, NGC 1399). The excess radio emission is not correlated with the far infrared emission. There may be a third population of early type galaxies which have significant far infrared emission but do not have radio emission. This group of galaxies may only produce low mass stars or they may not produce any stars at all.

If the excess radio emission is related to the hot gas in the sense that cooling flows onto the center are the fuel for the central radio source (Fabbiano *et al.* 1989), then it is expected that the galaxies which have hot gas should fall in the region above the linear relationship in the L_{FIR} - L_{radio} plane. Figure 3 shows the results for the galaxies observed in X-rays (Canizares *et al.* 1987). The galaxies with excess X-ray emission above that

expected from accreting X-ray binaries (see Fabbiano *et al.* 1989) are marked by filled circles and the others are marked by stars. In this diagram, the two groups of galaxies with large X-ray halos (hot gas) and with little or no halos are well segregated, suggesting that the presence of hot gas is important for the fueling of nuclear radio sources.

Table 1
Far Infrared Detection Rates^a

	#	12 μ m	25 μ m	60 μ m	100 μ m
Total	1153	256(22%)	217(18%)	530(45%)	561(48%)
HI sample ^b					
	321	98(30%)	71(22%)	176(54%)	179(55%)
detection	89	36(40%)	35(39%)	74(83%)	72(80%)
upper limit	232	62(26%)	36(15%)	102(43%)	107(46%)
Dust lane galaxies					
	68	30(44%)	26(38%)	49(72%)	53(78%)

a. Far infrared data are from Knapp *et al.* (1989).

b. HI data are from Knapp *et al.* (1985) and Wardle and Knapp (1986).

References

- Bally, J., and Thronson, H. A. 1989, *A. J.*, **97**, 69.
Canizares, C. R., Fabbiano, G., and Trinchieri, G. 1987, *Ap. J.*, **312**, 503.
Fabbiano, G., Gioia, I. M., and Trinchieri, G. 1989, *Ap. J. in press*
Forman, W., Jones, C., and Tucker, W. 1985, *Ap. J.*, **293**, 102.
Jura, M. 1986, *Ap. J.*, **306**, 483.
Jura, M., Kim, D.-W., Knapp, G. R., and Guhathakurta, P. 1987, *Ap. J. Lett.*, **312**, L11.
Knapp, G. R., Guhathakurta, P., Kim, D.-W., and Jura, M. 1989,
submitted to Ap. J. Suppl.
Knapp, G. R., Turner, E. L., and Cuniffe, P. E. 1985, *A. J.*, **90**, 454.
Kim, D.-W. 1988, Ph. D. dissertation
Kim, D.-W., Guhathakurta, P., van Gorkom, J. H., Jura, M., and Knapp G. R. 1988,
Ap. J., **330**, 684.
Schmitt, J. H. M. M. 1985, *Ap. J.*, **293**, 102.
van Gorkom, J. H., *et al.* 1986, *A. J.*, **91**, 791.
Veron-Cetty, M.-P., and Veron, P. 1988, *A. A.*, **204**, 28.
Wardle, M., and Knapp, G. R. 1986, *A. J.*, **91**, 23.
Walsh, D. E. P., Knapp, G. R., Wrobel, J. M., and Kim, D.-W. 1989, *Ap. J.*, **337**, 209.
Wrobel, J. M., and Heeschen, D. S. 1989, *in preparation*.
Wunderlich, E., Klein, U., and Wielebinski, R. 1987, *Astr. Ap. Suppl.*, **69**, 487. /par

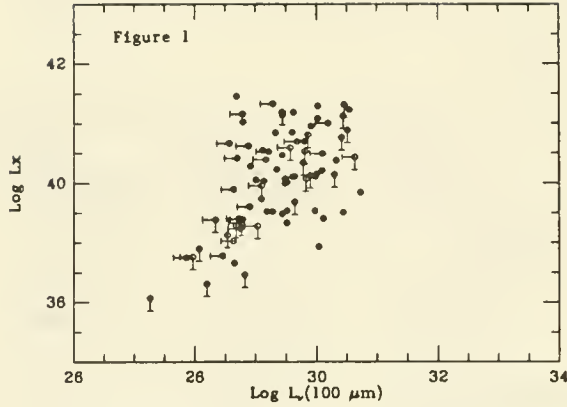


Figure 1. 100 μm luminosity vs X-ray luminosity for early type galaxies. Filled circles are detections and open circles are upper limits with bars indicating the limiting directions.

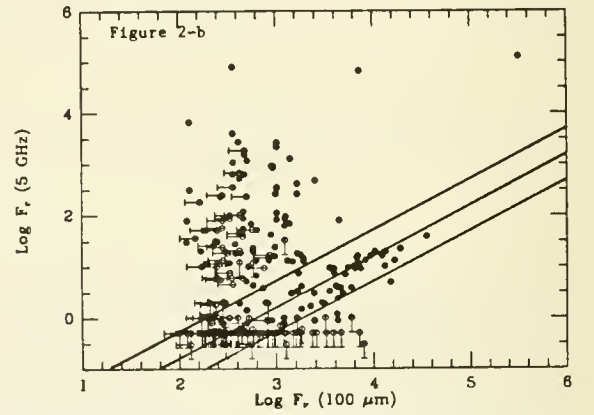
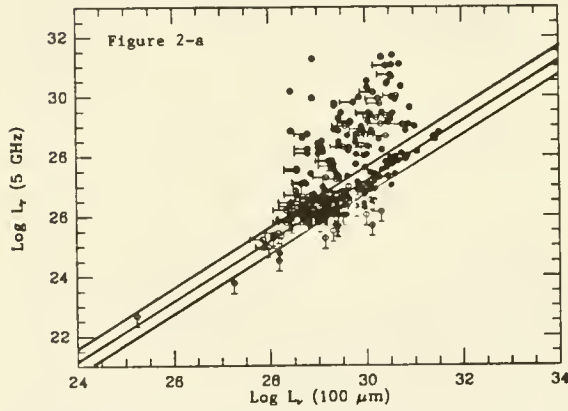


Figure 2. 100 μm luminosity vs 5 GHz radio continuum luminosity (a). The same but flux vs flux in (b). The symbols are the same as in Figure 1. The three lines indicate the location of spiral galaxies in this diagram.

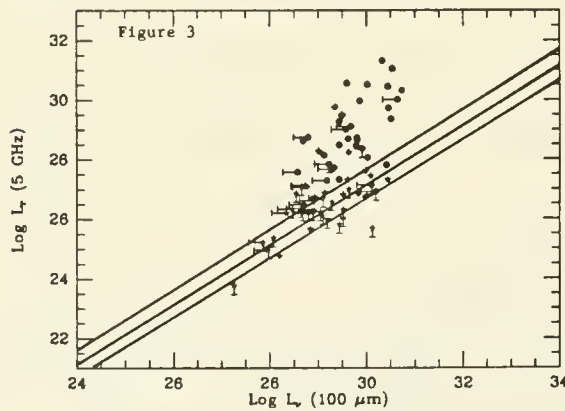


Figure 3. Same as Figure 2-a. Only galaxies with X-ray data are plotted. Filled circles are the galaxies with excess X-ray emission over that expected from stellar components and stars are those without the excess X-ray emission.

Physical Conditions in Photodissociation Regions: Application to Galactic Nuclei

M. G. Wolfire (U. of Chicago), A. G. G. M. Tielens, and D. Hollenbach (NASA/Ames)

Infrared and sub-millimeter observations are used in a simple procedure to determine average physical properties of the neutral interstellar medium in Galactic photodissociation regions as well as in ensembles of clouds which exist in the nuclei of luminous infrared galaxies. The relevant observations include the IRAS infrared continuum measurements, infrared spectroscopy of the fine-structure lines of SiII 35 μm , OI 63 μm , and CII 158 μm , and the 2.6 mm CO (J=1-0) rotational transition. The diagnostic capabilities of the OI 145 μm line is also addressed.

We attribute these emission lines as well as the continuum to the atomic/molecular photodissociation region on the surfaces of molecular clouds which are illuminated by strong ultraviolet fields. We use the theoretical photodissociation region models of Tielens and Hollenbach (1985, Ap. J., **291**, 722) to construct simple diagrams which utilize line ratios and line to continuum ratios to determine the average gas density n , the average incident far-ultraviolet flux G_0 , and the temperature of the atomic gas T . For example, the observed $[I_{\text{OI}(63\mu\text{m})} + I_{\text{CII}(158\mu\text{m})} + I_{\text{SiII}(35\mu\text{m})}]/I_{\text{IR}}$ and $I_{\text{CII}(158\mu\text{m})}/I_{\text{OI}(63\mu\text{m})}$ intensity ratios may be used to determine n and G_0 from Figure 1. The average atomic gas temperature near the cloud surface is easily determined from Figure 2 which shows T_s as a function of n and G_0 . In modeling the ensemble of clouds present in galactic nuclei, we adopt a global model of the interstellar medium, consisting of molecular cloud cores with atomic envelopes. In addition to n , G_0 , and T , we determine the mass of the molecular and warm atomic gas components as well as estimates of the area and volume filling factors and the number and radii of clouds.

As examples, the procedure is applied to the Galactic photodissociation region behind the Orion HII region as well as to ensembles of clouds in the Galactic center, and the nucleus of the starburst galaxy M82. We find that the Orion photodissociation region is composed of warm ($T \approx 500$ K) high density ($n \approx 10^5 \text{ cm}^{-3}$) gas which is illuminated by

a far ultraviolet radiation field of intensity $\sim 2 \times 10^4$ times the local Galactic field. Within 5 pc of the Galactic center we find ~ 100 clouds of size $r \approx 0.4$ pc, and density $n \approx 10^5 \text{ cm}^{-3}$. A far-ultraviolet radiation field, most likely from a central source with $L \approx 2 \times 10^7 L_\odot$, illuminates the clouds with an intensity $\sim 10^5$ times greater than the local Galactic field and heats gas in the surface layers to ~ 700 K. For the case of M82, we find that the neutral interstellar medium within the nuclear region of diameter < 650 pc consists of a large number, $N_{\text{cloud}} \approx 3 \times 10^5$, of small, $r \approx 0.4$ pc, dense, $n \approx 5 \times 10^4 \text{ cm}^{-3}$, clouds with a volume filling factor $\Phi_V \sim 10^{-4}$, and area filling factor $\Phi'_A \sim 0.3$, which are irradiated by a far-ultraviolet radiation field $\sim 10^4$ times larger than the local Galactic far-ultraviolet field. Thus, except for the scale size, the physical conditions in the center of our galaxy and of M82 are very similar to those in the region surrounding the trapezium stars in Orion. The physical conditions in the neutral atomic gas that we have estimated for the Orion photodissociation region, the Galactic center, and the nucleus of M82, are summarized in Table 1

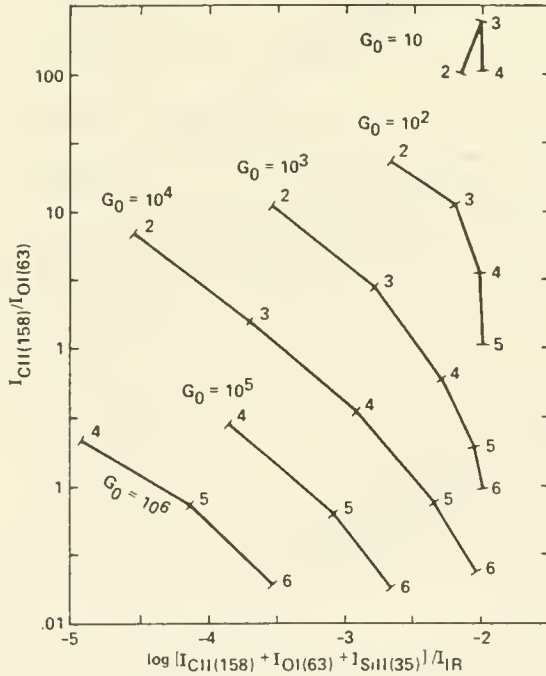


Figure 1 - The ratio of $I_{\text{CII}(158\mu\text{m})}/I_{\text{OI}(63\mu\text{m})}$ intensities versus the ratio of $[I_{\text{OI}(63\mu\text{m})} + I_{\text{CII}(158\mu\text{m})} + I_{\text{SII}(35\mu\text{m})}]/I_{\text{IR}}$ intensities. Tick marks are labeled with $\log n \text{ cm}^{-3}$ and are spaced at one decade intervals along lines of constant G_0 .

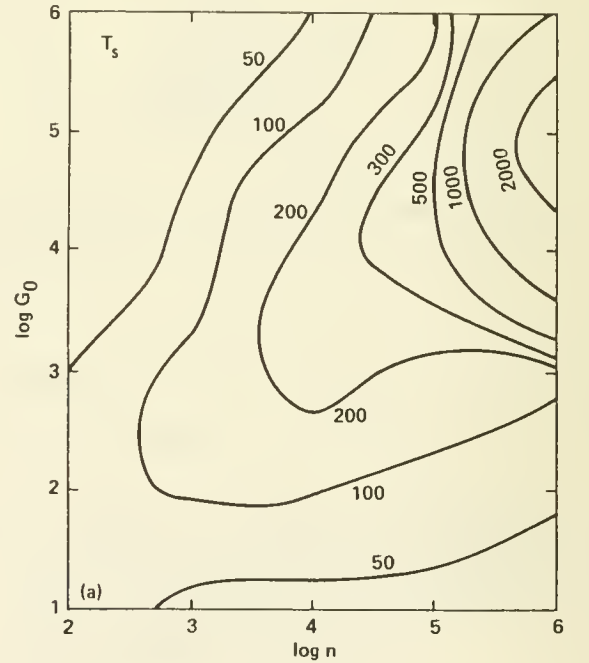


Figure 2 - Surface temperature, T_s ($^{\circ}\text{K}$), in the atomic gas as a function of n and G_0 .

Table 1

Derived Physical Conditions and Global Parameters

	Orion	Galactic Center	MS2
Gas density in clouds	$10^{4.8}$	$\lesssim 5$ pc	$\lesssim 330$ pc
Incident FUV field	n (cm^{-3})	$10^{5.0}$	$10^{4.7}$
Atomic gas temperature	G_o ($1.6 \times 10^{-3} \text{ erg cm}^{-2} \text{ s}^{-1}$)	$10^{4.9}$	$10^{3.9}$
Atomic gas mass	T_a (K)	730	370
Molecular gas mass	M_a (M_\odot)	3×10^3	6×10^6 ^b
Atomic to molecular mass ratio	M_m (M_\odot)	50 ^c	6×10^7
Volume filling factor of clouds	M_a/M_m (%)	4	10 ^d
Projected Area filling factor of clouds	Φ_V	...	6×10^{-2}
Atomic gas radius	Φ'_A	...	0.7
Thickness of atomic layer	r_a (pc)	...	0.4
Number of clouds	$r_a - r_m$ (pc)	...	0.005
	N_{cloud}	...	100
			3×10^5

^a Atomic gas in C^+ regions within $4' \times 8'$ beam $M_a \sim 40 M_\odot$.

^b Atomic gas in C^+ regions within $1'$ beam ($R \sim 500$ pc) $\sim 3 \times 10^7 M_\odot$.

^c Molecular gas within $4' \times 8'$ beam $M_m \sim 250 M_\odot$.

^d M_a/M_m ratio is $\sim 50\%$ within central $1'$ ($R \sim 500$ pc).

Far-Infrared Spectroscopy of NGC 6946, IC 342, and Arp 299

STEVEN D. LORD^{1,2}, DAVID J. HOLLENBACH¹, SEAN W.J. COLGAN^{1,3},
MICHAEL R. HAAS¹, ROBERT H. RUBIN¹ AND EDWIN F. ERICKSON¹

¹NASA/Ames Research Center

²National Research Council Research Associate

³University of California at Santa Cruz

ABSTRACT

We have investigated the physical conditions in the infrared bright galaxies NGC 6946, IC 342, and Arp 299 through measurements of far-infrared emission lines from Si II, O I, C II, and O III using the facility Cooled Grating Spectrometer on the Kuiper Airborne Observatory. These data are interpreted using our theoretical models for photodissociation regions and H II regions. For the central 45'' of these galaxies, we have determined that the dominant excitation mechanism for the FIR lines is FUV radiation from young stars, and we have derived the total mass, density, and temperature of the warm atomic gas and the typical sizes, number densities, and filling factors for the interstellar clouds.

I. INTRODUCTION

A determination of the physical parameters in the interstellar medium (ISM) of galactic nuclei requires far-infrared (FIR) line measurements. Observations at other wavelengths cannot adequately probe these heavily-obscured regions: optical lines are often so heavily reddened that large extinction corrections render interpretation difficult; radio continuum observations of the ionized gas are often confused by a large nonthermal component; and millimeter observations of molecular emission probe only the relatively cold gas component. However, FIR fine structure lines are relatively unaffected by extinction, so we can directly measure the physical state (composition, density, temperature) of the warm atomic gas component and indirectly infer some average properties of the molecular clouds.

We are conducting a survey of the FIR emission lines Si II (35 μm), O I (63 μm), C II (158 μm), and O III (52 and 88 μm) in infrared bright galaxies. The first three lines are important coolants of the atomic component of the ISM; the O III lines are important in the ionized component. We have compared the intensities and ratios of these lines with our theoretical models of photodissociation regions (PDRs) (Tielens and Hollenbach 1985a,b; Wolfire *et al.* 1989a,b), shocked gas (Hollenbach and McKee 1979, McKee *et al.* 1984), to determine the physical conditions in the nuclei of NGC 6946, IC 342, and Arp 299.

Table 1. Far Infrared Extragalactic Line Observations^a

Galaxy	Type	FIR Flux ^b ($10^{-16} \text{ W cm}^{-2}$)	Line Flux ($10^{-19} \text{ W cm}^{-2}$)				
			Si II (35 μm)	O I (63 μm)	C II (158 μm)	O III (52 μm)	O III (88 μm)
NGC 6946	Sc	3.3	8	9.6	7.5 ^c
IC 342	Scd	4.4	9.4	5.7	36 ^d
Arp 299	merger	4.9	3.7	3.8	8.5 ^c	8.2	3.6

Notes: a) Our recent results (45'' beam) are in boldface, b) FIR is the 44-123 μm integrated IRAS flux, c) From Stacey 1988, private communication (60'' beam), d) From Crawford *et al.* 1985 (60'' beam).

II. OBSERVATIONS

These observations were made in June 1988 and March 1989 using the facility Cooled Grating Spectrometer on the 91.4 cm telescope of the Kuiper Airborne Observatory. The effective beamsize was $45''$ (HPBW) and the velocity resolution ranged between 95 km s^{-1} and 120 km s^{-1} . Calibration and water vapor absorption corrections for each fine structure transition were accomplished through observations of K3-50A and Orion-KL. Total integration time per line was ~ 50 minutes. Table 1 shows the measured line fluxes.

III. RESULTS

In these three galaxies, the dominant excitation source for the FIR emission lines is identified as radiatively heated H II regions and PDRs (i.e., star formation regions). We are able to distinguish this form of excitation from other forms by the measurement of the FIR line and continuum ratios: $(\text{C II/O I}) \simeq 0.1 - 1.0$ and $(\text{C II} + \text{O I} + \text{Si II})/(\text{FIR Flux}) \sim 0.01$. These ratios are indicative of PDR emission, rather than excitation by AGN's or shocks. More quantitatively, the modeling procedures outlined in Wolfire *et al.* (1989a,b) can be applied to derive physical parameters for these galaxies. The models provide estimates of the ambient FUV radiation field and the density of the atomic gas from the flux ratios. These derived quantities, along with CO molecular mass estimates from the literature, and the individual line fluxes from Table 1, allow us to construct models of the ISM in these galactic nuclei, models which include the warm atomic gas component (the PDRs). Our results for these three galaxies are summarized in Table 2.

Table 2. Derived Astrophysical Quantities

Galaxy	n (cm^{-3})	T_a (K)	G_0 (ISRF)	M_a ($10^7 M_\odot$)	M_m ($10^7 M_\odot$)	ϕ_A	ϕ_V	N	r_{cl} (pc)	n_e (cm^{-3})
NGC 6946	10^4	200	10^3	1	100	0.1	3×10^{-5}	10^6	1.0	...
IC 342	10^4	100	10^2	2	5	2	10^{-4}	10^8	0.1	...
Arp 299	3×10^3	200	10^3	60	100	0.1	10^{-6}	6×10^8	0.2	600

Notes: Global parameters for gas clouds in the $45''$ beam: n is the gas density, T_a is the temperature of the warm atomic component, G_0 is the incident FUV flux in units of the average interstellar radiation field (ISRF), M_a is the mass of the warm atomic gas, M_m is the molecular mass from CO observations, ϕ_a is the area filling factor of the warm atomic component, ϕ_V is the volume filling factor of neutral cloud material (molecular and atomic), N is the number of clouds, r_{cl} is the radius of a typical cloud, and n_e is the H II region electron density.

For IC 342 and Arp 299, the warm ($T \sim 100$ – 200 K) atomic gas mass is comparable to the molecular mass and the fundamental "cloud building block" is a clump of radius 0.1 – 0.2 pc and mass $\sim 1 M_\odot$. Each clump is exposed to an average interstellar FUV flux of $\simeq 10^2 - 10^3$ times the ISRF. However, in NGC 6946, the fundamental unit is a cloud of radius 1 pc and a mass $10^3 M_\odot$, consistent with a more quiescent, less FIR bright central region than is seen in IC 342 and Arp 299.

An unexpected result of our study is that the Si II lines detected in each of these galaxies display Si II/C II and Si II/O I ratios (~ 1), which are comparable to those in M82. The relative Si II emission in all these galaxies is strong; comparable ratios in our galaxy are found only in high density, high FUV regions, such as M17 and the Galactic center.

REFERENCES

- Crawford, M. K., Genzel, R., Townes, C. H., and Watson, D. M. 1985, *Ap. J.* **291**, 755.
Hollenbach, D. J. and McKee, C. F. 1979, *Ap. J. Suppl.* **41**, 555.
McKee, C. F., Hollenbach, D. J. and Chernoff, D. F. 1984, *Galactic and Extragalactic Infrared Spectroscopy*, ed. M.F. Kessler and J.P. Phillips, Reidel:Dordrecht, 103.
Tielens, A. G. G. M. and Hollenbach, D. 1985a, *Ap.J.* **291**, 722.
Tielens, A. G. G. M. and Hollenbach, D. 1985b, *Ap.J.* **291**, 747.
Wolfire, M., Hollenbach D., and Tielens, A. G. G. M. 1989a, *Ap. J.* **344**, in press.
Wolfire, M., Tielens, A. G. G. M., and Hollenbach D. 1989a, *Ap. J.* submitted.

Neutral Atomic Absorption Lines and Far-UV Extinction: Possible Implications for Depletions and Grain Parameters

Daniel E. Welty
University of Chicago

Examination of the equation of ionization equilibrium: $n(\text{X I}) \Gamma = n(\text{X II}) n_e \alpha(T)$ suggests that absorption lines from neutral atoms whose first ions are dominant in H I regions are potentially significant diagnostic tools for determining the conditions within the densest portions of diffuse interstellar clouds. Ratios of this equation for different elements can give accurate relative abundances in those densest regions, as the generally poorly known electron density is eliminated and as uncertainties in Γ/α due to lack of specific knowledge of the temperature and radiation field within the cloud core would tend to cancel in the ratios (York 1980). Variations of this technique have been used to explore possible dependences of the depletions of various elements on the local gas density (Snow 1984; Snow, Joseph, and Meyer 1986), to infer characteristics of the grain mantle accretion process (White 1986), and to estimate grain scattering parameters (Jenkins and Shaya 1979). In this paper, we examine nine lines of sight within the Galaxy and one in the LMC for which data on both neutral atomic absorption lines (Snow 1984; White 1986; Welty, Hobbs, and York 1989) and far-UV extinction (Bless and Savage 1972; Jenkins, Savage, and Spitzer 1986) are available, in order to test the assumption that variations in Γ/α will cancel in taking ratios of the ionization balance equation and to try to determine to what extent that assumption has affected the aforementioned studies of depletions and grain properties.

The Galactic lines of sight seem to be naturally segregated into two distinct groups: one characterized by low (and generally shallow) far-UV extinction (LE) and small $N(\text{H}_2)/N(\text{H})$ (σ Sco, δ Sco, ρ Oph, β^1 Sco) and one characterized by higher (and generally steeper) far-UV extinction (HE) and larger $N(\text{H}_2)/N(\text{H})$ (χ Oph, ξ Per, σ Per, ζ Per, ζ Oph). Average ratios of the column densities of various neutral atoms with respect to $N(\text{K I})$ are presented for the two groups in columns 3 and 4 of Table 1. The ratios for Li I, Ca I, Mg I, and Fe I are all quite similar for both groups, given typical errors of ± 0.2 dex in the column densities. The ratios for Na I, S I, and C I, however, seem to be systematically larger by factors of 3 to 4 for the HE lines of sight than for the LE lines of sight. Although this could be indicative of different patterns of depletion in the two groups of clouds, examination of the ionization potentials of the various species suggests instead that the enhanced ratios for S I and C I reflect a substantially reduced far-UV radiation field in the cores of clouds characterized by higher far-UV extinction. This would not be entirely unexpected, as the calculations of Roberge, Dalgarno, and Flannery (1981; RDF) indicate reductions in Γ for S I and C I, relative to K I, by factors of ~ 2 and ~ 3 at the center of a cloud with $A_V = 1$ for their grain models 2 and 1, respectively. For clouds with appreciable $N(\text{H}_2)/N(\text{H})$, $\Gamma(\text{C I})$ will be further reduced due to the many strong absorption lines of H_2 shortward of 1110\AA , but probably not by more than a factor of ~ 1.5 . If the results of RDF, who used an average extinction curve, are crudely adjusted for variations in the observed $E(9-6.5)^\dagger$, and also for H_2 (factor 1.5 for the HE lines of sight), we estimate enhancements of $N(\text{S I})/N(\text{K I})$ and $N(\text{C I})/N(\text{K I})$, for the HE lines of sight relative to the LE lines of sight, of factors of ~ 1.4 and ~ 2.2 for their grain model 2 and ~ 1.9 and ~ 3.0 for their model 1. While much of the observed relative

[†] Although the available neutral species have ionization potentials corresponding to inverse wavelengths ranging from $3.5 \mu^{-1}$ (K I) to $9.1 \mu^{-1}$ (C I), inspection of their ionization cross sections as functions of energy suggests that the integrated Γ 's will be sensitive to radiation fields over restricted ranges near $\sim 5.5 \mu^{-1}$ (Ca I), 6.0 to $7.0 \mu^{-1}$ (K I, Na I, Li I, Mg I, Fe I), $\sim 8.5 \mu^{-1}$ (S I), and $\sim 9.2 \mu^{-1}$ (C I). We thus use $E(9-6.5)$, the difference in extinction between $9 \mu^{-1}$ and $6.5 \mu^{-1}$, to estimate the effect of the specific line of sight extinction on ratios of S I and C I with respect to K I.

enhancement of S I and C I might be explained by reduced Γ 's for the H&E lines of sight, however, the enhancement of Na I cannot - so that it still may be possible that much of the enhancement is due to differential depletion.

In principle, one can solve for n_e , assuming the radiation field is known, if data for adjacent ionization states are available for one element (*e.g.* Ca), and then obtain estimates for the absolute depletions of other elements (*e.g.* White 1986): $\delta_X = [N(X \text{ I})/N(\text{H I}) A_X] \times [N(\text{Ca II})/N(\text{Ca I})] \times [(\Gamma/\alpha)_X / (\Gamma/\alpha)_{\text{Ca I}}]$. The n_e 's calculated using Ca I and Ca II, however, seem consistently larger, by factors from ~ 4 to ~ 100 , than the n_e 's calculated from the neutral and first ionized states of Mg, Fe, and S, which typically agree to within a factor ~ 2 . Lower limits on n_e calculated from C, assuming C II dominant and C undepleted, are generally between the values derived from Ca and from Mg, Fe, and S - though if $\Gamma(\text{C I})$ is "corrected" for extinction the limits are reduced accordingly. Some error is introduced by using total line of sight column densities for the dominant first ions in such calculations, as the neutral species are presumably concentrated in the cloud cores. Analysis of the absorption-line profiles of the first ions, however, suggests that typically more than $\sim 70\%$ of the column density of the first ions is found at the same velocity as the dominant neutral component for these lines of sight (though see Snow and Meyers 1979 for ζ Oph). The absolute errors in n_e will thus be small, and the relative errors in comparing values of n_e determined from different elements will be smaller still. Other possible sources of error are incorrect atomic data, marked differences in the shape of the radiation field from the WJ1 field assumed, and differences in stratification of the various neutral and first ionized species within the clouds.

Since the uncertainties in n_e make estimates of the absolute depletions rather uncertain, we list in columns 6 through 8 of Table 1 the depletions relative to K, which seemed for any choice of n_e to be generally among the least depleted of the elements considered here. The second entries for S and C incorporate the extinction corrections described above, for grain model 1 of RDF. Comparison of these relative depletions with the depletions derived from the dominant first ions (columns 9 through 11 of Table 1) suggests that depletions of Mg, Fe, S, and C could be enhanced in the cloud cores if K is depleted by as much as a factor ~ 3 . The results for Ca, which would seem to imply much reduced depletion in the cloud cores, are puzzling; a substantially reduced $\Gamma(\text{Ca I})$ could, however, bring both the relative depletions and n_e determined from Ca into better agreement with those determined from the other elements.

The small number of lines of sight represented here makes it difficult to determine the relative importance of differential depletion and of differences in extinction in producing the observed differences in the ratios of various neutral species. Lines of both S I and Fe I should be detectable toward more stars; P I, also having a high ionization potential, may also be detectable. (Two very tentative detections of P I indeed seem to be consistent with behavior similar to that of S I and C I.) In any case, the specific extinction characteristics of individual lines of sight should be considered in attempts to use these trace neutral species to gain insights concerning depletion and/or the scattering and accretion properties of grains (see also Cardelli 1988 and van Dishoeck and Black 1988).

It is also of some interest to compare these Galactic lines of sight with the line of sight to SN 1987A in the LMC. If the dominant cloud in the LMC toward SN 1987A exhibits the steep far-UV extinction derived for the nearby 30 Doradus region (Fitzpatrick 1985), it would nonetheless be different from the Galactic lines of sight with steep far-UV extinction included here; it is likely to have a low $N(\text{H}_2)/N(\text{H})$ ratio (from the weak CH line observed by Magain and Gillet (1987) and from the lack of observed CO absorption in the UV (Welty, York, and Frisch 1989)), consistent with its low total extinction. Likewise, the $N(\text{C I})/N(\text{K I})$ and $N(\text{Na I})/N(\text{K I})$ ratios (~ 1100 and ~ 20) are similar to those of Galactic lines of sight with low far-UV extinction. The enhanced Mg I may be another indication of the high-pressure component implied by the C I fine structure level populations. In any case, the ambient radiation field is likely to be quite different from the typical Galactic interstellar radiation field.

I am grateful for discussions with D. G. York, L. M. Hobbs, T. P. Snow, and C. L. Joseph, and for atomic data provided by J. H. Black and W. H. Parkinson. This work has been supported by grants NAG5-255, NAG5-286, and CW-0001-85 to the University of Chicago.

Cardelli, J. A. 1988, *Ap. J.* **335**, 177.

Fitzpatrick, E. L. 1985, *Ap. J.* **290**, 219.

Grevesse, N., and Anders, E. 1988, in *Cosmic Abundances of Matter*, ed. C. Jake Waddington (New York: AIP), p. 1.

Jenkins, E. B., and Shaya, E. J. 1979, *Ap. J.* **231**, 55.

Jenkins, E. B., Savage, B. D., and Spitzer, L. 1986, *Ap. J.* **301**, 355.

Magain, P., and Gillet, D. 1987, *Astron. Ap.* **184**, L5.

Pequignot, D., and Aldrovandi, S. M. V. 1986, *Astron. Ap.* **161**, 169.

Roberge, W. G., Dalgarno, A., and Flannery, B. P. 1981, *Ap. J.* **243**, 817 (RDF).

Snow, T. P. 1984, *Ap. J.* **287**, 238.

Snow, T. P., and Meyers, K. A., 1979, *Ap. J.* **229**, 545.

Snow, T. P., Joseph, C. L., and Meyer, D. M. 1986, *Ap. J.* **303**, 433.

van Dishoeck, E. F., and Black, J. H. 1988, *Ap. J.* **334**, 771.

Welty, D. E., Hobbs, L. M., and York, D. G. 1989, in preparation.

Welty, D. E., York, D. G., and Frisch, P. C. 1989, in preparation.

White, R. E. 1986, *Ap. J.* **307**, 777.

York, D. G. 1980, in *Astrophysics from Spacelab*, ed. P. L. Bernacca and R. Ruffini (Dordrecht: Reidel), p. 609.

Table 1 - Ratios and Relative Depletions										
Element	Expected N(X I)/N(K I) (no depletion) ^a	Observed N(X I)/N(K I) (range)			log(δ_X/δ_K) ^d (average)			log($\delta_{X II}$) ^e		
		LE ^b	HE ^c	LMC	LE	HE	LMC	LE	HE	LMC ^f
Na	73	25±10	80±30	20	-0.5	0.0	-0.5	-	-	-
Li	.004	.007±.003	.003±.002	<.004	+0.1	-0.2	<-0.1	-	-	-
Ca	2.7	.015±.010	.012±.008	.10	-2.3	-2.5	-1.4	-3.9	-3.6	-3.2
Mg	220	55±25	70±30	525	-0.6	-0.5	+0.4	-0.7	-0.9	-
Fe	100	1.1±0.6	1.2±0.8	<8	-2.0	-2.2	<-1.1	-2.1	-2.1	-1.5
S	17	9±3	35±15	<18	-0.3 -0.7	+0.3 -0.4	<0.0 <-0.1	-	-	-
C	1170	1000±100	4300±300	1070	-0.1 -0.4	+0.5 -0.3	0.0 -0.2	-0.5	-	-

^a Γ and α (T=100 K) from Pequignot and Aldrovandi 1986, cosmic abundances from Grevesse and Anders 1988

^b low far-UV extinction: σ Sco, δ Sco, ρ Oph, β^1 Sco

^c high far-UV extinction: χ Oph, ξ Per, \circ Per, ζ Per, ς Oph

^d second entry for S and C "corrected" for far-UV extinction using RDF model 1 and E(9-6.5)

^e omitted where not observed or where so saturated as to be unreliable

^f assuming log(N(H)) = 21.0

Empirical Relationships Between Gas Abundances And UV Selective Extinction

Charles L. Joseph

Princeton University Observatory

The present paper summarizes several studies of gas-phase abundances in lines of sight through the outer edges of dense clouds. These lines of sight have $0.4 < E(B-V) < 1.1$ and have inferred spatial densities of a few hundred cm^{-3} . The primary thrust of these studies has been to compare gaseous abundances in interstellar clouds that have various types of peculiar selective extinction. To date, the most notable result has been an empirical relationship between the CN/Fe I abundance ratio and the depth of the 2200 Å extinction bump (see figure 1). It is not clear at the present time, however, whether these two parameters are linearly correlated or the data are organized into two discrete ensembles. Based on 19 samples and assuming the clouds form discrete ensembles, lines of sight that have a CN/Fe I abundance ratio greater than 0.3 (dex) appear to have a shallow 2.57 ± 0.55 bump compared to 3.60 ± 0.36 for other dense clouds and compared to the 3.6 Seaton (1979) average. The difference in the strength of the extinction bump between these two ensembles is 1.03 ± 0.23 . (Joseph, Snow, and Seab 1989).

Although a high-resolution IUE survey of dense clouds is far from complete, the few lines of sight with shallow extinction bumps all show preferential depletion of certain elements, while those lines of sight with normal 2200 Å bumps do not (see Joseph *et al.* 1986). Ca II, Cr II, and Mn II appear to exhibit the strongest preferential depletion compared to S II, P II, and Mg II. Fe II and Si II depletions also appear to be enhanced somewhat in the shallow-bump lines of sight. It should be noted that *Copernicus* data suggest all elements, including the so-called nondepletors, deplete in diffuse clouds (Snow and Jenkins 1980, Joseph 1988). Those lines of sight through dense clouds that have normal 2200 Å extinction bumps appear to be extensions of the depletions found in the diffuse interstellar medium. That is, the overall level of depletion is enhanced, but the element-to-element abundances are similar to those in diffuse clouds.

In a separate study, the abundances of neutral atoms were studied in a dense cloud having a shallow 2200 Å bump and in one with a normal strength bump (see Joseph 1986). Neutral atoms, which are selective tracers of the densest regions along the line of sight, are excellent interstellar probes since their absorption lines are normally free from saturation problems. While the abundances of neutral atoms depend on ionization equilibria (e.g., local flux densities and n_e), their ratios are meaningful because much of the uncertainty in the ionization equilibrium calculation cancels when two elements are compared. The abundances of neutral atoms in the shallow-bump line of sight indicate very strong (~ 1.0 dex) differences in the element-to-element depletions with respect to the integrated line-of-sight results. In the other line of sight, the Fe/P depletion ratio inferred from the neutrals is identical to the integrated line-of-sight measurements of the dominant, singly-ionized species. Previous studies of neutral atoms in diffuse clouds and in other dense clouds with normal extinction bumps also failed to find evidence of preferential depletion (Snow 1984, Snow, Joseph, and Meyer 1986).

Finally, there is one other potential difference, which may distinguish sight lines with shallow extinction bumps from those with ordinary ones. Despite several attempts to measure the 3.1μ ice feature in lines of sight with $E(B-V) \sim 1$, it has only been observed towards HD 29647, a line of sight with a shallow 2200 \AA extinction bump (Goebel 1983). Since it has been suggested that ice mantles on grains may suppress the 2200 \AA bump and since the observed preferential depletion of certain elements may be related to the formation of these ice mantles, a search for ice in lines of sight with shallow bump has been initiated (Joseph 1989).

Goebel, J.H. 1983, *Ap.J. (Letters)*, **268**, L41.

Joseph, C.L. 1986, poster paper presented at a workshop on *Interstellar Processes*, held at Grand Tetons National Park, Wyoming.

Joseph, C.L. 1988, *Ap.J.*, **335**, 157.

Joseph, C.L. 1989, *B.A.A.S.*, **21**, 762.

Joseph, C.L., Snow, T.P., Seab, C.G., and Crutcher, R.M. 1986, *Ap.J.*, **309**, 771.

Joseph, C.L., Snow, T.P., and Seab, C.G. 1989, *Ap.J.*, **340**, 314.

Seaton, M.J. 1979, *M.N.R.A.S.*, **187**, 73P.

Snow, T.P. 1984, *Ap.J.*, **287**, 238.

Snow, T.P., and Jenkins, E.B. 1980, *Ap.J.*, **241**, 161.

Snow, T.P., Joseph, C.L., and Meyer, D.M. 1986, *Ap.J.*, **303**, 433.

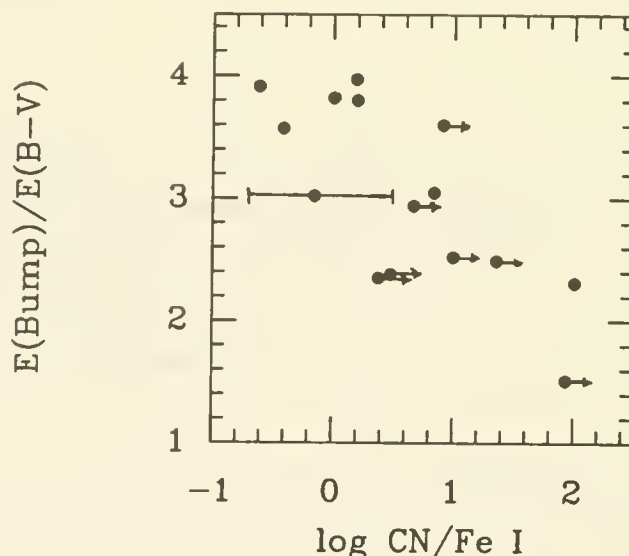


Figure 1: A scatter diagram, showing the relationship between the CN/Fe I abundance ratio and the strength of the 2200 \AA bump. Except for one line of sight, Fe I is not detected (typically at the 1 m\AA level) for all of the points with $E(\text{Bump})/E(B-V) < 3$. If these data form a linear correlation, many of the Fe I upper limits may be just above the detection threshold. If, however, future observations still fail to detect Fe I in the weak-bump lines of sight, then the data form discrete ensembles. The data are from Joseph, Snow, and Seab (1989, *Ap.J.*, **340**, 314). Most of the 2200 \AA Bump strengths are from Fitzpatrick and Massa (1988, *Ap.J.*, **328**, 734) or from Fitzpatrick (private communication).

I - THE COOL ISM

B - H₂, CO AND MOLECULAR GAS

The FCRAO Extragalactic CO Survey: Global Properties of Galaxies

J.S. Young, M. Claussen, N. Devereux, Y. Huang, J.D. Kenney, P. Knezek, L. Tacconi,
L. Tacconi-Garman, F.P. Schloerb, P. Viscuso, and S. Xie
University of Massachusetts Amherst, and
Five College Radio Astronomy Observatory

I. Introduction and Observations

Since stars form in molecular clouds, a critical element in studies of galaxy evolution is knowledge of the molecular content of a large sample of galaxies. To this end, we have undertaken a survey of CO emission from galaxies using the FCRAO 14-m millimeter telescope at 115 GHz. We aim to better understand the differences found among and within galaxies with regard to the efficiency of star and cloud formation.

The galaxies observed as part of the FCRAO Extragalactic CO Survey have been selected on the basis of their optical or infrared properties. The galaxies observed thus far are (1) brighter than $B_T^0 = 12.5$ in the blue, or (2) brighter than 20 Jy at 100 μ m. From major axis CO observations at 45" resolution and spacing in over 200 galaxies, we have determined the CO radial distributions, and derived global CO fluxes (cf. Kenney and Young 1988); H_2 masses were derived using the conversion factor $N(H_2)/I_{CO} = 2.8 \times 10^{20} \text{ cm}^{-2}/(\text{K km s}^{-1})$ (Bloemen et al. 1986).

Here, we concentrate on the global galaxy properties within the sample. HI masses for the sample galaxies were taken from Huchtmeier et al. (1983), blue luminosities and morphological types were taken from RC2. IR luminosities, colors, dust temperatures and dust masses were determined from coadded IRAS data (Young et al. 1989). We have chosen to first compare absolute luminosities and masses in order to determine the slope and scatter in each correlation; next we investigate luminosity independent ratios in order to intercompare large and small galaxies.

III. Results and Discussion

We find that the IR luminosities are related to the molecular gas and atomic gas masses and blue luminosities as follows:

$$\begin{aligned} L_{IR} &\propto M(H_2) 1.0 \pm 0.03 & (\text{corr. coeff.} = 0.93) & (1) \\ &\propto M(HI) 1.0 \pm 0.06 & (\text{corr. coeff.} = 0.81) & \\ &\propto L_B 1.2 \pm 0.05 & (\text{corr. coeff.} = 0.85). & \end{aligned}$$

Thus, we find the infrared luminosity to correlate better with the molecular content of galaxies than with the atomic gas content. Furthermore, the scatter in the L_{IR} - $M(H_2)$ correlation is found to depend on the temperature of the dust, whereas the scatter in the L_{IR} - $M(HI)$ correlation does not (Young et al. 1989). We conclude that the IR emission is closely tied to the molecular content of galaxies. We find no difference in the L_{IR} - $M(H_2)$ correlation for early and late spiral types.

We find the blue luminosities to be related to the molecular and atomic gas masses as follows:

$$\begin{aligned} L_B &\propto M(H_2)^{0.7 \pm 0.03} & (\text{corr. coeff.} = 0.91) \\ &\propto M(HI)^{0.7 \pm 0.04} & (\text{corr. coeff.} = 0.79). \end{aligned} \quad (2)$$

We suggest that the shallower slope of the L_B - $M(H_2)$ correlation relative to the L_{IR} - $M(H_2)$ correlation is due to extinction lowering the blue luminosities in the most luminous galaxies, since these galaxies have higher H_2 surface densities and therefore larger dust column densities in their central regions (Young et al. 1989). Some of the scatter in the L_B - $M(HI)$ correlation arises from the morphological type dependence of the $M(HI)/L_B$ (cf. Roberts 1969); we find a much weaker type dependence in the L_B - $M(H_2)$ correlation. The combination of these two effects gives rise to a morphological type dependence to the $M(H_2)/M(HI)$ ratio (see Knezek and Young 1989, this conference).

The best correlation we find is that between the warm dust masses inferred from IRAS data with the molecular masses (see Figure 1), such that

$$\begin{aligned} M(H_2) &\propto M_{\text{dust}}^{1.0 \pm 0.02} & (\text{corr. coeff.} = 0.97) \\ M(HI) &\propto M_{\text{dust}}^{0.7 \pm 0.04} & (\text{corr. coeff.} = 0.79). \end{aligned} \quad (3)$$

The tight $M(H_2)$ - M_{dust} correlation and the unity slope suggest that the gas to dust ratio is constant from galaxy to galaxy and that the H_2 mass derivations are reasonably accurate even though the cloud properties may be different from galaxy to galaxy. This can be understood because the $CO \rightarrow H_2$ conversion depends on $T_{\text{gas}} \rho^{-1/2}$ (Dickman, Snell, and Schloerb 1986), and both the gas temperature and density are likely to be higher in actively star forming regions. The total gas to dust ratio is discussed elsewhere (Devereux and Young 1989, this conference).

Among 50 of the galaxies for which published $H\alpha$ fluxes are available in the literature (Kennicutt and Kent 1983; Bushouse 1986), we find $L_{IR} \propto L(H\alpha)^{1.0 \pm 0.1}$ (corr. coeff. = 0.78). Although $H\alpha$ suffers extinction, and there may be old as well as young stars contributing to the IR luminosity, we suggest that both $H\alpha$ and IR luminosities are reasonable tracers of high mass star formation. We find the ratio $L_{IR}/M(H_2)$ varies with environment, such that merging/interacting galaxies have star formation efficiencies ~ 7 times higher than isolated galaxies (Young et al. 1986, 1989; Solomon and Sage 1988). We find *no* evidence for a type dependence to the star formation efficiency deduced from the global $L_{IR}/M(H_2)$, $L(H\alpha)/M(H_2)$, or Radio Continuum/ $M(H_2)$ ratios (Allen and Young 1989, this conference; Devereux and Young 1989, this conference).

IV. Conclusions

We conclude that star formation is generally a local process, dependent on the amount of gas available to form stars and not the galaxy morphology. The relative amount of gas in molecular versus atomic form does appear to depend on morphology (Knezek and Young 1989, this conference). The single property which appears to influence both the H_2/HI ratio and $L_{IR}/M(H_2)$ ratio is environment; we find both higher star formation efficiencies and higher molecular gas fractions in interacting/merging galaxies.

References

- Bloemen, J.B.G., et al. 1986, Astr.Ap., **154**, 25.
 Bushouse, H. 1986, Ph.D. thesis, Univ. of Illinois.
 Dickman, R.L., Snell, R.L., and Schloerb, F.P. 1986, Ap.J., **309**, 326.
 Huchtmeier, W.K., Richter, O.-G., Bohnenstengel, H-D., and Hauschildt, M. 1983, ESO preprint.
 Kenney, J.D.P., and Young, J.S. 1988, Ap.J.Suppl., **66**, 261.
 Kennicutt, R., and Kent, S. 1983, A.J., **88**, 1094.
 Roberts, M.S. 1969, A.J., **74**, 859.
 Solomon, P., and Sage, L. 1988, Ap.J., **334**, 613.
 Young, J.S., Xie, S., Kenney, J., and Rice, W. 1989, Ap.J.(Suppl.), In press (July 1989).

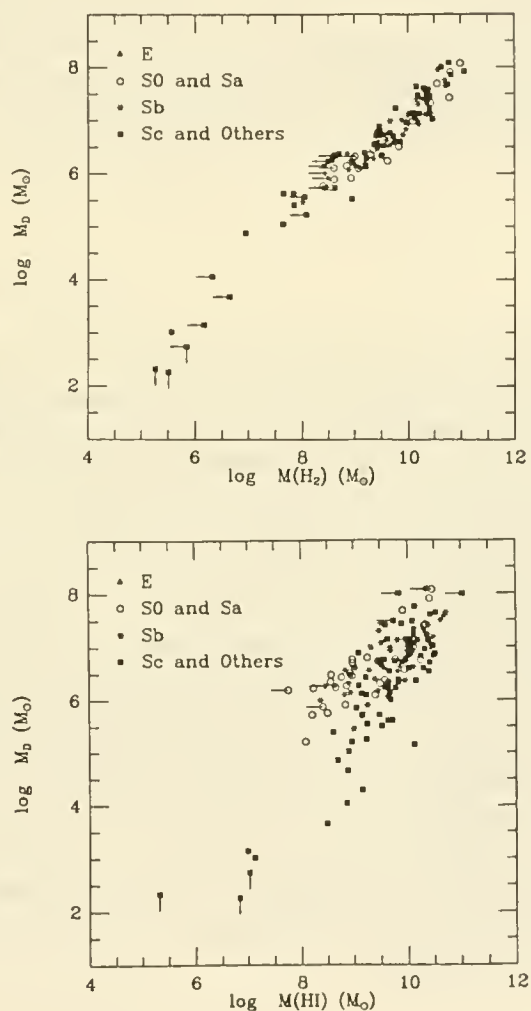


Figure 1. Comparison of dust masses derived from IRAS observations with H_2 and HI masses.

A survey of galaxies in CO

Torsten Elfhag
Stockholm Observatory
S-133 36 Saltsjöbaden
Sweden

Abstract. A large survey of galaxies in the CO ($J=1-0$) line is presented. Among different types of active galaxies, within the sample, the detection rate is found to be: Starbursts (15%), Liners (60%), Seyferts (30%). A look at the subsample that is located within 40 Mpc ($H_0 = 75 \text{ km s}^{-1} \text{ Mpc}^{-1}$) regarding local density of galaxies reveals no substantial difference between detections and non-detections.

1. Introduction.

In the literature there has been some discussion regarding a possible evolution of galaxies where the primary driving force is thought to be large scale star formation (Balzano (1983), Weedman (1983)). When the burst of star formation is completed the accumulation of compact remnants, especially in the central region, would lay the foundation for an active galaxy.

The general belief regarding Seyferts, and even more strongly active galaxies, is that a single central black hole (truly a monster with M in the range of 10^7 - $10^8 M_\odot$) is the cause of the observed events. But it is not implausible that a large amount of smaller black holes (or even neutron stars) clustered within a rather small volume close to the galactic centers also could explain the observations. Since extended radio emission can be observed in some of these sources (where the emission is thought to emerge from supernova remnants) it can be seen as evidence for a more extended active scenario in these galaxies.

Also, the trigger of the burst is supposed to be anything from a close encounter to merging with another galaxy. It could therefore be expected that some correlation would occur, within parts of the sample, with the surrounding density of galaxies.

2. Observations and data reduction.

The observations of ^{12}CO ($J=1-0$, $\nu = 115271.204 \text{ MHz}$) emission from 120 galaxies were performed during 1985 - 1987 using the 20m millimeterwave radome enclosed telescope of the Onsala Space Observatory (OSO). During

1988 additional observations were done of some low declination objects and one southern object (NGC 1365) with the 15m Swedish - ESO Submillimeter Telescope (SEST) at La Silla, Chile.

As the OSO telescope became equipped with a SIS - mixer in 1986 approximately the first half of the observations were performed with a Schottky barrier diode mixer and the latter half with the SIS. Receiver temperatures ranged from 300 to 500 K for the Schottky and 150 to 300 K for the SIS. A dual beamswitch method was used to obtain the spectra with a 512×1 MHz filter bank giving a resolution of 2.6 km s^{-1} . The beamwidth of the 20m at 115 GHz is $33''$.

SEST is equipped with a Schottky barrier diode mixer and is used together with a 728-channel acousto-optical spectrometer, which yields a velocity resolution of 1.8 km s^{-1} . The receiver temperature was about 370 K and the beamwidth of the telescope is $44''$.

All galaxies were observed at their central position. Mapping was done on 11 of the detections, but those results will be discussed elsewhere. The galaxies were primarily chosen from the samples of Balzano (1983), Hummel (1980), Keel (1983) and Stauffer (1982). Of the 120 galaxies observed roughly 50% were detected in CO.

3. Results and Discussion

Interaction between galaxies is generally thought to be one of the prime causes for increased star formation. The resulting shocks would heat and compress the gas. In the denser parts of the clouds the gas would cool rapidly and fragment into new stars. Since CO is the second most common molecule formed in these clouds after H_2 , and the easiest one to observe, it would be observable if we had a major outburst of star formation.

Nilson (1973) gives in his catalogue a note, "Pw", for each galaxy that he can identify with an optical companion. He describes the galaxies as a pair whenever there are no other nearby objects of similar size or brightness and it is deemed possible that they might form a physical pair. Among the surveyed galaxies 24 has such a designation, 17 of them are not detected in CO, i.e. 70%. Of course caution must be taken when interpreting the data since closeness on a photographic plate not necessarily means a physical one.

Tully (1988), though, gives in his catalogue a parameter called the local density ρ_{xyz} , the density of galaxies brighter than $M_{\text{B}}^{\text{b},i} = -16$ in the vicinity of each entry in the catalogue. The local density at each specified location is

$$\rho_{xyz} = \sum_i \rho_i. \quad (\text{see Tully for the def. of } \rho_i)$$

An isolated galaxy will have $\rho_{xyz} = 0.06 \text{ galaxies Mpc}^{-3}$ and in the center of the Virgo cluster the value will be $5 \text{ galaxies Mpc}^{-3}$. The mean result for galaxies within the survey that are at distances less than 40 Mpc (the limit of the catalogue) is:

$$\begin{array}{ll} \text{detected in CO } \rho_{xyz} = 0.47 & (47 \text{ galaxies}) \\ \text{not detected in CO } \rho_{xyz} = 0.58 & (30 \text{ galaxies}). \end{array}$$

These values must also be taken with some caution since we have some ellipticals among the non-detections (we only expect low amounts of gas in ellipticals). If they are sorted out we get $\rho_{xyz} = 0.48$ galaxies Mpc^{-3} (22 galaxies), i.e. essentially the same value as for the detections. It therefore seems like that we do not have any substantially different local environment between the two groups.

Within the sample we have 25 Starburst galaxies (chosen from Balzano (1983) list), 15 Liners and 16 Seyferts. The detection rates among the different types are: Starbursts 15%, Liners 60%, Seyferts 30% (values have been rounded off). In other words, we find the smallest amount of molecular gas where we perhaps should expect the most. Either the star burst phenomenon is a rapid event where the clouds form stars efficiently or these galaxies are not what we think they are. They have been chosen because of their blueness and stellarlike nucleus and these criteria might simply express the lack of large amounts of gas. Also, if we believe in the star burst scenario, these bursts must occur several times to explain such Seyfert galaxies as NGC 1365 and NGC 7469 which both contains huge amounts of gas and both are strong infrared emitting galaxies.

References.

- Balzano, V.: 1983, *Astrophys. J.* **268**, 602.
Hummel, E.: 1980, *Astronomy & Astrophys. suppl.* **41**, 151.
Keel, W.: 1983, *Astrophys. J. suppl.* **52**, 229.
Nilson, P.: 1973, *Uppsala General Catalogue of Galaxies*.
Stauffer, J.: 1982, *Astrophys. J. suppl.* **50**, 517.
Tully, B.: 1988, *Nearby Galaxies Catalog*.
Weedman, D.: 1983, *Astrophys. J.* **266**, 479.

The Ratio of Molecular to Atomic Gas in Spiral Galaxies as a function of Morphological Type

Patricia M. Knezek and Judith S. Young

University of Mass., Amherst, and Five College Radio Astronomy Observatory

I. Introduction

In order to gain an understanding of the global processes which influence cloud and star formation in disk galaxies, it is necessary to determine the relative amounts of atomic, molecular, and ionized gas both as a function of position in galaxies and from galaxy to galaxy. While atomic gas studies of galaxies have been underway for 30 years, the relative youth of the field of extragalactic molecular studies has meant that knowledge of the relative amounts of molecular and atomic gas in galaxies is limited by the relatively small number of galaxies observed in CO.

Ever since the pioneering work in the 1950's and 1960's, it has been recognized that there is a morphological type dependence to the atomic gas content of galaxies. In particular, Roberts (1969) showed that the HI mass to blue luminosity ratio, $M(\text{HI})/L_B$, increases by a factor of 5 among spiral galaxies from types Sa through Scd. With observations of the CO distributions in over 200 galaxies now completed as part of the FCRAO Extragalactic CO Survey (Young et al. 1989), we are finally in a position to determine the type dependence of the molecular content of spiral galaxies, along with the ratio of molecular to atomic gas as a function of type. Do late type spirals really have more gas than early types when the molecular gas content is included?

II. Sample and Analysis

The galaxies observed as part of the FCRAO Extragalactic CO Survey are either (1) brighter than $B_T^0 = 12.5$ in the blue, or (2) brighter than 20 Jy at 100 μm . From major axis CO observations at 45" resolution and spacing in over 200 galaxies, we have derived global CO fluxes (cf. Kenney and Young 1988); H_2 masses were derived using the conversion factor $N(\text{H}_2)/I_{\text{CO}} = 2.8 \times 10^{20} \text{ cm}^{-2}/(\text{K km s}^{-1})$ (Bloemen et al. 1986). HI masses for the sample galaxies were taken from Huchtmeier et al. (1983), and morphological types are from RC2.

III. Results and Discussion

Within our galaxy sample, we confirm the previously found trend of $M(\text{HI})/L_B$ to increase with increasing type from Sab-Sdm. We find the mean ratio of $M(\text{H}_2)/L_B$ to be roughly constant

for types Sa-Sc, with a decrease of a factor of >3 for types Scd-Sdm. The combination of these two effects is that *the mean value of the ratio of molecular to atomic gas decreases smoothly by a factor of ~ 20 as a function of morphological type for types Sa-Sd* as shown in Figure 1.

We have verified that the observed H_2/HI ratio variation with type is not due to the inclusion of Virgo cluster spiral galaxies, many of which are HI-deficient early type galaxies with high H_2/HI ratios (van Gorkom and Kotanyi 1985; Kenney and Young 1986, 1988; Stark et al. 1986). We have also verified that the observed decrease of H_2/HI is not the result of a Malmquist bias, since the observed trend is also found in the subset of galaxies more nearby than the Virgo cluster. We argue that metallicity variations with type among the galaxies in our sample will be small, since the mean mass for types Sa-Scd changes by only a factor of 4 and the $[O/H]$ ratio shows almost no variation with mass for spirals between 10^{10} and $10^{12} M_\odot$ (Pagel and Edmunds 1981).

In order to ascertain whether the observed H_2/HI variation is due to systematic changes in molecular cloud properties, and thereby in the $CO \rightarrow H_2$ conversion as a function of morphological type, we have determined the mean dust temperature for the galaxies in our sample as a function of type. We find T_{dust} to be 1.2 times higher in the Sa-Sab galaxies in the sample than in the Sb-Sdm galaxies. If we assume that the gas and dust temperatures are equal, then we will have overestimated $M(H_2)$ in the early type spirals by a factor of 1.2, since $M(H_2) = L_{CO} \sqrt{\rho} / T_{gas}$ (Dickman, Snell, and Schloerb 1986; Maloney and Black 1988; Elmegreen 1989). Correcting the observed $M(H_2)/M(HI)$ ratio in each galaxy by the observed dust temperature leaves a factor of 17 variation in the ratio $M(H_2)/M(HI)$ with morphological type.

IV. Conclusions

We conclude that there is more than an order of magnitude decrease in the ratio of molecular to atomic gas mass as a function of morphological type from Sa-Sd; an average Sa galaxy has more molecular than atomic gas, and an average Sc has less. Therefore, *the total interstellar gas mass to blue luminosity ratio, M_{gas}/L_B , increases by less than a factor of two as a function of type from Sa-Sd*. The dominant effect we find is that the *phase* of the gas in the cool ISM varies along the Hubble sequence.

We suggest that the more massive and centrally concentrated galaxies are able to achieve a molecular-dominated ISM through the collection of more gas in the potential. That gas may then form molecular clouds when a critical density is exceeded. The picture which these observations support is one in which the conversion of atomic gas to molecular gas is a global process which depends on large scale dynamics (cf. Wyse 1986).

Among interacting and merging systems, we find considerable scatter in the $M(H_2)/M(HI)$ ratio, with the mean ratio similar to that in the early type galaxies. These high global ratio of molecular to atomic gas could result from the removal of HI gas, the enhanced conversion of HI into H_2 , or both.

References

- Bloemen, J.B.G., et al. 1986, *Astr.Ap.*, **154**, 25.
 Dickman, R.L., Snell, R.L., and Schloerb, F.P. 1986, *Ap.J.*, **309**, 326.
 Elmegreen, B.G. 1989, *Ap.J.*, **338**, 178.
 Huchtmeier, W.K., Richter, O.-G., Bohnenstengel, H-D., and Hauschildt, M. 1983, ESO preprint.
 Kenney, J.D.P., and Young, J.S. 1988, *Ap.J.Suppl.*, **66**, 261.
 Maloney, P., and Black, J.H. 1988, *Ap.J.*, **325**, 389.
 Pagel, B.E.J., and Edmunds, M.G. 1981, *Ann.Rev.Astr.Ap.*, **19**, 77.
 Roberts, M.S. 1969, *A.J.*, **74**, 859.
 van Gorkom, J., and Kotanyi, K. 1985, in *ESO Workshop on the Virgo Cluster of Galaxies*, p. 61.
 Wyse, R. 1986, *Ap.J.(Letters)*, **311**, L41.
 Young, J.S., Claussen, M., Devereux, N., Huang, Y., Kenney, J., Knezek, P., Tacconi, L., Tacconi-Garman, L., Schloerb, P., Viscuso, P., and Xie, S. 1989, in preparation.

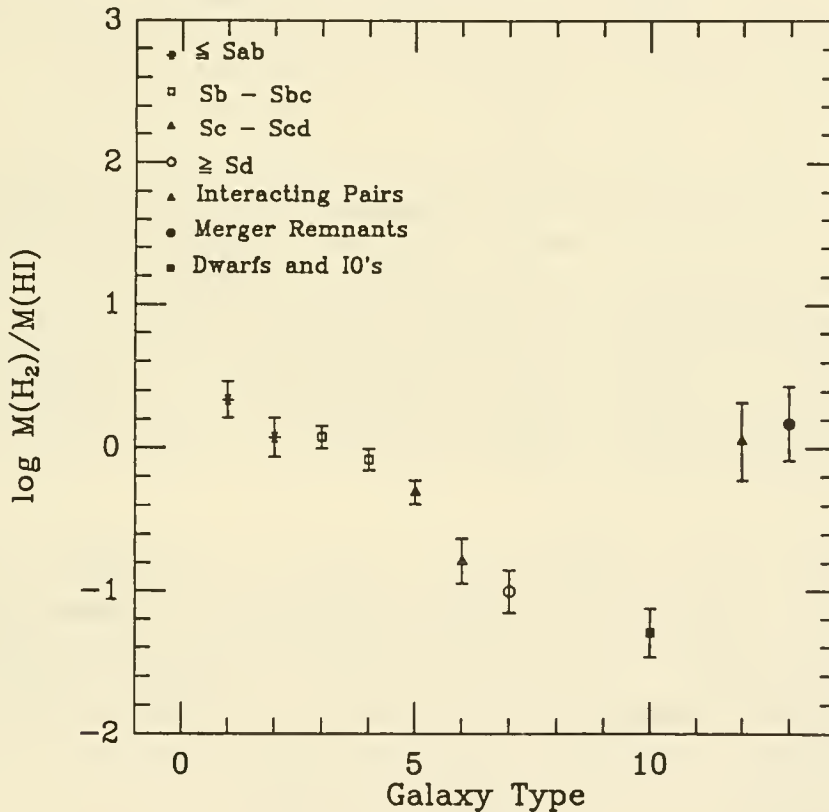


Figure 1. Ratio of molecular to atomic gas mass as a function of morphological type among 200 galaxies. We have combined RC2 types 0 and 1, types 7 and 8, and types 9 and 10. Also included in category 9-10 are dwarf galaxies and IO galaxies (i.e. M82). Type 12 represents interacting galaxy pairs and type 13 represents merger remnants. The error bars shown represent the error in the mean $M(H_2)/M(HI)$ ratio for each type.

CIRCUMNUCLEAR MOLECULAR GAS IN STARBURST AND SEYFERT GALAXIES

YOSHIKAKI TANIGUCHI

*Kiso Observatory, Institute of Astronomy, University of Tokyo
Mitake, Kiso, Nagano 397-01, JAPAN*

OSAMU KAMEYA and NAOMASA NAKAI

*Nobeyama Radio Observatory, National Astronomical Observatory of Japan
Minamimaki, Minamisaku, Nagano 384-13, JAPAN*

In order to investigate circumnuclear molecular gaseous contents and its relation to the nuclear activity, we made a search for circumnuclear ^{12}CO ($J=1-0$) emission from 28 starburst-nucleus galaxies (SBNs) and 12 Seyfert galaxies with the recession velocities less than 5000 km s^{-1} , using the Nobeyama Radio Observatory 45-m telescope. The full half-power beam width of 17 arcsec covers a region of less than about 5 kpc in diameter for the sample galaxies. The circumnuclear CO emission has been detected from twelve SBNs (one is marginal) and four Seyfert galaxies. Our main results and conclusions are summarized as follows.

I. Starburst-Nucleus Galaxies

(1) We study a relation between $M_{\text{H}_2}/M_{\text{HI}}$ and $[\text{OIII}]/\text{H}\beta$, where the latter ratio provides a measure of excitation condition of the ionized gas. It is indicated that the galaxies in which the circumnuclear gas is less abundant have higher-excitation emitting regions in general. This implies that molecular gas clouds are dissociated by strong radiation and/or supernova wind activity in such galaxies. Alternatively, we simply interpret that more intense starburst activity tends to have consumed more molecular gas.

(2) Comparing our results with previous CO studies made at radio observatories with larger beam sizes, we investigated the radial distribution of molecular gas in seven SBNs. We found that most of the SBNs show a tendency of central concentration of molecular gas in comparison to Seyfert galaxies.

(3) We found that two of the SBNs (Mrk 52 and Mrk 708) have very narrow CO line widths although they look like significantly inclined galaxies. This strongly suggests that the circumnuclear molecular gas clouds in these galaxies are kinematically independent from the host galaxies. Since these galaxies have prominent bar structure, it is considered that the bar shock cause forcing gas infall toward the nuclear regions, triggering the nuclear starburst activities.

II. Seyfert Galaxies

(1) We derived the circumnuclear surface density of molecular gas which is corrected for inclination of the galaxies. This analysis shows that the surface density span a wide range over two orders of magnitude. Further, there is no significant difference in the surface densities between types 1 and 2 Seyfert galaxies. Thus, we may conclude that the circumnuclear molecular content is not a key parameter producing the dichotomy of the Seyfert galaxies.

(2) It is also shown that there is no significant difference in the circumnuclear surface densities of molecular gas among the Seyfert, starburst, and normal galaxies. This implies that the circumnuclear gaseous content is not a key parameter determining which activity occurs in nuclei. We may conclude that more centrally condensed (*i. e.*, less than 10 - 100 pc in diameter) gas components play an essential role on the occurrence of nuclear activities.

(3) Comparing our results with the previous ones, we deduced radial distribution of surface density of molecular gases. We cannot obtain evidence for strong central concentration of molecular gas in our sample Seyfert galaxies except for NGC 3227. This is consistent with the previous result by Blitz, Mathieu, and Bally (1986).

(4) Comparing our CO emission line profiles with the previous ones taken with the larger beams, we discussed circumnuclear components of molecular gases. In particular, we found that molecular gas clouds may be absent in the SE of the nucleus of NGC 7469 where the high-excitation emitting region is discovered by Heckman *et al.* (1986). It is suggested that the nuclear activity (strong radiation and/or wind) may destruct the molecular clouds in that region.

REFERENCES

- Blitz, L., Mathieu, R. D., and Bally, J. 1986, *Ap. J.*, 311, 142.
 Heckman, T. M., Beckwith, S., Blitz, L., Skrutskie, M., and Wilson, A. S. 1986, *Ap. J.*, 305, 157.

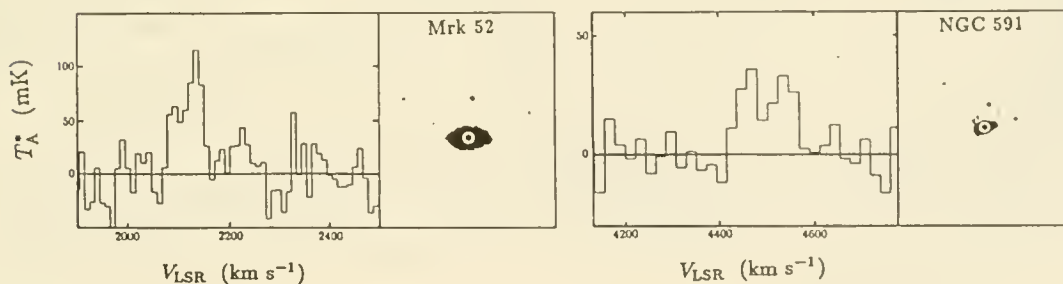


Fig. 1 . Examples of the observed ^{12}CO ($J = 1 - 0$) spectra of the starburst nuclei (Mrk 52) and Seyfert galaxies (NGC 591).

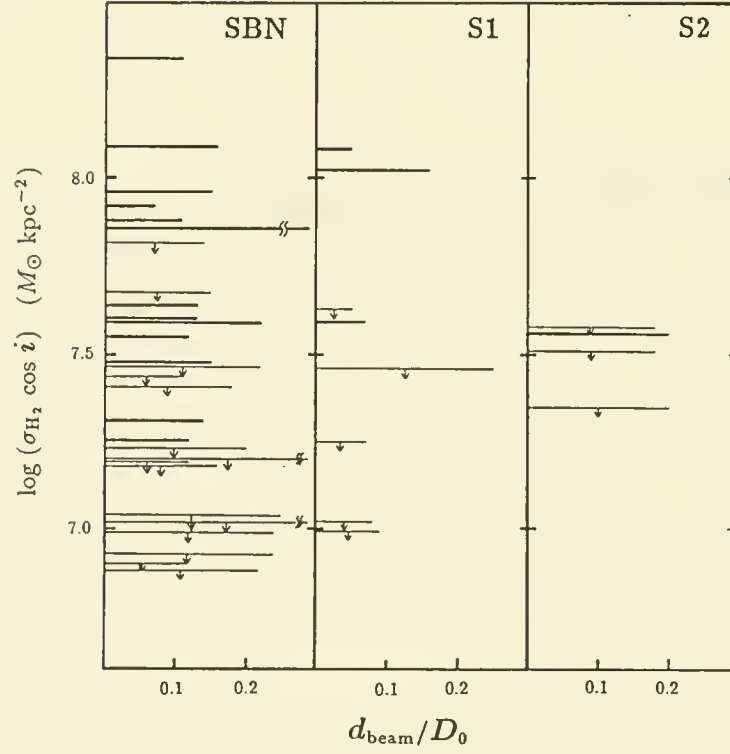


Fig. 2 . Circumnuclear surface densities of molecular gas corrected for the inclination of galaxies. The panels (a), (b), and (c) show the results of SBNs, Seyfert 1 (S1), and Seyfert 2 (S2), respectively.

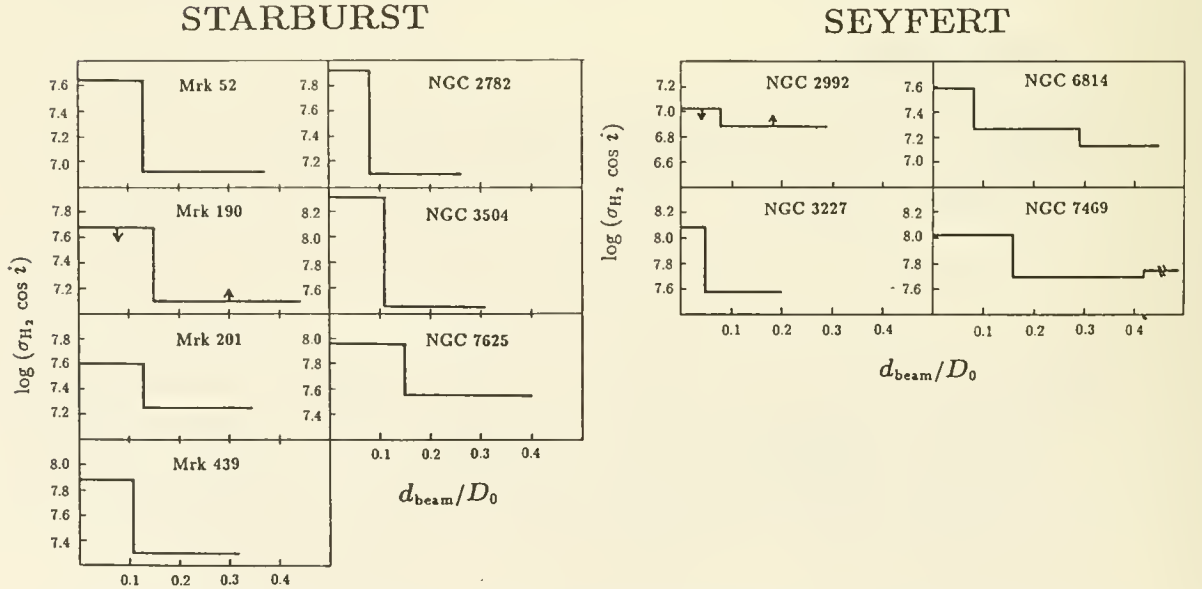


Fig. 3 . The radial distribution of surface molecular densities for seven SBNs and 4 Seyfert galaxies.

High Resolution CO Images of Seyfert Galaxies

M. Meixner (U. Maryland & U. California, Berkeley)

R. Puchalsky and L. Blitz (U. Maryland)

M. Wright (U. California, Berkeley)

One of the current problems in research on active galaxies is to determine to what degree one can separate Seyfert and starburst activity. It has been suggested that these two phenomena are related in an evolutionary sense (Norman and Scoville 1988; Weedman 1983) and N-body simulations have been performed to demonstrate this possibility in the case of interacting galaxies (Hernquist 1989). In this study, we investigate the role of molecular gas in fueling the activity in three Seyfert nuclei.

The Berkeley-Illinois-Maryland millimeter array (BIMA) has been used to image the ^{12}CO ($J=1-0$) emission of three relatively close (12-64 Mpc) Seyfert 1 galaxies, NGC 3227, NGC 7469 and NGC 5033, chosen for their strong single dish CO detections (Heckman *et al.* 1989). Extensive u-v coverage was obtained for all three galaxies resulting in $2''$ - $3''$ resolution.

The integrated intensity images of CO emission in NGC 3227, overlaid on H α emission, and in NGC 7469, overlaid on red continuum, are shown in figures 1 and 2 respectively. The CO emission in NGC 3227 and NGC 7469 appear as compact structures with respective scale sizes of 1.2 and 5 kpc, centered on the active nuclei, and containing substantial fractions ($\sim 80\%$ and $\sim 50\%$) of the single dish flux. The CO emission in NGC 5033 is not detected at such high resolution, implying a CO structure size of $20''$ - $60''$ (1.2-3.6 kpc). Table 1 lists the integrated CO fluxes and comparison single dish measurements.

The H_2 masses (Table 1) are estimated using the $\text{N}(\text{H}_2)/\text{I}(\text{CO})$ conversion factor, $2.5 \times 10^{20} \text{ H}_2 \text{ cm}^{-2} (\text{K km s}^{-1})^{-1}$ (Bloemen *et al.* 1986), that was derived from Galactic giant molecular clouds. As a comparison, the dynamical masses (Table 1) were computed assuming a gravitationally bound rotating disk model ($M = v^2 R/G$), which is consistent with the kinematics of the gas. The estimated H_2 masses for both NGC 3227 and NGC 7469 are a rather large fraction of the dynamical mass. In fact the H_2 mass for the unresolved component of NGC 7469 is comparable to the dynamical mass. This result is improbable because we know that stars, which are concentrated towards the galactic center, contribute to the mass. In light of recent theoretical and observational studies of the $\text{N}(\text{H}_2)/\text{I}(\text{CO})$ ratio, the CO luminosity seems to be enhanced resulting in an overestimate of the H_2 mass if the "standard" conversion factor is applied (Maloney and Black 1988; Crawford *et al.* 1985).

The blue- and red-shifted CO emission in NGC 3227 (fig. 3) and in NGC 7469 (fig. 4) are shown overlaid at a lower ($\sim 5''$) resolution. In both cases, the displacement between the blue and red peaks is along the major axis and the gas moves in the same sense as rotation curves determined for the galaxies (NGC 3227: Rubin and Ford 1968, NGC 7469: Wilson *et al.* 1986) supporting the idea that the molecular gas has rotational motion about the nucleus. In the case of NGC 7469, this result confirms that the molecular gas is involved with the starburst component.

The results of this study are consistent with the scenario that interacting galaxies cause gas to concentrate in the nucleus thereby feeding starburst and Seyfert activity. Both Seyferts with high central concentrations of CO emission, NGC 3227 and NGC 7469, are interacting galaxies listed in Arp's catalogue (Arp 1966) as Arp 94 and Arp 298 respectively. Both of the galaxies are also known to have some starburst component (Kirkpatrick 1989; Wilson *et al.* 1986). The third Seyfert, NGC 5033 has no

detectable centrally concentrated gas emission implying either an alternate mechanism of feeding the central blackhole or perhaps an exhaustion of the molecular gas fuel.

REFERENCES

- Arp, H. 1966, *Ap. J. Suppl.*, **14**, 1.
 Blitz, L., Mathieu, R.D. and Bally, J. 1986, *Ap. J.*, **311**, 149.
 Bloeman, J.B.G.M., Strong, A.W., Blitz, L., Cohen, R.S., Dame, T.M., Grabelsky, D.A., Hermsen, W., Lebrun, F., Mayer-Hasselwander, H.A., Thaddeus, P. 1986, *Astr. Ap.*, **154**, 25.
 Crawford, M.K., Genzel, R., Townes, C.H., and Watson, D.M. 1985, *Ap. J.*, **291**, 755.
 Heckman, T.M., Blitz, L., Wilson, A.S., Armus, L. and Miley, G.K. 1989, *Ap.J.*, *in press*.
 Hernquist, L. 1989, *Annals of the New York Academy of Sciences*, *in press*.
 Kirkpatrick, H., *private communication*.
 Maloney, P. and Black, J.H. 1988, *Ap. J.*, **325**, 389.
 Norman, C. and Scoville, N. 1988, *Ap. J.*, **332**, 124.
 Rubin, V.C., and Ford, W.K., Jr. 1968, *Ap. J.*, **154**, 431.
 Weedman, D.W. 1983, *Ap. J.*, **266**, 479.
 Wilson, A.S., Baldwin, J.A., Sun, S.-D., and Wright, A.E. 1986, *Ap. J.*, **310**, 121.

TABLE 1
RESULTS

	NGC 3227	NGC 7469	NGC 5033
Source size, maj. axis (kpc)	1.2	5	...
ΔV_{CO} (km s ⁻¹)BIMA	400±30	310±30	...
Integrated CO Flux (Jy km s ⁻¹)			
BIMA	470±140	320±70	<40 ^b
NRAO ^a	600	660	440
% NRAO detected by BIMA	80±20	50±10	<10
H ₂ mass (10 ⁹ M _o)			
Total	2	20	< 0.08
Unresolved Component	0.6	6	...
Dynamical mass (10 ⁹ M _o)			
Total	10	30	...
Unresolved Component	3	5	...

^aBlitz *et al.* 1986 and Heckman *et al.* 1989

^bunits are Jy km s⁻¹/3''beam

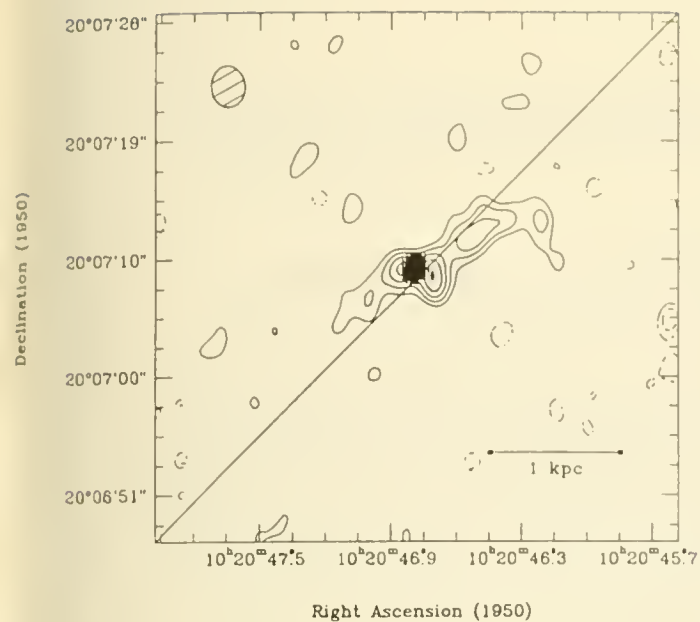


Fig. 1 NGC 3227: Total CO intensity contours overlaid on H α .

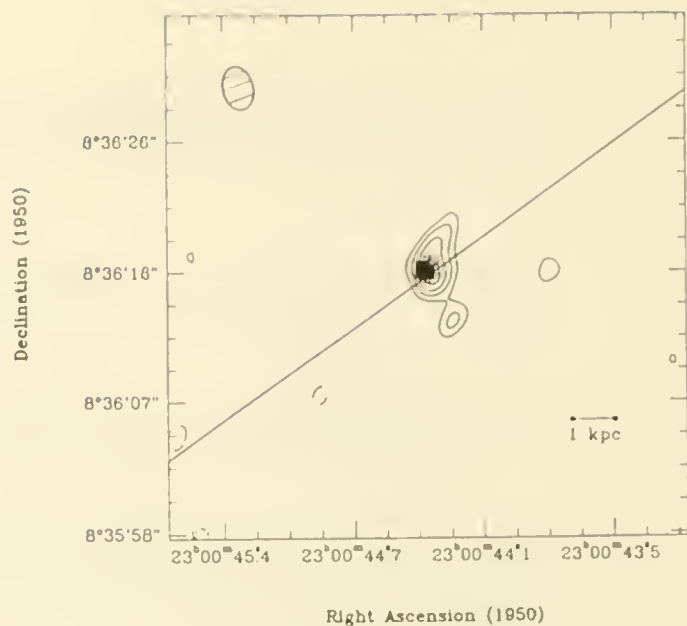


Fig. 2 NGC 7469: Total CO intensity contours overlaid on red continuum.

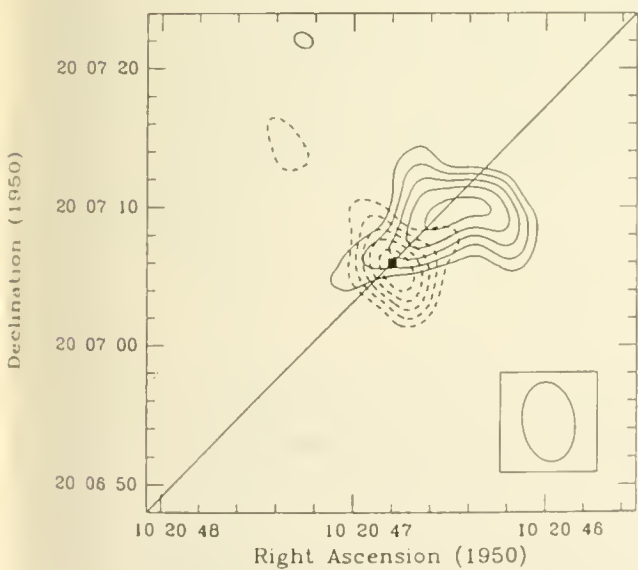


Fig. 3 NGC 3227: Blue-shifted (solid) and red-shifted (dashed) CO.

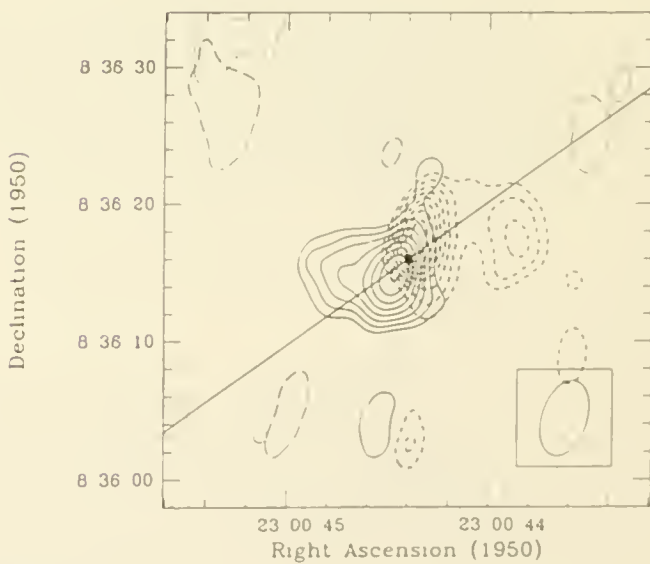


Fig. 4 NGC 7469: Blue-shifted (solid) and red-shifted (dashed) CO.

Aperture Synthesis CO Observations of the Inner Disk of NGC 1068

P. Planesas, N. Z. Scoville, S. T. Myers

Owens Valley Radio Observatory 105-24, Caltech, Pasadena, CA 91125

NGC 1068 is probably the nearest galaxy with both a high rate of star formation and a high luminosity active nucleus. About one-half of the total IR luminosity originates in a disk approximately $30''$ in size, which has been taken as evidence for a high rate of massive star formation (Telesco *et al.* 1984). Previous CO line observations have shown the existence of a ring at the outer boundary of the inner disk (Myers and Scoville 1987). Although these observations have proved that this ring is extremely rich in molecular gas (as suggested by Scoville *et al.* 1983), the angular resolution ($\sim 6''$) was not high enough to resolve its structure.

New aperture synthesis observations of the CO ($J=1-0$) emission in the inner disk of NGC 1068 have been carried out with the OVRO mm Interferometer. The new receivers installed for the 88/89 season have allowed us to obtain a high sensitivity map of the CO emission. The molecular cloud ring has been resolved and continuum as well as line emission from the nucleus of the galaxy have been detected.

OBSERVATIONS

The observations were made from November 1988 to March 1989 with the Owens Valley Radio Observatory (OVRO) millimeter-wave interferometer. Spectral coverage was provided by a filterbank consisting of 32 5-MHz channels giving a resolution of 13 km s^{-1} and a coverage of 416 km s^{-1} in the CO $J=1-0$ transition. Radio continuum measurements in both sidebands were simultaneously obtained using ~ 500 MHz continuum channels. NGC 1068 was observed in six different configurations with baselines out to 200 m east-west and 140 m north-south. The synthesized beam was $2.9'' \times 2.9''$, corresponding to a linear size of 260 pc at a distance of 18.1 Mpc (Sandage and Tammann 1975). The average rms was 60 mJy/beam in the 5 MHz channels, a factor of four lower than in previous observations done in 1986 with the same instrument.

RESULTS

The resulting contour map of the integrated CO intensity (in the range 917 to 1333 km s^{-1}) for NGC 1068 is shown in Figure 1. The shape and intensity of the CO emission distribution agree very well with the results of a previous observation (Myers and Scoville 1987) when convolved to a resolution of $5'' \times 7''$ or $7'' \times 11''$, showing two dominant emission peaks located at distances of $14''$ north and south of the nucleus. The new higher resolution map shows a much more complex structure for the ring, with ten or more peaks of emission. Some of them seem to be originated in unresolved sources, but others extend to linear sizes of ~ 600 pc, so they possibly correspond to complexes of giant molecular clouds.

The overall shape of the emission distribution closely matches that of a ring encircling the nucleus. Part of the emission extends out of such a ring, suggestive of the start of spiral arms. The

whole structure could equally well be constituted by two spiral arms, that start at the ends of the stellar bar found at $2.2\ \mu\text{m}$ (Scoville *et al.* 1988) and they extend for at least 5 kpc in length and ~ 300 pc in width.

The total mass of the molecular gas detected in the ring feature may be estimated using the relation between integrated CO emission and molecular mass derived from observations of giant molecular clouds in our Galaxy. We use the relation $N_{H_2}/I_{CO} = 3.6 \times 10^{20}\ \text{cm}^2\ (\text{K km s}^{-1})^{-1}$. The total H_2 mass in the ring is approximately $3.8 \times 10^9\ M_\odot$. This corresponds to $\sim 25\%$ of the total molecular mass of the galaxy as derived from single dish observations (Scoville, Young, and Lucy 1983; Planesas, Gomez-Gonzales, and Martin-Pintado 1989).

A very good spatial correlation exists between the CO distribution and the $10.8\ \mu\text{m}$ emission determined by Telesco and Decher (1988). Almost all the IR peaks lay very close to CO peaks of emission, which supports the interpretation of the disk IR emission as originating from young massive stars. In some regions (west, southeast), however, CO emission exists without any IR counterpart.

Radio continuum emission from the nucleus has been clearly detected at 2.6 mm in both sidebands. The northeast lobe of the radio jet has also been detected in the lower sideband because of the lower noise level at this frequency. The intensity of the central peak (31 mJy/beam) is consistent with the fluxes and spectral index measured at 15 and 22 GHz (Ulvestad, Neff, and Wilson 1987). The flux measured in the upper sideband is significantly larger (50 mJy/beam), which might indicate that a substantial contribution to this flux comes from CO molecular emission from the nucleus. If so, an estimate of the H_2 mass of $8 \times 10^7\ M_\odot$ is derived assuming that the same N_{H_2}/I_{CO} can be applied to the gas located in the nucleus, although the physical conditions of the molecular gas in the nucleus of NGC 1068 and in the giant molecular clouds in our galaxy are probably different. In fact, the dust temperature in the center of NGC 1068 is ~ 40 K (Young and Sanders 1986), so the value given for the mass should be considered as an upper limit. If the molecular gas is uniformly distributed in a 260 pc diameter sphere, an average density of $175\ H_2\ \text{cm}^{-3}$ and a peak extinction of 140 mag are deduced.

REFERENCES

- Myers, S.T., Scoville, N.Z. 1987, *Ap. J. (Letters)*, **312**, L39.
 Planesas, P., Gomez-Gonzales, J., Martin-Pintado 1989, *Astron. Astrophys.*, in press.
 Sandage, A., Tammann, G.A. 1975, *Ap. J.*, **196**, 313.
 Scoville, N.Z., Young, J.S., Lucy, L.B. 1983, *Ap. J.*, **270**, 443.
 Scoville, N.Z., Matthews, K., Carico, D.P., Sanders, D.B. 1988, *Ap. J. (Letters)*, **327**, L61.
 Telesco, C.M., Becklin, E.E., Wynn-Williams, C.G., Harper, D.A. 1984, *Ap. J.*, **282**, 427.
 Telesco, C.M., Decher, R. 1988, *Ap. J.*, **334**, 573.
 Ulvestad, J.S., Neff, S.G., Wilson, A.S. 1987, *Astron. J.*, **92**, 22.
 Young, J. S., Sanders, D. B. 1986, *Ap. J.*, **302**, 680.

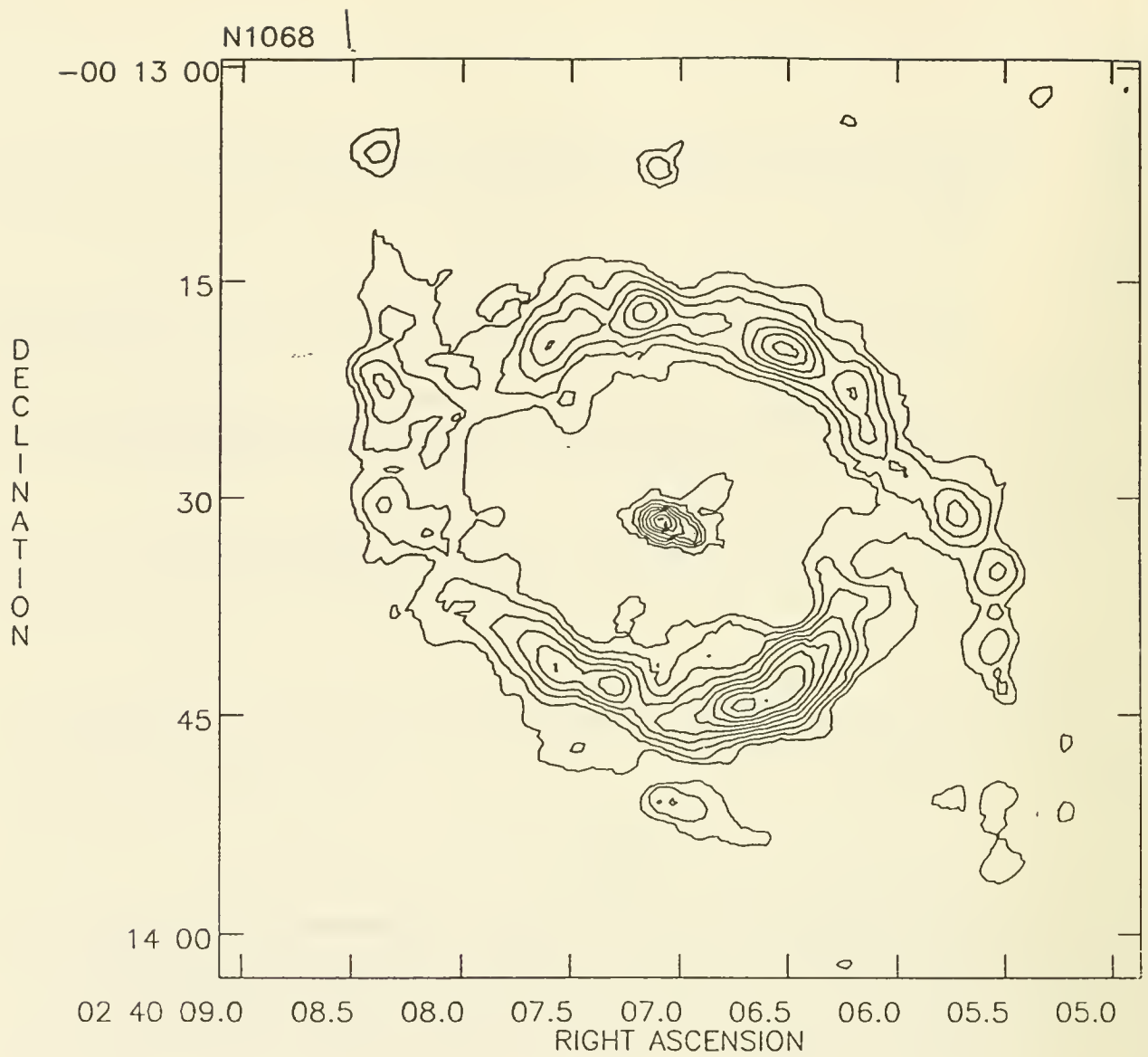


Fig. 1. Contours of the integrated CO emission mapped by the interferometer at $2.9'' \times 2.9''$ resolution. The lowest contour and the contour interval are 5 Jy km s^{-1} per beam. Emission at the nucleus includes radiocontinuum.

CO APERTURE SYNTHESIS OF NGC 4038/9 (ARP 244)

S.A. STANFORD
University of Wisconsin
AND

D.B. SANDERS, A.I. SARGENT, AND N.Z. SCOVILLE
California Institute of Technology

ABSTRACT

We present high-resolution ($\sim 6''$) CO observations of the merging galaxies NGC 4038/9 made with the Owens Valley Millimeterwave Interferometer.

I. INTRODUCTION

Arp 244 comprises the two galaxies NGC 4038 and 4039. At a distance of 21 Mpc ($V_{\text{LSR}}=1550$ km s $^{-1}$, $H_0=75$ km s $^{-1}$ Mpc $^{-1}$) this pair, popularly known as the Antennae, is the nearest example of merging disk galaxies. Previous observations of Arp 244 suggest the presence of several regions of active star formation, which could be due to the collision. Rubin, Ford, and D'Odorico (1970) observed many knots of H α emission throughout both northern and southern galaxies. Most of these knots also show up as strong sources at 6 and 20 cm (Hummel and van der Hulst 1986). Single-dish CO data at one position between the two nuclei show $M(\text{H}_2)=2.6 \times 10^9 M_\odot$ (Sanders and Mirabel 1985). Finally, IRAS observations show the system to be moderately strong in the infrared, with $L(40\text{-}400 \mu\text{m})=4.0 \times 10^{10} L_\odot$ compared to $L_B=2.9 \times 10^{10} L_\odot$.

II. OBSERVATIONS and RESULTS

The CO observations of Arp 244 were obtained between April and June 1988 using the OVRO Millimeter Wave Interferometer. Two fields with phase centers near the NGC 4039 nucleus and near the NGC 4038 nucleus were observed. The size of the synthesized beam is approximately $6.5'' \times 7''$ at PA= 72° . The rms in a single cleaned channel map is 0.06 Jy beam $^{-1}$, corresponding to a brightness temperature of 0.12 K over the synthesized beam.

Contour maps of the integrated CO intensity for both interferometer fields are shown in Figure 1. Three CO concentrations are evident. Two are centered near the nuclei of NGC 4038 and NGC 4039, closely correlated with H α and radio continuum maxima. A third CO emission region lies about $25''$ northeast of the NGC 4039 nucleus. A number of radio continuum, H α , and $10 \mu\text{m}$ emission knots appear in this region. The total integrated intensity at the northern nuclear source, 302 K km s $^{-1}$, leads to a molecular mass of $8.3 \times 10^8 M_\odot$ assuming a Galactic CO to H $_2$ conversion factor of 3.0×10^{20} H $_2$ cm $^{-2}$ (K km s $^{-1}$) $^{-1}$. The integrated CO intensity of the southern nuclear source leads to a molecular mass of $2.4 \times 10^8 M_\odot$. The extranuclear CO concentration contains $1.2 \times 10^9 M_\odot$ of molecular gas, extending over 170 km s $^{-1}$, and is resolved in a number of channels. Its large size, mass, and morphology strongly suggest that it is an agglomeration of several clumps.

III. DISCUSSION

At the NGC 4038 nucleus the average surface density of molecular gas, $\sigma(\text{H}_2)$, is $470 M_\odot \text{pc}^{-2}$ over the source diameter of 1.5 kpc, and at the CO peak $\sigma(\text{H}_2)$ is $880 M_\odot \text{pc}^{-2}$. In the NGC 4039 nucleus, the H $_2$ surface density is $310 M_\odot \text{pc}^{-2}$ over the 1.3 kpc source. These densities are 2 - 4 times higher than in comparably sized regions at the nucleus of the Galaxy (Sanders, Solomon, and Scoville 1984), which could be due to the collision. The narrow velocity width (104 km s $^{-1}$) of the CO emission in the NGC 4038 nucleus is consistent with a relatively small inclination angle for the northern galaxy. The NGC 4039 nuclear source shows emission over a broader range of velocity (156 km s $^{-1}$) consistent with a larger inclination angle for the southern galaxy.

The high $\sigma(\text{H}_2)$ at both nuclei supports the view that the nuclear luminosity is due to intense star formation rather than nonstellar activity. The radio continuum source at the NGC 4038 nucleus is

resolved at 20 cm. The nuclear source has a deconvolved half power size of 10" and a spectral index $\alpha = -0.62$. Likewise, the radio continuum source at the NGC 4039 nucleus has a deconvolved half power size of 9" and $\alpha = -0.52$. Hummel and van der Hulst (1986) estimated that for the NGC 4038 nucleus 10% of the total radio flux is thermal, and for the NGC 4039 nucleus 23% of the flux is thermal. These characteristics suggest that most of the radio emission is generated by HII regions and supernovae rather than by AGN.

A massive, $\sim 1.2 \times 10^9 M_{\odot}$, concentration of molecular gas was detected about 3 kpc from the NGC 4039 nucleus in the region where the disks of the two galaxies overlap. The concentration comprises a number of distinct clumps in the channel maps; one each at the south, west, north and east sides of the extranuclear concentration. Several observations suggest that the gas in each of these clumps is actively forming stars. In the southern clump, a radio emission knot lies near the highest CO contour and has a relatively flat spectral index, -0.43 , which implies 36% of the radio flux is thermal. Tesesco and Bushouse (1989) report 10 μm detections at 4 pixels in an image taken with a 20 pixel array bolometer (1 pixel = 4.5") centered on the southern clump, as shown by the crosses in Figure 1b. One other detection of 10 μm emission at the southern clump, from Wright *et al.* (1988), coincides with a strong H α knot. The total 10 μm emission, coupled with the implied thermal radio flux and H α emission for several sources in the southern clump, suggest that enhanced star formation exists in the southern clump. If we assume that the IR emission arises from dust heated by massive stars, we can estimate the current instantaneous rate of star formation in the southern clump of the extranuclear source following the method detailed in Hunter *et al.* (1986). Using the Salpeter IMF with an upper mass limit of 100 M_{\odot} and a lower mass limit of 0.1 M_{\odot} , we find a SFR of 4.1 $M_{\odot} \text{ yr}^{-1}$. It is interesting to compare this with the SFR calculated from the observed H α emission in the southern clump. Using the same assumptions, we calculate a SFR of 0.5 $M_{\odot} \text{ yr}^{-1}$ from the H α emission. If we were to correct the observed H α emission for the strong absorption expected in the clump then the two values would probably be in close agreement.

The other three clumps also show signs of active star formation. The radio knot at the western clump has a spectral index indicating about 10% of the emission at 20 cm to be of thermal origin. In the eastern clump, the radio knot has a spectral index which predicts a thermal to total flux density ratio of 1/3. Two H α knots also lie at the same position as the eastern clump. Their observed flux may be used as above to calculate a SFR for this clump of 0.4 $M_{\odot} \text{ yr}^{-1}$. This value is a lower limit because the H α flux has not been corrected for absorption. At the northern clump there is only a weak region of H α emission. No 10 μm data have yet been obtained for the northern, eastern and western clumps. The total SFR of the regions in the extranuclear source is about 5 $M_{\odot} \text{ yr}^{-1}$ based on the H α and 10 μm data, as compared with $\sim 5 M_{\odot} \text{ yr}^{-1}$ for the entire Milky Way. However, these SFR estimates are uncertain because of possible variations in the IMF. Evolutionary synthesis studies of young stellar populations in interacting systems suggest that the IMF of a starburst may not be the same as the Salpeter law (Stanford and Code 1989). Careful calculation of an evolutionary synthesis fit to properly extinction-corrected multiwavelength data for the individual regions is necessary to draw meaningful conclusions about their SFR.

In Figure 2, the velocity contours of the southern field are shown. At the northern edge of the extranuclear source there appears to be a separate clump as can be seen from the velocity gradient between it and the bulk of the emission region to the south. The velocity range 1550 to 1590 km s^{-1} of this clump is more similar to the 1550 km s^{-1} velocity of an H α knot in the southeastern part of NGC 4038 than to the velocities of 1451 km s^{-1} of the H α knots in the northeastern part of NGC 4039. The implication is that this clump is associated with NGC 4038 and has collided with the larger clumps in the extranuclear CO source. The second interesting feature in Figure 2 is the gradient seen in the emission region at the nucleus in NGC 4039. This gradient suggests that the molecular gas is rotating about the nucleus. The increase in the velocity of the CO emission with distance from the 2.2 μm peak of the nucleus agrees with the velocities of the H α emission knots in the same area. The sense of this rotation of the molecular gas in the NGC 4039 disk agrees with that of the stellar disk in the dynamical simulation of the collision by Barnes (1988).

One of us (SAS) thanks the Graduate School of the University of Wisconsin and the Organizing Committee of this conference for financial support enabling him to attend.

REFERENCES

- Barnes, J.E. 1988, *Ap.J.*, **331**, 699.
Hummel, E. and van der Hulst, J.M. 1986, *Astr. Ap.*, **155**, 151.
Hunter, D.A., Gillett, F.C., Gallagher, J.S., Rice, W.L., and Low, F.J. 1986, *Ap. J.*, **303**, 171.
Kennicutt, R.C. and Keel, W.C. 1989, private communication.
Rubin, V.C., Ford, W.K., and D'Odorico, S. 1970, *Ap.J.*, **160**, 801.
Sanders, D.B. and Mirabel, I.F. 1985, *Ap. J. (Letters)*, **298**, L31.
Sanders, D.B., Solomon, P.M., and Scoville, N.Z. 1984, *Ap.J.*, **276**, 182.
Stanford, S.A. and Code, A.D. 1989, in preparation.
Telesco, C.M. and Bushouse, H.A. 1989, private communication.
Wright, G.S., Joseph, R.D., Robertson, N.A., James, P.A., and Meikle, W.P.S. 1988, *M.N.R.A.S.*, **233**, 1.

Figure 1a (upper left). Integrated CO intensity map of the northern field. The velocity range is 1350 to 1750 km s⁻¹. Contour levels are 5, 10, 20, 30, 40, 50, 60, 70, 80, and 90 % of the peak flux of 79 Jy km s⁻¹/beam. A radio (Hummel and van der Hulst 1986) and H α (Kennicutt and Keel 1989) knot is marked by a filled circle, and the 2.2 μ m peak of NGC 4038 by an X.

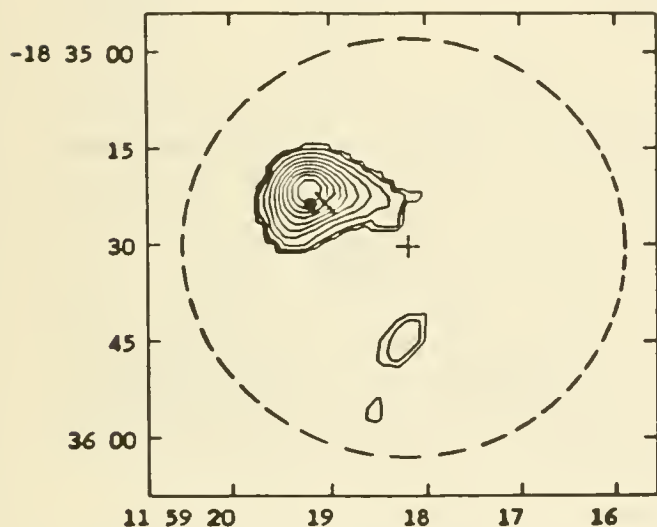


Figure 1b (lower left). Integrated CO intensity map of the northern field. The velocity range is 1350 to 1750 km s⁻¹. Contour levels are 5, 10, 20, 30, 40, 50, 60, 70, 80, and 90 % of the peak flux of 89 Jy km s⁻¹/beam. Radio/H α knots and the 2.2 μ m peak of NGC 4039 are marked by filled circles and an X, respectively. 10 μ m detections (Telesco and Bushouse 1989; Wright *et al.* 1988) are represented by crosses whose size corresponds to the IR beam. In each map, the dashed circle indicates the interferometer primary beam size, and a small cross the phase center.

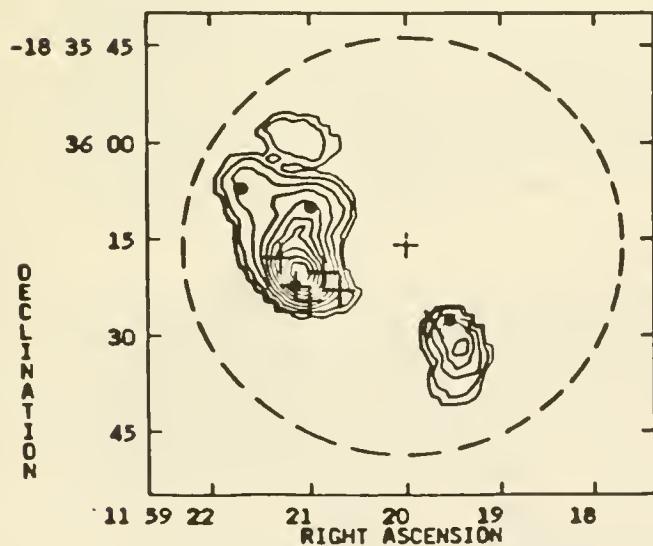
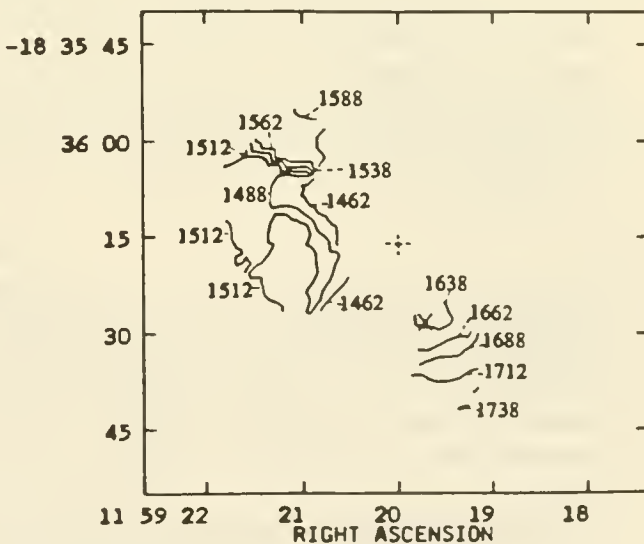


Figure 2 (lower right). A plot of CO velocity contours in the southern field. An X marks the position of the 2.2 μ m peak of NGC 4039. The velocity of each contour is indicated.



Observations of CO in the Magellanic irregular galaxy NGC 55*

Andreas Heithausen[§], Center for Astrophysics, Cambridge, Mass.,
and

Ralf-Jürgen Dettmar[§], Lowell Observatory, Flagstaff, Arizona

Introduction

The content of molecular gas in galaxies, mainly H_2 , is one of the key observations to understanding the star formation processes and history. As the CO molecule is the most widely distributed molecule after H_2 and has easily observable mm lines, it is used as a tracer for the molecular gas. The molecular hydrogen column density, $N(H_2)$, is usually derived by scaling the velocity integrated CO line, $W(CO) = \int T_R^* dv$. A typical factor, $X(W(CO)) = N(H_2)/W(CO)$, found for the Milky Way is $X_G(W(CO)) = 2.6 \times 10^{20} [\text{molecules cm}^{-2} (\text{K km}^{-1})^{-1}]$ (e.g. Bloemen et al. 1986) and very similar values, derived from Milky Way clouds, are used for normal spiral galaxies (e.g. Young et al. 1989). But this factor is not commonly accepted for all regions of our Galaxy. De Vries et al. (1987) found values of $0.5 \times 10^{20} [\text{molecules cm}^{-2} (\text{K km}^{-1})^{-1}]$ for a number of cirrus clouds (see also Heithausen and Mebold (1988) for a discussion of Galactic $X(W(CO))$ factors).

The basic explanations for the observed higher X values are excitation conditions due to an increased intensity of the ultraviolet (UV) radiation field and abundances effects. This effects are discussed in detail by Maloney and Black (1988). The observed low CO intensities of irregular (Irr) galaxies (Elmegreen et al., 1980, Young et al. 1984, Tacconi and Young 1985, 1987) have been discussed in this context and higher $X(W(CO))$ values by up to a factor of 10 were suggested by several authors for this type of galaxy (Thronson et al. 1987, Israel 1988, Cohen et al. 1988).

For most Irr galaxies the mass of H_2 is derived by indirect and global methods. Only for nearby objects, like the Small and Large Magellanic Clouds (SMC and LMC), is it possible to get dynamical masses if the molecular clouds are assumed to be in virial equilibrium. This assumption works very well within the Galaxy and if applied to the Magellanic Clouds, the resulting $X(W(CO))$ values are 6 times higher for the LMC (Cohen et al. 1988) and 25 times higher for the SMC (Rubio et al., 1988) than the average X_G value for our Galaxy.

Observations

NGC 55 is the nearest giant Magellanic-type galaxy beyond the Local Group. It is classified as SBm and shows similarities to the LMC. In order to study the distribution and properties of molecular gas within Magellanic type galaxies in more detail we observed this galaxy in July 1988 in the $J=1 \rightarrow 0$ CO line with the 15m Swedish-ESO Submillimeter Telescope (SEST). Spectra were taken with a low resolution acousto optical spectrometer using 728 channels and a velocity resolution of 1.792 km s^{-1} at 115GHz. The integration time was 40 minutes (on+off) resulting in an rms noise of about 15mK.

Results

CO was detected towards the direction where the $H\alpha$ and 6 cm radiocontinuum emission is strongest (Hummel et al. 1986). We present the gaussian line parameters in Table 1. The distribution of CO corresponds well with the intense HI cloud near the bar of NGC 55. The extent of the CO cloud is about 975 pc along the major axis and 390 pc perpendicular to the major axis. As the radio-continuum and $H\alpha$ emission also peaks in this region, it is most probably associated with the dominant star forming region in NGC 55. Assuming that the molecular gas is in virial equilibrium,

* Based on observations obtained with the SEST telescope at ESO/La Silla, Chile

[§] on leave from: Radioastronomisches Institut der Universität Bonn, Bonn, FRG

we derive a mass of about $8 \times 10^7 M_{\odot}$. The comparison to the III mass of $1.7 \times 10^7 M_{\odot}$ for this complex found by Hummel et al. (1986) shows that this cloud is mainly molecular.

Table 1: CO line parameters for NGC 55

$\Delta(RA)$ ["]	$\Delta(Decl)$ ["]	T_A [mK]	$v_{cent}(Hcl)$ [km s ⁻¹]	$FWHM$ [km s ⁻¹]	rms [mK]
0	0	32	108	43	11
12	-25	41	117	38	16
25	12	57	109	20	20
31	-31	90	121	38	15
37	-13	57	116	43	19
43	-57	33	129	34	10
50	-38	94	129	35	16
69	-44	61	133	32	15
75	-26	60	130	31	16
88	-51	44	138	35	13

Notes: Positions are offsets in arcseconds relatively to $RA = 00^h 12^m 23^s .5$, $Decl. = -39^{\circ} 28' 30''$

a) The $N(H_2)W(CO)$ Ratio

Comparing this mass to an averaged $W(CO)$ value of about 3 K km s^{-1} , we derive a $X(W(CO))$ ratio of $60 \times 10^{20} [\text{molecules cm}^{-2} (\text{K km}^{-1})^{-1}]$. This is approximately 20 times the average value for our Galaxy.

An independent estimate for the mass of the molecular gas can be obtained from the *IRAS* FIR fluxes. The use of the $S(60)/S(100)$ flux ratio results in a dust temperature of $T_D = 29 \text{ K}$ and finally in a dust mass of $M_d = 3.37 \times 10^5 M_{\odot}$.

If we make use of the relation $M(H_2) \sim 500 M_d$ (Young et al. 1989) that holds for a wide range of spiral galaxies, including the Milky Way, we find $M(H_2) \simeq 1.7 \times 10^8 M_{\odot}$. The molecular mass found indicates that the conversion factor for the molecular mass in Irr galaxies as inferred from CO line emission is indeed higher by up to a factor of 20 compared to the canonical value for the Galaxy.

b) Dependence on Metallicity

Metal abundances are considered to be the most important controlling parameters for the relation between the observable CO and the total content of molecular gas (e.g. Maloney and Black 1988). NGC 55 has low metallicity III regions (Webster and Smith 1983, Vigroux et. al. 1988, and references therein).

In the absence of known carbon abundances we can only compare the different X values with oxygen and nitrogen abundances directly. In Figure 1 we have plotted X/X_G against O/H and N/H abundances. For comparison with the Milky Way we have also included the values for the Orion nebula from Dufour et al. (1982). While a rough dependence of X/X_G on O/H abundances is found for the whole range of metallicities, a good correlation exists between X/X_G and N/H for the low metallicity Irr galaxies.

The dependence on metallicity discussed here can only be indicative and it is of course still possible that the radiation field plays an important role.

Acknowledgments. The authors are supported by the Deutsche Forschungsgemeinschaft and want to thank their host institutes for the kind hospitality.

REFERENCES

- Bloemen, J.B.G.M., et al. 1986, *Astr.Ap.*, **154**, 25.
- Cohen, R.S., Dame, T., Garray, G. Montani, J., Rubio, M., and Thaddeus, P. 1988, *Ap.J.*, **331**, L95.
- De Vries, H.W., Heithausen, A., and Thaddeus, P. 1987, *Ap.J.*, **319**, 723.
- Dufour, R.J., Shields, G.A., and Talbot, R.J. 1982, *Ap.J.*, **252**, 461.
- Elmegreen, B.G., Elmegreen, D.M., and Morris, M. 1980, *Ap.J.*, **240**, 455.
- Heithausen, A., and Mebold, U. 1988, *Astr.Ap.* in press.
- Hummel, E., Dettmar, R.-J., and Wielebinski, R. 1986, *Astr.Ap.*, **166**, 97.
- Israel, F. 1988, preprint.
- Maloney, P., and Black, J.H. 1988, *Ap.J.*, **325**, 389.
- Tacconi, L.J., and Young, J.S. 1985, *Ap.J.*, **290**, 602.
- Tacconi, L.J., and Young, J.S. 1987, *Ap.J.*, **322**, 681.
- Thronson, H.A., Hunter, D.A., Telesco, C.M., Harper, D.A., and Decher, R. 1987, *Ap.J.*, **317**, 180.
- Rubio, M. 1988, in "The Physics and Chemistry of interstellar Molecular Clouds", ed. G. Winnewisser, New York.
- Vigroux, L., Statsińska, G., and Comte, G. 1987, *Astr.Ap.*, **172**, 15.
- Webster, B.L., and Smith, M.G. 1983, *M.N.R.A.S.*, **204**, 743.
- Young, J.S., Gallagher, J.S., and Hunter, D.A. 1984, *Ap.J.*, **276**, 476.
- Young, J.S., Xie, S., Kenney, J.D., and Rice, W.L. 1989, *Ap.J.Suppl.* in press.

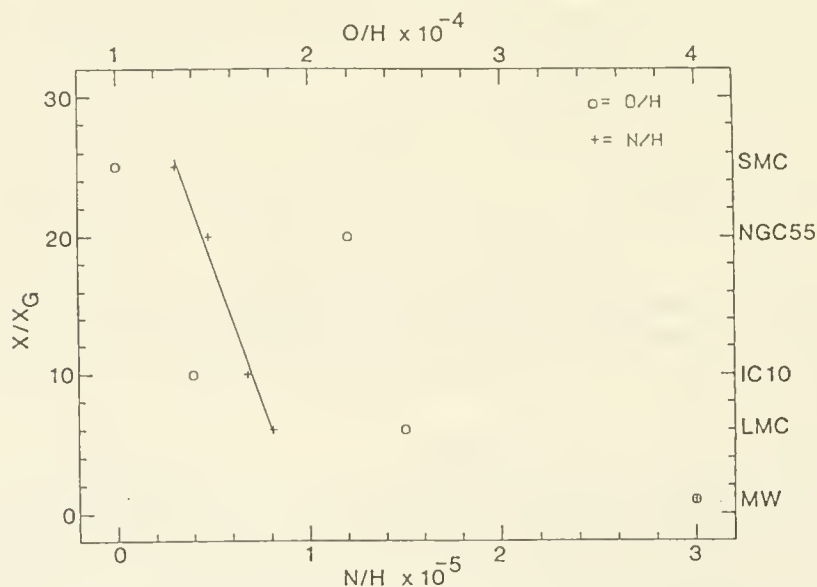


Figure 1: The dependence of X/X_G , the conversion factor $X(W(CO))$ scaled to the average value of our Galaxy, on O/H and N/H abundances. For comparison with the Galaxy abundances for the Orion nebula from Dufour et al. (1982) are included. The continuous line indicates the dependence of X/X_G on N/H for Irr galaxies.

Observations of CO Isotopic Emission and the Far-Infrared Continuum of Centaurus A

A. Eckart¹, M. Cameron¹, H. Rothermel¹, W. Wild¹, H. Zinnecker¹,
M. Olberg², G. Rydbeck², T. Wiklind²

¹ Max Planck Institut für Physik und Astrophysik,
Institut für extraterrestrische Physik, 8046 Garching, FRG

² Onsala Space Observatory, 34 Onsala, Sweden

We present maps of the $^{12}\text{CO}(1-0)$ line and the 100 μm and 50 μm far-infrared emission of Centaurus A, as well as measurements of the $^{12}\text{CO}(2-1)$, $^{13}\text{CO}(1-0)$, and the $\text{C}^{18}\text{O}(1-0)$ lines at selected positions. The observations were taken with the Swedish-ESO Submillimeter Telescope (SEST) and the CPC instrument on board *IRAS*.

The millimeter data show that the bulk molecular material is closely associated with the dust lane and contained in a disk of about 180'' diameter and a total molecular mass of about $2 \times 10^8 M_{\odot}$. The total molecular mass of the disk and bulge is of the order of $3 \times 10^8 M_{\odot}$. The molecular gas in the nucleus is warm with a kinetic temperature of the order of 15 K and a number density of 10^3 to $3 \times 10^4 \text{ cm}^{-3}$. Absorption features in the ^{12}CO and ^{13}CO lines against the nuclear continuum emission indicate that the properties of giant molecular clouds are comparable to those of the Galaxy.

The far-infrared data show that to a good approximation the dust temperature is constant across the dust lane at a value of about 42 K. The ratio between the far-infrared luminosity and the total molecular mass is $18 L_{\odot}/M_{\odot}$ and close to the mean value obtained for isolated galaxies. A comparison of the $^{12}\text{CO}(1-0)$ and the far-infrared data indicates that a considerable amount of the far-infrared emission is not intimately associated with massive star formation.

^{12}CO AND ^{13}CO J=2-1 AND J=1-0 OBSERVATIONS OF HOT AND COLD GALAXIES

Shuding Xie, F. Peter Schloerb and Judith Young

Department of Physics and Astronomy
University of Massachusetts

I. INTRODUCTION

We have observed the nuclear regions of the galaxies NGC 2146 and IC 342 in ^{12}CO and ^{13}CO J=1-0 and J=2-1 lines using the FCRAO 14m telescope. NGC 2146 is a peculiar Sab spiral galaxy. Its complex optical morphology (Pease 1920; de Vaucouleurs 1950; Bevenuti et al. 1975; Young et al. 1988) and strong nuclear radio continuum emission (Condon et al. 1982) suggest that it is experiencing a phase of violent activity and could have a polar ring (Schweizer et al. 1983) which may have resulted from an interaction. IC 342 is a nearby luminous Scd spiral galaxy. Strong CO, infrared and radio continuum emission from the nuclear region of IC 342 indicate enhanced star-forming activity, and interferometric ^{12}CO J=1-0 observations reveal a bar-like structure centered on the nucleus, along the dark lane in the NS direction (Lo et al. 1984). These two galaxies are selected based on their different dust temperatures and star formation efficiencies (SFE) as derived from the IRAS $S_{60\mu}/S_{100\mu}$ flux density ratio and $L_{\text{IR}}/M(\text{H}_2)$, respectively, with a relatively high SFE and dust temperature of 45K in NGC 2146 and a relatively low SFE and dust temperature of 35K in IC 342.

The data from the different ^{12}CO and ^{13}CO lines are used to study the physical conditions in the molecular clouds in the galaxies. We also consider the radiative transfer to determine whether a warm and optically thin gas component exists in these galaxies, as has been suggested in the case of M82 (Knapp et al. 1980), and whether the warm gas is related to the dust properties. Since optically thin ^{12}CO gas is rarely detected in our own Galaxy (except in outflow sources), to confirm its existence in external galaxies is very important in understanding the molecular content of external galaxies and its relationship to star formation activity.

The present ^{12}CO J=2-1 and ^{13}CO J=2-1 and J=1-0 data for NGC 2146 are the first detections of this galaxy to our knowledge. The ^{12}CO J=1-0 distribution in NGC 2146 has been measured as part of the FCRAO Extragalactic Survey. For the well-studied IC 342, our data are compared with the IRAM 30m observations (Eckart et al. 1989) and other available data. Here we present the observed results.

II. OBSERVATIONS

The observations were carried out during the periods of January - March in 1988 and 1989 using the 14m radome-enclosed FCRAO telescope. In order to avoid the calibration and pointing uncertainties associated with daily heating of the antenna, we only observed during the night time between 6p.m. and 6a.m. The data were calibrated by the chopper wheel method. Pointing was checked periodically on IRC+10216 and Jupiter with an rms of $\sim 5''$, and confirmed by monitoring the line profile of the central position of the galaxy. The HPBW of the 14m antenna at the ^{12}CO J=1-0 frequency (115.2712 GHz) and J=2-1 frequency (230.5379 GHz) are $45''$ and $23''$, respectively. All spectra were taken using double beam switching procedure so that flat baselines were achieved.

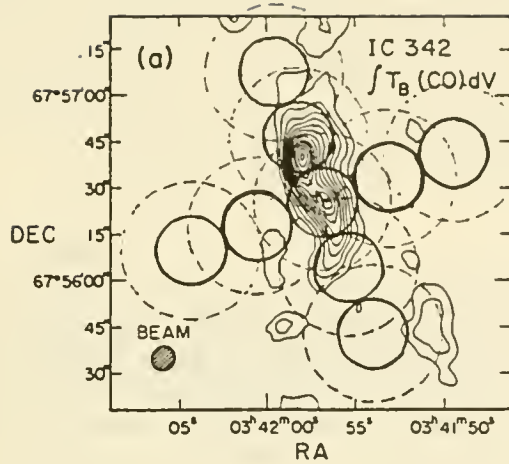


Fig. 1. The locations of our ^{12}CO and ^{13}CO J=2-1 and J=1-0 observations of IC 342 superposed on the integrated contour maps made with OVRO interferometer (Lo et al. 1984). The smaller circles show the 23" beam of the 14m FCRAO telescope for the J=2-1 emission and the larger one is the 45" beam for the J=1-0 line. The shaded circle on the lower left corner indicates the 7" beam of the interferometer. The cross represents the peak of 2.2 μm emission (Becklin et al. 1980).

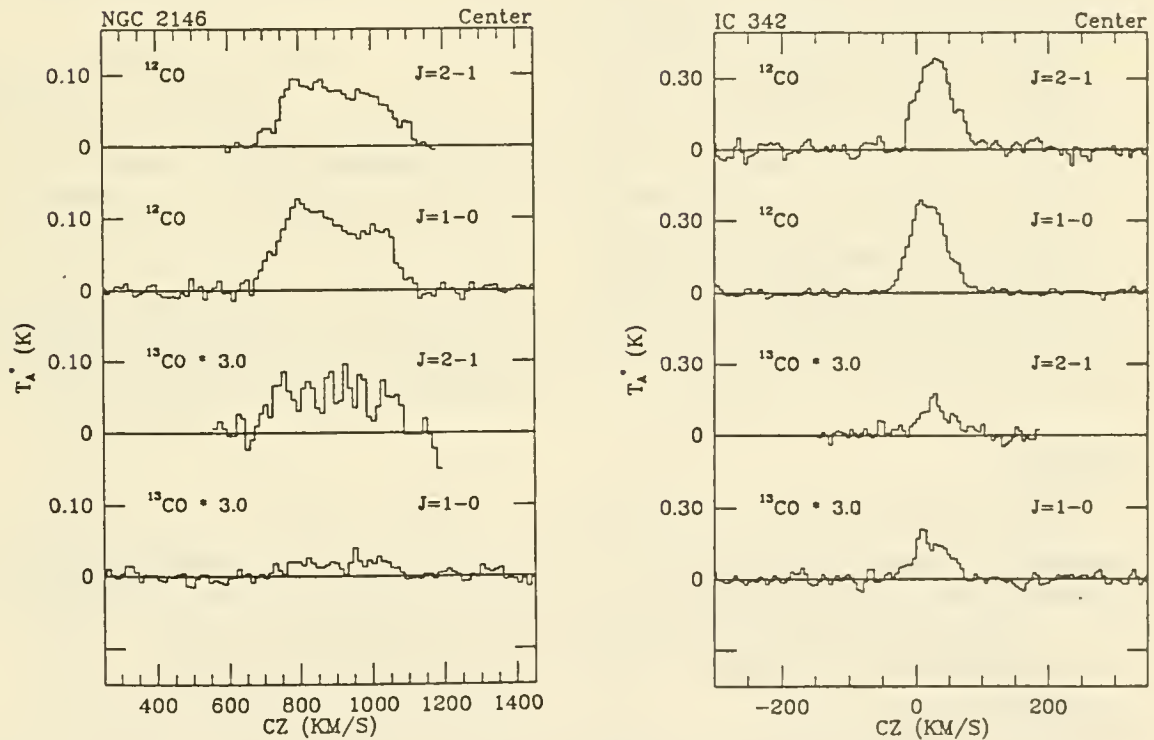


Fig. 2. Spectra of ^{12}CO and ^{13}CO J=2-1 and J=1-0 emission at the centers of the galaxies NGC 2146 and IC 342. The data are smoothed to a final velocity resolution of 15.6 km s^{-1} for NGC 2146 and 7.8 km s^{-1} for IC 342. The vertical scale is the antenna temperature uncorrected for the telescope efficiencies of the 14m antenna at the corresponding frequencies. In order to present the spectra from different species at the same scale, the weaker ^{13}CO emission has been enlarged by a factor of 3.

The coordinates and position angles used for NGC 2146 are same as those used in the FCRAO Extragalactic Survey (position angle of 128°). The central position of IC 342 was chosen based on the interferometer map (Lo et al. 1984) in which there were two peaks spaced by $\sim 15''$. We selected the peak which was closer to the optical center as our observing center. A position angle of 20° was also adopted based on the interferometer map. Fig. 1 illustrates the locations of our ^{12}CO and ^{13}CO J=2-1 and J=1-0 observations in the galaxy IC 342.

III. RESULTS

The preliminary comparisons of the different lines and isotopes show that:

(1) For IC 342, the ^{12}CO J=2-1 and J=1-0 integrated intensities peak at different positions. The J=1-0 data follow the NS gas bar, with a stronger peak located at about $15''$ north-east of the center. This is consistent with the Owens Valley Millimeter-Wave Interferometer J=1-0 map ($7''$ resolution; Lo et al. 1984) and the Nobeyama J=1-0 map ($15''$ resolution; Hayashi et al. 1986), which both show a double-peaked structure with the NE component stronger (for example, see Fig. 1). On the other hand, the IRAM $21''$ resolution J=1-0 map (Eckart et al. 1989) is centrally peaked and differs from the above data. However, since the first three results were obtained independently, we regard the double-peaked structure as real.

The ^{12}CO J=2-1 emission peaks at the center. Although the center position used at IRAM is slightly different from ours, both data show a symmetric distribution in the NS direction. Along the EW direction, we find the emission to be stronger in the west than in the east. The elongated NS bar-like structure is obvious.

(2) For NGC 2146, both transitions are centrally peaked with a decrease in integrated intensity of a factor of ~ 2 in $23''$. The ^{12}CO J=2-1 observations show strong emission along the major axis.

(3) The optical depths for the J=2-1 and J=1-0 lines in NGC 2146 and IC 342 are estimated from the ^{12}CO to ^{13}CO intensity ratios. Fig. 2 shows the spectra of ^{12}CO and ^{13}CO J=2-1 and J=1-0 emission at the centers of the two galaxies. In general, it is found that the ^{12}CO emission is consistent with optically thick gas.

REFERENCE

- Benvenuti, P., Capaccioli, M., and D'Odorico, S. 1975, *Astron. Astrophy.*, **41**, 91.
 Condon, J.J., Condon, M.A., Gisler, G., and Puschell, J.J. 1982, *Ap.J.* **252**, 102.
 de Vaucouleurs, G., de Vaucouleurs, A., and Corwin, H.G. 1976, *Second Reference Catalog of Bright Galaxies* (Austin: University of Texas Press) (RC2).
 Eckart, A., Downes, D., Genzel, R., Harris, A.I., Jaffe, D.T., and Wild, W. 1989, preprint.
 Hayashi, M., Handa, T., Sofue, Y., Nakai, N., Hasegawa, T., Lord, S., Young, J. 1986, *IAU Symp. No. 115*, *Star Forming Regions*, ed. M. Peimbert, J. Jugaku (Dordrecht: Reidel), p. 631.
 Lo, K.Y., Berge, G.L., Claussen, M.J., Heiligman, G.M., Leighton, R.B., Masson, C.R., Moffet, A.T., Philipps, T.G., Sargent, A.I., Scott, S.L., Wannier, P.G., and Woody, D.P. 1984, *Ap.J. (Letters)* **282**, L59.
 Knapp, G.R., Phillips, T.G., Huggins, P.J., Leighton, R.B., and Wannier, P.G. 1980, *Ap.J.* **240**, 60.
 Pease, F.G. 1920, *Ap.J.*, **51**, 276.
 Schweizer, F., Whitmore, B.C., and Rubin, V.C. 1983, *Astron.J.*, **88**, 909.
 Young, J.S., Claussen, M.J., Kleinmann, S.G., Rubin, V.C., and Scoville, N. 1988, *Ap.J. (Letter)*, **331**, L81.

The molecular cloud content of early type galaxies

Tommy Wiklund¹ and Christian Henkel²

¹) Onsala Space Observatory, S-43900 Onsala, Sweden

²) Max-Planck-Institute für Radioastronomie, Auf dem Hügel 69, 5300 Bonn, FRG

1. Introduction

A survey of the CO content of early type galaxies has led to 24 new detections, mostly lenticular galaxies. The galaxies, which are situated in both the northern and southern hemispheres, have been selected as being far-IR luminous compared to their blue luminosity, and situated at distances less than about 50 Mpc ($H_0=100 \text{ km s}^{-1} \text{ Mpc}^{-1}$).

2. Global properties

The typical H_2 masses, estimated from the CO integrated intensities, using a conversion ratio $N(H_2)/I_{CO}=2 \cdot 10^{20} \text{ cm}^{-2} (\text{K km s}^{-1})^{-1}$, fall between 10^7 - $10^9 M_\odot$. Since we have used a conservative conversion ratio and a large Hubble constant, these mass estimates can be regarded as lower limits to the molecular masses as long as the CO emission is optically thick.

The far-IR luminosities of the early type galaxies are, on average, an order of magnitude lower than for a sample of 121 spiral galaxies (including field and interacting systems). The spiral sample have been compiled from the literature and the relevant parameters are transformed to the same conversion ratio $N(H_2)/I_{CO}$ and the same Hubble constant as the early type sample. The current star formation rate for the early type galaxies, assumed to be proportional to the far-IR luminosity, are typically $0.1 - 1 M_\odot \text{ yr}^{-1}$, i.e. an order of magnitude lower than for spiral galaxies. The distribution of the ratio of 60 mm and 100 mm IRAS fluxes shows that the dust temperatures of the early type galaxies are similar to those of the spiral sample, indicating that the heating mechanism is of similar efficiency for both samples. The star formation efficiencies have been estimated through

the ratio of far-IR and CO luminosities, and have been found to be similar for the early type and spiral samples. Furthermore, weighting the far-IR and CO luminosities with their temperature dependences (T^5 and T , respectively), we find a linear correlation between these quantities. These results imply that the presence of spiral arm density waves is not necessary for efficient formation of massive stars on a global scale. The presence of massive molecular cloud complexes in these early type galaxies implies that spiral density waves are not necessary for molecular cloud formation either.

The ratio L_B/L_{FIR} , measuring the ratio of star formation rates averaged over approximately 10^9 and 10^6 years, indicate that the star formation history of the early type galaxies are similar to the spiral galaxies, i.e. more or less constant over time periods of at least 10^9 years.

3. Individual sources

We have mapped some early type galaxies in more detail, using both the $^{12}\text{CO}(1-0)$ and $(2-1)$ transitions, as well as observing $^{13}\text{CO}(1-0)$ and $(2-1)$. Here we present results for the lenticulars NGC 404, NGC 3593 and NGC 4369.

NGC 404. This peculiar S0 galaxy with a previously unknown distance has the molecular gas distributed in a broken ring close to the nucleus. The gas seems to be situated in the plane of the disk. Our CO observations together with observations of the HI content, using the VLA, indicate that NGC 404 is situated at a distance of approximately 10 Mpc. The total H_2 mass is estimated to be $7 \cdot 10^7 M_\odot$. The star formation rate, derived from the far-IR luminosity, is found to be $0.2 M_\odot \text{ yr}^{-1}$, which is less than the estimated rate of return of

processed stellar material to the interstellar medium. The $^{12}\text{CO}(2-1)/(1-0)$ line intensity ratio is found to be about 0.8. From a $^{13}\text{CO}(1-0)$ observation we estimate the optical depth of the ^{12}CO line to be 10

NGC 3593 This edge-on S0 galaxy has the molecular gas distributed in a disk-like configuration. The total molecular mass is found to be $2 \cdot 10^9 M_\odot$, with an assumed distance of 11 Mpc. The $^{12}\text{CO}(2-1)/(1-0)$ line intensity ratio is close to 1. Together with a $^{13}\text{CO}(2-1)$ observation this result indicates that the ^{12}CO emission is optically thick with an excitation temperature $>15\text{-}20$ K. The kinematical properties of the molecular gas indicate solid body rotation out to a distance of 0.8 kpc from the nucleus and constant rotational velocity at larger distances.

NGC 4369 This face-on S0 galaxy has the molecular gas distributed in a bar-like structure in the center region. The iso-velocity contours run parallel to the bar. The total molecular mass is estimated to be $2 \cdot 10^8 M_\odot$. The $\text{CO}(2-1)$ and $(1-0)$ distributions indicate that the line intensity ratio vary over the face of the galaxy. The $(2-1)$ and $(1-0)$ observations were done simultaneously thus eliminating pointing offsets as the cause for this effect. Whether this varying line ratio is due to different optical depths or excitation temperatures over the face of the galaxy is not known at the present since we do not yet have ^{13}CO observations of this galaxy.

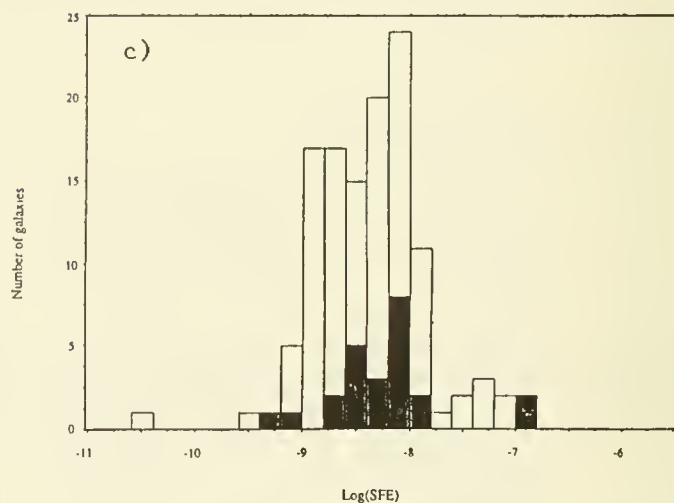
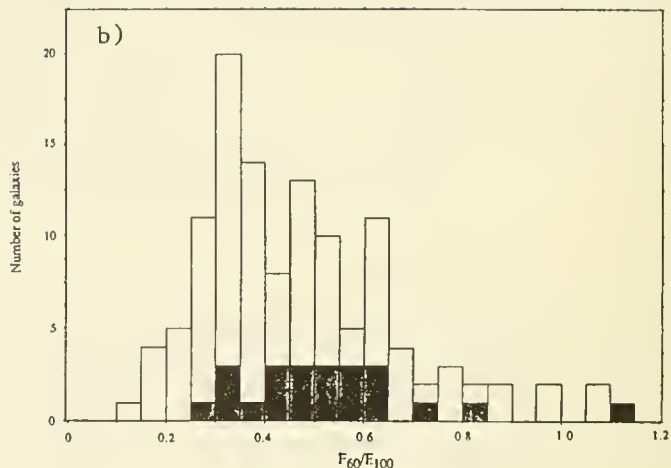
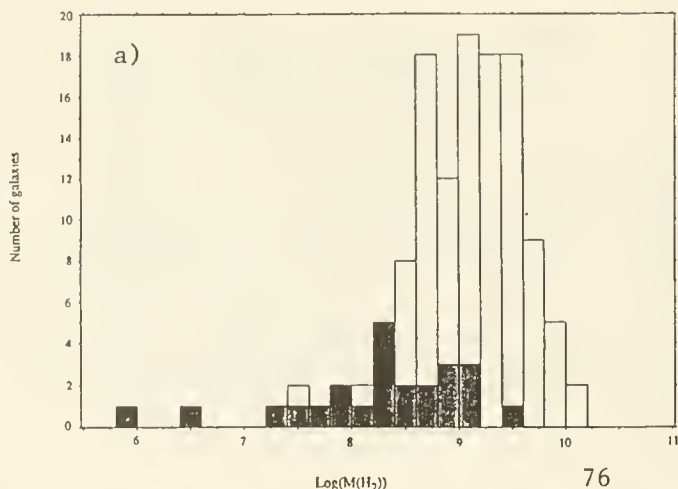


Figure 1. The distributions of a) $\log(M(\text{H}_2))$, b) F_{60}/F_{100} , and c) $\log(\text{SFE})$ for the early type galaxies (dark bars) and the spiral sample (unfilled bars).



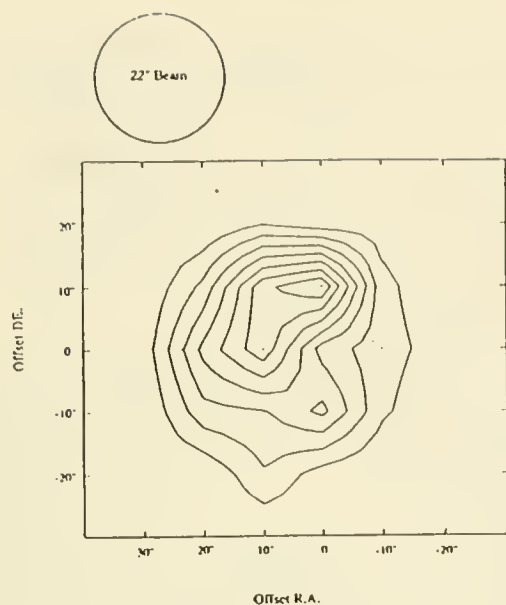


Figure 2. The $^{12}\text{CO}(1-0)$ integrated intensity distribution in NGC 404. The map spacing is $10''$. The lowest contour is 3.5 K km s^{-1} , and contours are spaced 1.5 K km s^{-1} apart.

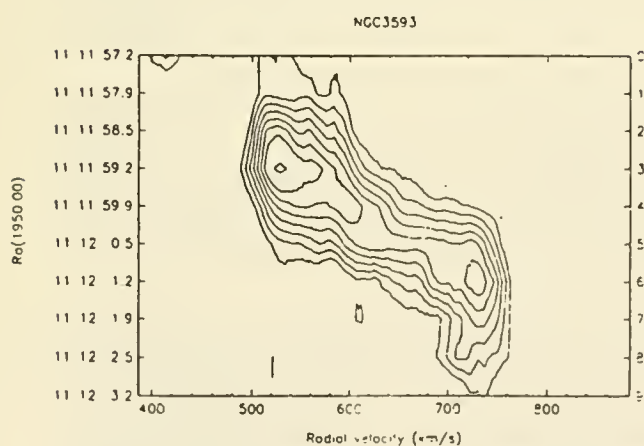


Figure 3. A position-velocity diagram along the major axis of NGC 3593.

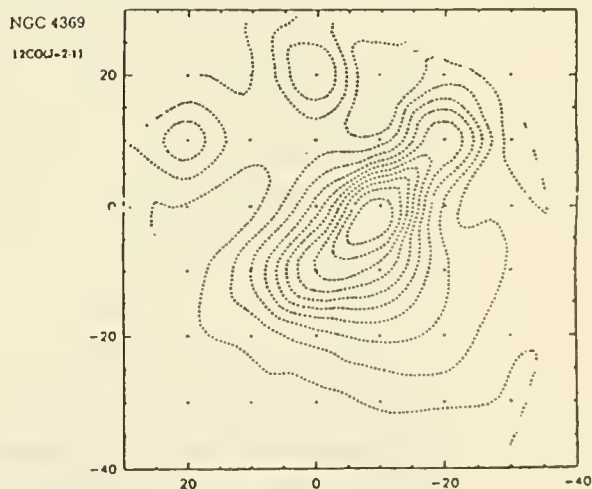
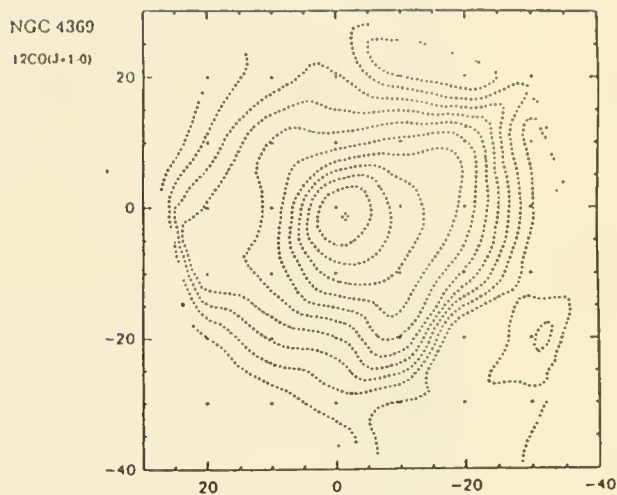


Figure 4. The $^{12}\text{CO}(1-0)$ and the $^{12}\text{CO}(2-1)$ integrated intensity distributions for NGC 4369.

CS $J=2 \rightarrow 1$ Emission Toward the Central Region of M82

C. E. Walker (Steward Obs.), C. K. Walker (Caltech), J. E. Carlstrom (U.C. Berkeley), and R. N. Martin (Steward Obs.)

M82 is an irregular (Type II) galaxy located at a distance of approximately 3.5 Mpc. Its unusual appearance and high luminosity, particularly in the infrared, has led many astronomers to classify it as a starburst galaxy. This interpretation is supported by the observation of a large number of radio continuum sources within the central arcminute of the galaxy. These sources are thought to be associated with supernova remnants (Kronberg *et al.* 1985). The starburst in the central region of the galaxy is believed to have been triggered by tidal interaction with either M81 or the H I cloud surrounding the M81 group.

High angular resolution ^{12}CO $J=1 \rightarrow 0$ maps by Nakai (1984) and Lo *et al.* (1987) indicate the existence of a 400-450 pc rotating ring of molecular material about the central region of M82. Red- and blue-shifted absorption components of the H I and OH lines measured by Weliachew *et al.* (1984) provided the first evidence for the presence of the ring. Many astronomers, each using a different angular resolution, have compared ^{12}CO $J=1 \rightarrow 0$, $J=2 \rightarrow 1$, and $J=3 \rightarrow 2$ emission and concluded that a large fraction of the CO emission is optically thin (Knapp *et al.* 1980; Sutton *et al.* 1983; Olofsson and Rybeck 1984; Turner *et al.* 1989). Additional observations suggest that the molecular material toward the center of M82 is clumpy and dense (Loiseau *et al.* 1988 and Carlstrom 1988).

Unlike the lower rotational transitions of CO, CS is excited only at relatively high densities, $n_{\text{H}_2} \geq 10^4 \text{ cm}^{-3}$. It is in clouds with these densities that stars are expected to form. This makes CS an excellent probe of star formation regions. We have observed the CS $J=2 \rightarrow 1$ transition (97.981 GHz) toward 52 positions in M82 using the NRAO 12 m telescope. The beamsize was $\approx 63''$ and the spacing between observed positions was $20''$. The spectral resolution was 6.1 km/s. An rms noise level of 4 mK per channel was obtained. CS was detected over a $160''$ square region roughly centered on the $2 \mu\text{m}$ peak (0,0 offset). The emission is extended along the major axis of the galaxy. The map of the CS integrated intensity is shown in Figure 1.

The velocity centroid of each observed spectrum was computed. The observed velocity gradient closely resembles that observed in CO $J=1 \rightarrow 0$, (Young and Scoville 1984) and appears to be dominated by rotation about the minor axis of the galaxy. The similarity between the two velocity maps suggests that the CS and CO emission are arising from molecular clouds located at similar positions in the galaxy.

Estimates of the molecular column density along the lines of sight that CS $J=2 \rightarrow 1$ was detected can be made if we assume the emission is optically thin. By adopting an excitation temperature of 40 K and $\tau < 1$, we can estimate the CS column density across our beam. In this type of derivation the molecular column density toward a given position is proportional to the CS integrated intensity observed there. The peak column density is $3 \times 10^{13} \text{ cm}^{-2}$ and occurs $\approx 20''$ east of the central position. For a fractional CS/H₂ abundance of 10^{-9} (Graedel *et al.* 1982), the corresponding H₂ column density is $3 \times 10^{22} \text{ cm}^{-2}$.

As mentioned earlier, the presence of CS emission indicates the presence of gas with a density $\geq 10^4 \text{ cm}^{-3}$. If such high density gas uniformly fills the region over which CS was detected, then this implies a gas mass of $\approx 2 \times 10^{12} M_{\odot}$. The dynamical mass of the region is only $\approx 4 \times 10^9 M_{\odot}$ (Young and Scoville 1984). The difference between the two mass estimates indicates that the dense gas is clumpy, with a filling factor $\leq 2 \times 10^{-3}$.

In Figure 2 we present a surface plot which shows the variation in the CO to CS integrated intensity ratio over the central region of M82. The CO data is from Young and Scoville ($\approx 50''$ resolution). The 0,0 position in Figure 2 is $\approx 15''$ west of the $2 \mu\text{m}$ peak. Along the major axis the $I_{\text{CO}}/I_{\text{CS}}$ ratio peaks near the center and the edges of the map and has minima about $50''$ east and $30''$ west. In contrast, the $I_{\text{CO}}/I_{\text{CS}}$ ratio reaches its lowest values at the edges of the map along a position angle close to that of the minor axis. Since the characteristic density of CO is much less than that of CS, lower values of $I_{\text{CO}}/I_{\text{CS}}$ may indicate that a higher percentage of the gas is in dense clouds. The minima in Figure 2 are at the outer boundary of the dense molecular ring observed both in high resolution single dish (Nakai *et al* 1987; Loiseau *et al.* 1988) and interferometer (Carlstrom 1988) maps. Therefore, if a low value of the $I_{\text{CO}}/I_{\text{CS}}$ ratio does indicate a large percentage of dense gas, then Figure 2 shows *there is a reservoir of dense gas located just outside the molecular ring found*. The peak $I_{\text{CO}}/I_{\text{CS}}$ ratio at the map center would then suggest that although the largest column density of dense gas occurs toward the center (see Figure 1), the percentage of molecular gas in dense clouds within our beam is lower there than in the surrounding region.

The variation in the $I_{\text{CO}}/I_{\text{CS}}$ ratio in Figure 2 could in principle be due to a variation of the CS fractional abundance across the source, perhaps due to shocks. However, model calculations by Hartquist *et al.* (1980) indicate that sulfur bearing molecules could be overabundant in shocked regions. Since the central region has a peak in the $I_{\text{CO}}/I_{\text{CS}}$ ratio and is probably the most heavily shocked, it is unlikely that shock chemistry is significantly effecting the fractional abundance of CS.

A drop in the $I_{\text{CO}}/I_{\text{CS}}$ ratio from a central peak could also occur if the gas temperature dropped as a function of distance from the center. In this situation the opacity in the CO $J=1 \rightarrow 0$ and the CS $J=2 \rightarrow 1$ lines would increase and may eventually saturate at larger radii. However, the more density sensitive CS would feel the effects of the decreasing temperatures more slowly than CO. The $I_{\text{CO}}/I_{\text{CS}}$ ratio would decrease at increasing radii and eventually level off. However, this is not what is observed. Inspection of Figure 2 shows that the $I_{\text{CO}}/I_{\text{CS}}$ ratio goes through a minimum and then sharply increases again along the major axis in both directions from the nucleus.

Different spatial resolution of CO and CS observations combined with a brightness gradient may also produce variations in $I_{\text{CO}}/I_{\text{CS}}$. We are currently investigating the effect of the $\approx 30\%$ difference between the NRAO and FCRAO beamwidths.

REFERENCES

- Carlstrom 1988, *Galactic and Extragalactic Star Formation*, ed. Pudritz and Fich, Dordrecht: Reidel.
 Graedel, Langer and Frerking 1982, *Ap. J. Supp.*, 48, 321.
 Hartquist, Oppenheimer and Dalgarno 1980, *Ap. J.*, 236, 182.
 Knapp *et al.* 1980, *Ap. J.*, 240, 60.
 Kronberg, Biermann and Schwab 1985, *Ap. J.*, 291, 693.
 Lo *et al.* 1987, *Ap. J.*, 312, 574.
 Loiseau *et al.* 1988, *Astron. Astrophys.*, 200, L1.
 Nakai 1984, *Ph.D. thesis*, University of Tokyo, Japan.
 Nakai *et al.* 1987, *P. A. S. J.*, 39, 685.
 Olofsson and Rydbeck 1984, *Astron. Astrophys.*, 136, 17.
 Sutton, Masson and Phillips 1983, *Ap. J.*, 275, L49.
 Turner, Martin and Ho 1989, *Ap. J.*, submitted.
 Weliachew, Fomalont and Greisen 1984, *Astron. Astrophys.*, 137, 335.
 Young and Scoville 1984, *Ap. J.*, 287, 153.

Figure 1 The CS $J=2 \rightarrow 1$ integrated intensity map of M82. The minimum contour level is 0.2 K km/s and the contour interval is 0.6 K km/s. The rms noise level is ≈ 0.06 K km/s. The 0,0 point is located at the $2\mu\text{m}$ peak.

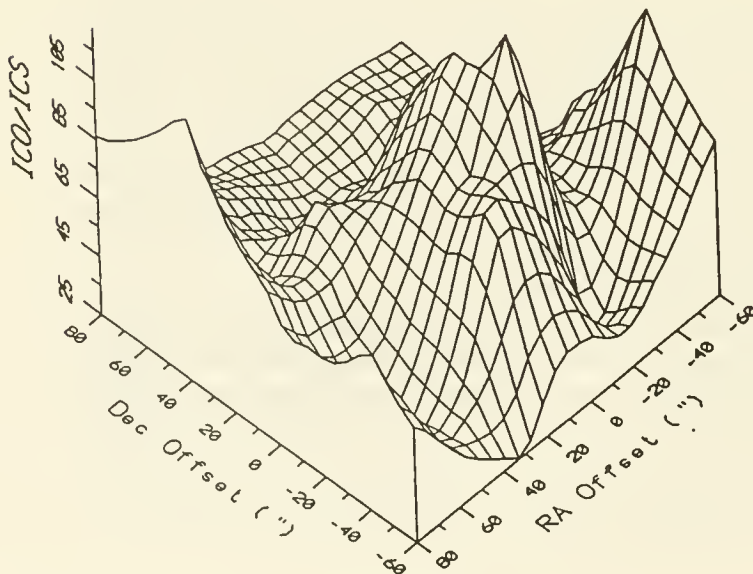
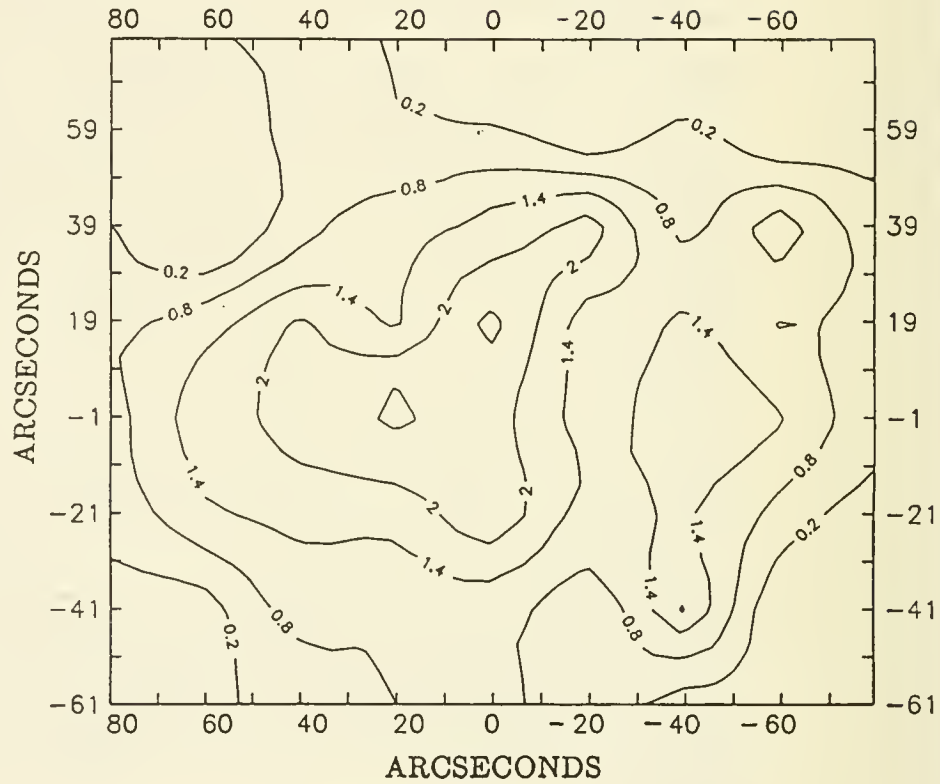


Figure 2 Surface plots showing the variation in the I_{CO}/I_{CS} ratio across M82.

I - THE COOL ISM

C - INTERSTELLAR DUST

High resolution sub-millimetre mapping of starburst galaxies: Comparison with CO emission

P.A. Smith, P.W.J.L. Brand & P.J. Puxley¹
Dept. of Astronomy, University of Edinburgh, U.K.

C.M. Mountain
Royal Observatory, Edinburgh, U.K.

N.Nakai
Nobeyama Radio Observatory, Japan.

Abstract

We present first results from a programme of submillimetre continuum mapping with the JCMT of starburst galaxies, and comparison of their dust and CO emission. This project was prompted by surprising results from our first target, the nearby starburst M82, which shows in the dust continuum a morphology quite unlike that of its CO emission, in contrast to what might be expected if both CO and dust are accurately tracing the molecular hydrogen. Possible explanations for this striking difference are discussed. In the light of these results, the programme has been extended to include sub-mm mapping of the nearby, vigorously star forming spirals, M83 and Maffei 2. The latter we have also observed extensively in CO, in order to study excitation conditions in its central regions.

Introduction

An important step towards an understanding of star formation in galaxies would be the ability to accurately determine the mass and distribution of available raw material (mostly H_2) in molecular clouds. The two commonest methods utilise tracers of the H_2 – either rotational transitions of the CO molecule, or sub-mm continuum emission from dust re-radiating the stellar UV. Recently, doubts have arisen over the reliability of these methods as applied to extragalactic molecular clouds, particularly in the extreme environments of ‘starburst’ galaxies, where vigorous star formation may significantly influence conditions in the clouds (*e.g.* Maloney & Black 1988). If the CO and sub-mm emission are both reliably tracing H_2 we may expect their morphologies to be similar. We tested this by sub-mm mapping of M82, a ‘classic’ starburst galaxy, and comparison with existing CO observations.² The results demonstrated an urgent need for more high resolution sub-mm maps, and detailed study of the excitation conditions of the CO, and the programme has been extended to include M83 and Maffei 2.

Results & Discussion

(i) M82

The central $40'' \times 40''$ of M82 was mapped at $450\mu m$ in the dust continuum, using the 15-m James Clerk Maxwell Telescope on Mauna Kea, Hawaii, with a beamsize at $450\mu m$ of $13''$.

Our $450\mu m$ map is presented in Fig. 1a. Fig. 1b, to the same scale, shows the ^{12}CO J=1–0 interferometer map of Lo *et al* (1987). There is a significant morphological difference between the two maps. The ^{12}CO map shows two distinct peaks, $25''$ apart, either side of the dynamical nucleus ($2.2\mu m$ peak). This dual peak structure has been interpreted as a 400 pc molecular ‘ring’ enclosing the starburst (Nakai *et al* 1987). In contrast, our sub-mm map shows only one peak, situated *inside* the ‘ring’, $\sim 7''$ SW of the nucleus. We believe that the difference is real, and not a result of poor resolution or pointing.

The integrated flux density from our map is 49 ± 21 Jy. Using the equations of Hildebrand (1983), and Gear (1988), with an adopted dust temperature of 47 K (Hughes *et al* 1989), we confirm that the sub-mm

¹Present Address : *University of Hawaii Institute for Astronomy, Honolulu, Hawaii, U.S.A.*

²This part of the work has been submitted to the *Monthly Notices of the Royal Astronomical Society*.

emission is optically thin, and derive a total gas mass in the mapped region of $(2.0 \pm 0.8) \times 10^8 M_{\odot}$.

The difference in morphology between the CO and sub-mm maps is surprising if, as is commonly assumed, the CO and dust continuum are both reliable tracers of the molecular hydrogen. Our $450 \mu\text{m}$ map shows similar morphology to $800 \mu\text{m}$ and $100 \mu\text{m}$ observations (Hughes *et al* 1989, Joy *et al* 1987). The $450 \mu\text{m}$ and $100 \mu\text{m}$ peaks are close to a region of vigorous star formation $10''$ SW of the nucleus. A possible explanation of the differing morphologies, then, is that two dust lobes are present, but are ‘swamped’, due to enhanced dust temperature, by emission from this region. However, from comparison of $100 \mu\text{m}$ and $40 \mu\text{m}$ profiles of M82 (Joy *et al* 1987) we infer no temperature variations greater than $\sim \pm 5$ K over the central regions, too small to ‘fill in’ the central depression seen in the ^{12}CO J=1–0 map. Therefore we believe it likely that the sub-mm is tracing predominantly column density variations.

If the dust continuum is accurately tracing the H_2 , then some process must be enhancing the CO emission in the lobes or depressing it in the interior. The integrated intensity of CO emission, I_{CO} , is critically sensitive to conditions in the molecular clouds. Large-beam ^{12}CO J=2–1, ^{12}CO J=1–0 and ^{13}CO J=1–0 observations suggest that the ^{12}CO emission in M82 may be at least partially optically thin, quite unlike Galactic clouds (Knapp *et al* 1980, Stark & Carlson 1982). The situation in M82 is far from simple, however. A recent ^{13}CO J=2–1 map (Fig. 1c) displays a large central peak, spatially coincident with our $450 \mu\text{m}$ peak and the SW star forming region, which dominates over the two peaks of the ‘ring’. As ^{13}CO is usually optically thin, the $^{12}\text{CO}/^{13}\text{CO}$ ratio traces changes in ^{12}CO optical depth. The morphology of the ^{13}CO map therefore suggests significant optical depth variations across M82 (Loiseau *et al* 1988).

I_{CO} is also sensitive to changes in CO excitation temperature. One factor which could have a marked effect on the gas temperature is the presence of intense UV fields. $\text{H}53\alpha$ measurements of M82 (Fig.2, Puxley *et al* 1989) imply a UV field 10^3 times that in the solar neighbourhood. In such an intense field, the CO may originate from warm (100 K), dense (10^3 cm^{-3}) photodissociation regions at the interface between HII regions and molecular clouds, where the gas temperature greatly exceeds the dust temperature (*e.g.* Tielens & Hollenbach 1985). The existence of such photodissociation zones in starburst galaxies is implied by the detection of $158 \mu\text{m}$ [CII] emission from M82 and other systems (Crawford *et al* 1985, Stacey *et al* 1989).

(ii) M83 and Maffei 2

It is apparent from the above results that CO and dust cannot both be accurately tracing H_2 across the central regions of M82. It cannot be assumed that M82 is unique in this, indeed, as it seems likely that the CO emission is strongly affected by the vigorous nature of the star formation in M82, it is clear that detailed knowledge of excitation conditions in other such ‘starburst’ galaxies are required for the correct interpretation of CO data and line ratios. We have therefore extended our study to two other IR- and CO-bright starbursts, M83 and Maffei 2. We have mapped M83 and Maffei 2 at $800 \mu\text{m}$ in the dust continuum with the JCMT (resolution $16''$). Additionally, we have obtained high resolution observations of Maffei 2 in the J=1–0 and J=2–1 transitions of both ^{12}CO and ^{13}CO , using the IRAM 30-m and Nobeyama 45-m telescopes (Smith *et al* 1989). Observations of two transitions in each of the two commonest isotopes of CO enables us to get a good handle on excitation and optical depth variations across the starburst regions, while the $800 \mu\text{m}$ mapping is invaluable as an independent tracer of the molecular gas and a test of the reliability of the CO morphology.

Acknowledgements

We thank the staff of the Joint Astronomy Centre in Hawaii, the Nobeyama Radio Observatory in Japan, and IRAM in Spain, for their valuable technical support, and the various selection committees for allocation of observing time on their facilities. PAS and PJP acknowledge SERC studentships.

References

Crawford *et al* 1985, *Ap.J.* 291, 755; Gear 1988, *Summer School on Millimetre and Submillimetre Astronomy, Stirling*, p307; Hildebrand 1983, *Q.J.R.A.S.*, 24, 267; Hughes *et al* 1989, in preparation; Joy *et al* 1987, *Ap.J.* 319, 314; Knapp *et al* 1980, *Ap.J.* 240, 60; Lo *et al* 1987, *Ap.J.* 312, 574; Loiseau *et al* 1988, *A.A.*, 200, L1; Maloney & Black 1988, *Ap.J.* 325, 38; Nakai *et al* 1987, *P.A.S.J.*, 39, 685; Puxley *et al* 1989, *Ap.J.* in press; Smith *et al* 1989, in preparation; Sofue *et al* 1987, in *Star Formation in Galaxies*, p179; Stacey *et al* 1989, *Ap.J.* submitted; Stark & Carlson 1982, *Ap.J.* 279, 122; Tielens & Hollenbach 1985, *Ap.J.* 291, 722.

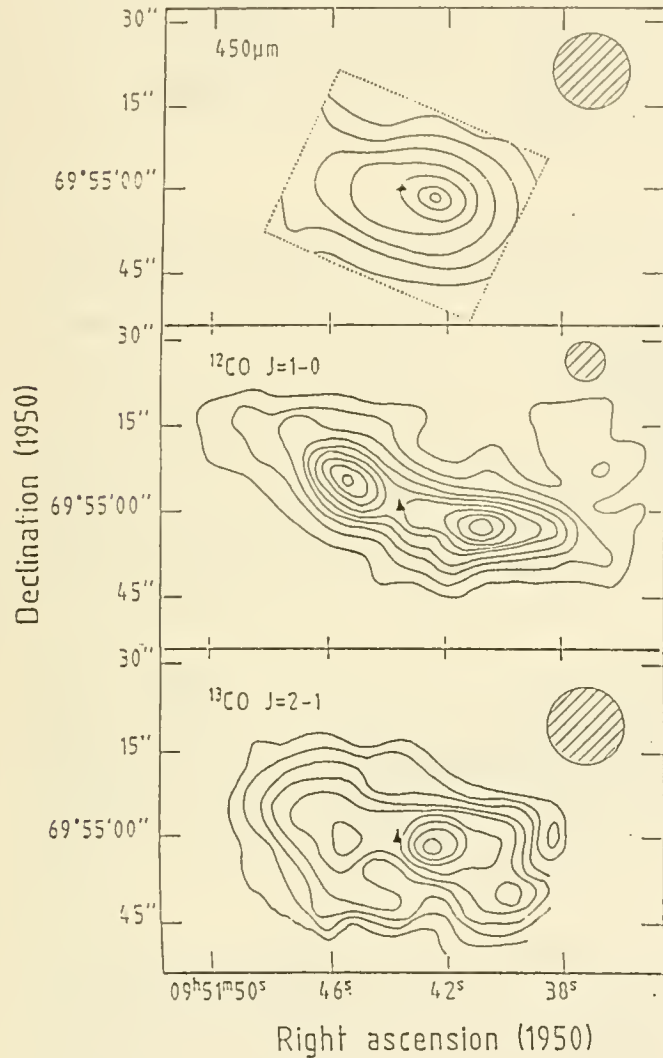


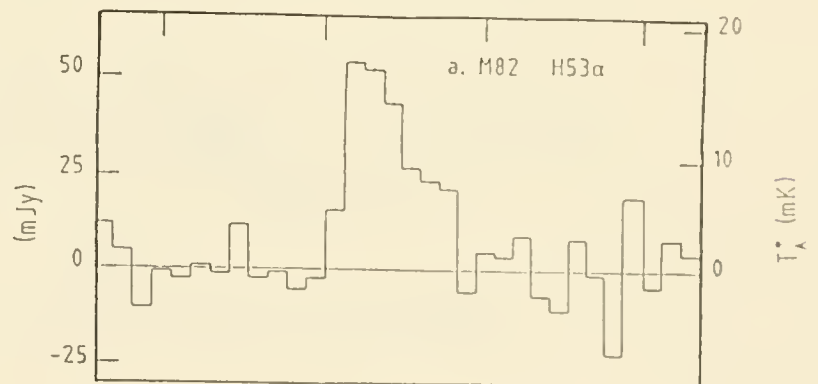
Figure 1

- a) 450 micron map of M82, 13'' resolution (Smith *et al* 1989, MNRAS, submitted).
- b) ^{12}CO J=1-0 interferometer map of M82, beamsize 7'', taken from Lo *et al* (1987).
- c) ^{13}CO J=2-1 map of M82, beamsize 13'', from Loiseau *et al* (1988).

The solid triangle marks the position of the 2.2 micron nucleus.

Figure 2

H53 α profile, measured with a 41'' beam. From Puxley *et al* (1989).



HIGH SPATIAL RESOLUTION 100 μm OBSERVATIONS OF THE M83 BAR

B. J. Smith, D. F. Lester, and P. M. Harvey (University of Texas)

We have been conducting a program of high spatial resolution far-infrared observations of galaxies using the Kuiper Airborne Observatory (KAO), to better understand the role of star formation, the general interstellar radiation field, and non-thermal activity in powering the prodigious far-infrared luminosities seen in spiral and interacting galaxies. Here, we present observations of the central region of the well-known barred spiral M83 (NGC 5236).

The observations were made April 22, 1988, using an 8-channel germanium bolometer array mounted at the straight Cassegrain focus of the 0.9m KAO telescope. This array was provided for our use by Frank Low of Infrared Laboratories. The 8 channels are spaced $12.8''$ apart at 100 μm , and 8 simultaneous $3.2'$ scans were made across the galaxy. The positions of the scans on M83 are shown in Figure 1, where they are superimposed on the CO $J = 1 - 0$ contours from Sofue *et al.* (1986). Eighteen back and forth sweeps were made across this region during the 35 minute M83 flight leg, with a total integration time on source of 18 minutes. The array was positioned such that channel 3, the most sensitive detector, was centered on the nucleus of M83. For calibration and to obtain the point spread function of the detectors, IRC+10216 was observed on the same flight. IRC+10216 has been shown to be a suitable point source at 100 μm (Lester, Harvey, and Joy 1985).

The resultant channel 3 scans for M83 and IRC +10216, after co-addition and smoothing, are shown in Figure 2. These data show that M83 is extended at 100 μm compared to a point source. A simple gaussian deconvolution of the M83 data with the point source profile from IRC+10216 gives a FWHM of $\sim 19''$ for M83. By comparison with IRC+10216, we obtain a flux for the unresolved component in M83 of ~ 110 Jy. This is $\sim 1/6$ the total flux for M83 (Rice *et al.* 1988) and $\sim 1/2$ the PSC flux.

The M83 and IRC+10216 profiles in the cross-scan direction (SE-NW) were also compared, and show that M83 is extended in this direction as well, with a width of $\sim 18''$. A comparison of the different channel profiles for M83 and IRC+10216 shows that there is an asymmetry in the M83 data, in that the maximum in the profiles shifts from southeast to northwest as channel number increases. This corresponds to the extension in the bar seen in the CO data in Figure 1. Thus the far-infrared emission in the central region of M83 tends to trace the CO bar.

The new 100 μm data is also compared with previous BVRIJK $H\alpha$ observations from the literature, to determine how well the far-infrared traces the stellar structure, the star formation as measured by $H\alpha$, and the optical colors.

REFERENCES

Lester, D. F., Harvey, P. M., and Joy, M. 1986, *Ap. J.*, 304, 623.

Rice, W., *et al.* 1988, *Ap. J. Supp.*, 68, 91.

Sofue, Y., Handa, T., Hayashi, M. and Nakai, N. 1986, in *Proceedings of the Star Formation in Galaxies Conference*, ed. C. J. L. Persson, (Pasadena: California Institute of Technology), p. 179.

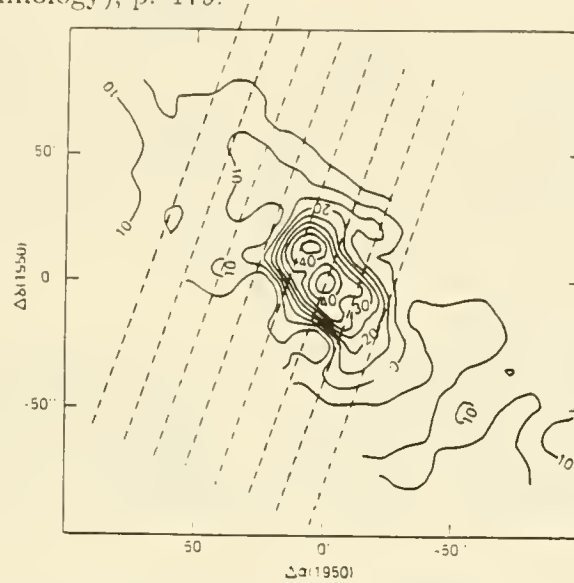


Figure 1. The positions of our scans across the central (bar) region of M83, superimposed on the CO $J = 1 - 0$ contours from Sofue *et al.* (1986). Detector #1 is the southernmost scan, while detector #8 is the most northern.

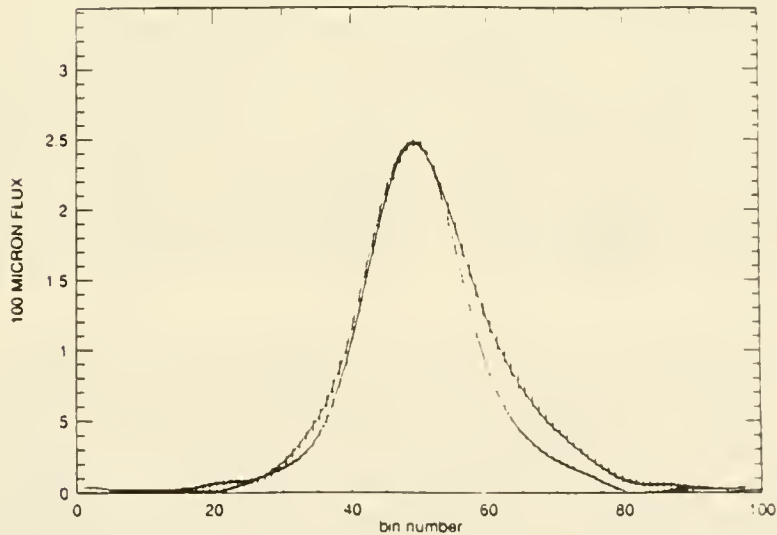


Figure 2. A comparison of the channel 3 final scans for M83 and IRC+10216.

FAR-INFRARED OBSERVATIONS OF CIRCINUS AND NGC 4945 GALAXIES

R.S. Bisht, S.K. Ghosh, K.V.K. Iyengar, T.N. Rengarajan
S.N. Tandon and R.P. Verma

Tata Institute of Fundamental Research, Bombay 400 005, India

I. INTRODUCTION

Circinus and NGC 4945 are two galaxies luminous in the infrared and are characterised by compact non thermal radio nuclei, deep silicate absorption features and unusually strong water vapour maser luminosities. Moorwood and Glass (1984) have observed these galaxies extensively in the 1-20 μm range. In the far-infrared, observations upto 100 μm are available from IRAS. In order to study the cool dust component of these galaxies, we have observed them at 150 μm using the TIFR 100 cm balloon-borne telescope. Here, we report our observations along with deconvolved maps at 50 and 100 μm obtained from the Chopped Photometric Channel (CPC) on board IRAS.

II. OBSERVATIONS AND RESULTS

Circinus galaxy was observed in a balloon flight in March 1985 using a single band (120-300 μm) photometer. NGC 4945 was observed in Nov. 1988 using a two band photometer which simultaneously viewed the same sky field in two bands of 45-75 μm and 110-210 μm . The field of view and chopper throw were 2'.4 and 3'.6. Intensity maps were obtained by deconvolving the observed signals using an MEM procedure resulting in a spatial resolution of 1'.5 (see Ghosh et al. 1988 for details).

No positive flux was observed from Circinus; the 3 σ upper limit to $F(150)$, the 150 μm flux density is 150 Jy. For NGC 4945, the deconvolved maps at effective wavelengths of 59 μm and 150 μm (for $T=35\text{K}$ and $\epsilon \propto \lambda^{-n}$, $n=1$) are shown in Fig. 1 a-b. The CPC data on these two galaxies were deconvolved using the point source profile of Ceres to get maps with a resolution of 1' at 50 and 100 μm and these are shown in Fig. 1 c-f. It is clearly seen that while Circinus exhibits only central emission, NGC 4945 is characterised by a nuclear source and disc emission. The IRAS COADD data also show that Circinus has very little extended emission (W. Rice, private communication) while NGC 4945 is extended at all IRAS wavebands. From the CPC maps we determine the flux densities in the central region as well as the total by integrating upto meaningful contour levels and subtracting a uniform background. The photometric growth curves for the central sources are shown in Fig. 2. The flux densities for the central source and the total are summarised in Table 1. The CPC data are means of 5 maps for Circinus and of 2 maps for NGC 4945. IRAS data have been color corrected.

For NGC 4945 both our and CPC data show that the central source is more extended at 100 μm than at 50 μm . Due to high pick up noise in the 59 μm channel, our signal to noise ratio is not high and we are likely to miss extended emission at 59 μm . However, the IRAS COADD data clearly indicate extended emission both at 50 and 100 μm . Brock et al (1988) found only a compact (20") nuclear source at 100 μm . Apparently they have missed the extended emission. Using the central 2' CPC data and taking the emissivity index $n=1$, the central source has $T=39\text{ K}$, while the extended emission (total-central) has $T=33\text{K}$. Using these values, we compute $F(150)$ to be 400 Jy

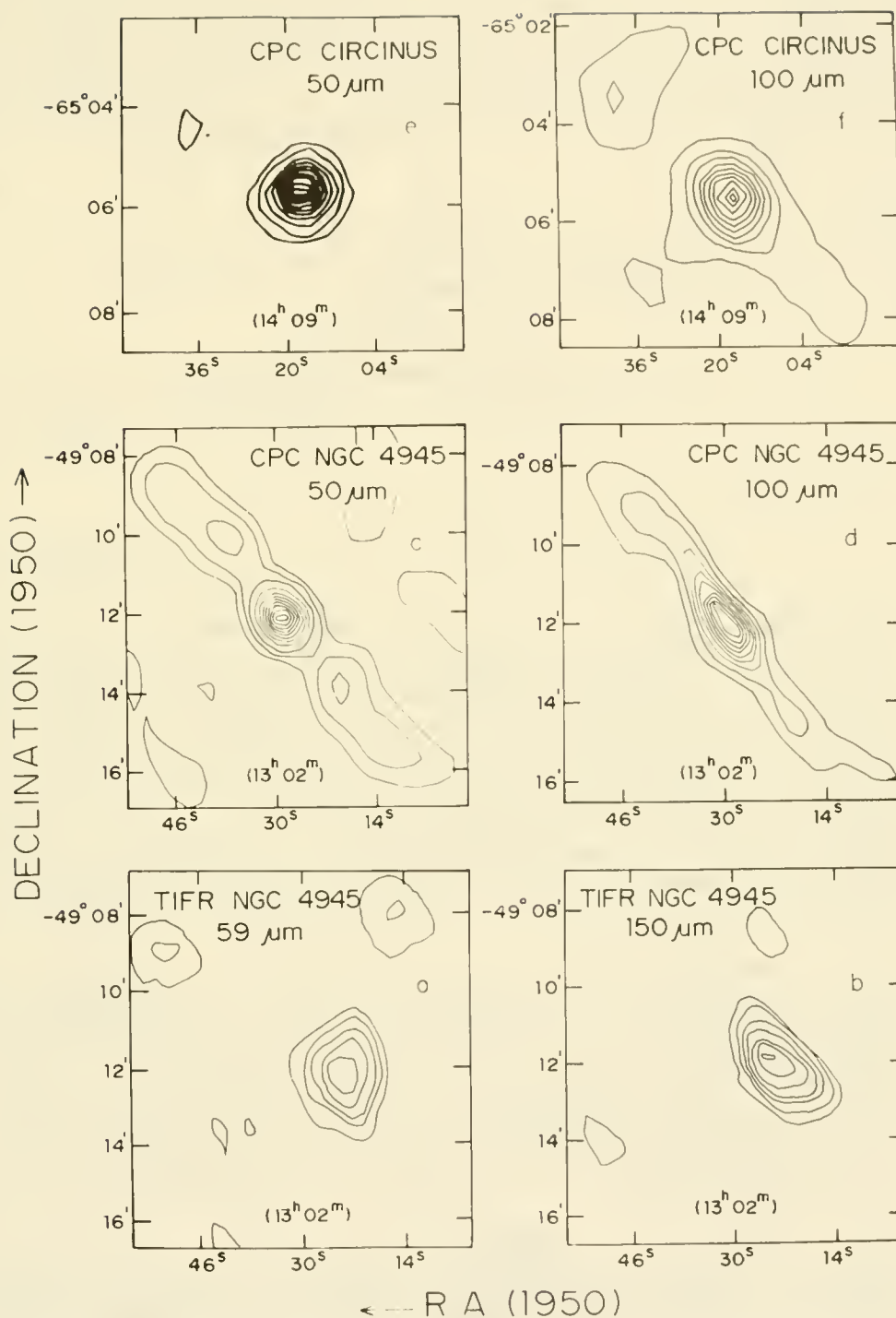


Fig.1. Deconvolved intensity maps of NGC 4945 and Circinus galaxies. The peak flux density (Jy) per pixel of $0.''3 \times 0.''3$ are a) 4.1; b) 83. The contour levels are 95,70,50,30,20 and 10 percent of peak; for b) 5 % also. c-f are CPC maps. Peak flux density (Jy) per pixel of $20'' \times 20''$ are c) 25.9; d) 32.2; e) 26.9; f) 21. Contour levels are 95,90,80,70,60,50,40,30,20,10 percent of peak. Also plotted for c) 5 and 2.5 percent and e) 5 percent.

and 550 Jy for the central and extended emissions and the total to be 950 Jy. Using a similar procedure, but using IRAS PSC and (total-PSC) fluxes we get total $F(150) = 1310$ Jy. These can be compared with our observed total $F(150) = 1605$ Jy. Thus, there seems to be more cool dust than that implied by IRAS data. For Circinus, the extended emission given by COADD data is $< 20\%$. While from IRAS 60 and 100 μm data one gets $T(60-100) = 43$ K ($n=1$) and 35 K ($n=2$), using the 100 μm flux density and our 150 μm limit we get $T(100-150)$ is >60 K ($n=1$) and >38 K ($n=2$).

REFERENCES

- Brock, D. et al, 1988, Ap.J., 329, 208.
 Ghosh, S.K. et al, 1988, Ap.J., 330, 928.
 Moorwood, A.F.M. and Glass, I.S., 1984, Astr. Ap., 135, 281.
 Rice, W. et al, 1988, Ap.J. Suppl., 332, 1093.

Table 1							
Galaxy	$\lambda(\mu\text{m})$	IRAS FD(Jy)		CPC FD(Jy)		TIFR FD(Jy)	
		PSC	Tot	2'Dia.	Tot	3'Dia.	Tot
Circinus	50	-	-	157	157	-	-
	60	246	255	-	-	-	-
	100	323	381	244	300	-	-
	150	-	-	-	-	<150	-
NGC 4945	50	-	-	200	330	-	-
	59	-	-	-	-	103	110
	60	379	639	-	-	-	-
	100	684	1465	550	1170	-	-
	150	-	-	-	-	1465	1605

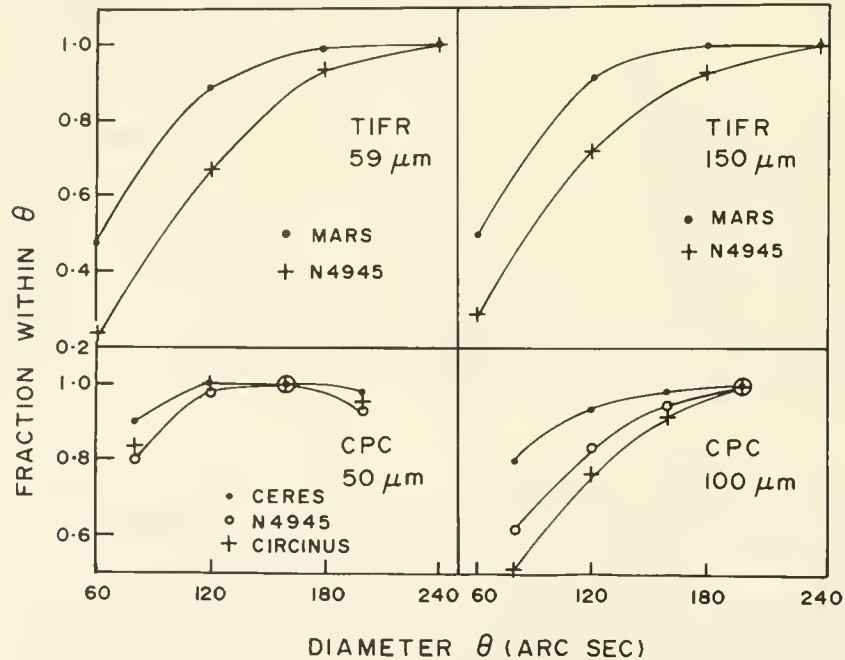


Fig. 2. Growth curves for the fraction of flux density within diameter θ . The decrease at large θ is due to background subtraction errors.

The 3 μ m Spectrum of NGC 4565 *

A. J. Adamson

School of Physics & Astronomy, Lancashire Polytechnic, Preston

AND

D. C. B. Whittet †

Physics Department, York University, Toronto; and
Canadian Institute for Theoretical Astrophysics, University of Toronto

1 Introduction

Three-micron spectroscopy of obscured galactic nuclei may provide important clues on the nature of the intervening dust material. Observations of the infrared sources in our own Galactic Centre (GC) have revealed the presence of absorption features at 3.0 and 3.4 μ m (e.g. Whittet 1988). The strengths of these features vary independently, and they cannot therefore be produced by the same grain component (McFadzean *et al.* 1989). The 3.0 μ m ‘ice’ feature indicates the chance occurrence of a molecular cloud in the line of sight, whereas the 3.4 μ m feature is attributed to carbonaceous dust in the diffuse ISM (e.g. Schutte & Greenberg 1988). Recent observations of highly-reddened field stars in the Galaxy (Tapia *et al.* 1989; Adamson *et al.* 1989) show that the 3.4 μ m feature is also present in other lines of sight, strengthening the conclusion that it is a characteristic signature of diffuse-cloud dust.

Infrared spectroscopy of normal spiral galaxies is potentially invaluable as an aid to understanding the significance of the dust features observed in the Milky Way, and as a means of comparing the interstellar media of separate systems. Since the composition of dust in the Galaxy is a function of galactocentric distance (Thronson *et al.* 1987), it is important to obtain spectra of relatively unobscured external galactic nuclei as a check that the 3.4 μ m absorption is not an intrinsic feature of the ISM at small galactocentric radii. It may be possible to measure directly the 3.0 and 3.4 μ m features in spirals which are seen edge-on.

NGC 4565 is a relatively nearby (~ 10 Mpc) field spiral of high inclination ($i \simeq 87^\circ.6$). Its Hubble type (Sb) matches that of the Galaxy, and it displays no obvious nuclear activity. Whilst a substantial number of optical and I-band images exist in the literature, they are

*Based on data obtained with the United Kingdom Infrared Telescope, Mauna Kea, Hawaii.

†On leave from: School of Physics & Astronomy, Lancashire Polytechnic.

2 THE SPECTRUM

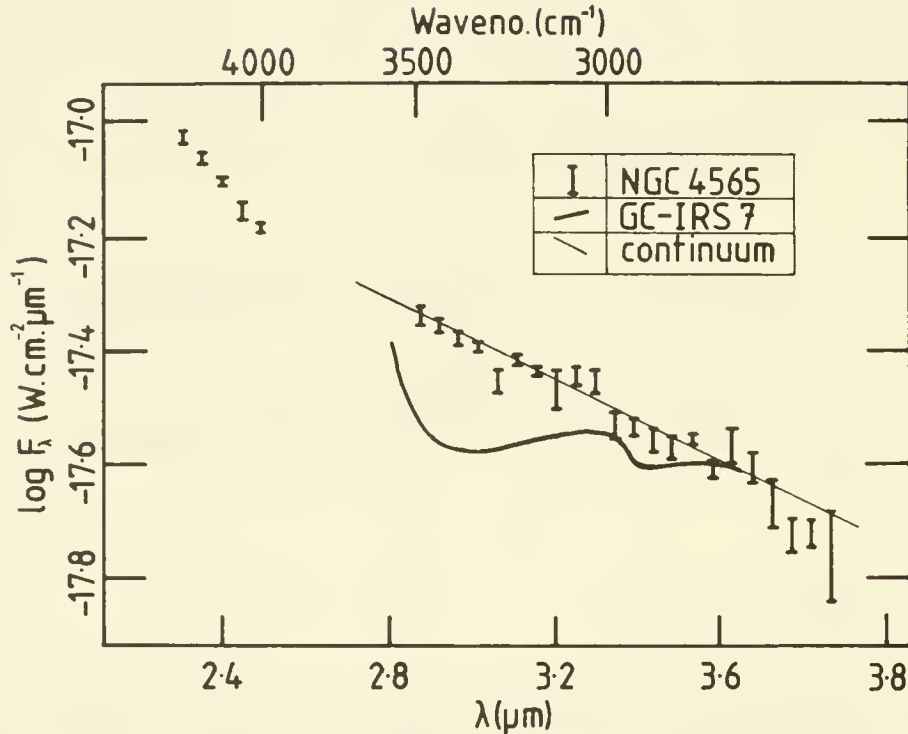


Figure 1: The 2.3–3.7 μm spectrum of NGC 4565. GC-IRS7 is also shown for comparison.

mainly deep exposures conveying little of use on the properties of the nucleus. Only two studies (Frankston & Schild 1976; Jensen & Thuan 1982) provide any real information on the obscuration of the nucleus, and to some extent they conflict as to whether it is situated behind the dust lane or not. However, following Schweizer (1978), a lower limit can be placed upon the extinction to the nucleus (excluding contributions from localized dark clouds) by adopting the observed dependence of extinction on galactic latitude in the solar-neighbourhood ($A_{pg} \simeq 0.25 \csc |b^{II}|$) within NGC 4565 itself. With the estimated inclination noted above, this gives $A_{pg} \geq 6^m$, or $A_V \geq 4^m.5$. Intrinsically weak interstellar features would be difficult to detect if this were the total extinction to the nucleus, but the proximity, brightness and high galactic latitude of NGC 4565 nevertheless make it the best available target for this type of observation outside our own Galaxy.

2 The Spectrum

The nucleus of NGC 4565 was observed with UKIRT in 1986 December, using a cooled CVF spectrometer with a 12" aperture and 40" E-W chop. The spectral range from 2.3 to 3.8 μm was covered at 1% spectral resolution and half-sampling. Figure 1 shows the resulting spectrum. For comparison, a schematic representation is included of the spectrum of GC-IRS7 between 3.0 and 3.6 μm , with an adjusted continuum slope.

3 CONCLUSIONS

Our spectrum of NGC 4565 is essentially featureless. The absence of the $3.0\ \mu\text{m}$ feature ($\tau_{3.0} < 0.05$) implies that the extinction to the nucleus does not arise to a significant degree in molecular clouds. We deduce $\tau_{3.0}/A_V < 0.01$, compared with ~ 0.022 for GC-IRS7. These results support the conclusion (McFadzean *et al.* 1989) that the $3.0\ \mu\text{m}$ absorption in the GC-IR sources is due to the presence of ice in a (probably single) foreground molecular cloud. The $3.4\ \mu\text{m}$ feature is also weak or absent in our spectrum of NGC 4565 ($\tau_{3.4} \leq 0.07$). Hence, $\tau_{3.4}/A_V \leq 0.016$, compared with ~ 0.008 towards GC-IRS7. The absence of the feature in NGC 4565 at the signal-to-noise level of the current observations is consistent with a probable moderate degree of extinction towards the nucleus.

3 Conclusions

Our observations of NGC 4565 provide a useful comparison for studies of dust in the Galaxy. Limits have been set on the strengths of the 3.0 and $3.4\ \mu\text{m}$ features in NGC 4565. The absence of $3.0\ \mu\text{m}$ absorption is significant, and supports the view that the feature at this wavelength in the Galactic Centre is due to water-ice absorption in a foreground molecular cloud. The non-detection of the $3.4\ \mu\text{m}$ absorption is less surprising and provides indirect support for the association between this feature and the diffuse interstellar medium. The current spectrum probably represents the best that can be achieved with a single-detector instrument within reasonable integration times. It will clearly be of interest in the future to obtain spectra of higher signal-to-noise, as a positive detection of the $3.4\ \mu\text{m}$ feature in an external galaxy, even at a low level, would be of considerable astrophysical significance.

REFERENCES

- Adamson, A.J., Whittet, D.C.B., & Duley, W.W., 1989. *Mon. Not. R. Astr. Soc.*, submitted.
- Frankston, M., & Schild, R., 1976. *Astr. J.*, **81**, 500.
- Jensen, E.B., & Thuan, T.X., 1982. *Ap. J. Suppl.*, **50**, 421.
- McFadzean, A.D., Whittet, D.C.B., Longmore, A.J., Bode, M.F., & Adamson, A.J., 1989. *Mon. Not. R. Astr. Soc.*, in press.
- Schutte, W.A., & Greenberg, J.M., 1988. *Dust in the Universe*, eds. M.E. Bailey & D.A. Williams, p. 403.
- Schweizer, F., 1978. *Ap. J.*, **220**, 98.
- Tapia, M., Persi, P., Roth, M. & Ferrari-Toniolo, M., 1989. *Astr. Ap.*, in press.
- Thronson, H.A., Latter, W.B., Black, J.H., Bally, J., & Hacking, P., 1987. *Ap. J.*, **322**, 770.
- Whittet, D.C.B., 1988. *Dust in the Universe*, eds. M.E. Bailey & D.A. Williams, p. 25.

THE GAS/DUST RATIO IN SPIRAL GALAXIES

N.A. DEVEREUX and J.S. YOUNG

Dept. of Physics and Astronomy

and the Five College Radio Astronomy Observatory

University of Massachusetts

Graduate Research Center

Amherst, MA 01003.

1. Introduction

Comparison of molecular gas masses from the FCRAO Extragalactic Survey with the dust masses that are required to produce the emission measured by IRAS lead to gas/dust ratios for spiral galaxies that are a factor of five higher than that measured for the Galaxy (Young et al. 1986; Stark et al. 1986). The inclusion of the atomic gas, which can contribute as much mass as the molecular gas, will only accentuate the discrepancy. One plausible explanation for the high gas/dust ratio is that the bulk of the dust mass is not contributing to the emission measured by IRAS and must therefore be radiating at $\lambda > 100\mu\text{m}$. *The high gas/dust ratio would then suggest significant quantities of cold, $< 30\text{K}$, dust.* On the other hand, recent observations (Telesco and Harper 1980; Stark et al. 1989; Eales, Wynn-Williams and Duncan 1989) have shown that the far infrared continuum energy distributions of spiral galaxies can be represented by a single temperature component over the wavelength range $60\mu\text{m}$ to $\sim 450\mu\text{m}$ with dust temperatures that typically range from 30K to 50K. *The far infrared continuum emission therefore provides no direct evidence for cold dust in spiral galaxies.* The goal of the present contribution is to reconcile these two apparently conflicting results concerning cold dust in galaxies.

2. Sample and Analysis

Coadded IRAS data are used to calculate dust masses (Hildebrand 1983) for 63 spiral galaxies in which the distributions of atomic and molecular gas have been measured. The dust masses are compared with the atomic and molecular gas masses in order to constrain the *amount* of cold dust in galaxies. Published far infrared photometry is used to constrain the *temperature* of the cold dust. The reader is referred to Devereux and Young (1989) for a full discussion of the sample and analysis.

3. Results and Discussion

The dust masses are highly correlated with the sum of the molecular and atomic gas mass and consequently the gas/dust ratio is well determined (Figure 1). The globally averaged gas/dust ratio for spiral galaxies is ~ 1400 ; over a factor of ten higher than that measured within the Galaxy. The high gas/dust ratio leads us to conclude that $\sim 90\%$ of the dust mass is radiating at $\lambda > 100\mu\text{m}$ and is therefore colder than 30K.

The shape of the far infrared continuum emission of galaxies indicates dust temperatures in the range 30K to 50K (Telesco and Harper 1980; Stark et al 1989; Eales et al 1989) and therefore provides no direct evidence for cold, $< 30\text{K}$, dust. It is important to note, however, that because of the strong temperature dependence of thermal emission the far infrared continuum observations do not necessarily rule out large quantities of cold dust. By way of illustration, we have reanalyzed the $160\mu\text{m}$ and $360\mu\text{m}$ data of Stark et al. (1989) in order to constrain the temperature of the cold dust if 90% of it is, in fact, radiating at $\lambda > 100\mu\text{m}$ as indicated by the gas/dust ratio calculation.

The *global* 160 μ m and 360 μ m fluxes of Stark et al., derived from maps obtained using the KAO, are presented in Figure 2 along with the *global* IRAS fluxes for the four Virgo spirals that were observed. Also shown is the sum of the emission expected if 90% of the dust mass is radiating as a "cold" component and the remainder is at a temperature derived from the IRAS $S_{100\mu\text{m}}/S_{60\mu\text{m}}$ flux ratio. Temperatures of 15K and 10K were adopted for the temperature of the cold component. The figure shows that *the IRAS data together with the 160 μ m and 360 μ m observations of Stark et al. are not inconsistent with the emission expected if 90% of the dust mass were radiating at a temperature of 10K or 15K.*

Thus it is possible to reconcile *both* the high gas/dust ratio and the shape of the far infrared continuum emission of spiral galaxies with the view that the bulk of the interstellar medium radiates at a temperature of 10K to 15K. Additionally, such low dust temperatures are expected for the dust in the interstellar medium of galaxies since model calculations indicate a temperature of 10K - 20K for HI associated dust that is exposed to the heating effect of the interstellar radiation field (Drain and Lee 1984) and even lower dust temperatures are expected within molecular clouds.

4. Conclusion

The high gas/dust ratio determined for spiral galaxies leads us to conclude that $\sim 90\%$ of the dust mass is radiating at $\lambda > 100\mu\text{m}$. The dust temperature must therefore be colder than 30K. Both the high gas/dust ratio and the shape of the far infrared continuum emission of spiral galaxies can be reconciled with the view that the bulk of the interstellar medium radiates at a temperature of 10K to 15K.

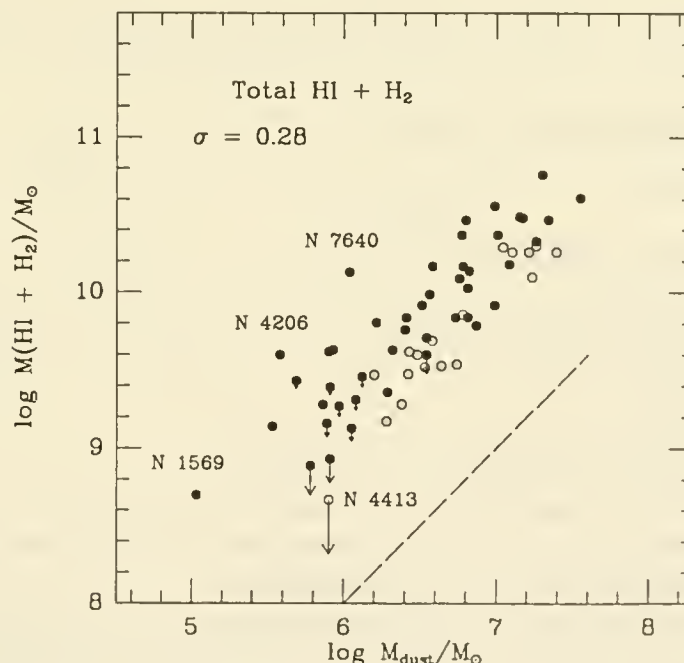


Figure 1. The correlation between dust mass and the sum of the molecular and atomic gas mass. Open circles indicate that $\geq 50\%$ of the gas mass is molecular, filled circles indicate $> 50\%$ of the gas mass is atomic. The arrows indicate upper limits to the molecular gas mass. The length of the arrow corresponds to the total displacement if the molecular gas mass were zero. The dashed line corresponds to gas/dust = 100; a value that is typical for the Galaxy.

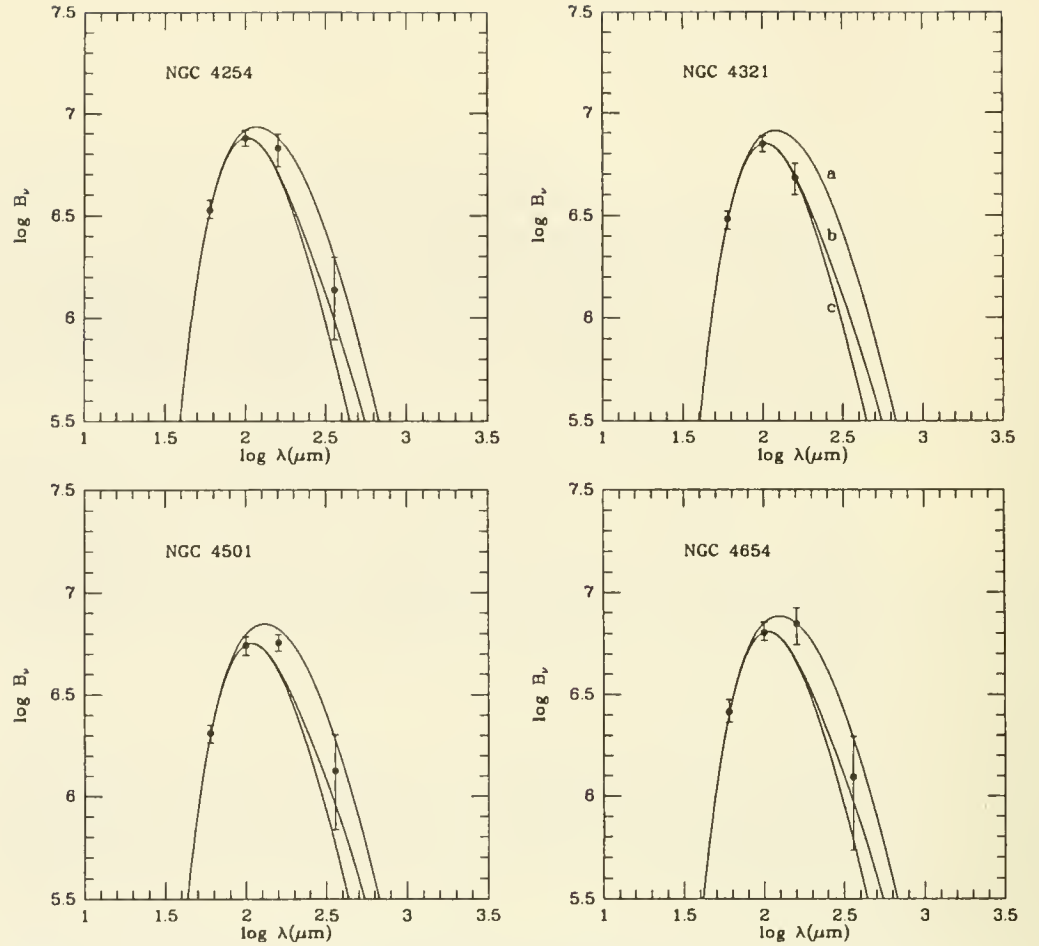


Figure 2. Comparison of far infrared photometry with models for the far infrared emission. A λ^{-2} emissivity law has been adopted for the model calculations.

model a. 90% of the dust mass at 15K, 10% of dust mass is warm *

model b. 90% of the dust mass at 10K, 10% of dust mass is warm *

model c. 100% of dust mass is warm *

* The temperature of the warm dust component is derived from the IRAS $S_{100\mu\text{m}}/S_{60\mu\text{m}}$ flux ratio and corresponds typically to $\sim 30\text{K}$.

5. References

- Devereux, N.A., and Young, J.S., 1989, *ApJ Submitted*
- Drain, B.T., and Lee, H.M., 1984, *ApJ* **285**, 89.
- Eales, S.A., Wynn-Williams, C.G., and Duncan, W.D., 1989, *ApJ* **339**, 859.
- Hildebrand, R.H., 1983, *Q.J.R. Astr. Soc.* **24**, 267.
- Stark, A.A., Knapp, G.R., Bally, J., Wilson, R.W., Penzias, A.A., and Rowe, H.E., 1986, *ApJ* **310**, 660
- Stark, A.A., Davidson, J.A., Harper, D.A., Pernic, R., Loewenstein, R., Platt, S., Engargiola, G., and Casey, S., 1989, *ApJ* **337**, 650.
- Telesco, C.M., and Harper, D.A., 1980, *ApJ* **235**, 392.
- Young, J.S., Schloerb, F.P., Kenney, J.D., and Lord, S.D., 1986, *ApJ* **304**, 443.
- Young, J.S., Xie, S., Kenney, J.D., and Rice, W.L., 1989, *ApJ Supp.* in press.

Spatial Analysis of IRAS Observations of Nearby Spirals

Roger Ball
Institute of Geophysics and Planetary Physics
Lawrence Livermore National Laboratory
and
Space Sciences Laboratory
University of California

and
K. Y. Lo
Department of Astronomy
University of Illinois

The unbiased survey of the infrared sky carried out by the IRAS satellite has greatly accelerated advances in understanding the dust component of our own and external galaxies. However, most extragalactic studies to date have been based on the IRAS Point Source Catalog (PSC), which has two serious limitations. First, in sources where a significant fraction of the flux is extended, significant errors may result from using PSC fluxes in comparative studies, and these errors could be systematic if the tendency to be non-pointlike depends on physical properties of the galaxy. Additionally, use of PSC fluxes rules out any direct investigation of the spatial distribution of the IRAS emission from disks in external galaxies. Since work on the Galactic IRAS results has shown that very different physical processes (star formation, quiescent cold dust emission, and AGN processes) can make varying contributions to the observed flux, it is important to look at a wide sample of galaxies with some spatial resolution to study the relative dominance of these processes under a variety of conditions. We report on work we are doing to carry out this program for many nearby spirals, using an analysis package that we have developed for this purpose.

We have used detailed models of the point spread functions of the individual IRAS focal plane detectors to investigate the spatial distribution of the fluxes measured for a sample of nearby spiral galaxies. These objects are selected to have large enough angular diameters to be resolvable, in principle, by IRAS at $60\text{ }\mu\text{m}$. The detector maps have kindly been provided by M. Moshir of IPAC. Our method works with single survey scans in the ADDSCAN format also provided by IPAC. The several such scans in each band over an object of interest give several independent measurements of the convolved galaxy and instrumental profiles, so that the results can be checked for consistency. As a first step in our analysis, we use a nonlinear least squares technique to make a best fit of the detector profile to the observed scan, in order to overcome the errors in the nominal pointing of the satellite and hence center our profile analysis accurately on the galaxy nucleus, empirically defined as the most pointlike object near the nominal galaxy position. We then determine the fluxes of the galaxy's pointlike and extended components. Here we will confine our attention to the question of what fraction of the $60\text{ }\mu\text{m}$ flux is contained in a pointlike nucleus, as seen by IRAS (i.e., FWHM about 1.5 arc minutes).

We have carried out this analysis for a sample of 121 nearby spirals. The fraction of the flux contained in a point source varies from 0 to 1 across the sample, all of which are well resolved at their nominal optical diameters. There is no evidence that the galaxies of smaller angular size are less likely to be resolved by IRAS at this level. Our program gives results which are quite repeatable from scan to scan; the fraction f (point source flux over total flux) at $60\text{ }\mu\text{m}$ has typical errors of 0.03 when different scans are combined.

Approximately two-thirds of the sample have more flux in the extended than in the nuclear component. There is a tendency for earlier-type spirals to be less centrally concentrated, but this effect is slight and the degree of variation is large for all types. Barred spirals are also found across the spectrum of f , but are much more likely to have little or no nuclear emission. More detail on individual unusual objects will be presented in the poster.

Contribution of Cool Dust to the FIR Brightness Distribution of NGC 6946 Sc(s)II

G. Engargiola and D.A. Harper
University of Chicago, Yerkes Observatory
Williams Bay, WI

I. Introduction

A few galaxies have been observed at submillimeter wavelengths (Stark et al., 1988; Eales, Wynn-Williams, and Duncan, 1988). These observations do not support the hypothesis that there exist substantial amounts of cool dust generating submillimeter radiation in excess of predictions from modified blackbody curves of the form $(1/\lambda)^{1.5} B_{\nu}(\nu, T)$ fit to total 100 and 160 μm fluxes. However, we find relatively cold dust ($\sim 17\text{-}23^{\circ}\text{K}$) at several interarm locations in the central $5' \times 5'$ region of NGC 6946 Sc(s)II. Since molecular gas is the predominate constituent of the ISM in this region, such low dust temperatures are indicative of quiescent molecular clouds and low star formation rates. Based on the contribution of cool grains to the 160 μm surface brightness distribution, regions of low star formation activity can be identified. A $1/\lambda^{1.5}$ emissivity law is assumed for this analysis.

II. Far Infrared Emission from NGC 6946

The central $5' \times 5'$ region of NGC 6946 has been mapped at 100 and 160 μm with the 32 channel U.Chicago FIR Camera on the KAO. The beamsize was $45''$. The far infrared brightness distributions are shown in Fig. 1. The peak brightnesses of the 100 and 160 μm maps are 65 Jy/beam and 59 Jy/beam, respectively. The contour spacings are 2 Jy/beam. A nuclear excess and a bisymmetric spiral pattern superimposed on an exponential disk are apparent at both wavelengths. The hydrogen alpha (Bonnerel and Boulsteix), radio continuum (van der Kruit, Allen, and Rots), integrated CO $J=1 \rightarrow 0$ (Young and Scoville; Tacconi and Young), and far-infrared distributions of NGC 6946 (Engargiola, Harper, and Jaffe) have average radial profiles which peak strongly at $r=0$. The 100 μm flux follows the resolved hydrogen alpha distribution more closely than the 160 μm flux, which more faithfully traces the I-band intensity distribution (Tacconi and Young). About 75% of the far-infrared luminosity of NGC 6946 originates from the central $5'$ of the disk.

III. Two Temperature Decomposition of 160 μm Flux

The far infrared brightness distribution can be represented at each position by a sum of two modified blackbody components, $f_{\nu}[T(1), T(2)] = a(1)\nu^{1.5}B_{\nu}[T(1)] + a(2)\nu^{1.5}B_{\nu}[T(2)]$ [Jys/beam], where $T(1,2) = 20, 35^{\circ}\text{K}$, $\tau_{\nu}(1,2) = a(1,2)\nu^{1.5}$. One solves for two optical depths, the 'a' coefficients, using both the 100 and 160 μm maps. The pair of temperatures were empirically chosen to maximize the contribution of the lower temperature component, subject to the constraint that the components $a(i)\nu^{1.5}B_{\nu}[T(i)]$ be greater than zero over the entire map and that the ratio of the integrated fluxes $F_{\nu}(350\mu\text{m})/F_{\nu}(160\mu\text{m}) \approx 5.0 \pm 1.0$, so as to be consistent with integrated far infrared and submillimeter measurements of other spiral galaxies e.g. NGC 4254, NGC 4501, NGC 4654 (Stark

et al.), and NGC 4736 (Jaffe, Engargiola, and Harper). Increasing the difference $\Delta T = T(2) - T(1)$ increases the cold component but results in a warm component which is less than zero over portions of the map if $\Delta T > 16^\circ\text{K}$. The decomposition will filter the brightness distribution into parts where the effects of warm and cool dust are enhanced. The results of this decomposition are shown in Fig 2. The warm and cold dust component contours are superimposed on a grey scale representation of the hydrogen alpha - smoothed to $45''$ resolution - and are labelled Fig. 2a. and 2b., respectively; the contour spacing is 2Jy/beam.

The average surface brightness of the cold dust $160\mu\text{m}$ component is 1.5 Jys/('')^2 . The ratio of this to the average total $160\mu\text{m}$ surface brightness is $[f_v(160)]_{20^\circ\text{K}}/f_v(160) = 0.14$. The total flux from the 20°K dust component from the central $5'.0 \times 5'.0$ region of the galaxy is 39 Jys. This component peaks at 14 Jys/('')^2 about $0.5'$ east of the galaxy center; other peaks of 6 Jys/('')^2 occur in interarm regions to the E and NW at $r > 6 \text{ kpc}$. Extrapolating the 20 and 35°K flux components with the model from 160 to $350\mu\text{m}$ yields an average surface brightness of 2.1 Jys/('')^2 , hence the ratio of the total 160 to $350\mu\text{m}$ flux is 5.3 and the decomposition yields a spectrum consistent with blue Virgo Cluster spirals. The total $160\mu\text{m}$ flux from cool dust is estimated to be 45 Jys; extrapolating to $100\mu\text{m}$ gives 25 Jys or 7% of the total $100\mu\text{m}$ flux of 344 Jys measured by IRAS (Rice et al). Hence, this emission model predicts a small contribution by 20°K grains to the total $100\mu\text{m}$ luminosity $f_v(100)$.

a) Spatial Relation of Cool Dust Emission to Regions of Massive Star Formation

The number surface density of HII regions - with luminosities $> \sim 10^{38} \text{ ergs/s}$ - for the central $5'.0 \times 5'.0$ of the galaxy is $8/('')^2$. This surface density has a range $3\text{-}10/('')^2$ for the inner disk and interarm regions and $10\text{-}20/('')^2$ for the spiral arms; the highest surface density of HII regions, $40/('')^2$, occurs at the center of the galaxy. The strongest peaks in the cold dust distribution occur where the number surface density is $6\text{-}7/('')^2$, slightly below average. Also, the HII regions are on average 3-10 more luminous in hydrogen alpha for positions along the spiral arms than for positions where the 20°K dust component is detected at $160\mu\text{m}$. It can be seen that (1) the 20°K dust component contributes over half the infrared luminosity from certain regions of NGC 6946 and (2) the relative size of the cold dust contribution is related to the amount of ionizing radiation, to the extent that hydrogen alpha is a measure of the ionizing UV continuum i.e. where there are fewer massive stars powering the ISM, there is more 20°K dust, not too surprising.

The average radial profiles of the 20°K and 35°K $160\mu\text{m}$ components appear in Fig. 3a. The 35°K component drops steeply with radius from the center of the galaxy but levels off beyond radius $1.5'$, where increasing numbers of HII regions resolved in hydrogen alpha light are found. The 20°K component peaks between the galaxy center and radius $1.0'$, dips to a minimum at radius $2.2'$ and begins to increase past $2.5'$. Cool dust appears to contribute a higher fraction of the total $160\mu\text{m}$ surface brightness at large radii. The radial profiles are uncorrected for the inclination of the galaxy.

b) Expected Cool Dust Contribution to $350\mu\text{m}$ Flux

Fig. 3b is the average radial submillimeter brightness profile of NGC 6946 obtained by extrapolating the 20°K and 35°K emission components to

350 μ m. The submillimeter profile has been normalized to the predicted peak value of 11 Jys/beam. The intervals plotted along with the submillimeter profile represent the span over position angle of the fractional contribution by the 20°K component to the 350 μ m flux. About 40% of the total 350 μ m flux is predicted to arise from cold dust. Also clear from Fig. 3b is that cold dust may produce as much as 60% of the submillimeter flux at galactocentric distances greater than 9 kpc.

IV. Recent Observations at 200 μ m

During a KAO flight series this past May, Engargiola and Harper observed NGC 6946 at 200 μ m. The data have yet to be calibrated. A preliminary contour map, where the contour levels are linear in raw signal, is shown in Fig. 4. Similarity is clear between the 200 μ m brightness distribution and the 20°K 160 μ m emission component, possibly indicating a higher relative fraction of the far infrared/submillimeter emission from cool grains in quiescent molecular clouds.

V. Conclusions

We have assumed a two temperature grain model in an effort to decompose the far infrared surface brightness distribution of NGC 6946 into contributions from cool, quiescent and active, star forming regions. This model has some validity; although an oversimplification of the dust energetics, we find from it that, where giant HII regions are sparse, a significant fraction of the 160 μ m emission is emitted by a cool grain component which IRAS could barely detect.

References

- Bonnarel, F., Boulesteix, J., and Marcelin, M. 1986, *Astron. Astrophys.*, **66**, 149
 Eales, Wynn-Williams, and Duncan, 1988, *Ap. J.*, in press
 Engargiola, G., Harper, D.A., and Jaffe, D.T. 1989, in preparation.
 van der Kruit, P.C., Allen, R.J., and Rots, A.H. 1977, *Astron. Astrophys.*, **55**, 421
 Rice, W., Lonsdale, C.J., Soifer, B.T., Neugebauer, G., Kopan, E.L., Lloyd, L.A., de Jong, T., and Habing, H.J. 1988, *Ap. J. (supplement)*, **68**, 91
 Stark, A.A., Casey, S., Davidson, J.A., Engargiola, G., Harper, D.A., Loewenstein, R.F., Pernic, R., and Platt, S. 1989, *Ap. J. (letters)*, **337**, 650
 Tacconi, L., and Young, J.S. 1989, *Ap. J. (Supplement)*, in press
 Young, J.S., and Scoville, N. 1982, *Ap. J.*, **258**, 467

NGC 6946 Sc(s)II λ 100 μ m

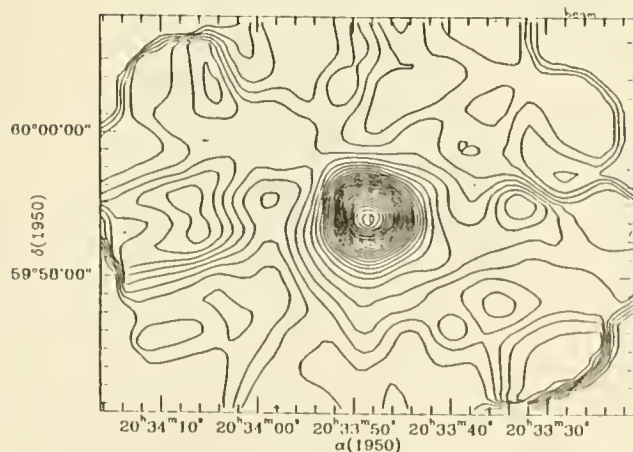


Fig. 1a

NGC 6946 Sc(s)II λ 160 μ m

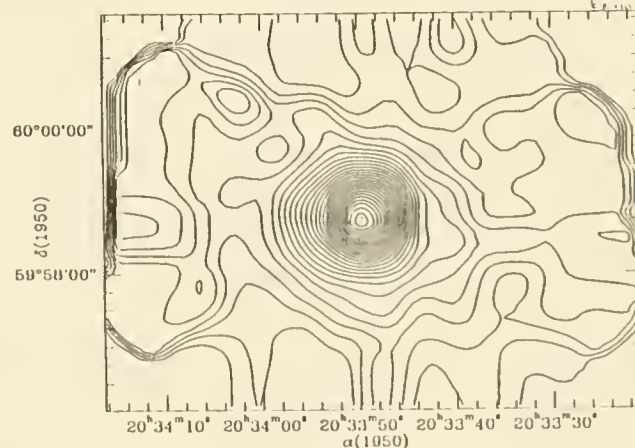


Fig. 1b

Far Infrared Luminosity Functions of Normal Galaxies

Takashi Isobe and Eric D. Feigelson
The Pennsylvania State University
Department of Astronomy
525 Davey Lab., University Park, PA 16802

Abstract : We construct a volume limited sample of 443 optically selected nearby galaxies from the Zwicky catalog to study far infrared luminosity functions. Schechter function fits and integrated luminosity densities are calculated. Comparing the resulting infrared spectrum with the infrared spectrum for interstellar matter in the solar neighborhood, we find most of the infrared emission is due to dust heated by the interstellar radiation field, except at 60 μ m emission where star forming regions contribute significantly.

We constructed a volume limited sample ($v < 1400 \text{ km s}^{-1}$) of 443 nearby galaxies from the Zwicky catalog (Huchra *et al.* 1983) to study far infrared luminosity functions of optically selected galaxies. The infrared data are obtained from the *IRAS Point Source Catalog II* and ADDSCAN pocessing. Detailed descriptions of the selection and processing of the sample are presented in Isobe and Feigelson (1989). Since many of the galaxies are not detected in the infrared, the non-parametric survival analysis Kaplan-Meier estimator (Feigelson and Nelson 1985; Isobe, Feigelson, and Nelson 1986) is used to calculate normalized integrated luminosity functions. The luminosity functions based on the volume limited sample show good agreement with those based on magnitude limited samples. Since survival analysis can be directly applied to the volume limited sample, the luminosity function based on the volume limited sample is the better choice for the samples selected in other wavebands.

The luminosity functions at 12, 25, 60, and 100 μ m Kaplan-Meier estimator are shown in Fig. 1. $H_0 = 75 \text{ km s}^{-1} \text{ Mpc}^{-1}$ is assumed throughout. Schechter functions (Schechter 1976) are fitted to these luminosity functions to find luminosity density per Mpc^3 . Since many galaxies are not detected, a simple sum of detected galaxies does not give total luminosities. Results are listed in Table 1. The fourth to sixth columns list the Schechter function parameters for

$$\phi d(L/L^*) = \phi^* (L/L^*)^{\alpha+1} \exp(-L/L^*) d(L/L^*), \quad (1)$$

Table 1: Mean Luminosities and Parameters of Schechter Functions of Four IRAS Bands

Band	Upper Limits	Mean ($\text{erg s}^{-1} \text{ Hz}^{-1}$)	α	$\log L^*$	ϕ^*	Total Luminosity Density ($\text{erg s}^{-1} \text{ Hz}^{-1} \text{ Mpc}^{-3}$)
1	323	28.14 ± 0.12	-1.67	29.0	1.7×10^{-1}	3.3×10^{27}
2	303	28.37 ± 0.09	-1.69	29.2	1.8×10^{-1}	5.1×10^{27}
3	121	29.46 ± 0.04	-1.59	30.1	1.5×10^{-1}	4.7×10^{28}
4	118	29.88 ± 0.04	-1.41	30.4	1.2×10^{-1}	1.3×10^{29}

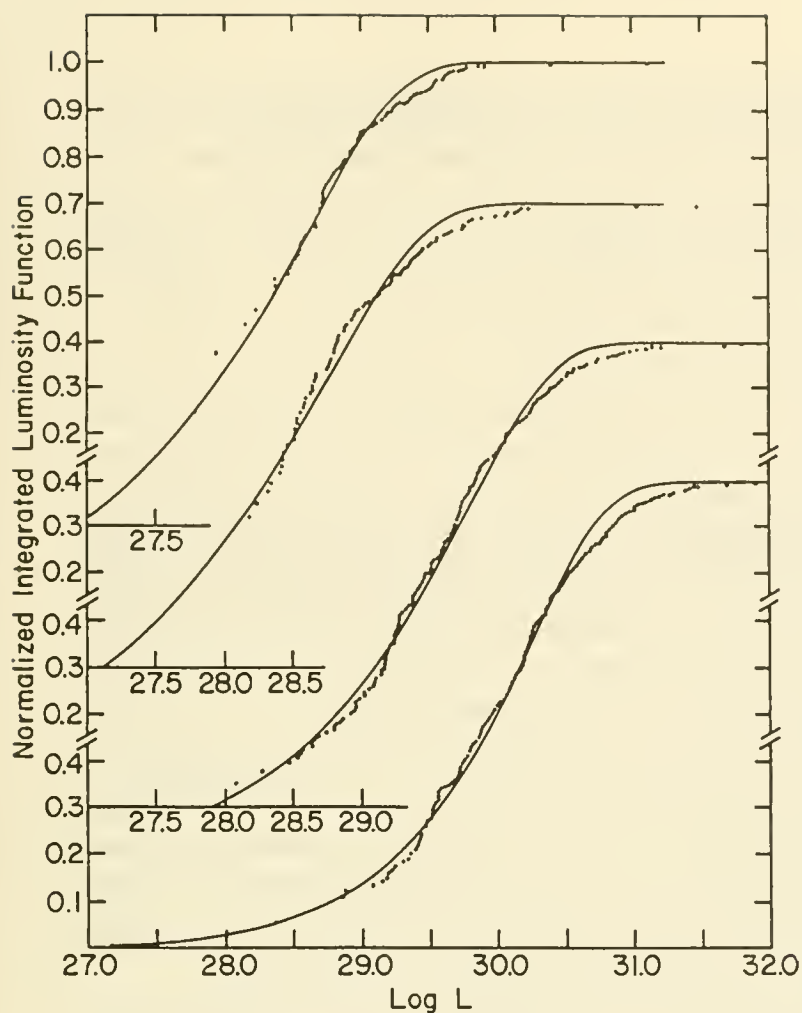
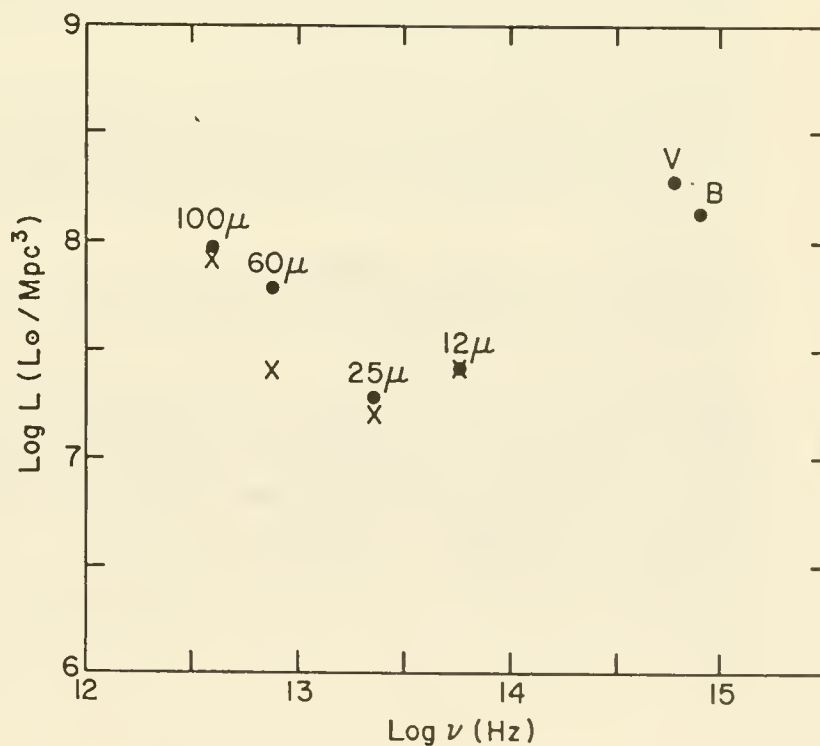


Figure 1 :
The luminosity functions for 12, 25, 60, and 100 μm from top to bottom. The fitted lines are Schechter functions.

Figure 2 :
The luminosity densities per Mpc^3 in solar luminosity units. The filled circles are obtained from Table 1, Felten (1977; V band) and Kirshner *et al.* (1983; B band), respectively. The crosses are obtained from Boulanger and Péroult (1988) normalized at 12 μm .



where ϕ^* is in number of galaxies per Mpc^3 , L^* is in $\text{erg s}^{-1} \text{Hz}^{-1}$. The last column lists the total luminosity density of optical galaxies in the local Universe of the band in $\text{erg s}^{-1} \text{Hz}^{-1} \text{Mpc}^{-3}$. Note, bands 1 and 2 have very low detection rates ($\sim 30\%$) and if survival analysis is not used, computations of luminosity functions are impossible. We find the mean L^* and integrated luminosities increase a factor of ~ 40 between 12 and $100\mu\text{m}$ monotonically with wavelength. The slope α is always steeper than seen at optical wavelengths where $\alpha \approx -1.25$.

The luminosity densities per Mpc^{-3} in Table 1 can be seen as a spectrum of a 'typical' galaxy. Boulanger and Péroult (1988; hereafter BP) present the infrared emission originating in the solar neighborhood based on IRAS data, and present the infrared spectrum of emission normalized per hydrogen atom. If we assume that a typical galaxy has a similar environment, their values can be used as a reference spectrum which represents the emission of dust heated by the interstellar radiation field. Since $12\mu\text{m}$ emission is almost certainly due to very small grains (e.g. polycyclic aromatic hydrocarbon; Léger and Puget 1984), we normalize the $12\mu\text{m}$ point of BP to that of our typical galaxy in Fig. 2 ($L_{12\mu\text{m}} = 2.6 \times 10^7 L_{\odot}$). They agree very well with the solar neighborhood spectrum, except at $60\mu\text{m}$. Our $60\mu\text{m}$ emission is 2.5 times higher than of BP.

Since some galaxies are not detected both at $L_{100\mu\text{m}}$ and $L_{60\mu\text{m}}$, we cannot compute the distribution of $L_{100\mu\text{m}}/L_{60\mu\text{m}}$ color correctly. Nonetheless we attempt to compute the luminosity density of galaxies with $L_{100\mu\text{m}}/L_{60\mu\text{m}} < 2.5$ which are supposed to be dominated by star formation. The contribution from these galaxies in our sample is $2.1 \times 10^7 L_{\odot}$ at $60\mu\text{m}$, and that from the galaxies not dominated by star formation is $2.6 \times 10^7 L_{\odot}$ which is exactly BP's predicted value. These results support a model suggested previously (e.g. Bothun, Lonsdale, and Rice 1989) in which most of the infrared emission in a typical galaxy is due to dust heated by the diffuse interstellar radiation field, except at $60\mu\text{m}$ where the emission is approximately doubled by contributions from star forming regions.

Acknowledgments: We thank the staff of *IPAC* for helping us during our visit. This work was supported by NASA's IRAS Data Analysis Program funded through JPL, and by a NSF PYI Award. Additional support was provided by a Zaccheus Daniel Foundation award to T. I.

References

- Bothun, G. D., Lonsdale, C. J., and Rice, W. 1989, *Ap. J.*, **341**, 129.
 Boulanger, F., and Péroult, M. 1988, *Ap. J.*, **330**, 964.
 Feigelson, E. D., and Nelson, P. I. 1985, *Ap. J.*, **293**, 192.
 Felten, J. E. 1977, *A. J.*, **82**, 861.
 Huchra, J., Davis, M., Latham, D., and Tonry, J. 1983, *Ap. J. Suppl.*, **52**, 89.
 IRAS Point Source Catalog, Version 2 1987 (Washington: Government Printing Office).
 Isobe, T., and Feigelson, E. D. 1989, in preparation.
 Isobe, T., Feigelson, E. D., and Nelson, P. I. 1986, *Ap. J.*, **306**, 490.
 Kirshner, R. P., Oemler, A. Jr., Schechter, P. L., and Shectman, S. A. 1983, *A. J.*, **88**, 1285.
 Léger, A., and Puget, J. L. 1984, *Astr. Ap.*, **137**, L5.
 Schechter, P. L. 1976, *Ap. J.*, **203**, 297.

Evidence against a simple two-component model for the far-infrared emission from galaxies

Stephen A. Eales
Space Telescope Science Institute

&

Nicholas A. Devereux
Five Colleges Radio Astronomy Observatory

Two of the first *IRAS* results were that galaxies have a wide range of values for the ratio of 60 μm to 100 μm flux density ($0.2 \leq S_{60}/S_{100} \leq 1.0$) and that this ratio is correlated with L_{fir}/L_b , L_{fir} being the total far-infrared luminosity and L_b being the luminosity at visible wavelengths (de Jong et al. 1984; Soifer et al. 1984). From these results arose the following simple model for the far-infrared emission from galaxies (de Jong et al. 1984), which has remained the standard model ever since. In this model, the far-infrared emission comes from two dust components: warm dust ($T \approx 50$ K) intermingled with, and heated by, young massive OB stars in molecular clouds and HII regions, and colder dust ($T \approx 20$ K) associated with the diffuse atomic hydrogen in the interstellar medium and heated by the general interstellar radiation field. As the number of young stars in a galaxy increases, S_{60}/S_{100} increases, because there is a greater proportion of warm dust, and so does L_{fir}/L_b , because most of the radiation from the young stars is absorbed by the dust, leading to a swifter increase in far-infrared emission than in visible light. Although this model explains the basic *IRAS* results, it is inelegant—it uses two free parameters to fit two data (the 60 and 100 μm flux densities)—and there are now several observations that contradict it:

- (1) Since the end of the *IRAS* mission, several groups have measured the submillimetre emission from galaxies, so there are now sufficient data to test a two-parameter model. Eales, Wynn-Williams & Duncan (1989), rather than needing two dust components, found that the 60-1100 μm flux densities of the 11 galaxies in their sample could be well-fitted by thermal emission from dust at a single temperature ($T \approx 30$ -50 K). Devereux and Young (this conference), using the submillimetre data of Stark et al. (1989), have demonstrated the same thing for a different sample.
- (2) If the two-component model is correct, one expects galaxies with few molecular clouds and most of their gas in atomic form to have low values for S_{60}/S_{100} . On the contrary, there appears to be no correlation between S_{60}/S_{100} and the relative proportions of molecular and atomic gas (Young et al. 1989).
- (3) A less direct but still highly suggestive argument comes from a study of the correlation between far-infrared and radio emission. Cox et al. (1988) and Devereux & Eales (1989) have shown that the slope of this relation is significantly different from unity, in the sense that $L_{\text{radio}}/L_{\text{fir}}$ increases with luminosity. At first glance, this is what one might expect from the two-component model. The radio emission from galaxies probably arises, directly or indirectly, from the supernova explosions of massive stars. Therefore, as the number of young massive stars in a galaxy increases, the radio

emission will increase in proportion to the number of young stars, but the far-infrared emission will increase at a slower rate because of the underlying contribution to the far-infrared emission from the cold dust component. Nevertheless, at second glance this scheme doesn't work, because it predicts a correlation between S_{60}/S_{100} and L_{radio}/L_{fir} that isn't observed (Devereux & Eales 1989).

Despite these major problems with the two-component model, it is not clear what should be put in its place. The basic *IRAS* results can be explained by other models. As an example of one possible model, imagine that *all* the far-infrared emission from galaxies is from dust heated by young stars in molecular clouds and HII regions. If the number-density of young stars in a galaxy is increased, the radiation field will be more intense and so S_{60}/S_{100} will be higher; both the far-infrared emission and the visible light from the galaxy will increase, but the far-infrared emission will increase more swiftly because of the contribution to the visible light from old stars and because most of the visible light from the young stars is absorbed by dust: and so L_{fir}/L_b will be correlated with S_{60}/S_{100} . A model like this would also be more in accord with the studies of galaxies that have been made in the CO 1-0 line by Young and collaborators (Young 1986). When considering possible models for the far-infrared emission from galaxies, the observational evidence for our own galaxy must be considered. We suspect that the study by Boulanger & Pérault (1988) of the far-infrared properties of the local interstellar medium may be particularly relevant. They showed that molecular clouds are leaky—that most of the light from OB stars in molecular clouds does not heat the dust in the clouds, but instead leaks out—and also the consequence of this: that while most of the far-infrared emission from the solar neighbourhood is from dust associated with diffuse HI, this dust is mostly heated by young stars.

Boulanger, F. & Pérault, M., 1988. *Astrophys. J.*, 330, 964.

Cox, M., Eales, S.A., Alexander, P.A. & Fitt, A., 1988. *Mon. Not. R. astr. Soc.*, 235, 1227.

de Jong, T., Clegg, P.E., Soifer, B.T., Rowan-Robinson, M., Habing, H.J., Houck, J.R., Aumann, H.H. & Raimond, E., 1984. *Astrophys. J.*, 278, L67.

Devereux, N.A. & Eales, S.A., 1989. *Astrophys. J.*, 340, 708.

Eales, S.A., Wynn-Williams, C.G. & Duncan, W.D., 1989. *Astrophys. J.*, 339, 859.

Soifer, B.T., 1984. *Astrophys. J.*, 278, L71.

Stark, A.A., Davidson, J.A., Harper, D.A., Pernic, R., Loewenstein, R., Platt, S., Engargiola, G. & Casey, S., 1989. *Astrophys. J.*, 337, 650.

Young, J.S., 1986 *IAU Symposium 115, Star Forming Regions*, eds M. Peimbert and J. Jugaku (Dordrecht: Reidel), p. 557.

Young, J.S., Xie, S., Kenney, J.D. & Rice, W., *Astrophys. J. suppl.*, (in press).

EMISSION FROM SMALL DUST PARTICULES IN DIFFUSE AND MOLECULAR CLOUD MEDIUM

J.P. Bernard¹, X. Désert²

¹ Institut d'Astrophysique Spatiale, Université Paris XI, bât. 210, 91401 Orsay Cedex, France

² NASA Goddard Space Flight Center, Code 685, Greenbelt, MD 20771, USA

IRAS observations of the whole galaxy has shown that long wavelength emission (100 and 60 μm bands) can be explained by thermal emission from big grains ($\approx 0.1 \mu\text{m}$) radiating at their equilibrium temperature when heated by the Inter Stellar Radiation Field (ISRF). This conclusion has been confirmed by continuum sub-millimeter observations of the galactic plane made by the EMILIE experiment at 870 μm (Pajot et al 1986). Nevertheless, shorter wavelength observations like 12 and 25 μm IRAS bands, show an emission from the galactic plane in excess with the long wavelength measurements which can only be explained by a much hotter particles population. Because dust at equilibrium cannot easily reach high temperatures required to explain this excess, this component is thought to be composed of very small dust grains or big molecules encompassing thermal fluctuations.

We present here a numerical model that computes emission, from NIR to Sub-mm wavelengths, from a non-homogeneous spherical cloud heated by ISRF. This model fully takes into account the heating of dust by multi-photon processes and back-heating of dust in the VIS-IR so that it is likely to describe correctly emission from molecular clouds up to large A_V and emission from dust experiencing temperature fluctuations. The dust is a three component mixture of PAHs (Polycyclic Aromatic Hydrocarbons), VSGs (Very Small Grains) and classical BGs (Big Grains) with independent size distributions (cut-off and power law index) and abundances.

The presence of PAHs in the ISM has been inferred for the first time to explain the unidentified IR bands at 3.3, 7.6, 7.7, 8.6 and 11.3 μm (Léger, Puget 1984, Allamandola et al 1985) observed in various objects ranging from planetary nebulae to external galaxies. They seem to be ubiquitous in the extended ISM of our galaxy as revealed by the AROME experiment which as mapped the galactic disk in the 3.3 μm band (Giard et al 1988). This plane molecules are so small dust particles that they can reach high vibrational temperatures (once a day in ISM environment) after absorption of a single UV photon by electronic transitions followed by internal redistribution of its energy between the vibrational modes. The molecule therefore cools by emitting IR photons (most of them in the 12 μm IRAS band) during only a few seconds so

that PAHs are the most extreme case of ISM particles emitting IR energy in an out-of-equilibrium stage. Moreover, recent laboratory measurements have shown that this molecules absorbs significantly in the non-linear FUV rise part of the extinction curve (Léger et al 1988) so that they play an important role in the radiation transfer from the edge of a cloud towards the center.

To account for the 12 μm emission, bigger grains are needed that are no longer two dimensional but three dimensional (VSGs). They are supposed to be carbon-dominated in the model and to account for most of the 2200 Å bump observed in the extinction curve.

BGs are considered as the carrier of the visible part of the extinction curve. As proposed by Chlewicki and Greenberg (1988), we have supposed that they are made of silicates coated by carbon dominated material. This has the advantage to explain both the width of the 9.7 and 18 μm absorption of silicates and the 3.4 μm absorption towards the galactic center.

The mass abundance relative to hydrogen (Y) and the size distribution parameters (radius cut-off a_{min} and a_{max} and size distribution power law index α) of each component has been optimized to fit the emission and extinction observed in the diffuse HI medium of our galaxy (see Table 1).

Fig 1 is a plot of IRAS brightness against position of the line of sight toward various A_V clouds with r^{-2} gas density distribution and dust characteristics of table 1. The separation of the curves at low radii is due to including back-IR heating. No limb brightening effect at 12 μm is obtained until high A_V are reached. Fig 2 shows the incident spectrum at various positions inside the $A_V=100$ mag cloud. The initial ISRF is progressively attenuated when penetrating into the cloud. The hatched area represents the effect of including back-IR heating.

Real cases of clouds with observed colors variations have also been emphasized. We find that IRAS colors variations with position in the cloud are not likely to be due to transfer effects but to abundance variations of the various dust species. For instance, G299-16, an high 12/100 cloud of the Chameleon complex, shows a decrease of 12 and 25 μm at the center which can only be explained by a strong decrease of PAHs abundance at $n_H > 400\text{-}500 \text{ H/cm}^3$ in the cloud.

References:

- Allamandola L. J., Tielens A.G.G.M. and Barker J.R. 1985, *Astrophys. J. (Letters)*, **290**, L25
 Chlewicki G. and Greenberg M. 1988, *Astrophys. J.*, submitted
 Giard M., Pajot F., Lamarre J.M., Serra G., Audouze J., Caux E., Combes M., Gispert R., Léger A. and Rouan D. 1988, *Astron. & Astrophys. Let.* **201**, L1
 Léger A., Puget J.L. 1984, *Astron. & Astrophys.*, **137**, L5
 Léger A., d'Hendecourt L. and Defourneau, D. 1988 *Astron. & Astrophys.*, submitted
 Pajot F., Gispert R., Lamarre J.M., Peytureaux R., Puget J.L., Serra G., Coron N., Dambier G., Leblanc J., Moalic J.P., Renaud J.C. and Vitry R. 1986, *Astron. & Astrophys.*, **154**, 55.

Table 1

	Y (10^{-4})	a_{\min} (nm)	a_{\max} (nm)	α
PAHs	4.6	.4	12	-3.0
VSGs	4.7	12	15	-3.1
BGs	64	15	110	-2.8

H-coverage for PAHs: 0.4

Fig 1

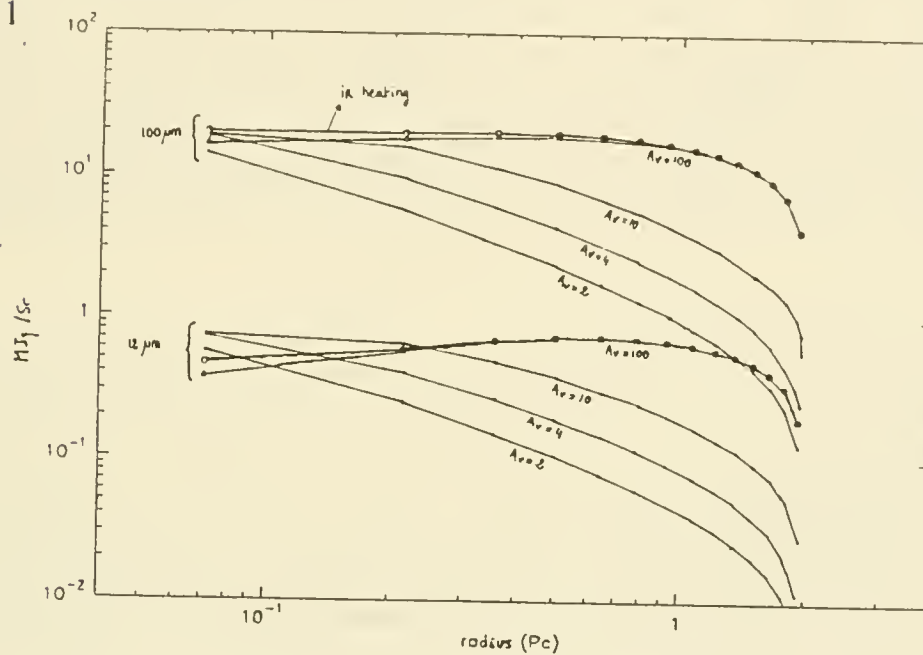
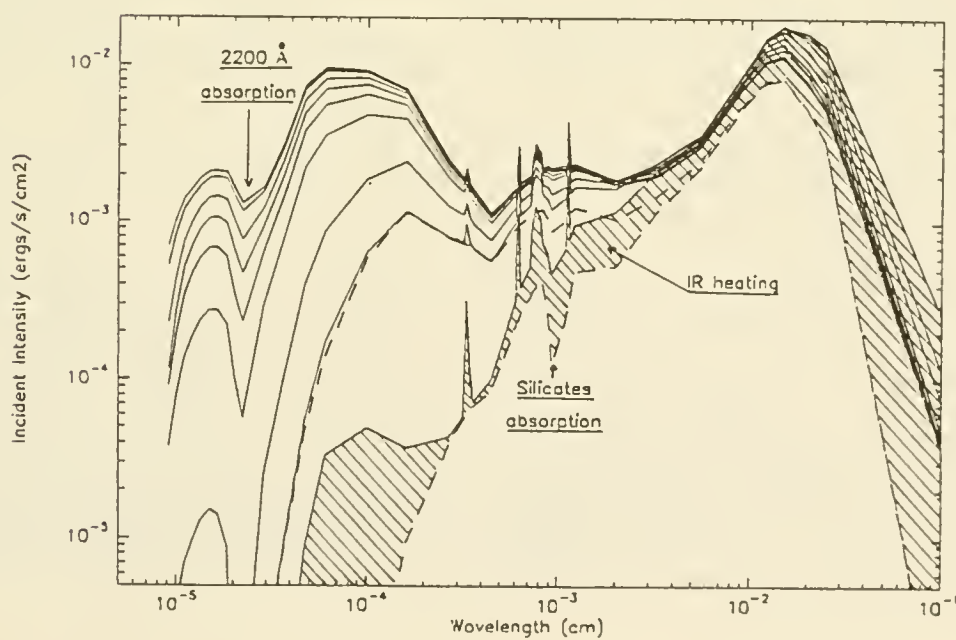


Fig 2



Very Small Grains in the Milky Way and External Galaxies

L. Luan (UC Berkeley), M.W. Werner (NASA/Ames), C. Heiles (UC Berkeley), K. Sellgren (U. of Hawaii)

I. Introduction

Excess emission at near- to mid-infrared wavelengths, over that expected from dust grains which are heated in equilibrium with the radiation field, has been observed from astronomical objects ranging from diffuse interstellar clouds to external galaxies. This excess emission has been attributed to a population very small grains (VSGs) which produce the emission in a non-equilibrium process. Theoretical, observational and laboratory studies have suggested that the VSGs may include both Polycyclic Aromatic Hydrocarbon (PAH) molecules (Léger and Puget 1984, Allamandola, Tielens and Barker 1985) and thermally fluctuating small dust grains (Draine and Anderson 1985). Because of the superb sensitivity of the Infrared Astronomical Satellite (IRAS) and its large data sample, IRAS data are very useful for studying this aspect of dust emission.

For many objects of interests, the IRAS $12\mu\text{m}$ band emission (from $7.5\mu\text{m}$ to $15.5\mu\text{m}$) arises primarily from the VSG component. The ratio $R = \nu F_\nu(12)/F(\text{farIR})$ is indicative of the ratio of the emission from VSGs to the total far-infrared emission, where $F(\text{farIR})$ is obtained from the IRAS 60 and $100\mu\text{m}$ fluxes. The ratio $F_\nu(60)/F_\nu(100)$ is taken as a measure of the temperature of larger dust grains which are heated in equilibrium with the radiation field; this ratio is thus indicative of the energy density of the heating radiation.

II. Data Sample and Results

We have measured the IRAS fluxes of 28 visibly bright reflection nebulae illuminated by B stars, by carrying out surface photometry on the co-added IRAS flux density maps. We compare these data with previously published IRAS measurements of high latitude HI clouds heated by the general interstellar radiation field (Heiles, Reach and Koo 1988), and of compact HII regions illuminated by O stars (Antonopoulou and Pottasch 1987). We also discuss in this paper the implication of comparison of infrared colors of these galactic objects with those of external galaxies.

Figure 1 presents a “color-color” diagram, $\nu F_\nu(12)/F(\text{farIR})$ vs $F_\nu(60)/F_\nu(100)$, for several classes of objects, while the mean colors are listed in Table 1. These data show that $\langle R \rangle = 0.31$ for reflection nebulae and $\langle R \rangle = 0.38$ for High Latitude (HL) HI clouds, while $\langle R \rangle = 0.044$ for compact HII regions. The separation between the compact HII regions and the more diffusely heated clouds in Figure 1 is quite striking and apparently independent of the starlight energy density as measured by the $60/100\mu\text{m}$ grain temperature. The fact that R in HII regions is about 8 times smaller than in reflection nebulae and HI clouds may be explained in terms of the destruction of VSG’s in HII regions or in the immediately adjacent neutral material. This has previously been suggested by Boulanger *et al.* (1988) and Ryter *et al.* (1987) from the studies of the spatial distribution of infrared radiation from extended HII regions. They have shown that the ratio R decreases significantly towards the central ionizing star, where the UV energy density of the stellar radiation field is very high. In the PAH model, this can be interpreted as the breaking of C=H bonds and the suppression of the associated vibrational modes (Allamandola 1988), while in the model of small grains undergoing temperature fluctuations, it implies that smaller grains are preferentially destroyed by hard UV photons or by electron and/or ion impact. A possible alternative explanation of the low value of R for HII regions is that it is due to a high optical depth at $\sim 10\mu\text{m}$ of the enveloping dust cloud through which the compact HII regions might be viewed in many cases.

Since both HII regions and more diffusely heated material presumably contribute to the infrared radiation from galaxies, we expect the value of R for an entire galaxy Way to lie between those for compact HII regions and for the reflection nebulae and HI clouds. Figure 1 shows that R for a sample of non-interacting spiral galaxies is fairly constant and lies in the expected range. This suggests that: 1) The $12\mu\text{m}$ band emission seen from these galaxies is predominantly from the VSG population; 2) since R is also proportional to the mass ratio $b = \text{Mass(VSG)}/\text{Mass(dust)}$, b is approximately uniform in this population of normal spiral galaxies. From the above arguments, we further estimate that $R \sim 0.14$ for the Milky Way.

We have also extended our investigations into interacting galaxies. The high $L(\text{IR})/L(\text{B})$ (> 35) galaxies studied by Bushouse, Lamb and Werner (1988) have $\langle R \rangle = 0.089$. These group of galaxies are merger-type objects, contact pairs or very closely interacting pairs. They have nuclear region optical spectra indicative of high levels of current star-formation activity, with very hot stars being the dominant ionization source. Thus it is not surprising that they have values of R comparable to those seen in the warmer HII regions.

III. Summary

In summary, our studies of the infrared colors of reflection nebulae, HL HI clouds, HII regions and external galaxies have shown the following:

1. Different classes of objects locate in different regions on the R vs $F_\nu(60)/F_\nu(100)$ diagram. This is determined both by differences in dust properties and by differences in the illuminating radiation field. For example, HL clouds and reflection nebulae almost have the same behavior since both are in the diffuse ISM and can be expected to have similar grain populations; the small difference in their infrared colors can be explained by the difference of the illuminating radiation field. On the other hand, the dramatic difference of $R = \nu F_\nu(12)/F_\nu(\text{farIR})$ between HII region and diffuse ISM may be due to the destruction of the VSG component in the HII regions, although radiation transfer effects may play a part as well.

2. The ratio $R = \nu F_\nu(12)/F_\nu(\text{farIR})$ is approximately constant in normal spiral galaxies. This implies that the mass ratio $b = \text{Mass(VSG)}/\text{Mass(dust)}$ does not vary greatly from one galaxy to another.

Further implications of these results and an extension to include the $25\mu\text{m}$ IRAS data in the comparisons will be presented in a more complete paper currently in preparation.

This work is supported by NASA Ames University Consortium NCA2-279 and by IPAC.

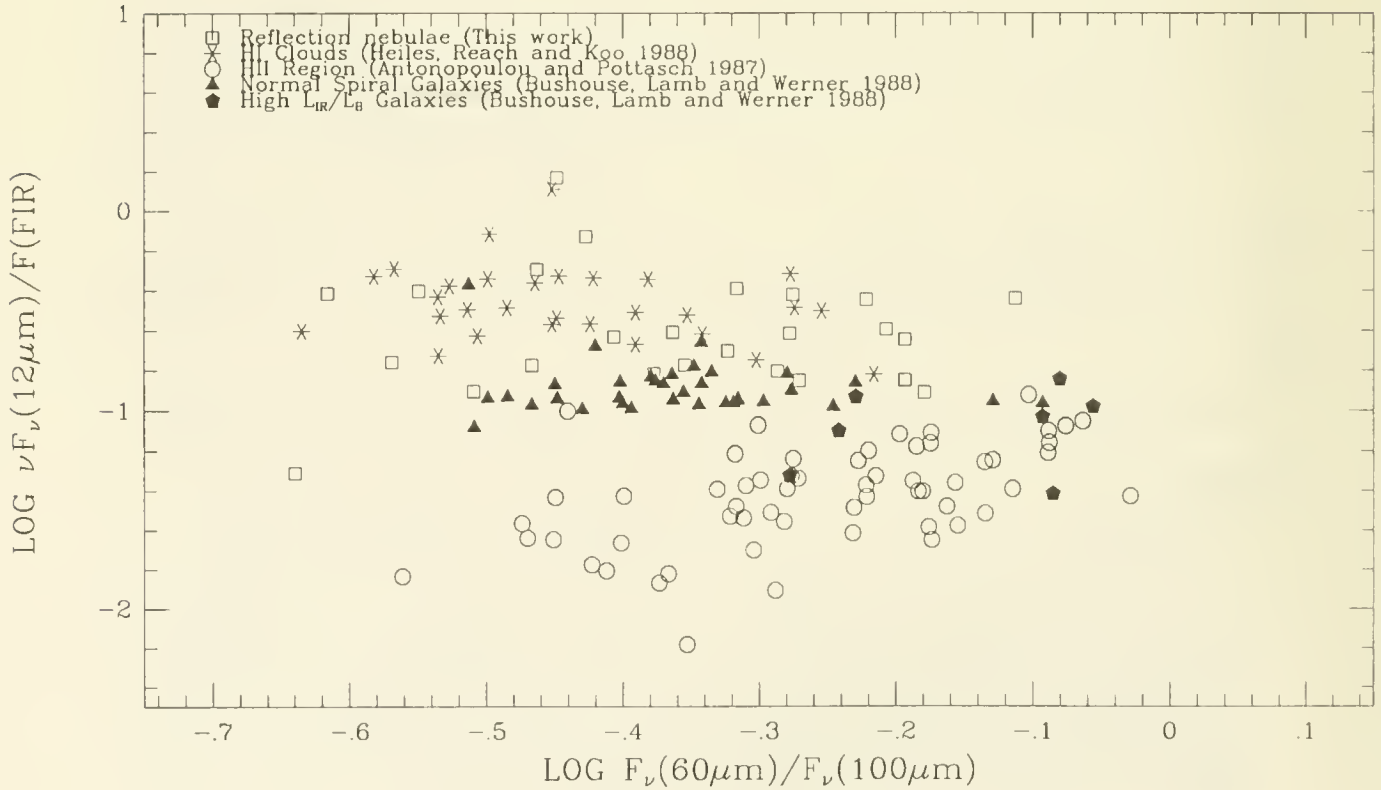
Reference

- Allamandola, L.J., Tielens, A.G.G.M., and Barker, J.R. 1985, *Ap.J.Lett.*, **315**, L61.
Allamandola, L.J. 1988, *Proceedings of IAU Symposium 135 (Interstellar Dust)*, Santa Clara, July 1988.
Antonopoulou, E., and Pottasch, S.R. 1987, *Astr.Ap.*, **173**, 108.
Boulanger, F., Beichman, C., Désert, F. X., Helou, G., Péroult, M., and Ryter, C. 1988, *Ap.J.*, **332**, 328.
Bushouse, H.A., Lamb, S.A., and Werner, M.W. 1988, *Ap.J.*, **335**, 74.
Draine, B.T., and Anderson, N. 1985, *Ap.J.*, **292**, 494.
Heiles, C., Reach, W. T., and Koo, B. 1988, *Ap.J.*, **332**, 313.
Léger, A., and Puget, J.L. 1984, *Astr.Ap.*, **137**, L5.
Ryter, C., Puget, J.L., and Péroult, M. 1987, *Astr.Ap.*, **186**, 312.

TABLE 1
MEAN PROPERTIES OF SAMPLES

Sample	$\frac{\nu F_\nu(12\mu\text{m})}{F(\text{FIR})} \pm \sigma$	$\frac{F_\nu(60\mu\text{m})}{F_\nu(100\mu\text{m})} \pm \sigma$	T_{dust}^a
Reflection Nebulae.....	0.30 ± 0.27	0.44 ± 0.16	33
HL HI Clouds ^b	0.38 ± 0.21	$0.23 \pm .057$	27
HII Regions ^c	$.044 \pm .024$	0.58 ± 0.15	37
Normal Spiral Galaxies ^d	$0.14 \pm .057$	0.45 ± 0.11	34
High $L_{\text{IR}}/L_{\text{B}}$ Galaxies ^d .	$.089 \pm .035$	0.72 ± 0.14	41

Note: ^a Dust temperature computed from the 60/100 μm flux ratio assuming emissivity proportional to frequency. ^b From Heiles, Reach and Koo (1988). ^c From Antonopoulou and Pottasch (1987). ^d From Bushouse, Lamb and Werner (1988).



A MODEL FOR THE INFRARED EMISSION FROM AN OB STAR CLUSTER ENVIRONMENT

D. Leisawitz
NASA/Goddard Space Flight Center
Laboratory for Astronomy and Solar Physics

We have developed an interactive radiative transfer code that predicts the infrared emission from an H II region containing diffuse ionized and atomic gas and dense molecular clouds. This model complements our investigation of the redistribution of OB star luminosity in the interstellar medium (Leisawitz and Hauser 1988, Ap. J., 332, 954). The model can be used as a diagnostic tool to probe the radiation field and matter density in an H II region, place constraints on the proximity and orientation of an illuminated molecular cloud with respect to the ionizing stars, test for the presence of small, transiently heated dust grains, and determine whether the dust-to-gas ratio is normal.

Predictions of the model agree qualitatively and quantitatively with observations of blister-type H II regions ionized by well-studied OB clusters in which the distribution of dense neutral material is known. This is illustrated by a model for IRAS observations of the region around NGC 7380 (S142).

We plan to use the model in our survey of regions of massive star formation in the outer Galaxy to study OB stars embedded to various degrees in their parental molecular clouds.

On this poster, the model is illustrated in a series of figures. Here we model the environment of a $1.7 \times 10^6 L_{\odot}$ cluster with 46% of the starlight radiated shortward of the Lyman limit. The ionizing (L_{yc}) photon production rate is $8.3 \times 10^{49} \text{ s}^{-1}$. These stellar parameters are based on spectrophotometric observations of NGC 1893 (see Mermilliod 1976, Astr. Ap. Suppl., 24, 159), a cluster rich in early spectral type stars. The interstellar radiation field (ISRF) energy density is assumed to be the same as that in the solar neighborhood (0.44 eV cm^{-3}).

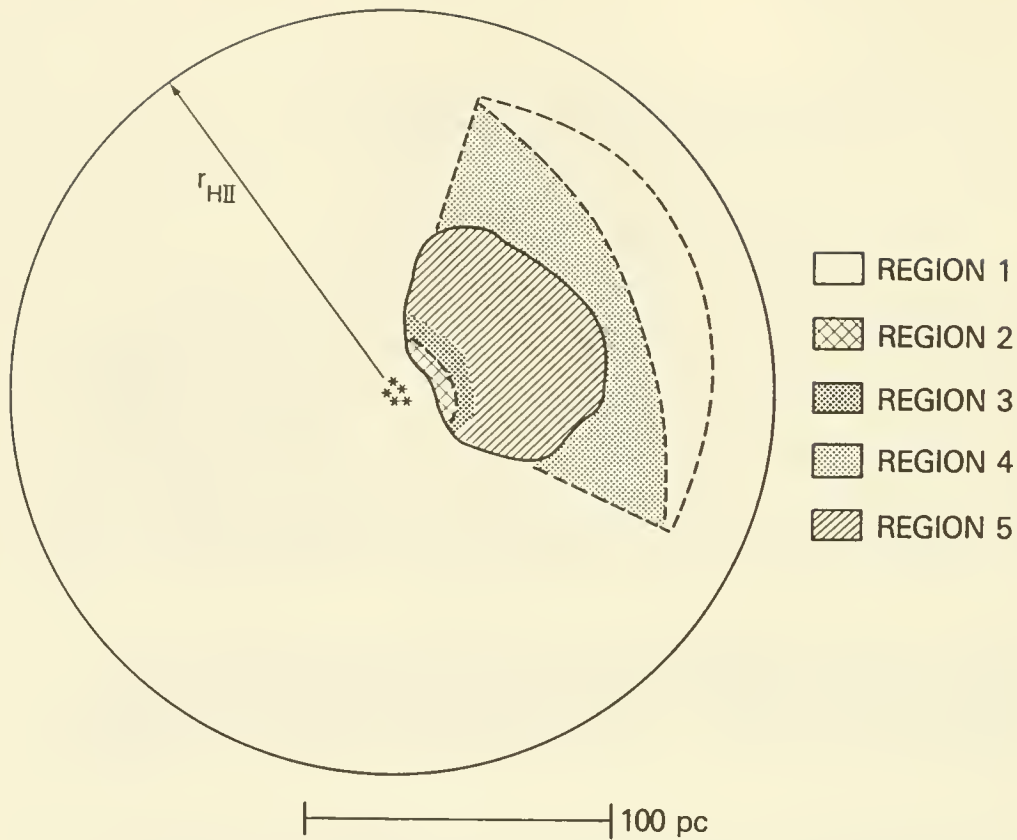


Figure 1: Elements of a typical model

The model has two components: a dense molecular cloud and a diffuse intercloud medium (ICM). Region 1 contains the ICM. Ionized gas is present in the ICM ($n = 1 \text{ cm}^{-3}$; Strömgren sphere radius, $R_S = 130 \text{ pc}$) and in a 4.8 pc thin layer (Region 2) on the illuminated surface of the nearby molecular cloud ($n = 30 \text{ cm}^{-3}$). Non-ionizing radiation from the central cluster penetrates the cloud to a greater depth (Region 3) and the entire cloud is heated externally by the ISRF. The molecular cloud surface is 6 pc from the cluster and the thickness of the cloud is 30 pc. Because of direct absorption of some of the Lyc radiation by dust, the ICM is ionized to a radius $r_{\text{H II}} = 104 \text{ pc}$, somewhat smaller than R_S . The cloud is opaque at UV and visible wavelengths, so it casts a shadow in the ICM (Region 4) and its interior (Region 5) is relatively cold. Two radiative transfer calculations are done. The first is along a line from the cluster through Region 1; the second calculation starts at the cluster and follows a line through Regions 1, 2, 3, 5, and 4.

IRAS OBSERVATIONS of the ISM in the γ CAS REFLECTION NEBULA

Richard H. Buss Jr.

Michael W. Werner

NASA Ames Research Center, Moffett Field, CA

1 Introduction

Mid-infrared emission from other galaxies originates both from interstellar grains heated by diffuse starlight and local excitation of grains by hot OB stars. Thus, a detailed examination of the *IRAS* data from a B star interacting with the interstellar medium (ISM) could provide insight into infrared (IR) emission processes in external galaxies. We have therefore used *IRAS* data to study the B0 IVe star γ Cas and its surroundings, which we find to exhibit evidence of grain heating, destruction, and possible star formation.

2 Background

γ Cas lies at a Galactic $b = -2^\circ$ and is associated with the visual reflection/emission nebulae, IC 59 and IC 63 (Witt *et al.* 1989), and an H II region (S185) 120' in extent. γ Cas lies ($d=200$ pc) at the edge of the local interstellar cavity, with little intervening dense molecular or atomic material (Paresce 1984; Jenkins, Savage, and Spitzer 1986). Recently, Witt *et al.* have detected H_2 emission in the ultraviolet and "extended red emission [ERE]" at 8000 Å from IC 63 but not from IC 59. They attribute both phenomena to ISM fluorescence excited by γ Cas.

Like other stars of its spectral type, γ Cas is known to have a strong stellar wind (Grady, Bjorkman, and Snow 1987). Moreover, γ Cas has a neutron star companion (Frontera *et al.* 1987), implying that a supernova occurred less than 10^6 years ago. Adopting a luminosity of $8 \times 10^4 L_\odot$ for γ Cas, the effective energy density of its radiation will equal that of the interstellar radiation field (8×10^{-13} ergs cm $^{-3}$) at a distance of 11 pc from the star, corresponding to 3 degrees at 200 pc. Thus, γ Cas should be the dominant heat source over the $2.25^\circ \times 2.25^\circ$ *IRAS* image that we have studied.

3 *IRAS* Data

We have examined 2.25×2.25 square degree co-adds centered near γ Cas in all 4 *IRAS* wavelength bands (*e. g.* Figures 1, 2). The principal features of the data are: 1) A promi-

ment 12 and 25 μm point source at the position of γ Cas; 2) Extended emission which shows positional associations with γ Cas, IC 59, and IC 63, yet which is very bright elsewhere in the field; 3) A second point source, which lies halfway between IC 59 and IC 63, and which is extremely bright, increasing in intensity from 12 to 100 μm .

The *IRAS* energy distribution and LRS spectrum of γ Cas (*cf.* Schaeffer 1986; Coe 1986) resemble those of other Be stars and appear to be due to the combination of black-body emission from the stellar photosphere and free-free emission from the circumstellar wind.

The extended IR emission associated with IC 59 and IC 63 shows a color temperature $T(60\mu\text{m}/100\mu\text{m})$ decreasing with increasing distance from γ Cas, as would be expected if it is primarily responsible for heating the radiating dust in these clouds. The energy distributions of the two nebulae, however, show slight differences that could be associated with the differing amounts of fluorescent emission found by Witt *et al.* Both show strong emission at 12 μm due to nonequilibrium radiation from tiny grains, yet the large grains radiating at longer wavelengths have $T(60\mu\text{m}/100\mu\text{m}) = 55$ K for IC 63 vs. $T(60\mu\text{m}/100\mu\text{m}) = 45$ K for IC 59. In the visible (Witt *et al.*) and the IR (Figs. 1 and 2), the two nebulae show sharp edges on the sides facing γ Cas; on other sides, the emission is diffuse (Figs. 1 and 2). This morphology suggests the nebulae are shaped by radiation pressure from γ Cas. At 60 μm (Figure 2), a bright emission region extends 10' from γ Cas toward IC 59 and IC 63. Because $T(60\mu\text{m}/100\mu\text{m}) = 60$ K in this extension indicates that γ Cas is heating the large, nearby interstellar grains, the weakness of *IRAS* 12 μm (Figure 1) emission from this region adjacent to γ Cas suggests that small grains have been destroyed in — or swept out of — a 10-15' (0.6 pc) radius region around γ Cas.

An extremely bright source ($F_{60} = 108$ Jy), cataloged as *IRAS* 00556+6048, appears between IC 59 and IC 63. *IRAS* 00556+6048 is not associated with any known PN, H II region, strong radio source, or near-IR bright star. Its IR colors [and possibly most of its spectrum (*cf.* Volk and Cohen 1989)] resemble those of a "red-reflection nebula" or a Herbig-Haro central star (Walker *et al.* 1989). The *IRAS* LRS (Olnon and Raimond; Beichman 1987) database spectrum for this object shows IR emission lines at 7.7, 8.6, and 11.3 μm attributed to macromolecules, as well as a Ne II 12.8 μm line on a red continuum. The spectrum resembles those of diffuse nebulae with spectra unlike those of H II regions or planetary nebulae (class 21: γ 03; Cheeseman *et al.* 1989). The Palomar Sky Survey R and B prints (*cf.* Witt *et al.* 1988) show faint nebulosity within 2' of the *IRAS* position. The nebula appears roughly elliptical on the red plate, the semimajor axis oriented east-west. We are currently investigating the nature of this object and its association (if any) with IC 59, IC 63, and γ Cas. Perhaps it is a compact, dust-embedded protostar or young stellar object induced to collapse by either the putative supernova or by the radiation pressure from Gamma Cas. In this case, ionization and excitation by γ Cas of the remnant outer fringes of the collapsing cloud might have produced the visible and ionized nebula.

IRAS 12 μm S/N MAP

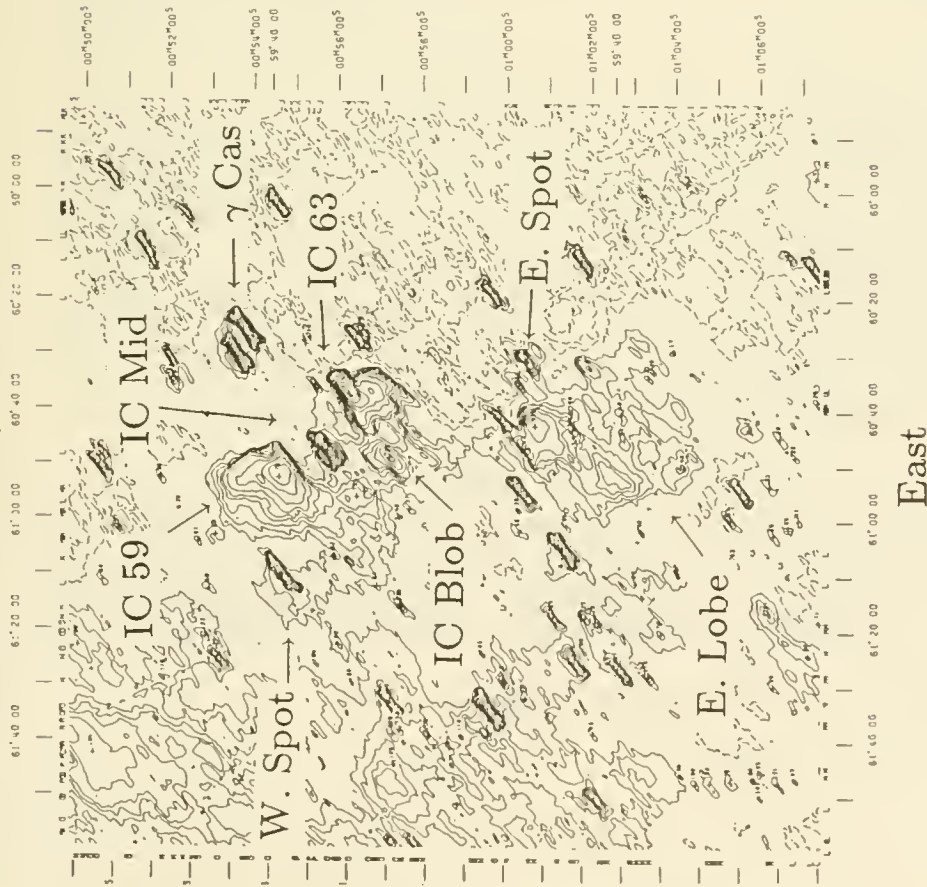


Figure 1 – The emission from IC 59 and IC 63 likely originates from intermittent photoexcitation of tiny interstellar grains by γ Cas. Note the hole of emission near γ Cas itself, showing that tiny grains have been destroyed (Maximum contour for IC 63 is 113.)

IRAS 60 μm S/N MAP

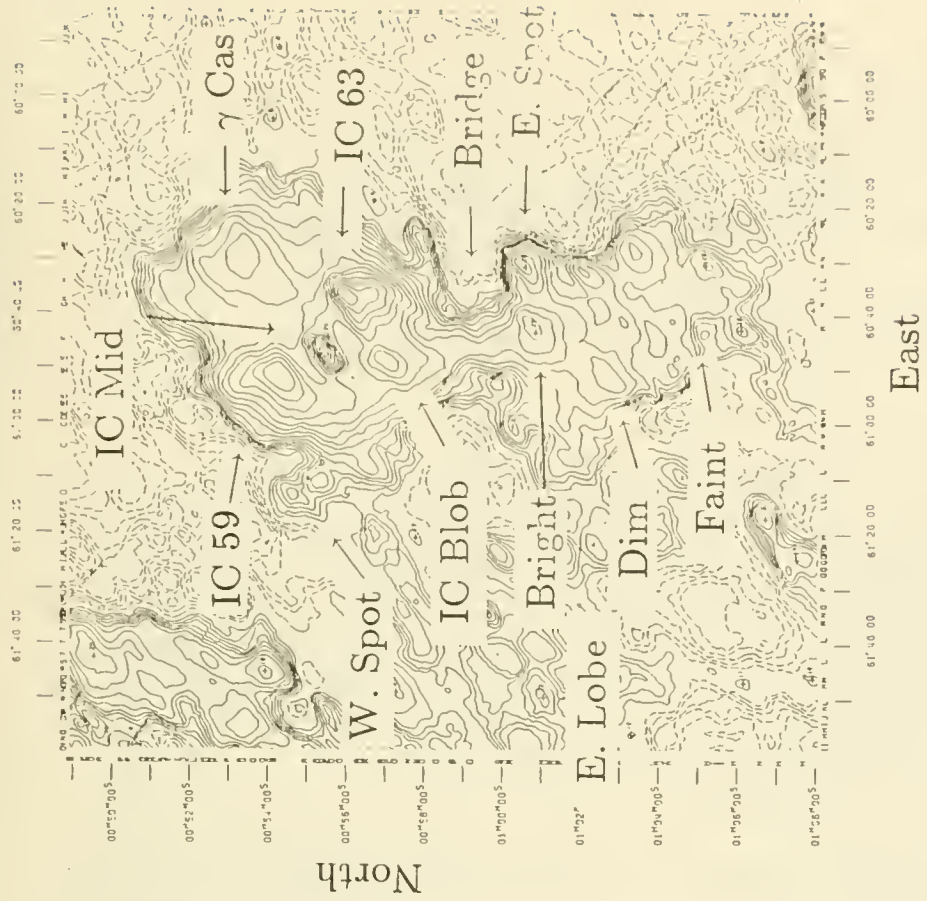


Figure 2 – The emission is highly extended, showing that an interstellar cloud is present. The mystery source, (“IC MID”), IRAS 00556+6048, is perhaps a protostar induced to collapse by γ Cas, as it lies between the IC nebulae. (Maximum contour for IC 63 is 640.)

Peering Beyond IRAS: The 100 - 350 μm Dust Emission from Galaxies

HARLEY A. THRONSON, JR.,¹ DEIDRE A. HUNTER,²
SEAN CASEY,³ GREG ENGARGIOLA,³ AND D. A. HARPER³

I. JUSTIFICATION AND RATIONALIZATION

Several arguments can be made to study the continuum emission from dust in galaxies at wavelengths between the cutoff of the *IRAS* survey (about 100 μm) and the shortest wavelength that is commonly accessible from the ground (about 350 μm). Some theoretical work (see the summary by Cox and Mezger 1989) indicates that there are very cool ($T_d \leq 25$ K) components to the dust emission that emit primarily at wavelengths between 100 μm and 250 μm . In fact, a significant fraction of the total luminosity, representing a large fraction of the dust mass in some types of galaxies, is emitted at long far-infrared wavelengths. In such cases, the cool dust must play a major role in regulation of the energy balance of the ISM and in shielding the cores of neutral clouds.

II. THE OBSERVATIONS

For four years we have been mapping the continuum dust emission from disk galaxies using the Yerkes Observatory 32-element far-infrared photometric array system onboard NASA's Kuiper Airborne Observatory (KAO). This array has a beam size of $45''$ and a set of filters that isolates the emission in bands from about 60 to 250 μm .

Our program has concentrated on irregular galaxies, especially Magellanic Irregulars, and lenticulars (S0), galaxies that until very recently had been widely believed to be devoid of a significant cool interstellar medium. We are particularly interested in both types of galaxies as they are often found to be forming stars in an environment devoid of spiral structure. The S0s were also observed because these galaxies are the only abundant morphological class that has shown all major components of the ISM.

Our conclusions discussed in this summary are based on the data summarized in Table 1, as well as the 160 μm /100 μm vs. 100 μm /60 μm color-color plot in Figure 1. We have not included our results for irregular galaxies in the table as H_2 masses derived from millimeter-wave CO observations are unreliable for these metal-poor systems.

III. THE SOURCE OF THE COOL DUST EMISSION

Based on the data available at present, a straightforward explanation for the source of the continuum emission from galaxies in the 100 - 350 μm range is dust mixed within both the diffuse atomic gas ("cirrus"?), as well as within the surface layers of molecular clouds. Dust in both locations will be heated by photons from the same sources: diffuse interstellar

¹Wyoming Infrared Observatory, University of Wyoming

²Lowell Observatory

³Yerkes Observatory, University of Chicago

radiation, augmented by light from massive stars if active star formation is widespread in the galaxy. This dust is distinct from that immediately associated with regions of active star formation or buried deep within molecular clouds. However, because it is part of a widely-distributed component of the cool ISM, these grains will intercept an important fraction of the galaxian radiation field and may interact strongly with X-ray-emitting, high-energy gas in the early-type galaxies in our sample.

Our conclusion on the location of the dust is based primarily on the very good correlation between the total 160 μm “luminosity” ($L_{160} \equiv 4\pi D^2 \nu F_\nu$) and the total derived HII mass for the galaxies presented in Table 1. In particular, we find $M(\text{HII}) = 0.34L_{160} + 6.5$, with a correlation coefficient of 0.86 for $M(\text{HII})$ and L_{160} in units of $10^8 M_\odot$ and $10^8 L_\odot$, respectively. We also derive an average $M(\text{HII})/M_d = 750$. Our sample showed a much poorer correlation between both L_{160} vs. $M(\text{H}_2)$, with the molecular mass derived from CO observations, and between L_{160} and $M(\text{HII}) + M(\text{H}_2)$.

In contrast, for some of the same galaxies, Maloney (1987) argued that the 160 μm flux was arising from molecular material, based on a good point-to-point correspondence between the H_2 column density derived from $J = 1 \rightarrow 0$ CO observations and the long-wavelength dust emission. If, as we suggest, the cool dust is mixed with both the HI gas *and* the outer part of the molecular clouds, a correlation will be found between the 160 μm emission and whichever cool gaseous component (HI or H_2) dominates. For many disk systems, $M(\text{H}_2) \gg M(\text{HI})$ over much of the inner radius of a galaxy, R , and a correlation will be found between the CO emission and the emission from the cool dust in surface layers of molecular clouds. However, since the gas mass increases in proportion to R^2 , for the entire galaxy, $M(\text{HI}) \sim M(\text{H}_2)$ (Table 1). Correlations between *global* parameters, such as that which we report, will then show a strong relation between the sub-millimeter emission and the HI mass.

IV. COMPONENTS OF THE SUB-MILLIMETER DUST EMISSION

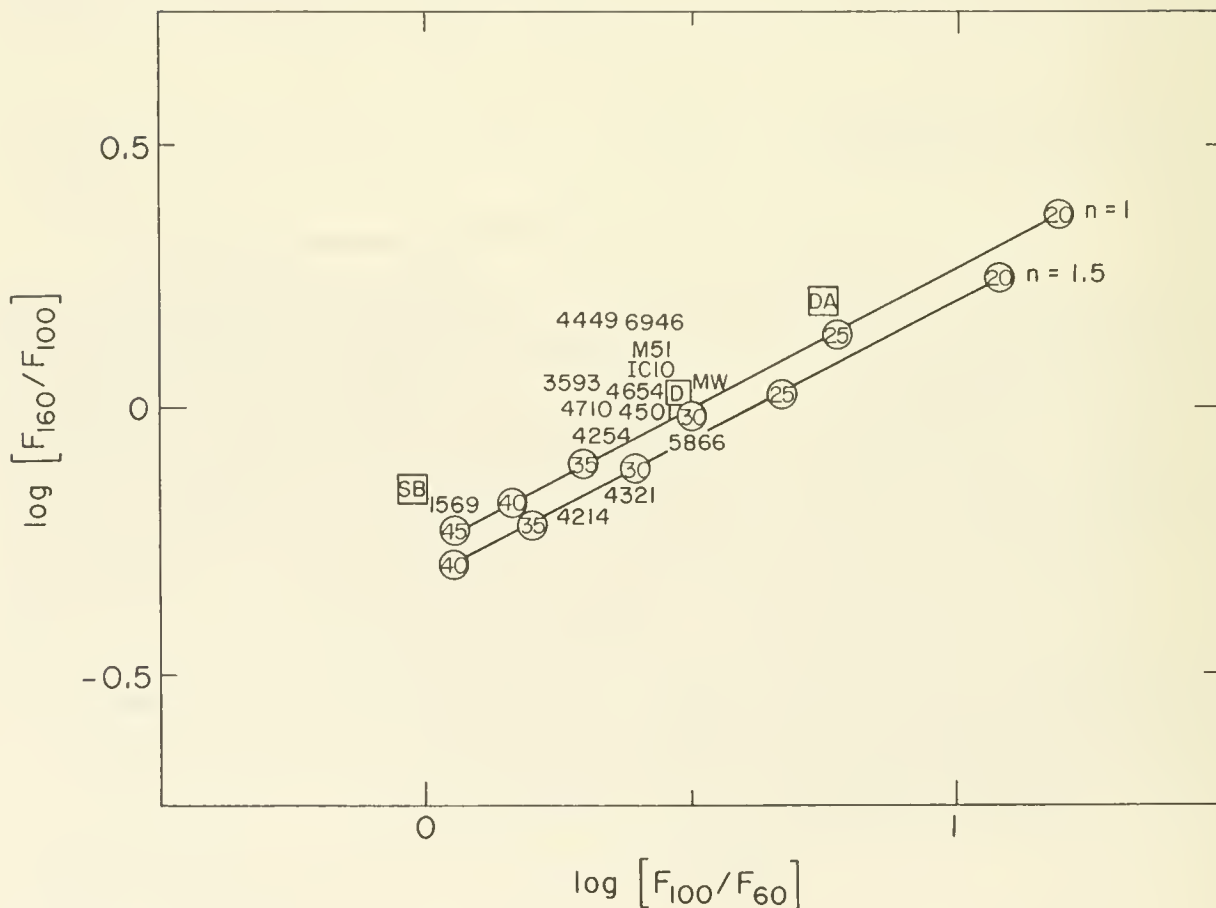
We suggest that emission from a minimum of two dust components is necessary to explain Figure 1 and the global spectra of galaxies between about 50 and 350 μm . Most of the emission longward of about 100 μm commonly arises from the cool dust that we describe above, while the emission over the range 50 - 100 μm includes a contribution from hotter grains, perhaps more intimately associated with HII regions. However, our color-color diagram indicates that as the average interstellar radiation field becomes more intense, as in a “starburst” system such as NGC 1569, the *cooler* dust component becomes more luminous and begins to also dominate the emission at shorter (50 - 100 μm) wavelengths. In our view, dust temperatures, T_d , derived at wavelengths longward of $\sim 100 \mu\text{m}$, including, perhaps, from the 160 $\mu\text{m}/100 \mu\text{m}$ ratio, are plausible estimates of a true dust temperature, as are estimates using wavelengths shorter than about 50 μm (see also Stark *et al.* 1989; Eales, Wynn-Williams, and Duncan 1989). However, T_d derived from emission in the $\sim 50 - 100 \mu\text{m}$ range are specious and are instead sensitive to the relative emission from multiple components of the dusty ISM.

This work was supported by NASA Grant NAG 2-134.

Object	Type	Dist Mpc	M(HI) 10^8 M_\odot	M(H ₂) 10^8 M_\odot	M_d 10^6 M_\odot	L_{160} 10^8 L_\odot	Refs
M51	Sbc(s)	9.6	50	90	18	200	1, 2, 3
NGC 3593	S0/a	12.4	7	15	2.3	3.5	4, 5, 6
NGC 4254	Sc(s)	20	90	110	6.0	180	7, 8, 9
NGC 4321	Sc(s)	20	65	190	3.2	110	7, 8, 9
NGC 4501	Sbc(s)	20	30	180	6.1	140	7, 8, 9
NGC 4654	SBc(rs)	20	55	50	5.1	90	7, 8, 9
NGC 4710	S0 _a (l)	20	0.28	8.8	0.5	25	10, 11
NGC 5866	S0 _a (S)	11	≤ 2.5	3.0	0.4	11	10, 11
NGC 6946	Sc(s)	10.1	110	120	44	300	12, 13

The 160 μm “luminosity” is defined as $L_{160} = 4\pi D^2 \nu F_{\nu}$, with $1 L_{\odot} = 3.85 \times 10^{33}$ ergs s^{-1} . We remind the casual reader who chances upon this note that there are wide, unexplained variations in the definitions of both “luminosity” and L_{\odot} in the literature.

References: (1) Weliachew and Gottesman 1973, (2) Young and Scoville 1983, (3) Smith 1982, (4) Hunter, Gallagher, and Rautenkranz 1982, (5) Thronson *et al.* 1989b, (6) Hunter *et al.* 1989, (7) Huchincier *et al.* 1983, (8) Stark *et al.* 1986, (9) Stark *et al.* 1989, (10) Kenney and Young 1988, (11) Thronson *et al.* 1990b, (12) Tacconi and Young 1986, (13) Smith, Harper, and Loewenstein 1984.



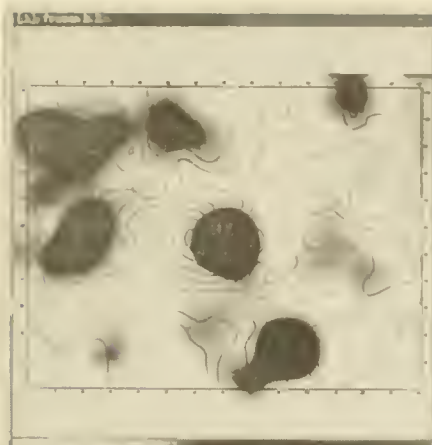


Fig. 2 a

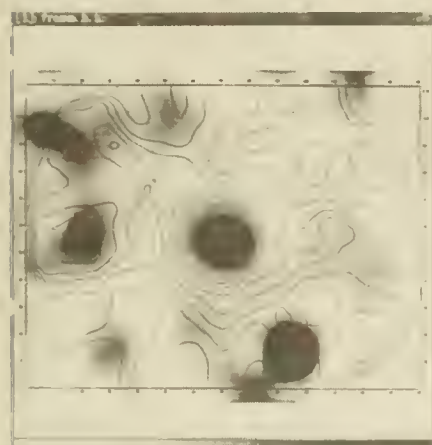


Fig. 2 b

n6946 (250 μ m) Ir=016
Monday, June 5, 1989, 3:33:34 AM

Verkes Infrared

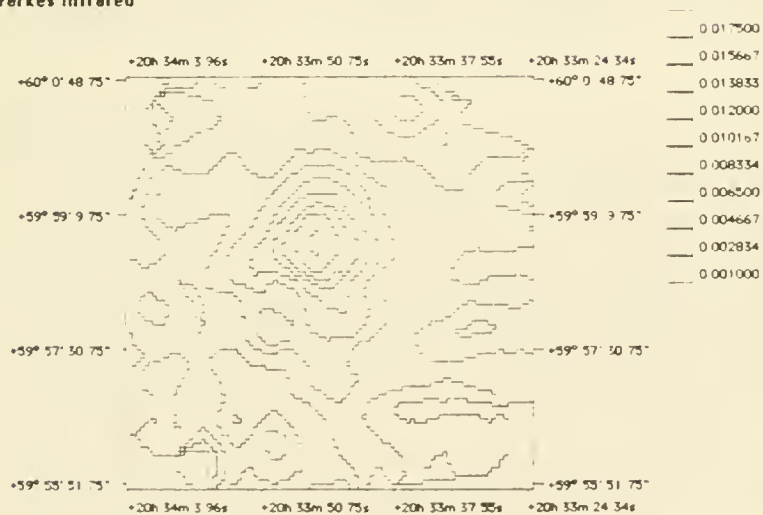


Fig. 4

Fig. 3 a

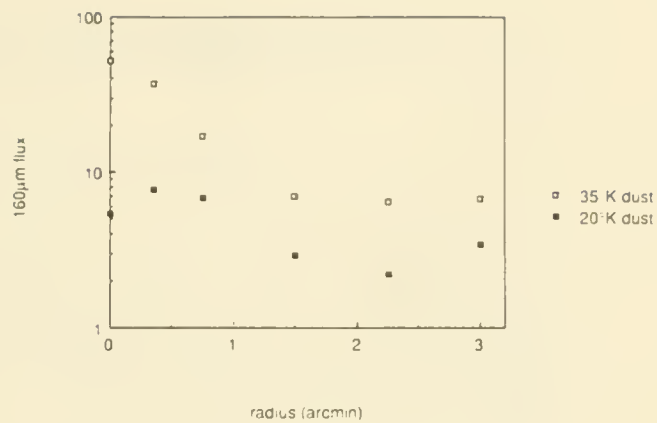
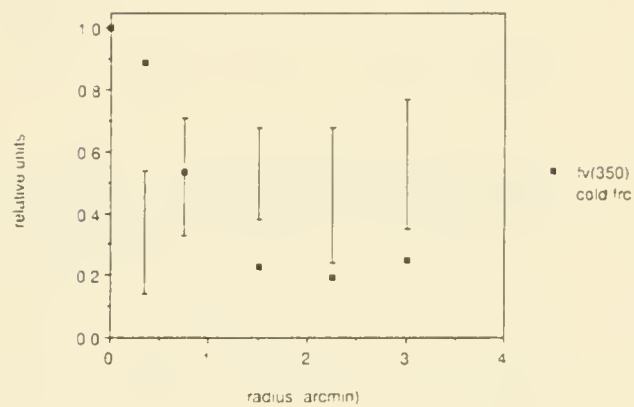


Fig. 3 b



FAR-INFRARED EMISSION FROM DUSTY ELLIPTICALS

DUNCAN WALSH AND JILL KNAPP
Princeton University Observatory

The incidence of dust lanes in elliptical galaxies has been estimated at $\sim 40\%$ by Sadler and Gerhard (1985), although the observed fraction is lower because of inclination effects. A similar percentage of ellipticals has been detected by *IRAS* at $100\ \mu\text{m}$ (Knapp *et al.* 1989); these have far-infrared colors expected for emission from cool dust ($S_{60\ \mu\text{m}}/S_{100\ \mu\text{m}} \sim 1/3$).

Table 1 shows the fractions of ellipticals detected at $100\ \mu\text{m}$ as a function of reported dust. The references are: EDD = Ebner, Djorgovski and Davis (1987); SG = Sadler and Gerhard (1985); Sp = Sparks *et al.* (1985); VC = Veron Cetty and Veron (1987); L = Lauer (1985); and EB = Ebner and Balick (1985). The classifications as ellipticals are taken from Knapp *et al.* (1989). In each case, the dusty galaxies are more often detected by *IRAS* than those with no optical evidence for dust. Part of the reason for this difference may be attributed to the fact that distant galaxies are not likely to be detected at $100\ \mu\text{m}$ or to show the presence of dust. However, it can be shown - by weighting galaxies according to distance - that this is not sufficient to account for the large differences. Hence, not surprisingly, DUST \Rightarrow Far-IR Emission.

For the far-infrared detected galaxies, neither $L_{100\ \mu\text{m}}/L_B$ nor $L_{60\ \mu\text{m}}/L_{100\ \mu\text{m}}$ is very dependent on dust content, suggesting that the source of the infrared luminosity is the same in both cases; and hence that dust is responsible even when not detected optically.

Despite this indication, $L_{100\ \mu\text{m}}$ does not prove to be a good indicator of the quantity of cool interstellar matter in elliptical galaxies, as measured by the mass of neutral hydrogen. (There even exist several examples of ellipticals with dust, strong $100\ \mu\text{m}$ flux density and sensitive limits on H I mass [Walsh *et al.* in preparation].) Chief reasons for the lack of correlation include (1) The existence of other important sources of far-IR power in ellipticals, such as nonthermal continuum emission extending from longer wavelengths in flat spectrum radio sources (Golombek, Miley and Neugebauer 1988). (2) Far-infrared luminosity per unit dust mass is extremely sensitive to the temperature of the ambient radiation field, which is not accurately known.

In addition to having their appearance distorted by dust, several ellipticals also show such features as shells, box-shaped isophotes or inner disks. These may be signatures of past mergers, which could also add to the ISM content of the system. Table 2 shows detection rates for samples of ellipticals belonging to each class. The shell galaxies are from the lists of Thronson, Bally and Hacking (1989); the others are from Nieto (1988). Both the shell galaxies and those with boxy isophotes show enhanced detections relative to the "expected" number (taken to mean the fraction from the comparison sample of Knapp *et al.* [1989] which would be detected if they had the same distance distribution as the small samples in question). However, since (at least for the boxy isophote galaxies) there is a correlation between presence of a "feature" and the blue luminosity, a larger number of ellipticals in each class is needed before the numbers are to be trusted.

This work was supported by NASA under the *IRAS* Extended Mission Project via grant 12010-87 to the University of California at Los Angeles, and by the NSF through grant AST86-02698 to Princeton University.

- Ebner, K., and Balick, B. 1985, *A. J.*, **90**, 183.
 Ebner, K., Djorgovski, S., and Davis, M. 1988, *Ap. J.*, **95**, 422.
 Golombek, D., Miley, G. K., and Neugebauer, G. 1988, *A. J.*, **95**, 26.
 Knapp, G. R., Guhathakurta, P., Kim, D. W., and Jura, M. 1989, *Ap. J. Suppl.*,
 in press.
 Lauer, T. R. 1985, *M.N.R.A.S.*, **216**, 429.
 Nieto, J. L. 1988, preprint.
 Sadler, E. M., and Gerhard, O. E. 1985, *M.N.R.A.S.*, **214**, 177.
 Sparks, W. B., Wall, J. V., Thorne, D. J., Jorden, P. R., van Breda, I. G., Rudd,
 P. J., and Jorgensen, H. E. 1985, *M.N.R.A.S.*, **217**, 87.
 Thronson, H. A., Bally, J., and Hacking, P. 1989, *A. J.*, **97**, 363.
 Veron-Cetty, M. P., and Veron, P. 1988, *Astr. Ap.*, **204**, 28.

TABLE 1
INFRARED DETECTION RATES FOR DUSTY ELLIPTICALS

Reference		Detected at 100 μ m	
EDD	Dust	7/12	(58%)
	Possible Dust	9/28	(32%)
	No Dust	27/78	(35%)
SG	Dust	4/4	(100%)
	No Dust	14/27	(52%)
Sp	Dust	6/7	(86%)
	Possible Dust	1/3	(33%)
	No Dust	8/21	(26%)
VC	Dust	9/10	(90%)
	Possible Dust	2/7	(29%)
	No Dust	24/38	(63%)
L	Dust	3/4	(75%)
	No Dust	18/36	(50%)
EB	Dust	18/23	(78%)

TABLE 2
ELLIPTICALS WITH “FEATURES”

	Detected at 100 μ m		“Expected”
Shells	14/23	(61%)	47%
Boxy Isophotes	13/21	(62%)	47%
Inner Disks	12/28	(43%)	43%
Comparison Sample	202/478	(42%)	—

OBSERVATIONS OF THE GALACTIC PLANE BY THE ZODIACAL INFRARED PROJECT

L. J. Rickard - E. O. Hulbert Center for Space Research
Naval Research Laboratory
Washington, DC

S. W. Stemwedel - Applied Research Corporation
Landover, MD

S. D. Price - Air Force Geophysical Laboratory
Hanscom AFB, MA

The two rocket flights of the Zodiacal Infrared Project (ZIP; Murdock and Price 1985, *Astr. J.*, 90, 375), flown 18 August 1980 and 31 July 1981, were intended to provide data on the near-infrared thermal emission of the interplanetary dust cloud over a broad range of ecliptic coordinates (latitudes -60° to $+85^\circ$, solar elongation angles 22° to 90° and 140° to 180°). In addition, their multiple crossings of the Galactic plane provided low resolution spectral data ($\Delta\lambda/\lambda$ ranging from 1. to 0.1, for effective wavelengths from 3 to 30 μm) for most of the first quadrant (longitudes 30 to 100 degrees). Examples are displayed in figure 1. Having made a thorough reanalysis of the calibration of the ZIP database, we present the salient features of the Galactic plane as observed by ZIP.

The binned, in-plane data, corrected for zodiacal emission, generally show an exponential decrease with increasing longitude. Figure 2 displays this for the 11 μm data. The fitted exponential scale-length is $0.038/^\circ$, and can be inverted to derive a radial density profile. Note as well the appearance of excess emission at 83° arising from material associated with the Cyg-X region.

Channel ratios are converted to temperatures by using model spectra in which thermal emitters with emissivity $\sim\lambda^{-1}$ are convolved with the filter responses. The results for channels 5 (11 μm) and 12 (21 μm) are shown in figure 3, along with similarly derived temperatures from IRAS 12 μm and 25 μm data. The ZIP data show little variation with longitude, consistent with IRAS results.

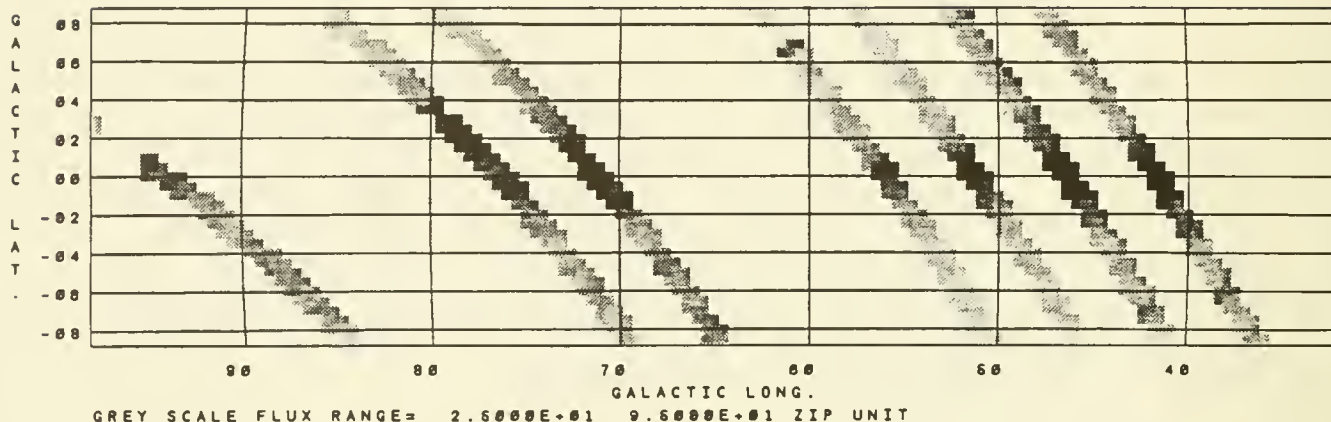
A narrow spectral feature at 13 μm appears consistently in data for the plane (uncorrected for zodiacal emission). However, this is strongly contaminated by calibration problems for channel 8. We suggest that residual emission at 13 μm arises from the [NeII] line at 12.8 μm .

OBSERVATIONS OF THE GALACTIC PLANE BY THE ZODIACAL INFRARED PROJECT

figure 1

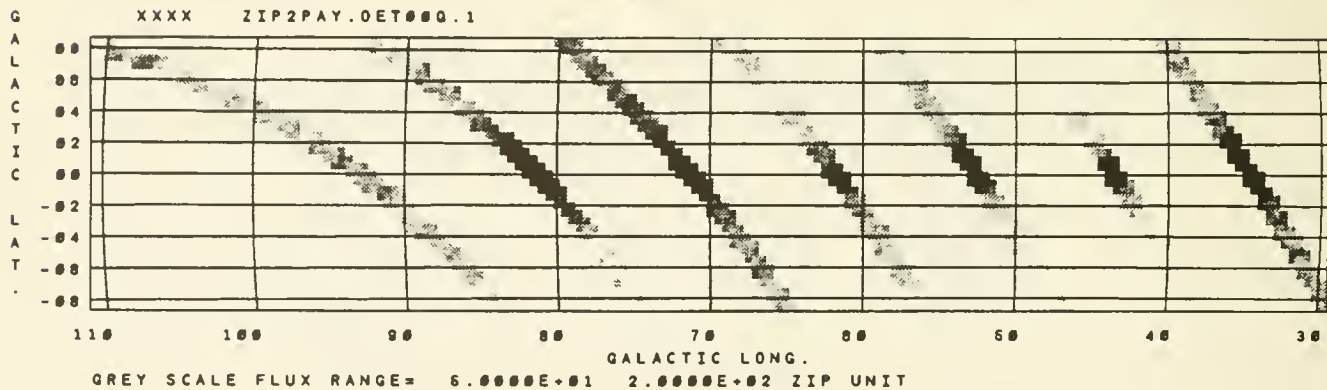
PLOT FILE VERSION 1 CREATED 22-FEB-1989 15:35:59

XXXX ZIP1PAY.DET10G.1

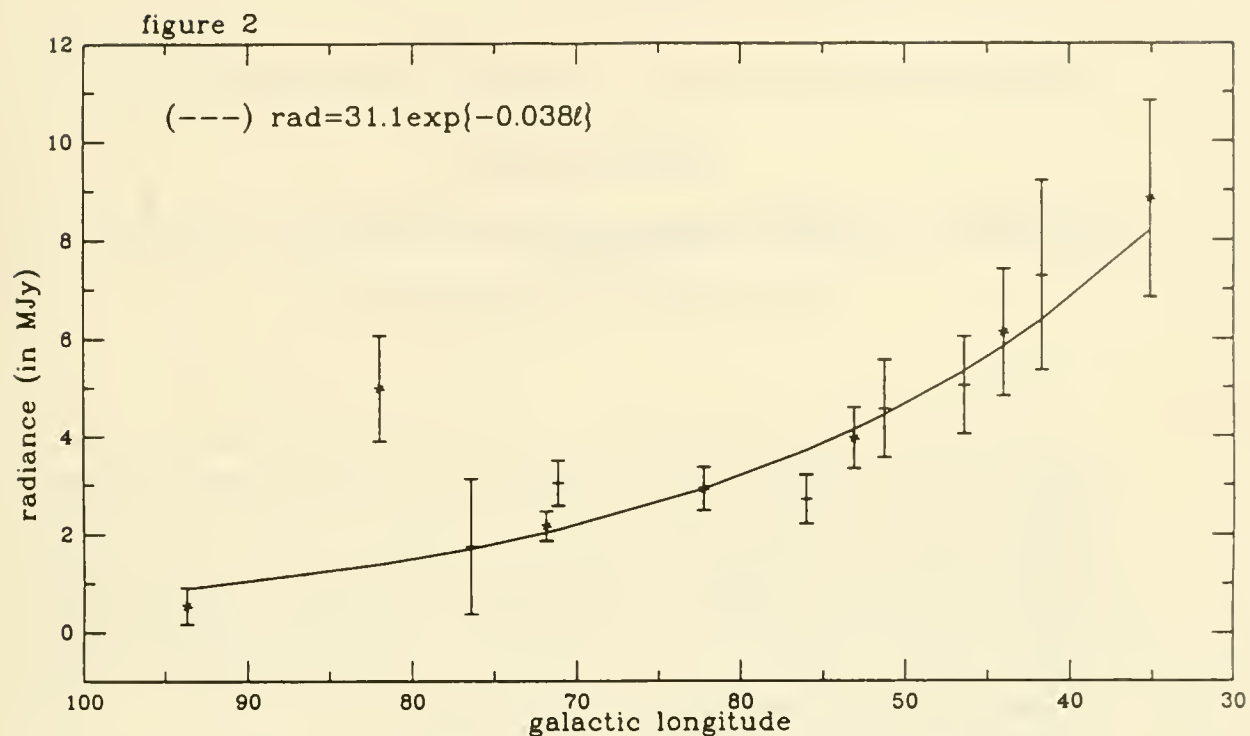


PLOT FILE VERSION 1 CREATED 23-FEB-1989 00:38:12

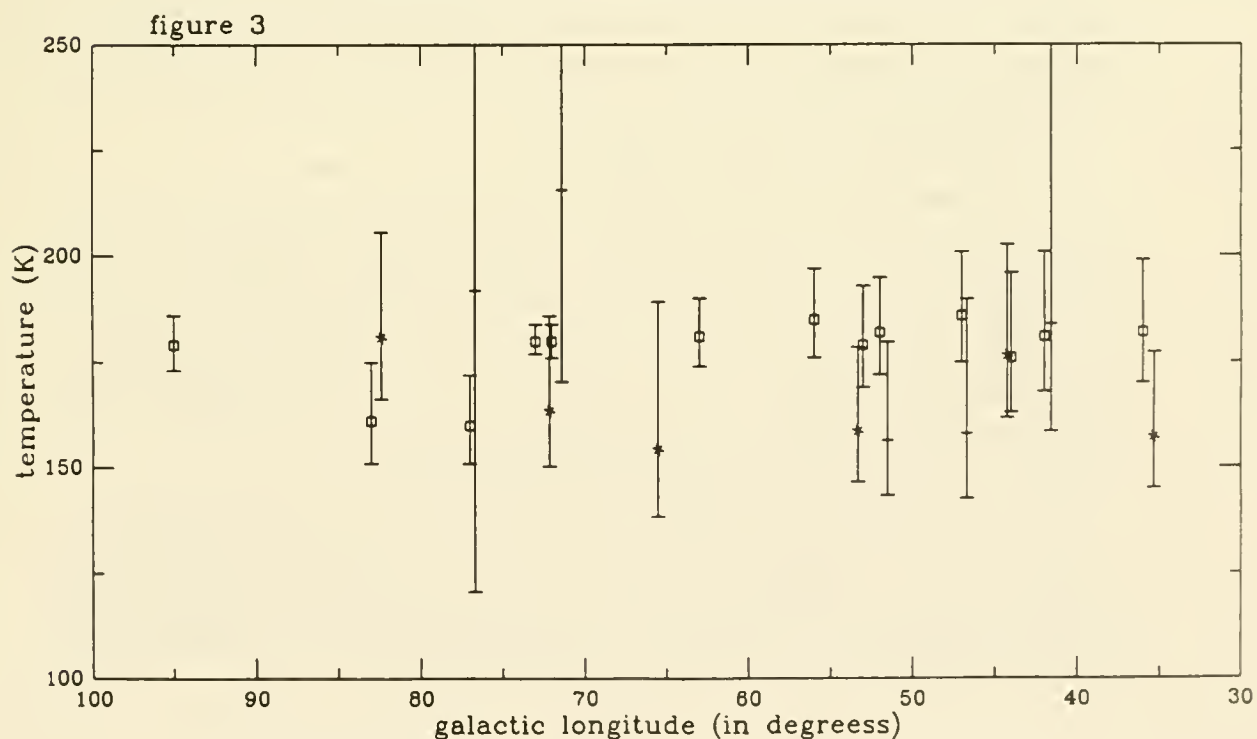
XXXX ZIP2PAY.0ET00Q.1



OBSERVATIONS OF THE GALACTIC PLANE BY THE ZODIACAL INFRARED PROJECT



ZIP 1(+) & 2(*)-DET. 10 GALACTIC CROSSING RADIANCE
WITH 95% CONFIDENCE INTERVAL INDICATED



ZIP TEMPERATURE ALONG GALACTIC PLANE (from D24/D10)

□ IRAS, + ZIP 1 & * ZIP 2 with 2σ indicated

The Infrared Continuum Spectrum of X-Ray Illuminated Molecular Gas

G. Mark Voit

Center for Astrophysics and Space Astronomy
and
Joint Institute for Laboratory Astrophysics
University of Colorado

In starburst galaxies, active galaxies, and the mysterious ultraluminous infrared galaxies, X-rays are likely to interact with molecular gas and dust, thereby inducing infrared emission. X-ray heated thermal dust will emit the IR continuum, and X-ray photoelectrons will excite an IR emission-line spectrum. In this work we model the IR continuum emission characteristic of some selected X-ray spectral fluxes, in particular the X-ray bremsstrahlung characteristic of supernova and stellar wind bubbles shocks in dense media and the power law spectra characteristic of active galactic nuclei. These models are part of a larger project to determine the complete IR spectra, lines plus continuum, of X-ray sources embedded in molecular gas.

For several reasons, the thermal continuum emitted by X-ray heated dust cannot be described by a single temperature. First, the temperatures of smaller grains will fluctuate radically because their typical thermal energy contents will be smaller than the X-ray energy doses they receive. Second, grains of different sizes will attain different temperatures when subject to the same incident flux. Third, as the X-ray flux penetrates the cloud, its intensity will degrade, and its spectrum will harden, giving cooler grains which suffer more extreme thermal transients.

We have modeled the thermal emission from grains by calculating a grain temperature/size/composition distribution function, $f(T, a, \text{Comp.})$, which accounts for temperature fluctuations by averaging over all grain thermal histories. In determining the grain thermal distribution, we account for both direct grain heating (by X-ray absorption and subsequent electron energy deposition) and indirect grain heating (by absorption of the UV emission stimulated by non-thermal photo- and Auger electrons in the gas phase). We let the grain size distribution be proportional to $a^{-3.5}$, and we consider two types of grain composition: graphites, which we assume to be pure carbon, and silicates, which contain all other depleted heavy elements. We derive the grain composition distribution function from solar abundances and interstellar depletion data.

From the function $f(T, a, \text{Comp.})$ we synthesize an emergent IR continuum. To derive an IR spectrum from this distribution, we employ the grain emission efficiencies of Draine and Lee. Therefore, our spectra exhibit the 9.7μ silicate band feature as well as continuum emission. Finally, to generate a complete IR spectrum, we calculate the IR spectra representative of the various column density layers in the cloud and combine them in proportion to the X-ray energy absorbed in each layer.

I - THE COOL ISM

D - THE COOL ISM AND THE NONTHERMAL RADIO CONTINUUM

A COMPARISON OF THE RADIAL DISTRIBUTION OF MOLECULAR GAS AND NON-THERMAL RADIO CONTINUUM IN SPIRAL DISKS.

N.A. DEVEREUX and J.S. YOUNG
*Dept. of Physics and Astronomy
and the Five College Radio Astronomy Observatory
University of Massachusetts
Graduate Research Center
Amherst, MA 01003.*

I. Introduction

Recent observational results suggest a close connection between non-thermal radio continuum emission and star formation in spiral galaxies. The small dispersion in the correlations of the globally integrated 1.49 GHz radio continuum emission with both the global H α emission (Kennicutt 1983) and thermal far infrared emission (Dickey and Salpeter 1984; Helou, Soifer and Rowan-Robinson 1985; Devereux and Eales 1989) constitute the primary evidence in support of a close correspondence between the non-thermal radio power and the intensity of star formation activity. Additionally the radial distribution of non-thermal radio emission closely traces the radial distribution of H α and far infrared emission within the disk of the late-type spirals M 51 (Scoville and Young 1983) and NGC 6946 (Tacconi and Young 1986). On a smaller (~ 0.5 kpc) scale a close correspondence is observed between the morphology of the non-thermal radio continuum and the infrared emission in the nuclei of galaxies (Rieke et al. 1980; Becklin et al. 1980; Gehrz, Sramek and Weedman 1983; Wynn-Williams and Becklin 1985). *Thus the radial distributions of non-thermal radio continuum emission should be viewed as a potentially valuable source of information on the radial distribution of star formation in spiral galaxies.* Furthermore, the radio continuum emission does not suffer from extinction as does the H α emission line tracer.

Since stars form in molecular clouds, the CO emission traces the sites of potential star formation. Following Israel and Rowan-Robinson (1984), it is of interest to compare the CO radial distributions measured in the course of the FCRAO Extragalactic CO Survey with the radial distributions of non-thermal radio continuum emission. Such a comparison will permit an investigation of whether the star formation rate per unit molecular gas, or equivalently, the star formation efficiency, varies with radius in spiral galaxies. A constant star formation efficiency would indicate that the star formation rate is determined by the local cloud properties; on the other hand, radial variations in the star formation efficiency may indicate that the star formation is regulated by a global process such as a spiral density wave or a galaxy-galaxy interaction.

2. Sample and Analysis

The present study includes 65 spiral galaxies selected from the FCRAO Extragalactic CO Survey for which the major axis distributions of CO emission and 1.49 GHz radio continuum emission are well determined. The radial distribution of the CO emission has been measured with the FCRAO at positions along the major axis that are spaced by one HPBW (45"). The radial profile of the 1.49GHz radio continuum emission was constructed by determining the radio emission at the location of the CO measurements from the 1.49 GHz maps of Condon (1987).

3. Results and Discussion

Although the radial distributions of radio continuum and CO emission both decrease by as much as a factor of 100 with increasing radius the *ratio* of radio emission to CO emission appears rather constant. The result is quantified in Figure 1. The histogram shows the mean change in the ratio of radio continuum emission to CO intensity across the disk of 46 spirals for which the CO and radio continuum was detected at at least three independent disk locations.

The histogram is centered on zero. Thus there is no evidence for a systematic increase or decrease in the ratio of radio continuum emission to CO intensity with radius.

The narrow width of the histogram indicates that the ratio of 1.49 GHz radio emission to CO intensity does not vary by more than a factor of three for the majority of spirals in this sample. The small radial gradient is comparable to the radial change in the infrared to radio continuum ratio observed for the disks of N 6946 and M 83. The radial gradient in the infrared to radio continuum emission has been interpreted in terms of cosmic ray diffusion (Bicay, Helou and Condon 1989). The cause for the small radial change in the ratio of radio continuum to CO intensity can not be due entirely to cosmic ray diffusion, however, because the ratio does not systematically increase with radius in all spirals.

The results indicate that the star formation efficiency is not a strong function of radius for the majority of the spirals included in the present study although there are some exceptions. The ratio of radio continuum to CO intensity decreases by over an order of magnitude across the disks of M 82, NGC 488, NGC 660, NGC 2841 and NGC 6503. The radial distributions of radio continuum and CO emission suggest large radially *decreasing* gradients in the star formation efficiency. Similarly large gradients in the H α to CO intensity ratio have been noted in M 82 and NGC 2146 (Young 1988).

Two of the galaxies M 82 and NGC 660 are notable for the high level of star formation in the central region (Rieke et al. 1980; Young, Kleinmann and Allen 1988). The ratio of radio continuum to CO intensity in the central 45" of M 82 and NGC 660 exceeds the mean measured for spiral disks by a factor of 10 and a factor of 3 respectively. Thus in the central region of M 82 and NGC 660 gas is converted into stars at a much higher efficiency than is typically observed for the disks of late-type spirals.

On the other hand NGC 488, NGC 2841 and NGC 6503 are distinguished by an uncharacteristically low star formation efficiency in the outer disk. The three spirals also share an unusual gas morphology in the form of a central depression in the molecular gas distribution or CO "hole". Collectively the five spirals exhibit a number of unique features although it is difficult to identify a single common property that may help explain why the radial gradient in star formation efficiency should be so much larger than that typically observed for spiral galaxies.

4. Conclusion

Large, greater than a factor of ten, radially decreasing gradients in the star formation efficiency are observed for a small percentage, $\sim 10\%$, of the spirals in this sample. The majority of spirals, however, are associated with small gradients in the star formation efficiency that do not systematically increase or decrease with radius. That the star formation efficiency does not systematically decrease with radius tends to argue against a global dynamical mechanism, such as a spiral density wave, for being the *dominant* mechanism triggering disk star formation for the majority of spirals in this sample. The results tend to support the view that the star formation in spiral disks is dominated by a local process that depends more on the molecular cloud properties than the dynamical structure of a galaxy.

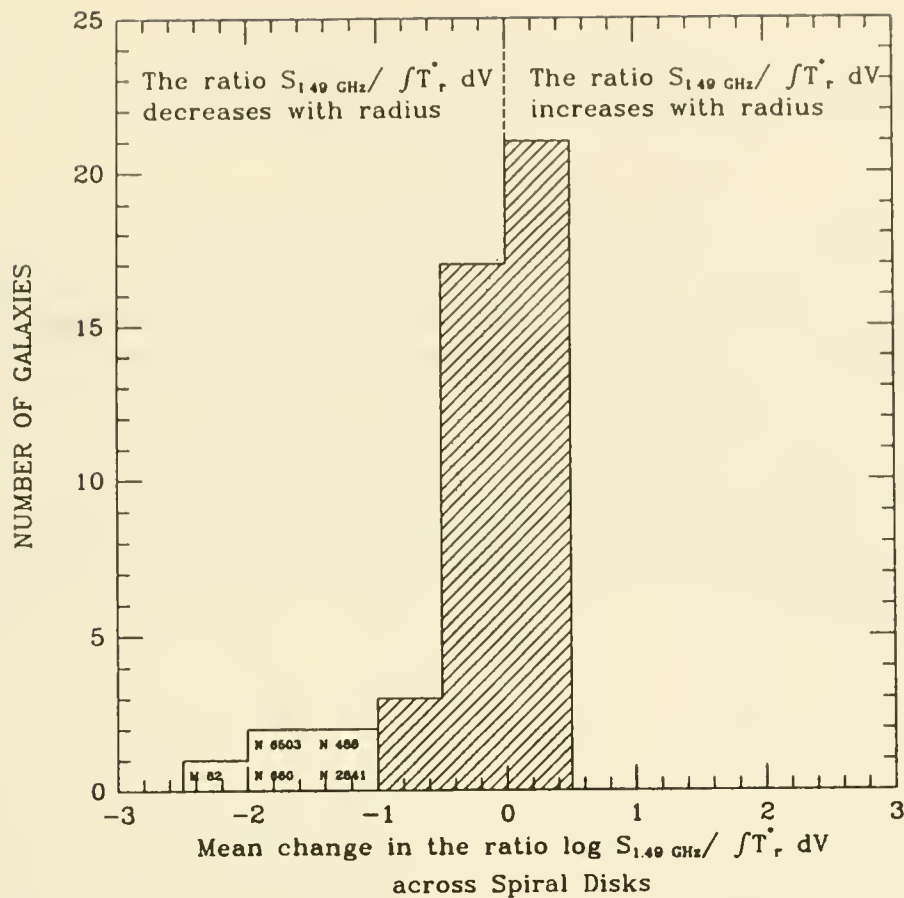


Figure 1. The histogram depicts the *mean* radial change in the ratio of 1.49 GHz radio continuum to CO line intensity across the disks of 46 spiral galaxies.

5. References

- Becklin, E.E., Gatley, I., Matthews, K., Neugebauer, G., Sellgren, K., Werner, M.W., and Wynn-Williams, C.G., 1980, *ApJ* **236**, 441.
- Bica, M.D., Helou, G., and Condon, J.J., 1989, *ApJ (Letters)* **338**, 53.
- Condon, J.J., 1987, *ApJ. Supp.*, **65**, 485.
- Devereux, N.A., and Eales, S. A., 1989, *ApJ* **340**, 708.
- Dickey, J.M., and Salpeter, E.E., 1984, *ApJ* **284**, 461.
- Gehrz, R.D., Sramek, R.A., and Weedman, D.W., 1983, *ApJ* **267**, 551.
- Helou, G., Soifer, B.T., and Rowan-Robinson, M., 1985, *ApJ (Letters)*, **298**, 7.
- Israel, F.P., and Rowan-Robinson, M., 1984, *ApJ* **283**, 81.
- Kennicutt, R., 1983, *Astron. Astrophys.* **120**, 219.
- Rieke, G.H., Lebofsky, M.J., Thompson, R.I., Low, F.J., and Tokunaga, A.T., 1980, *ApJ* **238**, 24.
- Scoville, N.Z., and Young, J.S., 1983, *ApJ* **265**, 148.
- Tacconi, L.J., and Young, J.S., 1986, *ApJ* **308**, 600.
- Wynn-Williams, C.G., and Becklin, E.E., 1985, *ApJ* **290**, 108.
- Young, J.S., 1988, in *Molecular Clouds in the Milky Way and External Galaxies* (ed R.D. Dickman, R.L. Snell, and J.S. Young)

A Relationship Between the Integrated CO Intensity and the Radio Continuum Emission in Spiral Galaxies

D.S. Adler, R.J. Allen, and K.Y. Lo

Department of Astronomy, University of Illinois

In an effort to determine the role played by cosmic ray electrons and interstellar radiation fields on the collapse of molecular clouds, a survey was begun to investigate the relationship between the radio continuum brightness emission and the integrated CO intensity in spiral galaxies. The investigation was done on two scales; a global galaxy to galaxy comparison of integrated disk values, and a ring-averaged study over the disks of individual galaxies.

For the large-scale survey, radio continuum flux densities integrated over the full disk at 1.49 GHz were taken from Condon (1987) and the total CO fluxes were taken from Verter (1985). The galaxies with values included in the two catalogs are displayed in Figure 1. It can be seen that a good correlation exists between the integrated CO emission and radio continuum emission.

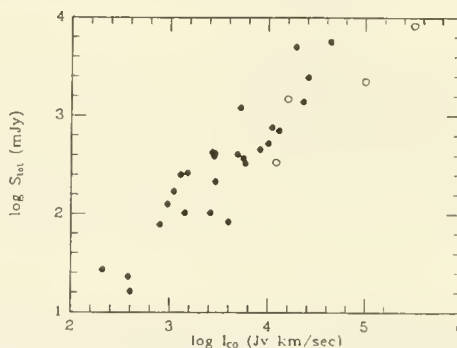


Figure 1. Total radio continuum flux versus total CO flux density for 31 spiral galaxies. Open circles denote galaxies which are missing radio continuum flux.

This is not an unexpected result since the total molecular emission of spiral galaxies has been shown to correlate with several other galactic features. Verter (1988) showed that the total molecular emission depends strongly on galactic scale, with less dependence on galactic morphology. The total CO emission in Verter's sample correlates well with the total HI, $H\alpha$, and far-infrared emission, as well as the blue luminosity. Wielebinski (1988) showed a strong linear correlation between CO luminosity and magnetic field strength for ten spiral galaxies. The non-thermal radio continuum of spirals has been shown to correlate well with the far-infrared luminosity (de Jong, *et al.* 1985). So it comes as no surprise to see the strong correlation between total radio continuum emission and integrated CO intensity as displayed in Figure 1. At least some fraction of these global correlations may be related to a "richness" effect: namely, larger galaxies have more of everything.

The next step was to determine if the relationship holds in the disks of individual galaxies. Since only a few spirals have been adequately observed in CO (see Verter 1985 for a list of galactic CO surveys), this part of the survey was limited to a few of the better studied systems. Table 1 lists the galaxies included in this part of the survey.

Table 1 Galaxy Parameters

Galaxy	D Mpc	i ($^\circ$)	l' on m.a. kpc	radio ref (ν_{GHz})	CO ref	radio beam ($''$) (kpc)	CO beam ($''$) (kpc)	$T_{20}(r/r_0=1)$ K	$\langle I_{\text{CO}}/T_{20} \rangle$ km/sec
M 51	9.6	20	2.8	C87 (1.49)	SY83	54 2.5	50 2.3	5.8	1.06 ± 0.14
NGC 6946	10.1	30	2.9	C87 (1.49)	YS82	48 2.3	50 2.4	4.8	0.96 ± 0.22
IC 342	1.5	25	1.3	GB88 (4.75)	YS82	147 3.2	50 1.1	2.3	1.37 ± 0.30
M 83	9.9	26	2.6	C87 (1.49)	L87	54 2.3	50 2.2	7.7	1.74 ± 0.62
					C78		64 2.8		0.85 ± 0.13
M 81	3.3	59	1.0	B85 (4.75)	B88	147 2.5	60 1.0	0.9	0.64 ± 0.26
M 101	7.2	22	2.1	I75 (1.41)	S83	66 2.3	60 2.1	0.6	1.64 ± 0.73
NGC 253	3.4	78	1.0	K83 (10.70)	S85	71 1.2	50 0.8	8.9	2.39 ± 1.03
M 31	0.7	78	0.2	B82 (2.70)	S85a	264 0.9	102 0.3	0.2	2.15 ± 0.91

The radio continuum data was usually presented in the literature in azimuthally-averaged form, corrected for the inclination of the galaxy. The data taken from Condon's (1987) survey was analyzed using an AIPS ring-averaging routine. Data taken at other frequencies was converted to 1.49 GHz using the published spectral index. Flux densities were converted to brightness temperatures when necessary.

The CO maps were generally less complete than the radio continuum maps. The data usually consisted of four or more radial cuts in a given galaxy. In some instances, exponentials were fit to the data (M 51, IC 342, and NGC 6946); these fits were used in this survey. In most cases, the data were converted to the plane of the galaxy and averaged in galactocentric radial bins. The sampling of the CO maps determined the sampling intervals of the CO to radio continuum ratios in the individual galaxies.

The ratio of integrated CO intensity to 20 cm radio continuum brightness temperature was calculated at each of the sampled radial points for the individual galaxies as shown in Figure 2. For the low-inclination galaxies, I_{CO}/T_{20} is roughly constant over the disk up to radii of 14 kpc. The highly inclined systems (NGC 253 and M 31) show a lot more scatter as well as higher I_{CO}/T_{20} values. In the case of M 31, the linear size of the CO beam (0.3 kpc) is much smaller than the other galaxies in the survey. We don't expect to see a CO - radio continuum correlation on this scale, because of the shift of the CO emission from other phases of the ISM seen in the spiral arm regions (Lo *et al.* 1988; Vogel *et al.* 1988). The radio continuum data for NGC 253 was presented only for the major axis, so the uncertainties with this galaxy may be due to a lack of completeness.

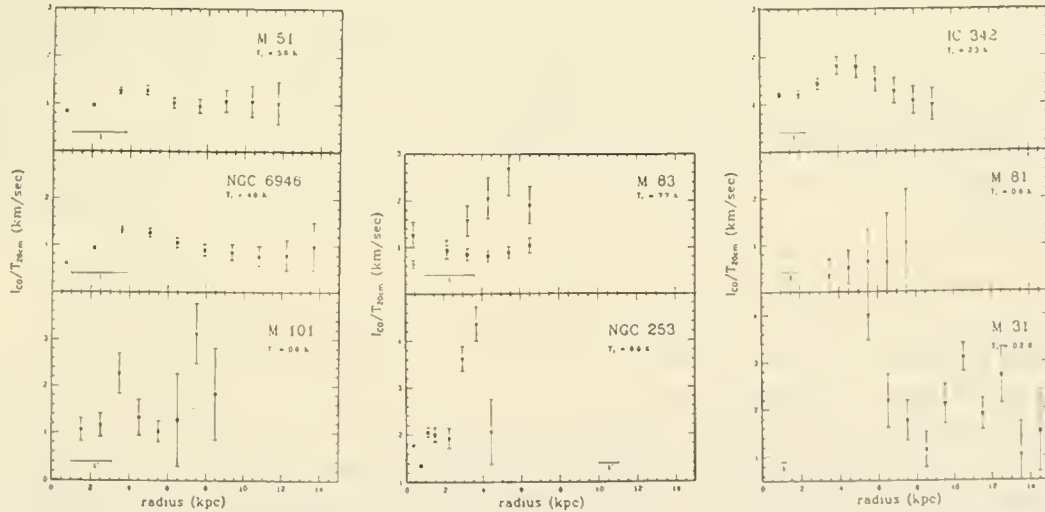


Figure 2. Ratio of integrated CO intensity to 20 cm radio continuum brightness temperature versus galactocentric radius. Error bars correspond to quoted values of the noise in the respective beams. The plot for M 83 includes CO data from L87 (filled circles) and C78 (open circles).

Not only is I_{CO}/T_{20} fairly constant in a given system, but *it also appears to be constant from galaxy to galaxy*. Table 1 lists the average value (and standard deviation) of I_{CO}/T_{20} for the individual galaxies. The average value of the eight galaxies is $I_{CO}/T_{20}=1.50\pm0.60$ km/sec; excluding the two high inclination systems gives a value of 1.35 ± 0.34 km/sec.

This constant value is remarkable when one considers that it holds for almost two orders of magnitude in surface brightness from galaxy to galaxy. Table 1 gives the surface brightness temperature for each galaxy at one scale length of the radio continuum emission. The range of surface brightnesses in the individual galaxies for which the ratio holds constant is also on the order of two magnitudes.

The standard models for the origin of the radio continuum emission relate it to the supernova rate, and therefore the rate of formation of massive stars. Similarly, models for the origin of CO emission relate it to the star formation rate through the formation of molecular clouds. Therefore, one possible explanation for the observed correlation is that these two apparently disparate quantities are both measures of the star formation rate. However, the correlation is all the more surprising when one considers the very different scale heights between the CO emission and radio continuum emission in spiral galaxies.

References

- Baudry, A., Brouillet, N., and Combes, F. 1988, in the Proceedings of the UMASS Conference on Molecular Clouds in the Milky Way and External Galaxies, Dickman, R., Snell, R., and Young, J. eds., Springer Verlag, Berlin, page 403. (B88)
- Beck, R. 1982, *Astron. and Astrophys.*, 106, 121. (B82)
- Beck, R., Klein, U., and Krause, M. 1985, *Astron. and Astrophys.*, 152, 237. (B85)
- Combes, F., Encrenaz, P.J., Lucas, R., and Weliachew, L. 1978, *Astron. and Astrophys.*, 67, L13. (C78)
- Condon, J.J. 1987, *Astrophys. J. Suppl.*, 65, 485. (C87)
- Grave, R., and Beck, R. 1988, *Astron. and Astrophys.*, 192, 166. (GB88)
- Israel, F.P., Goss, W.M., and Allen, R.J. 1975, *Astron. and Astrophys.*, 40, 421. (I75)
- de Jong, T., Klein, U., Wielebinski, R., Wunderlich, E. 1985, *Astron. and Astrophys.*, 147, L6.
- Klein, U., Urbanik, M., Beck, R., and Wielebinski, R. 1983, *Astron. and Astrophys.*, 127, 177. (K83)
- Lo, K.Y., Tilanus, R., Allen, R.J., Wright, M.H., and Jackson, J. 1988, in the Proceedings of the UMASS Conference on Molecular Clouds in the Milky Way and External Galaxies, Dickman, R., Snell, R., and Young, J. eds., Springer Verlag, Berlin, page 439.
- Lord, S.D. 1987, PhD thesis, University of Massachusetts. (L87)
- Scoville, N.Z., Soifer, N.T., Neugebauer, G., Young, J.S., Matthews, K. and Yerka, J. 1985, *Astrophys.J.*, 289, 129. (S85)
- Scoville, N.Z., and Young, J.S. 1983, *Astrophys. J.*, 265, 148. (SY83)
- Solomon, P.M., Barrett, J., Sanders, D.B., and de Zafra, R. 1983, *Astrophys. J.*, 266, L103. (S83)
- Stark, A.A. 1985, in "The Milky Way Galaxy", van Woerden, H., ed. p. 445. (S85a)
- Verter, F. 1985, *Astrophys. J. Suppl.*, 57, 261.
- Verter, F. 1985, *Astrophys. J. Suppl.*, 68, 129.
- Vogel, S.N., Kulkarni, S.R., and Scoville, N.Z. 1988, *Nature*, 334, 402.
- Wielebinski, R. 1988, in the Proceedings of the UMASS Conference on Molecular Clouds in the Milky Way and External Galaxies, Dickman, R., Snell, R., and Young, J. eds., Springer Verlag, Berlin, page 363.
- Young, J.S., and Scoville, N.Z. 1982, *Astrophys. J.*, 258, 467. (SY82)

RADIO CONTINUUM AND FAR-INFRARED EMISSION OF SPIRAL GALAXIES: IMPLICATIONS OF CORRELATIONS

T.N.Rengarajan and K.V.K.Iyengar

Tata Institute of Fundamental Research, Bombay 400 005, India

1. INTRODUCTION

We present a study extending the correlation seen between radio continuum and far-infrared emissions from spiral galaxies to a lower frequency of 408 MHz and also as a function of radio spectral index. The tight correlation seen between the two luminosities is then used to constrain several parameters governing the emissions such as the changes in star formation rate and mass function, frequency of supernovae that are parents of the interstellar electrons and factors governing synchrotron radio emission.

2. DATA

We make use of the 408 MHz catalog of Harnett (1982) and also the 1415 MHz sample of Hummel (1980) for galaxies common to both. The far-IR data are taken from IRAS SES Catalog wherever available, otherwise from IRAS PSC. Out of band correction is applied to get the total emission. In Figures 1 and 2 we show the plots of IR flux against radio flux at 408 and 1415 MHz, for two groupings of α , the radio spectral index. It is seen that at both frequencies there is an almost linear correlation fairly independent of α . We also find that the correlations are similar when derived luminosities are plotted. For both the 408 MHz and 1415 MHz samples, the exponent of correlation is close to unity and $\sigma(RI)$, the dispersion in $\log L(R)/L(IR)$ is 0.21 to 0.29. The 6.3 cm and 2.8 cm data of Wunderlich et al. (1987) also give a linear dependence with $\sigma=0.2$. For this sample also the correlations are independent of radio spectral index; further, they are also independent of morphological type of the galaxies. It is interesting to note that the spectral index between 408 MHz and 6.3 cm and 2.8 cm as derived from the ratio of means of radio to IR fluxes is 0.64, same as that measured from multi-frequency measurements of radio galaxies from a given sample.

3. DISCUSSION

Luminosities in different bands are sensitive to star formation rate (SFR) averaged over different periods (stellar masses). For example, the blue luminosity samples SFR over a few billion years, whereas the far-IR luminosity is an average over a much shorter period. If the SFR and the initial mass function (IMF) were to remain invariant over time, there will be tight correlations between luminosities in different bands. The dispersion in the correlations are, therefore, indicators of changes in SFR/IMF. For our discussion we take the IRAS emission to be a reasonable measure of the warm dust luminosity arising from OB stars (Rengarajan & Iyengar, 1988). We also assume that the radio emission is due to synchrotron radiation from interstellar electrons injected from supernovae (SNe). The IR luminosity is computed by integration over the

product of IMF, the stellar life time, bolometric luminosity and an efficiency factor decreasing inversely as the squareroot of mass. The radio luminosity is proportional to the integrated number of stars above a mass threshold. We summarise the inferences that can then be drawn from the tightness of the correlations.

a) Gavazzi et al.(1986) find that $\sigma(BI) = \sigma(RB) = 0.35-0.4$ where B refers to the blue band. The much higher values of these dispersions as compared to the dispersion in the radio to IR emission implies that unlike the blue emission from longlived stars, both radio and far-IR emissions result from stars of similar masses viz. the high mass OB stars. Since progenitors of Type I SNe are longliving low mass stars as compared to the shortlived parents of Type II SNe, we infer that in spiral galaxies the latter are dominant. This is in accord with the observations of van den Bergh et al. (1987) on SNe frequency.

b) While the far-IR emission results from present day stars, the radio emitting electrons are stored in the galactic disc for about 10 million years; further the SNe are produced at the end of main sequence life-time. The dispersion $\sigma(RI)=0.2$ then implies that bursts of star formation changing the SFR by a factor > 2 and lasting about 10 million years must be rare.

c) The dispersion in the exponent of the IMF for different spiral galaxies corresponding to $\sigma(RI)=0.2$ is 0.3 for $M > 8 M_{\odot}$.

d) The tight correlation of $L(R)$ and $L(IR)$, its lack of dependence on morphological type and the small dispersion in the mean values of $\log L(IR)/L(B)$ for different morphological types imply that the dispersion in the mean frequency of SNe as a function of morphology is 30 percent only.

e) Unless there are correlated variations, the logarithmic dispersion in the confinement life time of electrons is 0.2 while the dispersion in the mean value of magnetic field for different galaxies is still lower, only 0.11.

f) The radio spectral index has a spread from 0.2 to 1.2. Can this arise from a single injected spectrum with a changing power law of the type seen in our Galaxy? The equilibrium electron spectrum can change due to changes in photon density arising from bursts of star formation. It is found that such effects cannot explain indices less than 0.6 unless the magnetic field is \ll a microgauss.

REFERENCES

- Gavazzi, G. et al., 1986, Ap.J.Lett., 305, L15.
Harnett, J.J., 1982, Aust. J. Phys., 35, 321.
Hummel, E., 1980, Astr. Ap. Suppl. Ser., 41, 151.
Rengarajan, T.N. & Iyengar, K.V.K., 1988, J. Ap. Astr., 9, 79.
van den Bergh et al., 1987, Ap. J., 323, 44.
Wunderlich et al., 1987, Astr.Ap. Suppl. Ser., 69, 487.

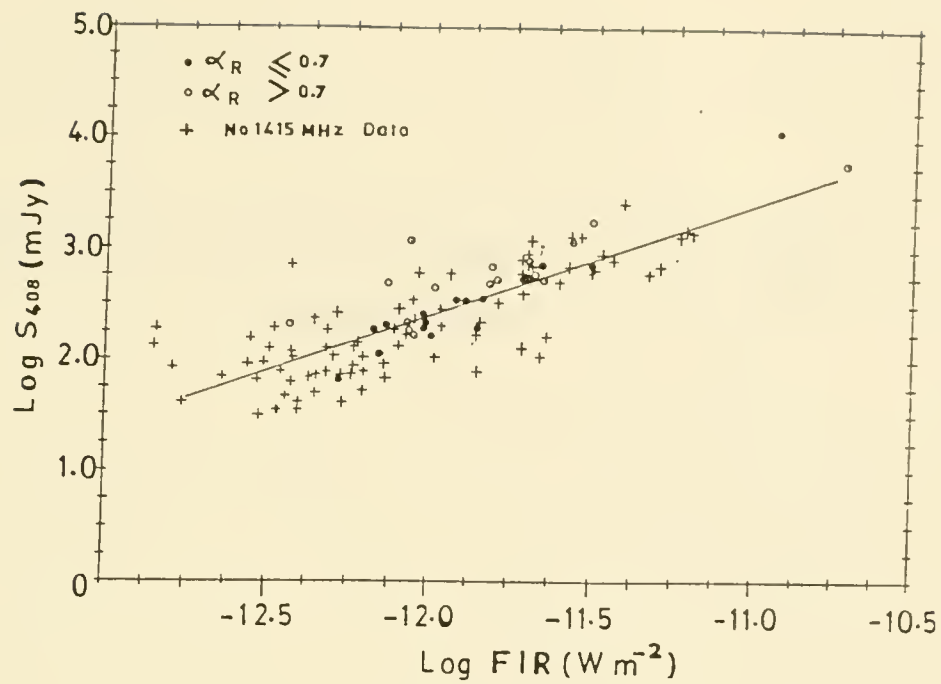


Figure 1

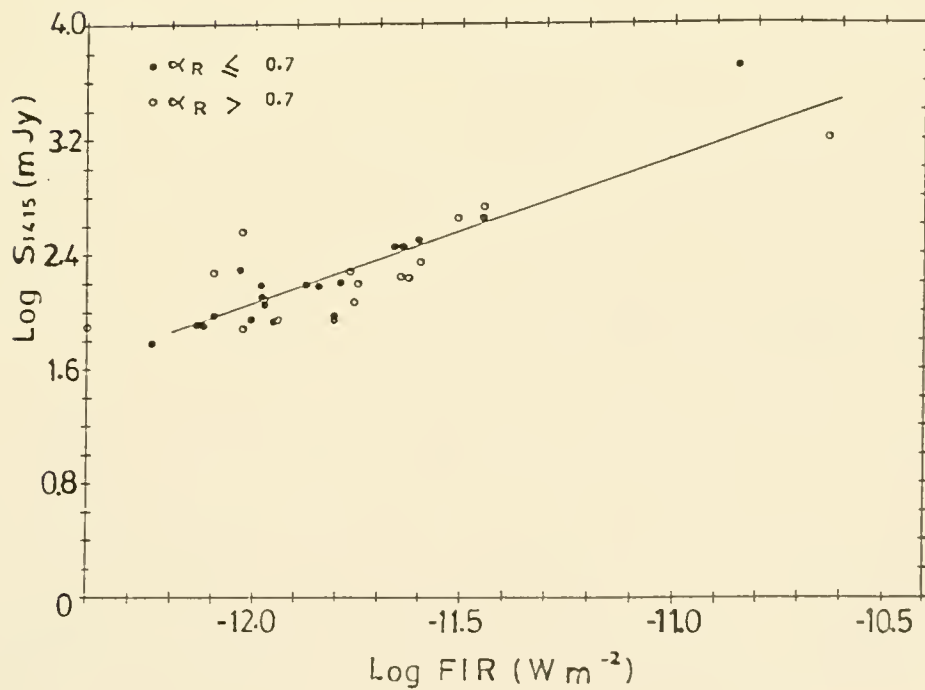


Figure 2

II - HII REGIONS, HALO AND HOT GAS, COOLING FLOWS

A - HII REGIONS

CIRCUMNUCLEAR IONIZED GAS IN STARBURST NUCLEI

YOSHIAKI TANIGUCHI

*Kiso Observatory, Institute of Astronomy, University of Tokyo
Mitake, Kiso, Nagano 397-01, JAPAN*

In order to study kinematical properties of starburst nuclei (SBNs), we made high-resolution spectroscopy of fifteen SBNs in the $H\alpha$ region using an intensified Reticon system attached to the coudé focus of the 188-cm reflector at the Okayama Astrophysical Observatory. The instrumental resolution is 21 km s^{-1} (FWHM) at $\lambda_{H\alpha}$. As for the archetypical SBN, Mrk 538 (=NGC 7714), we present high-resolution emission line profiles of several species of ions such as [OIII], [NII], [SII], and [OII]. Main results and conclusions are summarized as follows.

(1) It has been known that emission-line profiles of SBNs are symmetrical and narrow. However, our high-resolution spectroscopy shows that the observed emission-line profiles of the SBNs have the following asymmetrical patterns; a) *blueward*, b) *redward*, and c) *double-peaked*. It is known that such features have been observed for narrow line regions (NLRs) of active galactic nuclei (AGNs).

(2) There is no remarkable correlation between the asymmetry index (see Heckman *et al.* 1981) and the reddening indicator such as a Balmer decrement. Thus the line asymmetry is not attributed to inhomogeneous obscuration in the emitting regions. Some of the SBNs (*e. g.*, Mrk 52) have the blue wing emission in their spectra, providing evidence for starburst/supernova winds. The double-peaked emission line profiles show that there are more than a few distinct emitting clouds in the SBNs (eg Mrk 1021 and Mrk 1194).

(3) The observed FWHMs of the $H\alpha$ emission lines cover a range from 85 km s^{-1} to 318 km s^{-1} and are slightly larger than those of [NII] $\lambda 6584\text{\AA}$ emission except for the double-peaked SBNs. The FWHMs of $H\alpha$ emission show a good correlation with $\sin i$ (i is an inclination angle of galaxy). This correlation means that the FWHMs of the SBNs suffer significantly from rotational broadening. Mrk 52 is an anomalous SBN because it has narrow emission line widths for its high inclination angle (cf. Taniguchi 1987).

(4) From the above correlation, it is estimated that the intrinsic (*i. e.*, rotation free) FWHMs of $H\alpha$ emission are about 50 km s^{-1} . The least value of FWHMs is 85 km s^{-1} among the sample SBNs. In addition, the FWHMs of the resolved components in the double-peaked nuclei are about 100 km s^{-1} . Thus, we conclude that an intrinsic FWHM of the starburst

regions is about or less than 100 km s^{-1} (i. e., $\sigma \leq 40 \text{ km s}^{-1}$). In summary, a SBN consists of a few or a number of such starburst regions (clumps). The observed line widths suffer the rotational broadening to some extent.

(5) Note that the velocity dispersion of the starburst regions is quite smaller than that of bulges of spiral galaxies ($\sigma > 100 \text{ km s}^{-1}$: cf. Kormendy and Illingworth 1983). Thus the starburst regions are not in dynamical equilibrium with the bulge potential (cf. Feldman *et al.* 1982; Weedman 1983; Whittle 1985). Therefore, it is expected that the circumnuclear starburst regions may be self-gravitating in nature.

(6) As for Mrk 538, the several emission lines ([Osc iii], [NII], [SII], and [Osc ii]) have nearly the same line width (FWHM $\simeq 180 \text{ km s}^{-1}$). Therefore, there is no positive correlation between the line width and the critical density. This implies that the emitting region in this SBN has no stratified structure in contrast to the NLRs of AGNs.

REFERENCES

- Balzano, V. A. 1983, *Ap. J.*, 268, 602.
 Feldman, F. R., Weedman, D. W., Balzano, V. A., and Ramsey, L. W. 1982, *Ap. J.*, 256, 427.
 Heckman, T. M., Miley, G. K., van Bruegel, W. J. M., and Butcher, H. R. 1981, *Ap. J.*, 247, 403.
 Kormendy, J., and Illingworth, G. 1983, *Ap. J.*, 265, 632.
 Taniguchi, Y. 1987, *Ap. J. (Letters)*, 317, L57.
 Weedman, D. W. 1983, *Ap. J.*, 266, 479.
 Whittle, M. 1985, *M. N. R. A. S.*, 213, 1.

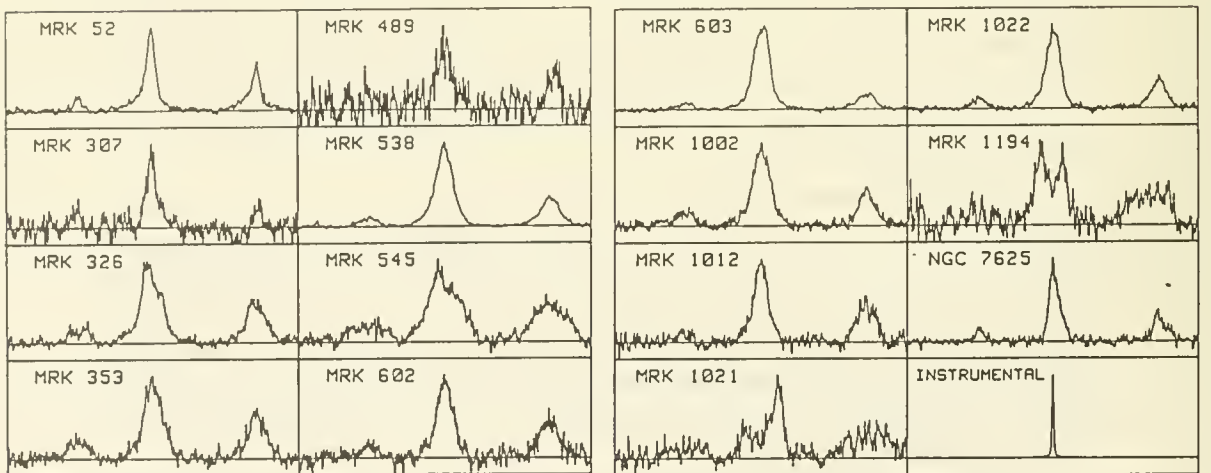


Fig. 1 . The emission line profiles of starburst nuclei in the $H\alpha$ region. A typical instrumental profile (FWHM = 21 km s^{-1}) is shown in the lower-right corner.

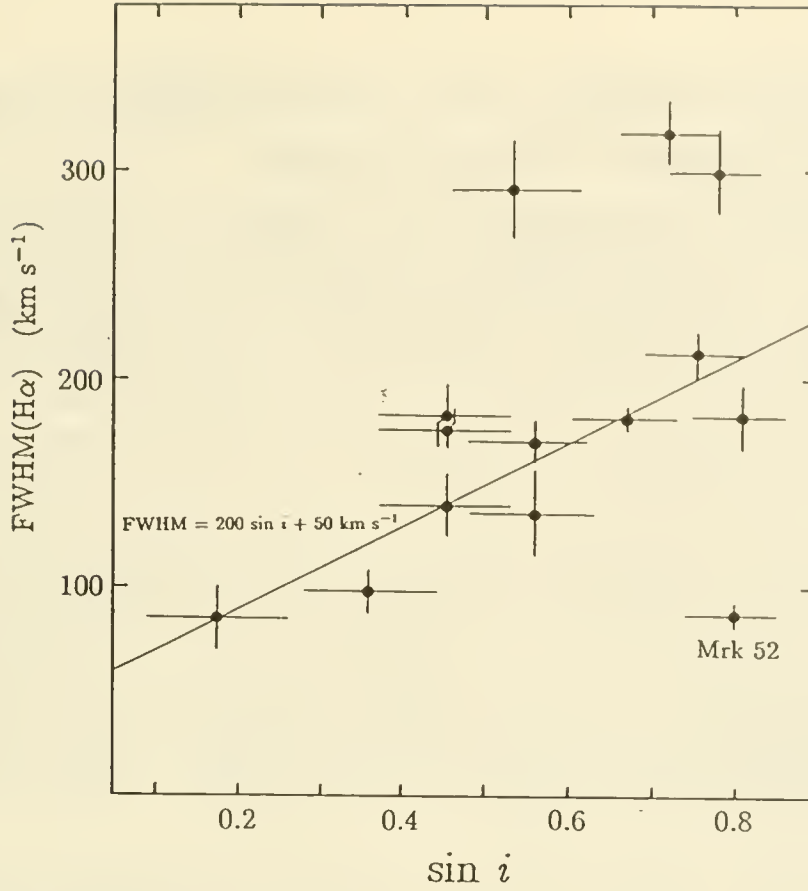


Fig. 2 . A diagram of FWHM versus $\sin i$ (i is an inclination angle of the galaxy. Except the double-peaked SBNs and Mrk 52, the data are approximately fitted by a relation $\text{FWHM} = 200 \sin i + 50 \text{ km s}^{-1}$.

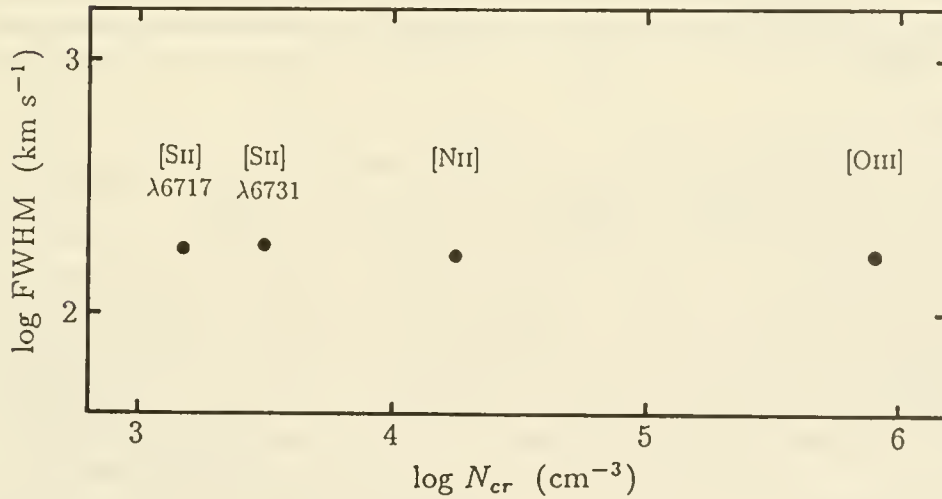


Fig. 3 . A diagram of FWHM versus critical density for the forbidden emission lines for Mrk 538 (= NGC 7714).

IMAGING SPECTROPHOTOMETRY OF THE NUCLEAR OUTFLOW OF NGC 1068

Gerald Cecil, *Institute for Advanced Study*, Princeton NJ 08540

This observational program (in conjunction with R. B. Tully [*IfA*, Honolulu], and J. Bland [*Rice U.*, Houston]) aims to constrain the kinematic organization and dominant excitation mechanisms of ionized gas in active galaxies. More generally, we are interested in the dynamics of radiative, supersonic flows in the ISM. Imaging Fabry-Perot interferometers and low-noise CCDs are used for complete spatial coverage of the complex gas distribution in circumnuclear narrow-line regions (NLRs). Extranuclear emission line widths in NLRs can exceed 3000 km s^{-1} , so to avoid inter-order confusion we use an etalon of 4000 km s^{-1} free spectral range to map $[\text{N II}]\lambda\lambda 6548, 6583$ and $\text{H}\alpha$. To maximize spatial resolution, we select nearby active systems independent of luminosity but known to possess interesting morphologies and/or high-velocity extranuclear ionized gas. Monochromatic images (FWHM $\sim 65 \text{ km s}^{-1}$) have thus far been obtained in $1''$ or better seeing at the U. Hawaii 2.2m, CFH 3.6m, and CTIO 4.0m telescopes. These are stacked into grids of line profiles, of spectrophotometric quality, at sub-arcsecond increments across a $3'$ field. To handle the $\sim 20,000 - 300,000$ useful spectra that arise from a typical night's work, we have developed a complete analysis and reduction package for VAX and Sun image workstations. Reduction involves parametrization of $\sim 10^8$ raw data points to a few maps (e.g. velocities of each kinematic subsystem, continuum-free line fluxes) containing $\sim 10^5$ pixels. We identify kinematic and structural symmetries by examining these maps and the point to point variations of the synthesized line profiles. The combination of monochromatic images and full spatial sampling of line profiles has allowed us to isolate such symmetries and has led to reliable kinematic deprojections.

The spatially extended NLR ($\sim 6''$ radius) of NGC 1068 was mapped in N^+ with high spatial resolution ($0.''8$ FWHM) at $f/8.6$ on the U. Hawaii 2.2m telescope. After subtracting the stellar continuum at each point, I summed the monochromatic images to generate a view equivalent to that obtained with traditional narrow-band interference filters. The NLR aligns with the jet axis, but correspondence to the radio structure is vague. The stacked images synthesize emission line profiles at sub-arcsecond spatial and $\sim 140 \text{ km s}^{-1}$ velocity resolution. Regularities in our spectra allow decomposition of the profiles into discrete kinematic subsystems. These were noted by other observers in slit spectra, but flux distributions and kinematics can now be tracked across the entire NLR and show obvious connections with the radio structure (Fig. 1). Our complete coverage allows detailed study of possible interactions of the prominent collimated radio "jet" and associated wind with the warm ionized component of the ambient ISM.

I find three major *dynamically distinct* kinematic subsystems in this NLR:

- 75% of the total dereddened NLR $[\text{N II}]$ flux ($\sim 12,000 [10^5 \text{ cm}^{-3} / n_e] M_\odot$) is contained in high-velocity gas (Fig. 1a), with approximately equal mass distributed a) to the NE, as a pair of components whose centroids are displaced symmetrically about systemic velocity by $\pm 500 \text{ km s}^{-1}$, with FWHMs $\sim 750 \text{ km s}^{-1}$; and, b) everywhere else within $4''$ radius, as a broad component with FWHM $\sim 1200 \text{ km s}^{-1}$. Double-peaked line profiles and rapid intensity gradients are found when the jet decollimates at hotspots NE and SW of the nucleus. The deprojected emission distribution shows that the radio jet is enveloped by a thick (FWHM $\sim 3.''3 = 230 \text{ pc}$), center-darkened, cylinder of line emission (Fig. 2). The most intense gas emission is concentrated in a thick, conical shell with Gaussian centroid and dispersion $1/4$ of the cylinder radius ($\approx 5'' = 370 \text{ pc}$). The cone has opening angle 85° and axial inclination 80° to the line of sight (so its axis is inclined $\sim 40^\circ$ above the disk plane in the NE quadrant); the jet axis lies closer to the disk plane. Intrinsic gas velocities approach 2000 km s^{-1} w.r.t. systemic; have form $r^{0.6}$ with r the cylindrical radius from the jet axis; and so are inconsistent with a

constant velocity conical outflow. The emitting filaments are optically thick (because [O III] and [N II] profiles are similar out to radii of several arcseconds), with internal extinction. The surprisingly good agreement between modeled and observed profiles shows that profile structure is here primarily driven by geometry. Because no line broadening is incorporated or required in the model, the large extranuclear line widths in this NLR arise exclusively from geometric projection and spatial averaging of an asymmetric, large-scale flow, with *no evidence for intrinsic “turbulence” in the outflowing material*. If the filaments are confined by a directed, outflowing thermal galactic wind, their masses are $\geq 10^{-2} M_{\odot}$, showing that they are not BLR clouds blown to observable radii. Instead it appears that molecular cloud cores with average densities of $\sim 10^3 \text{ cm}^{-3}$ (as derived from CO interferometry) are forced by the stellar bar (prominent in near-IR images) from radii $\sim 20''$ into the inner NLR. There they are exposed to the wind, and the resulting surface instabilities strip their envelopes. The envelope fragments are crushed to densities of $\sim 10^5 \text{ cm}^{-3}$ during wind acceleration, until each fragment attains pressure equilibrium with the shocked wind. The fragments are stable to thermal evaporation in the hot confining medium for the masses and velocities derived from our observations.

- Gas near systemic velocity is concentrated in the kinematic “flare” which coincides with the NE radio lobe (Fig. 1b); is edge-brightened, particularly along the NW edge of the lobe (leading w.r.t. galactic rotation); accounts for 8% of the total NLR [N II] flux ($\sim 1.2 \times 10^5 [10^3 \text{ cm}^{-3} / n_e] M_{\odot}$), but negligible kinetic energy; and is also apparent in H α images, so is a mass enhancement. In projection this component is contiguous with high-velocity gas in the NE radio lobe, yet the only kinematic deviation from the bar-forced flow field defined by gas in the large-scale disk is localized in an expanding “ripple” around the base of the NE cone (Fig. 1d), with kinetic energy $\sim 10^{51}$ ergs, which appears to be a stand-off shock between massive, inflowing molecular clouds and their wind-accelerated fragments.
- 9% of the total NLR [N II] flux ($\sim 1000 [10^5 \text{ cm}^{-3} / n_e] M_{\odot}$) is emitted by a component which dominates within $1''$ of the nucleus, and extends to $2''$ radius along $\sim 110^\circ$ P.A. (Fig. 1c). Its centroid is blue-shifted by $\sim 250 \text{ km s}^{-1}$ from systemic, and has line width $\sim 600 \text{ km s}^{-1}$ (i.e. typical of a Seyfert 2 galaxy). In the absence of a wind/ISM interaction we argue that this component would be the only manifestation of the active nucleus. Our highest-resolution images show a tight correlation of the brightest line emission with the nuclear triple radio-source ($\sim 0.''7$ extent), in agreement with speckle line-imaging.

In summary, the combination of monochromatic images and full spatial sampling of line profiles allows kinematic decomposition of this NLR into dynamically distinct subsystems, and mapping of the flux and velocity distributions of each component. The global kinematic structure of the high-velocity outflow shows well defined, large scale symmetry. Deprojection increases kinetic energies ten-fold to $\sim 2 \times 10^{53}$ ergs, and outflow velocities to 1900 km s^{-1} . The appearance of this NLR changes dramatically as the velocity resolution improves from the 1000 km s^{-1} (25 \AA) passbands traditionally employed in interference imaging to the 65 km s^{-1} resolution attained with our current etalon. Sharply defined, bright features exhibit sharp *kinematic* boundaries, and thus resemble not static, photoionized nebulae, but rather the shocked termini of hydrodynamic flows. These patterns indicate that, *down to the smallest observed scales*, the spatial morphology, kinematics, and bulk of the (kinetic and turbulent) energy of the near-nuclear ionized gas are apparently driven by the thermalization of a directed nuclear outflow along well-defined shock fronts in the ambient ISM. Relativistic electrons trace only a small fraction of the outflow. By its spatial extension the NLR of NGC 1068 provides a unique opportunity to study the dynamics of a supersonic flow in an active nucleus. *HST* will soon image NLRs in great detail, but only with second generation instrumentation will it be possible to produce kinematic maps.

We thank J. Ulvestad for the radio map and H. Thronson for the *K*-band image. This phase of our research was supported by grants NSF 86-15974 (Hawaii) and NAS8-32902 (IAS).



Fig. 1 Kinematic Subsystems in the NLR of NGC 1068

(Main figure) The large-scale disk kinematics in [N II] and H α . A total velocity range of $\pm 160 \text{ km s}^{-1}$ is spanned by 2 cycles of the grayscale, which wraps near systemic velocity. We find a (KMA, disk inclination) of $(85, 35)^\circ$ respectively, E approaching. The $2.2\mu\text{m}$ continuum image of the stellar bar is contoured on top. The Z-shape in the center is characteristic of a bar-forced gaseous disk; the boxed region is enlarged in inserts (a-d) which plot distributions of flux (a-c) and velocity centroid (d).

(a: upper left) High-velocity gas accounts for most of the NLR mass and kinetic energy, with $\sim 75\%$ tightly aligned with the linear part of the radio jet. Symmetries in the NLR profiles and monochromatic images suggest conical expansion of gas about the jet, with deprojected velocities $\sim 1900 \text{ km s}^{-1}$. 6cm continuum contours are overplotted.

(b: upper right) Ambient LSM interacting with the expanding radio lobes. Material is found:

a) NE of the nucleus in a narrow velocity ($< 60 \text{ km s}^{-1}$ FWHM) feature; and b) in an optical hotspot with somewhat broader lines, at the southern end of the linear part of the radio jet. In detail, both features are edge brightened along the leading side w.r.t. galactic rotation.

(c: lower right) The nuclear component has FWHM $\sim 600 \text{ km s}^{-1}$ and extends along 100° P.A.

(d: lower left) Kinematic response of the gaseous disk to the nuclear outflow. The 'ripple' across the base of the NE radio lobe (80 km s^{-1} difference) is the only deviation from the large-scale, bar forced flow.

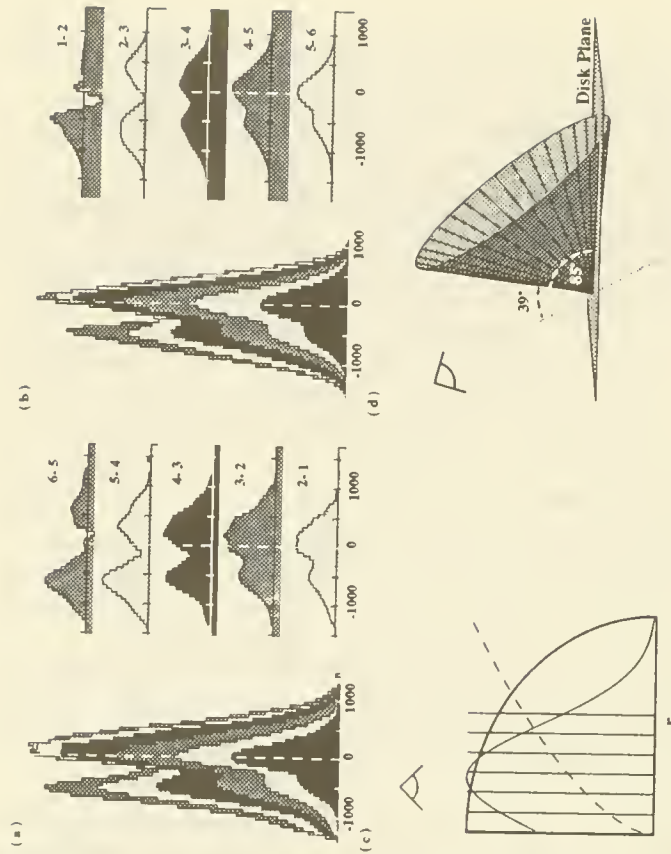


Fig. 2 Geometry of NGC 1068 Outflow

(a) Observed profile swath across the base of the NE radio lobe, averaged in a $(1, 0.5)''$ box (along, across) the jet. Velocities relative to systemic. This profile structure constrains the outflow geometry.

(b) Model profile swath from a cylindrically expanding flow, with velocity dependence $r_{0.6}^{0.6}$ and Gaussian emissivity centroid and dispersion 20% of the cylinder radius r ; smoothed to the velocity resolution ($\sim 140 \text{ km s}^{-1}$ FWHM) and spatial sampling ($0.48''$) of the data. The emitting clouds are assumed to be optically thick, and to absorb 60% of the incident nuclear ionizing flux.

(c) A slice through the outflowing cone, showing sample points (vertical bins) and the radial dependence of gas (emissivity, velocity) with (solid, dashed) lines. Note that emission drops on the jet axis.

(d) Schematic of inferred NLR geometry. Plane (c) intersects the cone parallel to the line of sight. The cone extends $\sim 6''$ NE of the nucleus.

LARGE SCALE EXCITATION OF THE ISM IN NGC 1068

J. Sokolowski,¹ J. Bland,¹ G. N. Cecil,² and R. B. Tully³
¹Rice University, ²Princeton University, ³University of Hawaii

ABSTRACT:

We have shown that photoionization by the continuum of the hidden Seyfert I nucleus in NGC 1068 can have a significant effect on the ionization state and energetics of this disk's ISM. Photoionization models with appropriate power law spectra can produce [NII] $\lambda\lambda$ 6538, 6584/H α line ratios of 1.25 for ionization parameters $Q \sim 10^{-12}$. However our data indicate large regions where the [NII]/H α ratio is 1-3. Since the abundances are known to be solar, there must be additional heating sources. Hardening of the incident radiation field by intervening absorption should be able to raise T_e , thereby raising the [NII]/H α ratio. Heating with moderate efficiency by the intense starburst ring should also be a significant factor in raising the temperature of the ISM. Our photoionization models with additional heating predict enhanced emission from other forbidden lines including [OII] λ 3727 and [SII] λ 6731.

INTRODUCTION:

NGC 1068 is a prototypical Seyfert II galaxy which has been the subject of considerable study due to its close proximity and wealth of interesting activity. There exists in the inner 15".0 a bipolar radio jet, a stellar bar as well as an elliptical ring of intense star formation, with semi-major axis parallel to both the bar and radio jets. That NGC 1068 harbors a hidden Seyfert I nucleus has been established by the detection of a typical broad-lined spectrum in scattered polarized light [Antonucci and Miller, 1985] as well as by the detection of broad Fe II nuclear line emission [Snijders, Netzer and Boksenberg, 1986]. Theoretical work [Krolik and Begelman, 1986] suggests that the Seyfert I nucleus is hidden from view by an optically and geometrically thick torus, which is the source of an electron wind boiled off of its inner surface. Detailed kinematical analysis of our Fabry-Perot data indicate that this torus has an opening angle of $\sim 85^\circ$, and symmetry axis inclined 35° out of the plane of the disk. This implies that the Seyfert I nucleus beams substantially into the disk. NGC 1068 has been found to contain considerable quantities of spatially extended high excitation gas, particularly toward the northeast quadrant. Evans and Dopita, studying HII regions in NGC 1068 [Evans and Dopita, 1986], have determined that their abundances are solar and their spectra are superpositions of a normal HII region component as well as a high excitation one, characterized by excessive [NeV] λ 3346, 3426 and He II λ 4686 emission.

Our data were obtained using the Hawaii Imaging Fabry-Perot Interferometer (HIFI) [Bland and Tully, 1988]. Summations over the separate monochromatic flux images in both H α and [NII] $\lambda\lambda$ 6538, 6584, produce complete H α and [NII] flux maps (see Fig. 1a). A flux ratio map of [NII]/H α (see Fig. 1b) is characterized by regions where [NII]/H α < 0.5 , with line widths of ~ 100 km/sec, and by kinematically distinct, high excitation regions where $0.5 < [NII]/H\alpha < 3.0$, with line widths typically ~ 350 km/sec.

LARGE SCALE EXCITATION:

1. Photoionization and heating by a Seyfert I power law continuum

The 100 eV to 10 keV nuclear spectrum of NGC 1068 can be characterized by a two component power law. To determine the shape of the spectrum throughout the disk of NGC 1068, we have employed a Monte Carlo calculation to simulate the scattering of radiation out of the beaming cone over the energy range of 7.5 eV - 1 MeV. The direct radiation within the beaming cone, as well as that scattered into the disk outside of the cone are given in Table I. Due to the

energy independence of low energy Compton scattering the spectral index for the 0-5 keV component does not change. At higher energies the energy dependence of both the cross-section and the energy transfer to the electron tend to steepen the spectral slope.

TABLE 1.		
ENERGY RANGE	SPECTRAL INDEX	FLUX AT 13.6 eV (ergs/cm ² sec Hz)
Within Cone		
0 - 5 keV	2.0	2×10^{-15} (1 kpc/D) ²
5 keV - 1 MeV	0.62	1×10^{-18} (1 kpc/D) ²
Outside Cone		
0 - 5 keV	2.0	1×10^{-17} (1 kpc/D) ²
5 keV - 1 MeV	0.81	5×10^{-21} (1 kpc/D) ²

We have used the general purpose ionization code MAPPINGS [Evans and Dopita, 1985] to investigate the ionizing effects of such an input spectrum. We have modeled the photoionization by a geometrically thin spherical shell with volume filling factor 0.1 and density 1 cm⁻³. Since the code has a high energy maximum of 5 keV we have chosen a spectral index of 2.0. We find that we are able to generate [NII]/H α ratios of up to 1.25 for ionization parameters $Q \cong 10^{-12}$ where Q is defined by

$$Q = \frac{1}{N_{\text{tot}}C} \int_{13.6\text{eV}}^{5\text{keV}} \frac{J_{\nu}}{h\nu} d\nu$$

However these models can not simultaneously generate the high values of [NeV] $\lambda\lambda 3346, 3426$ and HeII $\lambda 4686$ emission seen in the Evans and Dopita data. These values require ionization parameters an order of magnitude greater or more, indicating that these emissions may be spatially distinct.

We have calculated the Compton heating caused by photons of energies greater than 5 keV. For typical cooling rates for ionized gas of 10^{-24} N_e² ergs/cm³ sec, we find that the additional Compton heating in the cone will only be significant for ionization fractions less than 10^{-1} and/or at very low densities, whereas the Compton heating off of the cone should be negligible under all realistic physical conditions.

2. Heating by the Starburst Ring:

It is difficult to determine the direct heating effect of the starburst ring on the extended disk of NGC 1068 due to the undetermined geometric and starburst parameters. However an estimate may be made by scaling up the starburst of M82 which is better understood. Using a scaling factor equal to the ratios of the IR luminosities of these two starburst systems, we can determine the SN rate in NGC 1068 to be $\cong 0.75/\text{yr}$, which can generate $\cong 2 \times 10^{43}$ ergs/sec. Assuming a 3 kpc radius and 1 kpc thickness for the hot disk of NGC 1068 with a filling factor of 0.1 and mean filament density of 1 cm⁻³, we need $\sim 1\%$ efficiency in converting SN energy into heat in the disk, to have a heating rate of 10^{-24} ergs/cm³ sec, comparable to that of canonical heating/cooling rates.



Fig. 1a. Total H α Flux Map

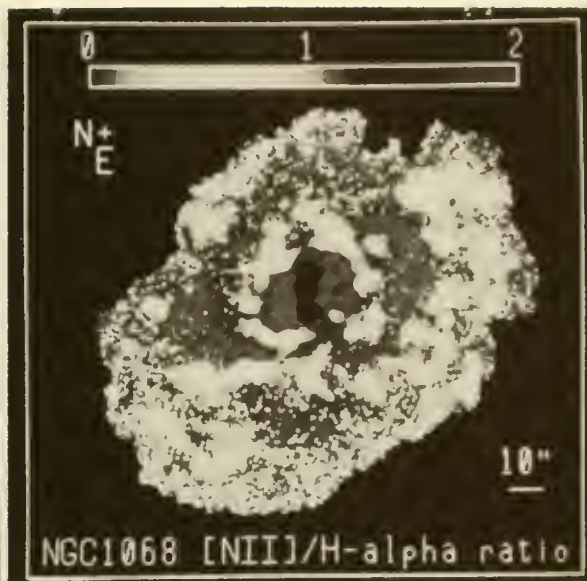


Fig. 1b: [NII]/H α Ratio Map

REFERENCES:

- Antonucci, R. R. J., and Miller, J. S., *Ap. J.*, **297**, 621, 1985.
 Bland, J., and Tully, R. B., *Astron. J.*, August, 1988.
 Evans, I. N., and Dopita, M. A., *Ap. J. Suppl.*, **58**, 125, 1985.
 Evans, I. N., and Dopita, M. A., *Ap. J. Lett.*, **310**, L15, 1986.
 Krolik, J. H., and Begelman, M. C., *Ap. J. Lett.*, **308**, L55, 1986.
 Snijders, M. A. J., Netzer, H., and Boksenberg, A., *M.N.R.A.S.*, **222**, 549, 1986.

Multiband Observations of Cygnus A: A Study of Pressure Balance in the Core of a Powerful Radio Galaxy

Chris Carilli (NRAO), Sam Conner (MIT),
John Dreher (NASA-Ames), and Rick Perley (NRAO¹).

Cygnus A is a powerful double radio source associated with a giant elliptical galaxy at the center of a poor cluster of galaxies (see figure 1). The radio source also sits within the core radius of a dense, ‘cooling flow’, X-ray emitting cluster gas¹. Optical spectroscopy and narrow band imaging have revealed copious amounts of narrow line emission from the inner 20 kpc of the associated galaxy^{2,3} (we assume $H_0 = 75 \text{ km sec}^{-1} \text{ Mpc}^{-1}$). In this short communication we discuss the pressures in the three components of the ISM (i.e. the radio, X-ray, and line emitting fluids) within a radius of about 15 kpc of the active nucleus of the Cygnus A galaxy.

In figure 2 we show the relative distribution of the narrow line emitting gas and the stars in the Cygnus A galaxy. Notice how the northwest peak of the broad band optical double nucleus is dominated by narrow line emission, while the southeast peak is dominated by continuum radiation (see ref. 3 for a detailed discussion). Also, notice the filamentary line emitting structures extending ≈ 10 kpc from the nucleus, to the northeast (NE) and south (S). The NE filament seems to end on a stellar like feature. This may be a foreground star, or it may be emission from something within the Cygnus A galaxy (perhaps star formation in the cooling flow?).

The integrated luminosity in $H\alpha$ and $[NII]$ from Cygnus A is $3.1 \times 10^{42} \text{ ergs sec}^{-1}$. An aperture spectrum of the inner 4" of this galaxy⁴ yields electron temperatures of 10^4 °K and densities of 300 cm^{-3} in the line emitting regions. We calculate a volume filling factor of 1.7×10^{-6} for the line emitting clouds, and pressures in the clouds of $8.4 \times 10^{-10} \text{ dynes cm}^{-2}$. Spatially resolved spectra of the various line emitting structures² show that the density varies spatially, with a value of about 200 cm^{-3} at the NW peak, and values of 500 cm^{-3} on the S filament, and $\leq 40 \text{ cm}^{-3}$ on the N filament (a corresponding study of the spatial variation of temperature cannot be made from existing spectra).

In figure 3 we show the relative distribution of the radio emitting fluid and the line emitting gas in the central regions of Cygnus A. A cross marks the position of the radio nucleus (which has been blanked in order to avoid obscuring the line emission). The radio nucleus sits between the two broad band optical peaks, and the radio jet can be seen extending from the nucleus to the northwest. Notice the tendency for the NE and S filaments to extend along the boundary of the radio source. This relative morphology could be a chance projection, or it may indicate an interaction between the two fluids. Minimum energy pressures in the radio lobes are about $7.7 \times 10^{-11} \text{ dynes cm}^{-2}$, while those in the jet are $3.1 \times 10^{-10} \text{ dynes cm}^{-2}$.

Lastly, we consider the X-ray emitting cluster gas enveloping the system. The pressure in the inner 10 kpc of the Cygnus A galaxy cannot be determined directly from existing X-ray observations. We estimate the pressure in the X-ray emitting gas by using the value at the cluster core radius (about 200 kpc¹), and then extrapolating the

¹The National Radio Astronomy Observatory (NRAO) is operated by Associated Universities, Inc., under contract with the National Science Foundation.

standard cooling flow model to small radii (which implies an increase in pressure by a factor of about 3 from the cluster core radius to the center of the cluster⁵). We find a pressure of 1.7×10^{-10} dynes cm^{-2} for the X-ray gas within 10 kpc of the nucleus.

Comparing the various pressures, we see that the line emitting clouds are overpressured with respect to the radio lobes by a factor of 11, with respect to the radio jet by a factor of about 3, and with respect to the X-ray emitting fluid by a factor of 5 (of course, given the observed variation in density for the line emitting clouds, we expect variations in pressure, e.g. the lower density on the NE filament suggests that this feature may be in equilibrium with the radio emitting fluid. A knowledge of the spatial variation in temperature is required for a more detailed comparison).

We can reconcile the pressure difference between the radio and line emitting fluids in a number of ways. First, we can assume large departures from minimum energy conditions in the radio source. Second, we can assume minimum energy holds, but that the volume filling factor for the synchrotron emitting fluid in the lobes is 0.015 (the filling factor for the jet would be 0.15). Third, we could assume that ram pressure of the back flowing radio emitting fluid dominates the pressure in the lobes. A rough estimate of the ram pressure can be made by assuming that the flow is driven by the high pressure heads of the radio lobes. Minimum energy pressures in the heads are a factor of 4 larger than in the bridge, which is still a factor of 3 below line cloud pressures. Lastly, we could assume that the radio lobes and line emitting gas are not interacting, and that the spatial coincidence is just a consequence of projection.

The most likely cause for the difference between the calculated pressures in the X-ray and line emitting fluids is that the cooling flow models are incorrect. We can think of a number of mechanisms which could alter the standard model. First, magnetic fields in the cluster gas⁶ may alter the heating and cooling of the gas through their influence on heat conduction. Also, if the fields are convected with the (hypothesized) flow, they may become dynamically important at small radii (within 15 kpc, depending on geometry³). Second, the active nucleus may heat its environs, which would also alter the standard model. Of course, we could always assume that pressure balance does not hold between the line clouds and their environs, and hence, that they are transient phenomena.

1. Arnaud, K.A., Fabian, A., Eales, S., Jones, C., and Forman, W. 1984, *M.N.R.A.S.*, **211**, 981.
2. Pierce, Michael J., and Stockton, Alan 1986, *Ap.J.*, **305**, 204 (PS).
3. Carilli, C.L., Dreher, J.W., Conner, Sam, Perley, R.A. 1989 *A.J.*, in press for August issue.
4. Osterbrock, D.E. 1989, *Astrophysics of Gaseous Nebulae and Active Galactic Nuclei*, University Science Books, Mill Valley, CA, p. 321.
5. Sarazin, C.L. 1986, *Rev. Mod. Phys.*, **58**, 1.
6. Carilli, C.L., Perley, R.A., and Dreher, J.W. 1988, *Ap. J. (Letters)*, **334**, L73.

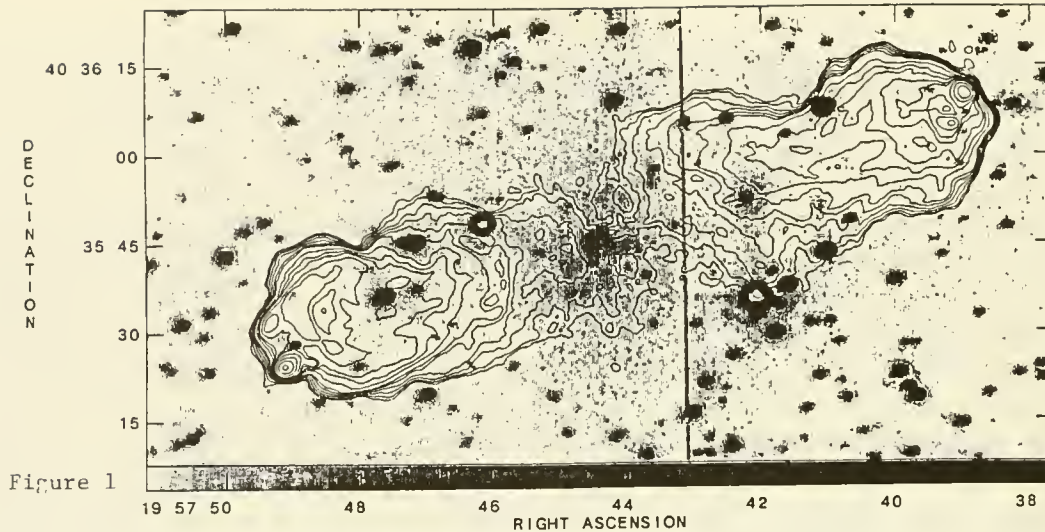


Figure 1: Gray Scale is an R band optical image (taken with McGraw Hill 1.3m telescope in 1.0" seeing), while contours are radio emission at 20cm (1.0" resolution VLA image). A cross marks the position of the radio core. Notice the large galaxy radius (about 40 kpc), and the way the radio lobes seem to avoid the central regions of the galaxy. Also notice the radio jet extending from the nucleus into the northwest lobe.

Figure 2: Grey scale is a broad band R image of the inner 30 kpc of the galaxy, while contoured is the optical line emission ($H\alpha$ and $[NII]$) at the redshift of the Cygnus A galaxy (with continuum subtracted). Note how the northwest broad band peak of the double optical nucleus is mostly narrow line emission, while the southeast peak is mostly continuum. Also, note how the line emitting filament to the northeast seems to end on a compact optical feature, which may be evidence for star formation in the cooling flow, or just a foreground star.

Figure 3: Contoured is the optical line emission ($H\alpha$ and $[NII]$) at the redshift of the Cygnus A galaxy (with continuum subtracted), while gray scale is the 20cm radio emission. Again, a cross represents the position of the radio core source (which has been blanked to better display the optical emission). Notice that the line emitting filaments extend from the nucleus both to the northeast and to the south by about 10", and seem to extend along the edge of the radio lobe.

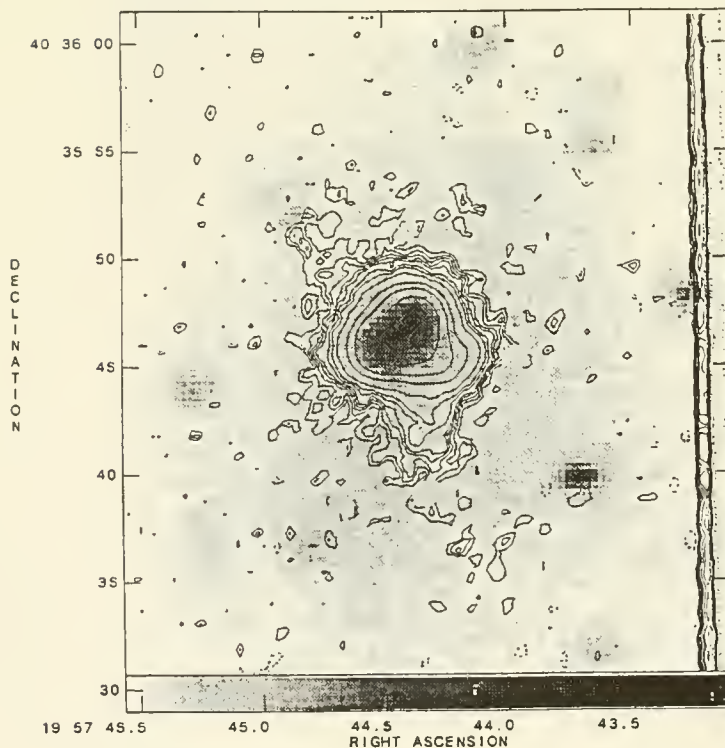


Figure 2



Figure 3

IONIZED INTERSTELLAR FROTH IN IRREGULAR GALAXIES

Deidre A. Hunter (Lowell Obs.) and John S. Gallagher, III (AURA, Inc.)

Introduction

The warm interstellar medium of galaxies is a complicated place. It is often full of holes, neutral and ionized loops and shells, and diffuse ionized gas (cf. Monnet 1971, Sivan 1974, Heiles 1979, Sabbadin and Bianchini 1979, Ogden and Reynolds 1985). Deep H α images of Magellanic-type irregular galaxies also reveal complex spatial structures consisting of loops and filaments in the interstellar gas outside of the boundaries of traditional HII regions (cf. Meaburn 1980). We refer to these ionized structures as "froth". Such structures could mark paths over which newly produced heavy elements are dispersed in irregular galaxies, and they could be the signatures of a feedback process related to star formation (cf. Dopita *et al.* 1985, McCray and Kafatos 1987). In order to investigate the physical nature of the froth we have obtained narrow-band images and high and low dispersion spectra from KPNO and deep blue-passband plates from the CFHT.

Description

Characteristics of typical filaments and loops are as follows: a) Dimensions: 0.5–1 kpc \times 15–150 pc; b) H α Surface Brightness: 6×10^{-16} ergs/cm²/s/arcsec²; EM ~ 230 cm⁻⁶ pc; c) Fraction of Total H α : 15–20%; d) Emission-line Ratios: [OII]/[OIII] ~ 3.5 (HII: ~ 1.5); [SII]/H α ~ 0.5 (HII: ~ 0.25); [NII]/H α ~ 0.2 (HII: ~ 0.1); [OII]/H α ≤ 0.05 ; e) Kinematics: FWHM(H α) ~ 40 –140 km/s; $\Delta v(\text{loops}) \sim 0$ –20 km/s.

We have superimposed the filamentary structures on prints of the CFHT plates in order to compare their locations to that of OB associations. We see that only one structure is centered around a young OB cluster. The loop around the giant HII region NGC 2363 in the dwarf irregular NGC 2366 has a similar structure, as does the outer structure of the 30 Doradus giant HII region in the LMC. In all other cases, including apparently coherent ionized loops, there is no stellar group of particular interest located *within* the feature.

In all cases, however, we find that the frothy structures are associated with HII regions. The loops and filaments appear to emanate from the HII regions with the filaments extending radially away and the loops being connected to the same HII complex on both footprints. Thus, while frothy ionized structures are associated with the presence of young, massive OB stars, their structures are inconsistent with simple models in which such features mark bubbles blown in the surrounding interstellar matter by stellar winds, supernovae explosions, and HII regions (Tenorio-Tagle and Bodenheimer 1988).

We have also compared the locations of the filaments with the distribution of the HII in the two galaxies for which high resolution maps exist (van Gorkom and Hunter, unpublished; Skillman *et al.* 1988). In NGC 4449 we see that the froth is generally located on the edges of HII complexes. None of the features is located within a cloud complex. In Sex A this general trend continues. The filaments extend from the eastern HII region and HII peak further west towards the HII hole.

Ionization and Pressure

The problem of ionization of interstellar froth in irregular galaxies parallels that of understanding the source of ionization for diffuse H α emitting gas in the Milky Way (e.g. Reynolds 1984, 1985; Sivan *et al.* 1986): (1) Interstellar froth in irregulars has lower excitation than classical HII regions in the same galaxies, although the excitation is higher than in the Milky Way diffuse ionized gas (e.g. much higher [OIII]/H β ; c.f. Reynolds 1985; Sivan *et al.* 1986). Froth therefore

cannot be due to light reflected from HII regions by interstellar dust. (2) Frothy matter shows large local velocity widths, and a shock-excited component therefore may also be present. (3) The higher surface brightnesses of the ionized froth in irregulars compared to that in the Milky Way exacerbates the problem of finding a suitable local ionization source as compared with the local Galactic disk (Reynolds 1984). A best model at present, therefore, appears to be the combined shock and photoionization interpretation proposed by Sivan *et al.* (1986). Shocks could produce enhanced emission from [S II], while photoionization contributes to the higher ionization species and depresses the amount of [O I] emission.

The pressures inferred in frothy structures studied here are 3–10 times *greater* than the estimated pressure in the local Galactic disk cloud layer (Kulkarni and Heiles 1988). We see no obvious reason why the mean pressure in the outer regions of an irregular galaxy with significantly lower surface mass density than the local Galactic disk should exceed the local value by a large factor. We therefore conclude that either (1) higher surface brightness (denser) ionized frothy structures in irregulars are not in pressure equilibrium with the surrounding interstellar medium, or (2) magnetic fields provide an additional confining force for these structures.

Preliminary Conclusions

Frothy features in irregular galaxies show that the influence of young stellar systems extends beyond the production of supershell bubbles around luminous OB associations. The origin of filaments extending out from HII regions is currently unclear, but these structures involve dynamic processes which produce comparatively large line velocity widths. Froth may possibly be produced from old supershells, in which case star formation must be spatially correlated to explain the proximity of HII regions and ionized froth. Alternatively, some form of magnetic structuring of gas is possible. That these features are more readily found in the ionized gas of irregulars than in spirals could reflect the high UV stellar output and small differential rotation in the irregulars.

We wish to thank KPNO and the CFHT for telescope time and the many people who supported the observing. This research was supported in part by the Lowell Observatory Research Fund.

References

- Dopita, M., Mathewson, D. and Ford, V. 1985, *Ap. J.*, **297**, 599.
 Heiles, C. 1979, *Ap. J.*, **229**, 533.
 Hunter, D. A. 1982, *Ap. J.*, **260**, 81.
 Kulkarni, S. and Heiles, C. 1988, in *Galactic and Extragalactic Radio Astronomy*, eds. G. Verschuur and K. Kellermann (New York: Springer-Verlag), p 95.
 McCray, R. and Kafatos, M. 1987, *Ap. J.*, **317**, 190.
 Meaburn, J. 1980, *M. N. R. A. S.*, **192**, 365.
 Monnet, G. 1971, *Astr. Ap.*, **12**, 379.
 Ogden, P. and Reynolds, R. 1985, *Ap. J.*, **290**, 238.
 Reynolds, R. J. 1984, *Ap. J.*, **282**, 191.
 ——— 1985, *Ap. J. (Lett)*, **298**, L27.
 Sabbadin, F. and Bianchini, A. 1979, *Pub. A. S. P.*, **91**, 280.
 Sivan, J. 1974, *Astr. Ap. Suppl.*, **16**, 163.
 Sivan, J., Stasińska, G., and Lequeux, J. 1986, *Astr. Ap.*, **158**, 279.
 Skillman, E., Terlevich, R., Teuben, P., and van Woerden, H. 1988, *Astr. Ap.*, **198**, 33.
 Tenorio-Tagle, G. and Bodenheimer, P. 1988, *Ann. Rev. Astr. Ap.*, **26**, 145.

Ar/S

Marshall L. McCall and Chris Stevenson

York University

Toronto, Ontario, Canada

and

Douglas L. Welch

McMaster University

Hamilton, Ontario, Canada

Summary

Near-infrared spectroscopy at high altitude and low humidity has been carried out to accurately measure [Ar III] λ 7136 and [S III] λ 9069 in the extreme metal-poor dwarf irregular galaxy IZw18. The ratio of the abundance of argon to the abundance of sulphur is within about 0.2 dex of the value for the solar neighbourhood. Since $n(\text{Ar})/n(\text{S})$ appears to be a universal constant, the line ratio [Ar III] λ 7136/[S III] λ 9069 may be a useful diagnostic of temperature in cool, metal-rich HII regions.

Background

For most HII regions with temperatures below about 8000 K, in particular metal-rich objects, standard temperature-sensitive lines such as [O III] λ 4363 are too weak to be detected in reasonable exposure times. As well, the sensitivity of auroral lines to temperature fluctuations compromises their value. Abundances have therefore been estimated indirectly through modeling the ratios of the stronger, primarily optical, observable lines. Considering the complexity of the objects, the number of free parameters in the models, and the small number of lines available, these abundances are very uncertain. The problem is particularly important because of the ubiquity of low-temperature giant HII regions in spiral galaxies, which play a pivotal role in studies of abundance gradients and chemical evolution.

In fact, it may be possible to observationally check the model abundances for cool HII regions by adopting a universal value for the ratio of the argon abundance to the sulphur abundance. To a good approximation,

$$\frac{I([\text{Ar III}]\lambda 7136)}{I([\text{S III}]\lambda 9069)} = 2.03 t^{+0.09} \exp(-0.453/t) \frac{n(\text{Ar}^{++})}{n(\text{S}^{++})}$$

where $n(\text{Ar}^{++})$ and $n(\text{S}^{++})$ are the number densities of doubly-ionized argon and sulphur, respectively, and where t is the electron temperature of the gas in units of 10^4 K (McCall, M. L. 1984, M.N.R.A.S., **208**, 253). The ionization potentials for Ar^+ and Ar^{++} are 2.0 and 3.0 Ryd, respectively, close to the ionization potentials of 1.7 and 2.6 Ryd for S^+ and S^{++} , respectively, so the Ar^{++} and S^{++} zones largely overlap. As a result, $n(\text{Ar}^{++})/n(\text{S}^{++})$ should be relatively insensitive to ionization structure, and, thus, directly related to $n(\text{Ar})/n(\text{S})$, particularly in low-excitation nebulae where little of the argon or sulphur is triply ionized. If $n(\text{Ar})/n(\text{S})$ is a constant, then the equation shows that the near-infrared line ratio should be a useful temperature diagnostic below 10,000 K. Most

importantly, the fact that the lines arise from upper levels with relatively low excitation potentials means that they remain fairly strong at low temperatures. The weak sensitivity to reddening is also a virtue. Whatever dependence there is on the ionization structure can be investigated (and corrected, if necessary) by studying correlations with $[\text{S III}]/[\text{S II}]$ or $[\text{O III}]/[\text{O II}]$ at fixed metallicity.

Both sulphur and argon are believed to be formed during explosive oxygen and silicon burning in massive stars. Since the two elements are synthesized under identical circumstances, it is reasonable to expect that $n(\text{Ar})/n(\text{S})$ should vary little from place to place in the universe. Indeed, it has been proven that the ratio varies by only about 0.05 dex from the Sun to the SMC, i.e. over a range of a factor of seven in the oxygen abundance. (Dufour, R. J. 1984, in *IAU Symp. 108: Structure and Evolution of the Magellanic Clouds*, eds. S. van den Bergh and K. S. de Boer (Dordrecht: Reidel), p. 353).

The authors are conducting an extended study of near-infrared argon and sulphur lines in extragalactic HII regions in order to verify the constancy of the abundance ratio and to evaluate its sensitivity to ionization details in order to derive metallicities of metal-rich giant extragalactic HII regions. Here, observations of IZw18 are presented in order to extend measurements of $n(\text{Ar})/n(\text{S})$ down to a metallicity more than a factor of forty below that of the solar neighbourhood.

Observations

Near-infrared CCD spectra of IZw18 were acquired at an altitude of 4200 meters with the Canada-France-Hawaii Telescope, while the relative humidity was 10%. A metal-poor red giant close in the sky was monitored during the observations in order to correct for the remaining atmospheric absorption. At this altitude and humidity the water vapour features that normally affect $[\text{Ar III}]\lambda 7136$ and $[\text{S III}]\lambda\lambda 9069, 9532$ are exceedingly weak. A total exposure of 3.3 hours over two nights led to the detection of $[\text{Ar III}]\lambda 7136$ and $[\text{S III}]\lambda 9069$. Reductions were carried out using IRAF, and measurements were made using software developed previously (McCall, M. L., Rybski, P. M., and Shields, G. A. 1985, *Ap. J. Suppl.*, **57**, 1).

Results

The final observed and reddening-corrected relative emission line intensities are listed in Table 1., the latter obtained by assuming $E(B - V) = 0.17$ (Dufour, R. J., Garnett, D. R., and Shields, G. A. 1988, *Ap. J.*, **332**, 752). The ratio $I([\text{Ar III}]\lambda 7136)/I([\text{S III}]\lambda 9069)$ is 0.31 ± 0.08 . From the strength of $[\text{S III}]\lambda 6312$ measured by Dufour, Garnett, and Shields (1988), the temperature of the S^{++} zone is of the order 18,000 K, which is consistent with O^{++} temperatures reported in the literature. Thus, the equation yields $n(\text{Ar}^{++})/n(\text{S}^{++}) = 0.19 \pm 0.05$. An O^+ temperature of $(14,300 \pm 3400)$ K is derived from our measurement of $[\text{O II}]\lambda\lambda 7320, 7330$ and the average published value for $[\text{O II}]\lambda\lambda 3726, 3729$. Based upon models by Dufour, Garnett, and Shields (1988), the ionization correction factor $X(\text{Ar}^{++})/X(\text{S}^{++})$ is 0.5 to 0.7, so $n(\text{Ar})/n(\text{S})$ is 0.40 ± 0.10 to 0.26 ± 0.07 . Referencing to the Sun, $[\text{Ar}/\text{S}] = 0.07 \pm 0.12$ to 0.26 ± 0.11 . The result seems to confirm the view that nucleosynthesis of argon goes hand in hand with sulphur, and gives further impetus to the employment of the abundance ratio to probe the temperatures of metal-rich nebulae.

Table 1
Relative Line Intensities for IZw18

line	wavelength	$F(\lambda)/F(\text{H}\alpha)$	$F(\lambda)/F(\text{H}\beta)$	$I(\lambda)/I(\text{H}\beta)^1$
[O II] ²	3727Å	—	—	31.9±5.6
He I	5876Å	2.164±0.100	7.27±0.34	6.27±0.29
[S III] ³	6312Å	—	0.9±0.8	0.7±0.6
H α	6563Å	100	336	277
He I	6678Å	0.865±0.073	2.91±0.25	2.38±0.20
[S II]	6723Å	1.054±0.088	3.71±0.30	3.02±0.24
He I	7065Å	0.663±0.100	2.23±0.34	1.77±0.26
[Ar III]	7136Å	0.389±0.088	1.31±0.30	1.04±0.23
[O II]	7326Å	0.396±0.100	1.33±0.34	1.04±0.27
[S III]	9069Å	1.438±0.216	4.83±0.73	3.40±0.51

¹ Corrected for reddening $E(B - V) = 0.17$.

² Average of values as reported from the literature by Davidson, K., and Kinman, T.D. 1985, *Ap. J. Suppl.*, **58**, 321.

³ Dufour, R.J., Garnett, D.R., and Shields, G.A. 1988, *Ap. J.*, **332**, 752.

Spatially Resolved Optical and Near Infrared Spectroscopy of I Zw 18

Evan D. Skillman

Astronomy Department, University of Texas

R. C. Kennicutt

Steward Observatory, University of Arizona

I MOTIVATION

For a long time, I Zw 18 has been recognized as the lowest abundance extragalactic H II region (with the possible recent exception of SBS 0335-052; Izotov 1989). As such, it is important for many studies, including the determination of the primordial helium abundance (e.g. Davidson and Kinman 1985; and references therein). Recent imaging studies of I Zw 18 (Davidson, Kinman, and Friedman 1989; Dufour and Hester 1989) have revealed a more complex structure to I Zw 18 than the simple two-component model previously assumed. This has given rise to concern about the reliability of chemical abundance measurements derived for I Zw 18. We have obtained long-slit spectra covering the wavelength range $\lambda 3650 - \lambda 10,000$, which allow us to measure physical parameters and chemical abundances as a function of position. With these new data we can investigate the SE component, which has not been studied previously, and we can address some of the concerns about abundance uncertainties.

II NEW OBSERVATIONS

The spectra were obtained with 3 different telescope/instrument combinations. All observations were made using a long slit spectrograph with a 2 arcsec slit width imaged onto a TI 800 x 800 pixel CCD. The position angle of -39° insured that the slit covered both the NW and SE components. The three data sets are summarized in Table 1. The MMT Red Channel Echellette (Schmidt, Weymann, and Foltz 1989) makes efficient use of the full format of the CCD by cross-dispersing 5 orders (of a 20 arcsecond long slit), allowing both large wavelength coverage and intermediate resolution. The high throughput of the Red Channel combined with the MMT allowed the detection of such faint lines as [N II] $\lambda\lambda 6548, 6584$, [O I] $\lambda\lambda 6300, 6363$, and [S III] $\lambda\lambda 6312, 9069, 9532$ in both the NW and SE components (see Figure 1).

III N/O, O/H, and He/H in I Zw 18

It is currently believed that while oxygen has dominantly primary nucleosynthetic origins, nitrogen benefits from both primary and secondary nucleosynthesis (cf. Pagel 1985). This is based on the observation that below $[O/H] \approx -0.6$, we see the primary ratio of $\log (N/O) \approx -1.54$, while above this N/O increases with increasing O/H (due to secondary nitrogen). Dufour, Garnett, and Shields (1988) presented the surprising value of $\log (N/O) = -1.25 \pm 0.18$ for I Zw 18. This lead

to speculation that in extreme dwarf galaxies supernovae may eject a significant fraction of their oxygen out of the galaxy, leading to a lower than expected value for the oxygen abundance. In fact, our new measurements (with a factor of 10 improvement in the s/n ratio in the [N II] $\lambda 6584$ line) yield $\log (N/O) = -1.5 \pm 0.1$. The N/O ratios are equal (within errors) in both components.

Campbell (1989) has proposed a radial density gradient model for I Zw 18 in which the central density is close enough to the critical density (7×10^5) to partially collisionally de-excite the [O III] $\lambda\lambda 4959, 5007$ lines. This results in a "true" oxygen abundance for I Zw 18 which is a factor of nearly 4 times higher than the generally accepted value. Figure 2 shows the density sensitive [S II] $\lambda 6717/\lambda 6731$ ratio as a function of position across I Zw 18. In all positions the ratio is close to the low density limit, and nowhere is there evidence of very dense gas. If the model of Campbell were correct we might expect some trace of high density gas in the [S II] ratio, such as a decrease in the ratio coincident with the continuum peak. In order for a density gradient not to effect the [S II] ratio would require that the high density region be confined to a very small fraction of the total volume of the nebula. In this case it would be visible in the imaging studies. The low value of O/H obtained by previous studies remains secure. We derive equivalent values of O/H (within errors) for the NW and SE components.

One of the motives of this study is to follow-up on the suggestion of Davidson and Kinman to provide additional observational material on I Zw 18 relevant to the study of the primordial helium abundance. These new observations provide three new tests: 1.) We have high s/n in the $\lambda 6678$ line. This is a singlet line, and should be immune from the effects of self-absorption. (previous studies concentrated on the $\lambda\lambda 5876, 4471$ triplet lines); 2.) We can study the $\lambda 6678/\lambda 6563$ line ratio as a function of position to test for the presence of neutral helium; and 3.) We have found the He II $\lambda 4686$ line (which is detected in the NW component, but not the SE component) to vary similarly to the Balmer emission. (The $\lambda 4686/\lambda 4861$ ratio shows a variation of only a factor of two - centrally peaked - over the NW component, while the $\lambda 4686/\text{continuum}$ ratio varies by more than a factor of 10.) This implies that the He II emission is nebular, and not circumstellar. This, in turn, implies two important results. The Helium abundance should be corrected for He^{++} (as discussed by Davidson and Kinman), and there is at least one very hot star ($T_{eff} \geq 70,000\text{K}$) in I Zw 18 (Bergeron, 1977).

Acknowledgements

This work was supported in part by Robert A. Welch Foundation grant F-910 to the University of Texas at Austin, and NSF grant AST-8613257 to RCK. Some of the observations reported here have been obtained at the Multiple Mirror Telescope, a joint facility of the University of Arizona and Smithsonian Institution.

References

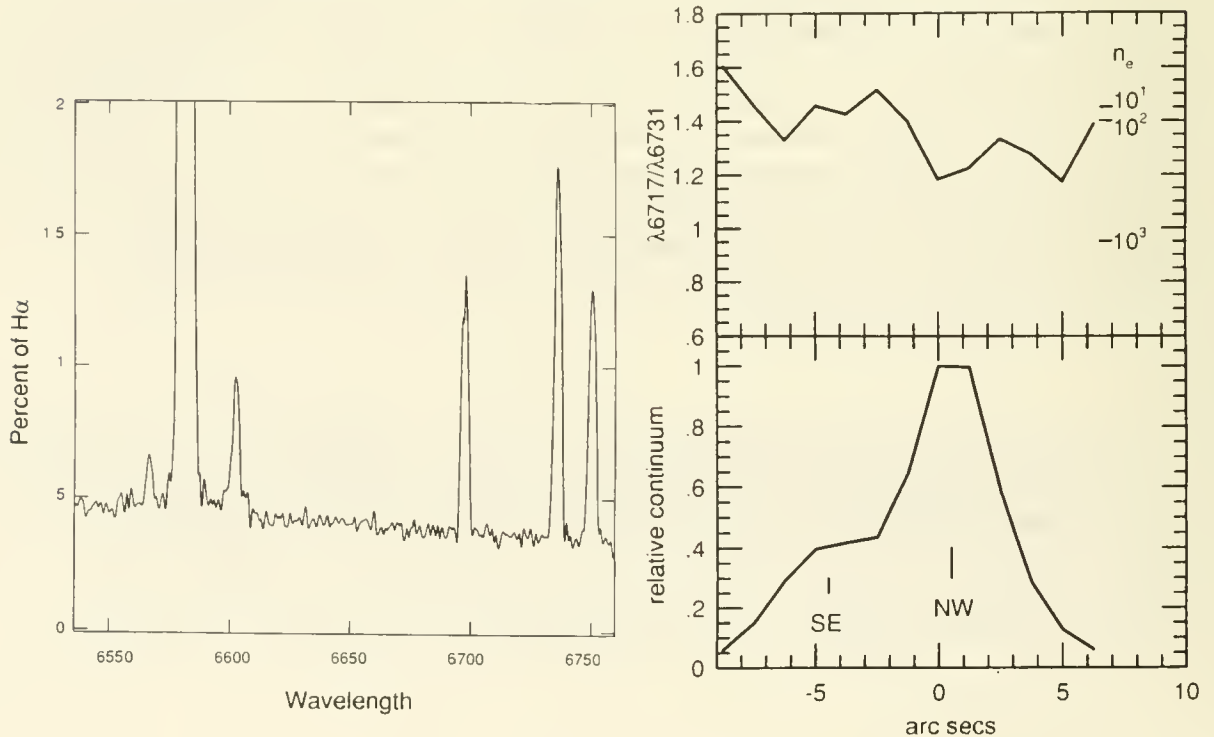
- Bergeron, J. 1977, *Ap. J.*, **211**, 62.
 Campbell, A. 1988, *B.A.A.S.*, **20**, 1038.
 Davidson, K., and Kinman, T.D. 1985, *Ap. J. Suppl.*, **58**, 321.
 Davidson, K., Kinman, T.D., and Friedman, S.D. 1989, *A. J.*, in press.
 Dufour, R.J., Garnett, D.R., and Shields, G.A. 1988, *Ap. J.*, **332**, 752.
 Dufour, R.J., and Hester, J.J. 1989, *Ap. J. (letts.)*, in press.
 Izotov, Y. 1989, private communication.
 Pagel, B.E.J. 1985, in *Production and Distribution of C, N, O Elements*, ed. I. J. Danziger, F. Matteucci, and K. Kjar (Munich: ESO), p.155.
 Schmidt, G.D., Weymann, R.J., and Foltz, G.B. 1989, *P.A.S.P.*, submitted.

Table 1

Telescope/ Instrument	Wavelength Coverage	Resolution
MMT/Red Channel	6200-6750Å	3.5Å
MMT/R.C. Echellette	4600-10,000Å	8-15Å
McDonald 2.7m/LCS	3650-5100Å	6Å

Figure 1.) Spectra in the region $\lambda 6500-6800$ for the SE component.

Figure 2.) The density dependent [S II] ratio as a function of position in I Zw 18. The relative stellar continuum is plotted below for reference.



Optical and Near-IR study of LMC HII Region N11AB

Myung Gyoon Lee (University of Washington)

I. Introduction

N11 (DEM 34), complex HII region located about 4 degrees from the center of the LMC bar, is very interesting giant interstellar shell. It has a complicated structure and motion (Meaburn *et al.* 1989, preprint). It is located on the edge of an HI concentration. This is the progress report of our study of its two components, A and B at the optical and near-IR wavelengths to investigate stars, dust and ionized gas associated with them. N11A is a compact high-excitation blob (Heydari-Malayeri 1985, *A. Ap.*, **144**, 98.) and N11B is a bright HII region in this complex, which embeds OB association Lucke-Hodge 10.

II. Observations and Data Reduction

We obtained H α , H β , [SII 6717/31], blue and red continuum, and UBV CCD frames by using CTIO 0.9-m plus TI CCD chip in Dec. 1987 and Jan. 1989. J, H, K, 1.99 μ m, Br γ , and 2.20 μ m images of N11A were obtained by using CTIO 1.5-m plus IR-imager in Jan. 1989. Flux calibration was done by using standard stars observed at the same night. Standard transformation error of UBV photometry is smaller than 0.03. UBV photometry of stars was derived by using DAOPHOT and ALLSTAR.

III. Results

1. Comparison of the $(U - B) - (B - V)$ diagram with the intrinsic relation of V and Ib gives the mean reddening value, $E(B - V) = 0.16 \pm 0.02$. There is a large scatter in the reddening.

2. By using the $V - (B - V)$ diagram, the $V - (U - B)$ diagrams, and the isochrones based on Maeder and Meynet (1989, *A. Ap. Suppl.*, **76**, 411), we estimated that the age of this area is 5 ± 5 Mys. $(m - M)_o = 18.5$, $E(B - V) = 0.16$, and $A_V = 3E(B - V)$ were assumed (Fig. 1a and 1b).

3. Stellar initial mass function for $9 \ m_{\odot} < m < 60 \ m_{\odot}$ was derived from the comparison of the evolutionary tracks (Maeder and Meynet 1989) and the $V - (U - B)$ diagram. The slope of the logarithmic IMF ($\Gamma = d \log N / d \log m$) is -1.8 ± 0.3 , which is very similar to that for Lucke-Hodge 117 and 118 associations (Massey *et al.* 1989, *A. J.*, **97**, 107).

4. Continuum-subtracted H α and H β maps of N11B show several peaks of emission around the inner boundary, while [SII 6717/31] emission is dominant at the outer boundary with a peak of emission at the NE boundary (Fig. 2a and 2b). The peak of [SII 6717/31] emission at the NE boundary is $\sim 5''$ away toward NE from the peak of H α and H β emission. These points show that the outer area is expanding outward colliding with surrounding material and that the curved feature at the NE is probably due to the interaction between N11B and the surrounding dust, instead of due to the nearby bright

star, Sk -6636. Note that [SII 6717/31] image of N11A blob shows a distinguishable spiral feature at the outer area, while Balmer emission line images do not.

5. Br γ map of N11A shows horizontally elongated emission, while J image shows a normal stellar profile. The second peak is $\sim 4''$ east of the stellar peak (Fig. 3a and 3b). We derived $K = 9.56$, $J - K = 1.05$, and $H - K = 0.46$ for N11A. The comparison of near-IR maps with optical maps is still in progress.

Figure Captions

Fig. 1 : (a) $V - (B - V)$ diagram of N11AB. Dashed lines represent evolutionary tracks of 40, 20, 12, 7, 4, and $2.5 m_{\odot}$ for $Z=0.02$ (Maeder and Meynet 1989), shifted according to $(m - M)_o = 18.5$, $E(B - V) = 0.16$ and $A_V = 3E(B - V)$. Filled circles represent the stars with photometric error smaller than 0.05. (b) $V - (U - B)$ diagram.

Fig. 2 : (a) Blue continuum (4650 Å) image overlapped with the contour map of continuum-subtracted and flux-calibrated H α image. The scale is $0.494''/\text{pixel}$. North is at the top and east is at the left. (b) Continuum-subtracted and flux-calibrated [SII 6717/31] image.

Fig. 3 : (a) J image of N11A. The scale is $0.92''/\text{pixel}$. (b) Continuum-subtracted Br γ image.

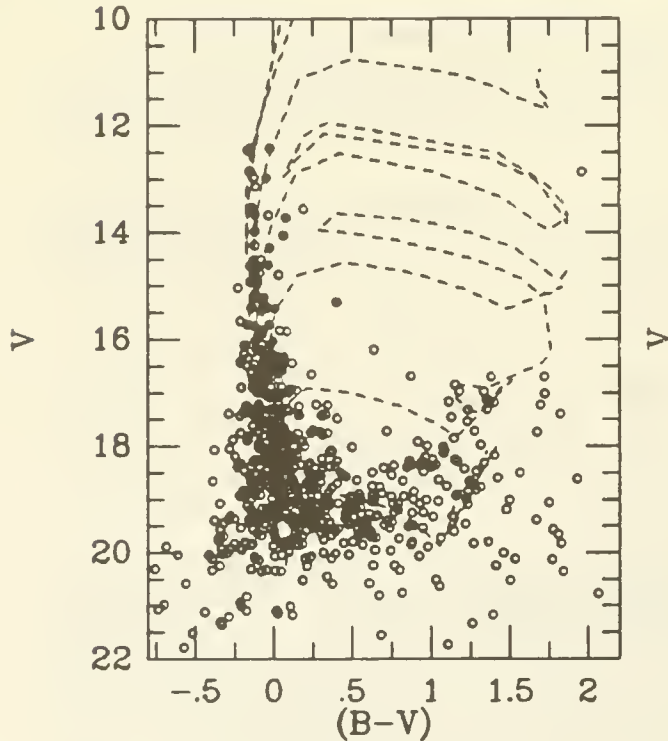


Fig. 1 (a)

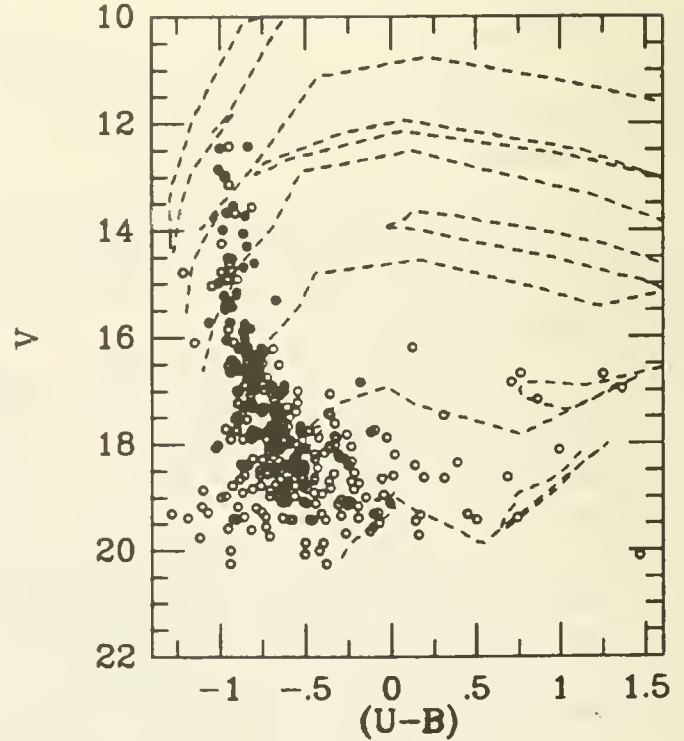


Fig. 1 (b)

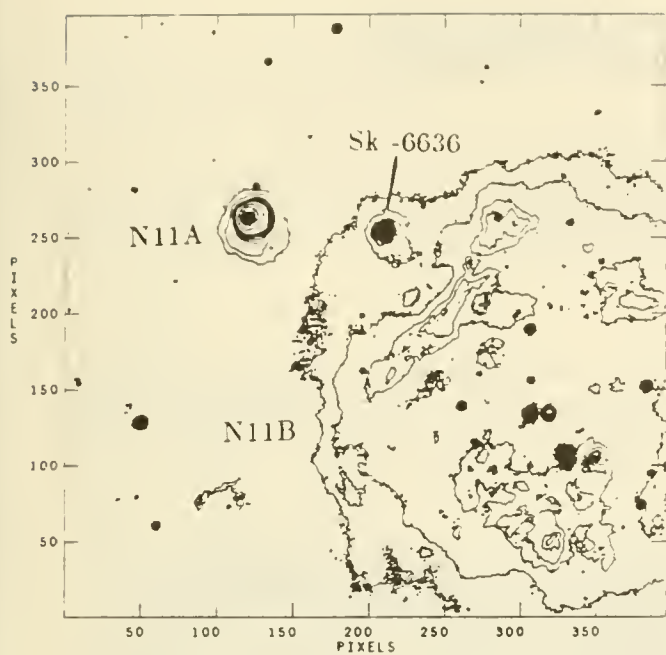


Fig. 2 (a)

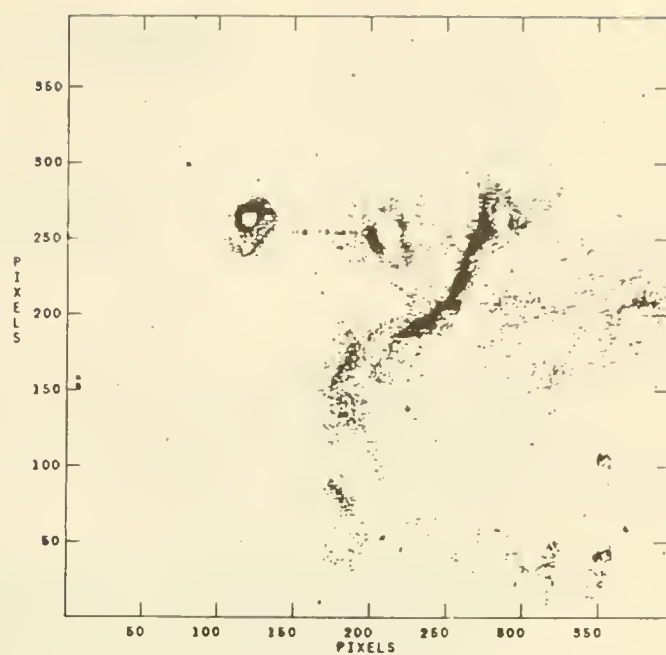


Fig. 2 (b)

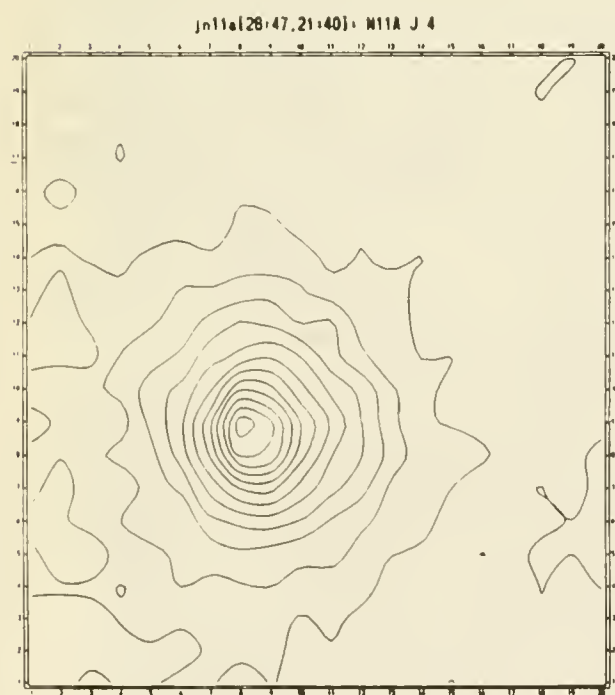


Fig. 3 (a)

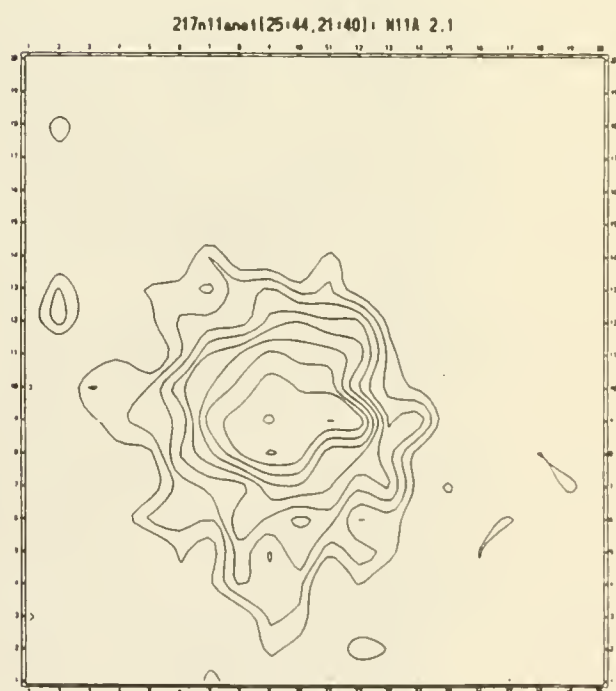


Fig. 3 (b)

H II REGIONS IN DWARF IRREGULAR GALAXIES OF THE LOCAL GROUP

Paul Hodge and
Myung Gyoon Lee
University of Washington

Deep, narrowband $H\alpha$ CCD surveys of H II regions have been carried out in several dwarf irregular galaxies in and near the local group. Data are now complete for these galaxies: NGC 6822, GR8, IC 10, IC 1613, Sextans A, Sextans B, and Sag Irr. Observations are complete for DDO 47, 53, 167, 168 and 187. Details of some of the results for the surveys completed so far are as follows:

NGC 6822. A CCD survey at $H\alpha$ resulted in the detection of 145 H II regions in the local group irregular galaxy NGC 6822. Most of them are newly detected, faint surface-brightness objects. Positions, maps, and dimensions are being published elsewhere.

Calibrated $H\alpha$ CCD images were used to obtain an absolute $H\alpha$ luminosity function and several versions of diameter distributions. The luminosity function reaches from the most luminous H II region, which has an $H\alpha$ flux of 4×10^{38} ergs/sec to the faintest limit yet obtained for an extragalactic H II region population, at a level of 5×10^{34} ergs/sec. We are exploring a portion of the H II region luminosity realm that has hitherto been largely unsampled, except in the solar neighborhood. Most of the H II regions are sufficiently faint to be explained by the excitation of a single early-type star, though some of the faintest are probably segments of diffuse galactic emission.

Although the bright end of the luminosity function can be fit satisfactorily to a power law, as found for most spiral galaxies, the curve has a peak at a flux of approximately 10^{36} ergs/sec, with a shallow decrease in number for fainter H II regions. This behavior results from the fact that the amount of ultraviolet energy released decreases more steeply than the number of stars increases for later type stars.

Three different definitions of sizes have been used to explore the properties of the H II region size distribution. As found for other galaxies, the size distribution can be fit by an exponential; the size scale is 33 pc. The fluxes are correlated to the 2.8 power of the diameter, but there is a large intrinsic scatter in this relationship.

GR8. Deep narrowband $H\alpha$ imaging of the nearby dwarf irregular galaxy GR8 has revealed a total of 32 H II regions. Positions, $H\alpha$ luminosities, and sizes of these objects have been determined. The $H\alpha$ luminosity function has the same shape as that for more luminous galaxies, except for size of sample effects. Most H II regions detected are at the very low luminosity end of the general luminosity function. The size distribution has an exponential shape, as for other galaxies, with a size scale of 17 pc. Candidates for the exciting stars can be identified for some of the H II regions; they are very blue, with $M_B = -5$ to -6 .

IC 10. Deep CCD narrowband $H\alpha$ imaging of the local group dwarf irregular galaxy IC 10 has revealed a total of 144 H II regions. Positions, $H\alpha$ luminosities, and sizes of these objects have been determined. The $H\alpha$ luminosity function has the same shape as that for more luminous galaxies. The faintest H II regions are at the low-luminosity end of the generally observed luminosity function for H II regions in galaxies, with fluxes of only $\sim 8 \times 10^{34}$ erg/sec. The size distribution has an exponential shape, as for other galaxies, with a size scale of 23 pc. Published radio continuum and CO maps compare well with the

H α emission distribution in the brightest areas, when smoothed to comparable resolution. The distribution of H I is similar in the central areas to the H II, but is much more widely distributed in the outer areas.

IC 1613. A deep search of 25 CCD fields centered on IC 1613 has resulted in a catalog of 71 H II regions, which include the 19 mapped by Sandage (1971) and most of the 26 measured by Price (1989). Our objects include several very low surface brightness rings and circular objects at large distance from the main body of the galaxy.

Sandage, A. R. 1971, *Ap. J.*, **166**, 13.

Price, J. 1989, this conference



Figure 1. Sample CCD frame showing central H II regions of IC 1613.

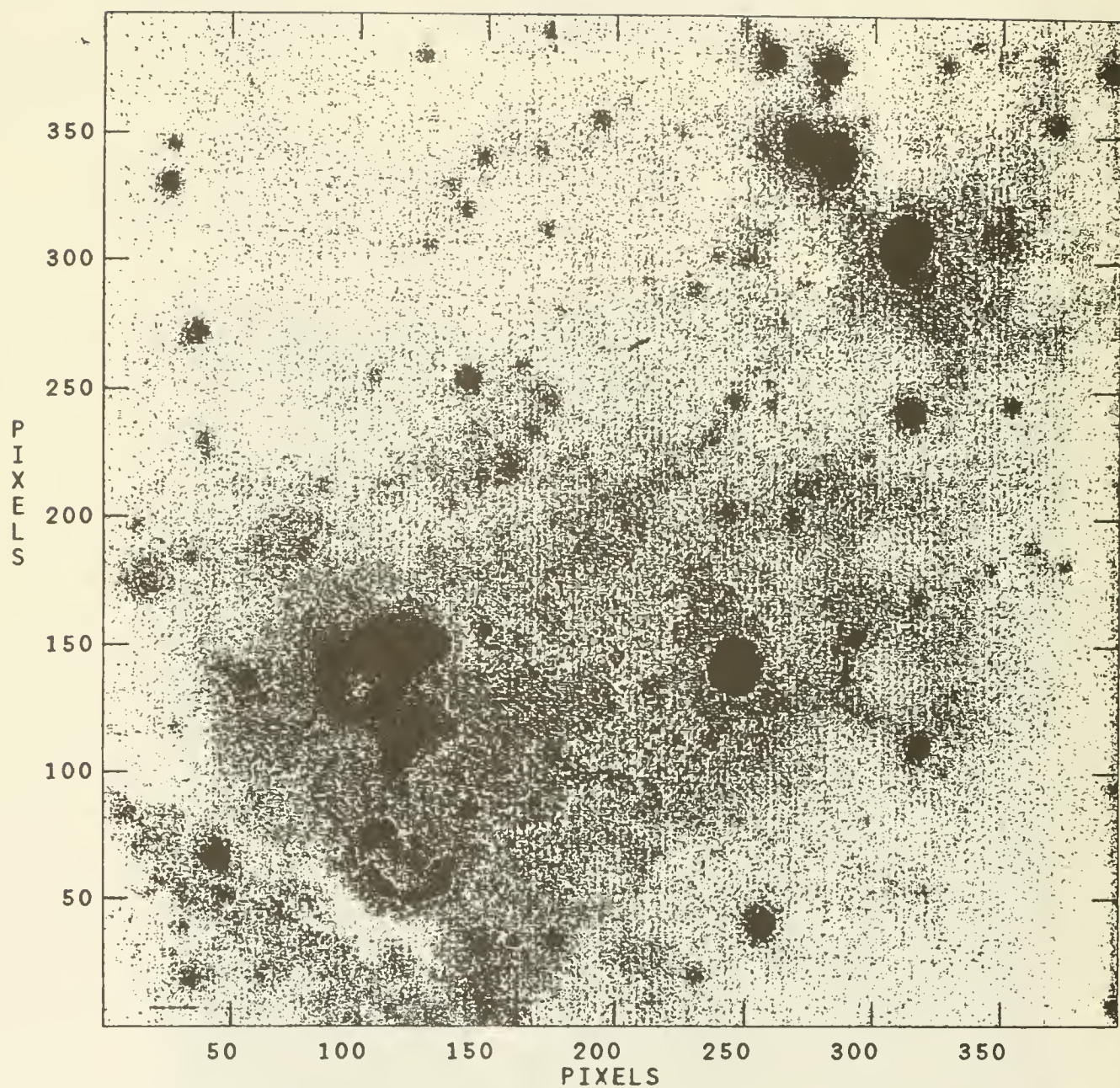


Figure 2. Sample CCD frame showing H II regions in IC 10.

HII Regions in IC 1613: The ISM in a Nearby Dwarf Irregular Galaxy

Jill S. Price (Bentley College), Stephen F. Mason (Prime Inc.), and Craig A. Gullixson (Lowell Observatory)

IC 1613, a nearby (725 kpc distant) dwarf irregular galaxy, has always been known to contain large, ring-shaped HII regions in its northeast corner. A new H_{α} image has been obtained using the Bell Labs CCD camera (on loan from J.A. Tyson), an RCA 320 X 512 pixel-thinned, back-illuminated CCD, an H_{α} filter of central wavelength 6562 Å and width (FWHM) of 30 Å, and the 42 inch telescope at Lowell Observatory. Our low resolution (2".6 pixels, 3".4 PSF) images exhibit many new, faint features. Figure 1 shows the entire CCD H_{α} image (11'.1 in R.A. by about 6'.1 in declination), on which HII regions are labelled: S1, S2, S3, etc. for HII regions catalogued by Sandage (1971, Ap. J., 166, 13); H1, HII, HIII, etc. for HII regions which are new to this study; and D1, D2, and D3 are some representative "diffuse" areas of emission, areas where the HII region boundaries are not clearly delineated, but there is emission nonetheless. In Figure 2, we compare our image (at high and low contrast) with Sandage's (1971) photo of the northeast corner of IC 1613. Hodge et al. (this volume) present higher resolution images of the same area. Figure 3 compares the H_{α} luminosity function for HII regions in IC 1613 (open squares) with that for the Small (filled squares) and Large (crosses) Magellanic Clouds. The last two figures compare observed size distributions- number of HII regions larger than a given diameter vs diameter- for IC 1613 (Figure 4) and NGC 6822 (Figure 5) with two models:

$$(1) \text{ Poisson distribution: } N^*(D) = \sum_n \frac{(D_0)^n \exp(-D_0)}{n!}$$

$$(2) \text{ exponential distribution: } N^*(D) = N_0 - N_0 \exp(D/D_0) ,$$

where $n = 0, 1, 2$, etc., and stands for the "bin number", ($n = 0$ for $D = 0-5$ pc, $n = 1$ for $D = 5-10$ pc, etc.), D_0 is the average HII region diameter, and N_0 is the total number of HII regions in the sample. We see that the Poisson models provide a better fit for IC 1613 and NGC 6822.

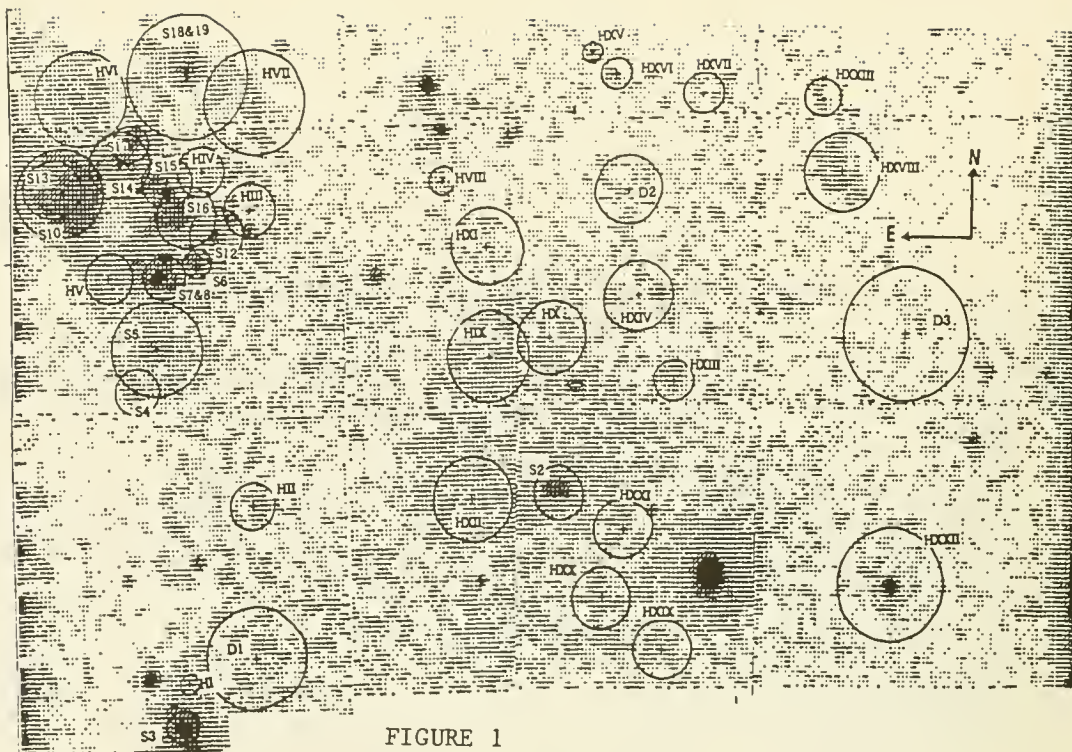


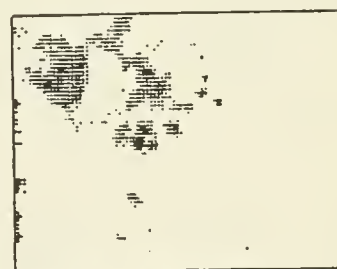
FIGURE 1



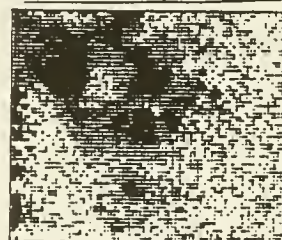
Sandage (1971)

Figure 2

All to the
Same Scale



This study (low contrast)



This study (high contrast)

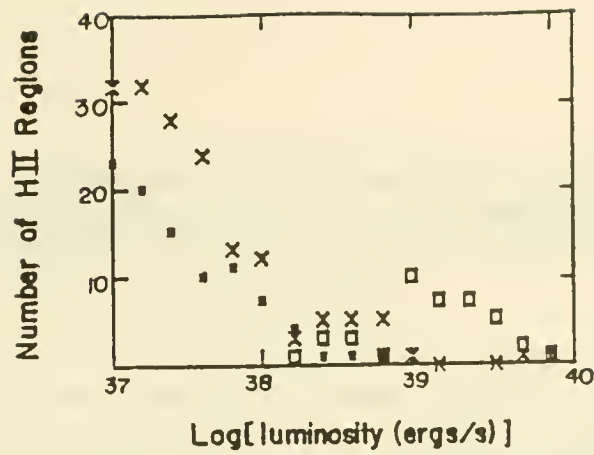


Figure 3. The $H\alpha$ luminosity function for: IC 1613 (open squares), the SMC (filled squares) and the LMC (crosses). The plot is the number of HII regions vs. $\log(H\alpha$ luminosity), binned every 0.2 dex. Data for the Magellanic Clouds from Kennicutt, Edgar, and Hodge's recent work (1989, Ap. J., 337, 761).

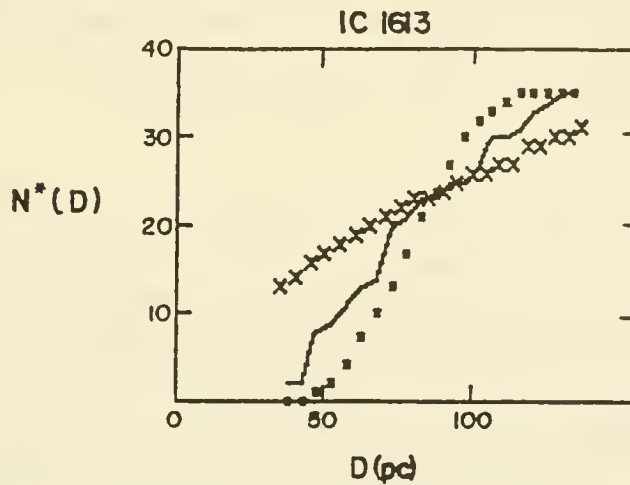


Figure 4. Size distribution for HII regions in IC 1613. The number of HII regions larger than diameter D is plotted vs. D for: data (solid line), Poisson distribution (filled squares), for an average diameter 83 parsecs, and exponential model with $N_0 = 35$, $D_0 = 63$ pc (crosses).

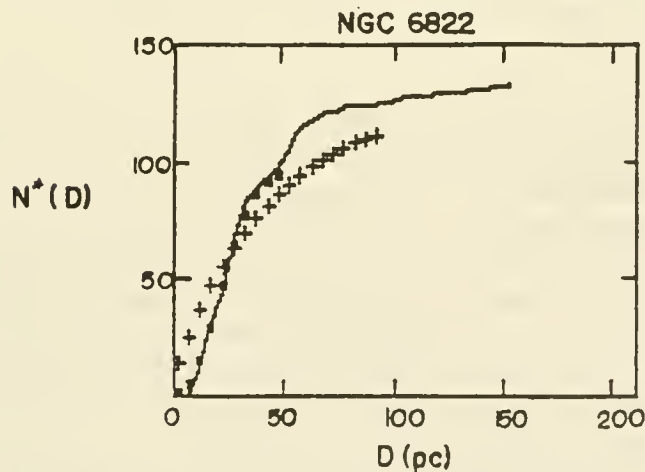


Figure 5. Size distribution for HII regions in NGC 6822 (data from the recent work by Hodge, Lee, and Kennicutt: 1988, P.A.S.P., 101, 32). The same symbols are used as in Fig. 4. For the Poisson distribution only the first ten bins were used, so the average HII region diameter is 24 pc. In the exponential model for the whole sample, $N_0 = 134$, and $D_0 = 43$ pc.

DIFFERENCES IN THE SIZE-INTERNAL VELOCITY RELATION OF GALACTIC AND EXTRAGALACTIC HII REGIONS

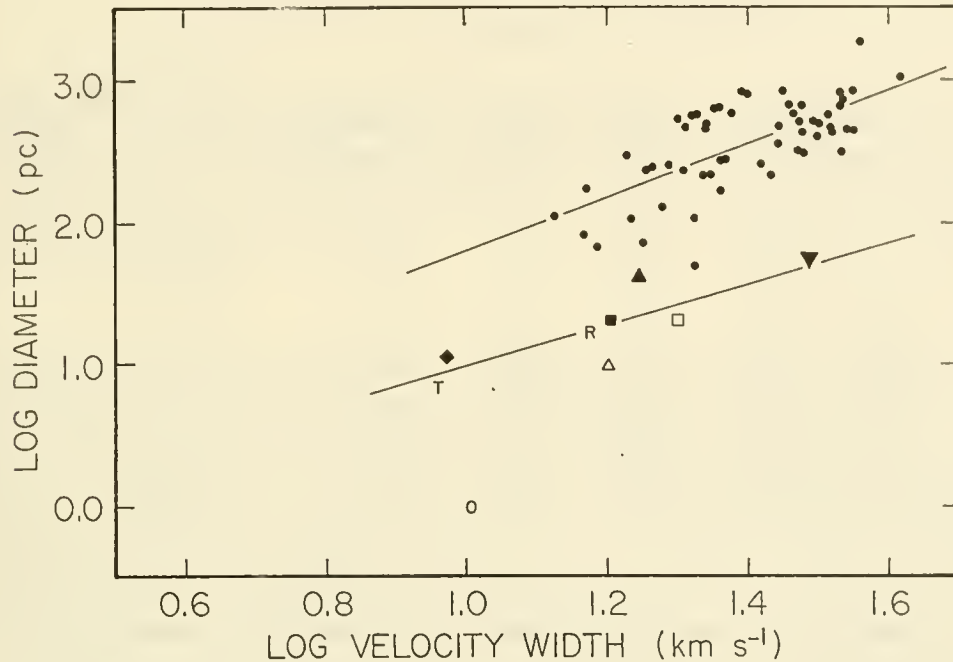
C. R. O'Dell
Rice University

SUMMARY: This study examines the nature of the size-internal velocity relation in extragalactic HII regions in order to improve their use as distance determinants. I have compared the relation between the linear size and the internal velocity for HII regions in the Galaxy and in external galaxies. Data for the former are from my own studies at high spatial resolution while the latter have been the subject of spectroscopy that includes almost the entire objects. The Galactic HII regions are corrected to values of the internal velocity that would be observed if they were at extragalactic distances. I find a very different size-internal velocity relation for the two types of objects in the sense that the extragalactic objects are some ten times larger at the same internal velocity. This is interpreted to mean that the extragalactic HII regions are actually complexes of small HII regions comparable in size to their Galactic counterparts.

EXTRAGALACTIC. The potential application of Giant Extragalactic HII Regions (GEHR) as distance determinants for galaxies is very great because of the ability to resolve them at large distances. The early studies that assumed limiting sizes for the largest objects have given way to methods that seek to determine the linear size from an observable quantity such as the emission line broadening. A linear relation between GEHR size and line width was first quantitatively advocated by Melnick (1977) and has since been refined (Roy, Arsenault, and Joncas 1986, Melnick et al. 1987, Arsenault and Roy 1988, Melnick 1988, Arsenault et al. 1988). The line width is usually expressed as the half width at which the intensity has dropped to a value $1/e$ that of the line peak. The line widths (β) are usually expressed in values corrected for the appropriate electron temperature, which allows the variable quantities to be more visible. The small angle of the GEHR means that values of β are usually determined from spectroscopic apertures that include most of a single object. The results of the study of Arsenault and Roy (1988) are shown in the figure, where we have used their sizes for the limiting H α isophotes. One finds a general relation of the form $\log D = -0.077 + 1.878 \log \beta$.

GALACTIC. My colleagues and I have studied the internal velocity in Galactic HII regions for over a decade, compiling observations at spatial resolutions that varied from about 1 to 10 percent of the size of the nebulae (Castañeda and O'Dell 1987, Castañeda 1988, Fountain, Gary and O'Dell 1979, 1983a, 1983b, Mufson et al. 1981, O'Dell, Townsley, and Castañeda 1988). In these studies we have found that there are velocities due to thermal gas motion, large scale flow of gas, and fine scale random motions usually referred to as turbulence. Since these observations were made at high spatial resolution, the data for each nebula must be corrected to what would have been observed had the entire nebula been observed, as was the case for the GEHR. The results are shown in the table and in the figure. One sees that the Galactic HII regions also fall into a linear relation with the exception of the Orion Nebula, which is substantially smaller than the other nebulae studied. Excluding the Orion Nebula from the set gives a relation $\log D = -0.46 + 1.43 \log \beta$ with a correlation similar to the GEHR. The slope in this relation is much less than the

value of three that would be expected for a Kolmogorov model of turbulence for HII regions having similar energy densities. This more rapid increase in turbulence with size is probably due to the large scale motions of the HII regions, which for the optically bright objects selectively includes objects in the champagne phase of their evolution.



The relation between size and l/e velocity for GEHR (filled circles), and Galactic HII regions NGC 1499 (open triangle), NGC 7000 (filled triangle), S252 (open square), NGC 6611 (filled square), NGC 6514 (T), IC 1318B/C (inverted filled triangle), NGC 6523 (filled diamond), the Rosette Nebulae (R) and NGC 1976 (O).

Comparison of the results for the two data sets shows that the GEHR are all larger than the Galactic HII Regions, the GEHR being about ten times larger at the same value of β , and that the slope of the relation is slightly different. Had we used the core diameters where available, the GEHR would have been only about three times smaller. The most straightforward interpretation of the difference is that the GEHR are actually complexes of HII regions like the Galactic objects. In this case the size would be determined by the “packaging” of the nebulae and the inferred velocities would be the addition of the values of the individual regions together with any random motions. A detailed numerical model with the number of HII regions decreasing in number with increasing sizes shows that the slope in the figure should vary between GEHR and HII regions in the same sense as shown. This interpretation could be tested by observing GEHR down to sizes that overlap the Galactic sample, in which case one would expect to see a wider spread of velocities in a given size range since individual large regions would begin to be observed in addition to the complexes.

In summary, we see that the size-internal velocity relation for GEHR that is used for extragalactic distance determination is based on the same physics that govern this relation for Galactic HII

regions, which makes this method much less *ad hoc* than first appears; however, the GEHR seem to be complexes of multiple HII Regions, which gives them a different zero point in their calibration.

TABLE 1
Expected Velocity Widths of Galactic HII Regions

Object	<u>Diameter (pc)</u> studied total		Log D (total)	β_{OBS} (km s ⁻¹)	Standard Deviation*	$\sqrt{\beta_{\text{OBS}}^2 + \text{SD}^2}$	References [†]
NGC2237-46	15.0	15.0	1.176	16.4	0.0	16.4	1
NGC1499	9.55	9.55	0.980	15.8	2.34	15.97	2
NGC7000	40.7	40.7	1.610	16.9	5.13	17.66	2
IC1318B/C	52.4	52.4	1.719	31.2	--	31.2	2
S252	19.5	19.5	1.290	19.3	4.79	19.89	3
NGC6611	20.1	20.1	1.303	16.5	4.62	17.13	4
NGC6514	0.71	7.0	0.845	8.8	2.48	9.11	5
NGC6523	1.0	11.6	1.064	7.42	5.65	9.33	5
NGC1976 A+B	0.3	1.0	0.0	7.05	7.29	10.14	6

*Calculated standard deviation in all radial velocities, scaled to the full size of the nebula.

[†](1) Fountain, Gary and O'Dell 1979, (2) Fountain, Gary and O'Dell 1983a, (3) Fountain, Gary and O'Dell 1983b, (4) Mufson et al., 1981, (5) O'Dell, Townsley & Castañeda 1987, (6) Castañeda 1988

REFERENCES

- Arsenault, R. and Roy, J.-R. 1988, *Astron. Ap.*, **201**, 199.
 Arsenault, R., Boulesteix, J., Georgelin, Y., and Roy, J.-R. 1988, *The Extragalactic Distance Scale*, S. van den Bergh and C. J. Pritchett, ed. (San Francisco, Astr. Soc. of Pacific) p. 303.
 Castañeda, H. O. 1988, *Ap. J. Suppl.*, **67**, 93.
 Castañeda, H. O., and O'Dell, C. R. 1987, *Ap. J. Letters*, **315**, L55.
 Fountain, W. F., Gary, G. A., and O'Dell, C. R. 1979, *Ap. J.*, **229**, 971.
 _____, 1983a, *Ap. J.*, **269**, 164.
 _____, 1983b, *Ap. J.*, **273**, 639.
 Melnick, J. 1977, *Ap. J.*, **213**, 15.
 _____ 1988, *The Extragalactic Distance Scale.*, S. Van den Bergh and C. J. Pritchett, editors (San Francisco, Astro. Soc. of Pacific) p. 157.
 Melnick, J., Moles, M., Terlevich, R., Garcia-Pelayo, J. M. 1987, *M.N.R.A.S.*, **226**, 849.
 Mufson, S. L., Fountain, W. F., Gary, G. A., Howard, W. E., III, O'Dell, C. R., and Wolff, M. T. 1981, *Ap. J.*, **248**, 992.
 O'Dell, C. R., Townsley, L. K., and Castañeda, H. O. 1988, *Ap. J.*, **317**, 676.
 Roy, J. R., Arsenault, R., and Jocas, G. 1986, *Ap. J.*, **300**, 626.

A Study of H II Regions in Spiral Galaxies Using Multiobject Spectroscopy

Dennis Zaritsky¹, Richard Elston^{1,2}, and J.M. Hill¹

¹*Steward Observatory, University of Arizona, Tucson AZ, 85721*

²*KPNO, Tucson AZ, 85721*

ABSTRACT

We present results from multiobject spectroscopy of H II regions in nearby late-type spiral galaxies. Our results include excitation measurements, $\log ([\text{O III}]/\text{H}\beta)$, for 81 regions in M 101, 30 regions in NGC 2403, and 13 regions in M 51. We conclude that late-type spirals can be classified into two distinct populations, examine possible causes of this division, and derive metallicity gradients for these galaxies. M 51 appears to have an anomalously shallow abundance gradient.

Before the advent of multiobject spectroscopy only one galaxy, M 33, had excitations, $\log ([\text{O III}]/\text{H}\beta)$, measured for more than 30 of its H II regions. In fact, excitation and metallicity gradients for most galaxies are derived from measurements of roughly 10 regions. Since the development of multiobject spectroscopy, we have presented excitation measurements for 45 regions in M 33 (Zaritsky, Elston, and Hill 1989a; Paper I) and Walsh and Roy (1989) have presented measurements for 49 regions in NGC 2997. In this paper, we present results from observations of 81 regions in M 101, 30 regions in NGC 2403, and 13 regions in M 51. Multiobject spectroscopy provides the opportunity to observe a large number of regions in a fraction of the observing time previously required.

The observations were made using the MX Spectrometer on the Steward Observatory 90 in. (2.3 m) telescope on Kitt Peak. MX is a multiaperture spectrometer equipped with optical fibers that are attached to microprocessor controlled mobile probes. There are 32, 4 arcsec aperture object-designated fibers. An 832 gpm grating in second order centered at $\approx 4800 \text{ \AA}$ provided a spectral scale of 0.7 \AA per pixel. Typical exposure times were about 1 hour. For more details of the observing procedure, data reduction, and error estimation see Paper I and Zaritsky, Elston, and Hill (1989b).

In Figure 1a we present the data for M 33 (from Paper I), M 51 (data from this study and from Searle (1971) and Smith (1975)), M 101, NGC 2403, and NGC 2997 (from Walsh and Roy 1989). It is apparent that these five galaxies can be sorted into two distinct groups with very little overlap. The demarcation between the two groups becomes more striking when one considers that the scatter in excitation measurements for a single galaxy at a given radius can be as large as 1 dex. We have used these data as the training sample with which to construct a classification scheme. The classification scheme was then applied to data from the literature for Sbc to Scd type galaxies for which at least five H II regions have been observed (from Searle 1971, Smith 1975, Pagel *et al.* 1979, Dufour *et al.* 1980, Edmunds and Pagel 1984, and McCall *et al.* 1985). The results are presented in Figure 1b. The misclassification percentage (a regions is termed misclassified if its classification is different than that of the majority of the regions in its parent galaxy) is less than 9%, with many of the misclassified regions being less than 1σ away from the dividing line. Even if with additional data the division between the groups disappears, it is clear that there are significant global differences in excitation among late-type galaxies.

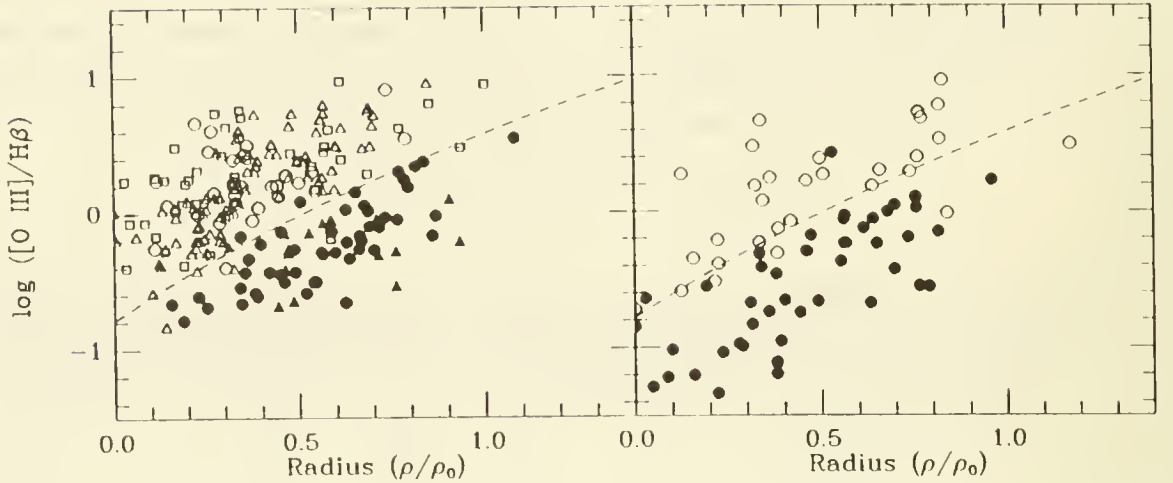


Figure 1a (left) - M 101 (open triangles), M 33 (open squares), NGC 2403 (open circles), NGC 2997 (solid circles), and M 51 (solid triangles). Dashed line indicates division between proposed populations. Figure 1b (right) - Data from literature for NGC 300, NGC 628, NGC 2403, NGC 3344, NGC 4736, NGC 5068, NGC 7793, M 33, and M 101 (open circles). Data from literature for NGC 1635, NGC 2903, NGC 2997, NGC 3184, NGC 3351, NGC 4254, NGC 4321, NGC 5055, NGC 6946, IC 342, M 51, and M 83 (solid circles).

Excitation is a function of the dust content, the ionizing radiation field, and the abundance of the H II region. Searle (1971) argued against the first two parameters when discussing the cause of the excitation gradients in galaxies by citing the lack of radial variations in either $H\alpha/H\beta$ (sensitive to dust), or in $I(\text{He I } \lambda 5876)/I(H\beta)$ (sensitive to high energy photons). We examined whether variations in dust content or ionizing field could produce the global excitation differences between galaxies. There is no clear division between the distributions of either $H\alpha/H\beta$ or $I(\text{He I } \lambda 5876)/I(H\beta)$ for the two groups; therefore, we conclude that neither dust content nor ionizing field is the primary cause of the grouping in Figure 1.

It has been suggested (McCall 1982) that metal abundance be plotted as a function of fractional effective radius or surface mass density instead of fractional isophotal radius. The reasoning is that both of these quantities provide better physical descriptions. In support of this, we find that when excitation is plotted against either of these quantities, the data fall more nearly on a single curve. However, there is still strong segregation between the groups and in the case of the relationship between excitation and fractional effective radius, more scatter than when excitation is plotted against fractional isophotal radius.

We have applied the empirical calibration of $\log([O \text{ III}]/H\beta)$ (Edmunds and Pagel 1984) to estimate the oxygen abundance of the observed H II regions. Empirical calibrations rely on a statistical relationship between the observed line ratios and abundance. Multiobject spectroscopy compliments this technique by providing a large number of measurements at a given radius, thereby allowing for an accurate statistical measurement of the metal abundance at that radius, provided the empirical calibration is correct. The abundance gradients we measure for M 33, M 51, M 101, NGC 2403, and NGC 2997 using this empirical calibration are -0.098 ± 0.027 , -0.042 ± 0.010 , -0.072 ± 0.006 , -0.089 ± 0.033 , -0.093 ± 0.010 dex kpc^{-1} , respectively. Previous measurements are -0.01 ± 0.03 (using

data from Kwitter and Aller 1981), -0.081 ± 0.027 (Tosi and Diaz 1985), -0.074 ± 0.006 (Evans 1986), -0.083 ± 0.032 (Tosi and Diaz 1985), and 0.084 (Walsh and Roy 1989), for M 33, M 51, M101, NGC 2403, and NGC 2997 respectively. The excellent agreement ($< 1\sigma$) between the gradients derived for M 33, M101, NGC 2403 and NGC 2997 imply that the empirical calibration for excitation when used in conjunction with measurements of over 30 H II regions produces results at least as accurate and precise as those obtained from a combination of the favored empirical calibration, that of $([\text{O II}] + [\text{O III}])/\text{H}\beta$, and detailed modelling. The derived gradient for M 51 is in marginal agreement ($< 2\sigma$) with the previous determination, but the difference is due entirely to the additional regions, not to the abundance calculations.

In conclusion, we have discussed briefly some of the preliminary results from multi-aperture spectroscopy of H II regions in some nearby late-type spiral galaxies, M 33, M 51, M 101, NGC 2403, NGC 2997. We conclude that late-type spirals can be classified into two distinct groups based on the excitation of their H II regions at a given fractional isophotal radius. We also conclude that neither dust nor ionizing field is the prime cause of this segregation.

We have also used an empirical calibration between excitation and abundance to measure the abundance gradients in these five galaxies. The agreement between our results using the empirical calibration of $\log([\text{O III}]/\text{H}\beta)$ and those of previous authors using detailed models and the calibration of $\log(([\text{O II}] + [\text{O III}])/\text{H}\beta)$ demonstrates that excitation can be used to measure abundance gradients as accurately and precisely as previously, provided measurements for many H II regions are used. M 51 apparently has a shallower gradient than the other galaxies, which we propose might be a result of the interaction with NGC 5195. Future work will include further analysis of the cause of the two populations, analysis of azimuthal variations in excitation and abundance, and a corresponding study of earlier-type galaxies.

DZ acknowledges support from a NSF Graduate Fellowship, and thanks the Minority Graduate Student Travel Fund at the U. of A. and the organizers of this meeting for travel support.

References

- Dufour, R.J., Talbot, R.J. Jr., Jensen, E.B., Shields, G.A. 1980, *Ap. J.*, **236**, 119.
 Edmunds, M.G., and Pagel, B.E.J. 1984, *M.N.R.A.S.*, **211**, 507.
 Evans, I.N. 1986, *Ap. J.*, **309**, 544.
 Kwitter, K.B., and Aller, L.H. 1981, *M.N.R.A.S.*, **195**, 939.
 McCall, M.L. 1982, Ph.D. dissertation, University of Texas.
 McCall, M.L., Rybski, P.M., and Shields, G.A. 1985, *Ap. J. Suppl.*, **57**, 1.
 Pagel, B.E.J., Edmunds, M.G., Blackwell, D.E., Chun, M.S., and Smith, G. 1979, *M.N.R.A.S.*, **189**, 95.
 Searle, L. 1971, *Ap. J.*, **168**, 327.
 Smith, H.E. 1975, *Ap. J.*, **199**, 591.
 Tosi, M., and Díaz, A.I. 1985, *M.N.R.A.S.*, **217**, 571.
 Walsh, J.R., and Roy, J.-R. 1989, *Ap. J.*, **341**, 722.
 Zaritsky, D., Elston, R., and Hill, J.M. 1989a, *A. J.*, **97**, 97; Paper I.
 Zaritsky, D., Elston, R., and Hill, J.M. 1989b, in preparation.

The diffuse ionized interstellar medium perpendicular to the plane of NGC 891

Ralf-Jürgen Dettmar[§], Lowell Observatory, Flagstaff, Arizona

Jean Keppel, NOAO, Tucson, Arizona

Morton S. Roberts, NRAO, Charlottesville, Virginia

and

John S. Gallagher III, Lowell Observatory, Flagstaff, Arizona

Introduction

The structure of the interstellar medium in galactic disks is very complex. Star formation processes affect the surrounding interstellar medium in galactic disks by means of energy inputs from stellar winds and supernovae. As a result of these processes the interstellar medium in the disk can connect to the galactic halo. One effect of this process is believed to be cosmic ray and hot gas leakage into the galactic corona, which is responsible for extended radio and X-ray emission above the plane.

This is described in terms of galactic fountains and loops by theorists and in terms of supershells and worm-structures by observers. Possible models depend on the energy input, gas temperature and density, and the presence of magnetic fields (e.g. Cox 1986).

Models of magnetic fields in galaxies show (e.g., Sawa and Fujimoto 1986) that axisymmetric magnetic fields in galactic disks can give rise to vertical field components. Such vertical components or Parker instabilities could build up magnetic flux tubes that possibly connect the processes within the disk to the halo.

Vertical magnetic fields could also explain observed vertical dust features which are most prominent in the edge-on galaxy NGC 891 (Sofue, 1987). Numerous dust filaments perpendicular to the plane are visible on plates taken under excellent seeing conditions. These dust structures can be traced out to 1.5 kpc above the plane. NGC 891 is a very promising candidate for studies of the so-called "disk-halo-connection" as it also possesses a thick radio continuum emitting disk.

In an attempt to study the structure and the properties of the diffuse ionized interstellar medium perpendicular to the plane of disk galaxies we have obtained H α images and spectra of NGC 891.

Observations

Our spectroscopic data consist of two sets of observations. All of these data were taken with the Mayall 4-m telescope at Kitt Peak National Observatory [†]. The first set, obtained between 1977 and 1979, contains eight photographic spectrograms taken with the R-C spectrograph. These spectra have a reciprocal dispersion of 26 Åmm⁻¹. A second set of spectra was obtained in 1989 and consists of CCD spectrograms in two positions, taken with the echelle spectrograph and UV camera. With this instrumentation the reciprocal dispersion was 8.0 Åmm⁻¹ at H α .

In addition H α images of NGC 891 were obtained in 1988 with the 42" telescope at Lowell Observatory. A 2:1 focal reducer was used with the f/8 secondary. A thinned 800x800 Tl chip was used resulting in an image scale of ~0.8 arcsec/pixel. The H α distribution was obtained by subtracting a scaled R band image from the image taken with the H α filter.

Results

Perhaps the most remarkable property of the H α emission line in NGC 891 is its extension out of the plane of the galaxy: we are able to measure the H α line out to more than 30" (1.4 kpc) from

on leave from: Radioastronomisches Institut der Universität Bonn, Bonn, FRG

Kitt Peak National Observatory, National Optical Astronomy Observatories, is operated by the Association of Universities for Research in Astronomy, Inc., under contract with the National Science Foundation

the midplane. This means that the ionized hydrogen extends at least four times higher than the neutral hydrogen layer. An anomalously large scale-height for the ionized gas of ≈ 1 kpc is also found in the Milky Way (Reynolds 1989).

The echelle spectra show a changing ratio of [NII] to $\text{H}\alpha$. This excludes the possibility that the large scaleheight of the emission is due to scattering of disk emission by dust high above the plane. The z-extent of the $\text{H}\alpha$ emission is confirmed by the imaging result. The large z-extent of the ionized gas is confined to the inner half of the visible disk. In this inner region the $\text{H}\alpha$ distribution also shows a filamentary structure of the diffuse ionized medium. These filaments, sticking out of the plane, originate in HII regions in the plane.

The $\text{H}\alpha$ image also shows a large scale asymmetry if the NE and SW parts of the disk are compared. The NE part is more prominent and extended in $\text{H}\alpha$. The same asymmetry is also seen in the radio continuum distribution (Hummel *et al.* 1989). This correlation between the diffuse ionized medium and the distribution of relativistic electrons is one example of a relation between star formation processes in the disk and the various components of the halo.

Thermal filaments or spurs which are related to HII regions are also known in the Galaxy (Müller *et al.* 1987). These filamentary structures perpendicular to the galactic planes may represent the *chimneys* which result in the supernova dominated model of the ISM by Norman and Ikeuchi (1989).

Acknowledgments. RJD has been supported by the Deutsche Forschungsgemeinschaft under De 385/2-1.

REFERENCES

- Cox, D. 1986, in NRAO workshop No. 12, "Gaseous halos of galaxies", eds. J.N. Bregman and F.J. Lockman, NRAO, p. 239.
Hummel, E., Dahlem, M., and Beck, R. 1989, in preparation.
Müller, P., Reif, K., and Reich, W. 1987, *Astr.Ap.*, **183**, 327.
Norman, C.A., and Ikeuchi, S. 1989, *Ap.J.* in press.
Reynolds, R.J. 1988, *Ap.J.*, **339**, L29.
Sawa, T., and Fujimoto, M. 1986, *P.A.S.J.*, **38**, 133.
Sofue, Y. 1987, *P.A.S.J.*, **39**, 547.

II - HII REGIONS, HALO AND HOT GAS, COOLING FLOWS

B - HALO AND HOT GAS

HOT INTERSTELLAR GAS AND IONIZATION OF EMBEDDED CLOUDS

K-P Cheng and F. Bruhweiler

Department of Physics, Catholic University of America

We present detailed photoionization calculations for the interstellar cloud in which the Sun is embedded. We consider the EUV radiation field with contribution from discrete stellar sources and from a thermal bremsstrahlung-radiative recombination spectrum emitted from the surrounding 10^6 K coronal substrate. We establish lower limits to the fractional ionization of hydrogen and helium of 0.17 and 0.29 respectively. The high He ionization fraction results primarily from very strong line emission below 500 Å originating in the surrounding coronal substrate while the H ionization is dominated by the EUV radiation from the discrete stellar sources. The dual effects of thermal conduction and the EUV spectrum of the 10^6 K plasma on ionization in the cloud skin are explored. The EUV radiation field and Auger ionization have insignificant effects on the resulting ionic column densities of Si IV, C IV, N V and O VI through the cloud skin. Our calculations show that the abundances of these species are dominated by collisional ionization in the thermal conduction front. Because of a low charge exchange rate with hydrogen, the ionic column density ratios of $N(\text{C III})/N(\text{C II})$ and $N(\text{N II})/N(\text{N I})$ are dominated by the EUV radiation field in the local interstellar medium. These ratios should be important diagnostics for the EUV radiation field and serve as surrogate indicators of the interstellar He and H ionization fraction respectively. Spacecraft such as Lyman which is designed to obtain high resolution spectral data down to the Lyman limit at 912 Å could sample interstellar lines of these ions.

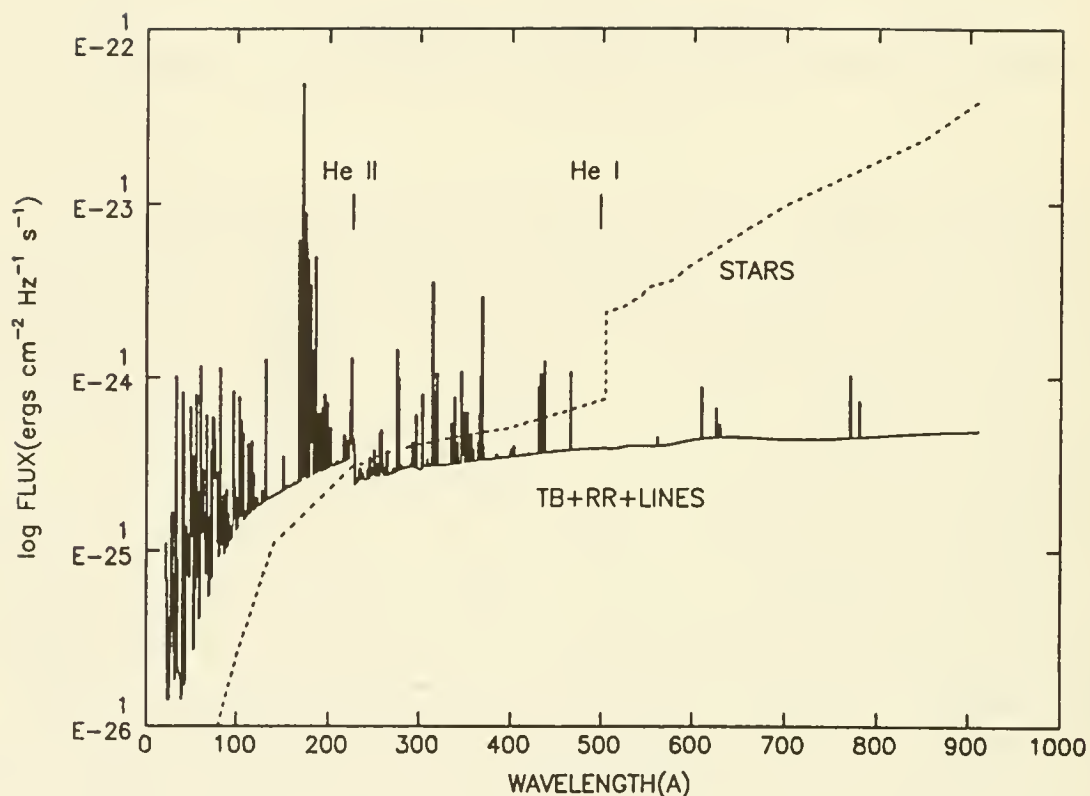


Fig. 1 - Unattenuated EUV flux distributions of the diffuse and discrete sources. The curve labeled "STARS" indicates the contribution from the dominant stellar sources. The diffuse X-ray background flux from the 10⁶ K gas is represented by the sum of three components: thermal bremsstrahlung, radiative recombination, and line emission. This is represented by the curve labeled "TB+RR+LINES". The important emission lines are summed into 1 Å bins. The ionization edges of He I (504 Å) and He II (228 Å) are indicated.

RADIATIVE THERMAL CONDUCTION FRONTS

Kazimierz J. Borkowski, Steven A. Balbus, and Carl C. Fristrom
Virginia Institute for Theoretical Astronomy, Department of Astronomy,
University of Virginia.

I INTRODUCTION

The discovery of the O VI interstellar absorption lines in our Galaxy by the *Copernicus* observatory was a turning point in our understanding of the ISM. It implied the presence of widespread hot ($\sim 10^6$ K) gas in disk galaxies. The detection of highly ionized species in QSOs absorption spectra may be the first indirect observation of this hot phase in external disk galaxies.

Previous efforts to understand extensive O VI absorption line data from our Galaxy were not very successful in locating the regions where this absorption originates. The location at interfaces between evaporating ISM clouds and hot gas was favored, but recent studies of steady-state conduction fronts in spherical clouds by Ballet, Arnaud, and Rothenflug (1986) and Böhringer and Hartquist (1987) rejected evaporative fronts as the absorption sites. We report here on time-dependent nonequilibrium calculations of planar conductive fronts whose properties match well with observations, and suggest reasons for the difference between our results and the above. We included magnetic fields in additional models, not reported here, and our conclusions are not affected by their presence.

II THE CONDUCTION FRONT

We consider the structure and evolution of a conduction front propagating between the hot ISM and a cold planar cloud. Gas at constant temperature and pressure is distributed uniformly in each phase. The hot phase cools through the emission of the optically thin radiation. As a result, the hot gas temperature T_h decreases with time from its initial value T_{h0} . The cold gas at temperature 10^4 K is assumed to be in a stable thermal equilibrium, with radiative losses balanced by energy sources. Initially, the temperature changes discontinuously from T_{h0} to 10^4 K at the transition between the two phases.

The early stage of the front evolution is dominated by conductive heating of the cold gas. Radiative losses can be neglected, and a self-similar solution (Balbus 1986) accurately describes the front evolution. Temperature profile in this stage in our representative model with $T_{h0} = 7.5 \times 10^5$ K and pressure of 3750 K cm^{-3} , somewhat modified by radiative losses, is shown in Figure 1 as a function of the hydrogen column density at 2.8×10^5 years. Note the front steepness at low temperatures. The conduction front broadens continuously, resulting in reduced conductive heating of the cold medium. Radiative losses eventually become important, first at temperatures $\sim 10^5$ K (where line cooling is particularly effective), and later throughout the whole front. Finally, the front becomes sufficiently broad for radiative losses to balance the rate at which energy is conducted from the hot gas. The front comes to a halt at this time, which we denote t_{rad} . We find that $t_{rad} \sim 2 \times 10^6$ years is an order of magnitude less than the cooling time $\sim 2 \times 10^7$ years of the hot gas. The temperature profile for the quasi-static front is shown in Figure 1 at 2.2×10^6 years.

At still later times $t \geq t_{rad}$, radiative cooling dominates the evolution. *The gas is now flowing from the hot phase towards the cold phase, rather than evaporating from the cold cloud.* This late-time evolution can be described as a cooling wave propagating into the hot gas (Doroshkevich

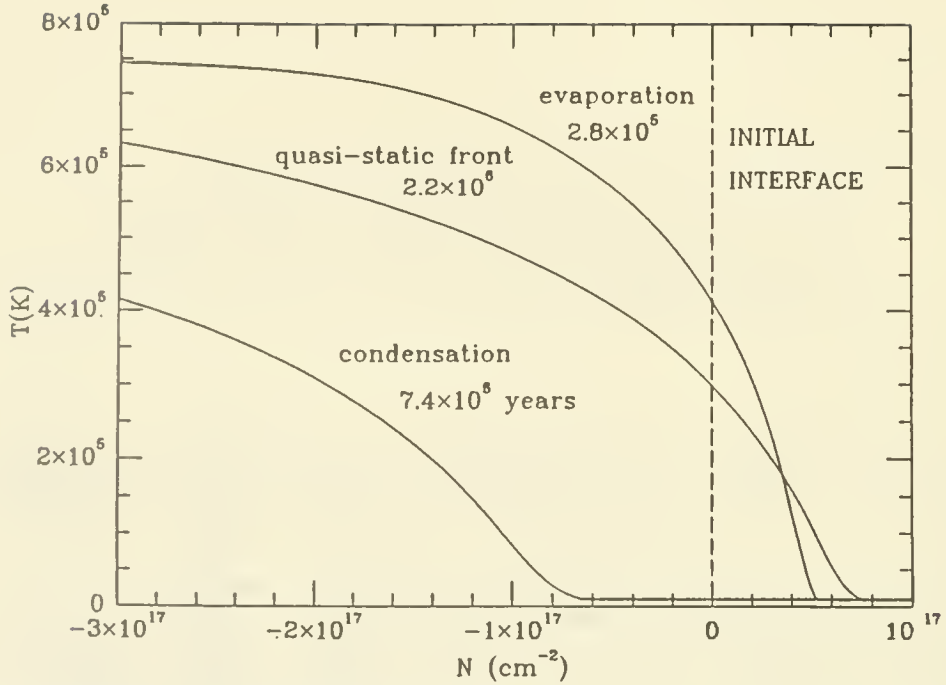


Figure 1: Temperature T vs. hydrogen column density N in a model with the initial hot medium temperature 7.5×10^5 K and pressure of 3750 K cm^{-3} .

and Zel'dovich 1981). The late-time temperature distribution is shown in Figure 1 at 7.4×10^6 years.

III COLUMN DENSITIES

In Figure 2, we present a plot of ionic column densities for selected species as a function of time t . Initially, the gas is underionized, and the front is deficient in highly ionized species. Their column densities increase with time, however, as the evaporated hydrogen column density increases and the collisional ionization becomes effective. The column density of each ion species i attains maximum at time $t_{i, \text{coll}} \sim (n_e C_i)^{-1} \approx T_{h0}/C_i(T_{h0}/2)P$, where C_i is the collisional rate coefficient ($\text{cm}^3 \text{s}^{-1}$) from state i .

At later times, the front has grown sufficiently broad that a quasi-steady state develops, and the column densities remain nearly constant, or gradually decrease as the gas flows from the cold to the hot phase. Finally, the structure of the front changes from an evaporative to a cooling front when the conductive heating is balanced by radiative losses. The column densities decrease (see dips in Figure 2 at $\sim 2 \times 10^6$ years), but as the cooling front continues to broaden the values again increase. However, the column number density of each ion species i is fairly constant after the time $t_{i, \text{coll}}$, and does not depend on pressure P .

Column number densities of important ions present in conduction interfaces are insensitive to the detailed structure of these interfaces, provided that the hot medium temperature T_{h0} exceeds 7.5×10^5 K. A detection of highly ionized species with the column densities such as in Figures 2 should be considered as a strong evidence for the presence of conduction interfaces in the ISM. Such quantities of O VI were detected by the *Copernicus* satellite (Jenkins 1978). Two-thirds of the O VI bearing gas originates in the discrete components with 10^{13} ions per cm^{-2} . This agrees very well with our results (Figure 2).

The observations of other highly ionized atoms are consistent with both evaporative and condensing interfaces, with the notable exception of Si IV. The N V/O VI column density ratio is equal to ~ 0.1 (York 1977), in agreement with our results shown in Figure 2. A recent survey

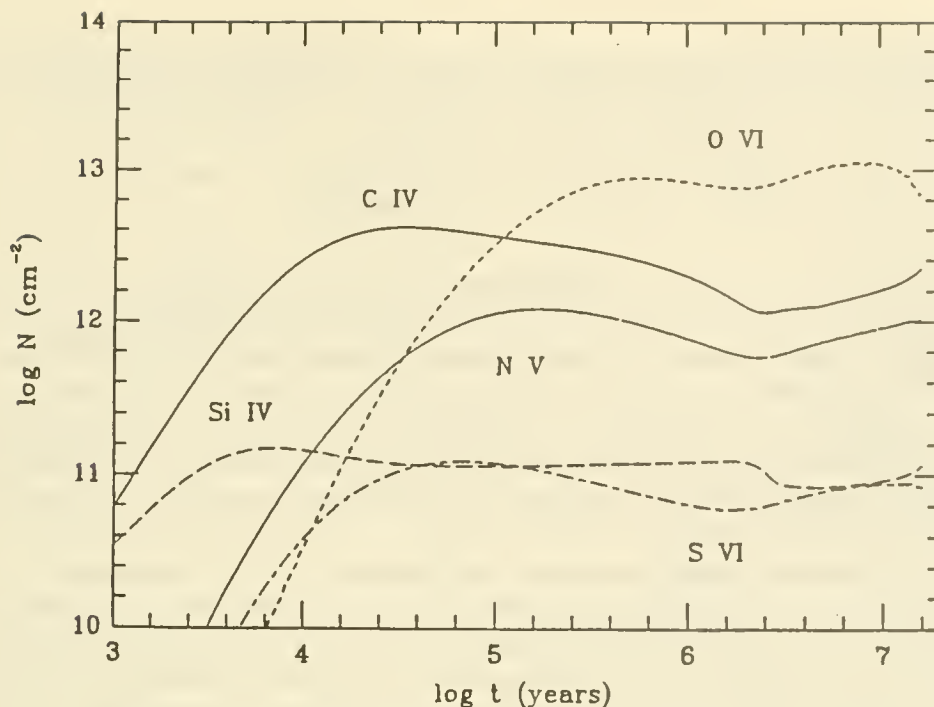


Figure 2: The ion column densities along the front normal vs. time t .

of N V, C IV, and Si IV interstellar absorption lines (Savage and Massa 1987) give an average number density ratio, relative to O VI, of 0.11, 0.25, and 0.07, respectively. The C IV/O VI ratio again agrees with our results, but Si IV absorption lines are an order of magnitude stronger than expected, indicating that Si IV is probably produced by photoionization.

IV DISCUSSION

Böhringer and Hartquist (1987) rejected evaporative fronts as the sites where the O VI absorption originates because the calculated line widths were larger than the observed widths. While this argument applies also to planar conductive fronts in the evaporative stage of their evolution, the temperature of the line formation region is lower in condensing fronts which results in better agreement with the observed line widths. The identification of condensing conductive fronts as the sites where highly ionized atoms, such as O VI, N V, and possibly C IV, are present, leads to interesting conclusions. Haloes of disk galaxies are thought to contain hot gas whose cooling onto embedded clouds could produce highly ionized ions seen in absorption in QSOs absorption systems. Condensing conductive fronts could also be present in clusters of galaxies (Doroshkevich and Zel'dovich 1981) and in elliptical galaxies which exhibit signs of cooling flows.

REFERENCES

- Balbus, S. A. 1986, *Ap. J.*, 304, 787.
 Ballet, J., Arnaud, M., and Rothenflug, R. 1986, *Astr. Ap.*, 161, 12.
 Böhringer, H., and Hartquist, T. W. 1987, *M. N. R. A. S.*, 228, 915.
 Doroshkevich, A. G., and Zel'dovich, Ya. B. 1981, *Soviet Physics — JETP*, 53, 405.
 Jenkins, E. B. 1978, *Ap. J.*, 220, 107.
 Savage, B. D., and Massa, D. 1987, *Ap. J.*, 314, 380.
 York, D. G. 1977, *Ap. J.*, 213, 43.

Energy Input and HI Spin Temperatures in Low Pressure Regions

E. Corbelli and E. E. Salpeter

CRSR, Cornell University, Ithaca, NY

We report on two recent (unpublished) HI emission/absorption studies, carried out with good sensitivity using the Arecibo 21cm beam. One study (Colgan, Salpeter and Terzian) looked for high velocity clouds of our own Galaxy in absorption in the directions of 63 of the brightest continuum sources reachable with the Arecibo telescope. HI emission mapping in the neighborhood of these directions was also carried out. The other study (Corbelli and Schneider) looked for absorption along lines of sight to about 50 weaker sources which pass within a few diameters of nearby disk galaxies. Neither study detected any absorption.

Three generalizations emerge from these and previous published absorption studies, as well as published emission mapping of high velocity clouds (HVC) and outer regions of disk galaxies. Qualitatively, at least, these properties are similar for HVCs and outer disks: (1) There is no evidence for any appreciable column densities of HI ($N_{\text{HI}} \gtrsim 5 \times 10^{18} \text{cm}^{-2}$, say) being “hidden” in emission studies by an extreme “subthermal effect” depressing the HI spin temperature T_S so far below the gas kinetic temperature T_K that it approaches the microwave background radiation temperature T_R . (2) While there is a wide dynamic range of values for N_{HI} , there is a tendency towards a “cut-off” on the lower end. One can state a related tendency for the (projected) shapes of iso-intensity contours: While the shapes of outer contours can be highly non-circular (e.g. irregular, long “plumes”), there is a tendency for fairly sharp intensity gradients near some lower “cut-off” value N_l of N_{HI} . For HVCs the column densities extend up to a few times 10^{20}cm^{-2} and N_l is of order a few times 10^{18}cm^{-2} ; for outer disks N_l is of order 10^{19}cm^{-2} . (3) For column densities N_{HI} up to $\sim 10^{20} \text{cm}^{-2}$ one usually sees no HI absorption at all. For total column densities a few times larger one may find appreciable absorption over a narrow velocity range, but still none for most of the HI over a wider velocity range (see, e.g., Carili, van Gorkom and Stocke, *Nature* **338**, 134 1989). Given the sensitivity for absorption studies, we see that most of the HI material for a column density of $N_{\text{HI}} \sim (1 \text{ or } 2) \times 10^{20} \text{cm}^{-2}$ must lie at a spin temperature T_S above some measurement threshold of at least a few hundred K. We thus have to consider appropriate heat sources.

Presumably neither HVCs nor outer disks and plumes have supernova remnants or hot stars inside them, so the energy source must come from the outside. We consider first two simple extreme cases (a) A ubiquitous flux of penetrating ionizing radiation (cosmic rays or X-rays with $h\nu \gtrsim 150 \text{ eV}$); (b) Some heat source, presumably coming from supernova energy release in the inner disk and moving upward and outward through a corona (“galactic fountain”), which ionizes only indirectly through collisions (e.g. hydrostatic waves, see Ferriere, Zweibel and Shull, *Ap.J.* **332**, 984, 1988). For thermal equilibrium at an assumed pressure p and gas kinetic temperature T_K , the required energy input rate ϵ per H-atom is appreciably larger for (a) than for (b), because the electron density is larger and free electrons lead to larger radiative cooling losses. The “subthermal effect”, the depression of spin temperature T_S below

T_K , depends on the Lyman-alpha pumping rate, which in turn depends on the ionizing flux and the column density; this depression is smaller for (a) than for (b). For $N_{III} \sim (1 \text{ or } 2) \times 10^{20} \text{ cm}^{-2}$, we have calculated the required values of ϵ for a number of assumed pairs of values of p and T_S ; for most cases the first effect dominates the second, so that ϵ is larger for (a) than for (b). The dependence on p and T_S is complex, but at $p \sim 100 \times k \times \text{cm}^{-3} \times K$ and $T_S \sim (100 \text{ to } 3,000) \text{ K}$ we have roughly $\epsilon \sim 3 \times 10^{-15} \text{ eV } H^{-1} s^{-1}$ for case (a) (the dependence on p is less than linear). The ϵ required for case (b) is smaller by a factor between 0.1 and 0.5.

We return to the observational generalizations, numbered (1), (2), (3) above, in relation to different models: (1) states that $T_S - T_R$ is not very small for $N_{III} \gtrsim 5 \times 10^{18} \text{ cm}^{-2}$, say. This is not surprising theoretically--such an extreme subthermal effect would arise only for very small pressures ($p \lesssim 1 \times k \times \text{cm}^{-3} \times K$) and if there is little energy input beyond starlight and the minimum extragalactic X-ray background. A practical consequence, however, is that HI emission brightness temperature measurements always give N_{III} (or an upper limit) correctly. (2) states that outer edges of HVCs and galactic disks or plumes tend to have sharp edges in N_{III} , at some column density level N_I (between $\sim 2 \times 10^{18}$ and 10^{19} cm^{-2}). This could have two types of explanations: (a) These structures could have been formed with sharp edges in total hydrogen (neutral plus ionized), although one would still have to explain why the edge has not broadened with time. (b) The edge could appear artificially sharp when viewed in HI because an ionizing flux or other energy input produces an ionized layer for column densities up to N_I . Because of the small value of N_I the pressure p , and hence the required flux, is quite uncertain. At these low column densities, "star-like" UV ($h\nu = 13.6$ to about 50 eV) could play a role. Sufficiently powerful heat sources for observational generalization (3; see below) are probably also sufficient to ionize a column density of $\sim N_I$. In view of the likely strong heat sources (and the empirical fact 1 above) we need not consider the alternative of very low T_S hiding emission for $N_{III} \lesssim N_I$.

(3) The minimum extragalactic cosmic ray and X-ray flux is not sufficient to keep spin temperatures above a few hundred K for a relatively thick layer with $N_{III} \sim (1 \text{ to } 2) \times 10^{20} \text{ cm}^{-2}$ (stellar UV photons with $h\nu < 50 \text{ eV}$ are irrelevant here since they could not penetrate). Fortunately, the uncertainty in the internal pressure is not very great in this case: Pressures must be appreciably smaller than in an inner galactic disk ($p \lesssim 10^3 k \text{ cm}^{-3} K$, say) and must exceed that due to self gravity alone ($p \gtrsim 10 k \text{ cm}^{-3} K$ for $N_{III} \sim 10^{20} \text{ cm}^{-2}$). The required flux of cosmic rays or medium-soft X-rays ($h\nu \gtrsim 150 \text{ eV}$) impinging from the outside is of order $10^{-6} \text{ erg cm}^{-2} s^{-1}$. This is not ruled out, but would represent an appreciable energy requirement if it were a cosmologically uniform extragalactic diffuse flux; e.g., it is larger by a factor of order 10 than an extrapolation of the known power-law X-ray flux at $h\nu > 1 \text{ keV}$ down to $\sim 150 \text{ eV}$. The overall energy budget is of course less severe if the energy flux is not ubiquitous but comes from the individual galaxy through its corona in a "galactic fountain" (see Ap. J. 326, 551, 1988). If the energy carried in such a stream were primarily in the form of hydromagnetic waves, electron heat conduction and cooling flows, the energy required would probably be slightly less than for ionizing radiation (intermediate between cases a and b). If spread over a radius of about 30 kpc, such a stream would require $\sim 5\%$ of the total galactic supernova energy output rate.

The Interstellar Halo of Spiral Galaxies: NGC 891

S. R. Kulkarni, R. J. Rand and J. J. Hester

California Institute of Technology, Pasadena, CA91125

Introduction.

It is now being increasingly recognized that the warm, ionized medium (WIM) is a major phase of the interstellar medium in our Galaxy. At the Solar circle, this medium has a mean density $\sim 0.03 \text{ cm}^{-3}$ and a temperature of $\sim 7500 \text{ K}$. This gas is detected by two principal techniques: dispersion of pulsar signals and faint, diffuse optical line emission due to recombination ($\text{H}\alpha$) and collisional excitation of metastable lines ($[\text{S II}]$ and $[\text{N II}]$). The power needed in the form of ionizing photons to match the observed recombinations exceeds the power injected by SNe. Consequently it is thought that the WIM is ionized by stars: young stars, hot white dwarfs, planetary nebulae etc. The unknown topology of the neutral ISM has so far prevented us from precisely identifying the dominant ionizing agents.

The vertical structure of the WIM is of considerable interest from many viewpoints. In our Galaxy, pulsar dispersion measure data appear to indicate that the local WIM layer is about 3 kpc thick (two-sided) and a filling factor, ϕ , somewhere between 10% and 30%. However, some WIM exists at $|z| > 3 \text{ kpc}$ as evidenced by UV absorption studies towards hot halo stars, stars in the Magellanic Clouds and nuclei of active galaxies.

The large scale distribution of the WIM phase can provide a crucial handle on our understanding of the WIM. For example, the radial variation of the WIM phase can throw considerable light on the nature of the ionizing sources. Knowledge of the vertical distribution of the WIM is certainly needed before issues of pressure support and ionization can be addressed. Unfortunately, our location prevents us from obtaining a comprehensive view of the large scale structure of the Galactic WIM. Consequently, we started a program of narrow band imaging in the $\text{H}\alpha$ line of nearby galaxies. NGC 891, an edge-on Sb galaxy and considered to be similar to our Galaxy, was our prime target.

Observations and Reduction

The observations were done at the 60-inch telescope of the Palomar Observatory. A reimaging camera followed by a CCD detector (TI 800²) enabled us to obtain a wide field, $16 \text{ arcmin} \times 16 \text{ arcmin}$. NGC 891 was observed with an $\text{H}\alpha$ filter of 15 \AA bandwidth and a much wider continuum filter.

All cameras, especially reimaging cameras, suffer from scattered light problem viz. light from a bright source is scattered over a large portion of the detector. For most normal imaging projects, this can be ignored. However, in our case, the expected WIM emission from NGC 891 is weak and light scattered from the bright HII regions which are confined to the disk of the galaxy could mimic diffuse emission at high $|z|$. Let $\epsilon(x)$ be the scattered PSF. Then the observed image, $B(x)$ is

$$B(x) = A(x) * [1 + \epsilon(x)]$$

where $A(x)$ is the image that one would have obtained in the absence of scattering. We observed a bright star and measured $\epsilon(x)$. (In reality, $\epsilon(x)$ is a function of the position of the

centroid of the bright star; we ignore this subtle but numerically unimportant correction in the analysis reported here). It is easy to show that to $O(\epsilon(x)^2)$, we can get a scatter corrected image:

$$\begin{aligned} A_{cor}(x) &= B(x) - B(x) * \epsilon(x) \\ &= A(x) - [A(x) * \epsilon(x)] * \epsilon(x). \\ &\simeq A(x) \end{aligned}$$

The on- and off-band images after the above deconvolution were registered, gain corrected by using a grid of stars and subtracted to yield a continuum subtracted H α image. In a similar manner, images were obtained in the $\lambda\lambda$ 6713Å and 6731Å line of [S II]. Here we present only the H α observations.

Assuming a distance of 9.5 Mpc to NGC 891 (equivalent to assuming a Hubble's constant of 50 km s⁻¹ Mpc⁻¹), our pixel of 1.2 arcsec translates to 57 pc. This resolution is more than sufficient to study the diffuse ionized gas in NGC 891. Indeed we purposely degrade the spatial resolution in one axis to further improve the sensitivity e.g. in order to study the z -distribution we divide the galaxy into five regions: the bulge, the mid-section (East and West) and the outer galaxy (East and West). The final reliable sensitivity achieved in such 1-dimensional slices is an emission measure limit of $EM \sim 0.3 \text{ cm}^{-6} \text{ pc}$ where we have assumed an temperature of 10⁴ K to convert the observed H α emission to EM .

Distribution of the Diffuse Ionized Gas

Our preliminary results show that NGC 891, a spiral galaxy considered to be rather similar to our Galaxy, has more WIM than our Galaxy. We readily detect strong integrated emission from the HII regions confined to the plane of the galaxy. Diffuse emission is easily detected out to a radial distance of 11 kpc and to $|z| \simeq 5$ kpc. The latter detection is perhaps the most significant result of our project.

Mid-Region ($3 < R < 6$ kpc). At our sensitivity limit, the gas is readily detected to $|z| \simeq 5$ kpc. Averaging the gas between galactocentric radius 2 and 5 kpc, the emission measure can be represented as

$$EM(z) = 75 e^{-|z|/2.2 \text{ kpc}} \text{ pc cm}^{-6}.$$

The above one-component fit clearly falls short of the observations for high $|z|$. A second component with a scale height larger than 2.2 kpc is needed to describe the very high $|z|$ emission. Since $EM(z) = \langle n_e^2 \phi \rangle(z) P$ where P is the effective path length and $\phi(z)$ is the filling factor of thermal electrons we deduce that the vertical density distribution of the electrons is given by

$$\langle n_e \phi \rangle(z) = 0.1 \sqrt{\phi(z)} e^{-|z|/4.4 \text{ kpc}} \text{ cm}^{-3}.$$

In arriving at the above equation we have used an effective path length $P = \sqrt{R_g^2 - R_0^2}$ where $R_0 = 3.5$ kpc, the mean galactocentric radius of the slice and R_g is the effective radius of the diffuse gas, assumed to be 12 kpc.

Assuming a $\phi \sim 0.25$ (the value appropriate for the Solar neighbourhood as estimated by Reynolds) we derive a mean density of 0.05 cm^{-3} which is about twice the mean density at the Solar circle.

The vertical column density of the electrons is given by $\int_{-\infty}^{+\infty} \langle n_e(z) \rangle dz$ which turns out to be $420 \sqrt{\phi/0.2} \text{ cm}^{-3} \text{ pc}$, considerably larger than the equivalent value of 70 to $100 \text{ cm}^{-3} \text{ pc}$ at the Solar circle of our Galaxy. While there is evidence that the WIM increases in the inner region of our Galaxy by a factor of perhaps 2 there is no doubt that the WIM layer in NGC891 is more massive than that in our Galaxy.

Outer Galaxy ($5 < R < 9 \text{ kpc}$). We detect $\text{H}\alpha$ emission out to $|z| \simeq 5 \text{ kpc}$. A one component fit to a slice averaged over galactocentric radius 5 and 9 kpc yields

$$EM(z) = 45 e^{-|z|/2.4 \text{ kpc}} \text{ pc cm}^{-6}.$$

As before, this model falls below the observed emission for large $|z|$. The surface density of the thermal electrons can be estimated as before and is found to be $376 \sqrt{\phi/0.2} \text{ cm}^{-3} \text{ pc}$ or $11 M_{\odot} \text{ pc}^{-2}$ (this includes correction from He). In contrast, the HI surface density in NGC 891 is $6 M_{\odot} \text{ pc}^{-2}$. These observations show the importance of the WIM in spiral galaxies like NGC891.

Beyond galactocentric radius of 9 kpc, it becomes quite increasingly hard to see the high- $|z|$ emission. Between 9 and 12 kpc, we detect emission quite easily to a z -height of 1.4 kpc. Study of the WIM in this region is important because ionization by young stars probably comparable to other sources such as the extragalactic UV background.

Inner Galaxy ($0 < R < 3 \text{ kpc}$). NGC 891, like our Galaxy, has a central hole in both HI and CO. Coincident with the inner edge of the molecular distribution (at $R = 3 \text{ kpc}$) there is an enhanced WIM emission. We are in the process of inferring the bulge ($R < 3 \text{ kpc}$) contribution from our data. Pending this we advise you to ignore any previous draft of this work that you may have seen.

Summary

We have detected the Warm Ionized Medium (WIM) phase in the galaxy NGC 891. We find that the radial distribution of the WIM follows the molecular or young star distribution – an expected dependence. The amount of the WIM in this galaxy exceeds that in our Galaxy. The major surprise is the large thickness of the WIM phase – about 9 kpc instead 3 kpc as in our Galaxy. Clearly, this is the most significant result of our observations.

The presence of low ionization gas at high $|z|$ as well as at large galactocentric radii (where young stars are rare) is an important clue to the origin of the halo and observations such as the one reported here provide important data on this crucial question. In particular, the ionization of gas at high $|z|$ imply that either the UV photons manage to escape from the disk of the galaxy or that the extragalactic UV background plays an important role.

Bulk of the WIM in spiral galaxies is a result of star-formation activity and thus our results can be understood by invoking a high star formation rate in NGC891. Only the concerted action of supernovae can get the gas to the large z -heights as is observed in this galaxy. Support for this view comes from our detection of many “worms” i.e. bits and pieces of supershells in the form of kilo-parsec long vertical filaments. We also see a 600-pc size supershell located nearly one kpc above the plane of the galaxy.

The Onset of Galactic Winds in Early-Type Galaxies

W. Forman, C. Jones, W. Tucker, and L. David
Harvard-Smithsonian Center for Astrophysics

Einstein x-ray observations have shown that bright elliptical galaxies contain extensive coronae of hot ($T \sim 10^7\text{K}$) gas. Prior to the Einstein observations, it was generally believed that early-type galaxies (ellipticals and S0's) contained little gas or dust. The discovery from Einstein observations that bright early-type galaxies, as a class, contain up to several $10^{10} M_{\odot}$ of hot gas (Forman, Jones and Tucker 1985) both demonstrated that these galaxies contained a substantial interstellar medium and provided a tool for measuring the total mass of these systems. While the x-ray emitting coronae seen in the Einstein images account for the bulk of the mass shed by the evolving stars, sensitive observations primarily in the optical and the infrared have shown that the interstellar medium in early-type galaxies is complex with components (gas and dust) at widely differing temperatures (e.g. Jura 1986, Jura et al. 1987, DeMoulin-Ulrich et al. 1984, Phillips et al. 1984).

In our initial x-ray survey (Forman, Jones and Tucker 1985), we showed that, if the hot coronae around luminous early-type galaxies were not in hydrostatic equilibrium, then the replenishment rates of the gas would have to be nearly 100 times higher than expected from the mass loss by the known stellar populations. Therefore, we concluded that these galaxies do not presently drive galactic winds. It is now generally agreed that a massive dark halo is required to gravitationally bind these hot coronae to the underlying galaxies (Forman, Jones, and Tucker 1985, Fabian et al. 1986, Mathews and Loewenstein 1986, Sarazin and White 1988; see Trimble 1987 for a review).

The status of the hot gas in lower luminosity (and hence lower mass) galaxies is less clear. Calculations show that, for a given supernova rate, a critical galaxy luminosity (mass) exists below which the gas cannot be gravitationally confined and a galactic wind is predicted to be effective in expelling gas from the galaxy (Loewenstein and Mathews 1987; David et al. 1988). Thus, galaxies which fall below a certain mass are expected to drive winds and should contain little or no hot gas. The critical galaxy luminosity which defines the transition from hydrostatic atmospheres to galactic winds depends on the type I supernova rate.

We report on a program using Einstein X-ray observations of the x-ray spectra and surface brightness profiles (or extents) of a large sample of early-type (elliptical and S0) galaxies for which our goal is to determine the critical optical luminosity

for which galactic winds are important. For galaxies in which the x-ray emission is dominated by hydrostatic coronae, the x-ray spectra will be relatively soft (characterized by a temperature of $\sim 10^7\text{K}$), while for galaxies with a galactic wind, the emission will be dominated by the spectrally harder discrete sources (since the x-ray emission from the wind is essentially negligible). Although galaxies in the transition region, those having subsonic or partial winds, may have spectra that are comparable to those with hydrostatic atmospheres, they are predicted to have flatter x-ray surface brightness profiles. Thus, with a combination of surface brightness profiles and x-ray spectroscopy, we should be able to determine the critical luminosity separating galaxies with winds from those with hydrostatic gaseous coronae. Gas temperatures have so far been published for only nine early-type galaxies (eight in Forman, Jones, and Tucker, 1985 and one additional galaxy spectrum in Trinchieri et al. 1986). These nine published spectra are all for quite luminous galaxies. In our new sample of 180 galaxies, there are 28 early type galaxies with sufficient counts to obtain a spectrum with the Einstein IPC (these galaxies are marked in Figure 1). This sample more than doubles the total number of early-type galaxies in earlier compilations (Forman, Jones, and Tucker 1985; Canizares et al. 1987). The new new spectral observations will help determine the critical optical luminosity for the onset of galactic winds which is important for understanding the chemical evolution of galaxies and of the intergalactic medium. The implications of galactic winds for the heavy element enrichment and energy content of the intracluster medium will be discussed.

REFERENCES

- Canizares, C., Fabbiano, G., and Trinchieri, G. 1987, *Ap.J.*, 312, 503.
David, L., Forman, W., and Jones, C. 1988, preprint.
DeMoulin-Ulrich, M.H., Butcher, H., and Boksenberg, A. 1984, *Ap. J.*, 285, 527.
Fabian, A.C., Thomas, P.A., Fall, S. M., and White, R. E. 1986, *MNRAS*, 221, 1049.
Forman, W., Jones, C., and Tucker, W. 1985, *Ap. J.*, 293, 102.
Jura, M. 1986 *Ap. J.* 306, 483.
Jura, M., Kim, D.W., Knapp, G.R., and Guhathakurta, P. 1987, *Ap. J.*, 311, L11.
Loewenstein, M. and Mathews, W. 1987, *Ap.J.*, 319, 614.
Mathews, W. and Loewenstein, M. 1986 *Ap.J.*, 306, L7.
Phillips, M. Jenkins, C., Dopita, M., Sadler, E., and Binette 1986, *AJ*, 91, 1062.
Sarazin, C. and White, R. 1988 *Ap.J.* 331, 102.
Trimble, V. 1987, *Ann. Rev. of Astr. and Astrophys.* 25, 425.
Trinchieri, G., Fabbiano, G., and Canizares, C. 1986, *Ap.J.*, 310, 637.

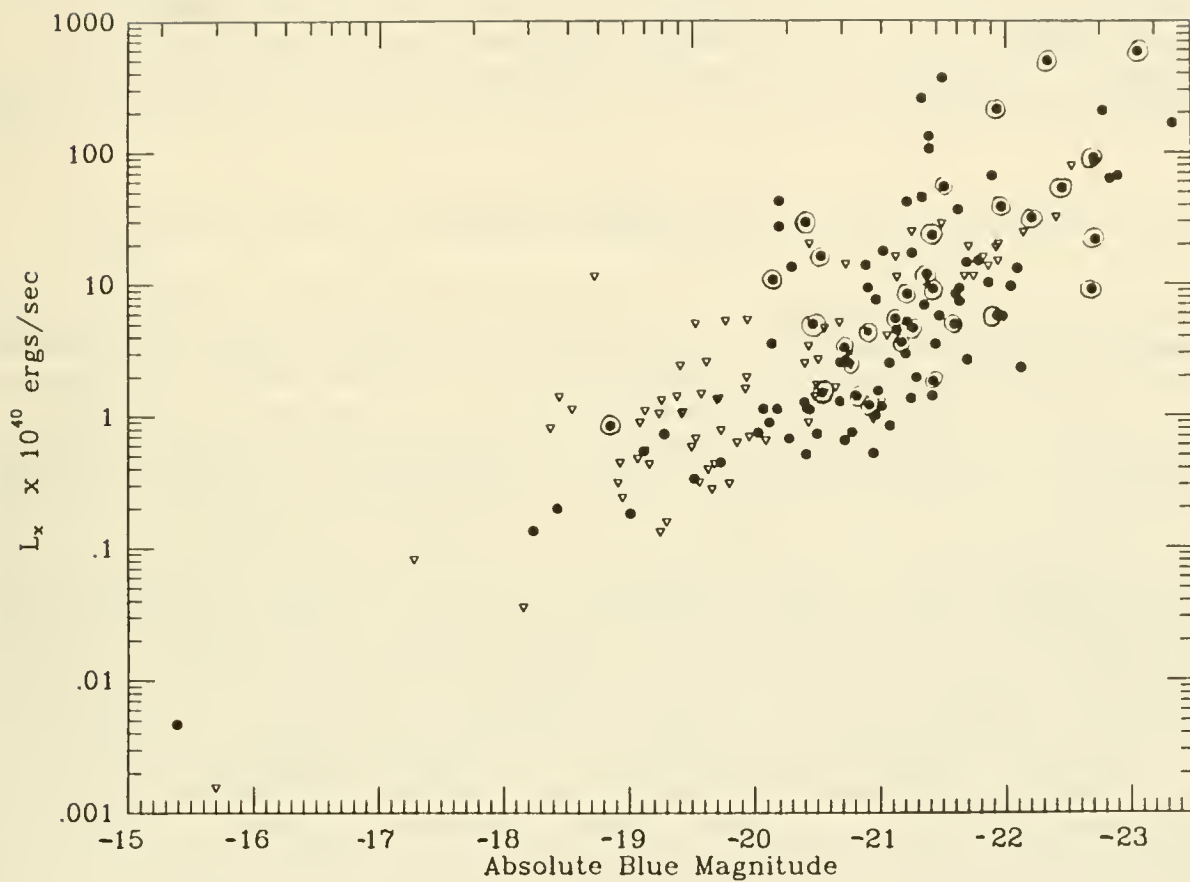


Figure 1 shows the correlation, for nearly 180 early type galaxies, of x-ray with optical luminosity. The solid circles are detections and the open triangles represent upper limits. Galaxies whose x-ray spectra can be determined are denoted with a second, open circle.

The environments of double radiogalaxies

Steve Rawlings, MRAO, Cavendish Laboratory, Cambridge, UK.

Abstract

I discuss simple methods by which the densities and pressures of the gas confining double radiogalaxies can be estimated from optical and X-ray data. By applying these methods to an unbiased sample of nearby ($z < 0.5$) double radiogalaxies, I quantify the empirical relation between the external confining pressure and the internal pressure of the lobes as inferred from the minimum energy argument. This relation is explained by an analytic model in which the lobes are statically confined by ambient material pre-heated in the bow-shock of the advancing radio source. Such a model allows one to: (a) estimate source expansion speeds from a combination of radio and environmental data; and (b) estimate properties of the environment from radio data alone providing expansion speeds can be estimated from multifrequency observations.

1 The empirical relation between internal and external pressure

In a study of the effects of the environment on the properties of radio sources three different classes of ambient material must be considered, namely the ISM, the ICM and the IGM. The detection of X-ray haloes out to radii ~ 100 kpc around nearby giant elliptical galaxies ¹ indicates that the lobes of radiogalaxies (typically ~ 300 kpc total size) will be confined by this circum-galactic material unless the galaxy is in the core of a reasonably rich cluster; only for low-redshift giant radio sources do we need to consider the effects of the IGM. Therefore, I have classified the environments of the unbiased sample of 39 double radiogalaxies studied optically by Rawlings et al. ² according to the number of galaxies (N_{250}) with $M_V < -21$ within 250 kpc of the radiogalaxy; the environments with $N_{250} > 5$ are termed cluster core (C) and those with $N_{250} < 4$ termed isolated (I), the remaining intermediate cases are termed group (G). Although crude, this classification scheme is systematic, repeatable and unbiased with respect to redshift; furthermore it was found to be almost perfectly correlated with the X-ray data available for the sample objects. Using the standard formulae relating X-ray properties to gas pressure as a function of radius ^{1,3}, and where necessary estimating the X-ray properties from established correlations with optical properties ^{1,4}, I estimated the pressure external to the source using the null hypothesis that properties of the ambient material are not influenced by those of the radio source. Completely independent estimates of the *internal* pressure of the radio-emitting plasma were made by applying the standard minimum energy arguments ⁵ to the radio data. I plot the external pressure versus the minimum internal pressure in Fig. 1 obtaining a strong empirical correlation. Two further aspects of Fig. 1 deserve emphasis: for the sources in clusters there is a rough equality between minimum-internal and external pressure while for those associated with isolated galaxies over-pressures in the lobe of ~ 10 are the norm. I now outline an analytic model that explains these features by rejecting the null hypothesis and allowing the radio source to influence its own environment.

2 An analytic model for radio source confinement

The similarity of derived internal and external pressures in the cluster doubles, as seen in cluster sources with other structures, argues strongly that the minimum-lobe pressure is in fact a reasonable approximation to the true internal pressure. With this in mind it is constructive to consider the model source of total linear size D illustrated in Fig. 2. I assume that the volume of gas shocked by the radio source (ϕ_{bs}) as

it expands supersonically into the ambient medium is a fraction f of the maximum (ϕ_{\max}) obtained by considering a sphere of radius $D/2$ centred on the radiogalaxy. Thus

$$\phi_{\text{bs}} = \frac{\pi D^3 f (2R_T^2 - 3)}{12R_T^2}$$

By assigning an average pressure \bar{p} to the gas in the shocked region, its gain in internal energy is

$$U_{\text{bs}} = \frac{3\pi D^3 f ((2pR_T^2 - 3p) - 2p_0 R_T^2)}{24R_T^2}$$

If this energy is supplied adiabatically by the work done on the gas by the expanding heads of the source then

$$U_{\text{bs}} = \frac{\pi D^3 \eta^2 V^2 \rho_0}{4R_T^2}$$

where η is the ratio of the width of the working surface (the compact hotspot?) to the width of the lobes. Thus in a constant pressure and density atmosphere

$$\frac{\bar{p}}{p_0} = \frac{\frac{1.4m_p \eta^2 V^2}{kT} + fR_T^2}{f(R_T^2 - 1.5)}$$

For $V^2 < \frac{fR_T^2 kT}{1.4m_p \eta^2}$ this pressure enhancement factor tends to unity whereas for larger V we obtain

$$\frac{\bar{p}}{p_0} = \frac{1.4m_p V^2 \eta^2}{fkTR_T^2} \quad (1)$$

which for typical values of the parameters ($V = 0.05c$; $T = 3\text{keV}$; $R_T = 5$; $f = 0.1$; $\eta = 0.1$) gives overpressures of ~ 10 ; this value will increase with the Mach number of the jet principally as f and V^2 vary.

Thus this simple analytic model can explain the distribution of sources in Fig. 1 by allowing the rapidly expanding isolated radiosources to modify their own environments and thereby obtain static pressure balance between the lobe plasma and the shocked ambient gas in the bow-shock. A source with similar jet properties in a cluster will expand at a slower speed and will not have an apparent over-pressure in the lobe. *Thus the resulting shapes and luminosities of the lobes of double radiosources are influenced by the properties of both the powering jets and those of the surrounding environment.* These features also appear, although in a less immediately accessible form, in numerical simulations of double radiosources ⁶.

By assuming that the lobes are in static pressure balance (e.g. measured lobe minimum pressure $\approx p$) it is possible, using a suitably calibrated version of equation 1, to estimate the expansion speed of a radiosource using radio and environmental data. Furthermore, if V is known from the spectral ageing analysis of multifrequency radio data ⁸, then radio data alone can be used to estimate the properties of the environment at all redshifts. Further details of these methods and their uses will be presented at the Conference.

References

- [1] Forman W. *et al.* Ap.J. 293, 102 (1985) [2] Rawlings S. *et al.* MNRAS, in press. [3] Jones C. & Forman W. Ap.J. 276, 38 (1984). [4] Bahcall N. Ap.J. 238, L117 (1980). [5] Miley G. Ann.Rev.Astron.Astrophys. 18, 16 (1980). [6] Leahy J. & Williams A. MNRAS 210, 929 (1984). [7] Rawlings S. & Saunders R., IAU 134, in press. [8] Alexander P. & Leahy P. MNRAS 225, 1 (1987) [9] Guilbert P. & Fabian A., MNRAS 220, 439 (1986).

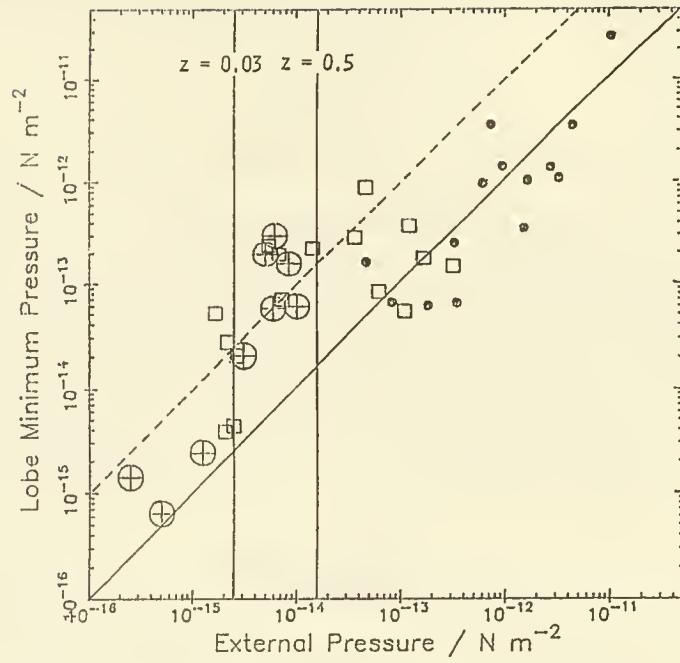
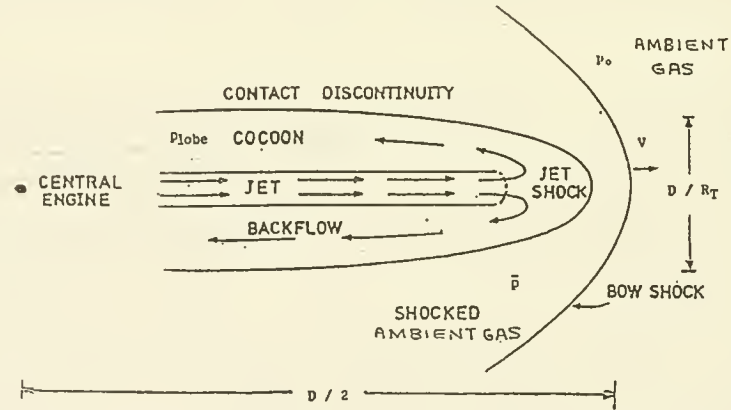


Fig.1 Lobe minimum pressure versus external pressure for sources in clusters (circles), groups (squares) and those that are isolated (crossed-circles). The vertical lines mark the pressure of the IGM at the redshift limits of the sample assuming the model of Guilbert & Fabian⁸; the diagonal lines mark apparent pressure balance and a lobe over-pressure of ~ 10 .



- D = largest projected linear size
- p_{lobe} = pressure in the radio lobe
- p_o = pressure of undisturbed ambient gas
- $\langle p \rangle$ = average pressure in the shocked gas
- ρ_o = density of undisturbed ambient gas
- R_T = ratio of largest projected size to width half way along the lobes
- T = temperature of undisturbed ambient gas
- v = rate of growth of the source, the true advance speed

Fig.2 Schematic diagram of the analytic model.

II - HII REGIONS, HALO AND HOT GAS, COOLING FLOWS

C - COOLING FLOWS

ORIGIN AND DYNAMICS OF EMISSION LINE CLOUDS IN COOLING FLOW ENVIRONMENTS

Michael Loewenstein

Joint Institute for Laboratory Astrophysics, University of Colorado

The interstellar environment of central dominant (cd) cluster galaxies is unique among ISM's in external galaxies as it is pervaded by hot, high pressure gas accreted from the surrounding intracluster medium. Typical average temperatures and pressures are $T \sim 310^7$ K and $P/k \sim 10^6$ K cm⁻³. Central peaks in the x-ray surface brightness distribution, and inwardly decreasing temperature profiles suggest that a massive, subsonic, cooling inflow is centered on the cd galaxy.

One of the intriguing aspects of the x-ray observations is that they cannot be fit by homogeneous steady-state cooling flow models. To date, the only models successful in explaining the observations in detail are those where the accretion rate decreases approximately linearly in radius – mass appears to be dropping out of the flow and forming (mostly low mass) stars. This scenario is independently supported by soft x-ray line measurements and by the existence of extended emission line regions of $T \sim 10^4$ K gas.

When first proposed, the mass deposition hypothesis seemed to be on a firm theoretical footing via the mechanism of thermal instability – comoving perturbations in pressure equilibrium exhibit the same kind of rapid growth as in static atmospheres (Mathews and Bregman 1978). However recent work has pointed out two important mitigating factors – conduction and, particularly, buoyancy. Since the ICM is stably stratified in a background gravitational field, linear perturbations are not in fact comoving but tend to oscillate buoyantly. This oscillatory behaviour dominates over cooling for the conditions appropriate to cooling flows – very modest growth rates are therefore inferred (Malagoli, Bodo, and Rosner 1987; Balbus 1988; Balbus and Soker 1989).

However, this is still not the final word on linear perturbations. Buoyancy forces can be supported if there are non-isotropic stresses. In particular, I have reconsidered Eulerian perturbations including the effects of magnetic fields self-consistently by perturbing the full MHD equations with gravity, thermal conduction, and radiative cooling (Loewenstein 1989a). The results are that there are comoving, thermally unstable modes for a finite region in wave number space in regions where (for a radial background magnetic field)

$$\lambda_B^2 + \frac{v_A^2}{c^2} \lambda_g^2 > \frac{\lambda_F^2}{(2 - \alpha)}.$$

Here λ_g is the pressure scale height, λ_B is the coherence length of the magnetic field, λ_F a local conduction length, α the slope of the cooling function, c the local adiabatic sound speed, and v_A the local Alfvén speed.

The relevance of all this linear analysis can be questioned since there are reasons to believe that the ICM is fundamentally inhomogeneous due to the effects of continued subcluster merging, galactic halo stripping, and possibly radio source-cooling flow interaction and central galaxy motion. A phenomenological, multi-phase, comoving flow model can reproduce the x-ray observations in a self-consistent way (Thomas, Fabian, and Nulsen 1987). Hydrodynamic calculations of finite perturbations have been performed by David, Bregman, and Seab (1988), by Loewenstein (1989b), and by Hattori and Habe (1989). Only the latter work is two-dimensional and illustrates the importance of lateral flows and the formation of vortex-like structures, although at the price of somewhat unrealistic background models. The former work has the most careful treatment of cooling and ionization; however, their choice of plane parallel symmetry precludes buoyancy. In Loewenstein (1989b), I found the same kind of thermal-convective oscillations that occur for infinitesimal perturbations to occur in finite, isolated inhomogeneities as long as the density contrast is

less than about 10. An additional mechanism must be included to induce "cooling out" – the coupling of inhomogeneities to the background flow via drag. This introduces a maximum length scale for thermally unstable perturbations of about 1 pc.

It also introduces an apparent paradox – in order to cool out, perturbations must be co-moving and yet the emission lines presumed to be their descendants have observed velocity widths of several hundred km s^{-1} . Since cooling flows are presumed to be nearly hydrostatic, these velocities are relative to a high pressure background so that severe survivability problems are created as a result of various shear instabilities. The parameter space (in the mass-temperature plane) of Jeans-stable clouds that can be stably accelerated is probably unrealistically small (Loewenstein and Fabian 1989). We have therefore suggested that clouds are born co-moving in a "turbulent" ICM – the allowed parameter space can now be opened up to a more acceptable range. Large-scale motions can be driven in the central parts of cooling flows by a number of mechanisms including the motion of the central and other galaxies, and the dissipation of advected, focussed rotational and magnetic energy. In addition to the velocity width paradox, two other paradoxes (Heckman *et al.* 1989) can be solved if the ICM is turbulent. Firstly, the heating source for the emission line regions has always been puzzling – line luminosities are extremely high for a given (optical or radio) galaxy luminosity compared to those in non-cooling flow galaxies, therefore a mechanism peculiar to cooling flows must be at work. However most, if not all, previously suggested heating mechanisms either fail to provide enough ionization or give the wrong line ratios, or both. The kinetic energy in the turbulence provides a natural energy source if it can be efficiently converted to cloud heat – we suggest this can be done via magneto-hydrodynamic waves through plasma slip. Secondly, while the x-ray observations indicate extended mass deposition, the optical line emission is more centrally concentrated. Since many of the turbulence-inducing mechanisms are strongest in the central regions of the ICM, so is the method of heating. In other words material is dropping out everywhere but only being lit up in the center.

REFERENCES

- Balbus, S. A. 1988, *Ap. J.*, **328**, 395.
 Balbus, S. A., and Soker, N. 1989, *Ap. J.*, submitted.
 David, L. P., and Bregman, J. N., and Seab G. C. 1988, *Ap. J.*, **329**, 66.
 Hattori, M., and Habe, A. 1989, *M. N. R. A. S.*, submitted.
 Heckman, T. M., Baum, S. A., van Breugel, W., and McCarthy, P. J. 1989, *Ap. J.*, **338**, 48.
 Loewenstein, M. 1989a, *Ap. J.*, submitted.
 Loewenstein, M. 1989b, *M. N. R. A. S.*, **238**, 15.
 Loewenstein, M., Fabian, A. C. 1989, *M. N. R. A. S.*, in press.
 Malagoli, A., Rosner, R., and Bodo, G. 1987, *Ap. J.*, **319**, 632.
 Mathews, W. G., and Bregman, J. N. 1978, *Ap. J.*, **224**, 308.
 Thomas, P. A., Fabian, A. C., and Nulsen, P. E. J. N., 1987, *M. N. R. A. S.*, **228**, 973.

NARROW BAND IMAGES OF SUSPECTED COOLING FLOW GALAXIES

Susana Deustua and Greg Bothun
Department of Astronomy
University of Michigan
Ann Arbor, MI 48109

ABSTRACT: We present narrow-band (H α and [NII]) CCD images of elliptical galaxies suspected of having cooling flows.

I. INTRODUCTION: Cooling flows analogous to those in clusters of galaxies are also present on smaller scales in isolated (i.e. not in the center of a cluster) early-type galaxies as evidenced by observed soft x-ray halo emission around these galaxies (Forman, Jones and Tucker (1985); Canizares, Fabbiano and Trinchieri (1987); Fabbiano et al (1987)). The typical luminosity in these halos is $L_x = 10^{39} - 10^{41}$ ergs s $^{-1}$. This gas most probably originates as mass loss from stellar evolution which has been driven out of the galaxy by supernovae induced winds and subsequently flows inward in a cooling flow (Mathews and Loewenstein 1986). These smaller flows should exhibit temperature and density gradients, optically emitting filaments and star formation (at the rate of up to a few M_\odot yr $^{-1}$). Therefore one expects to find cool gas ($T = 10^4$ K) in the inner few kpc of elliptical galaxies.

II. OBSERVATIONS: Narrow-band (20 Å bandpass) interference filter images in H α and [NII] of a subsample of 12 of approximately 40 cooling flow galaxies were taken at the MDM observatory with the 1.3m McGraw-Hill Telescope. Previous narrow-band imaging has been at a resolution insufficient to separate H α from [NII]. Typical exposure times are 900 seconds.

III. RESULTS and DISCUSSION: We find evidence of optical emission from cool gas which is most likely associated with a cooling flow. At least 4 galaxies (NGC3998, NGC4203, NGC4550 and NGC4697) show emission of [NII] and/or H α within the central 20", a fraction consistent with results from Phillips et al (1987) and Caldwell (1984). In these four, [NII] λ 6584Å emission is stronger than H α (which is often in absorption e.g. as seen in long slit spectra of NGC4697). From long slit spectra of these galaxies, Deustua and Teske (1989) infer electron densities, N_e , of order 1.2×10^3 cm $^{-3}$ assuming $T = 10^4$ K for the optically emitting gas. NGC 2685, NGC 3489 appear to have emission in [NII]; NGC 4636 may also, but, is difficult to see in our data (Demoulin-Ulrich, Butcher and Boksenberg (1984) did not see emission from this galaxy). NGC 4472, NGC 4473, NGC 4365, NGC 4638 and NGC 4649 show no emission.

Table 1

Parameters of the Sample Galaxies

OBJECT	type	$\log L_x$ erg/s	a_x kpc	$N_e(0)$ cm^{-3}	$t_{cl}(0)$ 10^7yr	M_{gas} $10^{10} M_\odot$
NGC 2685	S0	39.91	0.25	0.14	4.7	0.017
NGC 3489	S0/Sa	<39.80	0.24	0.13	5.2	0.015
NGC 3998	S0	41.74	0.44	0.50	1.4	0.338
NGC 4203	S0	41.34	0.40	0.36	1.9	0.186
NGC 4365	E3	40.29	0.65	0.05	13.2	0.117
NGC 4472	E1/S0	41.71	1.80	0.06	11.8	2.741
NGC 4473	E5	39.95	0.46	0.06	11.5	0.047
NGC 4550	E7/S0	<39.85	0.18	0.21	3.2	0.010
NGC 4636	E0/S0	41.64	0.70	0.22	3.1	0.618
NGC 4638	S0	39.59	0.22	0.11	5.9	0.011
NGC 4649	E0	41.40	1.16	0.08	8.7	0.988
NGC 4697	E6	40.27	0.95	0.03	23.4	0.199

Galaxy type is from the Revised Shapley-Ames Catalog. $\log L_x$ is given in Canizares, Fabbiano and Trinchieri (1987); the values of the core radius, a_x , central density, $N_e(0)$, central cooling time, $t_{cl}(0)$, and gas mass, M_{gas} , for the hot gas are calculated using their equations.

The best candidates for active cooling flows are NGC 3998 and NGC 4203. Both have H α and [NII] emission as well as large central densities and short central cooling times as calculated from their x-ray properties (Table 1), furthermore, van Driel *et al* (1988) observed an HI disk in NGC 4203. Whereas the galaxies with weaker [NII] emission and no H α have lower central densities and longer cooling times.

It has been suggested in the literature that distorted isophotes i.e. pointy or boxy, indicate the presence of accretion processes. Jedrzejewski (1987) found pointy isophotes for NGC 4473 and NGC 4697, and Mollenhoff and Bender (1986) found boxy isophotes in NGC 4365 and NGC 4472. However, while NGC 4697 has optical emission, its central $N_{eX\text{ray}}$ is small and $t_{\text{cool}X\text{ray}}$ is large. We find that broad-band U, B, and I images of 7 southern cooling-flow galaxies show that 3 have boxy isophotes at intermediate radii and pointy isophotes at the inner and outermost radii (i.e. mixed), two are essentially boxy, one has elliptical isophotes and one, PKS0745-191, is too small to fit. Three of the control galaxies

have isophotes which are essentially elliptical. However, IC 3370, while not a cooling flow candidate, also has very obvious boxy isophotes (Jarvis 1987).

Distorted isophotes probably confirm the presence of a cooling flow via its dynamical effect but do not alone provide sufficient evidence. Whether the presence of H α and [NII] emission alone are related to cooling flows is unclear (see also Donahue, Stocke and Voit this conference), though Hu, Cowie and Wang (1985) observed such emission filaments in several cluster cooling flows.

Acknowledgments : S. D. thanks the Astronomy Dept. at CWRU for use of their computing facilities, G. Aldering and R. E. Luck for useful suggestions. We also thank I. Thompson for obtaining some broad band images. Partial support for this research was provided by a Rackham Dissertation Grant from the University of Michigan.

REFERENCES:

- Caldwell, N., 1984 P. A. S. P., 96, 287
Canizares, C., Fabbiano, G. and Trinchieri, G., 1987 Ap. J., 312, 503
Demoulin-Ulrich, M-H., Butcher, H. R. and Boksenberg, A., 1984 Ap. J., 285, 527
Deustua, S. and Teske, R., 1989 in preparation
Fabbiano, G., Klein, U., Trinchieri, G. and Wielebinski, R., 1987 Ap. J., 312, 111
Forman, W., Jones, C. and Tucker, W., 1985 Ap. J., 293, 102
Hu, E., Cowie, L. and Wang, Z., 1985 Ap. J. Suppl., 59, 447
Jarvis, B., 1987 A. J., 94, 30
Jedrzejewski, R. I., 1987 M. N. R. A. S., 226, 747
Mathews, W. G. and Loewenstein, M., 1986 Ap. J. (Lett.), 306, L7
Mollenhoff, C., and Bender, R., 1986 in IAU Symposium 127: Structure and Dynamics of Elliptical Galaxies ed. T. de Zeeuw (Dordrecht: Reidel) p. 409
Phillips, M., Jenkins, C. R., Dopita, M. A., Sadler, E. M. and Binette, L., 1986 A. J., 91, 1062
van Driel, W., van Woerden, H., Gallagher III, J. S. and Schwarz, U. J., 1988 Astronomy and Astrophysics, 191, 201
Vedder, P. 1988 MIT thesis

OPTICAL EMISSION FROM COOLING FLOWS IN DISTANT X-RAY CLUSTERS OF GALAXIES

Megan Donahue, John T. Stocke, G. Mark Voit,
Center for Astrophysics and Space Astronomy, University of Colorado
and
Isabella Gioia
Harvard/Smithsonian Center for Astrophysics, Cambridge, MA

Although the *Einstein* satellite detected "cooling flows" in the X-ray emission from clusters of galaxies (cf. Sarazin, 1988) 10 years ago, the understanding of these flows remains incomplete. The x-ray emitting gas in the centers of these clusters is so dense that its cooling time is shorter than a Hubble time. Thus gas may cool and flow into the center of the cluster. This cooling gas is thermally unstable (e.g. Mathews and Bregman 1978) and should quickly become inhomogeneous. Optical filamentation (1-100 kpc scales) often appears near the centers of nearby clusters containing cooling flows, usually within the central galaxies accreting the gas (e.g. Ford and Butcher 1979; Hu *et al.* 1983, 1985). Indeed, only clusters with well-developed cooling flows seem to possess highly luminous, emission-line nebulae (Heckman, *et al.* 1989). We present here some results of our preliminary observational and theoretical studies of this class of emission-line objects.

We have observed a complete, X-ray selected sample of 25 distant ($0.07 > z > 0.35$) clusters of galaxies extracted from the Einstein Extended Medium Sensitivity Survey (Gioia, *et al.* 1989.) These clusters have $F_x(0.3 - 3.5 \text{ keV}) \geq 8 \times 10^{-13} \text{ erg/s/cm}^2$, declination $\geq -20^\circ$. We have discovered luminous ($\geq 10^{41} \text{ erg/s}$) extended $H\alpha$ emission in 10 of these clusters. (e.g. Figure 1.) Thus *at least* 40% of the clusters in our sample contain cool gas. If we crudely compare our sample to that of Arnaud (1988), in which $\sim 40\%$ of his 104 X-ray clusters have cooling flows, our result implies that cooling flows may actually be a more common phenomenon in the past than in the present.

The connection between the cooling flow and the $H\alpha$ emission is a mystery. The straightforward calculation of 1 (photoionization) to 3 (shocks) recombinations per H atom in the cooling flow gives mass infall rates 3 - 100 times greater than \dot{M} derived from X-ray observations (Heckman, *et al.*, 1989). We have made some preliminary theoretical calculations in an attempt to resolve this problem.

REFERENCES

- Arnaud, K. 1988 in *Cooling Flows in Clusters and Galaxies*, ed. A. Fabian, (Kluwer: Boston), p. 31.
Ford, H. C. and H. Butcher 1979, *Ap. J. Suppl.*, **41**, 147.
Gioia, I. *et al.* 1989, *Ap. J. Suppl.*, in press.
Heckman, T. *et al.* 1989, *Ap. J.*, **338**, 48.
Hu, E., Cowie, L, and Wang, Z. 1985, *Ap. J. Suppl.*, **59**, 447.
Hu, E. 1988 in *Cooling Flows in Clusters and Galaxies*, p. 121.
Mathews W.G., and J.N. Bregman 1978, *Ap. J.*, **224**, 308.
Sarazin, C. 1988, *X-ray Emissions from Clusters of Galaxies*, (Cambridge University Press: New York).

MS 0839 + 2938

$z = 0.194$

A) At right, R-
band full-field

B) Below left,
R-band, close-up

C) Below right,
H α , close-up

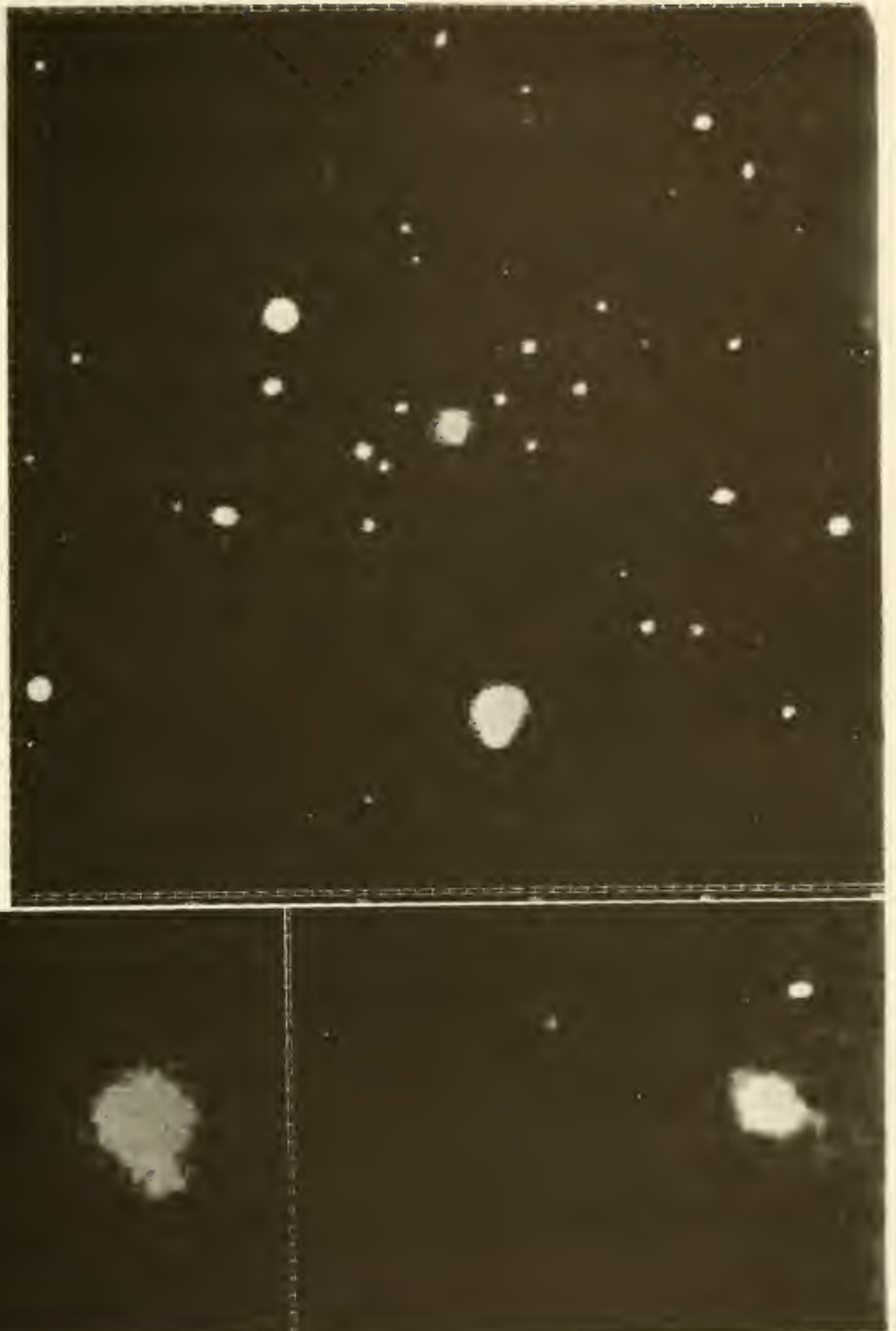


Figure 1: (A) A 3 arcmin x 3 arcmin R band CCD image of the X-ray selected cluster of galaxies MS 0839+2938 ($z = 0.194$). All images obtained with the KPNO 2.1m + Tektronix CCD (Seeing ~ 1.4 arcsecs.)

(B) The central 33 x 20 arcsecs of image (A) showing the red continuum of the central dominant (cD) galaxy.

(C) A pure H α image of the same field as (B) showing the very extended, luminous H α emission associated with the central galaxy and typical of our H α detections of "cooling flows." The bright spot on the upper right is a cosmic ray hit on the chip.

GAS FLOWS IN ELLIPTICAL GALAXIES

L.P. David, W. Forman, and C. Jones
Harvard-Smithsonian Center for Astrophysics

A great deal of information about the interstellar medium in elliptical galaxies has been acquired over the last decade through analysis of Einstein X-ray data. The X-ray emission from luminous elliptical galaxies arises through thermal emission from extended hot coronae in nearly hydrostatic equilibrium (Forman, Jones, and Tucker 1985; Canizares, Fabbiano, and Trinchieri 1987). Since the radiative cooling time of the hot gas in luminous elliptical galaxies is typically less than a Hubble time, the gas must be slowly cooling and accreting into the center of the galaxy through a cooling flow (Nulsen, Stewart, and Fabian 1984). For a given supernova rate, however, there must exist a critical galaxy luminosity below which ellipticals cannot retain the gas liberated by the stellar systems.

In preparation for the next generation of X-ray telescopes, we have begun a program investigating the evolving X-ray properties of elliptical galaxies (David, Forman, and Jones 1989a and b). Our galaxy models consist of a modified King profile for the luminous portion of the galaxy and can include an isothermal dark halo comprising 90% of the total mass. The stellar population is assumed to form at a rate which decreases exponentially on a dynamical time scale with a Salpeter initial mass function. Stellar mass loss occurs instantaneously as stars evolve off the main sequence. All stars more massive than $8M_{\odot}$ produce type II supernovae, while less massive stars loss mass through a planetary nebulae. The evolving rate of type I supernovae is normalized to a fraction, r_{snI} , of Tammann's (1974) value. All of this information is then incorporated into a one-dimensional hydrodynamics code to determine the evolving dynamical state of the interstellar medium.

The various evolutionary stages encountered in these models have been discussed elsewhere (David, Forman, and Jones 1989a and b). In this brief contribution, we discuss how the present state of the ISM depends on the galaxy luminosity L_B , the present epoch type I supernova rate, and the presence of a massive halo. The results of a large variety of models with massive dark halos are summarized in Figure 1. As can be seen from this figure, the ISM varies from pure accretion flows, to partial winds, to total subsonic winds, to total transonic winds as either L_B decreases or r_{snI} increases. Using the best estimate on the present type I supernova rate ($r_{snI} = 1/4$; van den Bergh, McClure, and Evans 1987), the critical optical luminosities separating these dynamic states are $L_B \approx 1.7 \times 10^{10}$, 5.5×10^9 , and $1.7 \times 10^9 L_{\odot}$, or equivalently $M_B \approx -20.2$, -18.9 , and -17.7 . These critical luminosities depend

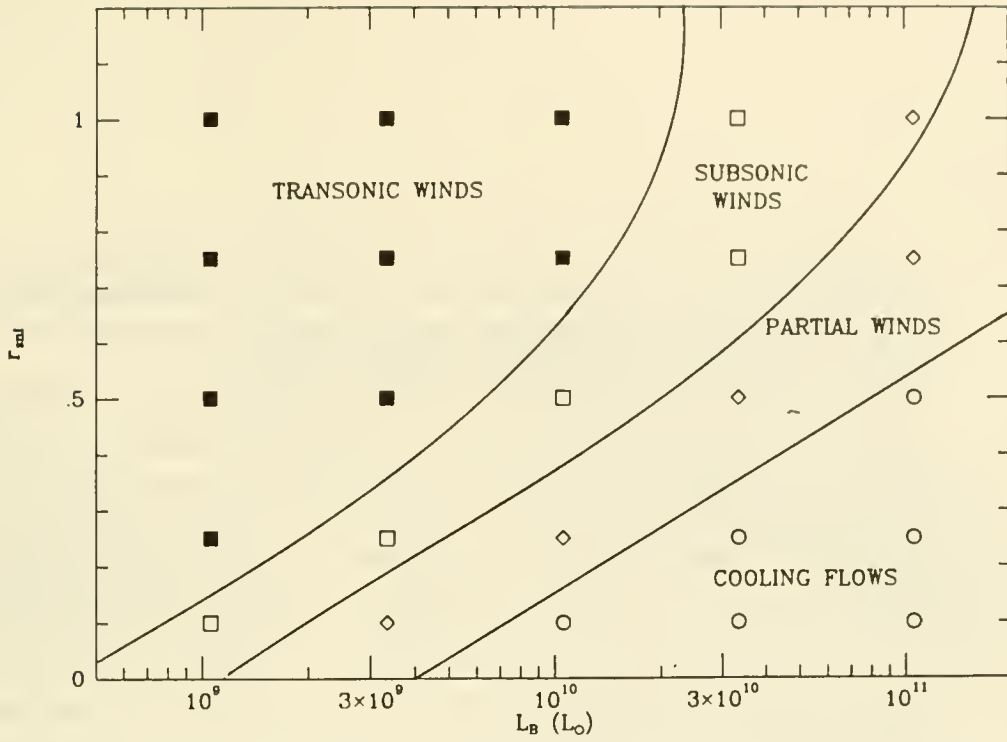


Figure 1. The present dynamic state of the hot ISM in a variety of galaxy models with massive halos. The supernova rate, r_{snI} , is normalized to Tammann's (1974) value. Partial winds have an inner accretion flow and an outer wind.

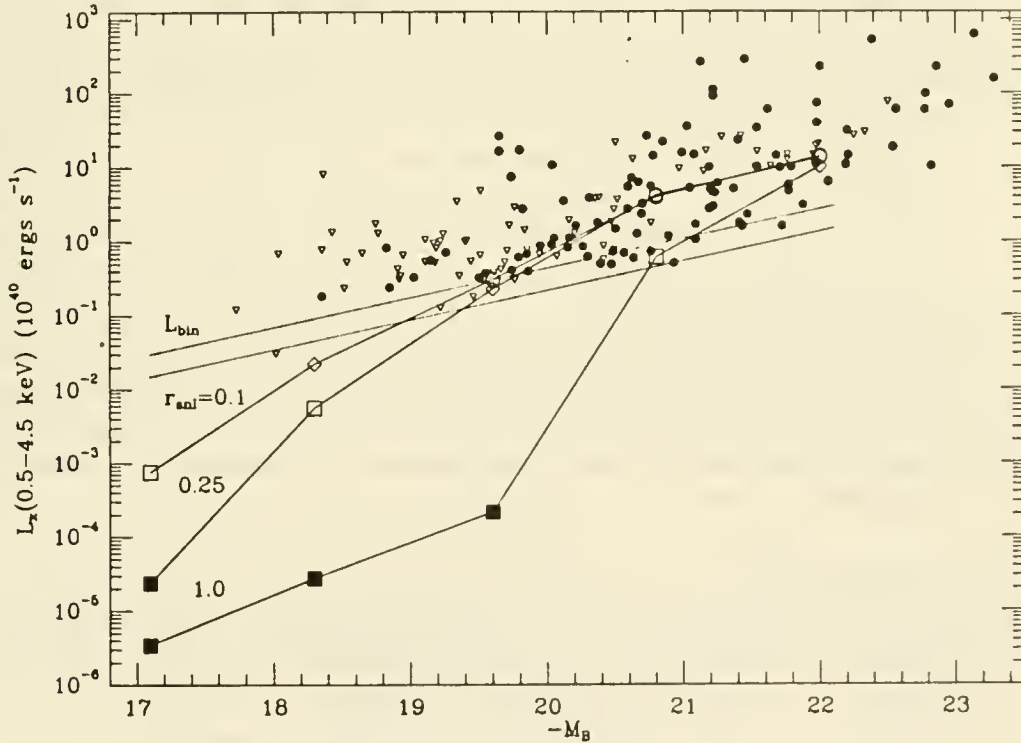


Figure 2. X-ray luminosity of the galaxy models with massive halos for three different supernova rates. For comparison, the Einstein X-ray data on early type galaxies and estimates on the X-ray luminosity from binaries, L_{bin} , are also given. The symbols indicate the dynamic state of the ISM in the models (see Figure 1).

on the ratio of dark to luminous mass and only strictly apply when the dark halo comprises 90% of the total mass of the galaxy. We also have simulated galaxy models without massive halos and find that galaxies with $M_B \gtrsim -20.5$ have total transonic winds at the present time for $r_{snI} = 1/4$.

The present 0.5-4.5 keV luminosity of the galaxy models is shown in Figure 2 along with the Einstein data for early type galaxies (Jones, Forman, and Tucker 1989). For comparison, estimates on the 0.5-4.5 keV luminosity from compact binaries in these galaxies also are shown (Forman, Jones, and Tucker 1985; Canizares, Fabbiano, and Trinchieri 1987). The present X-ray luminosity in our models is very sensitive to the assumed type I supernova rate. In general, the 0.5-4.5 keV luminosity in a given galaxy model increases slightly with increasing supernova rate until heating by supernovae dominates the energetics of the gas and winds develop. When this occurs, most of the supernova energy is converted into the mechanical energy of the wind and the X-ray luminosity decreases rapidly with any further increase in the supernova rate. As the present epoch type I supernova rate is increased, winds and lower X-ray luminosities are generated in increasingly more optically luminous galaxies (see Figure 2). The amount of scatter in the present data is too large to strongly constrain the present type I supernova rate, however, it is clear that Tammann's (1974) value is too high by a factor of at least four to account for the observed X-ray luminosity of galaxies with M_B between -20 and -21. If elliptical galaxies have massive halos and $r_{snI} = 1/4$, our models indicate that the X-ray emission from hot gas should dominate over emission from binaries in galaxies with $M_B \lesssim -19.6$. Galaxies with this absolute blue magnitude have partial winds.

The present 0.5-4.5 keV luminosity of elliptical galaxies also is very sensitive to the presence of a massive dark halo. Our models without halos have predominantly low X-ray luminosity, transonic winds. In models without halos and $r_{snI} = 1/4$, the X-ray emission from the hot ISM only dominates over the X-ray emission from binaries in galaxies more luminous than $M_B \approx -21.1$. Our models indicate that ellipticals with M_B between -20 and -21.5 must have massive dark halos in order to retain the large amounts of hot gas necessary to produce their observed 0.5-4.5 keV luminosities.

REFERENCES

- Canizares, C., Fabbiano, G., and Trinchieri, G. 1987, *Ap.J.*, 312, 503.
 David, L.P., Forman, W., and Jones, C. 1989a and b, *Ap.J.* (submitted).
 Forman, W., Jones, C., and Tucker, W. 1985, *Ap.J.*, 293, 102.
 Jones, C., Forman, W., and Tucker, W. 1989 (in preparation).
 Nulsen, P., Stewart, G., Fabian, A. 1984, *MNRAS*, 208, 185.
 Tammann, G.A. 1974, in *Supernovae and Their Remnants*, ed. C.B. Cosmovici (Dordrecht:Reidel), p.155.
 van den Bergh, S., McClure, R.D., Evans, R. 1987, *Ap.J.*, 323, 44.

STRIPPING OF GAS AND DUST FROM THE ELLIPTICAL GALAXY M86

D.A.White, A.C.Fabian

Institute of Astronomy
Madingley Road
Cambridge CB3 0HA
England

W.Forman, C.Jones, C.Stern

Centre for Astrophysics
60 Garden Street
Cambridge, Mass.
U.S.A.

1 Introduction

Past observations of the X-ray morphology of M86 have revealed that the galaxy is experiencing ram-pressure stripping due to its large velocity (1500 km s^{-1}) relative to the intracluster medium of Virgo (Forman *et al* 1979, Fabian, Schwartz, and Forman 1980).

Our observations indicate that the X-ray emitting gas in the plume of M86 is still being produced from the continual heating of gas and dust stripped from nearer the galaxy's centre.

2 Observations

We have obtained two-dimensional *IRAS* images of M86 which have revealed that there are two spatially separated regions of emission, one at 60μ and the other at 100μ of the *IRAS* wavebands. The 100μ emission, presumably from cool dust (at approximately 20K), appears to be located near the centre of the galaxy together with HI (detected by Bregman, Roberts and Giovanelli 1988), while the 60μ emission (whose origins of emission will be discussed later) appears to lie more than 3 arcminutes away from the optical 'centre' in a direction slightly South of the centre of the plume.

Optical images produced by scanning U.K.Schmidt plates with the A.P.M. at the I.o.A., reveal asymmetric isophotal contours along the major axis of the galaxy (first reported by Nulsen and Carter in 1987, which they propose as excess emission due to star formation). This excess optical emission is co-incident with the direction of the 60μ infra-red emission.

3 Discussion

M86 has an extended X-ray morphology, possibly characteristic of a cooling flow, with a distortion in the atmosphere caused by ram-pressure stripping. The $1.5 \cdot 10^8 M_{\odot}$ of HI detected in the centre of M86 is also interpreted by Bregman *et al* as resulting from a cooling flow, due to the lack of rotational support in the gas. The possible $3 \cdot 10^5 M_{\odot}$ of dust at the centre of M86 emitting at 100μ , has presumably accumulated from mass-loss from M-giant stars, and has been protected from sputtering by the cool HI gas. Both these accumulations could have occurred over less than a crossing-time, i.e. since M86 last passed through the dense medium of the cluster core where it had the majority of its gas removed.

Now that the galaxy is again approaching the cluster core, and has reached supersonic speeds relative to the cluster gas, first the gas in a shallow gravitational potential is stripped and heated to X-ray temperatures, as seen in the plume, and then gas deeper in the galaxy's potential well is removed and heated. It appears that we are now observing the continued stripping of the gas and dust in the centre of the galaxy, given that the 60μ emission is displaced from the galaxy centre in roughly the apparent direction of the plume.

The observed 60μ emission may be due to the heating of the cooler dust previously at the centre of the galaxy (i.e. at 90K compared to 20K), though the observed luminosity may be explained by OI line emission at 63μ . The OI emission could produce all the required luminosity from approximately $10^6 M_{\odot}$ of gas, though it would appear more plausible if the 60μ emission were due to a combination of gas and dust emission.

The picture of the gas and dust being forced out of the galaxy, presumably along the shallowest potential gradient i.e. the major-axis, is reinforced by the asymmetrical optical isophotes. Whether the extended optical emission in the direction of the infra-red emission is due to star formation still has to be investigated.

4 References

- Bregman J.N., Roberts M.S., & Giovanelli R., 1988. *Astrophys. J.*, **330**:L93-196.
- Fabian A.C., Schwarz J., & Forman W., 1980. *Mon. Not. R. Ast. Soc.*, **192**, 135-142.
- Forman W., Schwarz J., Jones C., Liller W., & Fabian A.C., 1979. *Astrophys J.*, **234**:L27-L31.
- Nulsen P.E.J., & Carter D., 1987. *Mon. Not. R. Ast. Soc.*, **225**, 939-945.

ISM STRIPPING FROM CLUSTER GALAXIES AND INHOMOGENEITIES IN COOLING FLOWS

NOAM SOKER¹, JOEL N. BREGMAN² AND CRAIG L. SARAZIN¹

¹DEPARTMENT OF ASTRONOMY, UNIVERSITY OF VIRGINIA

² NRAO, CHARLOTTESVILLE, VIRGINIA

Analyses of the X-ray surface brightness profiles of cluster cooling flows suggest that the mass flow rate decreases towards the center of the cluster. It is often suggested that this decrease results from thermal instabilities, in which denser blobs of gas cool rapidly and drop below X-ray emitting temperatures. If the seeds for the thermal instabilities are entropy perturbations, these perturbations must enter the flow already in the nonlinear regime. Otherwise, the blobs would take too long to cool. We suggest that such nonlinear perturbations might start as blobs of interstellar gas which are stripped out of cluster galaxies. Assuming that most of the gas produced by stellar mass loss in cluster galaxies is stripped from the galaxies, the total rate of such stripping is roughly $\dot{M}_{ISM} \sim 100 M_{\odot} \text{ yr}^{-1}$. It is interesting that the typical rates of cooling in cluster cooling flows are $\dot{M}_{cool} \sim 100 M_{\odot} \text{ yr}^{-1}$. Thus, it is possible that a substantial portion of the cooling gas originates as blobs of interstellar gas stripped from galaxies. The magnetic fields within and outside of the low entropy perturbations can help to maintain their identities, both by suppressing thermal conduction and through the dynamical effects of magnetic tension. One significant question concerning this scenario is: Why are cooling flows seen only in a fraction of clusters, although one would expect gas stripping to be very common. It may be that the density perturbations only survive and cool efficiently in clusters with a very high intracluster gas density and with the focusing effect of a central dominant galaxy. Inhomogeneities in the intracluster medium caused by the stripping of interstellar gas from galaxies can have a number of other effects on clusters. For example, these density fluctuations may disrupt the propagation of radio jets through the intracluster gas, and this may be one mechanism for producing Wide-Angle-Tail radio galaxies.

ACCOUNTING FOR THE DISPERSION IN THE X-RAY PROPERTIES OF EARLY-TYPE GALAXIES

Raymond E. White III (University of Alabama)
 Craig L. Sarazin (University of Virginia)

Early-type galaxies are found to have diffuse X-ray emission, with X-ray luminosities ranging from $L_X \approx 10^{39} - 10^{42}$ erg s⁻¹ (Forman, Jones and Tucker 1985; Canizares, Fabbiano and Trinchieri 1987 [CFT]). The source of X-ray emission is thought to be thermal radiation from hot gas permeating the galaxies; coarse X-ray spectra of the most luminous galaxies reveal gas temperatures of ~ 1 keV. The inferred amount of X-ray emitting gas, $10^9 - 10^{10} M_\odot$, is generally consistent with the amount expected from the integrated history of normal stellar mass loss in the galaxies. Since the cooling time of the hot gas is typically less than a Hubble time, the gas is likely to be involved in cooling flows (White and Chevalier 1984; Nulsen, Stewart and Fabian 1984; Thomas *et al.* 1986). For the *least* optically luminous early-type galaxies, it is not yet clear whether their X-ray emission is from diffuse gas or from (hotter) discrete sources.

The X-ray luminosities of early-type galaxies are correlated with their optical (e.g. blue) luminosities ($L_X \sim L_B^{1.6}$), but the X-ray luminosities exhibit considerable scatter for a given optical luminosity L_B . This dispersion in X-ray luminosity is much greater than the dispersion of other properties of early-type galaxies (for a given L_B), such as luminosity scale-length, velocity dispersion, color, and metallicity. In particular, early-type galaxies with blue luminosities of $L_B \approx 10^{11} L_\odot$ (assuming $H_0 = 50$ km s⁻¹ Mpc⁻¹) have X-ray luminosities which range nearly two orders of magnitude, from $L_X \approx 10^{40} - 10^{42}$ erg s⁻¹. It is not clear whether the scatter in L_X reflects variations in the *intrinsic* properties of galaxies (i.e. stellar mass loss rates, supernova rates, velocity dispersions, masses, etc.) or whether it reflects variations in the *environment* of the galaxies (i.e. variations in the amount of ram-pressure stripping). Therefore, when X-ray observations of early-type galaxies are used to constrain the intrinsic properties of early-type galaxies, it is not clear how theoretical models should properly be compared to the data. If the scatter in L_X is intrinsic, theoretical models should at least reproduce median values of L_X as a function of L_B . Alternatively, if the scatter is environmentally induced, theoretical models should provide an *envelope* for L_X as a function of L_B . This ambiguity has significant consequences: for example, the supernova rate in early-type galaxies as inferred from their X-ray properties is then uncertain by a factor of ~ 3 .

We consider several possible sources for the dispersion in X-ray luminosity:

Some of the scatter in X-ray luminosity may result from stellar population variations between galaxies with similar L_B . Since the X-ray emitting gas is from accumulated stellar mass loss, the L_X dispersion may be due to variations in integrated stellar mass loss rates. For example, more metal-rich galaxies of a given L_B may have more mass loss than less metal-rich galaxies, due to the increased stellar opacity at higher metallicities. Population variations may also affect supernova rates. Galaxies with higher supernova rates (at fixed L_B) will have larger L_X . Since significant stellar population differences should manifest themselves through color variations, we look for correlations between the X-ray luminosities and optical colors ($U - V$) of early-type galaxies for fixed L_B (that is, we look for a correlation between the residuals of the mean $L_X - L_B$ and $(U - V)$ - L_B relations).

Another possible cause of the L_X dispersion may be variations in the amount of cool material in the galaxies; cool gas may act as an energy sink for the hot gas. Sources of cool

(atomic or molecular) material include 1) the infall of gas-rich dwarf galaxies; 2) thermally unstable density perturbations in the hot gas; or 3) the incomplete thermalization of stellar ejecta. Infrared emission may be used to trace such cool material, so we look for a correlation between the infrared emission and the X-ray emission of early-type galaxies at fixed L_B .

Velocity dispersion variations between galaxies of similar L_B may also contribute to the L_X dispersion. Galaxies with greater stellar velocity dispersions will have the stellar mass loss heated to higher temperatures, which will also increase L_X for a given amount of gas. If velocity dispersions are well-correlated with the total masses of early-type galaxies, then galaxies with higher velocity dispersions will retain more gas in stripping encounters with other galaxies or with intracluster gas. Thus, higher velocity dispersions would again be correlated with higher L_X at fixed L_B .

The most likely *a priori* source of the dispersion in L_X is probably the varying amount of ram-pressure stripping in a range of galaxy environments (CFT, Sarazin and White 1988). The hot gaseous halos of early-type galaxies can be stripped in encounters with other galaxies or with ambient cluster gas if the intracluster gas is sufficiently dense. Since the timescale for a stripped galaxy to replenish its gas is much longer than a typical crossing time in a galaxy cluster or group, we do not expect a *tight* correlation between X-ray luminosity deficit (for a given L_B) and local galaxy density. Stripped, X-ray deficient galaxies need not remain near the spot where they were stripped in the distant past. However, if stripping is important, we may expect to find that the *least* stripped galaxies, i.e. the most X-ray luminous galaxies for a given L_B , will tend to be in less dense environments.

Of these various possibilities for the cause of the dispersion in the X-ray properties of early-type galaxies, we find that the most likely cause is probably the ram-pressure stripping of gaseous halos from galaxies. For a sample of 81 early-type galaxies with X-ray luminosities or upper limits derived from *Einstein Observatory* observations (CFT) we calculated the cumulative distribution of angular distances between the X-ray sample members and bright galaxies from the *Revised Shapley – Ames* catalog. Collectively, galaxies with low X-ray luminosities (for a given L_B) tend to be in denser environments than galaxies with higher X-ray luminosities: galaxies with low L_X have $\sim 50\%$ more neighbors between 1 and ~ 5 degrees than do galaxies with high L_X (for a given L_B). This is indicative of an environmental cause for the L_X dispersion. We are currently checking whether this dichotomy in the angular density of bright galaxies is manifested in the space density of bright galaxies, as well, or only in projection on the sky.

As for the other possibilities mentioned for the cause of the L_X dispersion, we find no compelling correlations which support any of the causes other than stripping for the dispersion in X-ray luminosity.

REFERENCES

- Canizares, C. R., Fabbiano, G. and Trinchieri, G. 1987, *Ap.J.*, **312**, 503 (CFT).
 Forman, W., Jones, C. and Tucker, W. 1985, *Ap.J.*, **293**, 102.
 Nulsen, P. E. J., Stewart, G. C. and Fabian, A. C. 1984, *M.N.R.A.S.*, **208**, 185.
 Sarazin, C. L. and White, R. E. III 1988, *Ap.J.*, **331**, 102.
 Thomas, P. A., Fabian, A. C., Arnaud, K. A., Forman, W. and Jones, C. 1986, *M.N.R.A.S.*, **222**, 655.
 White, R. E. III and Chevalier, R. A. 1984, *Ap.J.*, **280**, 561.

SEARCH FOR COLD GAS IN CLUSTERS WITH AND WITHOUT COOLING FLOWS

D.A. Grabelsky and M.P. Ulmer

Northwestern University, Department of Physics and Astronomy
Evanston, IL 60208

ABSTRACT. The dominant galaxy in each of ~ 40 clusters has been studied using co-added *IRAS* survey data, and 11 of these galaxies have been observed for CO ($J=1\rightarrow 0$) emission with the NRAO 12 m telescope at Kitt Peak. Half of the galaxies in our sample are in clusters reported to have cooling flows while the other half are not. Six of the galaxies appear to have been detected by *IRAS* at fairly low flux levels, in addition to one previously known strong detection; all seven have reported cooling flows. No detectable CO emission (to 2-3 mK) was found in any of the 11 galaxies observed. Assuming accretion rates of $\sim 100 M_{\odot} \text{ yr}^{-1}$, the star formation rates and efficiencies in these galaxies must be quite high in order to render the CO undetectable. At the same time, the infrared luminosities of these galaxies is unremarkable, suggesting that the correlation between star formation efficiency and infrared luminosity found for spirals may not hold for cooling flows.

INTRODUCTION. In the last fifteen years, X-ray observations of clusters of galaxies have led to the discovery that the hot intracluster gas in the cores of many clusters appears to be cooling on timescales short in comparison with the ages of the clusters. If not reheated, the gas will flow toward the cluster center where it may be accreted by the central dominant galaxy. Estimates of the mass-flow rates range over $5\text{-}500 M_{\odot} \text{ yr}^{-1}$ (cf. Sarazin 1986). Debate over the possible role of reheating (Bertschinger and Meiksin 1986; Silk *et al.* 1986), however, has cast some doubts on the existence of flowing – as opposed to simply cooling – gas in these clusters.

An important question related to the existence of cooling flows is the ultimate fate of the accreted material. The most obvious and generally assumed repository is stars. Since the gas must first pass through a cold, neutral phase, a fundamental test for the accumulation of cooling intracluster gas in cluster cores is the search for the cold gas that must feed the star formation. The *IRAS* and CO observations we present here are directed at detecting such a reservoir.

OBSERVATIONS. We co-added *IRAS* survey data about the central dominant galaxy in each of ~ 40 clusters, and observed a subset of 11 galaxies with the NRAO 12 m telescope at Kitt Peak for CO ($J=1\rightarrow 0$) emission. Our goal was to search for cold interstellar gas in these galaxies, with a focus on the possible contribution from accretion of the cooling intracluster gas. Our sample was drawn from the list of Stewart *et al.* (1984) of X-ray clusters; about half the clusters in their list show evidence for cooling flows (cooling times less than H_0^{-1}) while the other half do not. Additional cooling-flow clusters were taken from Sarazin (1986; and references therein) and Romanishin and Hintzen (1988).

RESULTS. Seven of the galaxies appear to have been detected by *IRAS*, although except for NGC 1275 (which is already in the *IRAS Point Source Catalog*), none can be classified as unquestionable detections. On the basis of signal strength, positional coincidence of the $60\mu\text{m}$ and $100\mu\text{m}$ sources, and proximity to the optical image of the galaxy, we ranked six sources as follows: A 1126 and A 2199, very probable detections; A 2063, A 576, and A 400,

likely detections; and A 1983, marginal detection. For these seven galaxies, the infrared luminosities range from $0.83 \times 10^{10} L_{\odot}$ (A 400) to $13 \times 10^{10} L_{\odot}$ (A 426); 3σ upper limits for the remaining galaxies range from $0.33 \times 10^{10} L_{\odot}$ to $22 \times 10^{10} L_{\odot}$. The median value of L_{IR} (detections and upper limits) is roughly $4.5 \times 10^{10} L_{\odot}$. (We have used $H_0 = 50 \text{ km s}^{-1} \text{ Mpc}^{-1}$ for all distant-dependent quantities.)

No CO was detected in any of the sources observed. (The data for NGC 1275 were lost due to a previously undiscovered software error in the telescope system; this galaxy has subsequently been detected in CO by Lazareff *et al.* [1989]). Upper limits to the total mass of molecular gas in each galaxy have been determined on the basis of the assumed proportionality of integrated CO line intensity and H_2 column density, where the conversion of Sanders *et al.* (1986) has been used. Our values are consistent with the observational results of Bregman and Hogg (1988) for the dominant galaxies in A 1126, A 2199, and 2A 035+096.

The CO luminosity upper limits are plotted against the IR luminosities (detections and upper limits) as open circles (\circ) in Figure 1. For comparison, the empirical L_{IR} - L_{CO} relation derived by Young *et al.* (1986), in three ranges of dust temperature, for spiral galaxies is also shown (dashed lines). The results for spirals are explained quite plausibly in terms of a correlation between molecular gas content and star formation. Evidently, the CO luminosities (and presumably the molecular gas masses) of the galaxies we observed would in many cases have to be substantially lower than our upper limits, in order for these galaxies to follow the same general trend found for spirals. If star formation is proceeding in these galaxies in a manner similar to that in spirals, then it is either doing so at fairly low rates, or not producing massive stars, or both. Any of these possibilities must be reconciled with the continuous influx of star-forming material if a cooling flow is believed to be present.

Also shown in Figure 1 are five galaxies which were either detected by *IRAS* but not observed in CO (\square -symbol), or observed in CO but no *IRAS* data were obtained (\times -symbol). The L_{IR} - L_{CO} relation of Young *et al.* has been used in these cases to predict the luminosity in the unobserved waveband based on the luminosity in the observed waveband. The predicted luminosities may provide sensitivity limits for future observations.

DISCUSSION. We use a simple formalism to estimate the amount of cold interstellar gas that we might expect from a cooling flow at the present time, t . Assuming $dU/dt =$ growth rate of the ISM, $dS/dt = \eta U/\tau =$ star formation rate, and $\dot{M} =$ mass-flow rate = constant, where η is the star formation efficiency, τ is the lifetime of the ISM against star formation and all masses are in units of M_{\odot} , then $dU/dt = -\eta U/\tau + \dot{M}$. Because both η and τ may vary with time, we use $\langle \eta/\tau \rangle = t^{-1} \int_0^t [\eta(t')/\tau(t')] dt'$, which allows the simplification

$$U(t) \approx U_0 \exp(-\langle \frac{\eta}{\tau} \rangle t) + \dot{M} \langle \frac{\eta}{\tau} \rangle^{-1} \approx \dot{M} \langle \frac{\eta}{\tau} \rangle^{-1}.$$

We therefore expect the size of the reservoir to scale with \dot{M} , τ , and inversely with the star formation efficiency η .

Figure 2 shows mass-flow rates taken from the literature, plotted against our derived ISM masses or mass upper limits (IR-determined masses were derived following Jura [1986]). There does not appear to be any correlation. (Note that both the derived \dot{M} and M scale with distance-squared.) Taken at face value, this lack of correlation seems to add to the doubts about the existence of cooling flows. Alternatively, the failure to detect CO and IR

LUMINOSITY COMPARISON

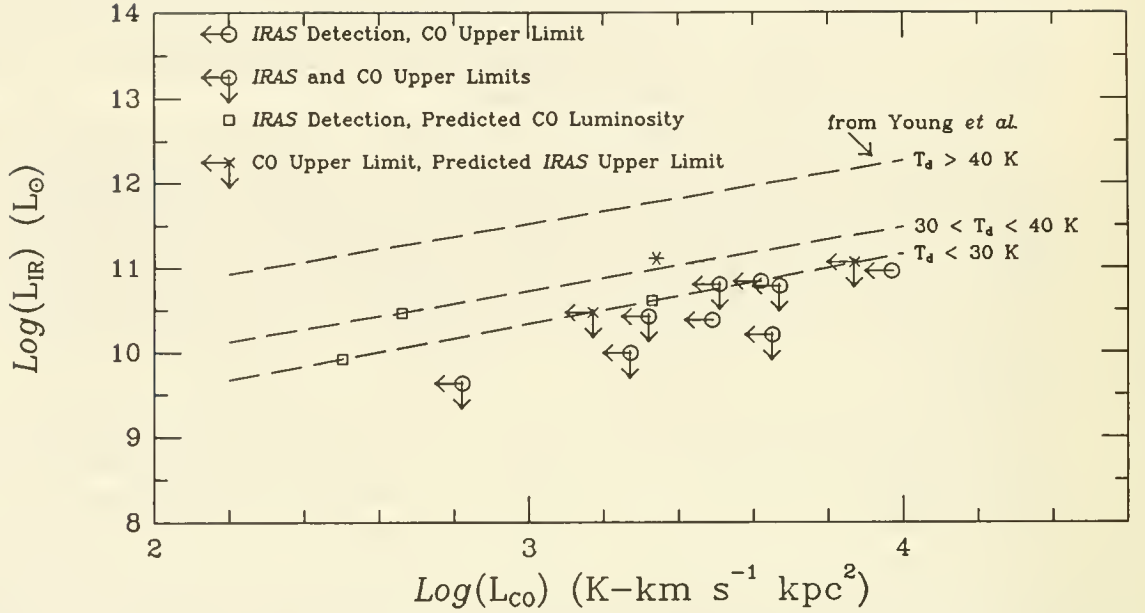


Figure 1. Luminosity comparison. The logarithms of L_{CO} and L_{IR} are plotted against each other. The symbols indicate whether only CO data (\times), only IRAS data (\square), or both (\odot) were obtained. The dashed lines show the $L_{\text{CO}}-L_{\text{IR}}$ relation determined by Young *et al.* (1986) for spirals; this was used to predict L_{IR} for \times 's and L_{CO} for \square 's. All upper limits are 3σ . The asterisk (*) is NGC 1275; L_{CO} is from Lazareff *et al.* (1989), scaled to $H_0 = 50 \text{ km s}^{-1} \text{ Mpc}^{-1}$.

MASS vs FLOW RATE

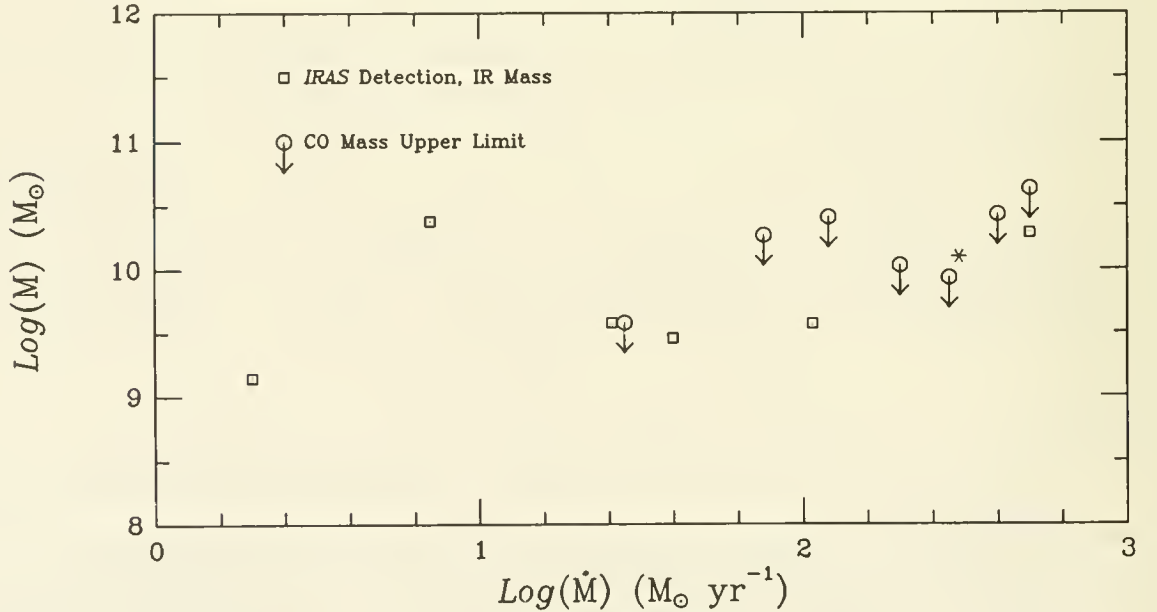


Figure 2. Mass vs flow rate. The logarithms of the mass-flow rates taken from the literature plotted against the logarithms of the IR-derived masses (\square) or 3σ CO mass upper limits (\odot). The asterisk (*) is NGC 1275; M_{CO} is from Lazareff *et al.* (1989), scaled to $H_0 = 50 \text{ km s}^{-1} \text{ Mpc}^{-1}$.

emission from most of the galaxies in our sample could indicate that the star formation rates and efficiencies are high, and the reservoir of star-forming gas is therefore relatively small. This possibility can be evaluated by deriving $\langle\eta/\tau\rangle^{-1}$ based on the assumed existence of cooling flows.

We redefine the quantity $\langle\eta/\tau\rangle^{-1}$ as $\tau_{SF} = 2M/\dot{M}$, where the factor of 2 is assumed to account roughly for the fraction of the cold ISM detected: only half in the form of H_2 in the case where M is derived from the CO upper limits; or only half the neutral gas being warm enough to be detected by *IRAS* at $100\mu\text{m}$ (cf. Jura 1986) in the case where M is derived from the *IRAS* data. For most of the clusters with reported cooling flows, we find $\tau_{SF} \sim 10^8$ yr, fairly short considering that this is a global value.

In spiral galaxies, high star formation efficiencies have been associated with high dust temperatures, high infrared luminosities, and large ratios of L_{IR}/L_{CO} (Young *et al.* 1986). Our results suggest that if cooling flows exist, then star formation fed by them is highly efficient. At the same time, however, the IR luminosities of the galaxies we observed are relatively low, a property which in spirals seems to indicate fairly low star formation rates. If the formation of massive stars is somehow suppressed in cooling flows, vigorous low-mass star formation might still proceed without significantly heating the interstellar gas and dust. This would be consistent with cooling flow models in which star formation is characterized by a truncated initial mass function (e.g., Sarazin and O'Connell 1983). Of course, if cooling flows are not actually present, or if mass-flow rates have been greatly overestimated, then the relatively small ISM masses and low infrared luminosities we find would be consistent with the results for spirals, without invoking different modes of star formation.

An additional question that can be addressed with our data, not directly related to cooling flows, is whether the FIR properties of cD galaxies differ from elliptical galaxies. To do this, we compared our results for cluster-dominant galaxies with those of Jura *et al.* (1987) for ellipticals. Using their findings for $F_\nu(B)$ versus $F_\nu(12\mu\text{m})$, the lack of detections in our sample at $12\mu\text{m}$ is consistent with cDs being scaled-up ellipticals. Similarly, the ISM masses we derived from the $100\mu\text{m}$ fluxes, a factor of ~ 100 greater than those found for ellipticals, are consistent with the typical mass estimates for cDs and ellipticals (cf. Sarazin 1986). Evidently, cD galaxies appear to be "oversized" ellipticals with regard to their FIR properties.

SUMMARY. Our results are summarized as follows:

1. About 40 clusters with and without cooling flows have been searched for IR emission with *IRAS* co-adds; 11 of these have also been observed for CO emission.
2. Six new *IRAS* detections have been discovered; no CO detections were made.
3. If cooling flows exist, star formation rates and efficiencies must be high in order to render the CO undetectable; yet at the same time IR luminosities are observed to be relatively low.
4. cD galaxies look like scaled-up ellipticals with regard to their FIR properties.

REFERENCES

- Bertschinger, E., and Meiksin, A. 1986, *Ap. J. (Letters)*, **306**, L1.
Bregman, J.N, and Hogg, D.E. 1988, *A. J.*, **96**, 455.
Jura, M. 1986, *Ap. J.*, **306**, 483.
Jura, M., Kim, D.W., Knapp, G.R., and Guhathakurta, P. 1987, *Ap. J. (Letters)*, **316**, L11.
Lazareff, B., Castets, A., Kim, D.-W., and Jura, M. 1989, *Ap. J. (Letters)*, **336**, L13.
Romanishin, W., and Hintzen, P. 1988, *Ap. J. (Letters)*, **324**, L17.
Sarazin, C.L. 1986, *Reviews of Modern Physics*, **58**, 1.
Sarazin, C.L., and O'Connel, R.W. 1983, *Ap. J.*, **268**, 552.
Sanders, D.B., Soifer, B.T., Elias, J.H., Madore, B.F., Matthews, K., Neugebauer, G., and Scoville, N.Z. 1988, *Ap. J.*, **325**, 74.
Silk, J, Djorзовski, S., Wyse, R.F.G., and Buzual, G. 1986, *Ap. J.*, **307**, 415.
Stewart, G.C., Fabian, A.C., Jones, C., and Forman, W. 1984, *Ap. J.*, **285**, 1.
Young, J.S., Schloerb, P.F., Kenney, J.D., and Lord, S.D 1986, *Ap. J.*, **304**, 443.

III - GAS DYNAMICS, HEATING, INTERACTIONS
A - GAS DYNAMICS AND MAGNETIC FIELDS IN GALAXIES

**AN INFRARED JET IN CENTAURUS A (NGC 5128):
EVIDENCE FOR INTERACTION BETWEEN THE ACTIVE NUCLEUS
AND THE INTERSTELLAR MEDIUM**

Marshall Joy

Space Science Laboratory, NASA Marshall Space Flight Center

P. M. Harvey and E. V. Tollestrup

Astronomy Department, University of Texas at Austin

P. J. McGregor and A. R. Hyland

Mt. Stromlo and Siding Spring Observatories, Australian National Observatory

Summary

The giant elliptical NGC 5128 (Centaurus A) is nearby radio galaxy containing a luminous active nucleus embedded in a broad dust lane (Graham 1979). A beam of relativistic particles emanates from the nucleus, generating X-ray and radio jets as well as extensive radio lobes and optical filaments in the outer parts of the galaxy (Burns, Feigelson, and Schreier 1983; Brodie, Konigl, and Bowyer 1983). The nature of this active galaxy has been studied at many wavelengths, but the nuclear region is rendered optically unobservable by heavy obscuration in the dust lane; therefore, studies of nuclear structure must be carried out at near-infrared wavelengths where the effects of extinction are greatly reduced. Giles (1986) constructed the first high resolution near-infrared maps of Cen A by scanning a small aperture across the source; this work pinpointed the location of the nucleus and also revealed unexpected asymmetries in the near-infrared light distribution.

In the present study, higher resolution near infrared images of the visually-obscured central region of Centaurus A have been obtained in order to investigate the effects of the active nucleus on the surrounding galaxy. We present J(1.25 μ m), H(1.65 μ m), and K(2.2 μ m) images of the central 40" of the galaxy, taken with the Univ. of Texas InSb array camera on the Anglo Australian 3.9 meter telescope. These images reveal a jet extending ~ 10 arcseconds to the northeast of the nucleus at the same position angle as the X-ray and radio jets. The infrared jet is most prominent at the shortest wavelength (1.25 μ m), where its brightness surpasses that of the nucleus (figure 2).

The blue appearance of the infrared jet is remarkable considering the heavy obscuration that is evident at visual wavelengths. The amount of reddening in the vicinity of the jet is determined from the measured colors of the stellar core of the galaxy (figure 3), and this value is used to generate an extinction-corrected energy distribution (figure 4). In contrast to previously studied optical and infrared jets in active nuclei, the short-wavelength prominence of the Cen A jet indicates that it cannot be attributed to synchrotron emission from a beam of relativistic electrons. The remaining viable mechanisms involve an interaction between the interstellar medium and the active nucleus: the infrared radiation from the jet may be due to emission from interstellar gas that has been entrained and heated by the flow of relativistic particles from the nucleus (cf. Brodie, Konigl, and Bowyer 1983); alternatively, luminous blue stars may have been created by compression of interstellar material by the relativistic plasma (De Young 1981). To investigate these proposed mechanisms, near-infrared spectroscopic studies of Cen A are in progress to look for collisionally excited molecular hydrogen emission lines and recombination lines from ionized gas.

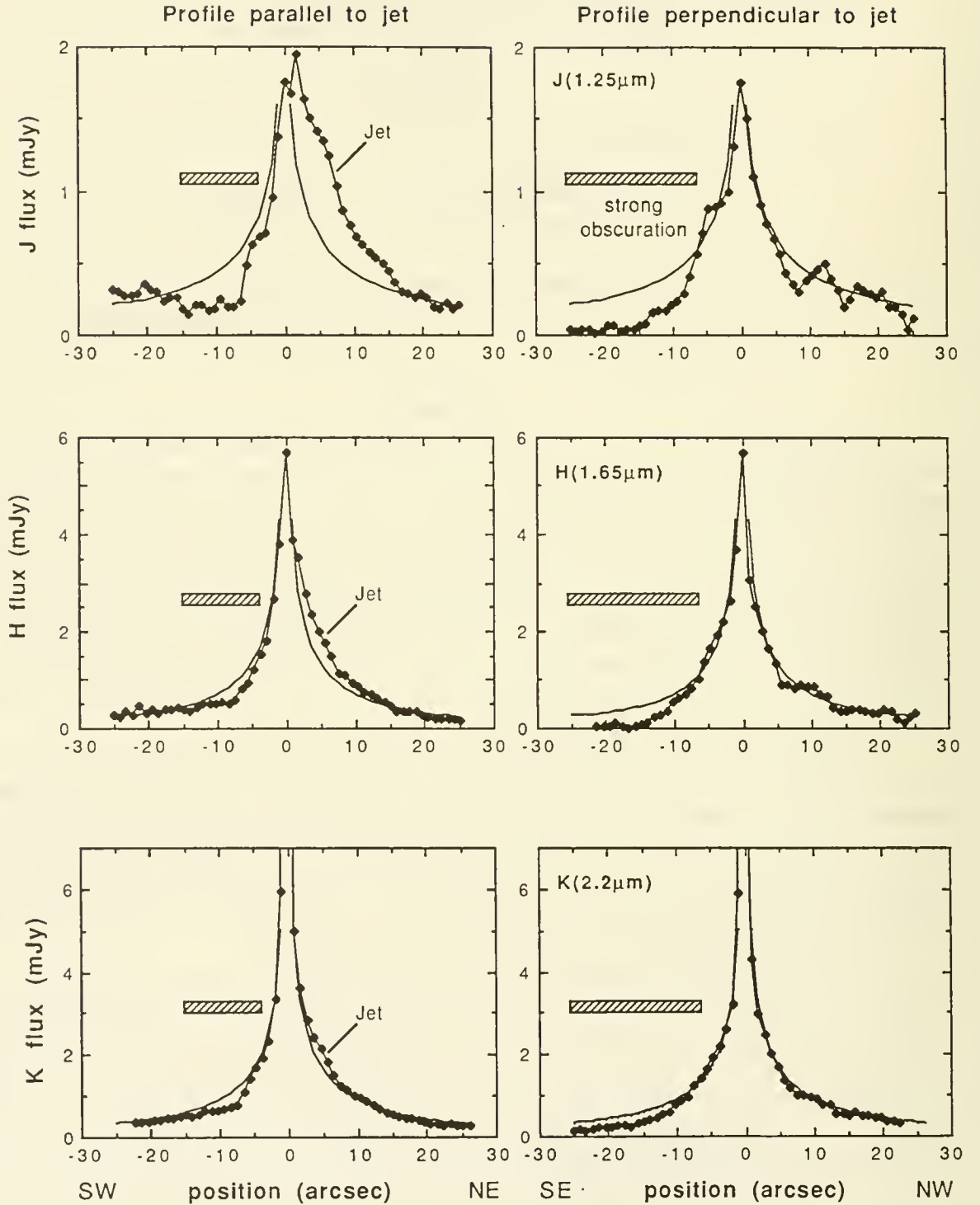


Fig. 2 – Slices through the infrared jet and the galaxy nucleus.

In order to compare the structure of the jet at all three wavelengths, we present slices directly through the nucleus and the jet (*left side of figure*); in the perpendicular direction, the slices pass through the nucleus alone (*right side*). All of the profiles intersect with the prominent dust lane; these regions of strong obscuration are indicated by cross-hatched bars in the figure. The underlying stellar bulge of the galaxy has been identified by fitting de Vaucouleurs $r^{1/4}$ profiles to the central region of the galaxy (*solid lines*); relative to these $r^{1/4}$ profiles, the jet is clearly seen in emission to the NE of the nucleus, and it is brightest at the shorter wavelengths.

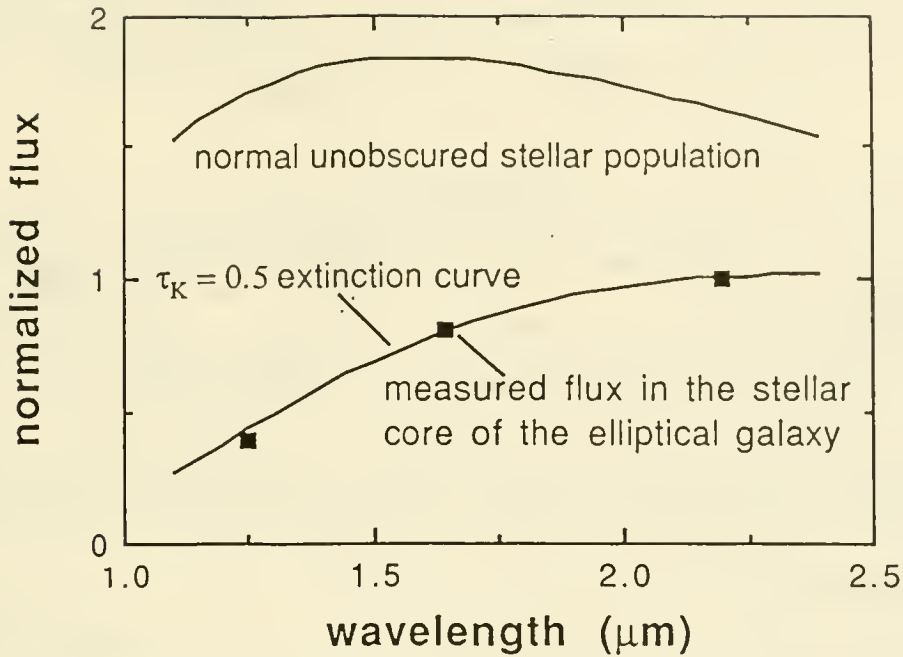


Fig. 3 – Near-infrared colors of the stellar core of Cen A.

The brightness of the stellar core of Cen A was derived from $r^{1/4}$ profiles fitted to the central region of the galaxy ($1'' < r < 6''$); these profiles yield colors that are much redder than those of a normal stellar population in an elliptical galaxy. The observed colors are consistent with a normal extinction law and a $2.2 \mu\text{m}$ optical depth of 0.5, which implies that the *visual* flux from the core of the galaxy is attenuated by a factor of ~ 50 ($A_V \sim 4$ mag). It is evident from figure 2 that the extinction is even greater within the dust lane.

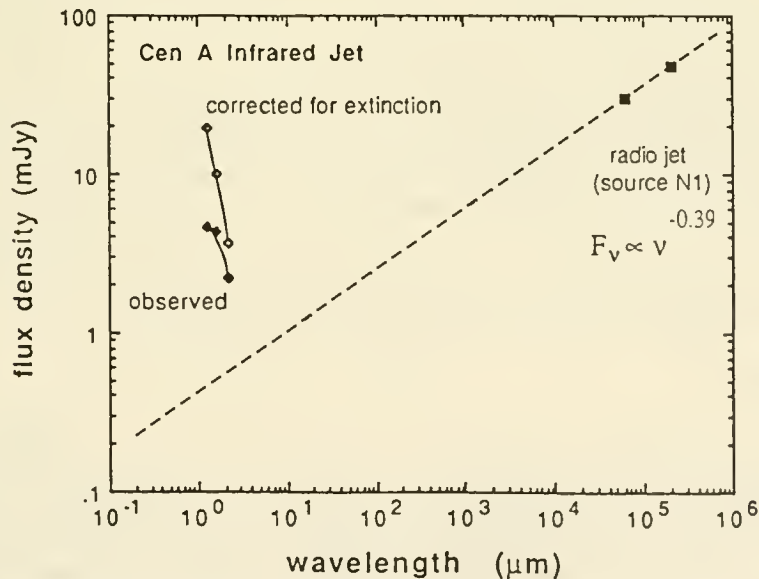


Fig. 4 – Energy distribution of the infrared jet.

The flux from the infrared jet was calculated by subtracting the underlying $r^{1/4}$ galaxy profile from the observed image, as indicated in figure 2. The infrared fluxes in this figure were computed for a $3.6'' \times 1''$ beam so that they could be directly compared with VLA measurements of the radio continuum jet N1 (Burns, Feigelson, and Schreier 1983). Filled triangles denote the measured flux of the jet, and open triangles represent extinction-corrected fluxes calculated using the optical depth from figure 3. It is evident from the figure that neither the slope nor the amplitude of the near-infrared emission is consistent with synchrotron emission from the radio jet.

NGC 4438: RAM PRESSURE SWEEPING OF A TIDALLY DISRUPTED GALAXY.

J. E. Hibbard, Columbia University
J. H. van Gorkom, Columbia University/NRAO*

ABSTRACT

NGC 4438 is the highly HI deficient peculiar spiral in the center of the Virgo cluster. In this paper we present observations of the neutral hydrogen emission obtained with the VLA in the D-array configuration. These observations map out the total HI as determined from single dish measurements, and show the hydrogen to be confined to a region about one third the size of the optical disk and displaced to the side of the galaxy opposite M87. The hydrogen content of the galaxy is over an order of magnitude less than that expected for a galaxy of its type.

The data suggest that the HI deficiency is a result of ram pressure stripping of the gas in the outer regions of the galaxy by the hot intracluster medium after being tidally perturbed.

I. INTRODUCTION

It is well known that the central galaxies in clusters with high X-ray luminosities are deficient in HI in comparison with galaxies in less volatile environments (Giovanelli and Haynes, 1985), suggesting that the hot intracluster medium plays a crucial role in removing the gas from these galaxies. This effect is most strikingly illustrated in figure 23 of Cayette et al. (1989) of HI observations of the galaxies within 5° of M87, a bright X-ray source. All of the galaxies within 2° of M87 have greatly reduced HI disks sizes.

NGC 4438 is in projection the closest spiral to M87 ($50' = 150$ kpc, assuming a distance to Virgo of 12 Mpc, used throughout this paper). If it is physically close to M87, it moves through that galaxy's X-ray halo at supersonic speeds, and is therefore a prime candidate to study for the effects of the sweeping of its interstellar medium (Kotanyi, van Gorkom and Ekers, 1981). Optically the galaxy looks disturbed, possibly caused by an interaction with NGC 4435, which is close in projection ($4.3'$) to NGC 4438. Yet the neutral hydrogen observations of NGC 4438 are not typical of tidally involved galaxies: clearly interacting systems with HI show the gas to be almost always extended, either in narrow tails or diffuse envelopes, and to have roughly the gas content expected for their morphological type.

The intent of this observation was to recover the full velocity width profile of NGC 4438, which previous synthesis observations failed to do. With the HI fully located it is now possible to address the cause of the peculiar hydrogen extent and content.

II. OBSERVATIONS

NGC 4438 was observed with the VLA of the NRAO* in the compact D-array configuration. The spatial resolution is $60''$ and the velocity resolution is 21 km/s. The rms noise in the channel maps is 0.75 mJy/beam. These observations are sensitive to hydrogen emission on scales less than $15'$ and column densities greater than 8.3×10^{17} atoms/cm² per channel (3σ). We recover the full profile width of 412 ± 21 km/s found from single dish observations, and find a total hydrogen content of $1.7 \times 10^8 M_\odot$.

III. DISTRIBUTION AND KINEMATICS OF THE GAS

The intensity distribution from the zeroth order moment is given in figure 1 overlaid upon the optical photograph from Arp (1966) and the CO observations of Combes et al. (1988).

The maximum has a peak of $4.9 \times 10^{20} \text{ cm}^{-2}$ and is displaced to the northwest of the galaxy, anti-correlated with the CO peaks. A secondary peak of $1.2 \times 10^{20} \text{ cm}^{-2}$ occurs towards NGC 4435 and coincides with the end of the swept back stellar arm. Similar peaks are found in the tail features of other interacting galaxies. The HI disk is only a third the size of the optical disk.

The line emission was detected in 21 channels, from 300 to -112 km/s. These channel maps are presented in figure 3. The intensity-weighted velocity field is given in figure 2. The velocity field is disturbed, but regular.

IV. DISCUSSION

The HI deficiency parameter, DEF, is defined by Haynes and Giovanelli (1983) as the difference in the logarithm of galaxy's observed HI mass from that expected for a normal galaxy of similar morphological type and optical diameter. Figure 4 plots the HI flux (which is proportional to HI mass) versus the corrected photometric diameter, D_0 , for late type galaxies of the comparison field sample used by Haynes and Giovanelli, as well as for several classes of interacting and peculiar galaxies from data presented by Davis and Seaquist (1983). It is found that the interacting and peculiar samples follow the same relationship as the comparison sample, albeit with a wider spread. NGC 4438 is found to lie over an order of magnitude off of the relationship, with a DEF of 1.44 ± 0.20 . This makes it one of the most hydrogen deficient galaxies measured.

Ablation processes, such as ram pressure sweeping (Gunn and Gott, 1972) and thermal evaporation (Cowie and Songaila, 1977) are expected at the gas densities and X-ray temperatures appropriate to NGC 4438, if it is within the X-ray halo of M87 (Kotanyi, van Gorkom and Ekers, 1981, Chincarini and de Souza, 1985). Yet these processes cannot mechanically affect the stellar component of the galaxy. The tidal encounter scenario of Combes et al. (1988) nicely reproduces the stellar and molecular features of NGC 4438, as well as the general distribution of the HI which is found. But simulations and observations show that interactions do not remove the HI, and they extend rather than truncate the size of the disk.

The best explanation of the data is that both effects are important in this case. We believe that NGC 4438 underwent a tidal encounter with NGC 4435 which displaced the hydrogen and molecular features and produced the sweptback arm. The hydrogen disk was extended, moreso nearest NGC 4435, where it became clumped along the northern arm. Since the galaxy was within the halo of M87 during or shortly after the encounter, this extended gas was easily removed by the hot IGM, since both the column densities and the gravitational pull of the galaxy were lower.

*The National Radio Astronomy Observatory is operated by AUI, Inc. under cooperative agreement with the National Science Foundation.

REFERENCES

- Arp, H. (1966). Atlas of Peculiar Galaxies (California Institute of Technology, Pasadena).
Cayette, V., van Gorkom, J.H., Balkowski, C., Kotanyi, C. (1989). In preparation.
Chincarini, G., de Souza, R. (1985). *Astr. Ap.*, **153**, 218.
Combes, F., Dupraz, C., Casoli, F., Pagani, L. (1988). *Astr. Ap.*, **203**, L9.
Cowie, L.L., Songaila, A. (1977). *Nature*, **266**, 501.
Davis, L.E., Seaquist, E.R. (1983). *Ap.J.Suppl.* **53**, 269.
Giovanelli, R., Haynes, M.P. (1985). *Ap.J.* **292**, 404.
Gunn, J.E., Gott, J.R. (1972). *Ap.J.* **176**, 1.
Haynes, M.P., Giovanelli, R. (1983). *A.J.* **88**, 881.
Kotanyi, C., van Gorkom, J.H., Ekers, R.D. (1981). PhD. Thesis, Kotanyi, Univ. Groningen, p. 17.

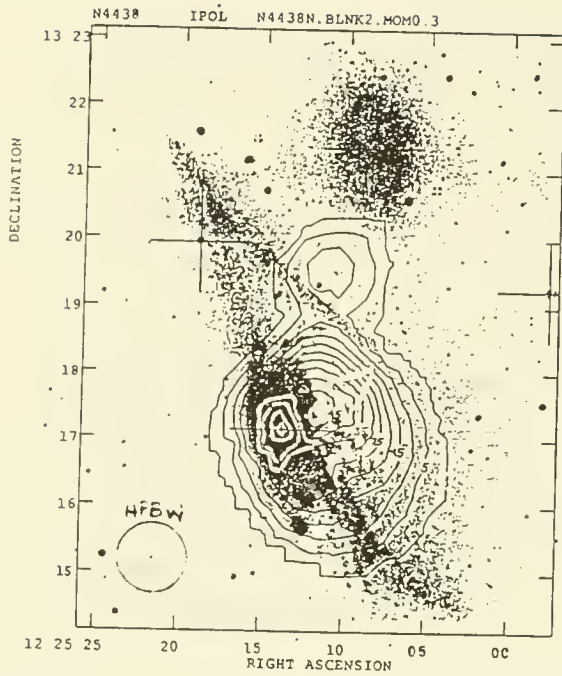


Figure 1: Hydrogen contours (black) for NGC 4438 superposed on the photograph from Arp (1966) and the CO(1-0) contours (white) from Combes et al. (1988). The Hydrogen contours are in units of 10^{19} atoms/cm², and the CO contours are at levels of 8, 20, and 50 *K km/s.

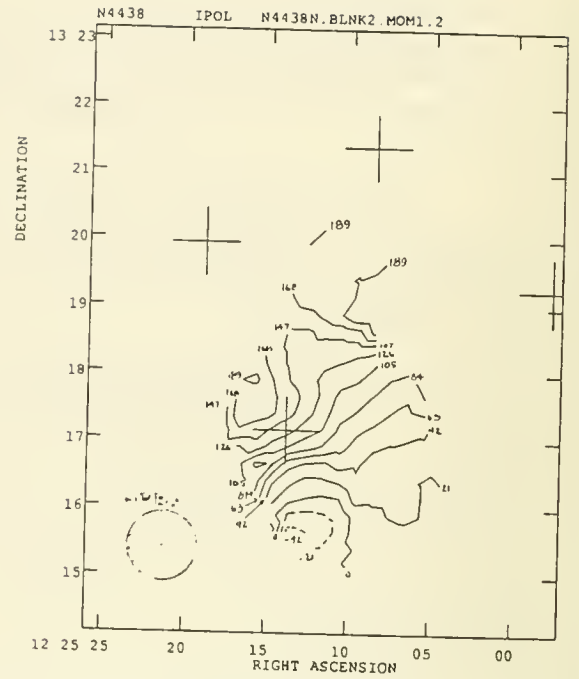


Figure 2: Intensity-weighted HI velocities (km/s) for NGC 4438. Crosses mark the optical centers of NGC 4438 and NGC 4435 and two reference stars.

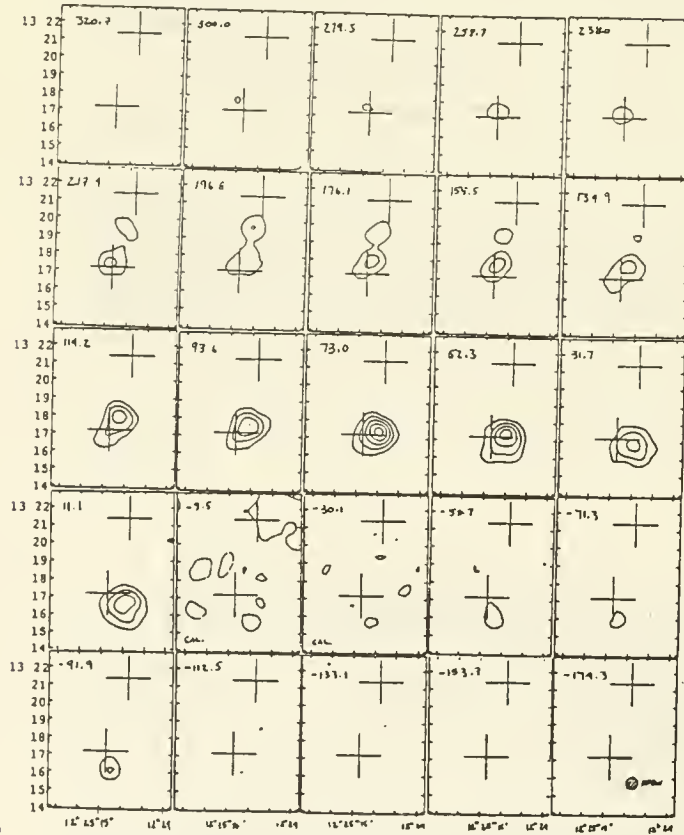


Figure 3: Channel maps of 21 cm-line radiation from MOC 4438. The contours are at steps of 1.7×10^{19} atoms/cm² [3σ]. Negative contours are dashed. The heliocentric radial velocity (km/s) of each channel is indicated at the top left of each frame. The channels at -9.3 and -30.1 km/s are contaminated by HI from the Galaxy. Crosses mark the optical centers of MOC 4438 and MOC 4435. The hatched ellipse in the final frame shows the size of the synthesized beam (HFBW).

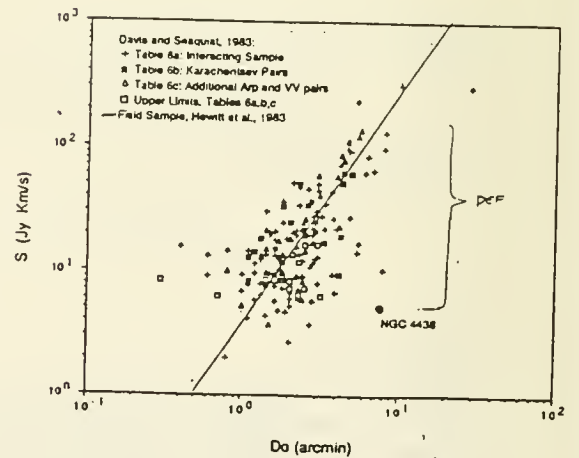


Figure 4: The relationship between single dish HI flux (Jy km/s) and corrected photometric diameter (arcmin) for the late-type interacting galaxies in the lists of Davis and Seagust (1983) and for the field sample of Hewitt et al. (1983). Notice that the interacting sample follows the same relationship as the field sample for optical diameters above 1". HI deficiency is measured by the vertical distance off of the mean relationship. As can be seen, MOC 4438 is HI deficient compared to either sample.

NGC 3312: A VICTIM OF RAM PRESSURE SWEEPING ?

P.M. McMahon¹, O.-G. Richter^{2*}, J.H. van Gorkom^{1,3}, and H.C. Ferguson⁴

1) Columbia University, New York

2) Space Telescope Science Institute, Baltimore

3) National Radio Astronomy Observatory, Socorro[†]

4) Johns Hopkins University, Baltimore

Introduction

We are undertaking a volume limited survey of the Hydra I cluster in neutral hydrogen using NRAO's Very Large Array (VLA). The main purpose is to study the effects of a dense environment on the gaseous component of the galaxies. Observational evidence has been accumulating recently that ram pressure sweeping does occur in the centers of clusters, but it is possible that tidal interactions play a role as well. In this paper we present results of high resolution H I imaging of NGC 3312, the large peculiar spiral near the cluster center. Hydra I (= A1060) is the nearest rich cluster beyond Virgo and, as such, presents a unique opportunity to do a complete survey of a cluster. It is similar to the Virgo cluster (*e.g.*, Richter 1985) in many of its general physical characteristics, such as, size, X-ray luminosity, velocity dispersion, and galaxy content (high spiral fraction). However, Hydra I appears to be more regular and relaxed. This is evident in the X-ray distribution in its central region, which is radially symmetric and centered on the dominant galaxy, NGC 3311, a cD-like elliptical. The observed X-ray luminosity implies a central gas density of $4.5 \times 10^{-3} \text{ cm}^{-3}$ (Jones and Forman 1984). Gallagher (1978) argued from optical images of NGC 3312 that this galaxy might be an ideal candidate to directly study effects of the ram pressure process; it might currently be undergoing stripping of its interstellar medium. Our data are consistent with this suggestion, but other origins of the peculiar appearance cannot yet be ruled out.

Observations

Forty-eight hours of observations were made at the VLA in both B/C and C/D configurations. The data were on-line Hanning smoothed and calibrated employing standard VLA calibration methods. The UV data from both hybrid arrays were then combined in order to form a high resolution high sensitivity 31 channel data cube. Two maps were created using both natural ($30''7 \times 17''2$ beam) and uniform ($14''2 \times 11''6$ beam) weighting. Line-free channels on either side of the band were combined to form a continuum map which was then subtracted from all channels, leaving a cube of H I emission. The central velocity of this cube is 2850 km s^{-1} and the channel spacing is 41.5 km s^{-1} . We present here the natural-weighted (higher sensitivity) H I images and the uniform-weighted (higher resolution) continuum image. The 3σ -level column density is $5.8 \times 10^{19} \text{ cm}^{-2}$.

Results and Discussion

NGC 3312 is a large peculiar spiral with apparently anemic arms on the west side and dust lanes on the east side. Fig. 1 shows a contour map of the radio continuum emission overlayed on an optical print. The continuum is composed of an unresolved core source of 24 mJy and an extended region associated primarily with the prominent eastern spiral arm(s) of the galaxy. With a cluster radial velocity of 3420 km s^{-1} and a Hubble constant of $50 \text{ km s}^{-1} \text{ Mpc}^{-1}$, this galaxy has a diameter of about 80 kpc. The radio continuum distribution is quite asymmetric. Except for an extension to the northwest (just outside a ridge along several H II regions), the emission is almost completely confined to the dust lanes at the east side of the galaxy. This side is also about 0.3 magnitudes bluer than the mean color of the galaxy as a whole.

The gas distribution is equally asymmetric. Fig. 2 shows the integrated H I emission for NGC 3312 as well as NGC 3314a (south) and a tiny ring galaxy (east). The neutral hydrogen in NGC 3312 is distributed asymmetrically across the disk of the galaxy, with a steep dense ridge on the bluer eastern side and weaker

*Also affiliated with the Astrophysics Division of the Space Science Department of E.S.A.

[†]The National Radio Astronomy Observatory is operated by AUI, Inc. under cooperative agreement with the National Science Foundation.

emission extending out to the region of the optical filaments noted by Gallagher (1978) in the west. In between lies a central depression. A slice through the center along the minor axis reveals two things: (a) the eastern (left) side rises from less than $6 \times 10^{19} \text{ cm}^{-2}$ to a column density of $1.4 \times 10^{21} \text{ cm}^{-2}$ in less than a beam width (4.3 kpc), while the western (right) side peaks at only $1.1 \times 10^{21} \text{ cm}^{-2}$ and falls off more gradually, and (b) the western side of the galaxy actually contains about 30% more H I than the eastern side. The H I, like the continuum emission, mostly coincides with the regions of active star formation, *e.g.*, no H I is seen coincident with the faint smooth optical extension in the north, which lacks the blue knotty appearance of other northern and eastern features. In general, the distribution of the red light is much more symmetric than that of the H I and radio continuum.

The channel maps and the intensity-weighted mean velocity field (Fig. 3) show that the kinematics are even more irregular than the H I distribution. Especially in the southwest, gas seems to be dragged out and moving at less negative velocities than expected from the underlying rotation pattern. We note here that this is exactly what would be expected from ram pressure sweeping if the galaxy is moving toward us with respect to the mean cluster motion. The changing orientation of the line of nodes in Fig. 3 indicates that this is not simply gas in a disk on circular orbits and it is even more complicated than a warped disk would be. Thus, non-circular motions are indicated in the outer parts.

Even if we take projection effects into account, the observed steep drop in H I surface density inside the optical image in the east is quite unusual. Isolated spiral galaxies usually show H I at higher column densities out to much larger radii than is seen here (*e.g.*, Sancisi 1982). Although sharp edges have been found in a few isolated galaxies, these occur at much larger radii and lower column densities (*e.g.*, Corbelli *et al.* 1989; van Gorkom *et al.* 1989). Although the H I morphology of NGC 3312 is very unusual, it is not unique. A similar morphology (sharp edge on one side and smooth extended H I on the other) has been found in a number of galaxies in the Virgo cluster (Cayatte *et al.* 1989) and in the relatively isolated galaxy NGC 1961 (Shostak *et al.* 1982). For all these examples ram pressure sweeping has been invoked as the most plausible explanation.

We, therefore, suggest that (a) the mechanism responsible for this gas pile-up and deficiency is ram pressure sweeping, and (b) a secondary effect may be enhanced star formation in the pile-up region, indicated by both the continuum distribution and the strong color gradient, and this may cause further gas depletion. A rough calculation of intracluster medium (ICM) densities needed to strip gas down to observed column densities produces values consistent with observations. Assuming NGC 3312 moves through the ICM with a velocity just equal to its radial velocity (-839 km s^{-1} relative to the cluster), and that its mass is uniformly distributed across the disk, the density needed for stripping is $3 \times 10^{-4} \text{ cm}^{-3}$, comfortably below that observed in X-rays.

It is still worthwhile to consider other mechanisms which may be consistent with the observations. Tidal interactions could also produce sharp edges, and an asymmetry in the H I distribution. The interaction could have occurred with the other peculiar spiral in the same field, NGC 3314a. It is located about 7.5 south of NGC 3312 and lies in the same velocity range. An additional reason to suspect an interaction between these two is that both exhibit tails of neutral hydrogen, indicative of tidal interaction. NGC 3314a has a long tail of emission pointing away from NGC 3312, while NGC 3312 has a short arm pointing toward NGC 3314a. Thus the tails are close to parallel; the momentum vectors of the galaxies are parallel as well. The alignment of the tails is not easily understood in a tidal interaction scenario, while it would be the most likely orientation if the two galaxies are moving together through an ICM and are being stripped.

There is also a finite chance that NGC 3312 along with the other galaxies detected (NGC 3314a, Ring, etc.) form a genuine foreground group. In this case, one might compare this "group" with the NGC 1961 group (Shostak *et al.* 1982). Since the X-ray emission is centered on NGC 3311, we must then conclude that no ICM of significance is present in the group, and the peculiar morphology of NGC 3312 must be due to a tidal interaction. Simulations are required to test this hypothesis. A bonus of the foreground hypothesis is that it would explain why these galaxies seem brighter and bigger than most Hydra I galaxies.

Given the study on cluster substructure by Fitchett and Merritt (1988) and keeping in mind that Hydra I is isolated in redshift space, the group hypothesis is perhaps plausible. However, a more likely interpretation is then, that the entire group is currently falling into Hydra I, thus it would be a background and not a foreground group. In such a situation the H I observations are pointing to ram pressure sweeping again. As mentioned above, the roughly parallel extensions of both NGC 3312 and NGC 3314a seem to favor this interpretation. Note, however, that in this scenario we can derive a lower limit for the transverse velocity

of NGC 3312 which is more than five times the radial velocity dispersion of the potential “group” members. This is done via a dynamic interpretation of the optical appearance of the eastern side of NGC 3312. Dust on the front side seems to absorb light from part of the bulge. Thus, it must have been moved – by ram pressure – above the disk. For this to happen, NGC 3312 must move into the ambient medium with some inclination with respect to edge-on. The inclination on the sky is about 72° therefore the transverse velocity must be at least 280 km s^{-1} ($= v_r \cdot \cot i$ with $v_r = -839 \text{ km s}^{-1}$). This seems unlikely and either a genuine foreground group with tidal interactions or genuine cluster members undergoing ram pressure sweeping (and, possibly, simultaneous tidal interactions) remain the plausible alternatives.

Conclusions

The results can be summarized as follows:

- A steep, smooth edge on the east side of the galaxy, seen in optical (B), radio continuum, and neutral hydrogen is consistent with NGC 3312 having its outer regions of gas stripped and its leading edge gas compressed as it moves through the cluster.
- The continuum distribution and new UBVR photometry indicate that recent star formation has occurred in the “piled-up” gas, which may have also contributed to the gas depletion.
- If it is being stripped, the proper motion of NGC 3312 can be inferred to be at least 280 km s^{-1} in a northeastern direction. This motion through the intracluster gas has moved the H I in the leading side out of the original disk.
- Gallagher (1978) proposed ram pressure sweeping to explain NGC 3312 based on faint filaments extending from the back side of the galaxy seen in the optical.

Although we cannot exclude the possibility that NGC 3312 and NGC 3314a are tidally interacting in a foreground group, we suggest, based on the above evidence, that NGC 3312 is, indeed, an ideal candidate to study the detailed effects of ram pressure sweeping.

References

- Cayatte, V., van Gorkom, J.H., Balkowski, C. and Kotanyi, C. 1989, preprint.
 Corbelli, E., Schneider, S., and Salpeter, E. 1989, *A.J.*, **97**, 390.
 Fitchett, M. and Merritt, D. 1988, *Ap.J.*, **335**, 18.
 Gallagher, J.S. 1978, *Ap.J.*, **223**, 386.
 Jones, C. and Forman, W. 1984, *Ap.J.*, **276**, 38.
 Richter, O.-G. 1985, *The Virgo Cluster of Galaxies, Proceedings of an ESO Workshop*, eds. O.-G. Richter and B. Binggeli, ESO, Garching, p. 427.
 Sancisi, R. 1982, IAU symposium No. 100, 57.
 Shostak, G.S., Hummel, E., Shaver, P.A., van der Hulst, J.M., and van der Kruit, P.C. 1982, *Astr.Ap.*, **115**, 293.
 van Gorkom, J.H., van Albada, T.S., Cornwell, T.J., and Sancisi, R. 1989, in preparation.

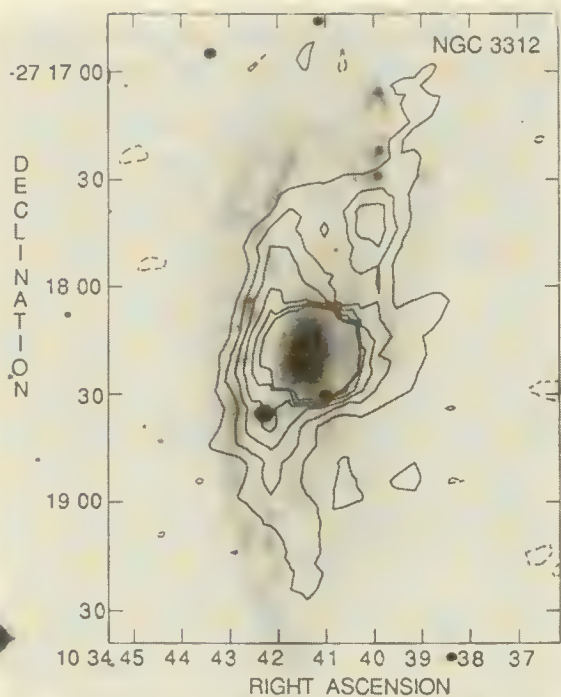


Fig. 1 Overlay of the radio continuum radiation at 21cm from NGC 3312 on an optical photograph taken by A. Sandage at the Las Campanas DuPont 2.5m telescope. Contour levels are -2, 2, 4, 6, 8, 10, and 12 σ , where $\sigma = 0.2$ mJy/Bm.

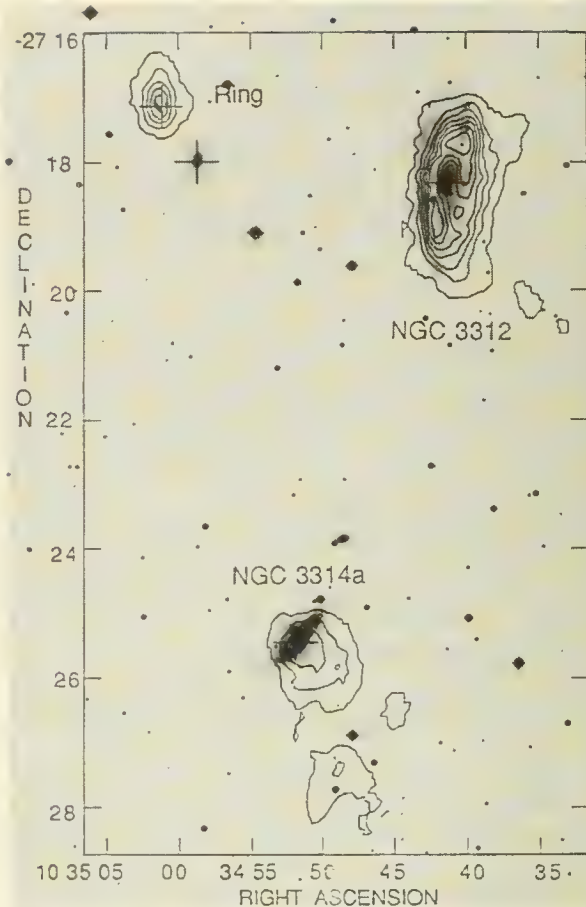


Fig. 2 Integrated H I distribution of NGC 3312, NGC 3314a, and the Ring galaxy overlaid on the optical photograph. The contour levels are in steps of $7 \times 10^{19} \text{ cm}^{-2}$ beginning at 10^{19} cm^{-2} .

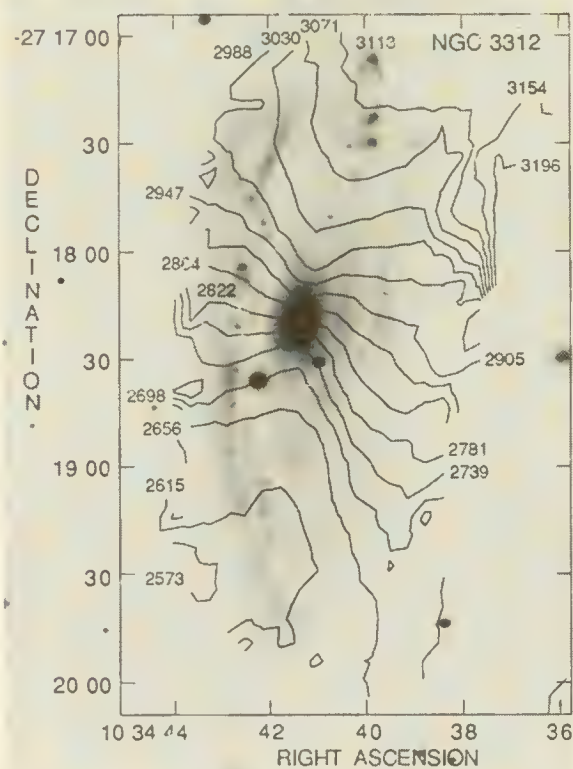


Fig. 3 The velocity field of NGC 3312. Note the strong asymmetry and the bent line of nodes. Velocities are in units of km/s.

THE VIOLENT INTERSTELLAR MEDIUM IN MESSIER 31

Elias Brinks¹, Robert Braun², Stephen W. Unger¹

¹*Royal Greenwich Observatory, Herstmonceux Castle, Hailsham BN27 1RP, England*

²*National Radio Astronomy Observatory, Very Large Array,
Socorro, New Mexico 87801-0387, U.S.A.*

ABSTRACT: TAURUS observations in the line of $H\alpha$ and VLA HI mapping of the HII complex No. 722 in M31, reveal what seems to be a spherical cavity 330 pc in diameter blown out by a stellar association of over 20×10^6 year old. Evidence of induced star formation which was initiated less than 5×10^6 years ago is present in the form of bright HII emission and numerous O, B and Wolf-Rayet stars which are found within the shell surrounding the cavity. The energy necessary to create the HI shell is estimated to be about 5×10^{51} erg.

Vast amounts of energy are pumped into the interstellar medium (ISM) by an OB association, firstly in the form of photons and stellar winds from the most massive stars and later by supernova explosions of all stars initially more massive than about $8 M_{\odot}$. The effects that this has on the ISM of spiral galaxies is the creation of large cavities filled with hot gas. Examples of this can be found in recent studies which identify numerous "holes" and shells within the neutral hydrogen (HI) distribution of our Galaxy (Heiles 1979, 1984), the LMC (Meaburn 1980, Dopita *et al.* 1985), M31 (Brinks and Bajaja 1986) and M33 (Deul 1988). There are a number of theoretical studies which describe the energy balance and structure of a supernova dominated ISM (Cox and Smith 1974; McKee and Ostriker 1977). Recently they have been extended to take into account the fact that supernovae occur clumped, *i.e.* they go off within their parent OB association (Heiles 1987; Norman and Ikeuchi 1989). Also, the most energetic events might cause a blow-out of the hot gas and fuel the halo (Bregman 1980; Corbelli and Salpeter 1987). However, what is lacking are observational constraints on these models such as: how is the energy input distributed among the primary sources, how much kinetic energy is dumped into the ISM, and what is the filling factor for each of them. Other interesting questions are: how does an evolving OB association shape its immediate surroundings and what happens at the interfaces of the various phases of the ISM. Again many models have been proposed (see Tenorio-Tagle and Bodenheimer (1988) for a recent review).

Attempts to answer these questions by studying our Galaxy are frustrated by our location within its disk. Extinction limits our optical horizon to the solar neighbourhood and at radio wavelengths the picture is confused by the lack of reliable distance determinations. We therefore decided to attempt a multi-frequency study of the violent ISM of M31. Part of this study consists of mapping some eight selected areas using TAURUS-I, the Fabry-Perot interferometer mounted at the Cassegrain focus of the 2.5-m INT telescope on La Palma to trace the distribution and kinematics of the ionised gas, or warm phase of the ISM, via its $H\alpha$ emission. Figure 1 shows a sequence of $H\alpha$ channel maps of a field located at a galactocentric distance of 9.7 kpc in the north-eastern arm of M31, encompassing region P722 from Pellet *et al.* (1978). The field of view of TAURUS-I is 5 arcmin which corresponds to 1000 pc at the assumed distance of M31 of 690 kpc. The heliocentric velocities corresponding to the channels are indicated

on top of each frame. This field coincides with OB48 (van den Bergh 1964; Efremov 1987) which was recently studied in greater detail by Massey *et al.* (1986). They found several Wolf-Rayet stars within its boundaries and estimated it to be young ($< 5 \times 10^6$ year). They also point out that the region seems to consist of subclusters with sizes of typically ~ 200 pc. The H α shell partly overlaps with an HI shell which was found in the new survey of part of M31 with the Very Large Array (Braun 1989). Its diameter is about 330 pc. Quite surprisingly the shells do not show any sign of expansion. Order of magnitude estimates for the age and energy requirement for the HI shell give 20×10^6 year and 5×10^{51} erg.

Our interpretation of this complex region is as follows. Some 20×10^6 year ago an OB association was formed. During its evolution it created an expanding HI shell. Eventually the shell swept up so much material that it stalled. Densities in this shell reached high enough values for star formation to take place and only 5×10^6 year ago new OB associations were formed which by their strong UV flux ionise most of the HI shell.

These first results illustrate that it is feasible with current instruments to study the violent ISM in nearby galaxies at linear resolutions which could hitherto only be achieved in our Galaxy. Further analysis of this and the other fields is currently in progress.

ACKNOWLEDGEMENTS

The Isaac Newton Telescope is operated on the island of La Palma by the Royal Greenwich Observatory in the Spanish Observatorio del Roque de los Muchachos of the Instituto de Astrofísica de Canarias. The National Radio Astronomy Observatory is operated by Associated Universities, Inc., under contract with the National Science Foundation.

REFERENCES

- Braun, R.: 1989, *Astrophys. J. Suppl.* (in preparation)
 Bregman, J.N.: 1980, *Astrophys. J.* **236**, 577
 Brinks, E., Bajaja, E.: 1986, *Astron. Astrophys.* **169**, 14
 Corbelli, E., Salpeter, E.E.: 1987, *Astrophys. J.* **326**, 551
 Cox, D.P., Smith, B.W.: 1974, *Astrophys. J. Letters* **189**, L105
 Deul, E.: 1988, *Ph. D. Thesis* (Leiden Observatory)
 Dopita, M.A., Mathewson, D.S., Ford, V.L.: 1985, *Astrophys. J.* **297**, 599
 Efremov, Yu.N., Ivanov, G.R., Nikolov, N.S.: 1987, *Astrophys. Space Sci.* **135**, 119
 Heiles, C.: 1979, *Astrophys. J.* **229**, 533
 Heiles, C.: 1984, *Astrophys. J. Suppl.* **55**, 585
 Heiles, C.: 1987, *Astrophys. J.* **315**, 555
 Massey, P., Armandroff, T.E., Conti, P.S.: 1986, *Astron. J.* **92**, 1303
 McKee, C.F., Ostriker, J.P.: 1977, *Astrophys. J.* **218**, 148
 Meaburn, J.: 1980, *Monthly Notices Roy. Astron. Soc.* **192**, 365
 Norman, C.A., Ikeuchi, S.: 1989, *Astrophys. J.* (submitted)
 Pellet, A., Astier, N., Viale, A., Courtès, G., Maucherat, A., Monnet, G., Simien, F.: 1978, *Astron. Astrophys. Suppl.* **31**, 439
 Tenorio-Tagle, G., Bodenheimer, P.: 1988, *Ann. Rev. Astron. Astrophys.* **26**, 145
 van den Bergh, S.: 1964, *Astrophys. J. Suppl.* **9**, 65

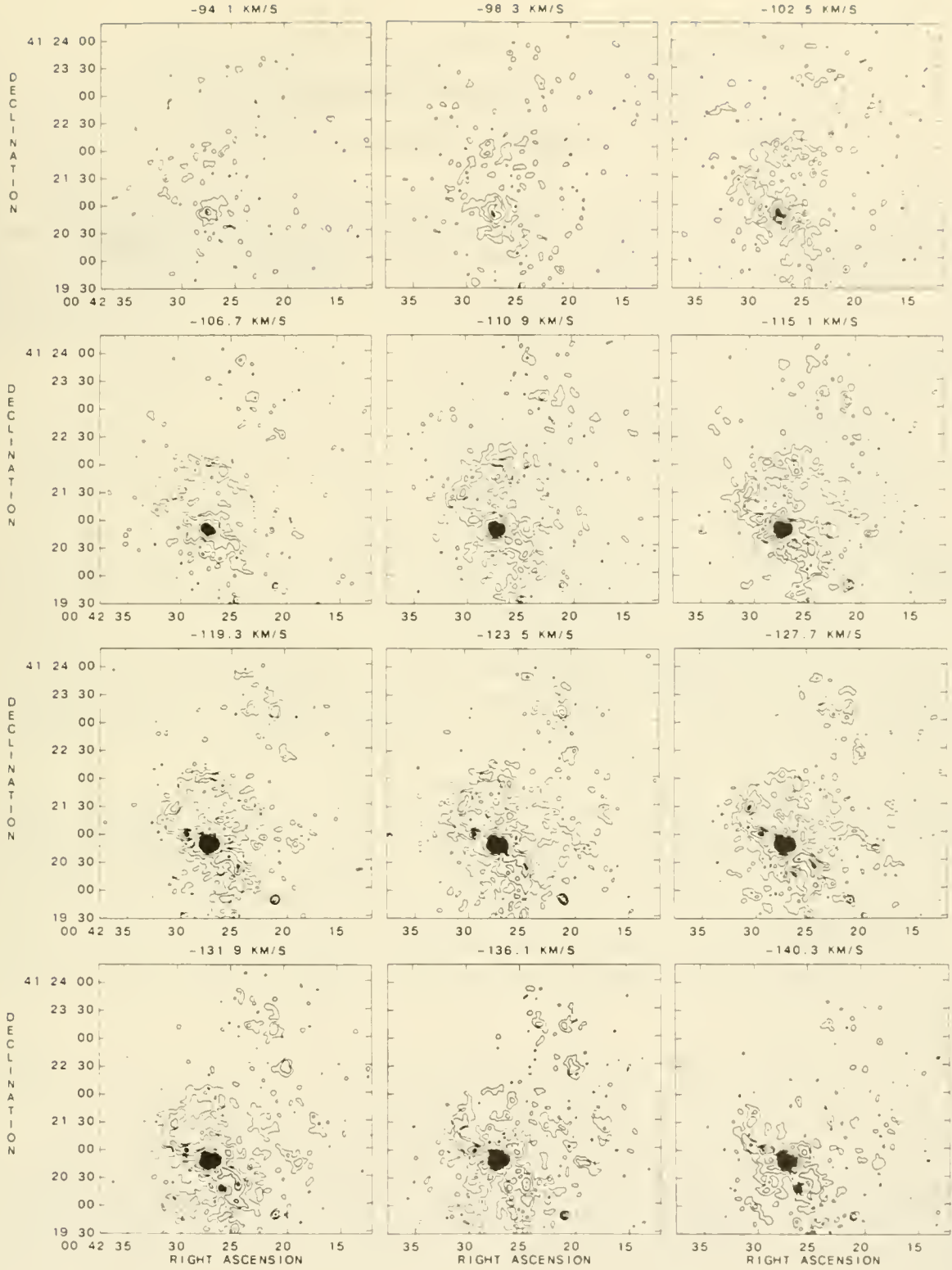


Figure 1: Sequence of $H\alpha$ channel maps. The heliocentric velocity of each channel in km s^{-1} is shown above each frame. Contour levels are at -1, 1, 2, 4, 8 and 16 in units of $2.14 \times 10^{-17} \text{ erg cm}^{-2} \text{ s}^{-1} \text{ arcsec}^{-2}$ per channel. The resolution is 5 arcsec, the channel separation 4.2 km s^{-1} .

Supernova Remnants and Diffuse Ionized Gas in M31

René Walterbos, University of California, Berkeley

Robert Braun, NRAO, Socorro and NFRA, Dwingeloo

Through its proximity, M31 offers us an ideal opportunity to study in detail the basic physical properties of the interstellar medium on a galactic scale, providing us with information that is difficult to obtain in our own Galaxy. We have completed a large radio and optical survey of the interstellar medium and young stars in the NE half of this nearby spiral. The VLA was used to map the 21-cm HI (Braun, 1989a) and the 20-cm radio continuum emission (Braun, 1989b) at high sensitivity and spatial resolution, 5" to 10", corresponding to 17 to 34 pc. The No1 36-inch telescope at Kitt Peak was used to obtain deep CCD-images of the H α and [SII] line emission, and broadband B and R exposures of the stellar associations in the main spiral arms. The line images reach emission measures of a few pc cm⁻⁶ and provide accurate absolute fluxes for about 1000 HII regions, supernova remnants (SNRs), and planetary nebulae (Walterbos and Braun, 1989). Here we will present new results on the SNRs in M31 and discuss the discovery of diffuse ionized gas with high [SII]- to H α intensity ratio in the spiral arms.

We have compiled an initial list of radio/optical SNRs in M31, by searching for radio identifications of emission-line sources with a high [SII]/H α ratio (> 0.60). (The [SII] filter included both sulfur lines and the H α filter did not include [NII]). This search revealed 11 SNRs, of which only two were known. An example of a new detection is shown in Fig. 1. In addition, we detected radio emission from 3 SNRs that were identified in previous optical surveys (D'Odorico *et al.*, 1980), but that were outside our CCD fields. The 14 objects only include the most obvious candidates, but a full search is in progress and we expect to find several more SNRs. Also not all optical SNRs show detectable radio emission and a pure optical list of SNR candidates based only on the ratio of [SII]/H α emission contains many more objects.

Two conclusions are apparent. First, the radio properties of the SNRs in M31 are quite similar to those of Galactic SNRs as can be seen from Fig. 2, where we show a surface brightness-diameter plot. The brightnesses are not systematically lower as has been suggested in the past (Dickel and D'Odorico, 1984). Second, the slope of the relation is close to -2 ; this slope is expected from the *intrinsic* dependence between surface brightness and diameter. Hence, as is shown in the right panel of Fig. 2., the radio luminosity of the SNRs does not seem to depend strongly on diameter, or age, contrary to model predictions (see *e.g.* S. Reynolds, 1988 for a review). Selection effects, however, play an important role in these plots and a complete discussion that includes the upper limits for non-detections will be presented elsewhere (Braun and Walterbos, in prep.).

The CCD images show widespread diffuse ionized gas with a ratio of [SII]/H α that is higher than that of discrete HII regions. This is illustrated in Fig. 3. Discrete HII regions typically show ratios between 0.2–0.3, while the diffuse gas in the arms consistently shows ratios of 0.5. We can trace this gas across the spiral arms to emission measures below 5 pc cm⁻⁶. Its properties seem to be similar to that of the diffuse gas in the solar neighborhood (R. Reynolds, 1988 and references therein). The importance of diffuse ionized gas in the ISM has often been pointed out (*e.g.* Kulkarni and Heiles, 1988), but this is the first time it has so clearly been detected and measured on a global scale in an external galaxy. A point of debate is the origin of the ionization of this gas. The constancy of the ratio of [SII]/H α in the diffuse medium displayed by our data, seems to favor photo ionization over shock ionization, since the ratio depends critically on shock

Fig. 1. One of the new SNRs in M31 that was detected in our survey. The sequence of images (from top left, in clockwise direction) shows the 20-cm radio continuum map, the R-band optical continuum, the [SII] emission-line image and the H α image. The field measures 250 by 250 pc. The SNR is in the center and is blended with a neighboring III region. It stands out as a source of relatively strong [SII] and radio continuum emission.

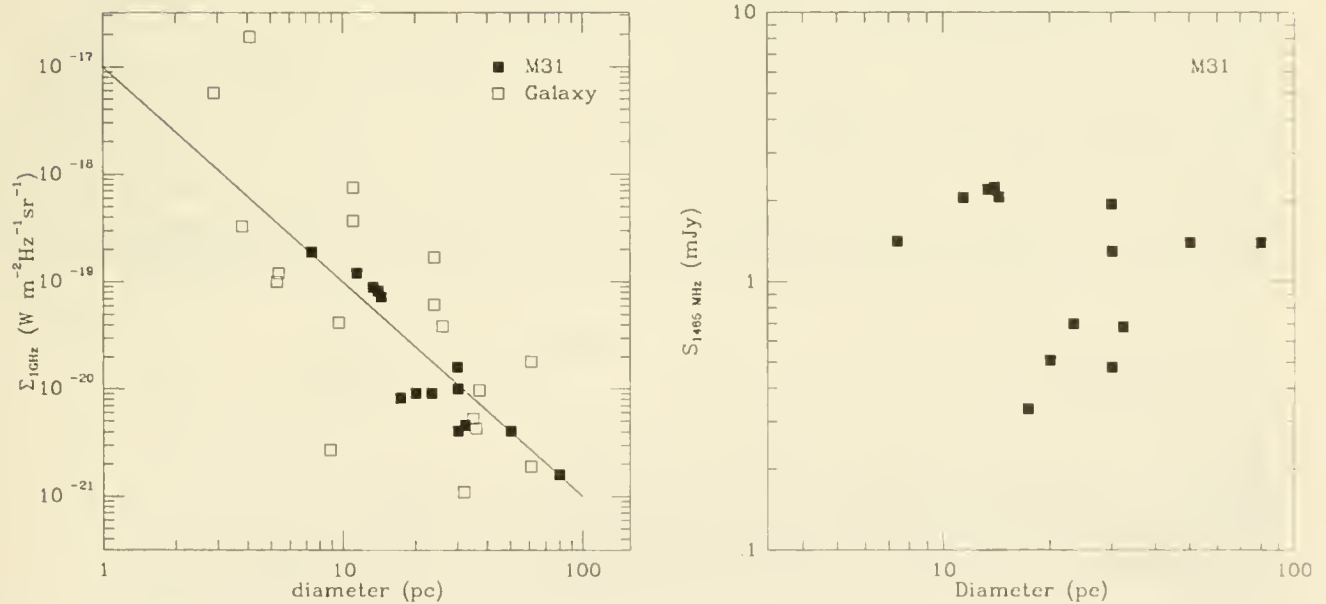
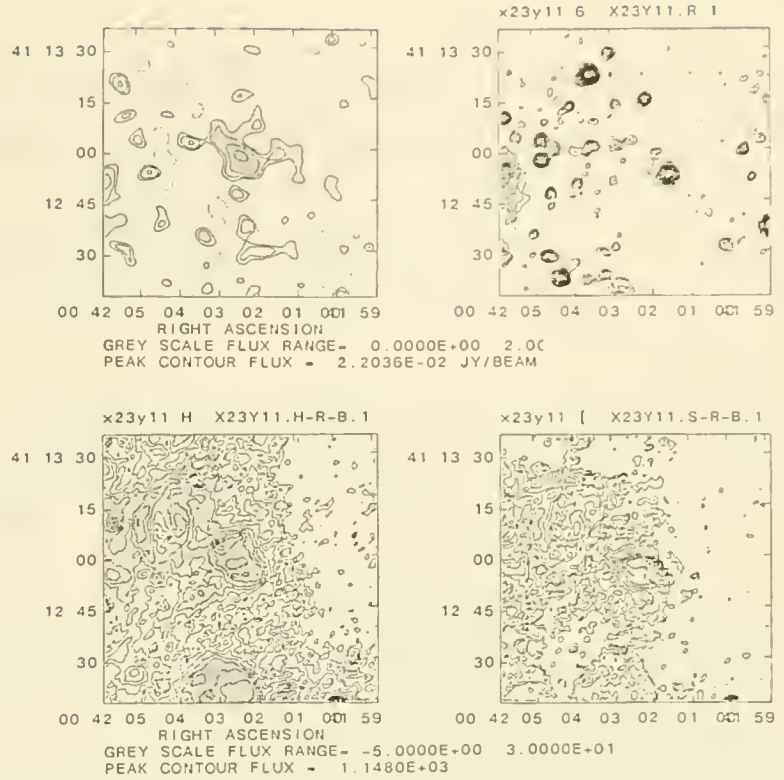


Fig. 2. The left diagram shows the (in)famous Σ -D relation for the new, as yet incomplete, sample of SNRs in M31 and for Galactic SNRs with reliable distances (Green, 1984). Most of the M31 objects are new detections. The radio properties of the M31 SNRs are quite similar to those in our Galaxy. The line is *not* a fit, but a line with slope -2, corresponding to the *intrinsic* dependency between the surface brightness and the diameter. Most of the correlation in this figure is due to the fact that the two quantities are related to each other, as is apparent from the diagram on the right, which plots the flux (which is proportional to luminosity since all remnants are at the same distance) as a function of diameter.

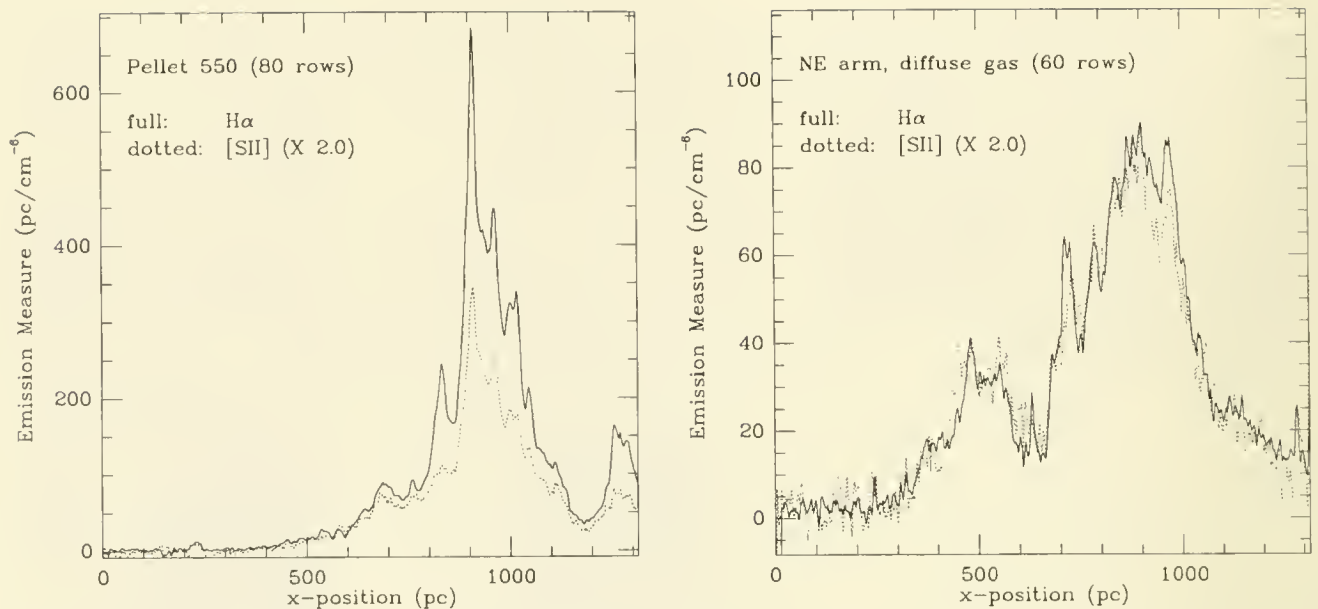


Fig. 3. Cross-cuts in $H\alpha$ and $[SII]$ emission lines through the 10-kpc spiral arm on the NE side of M31. The plots were obtained by averaging the indicated number of rows in the continuum-subtracted CCD images. The $[SII]$ intensities have been multiplied by two. The left diagram includes the large HII region complex Pellet 550, while the right diagram was obtained for a region with mainly diffuse ionized gas. The ratio of $[SII]/H\alpha$ intensities is typically about 0.2–0.3 in discrete HII regions but reaches a constant value of 0.5 in the diffuse medium.

velocities whereas it can be successfully reproduced by photo ionization models (*e.g.* Mathis, 1986). The gas is spatially correlated with the neighboring star forming regions in that it is more widespread around the larger HII complexes. This is to be expected in both shock and photo ionization models. Correlation of the diffuse gas distribution with the distribution of O and B stars, derived from the B and R frames, will establish if the photons responsible for the ionization have leaked out from the HII complexes, or if they come from older stars that have already dispersed the clouds in which they were formed. This study is in progress (Walterbos and Braun, in prep.).

We are currently extending our study of the interstellar medium to a sample of nearby galaxies of different Hubble types.

References

- Braun, R.: 1989a, submitted to *Astrophys. J. Suppl.*
- Braun, R.: 1989b, submitted to *Astrophys. J. Suppl.*
- Dickel, J.R., D'Odorico, S.: 1984, *Mon. Not. R. Astron. Soc.* **206**, 351.
- D'Odorico, S., Dopita, M.A., Benvenuti, P.: 1980, *Astron. Astrophys. Suppl.* **40**, 67.
- Green, D.A.: 1984, *Mon. Not. R. Astron. Soc.* **209**, 449.
- Kulkarni, S.R., Heiles, C.: 1988, in *Galactic and Extragalactic Radio Astronomy*, eds. G.L. Verschuur and K.I. Kellermann, p95.
- Mathis, J.S.: 1986, *Astrophys. J.* **301**, 423.
- Reynolds, R.J.: 1988, *Astrophys. J.* **333**, 341.
- Reynolds, S.P.: 1988, in *Galactic and Extragalactic Radio Astronomy*, eds. G.L. Verschuur and K.I. Kellermann, p439.
- Walterbos, R.A.M., Braun, R.: 1989, *Astrophys. J. Suppl.* . in preparation.

EVOLUTION OF A SUPERBUBBLE BLASTWAVE IN A MAGNETIZED MEDIUM.

Katia M. Ferriere , APAS Dept., University of Colorado
Ellen G. Zweibel , APAS Dept., University of Colorado
Mordecai-Mark MacLow , NASA Ames Research Center

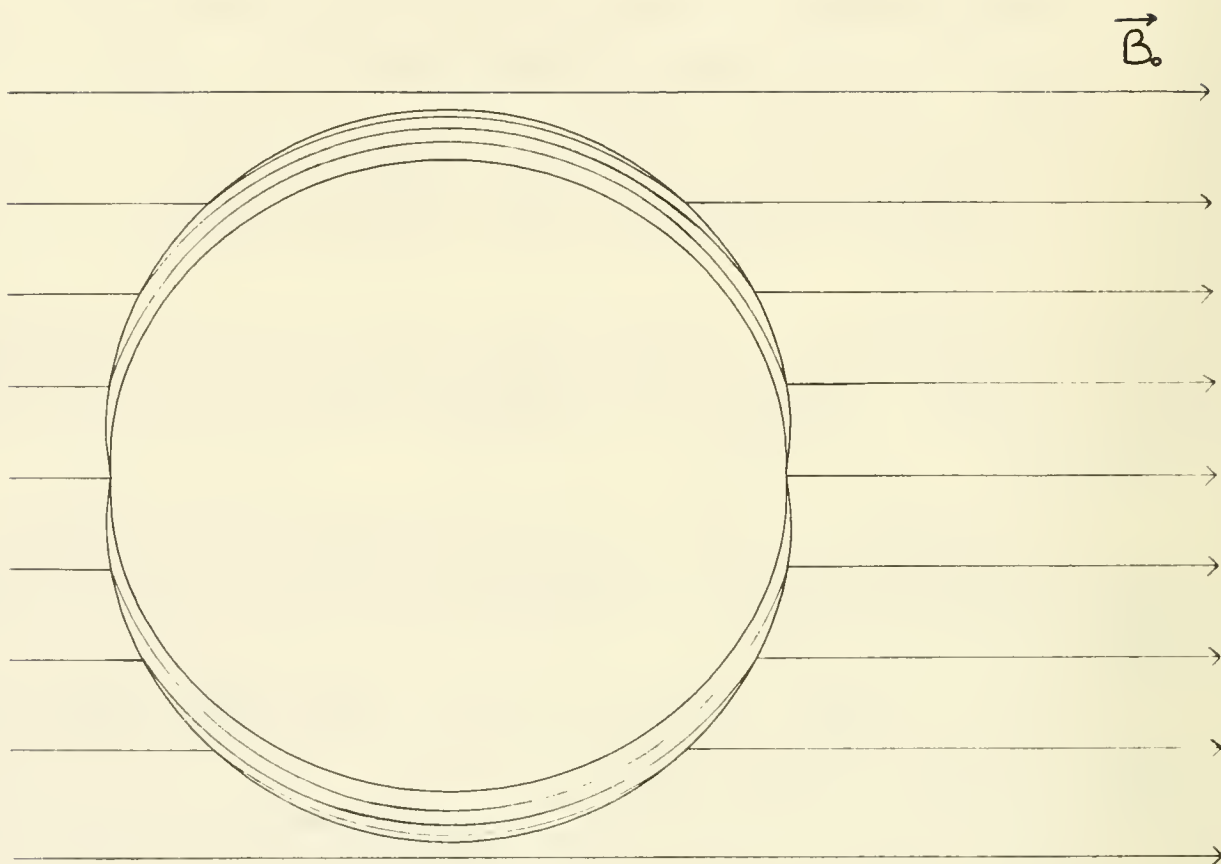
We investigate the effects of interstellar magnetic fields on the evolution and structure of interstellar “superbubbles”, using both analytic and numerical MHD calculations. These cavities of hot gas, surrounded by shells of cold dense material preceded by a shock wave result from the combined action of stellar winds and supernova explosions in OB associations.

If the medium in which a superbubble goes off is homogeneous and unmagnetized, the blast wave expands isotropically. As the interstellar gas flows through the shock, it cools significantly and gets strongly compressed such that thermal pressure remains approximately equal to ram pressure. Hence, the swept up material is confined to a very thin shell.

However, if the ambient medium is permeated by a uniform magnetic field $B_0 \sim 3\mu G$ (typical value for the ISM), the configuration loses its spherical symmetry, and, due to magnetic pressure, the shell of swept up material does not remain thin. We find the following qualitative differences:

1. Except in the immediate vicinity of the magnetic poles, the shell is supported by magnetic pressure. Its thickness, which is now determined by flux conservation, increases continuously from the poles to the equator.
2. The refraction of field lines at the shock and the thermal pressure gradient along the shell both contribute to accelerating the gas toward the equator. The resulting mass flux considerably decreases the column density at the magnetic poles.
3. Away from the poles, magnetic tension in the shell causes the field lines (particularly the inner boundary) to elongate in the direction of \vec{B}_0 . In contrast, the shock wave radius increases with increasing θ , as would be the case if the wave were linear. At late times, however, the shock surface tends to flatten near the equator.
4. The reduced inertia of a parcel in the polar neighborhood makes it easier to decelerate, and accounts for the dimple which appears at the poles in numerical simulations. This dimple also results from the necessity to call on intermediate shocks in order to insure a smooth transition between a purely thermal shock at the poles and a magnetic shock in the rest of the shell.
5. The shock wave propagates faster than in the absence of magnetic field, except near the poles where the reduced mass of the shell allows it to be more efficiently decelerated. The shell inner boundary travels slower in a magnetized medium, regardless of the value of θ .

Acknowledgment: This research was supported by the NASA Astrophysical Theory Program, NAGW-766, at the University of Colorado.



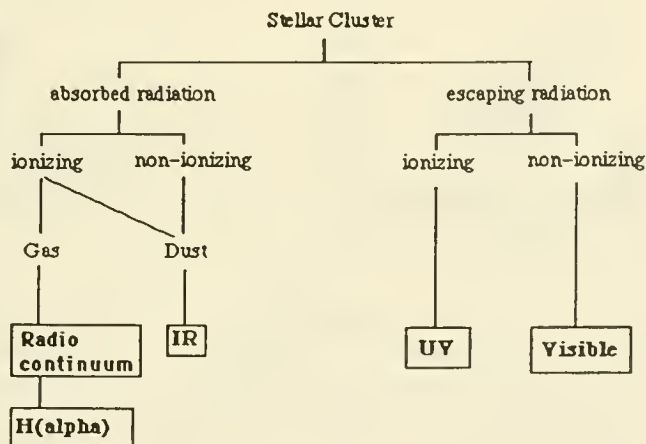
Shape of a superbubble in a medium with $n_0 = 0.324 \text{ cm}^{-3}$, $T_0 = 8000 \text{ K}$, $B_0 = 3 \mu\text{G}$, at $t = 3 \times 10^6 \text{ yr}$.

Infrared Analysis of LMC Superbubbles

Fran Verter and Eli Dwek
NASA Goddard Space Flight Center

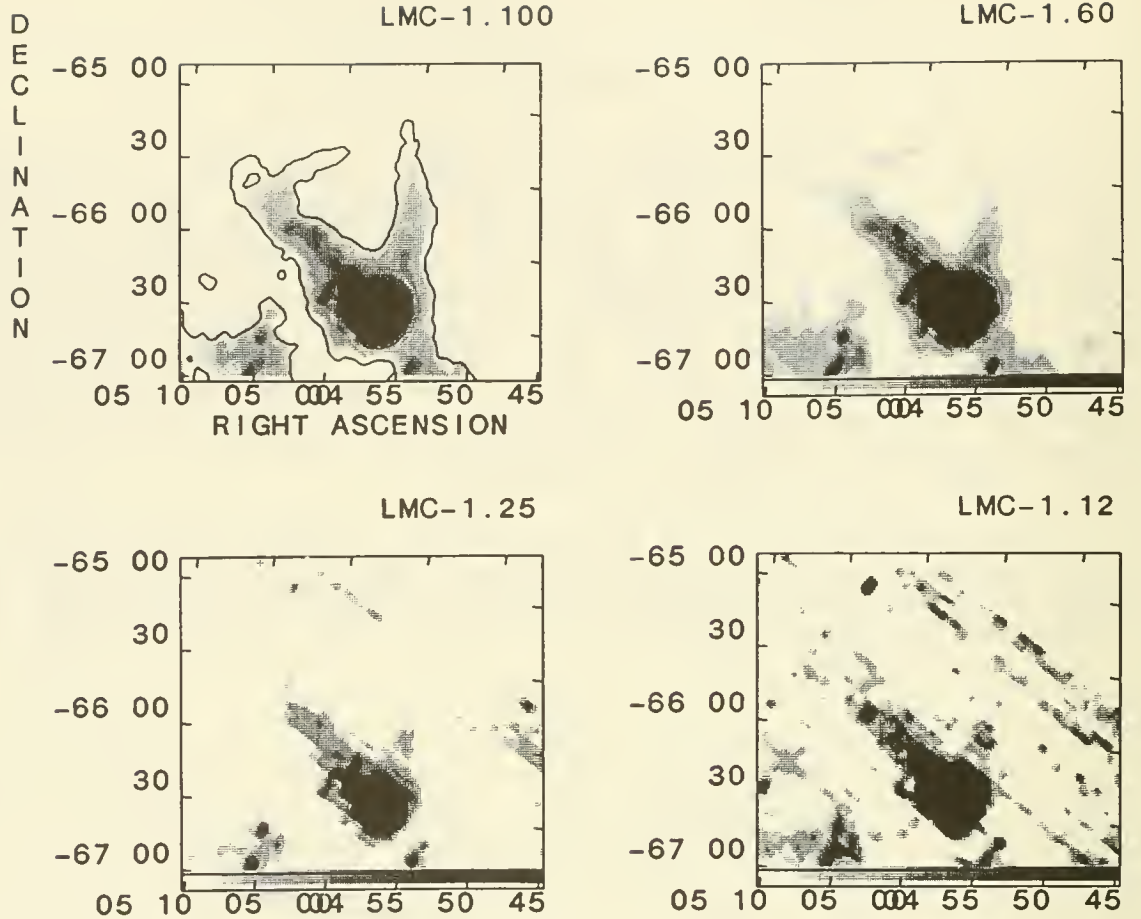
We are analyzing three superbubbles in the LMC, those cataloged by Meaburn (1980) as LMC-1, LMC-4 (a.k.a. Shapley Constellation III), and LMC-5. Superbubbles are the largest infrared sources in the disks of external galaxies. Their expansion requires multiple supernovae from successive generations of star formation. In LMC superbubbles, the grains swept up by shocks and winds represent an ISM whose abundances are quite different from the Galaxy. By applying the Dwek (1986) grain model, we can derive the composition and size spectrum of the grains. The inputs to this model are the dust emission in the four IRAS bands and the interstellar radiation field (ISRF) that provides the heating.

The first step in our project is to derive the ISRF for star-forming regions on the periphery of superbubbles. We are doing this by combining observations at several wavelengths to determine the energy budget of the region (see the flowchart).



We will use a UV image to trace the ionizing stellar radiation that escapes (Smith, Cornett, and Hill 1987), an $H\alpha$ image to trace the ionizing stellar radiation that is absorbed by gas (Kennicutt and Hodge 1986), and the four IRAS images to trace the stellar radiation, both ionizing and non-ionizing, that is absorbed by dust. This multi-wavelength approach has the advantages that we do not have to assume the shape of the IMF or the extinction of the source.

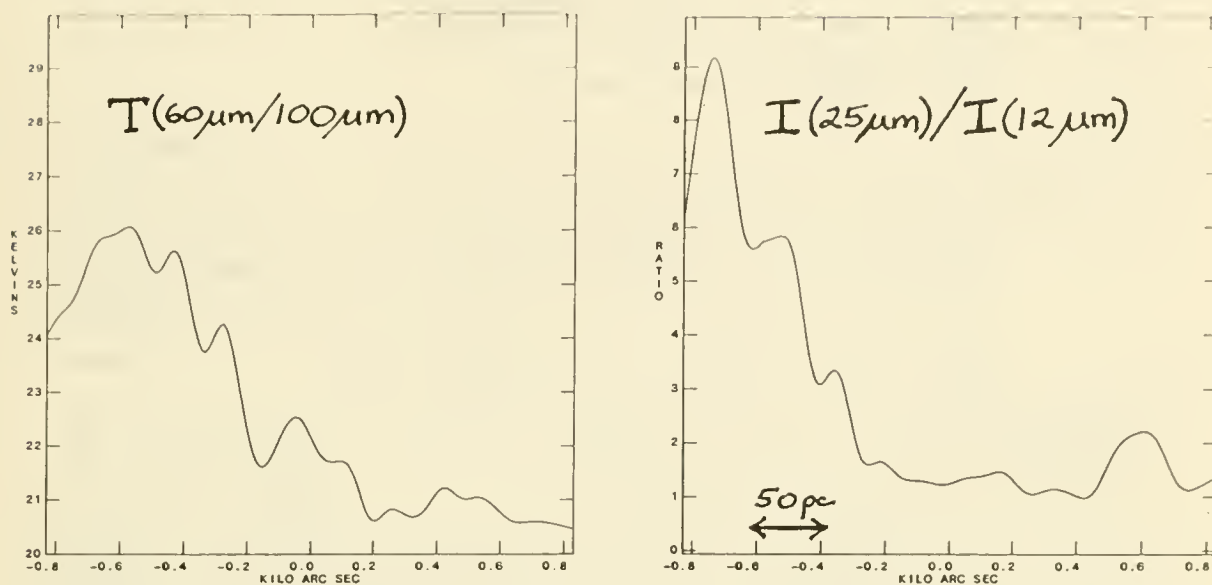
We have only just begun this project, so for now we present some preliminary results on the superbubble LMC-1. IRAS coadds, shown below, provide a resolution of 1' or 15 pc. This bubble has a roughly triangular shell of diffuse emission, with one strong infrared peak associated with the HII region DEM 34 (Davies Elliott, and Meaburn 1980).



The diffuse emission of LMC-1 is not detectable at 12 and 25 μ m. We modeled the grain content of the northernmost leg of the diffuse shell by assuming the ISRF of the local Galaxy, and taking into account the known differences in the LMC grain abundances: The dust/gas ratio is 4 times lower than in the Galaxy (Koornneef 1982), and the graphite/silicate ratio is 3 times lower than in the Galaxy (Nandy 1984). In order to fit the observed spectrum, the grain size distribution must be cut off below 30 to 100 \AA . By comparison, Galactic clouds are usually modeled with grain distributions containing graphite particles down to 3 \AA size (Verter 1989).

From our grain model and the LMC dust/gas ratio, we find that the total mass of the cloud corresponding to this leg of the diffuse emission is $1.6 \times 10^6 M_{\odot}$. This cloud was mapped in CO emission by Cohen et al. (1987). The standard Galactic conversion from CO emission to molecular hydrogen mass would have calculated the cloud mass to be 2.0×10^5 , an order of magnitude underestimate.

The peak emission of LMC-1 at DEM 34 shows clear evidence for destruction of very small grains. This is best seen in plots of the flux ratios $I(60\mu\text{m})/I(100\mu\text{m})$ and $I(25\mu\text{m})/I(12\mu\text{m})$ along a slice through the peak.



The increase in $I(60\mu\text{m})/I(100\mu\text{m})$ towards the luminosity peak indicates that the big ($> 200 \text{ \AA}$) grains are hotter in the vicinity of DEM 34. The contribution to $I(25\mu\text{m})/I(12\mu\text{m})$ from stochastically heated very small ($< 200 \text{ \AA}$) grains is near unity for all small grain temperatures. Thus the increase in this ratio is driven by increasing contributions to $I(25\mu\text{m})$ from big grains. But the temperature of the big grains in this vicinity, derived from $I(60\mu\text{m})/I(100\mu\text{m})$, is at most 30 K. Under such heating, $I(25\mu\text{m})/I(12\mu\text{m})$ should be only 1.1 (see Figure 4 of Boulanger et al. 1988). The factor of 9 increase in $I(25\mu\text{m})/I(12\mu\text{m})$ that is seen implies that the big grains are dominating the ratio because the very small grains are being destroyed in the vicinity of DEM 34.

- Boulanger, F., Beichman, C., Desert, F. X., Helou, G., Perault, M., and Ryter, C. 1988, Ap.J., 332, 328
 Cohen, R. S., Dame, T. M., Garay, G., Montani, J., Rubio, M., and Thaddeus, P. 1988, Ap.J. Lett., 331, L95
 Davies, R. D., Elliott, K. H., and Meaburn, J. 1980, M.N.R.A.S., 81, 89
 Dwek, E. 1986, Ap.J. 302, 363
 Kennicutt, R. C., Jr., and Hodge, P. W. 1986, Ap.J., 306, 130
 Koornneef, J. 1982, Astron. Ap., 107, 247
 Meaburn, J. 1980, M.N.R.A.S., 192, 365
 Nandy, K. 1984, in "Structure and Evolution of the Magellanic Clouds", proc. IAU Symp. 108, ed. K. de Boer and S. van den Bergh, p.341
 Smith, A. M., Cornett, R. H., and Hill, R. S. 1987, Ap.J., 320, 609

MAGNETIC COLLIMATION OF PROTOSTELLAR WINDS INTO BIPOLAR OUTFLOWS

Michael L. Norman and James M. Stone
National Center for Supercomputing Applications
and Department of Astronomy
University of Illinois, Urbana-Champaign
Urbana, IL 61801

Abstract: We describe self-consistent 2-D MHD simulations of the collimation of an isotropic protostellar wind into bipolar outflows by magnetic stresses in the ambient medium. A variety of ambient field strengths, wind luminosities, and density profiles have been studied. Collimation occurs when the energy of the magnetic field swept up by the expanding bubble approaches the bubble thermal energy. Measured axial and radial expansion rates are in good agreement with the analytical predictions of Königl (1982).

Introduction: Energetic mass ejection, frequently in the form of bipolar outflows, is now a well-established characteristic of low-to-intermediate mass star formation in our Galaxy (Lada 1985). The collimating mechanism for these outflows is uncertain, however, as is the physical relationship between the high-velocity molecular lobes, ionized jets, Herbig-Haro objects, water masers, etc. One possibility suggested by Königl (1982) which we explore here is that an isotropic protostellar wind may be collimated into bipolar outflows by a strong magnetic field which threads the ambient molecular cloud. This mechanism is attractive due to the good correlation between observed molecular outflow axes and magnetic axes inferred from optical polarization measurements of background stars (e.g., Vrba, Strom and Strom 1976).

Simulations: Here we solve the time-dependent equations of ideal MHD in axisymmetric, cylindrical (RZ) geometry for an unmagnetized, isotropic wind inflating a cavity within a magnetized external medium. In this preliminary study, radiative cooling is not included, hence both media are assumed adiabatic with $\gamma=5/3$. The ambient magnetic field is taken to be uniform with strength B_0 parallel to the Z axis. The ambient gas is isothermal with sound speed C_0 and plane-stratified according to $\rho(Z)=\rho_0/[1+(Z/a)^2]^{m/2}$, $0 \leq m \leq 2$, where a is the core radius. The stellar wind is modeled by continuously adding mass into a small spherical source region with internal energy $\epsilon_w=C_0^2/\eta$, with $\eta=.01$ and at a rate such that the desired mechanical luminosity is produced. The initial source region excludes magnetic flux. Because of the adiabatic assumption, the simulations are parameterized by two dimensionless ratios involving the ambient conditions and the source radius r_0 : $\beta=(\rho_0 C_0^2/\gamma)/(B_0^2/8\pi)$ -- the plasma parameter, and $L=\dot{m}_w \epsilon_w/(4\pi \rho_0 V_{ms}^3 r_0^2)$, where $V_{ms}=(C_0^2+B_0^2/4\pi\rho_0)^{1/2}$ is the magnetosonic speed.

The simulations were performed using the ZEUS-2D code developed by the authors, which incorporates the hydrodynamic algorithms described in Norman and Winkler (1986) as well as the CT method of Evans and Hawley (1988) for magnetic field evolution. ZEUS-2D is a time-explicit, Eulerian ideal MHD code which has been tested against a battery of problems including the 1-D magnetic Riemann problem of Brio and Wu (1988), a 1-D Weber-Davis (1967) wind solution, and the 2-D solar transient solution of Low (1984). Typically, a grid of 256x128 zones were used in these calculations.

Results: The effects of varying field strength and wind luminosity on collimation in a constant density medium ($m=0$) were investigated in a series of runs having parameters $(\beta, L)=(0.2, 1), (1, 1), (5, 1), (1, 0.1), (1, 10)$. Magnetic collimation occurs in each case, producing a smooth-surfaced bubble elongated in the direction of the magnetic field with eccentricity increasing in time at a rate determined by β and L . Fig. 1 shows a case with parameters representative of observed bipolar outflows. The early expansion of the bubble is quasi-spherical and drives a shock wave into the surrounding gas. The shock propagates faster perpendicular to the magnetic field lines than along them because $V_{ms} > C_0$ and soon becomes highly oblate. At later times, the shock is quasi-planar and advances parallel to the field lines with the tip of the bubble. Behind the shock, a dense cap of material is accumulated near the bubble apex. The wind density distribution inside the bubble is smooth, however the velocity field contains eddies.

The bubble eccentricity is found to increase linearly in time, in agreement with the analytical predictions of Königl (1982; cf. Appendix). Fig. 2 shows this result for three values of β . The linear behavior is due to the fact that at late times, the bubble elongates at a constant rate while maintaining a constant equatorial radius. This result is only true in uniform density ($m=0$) clouds; for $m>0$, both the equatorial and axial radii obey separate expansion laws (Königl 1982):

$$Z_0(t) \propto t^{2/(2-m)}; \quad R_0(t) \propto t^{-m/(4-m)}; \quad (0 \leq m < 2).$$

We have confirmed these relations numerically for $m=1$, and have also computed the case $m=2$. In both cases, the bubble tip accelerates whereas the equatorial radius eventually decreases (cf. Fig. 3). Despite the reduced pressure at large Z , the bubble does not flare and "blow out" owing to the strong lateral magnetic confinement.

Future prospects: We have demonstrated that an ambient magnetic field is capable of collimating an isotropic protostellar wind into an elongated bubble resembling bipolar outflows. Future work will consider radiative cooling in the wind and cloud regions, and different magnetic field geometries. However, using the simplified assumptions of the present model, we are already able to obtain collimation ratios $R_{coll}=Z_0/R_0$ well within the observed range of 2-4 for majority of highly-collimated flows (Lada 1985).

Acknowledgements: These simulations were performed using the CRAY X-MP system of the National Center for Supercomputing Applications, University of Illinois, Urbana-Champaign. We gratefully acknowledge John Hawley for his assistance with testing the MHD algorithm.

References:

- Brio, M. and Wu, C. 1988, *J. Comp. Phys.* **75**, 400.
- Evans, C. and Hawley, J. 1988, *Ap. J.*, **332**, 659.
- Lada, C.J. 1985. *Ann. Rev. Astron. Astrophys.* **23**, 267.
- Low, B.C. 1984, *Ap. J.*, **281**, 392.
- Königl, A. 1982, *Ap. J.* **261**, 115.
- Norman, M.L. and Winkler, K.-H.A. 1986, in *Astrophysical Radiation Hydrodynamics*, eds. K.-H. Winkler & M.L. Norman, (Reidel: Dordrecht), 187.
- Vrba F.J., Strom, S.E., and Strom, K.M. 1976, *A. J.* **81**, 958.
- Weber, E. and Davis, L. 1967, *Ap. J.* **148**, 217.

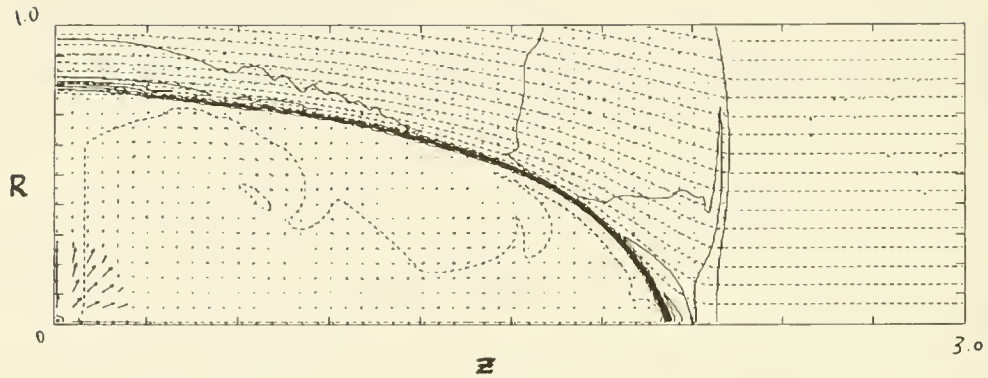
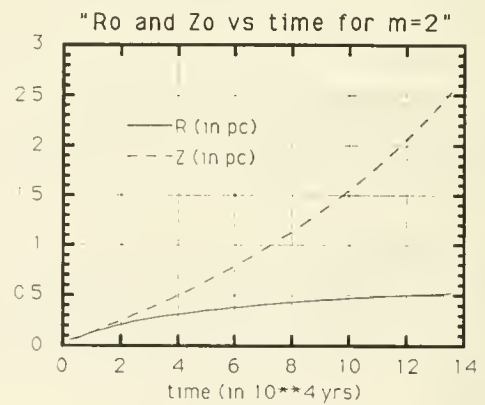
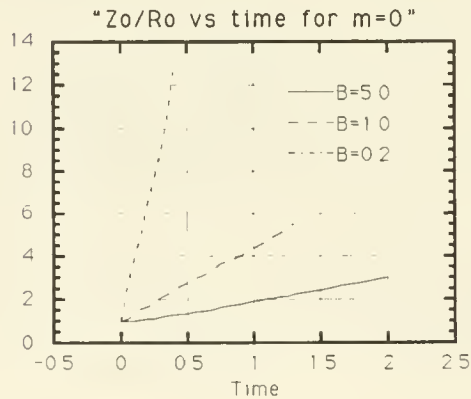


Fig. 1 - Magnetic collimation of a protostellar wind creates an elongated bubble in the direction of the ambient magnetic field. Density contours (solid lines) are superposed on the displaced magnetic field lines (dashed lines) and velocity vectors, and show the near planar MHD shock being driven by the advancing bubble apex. The parameters are $\beta=1$, $L=10$.



Figs. 2 - Ratio of axial to equatorial radius versus time for $L=1$ varying β in constant density ($m=0$) atmosphere.

Fig. 3 - Axial and equatorial radius versus time for $m=2$ atmosphere for $L=1$, $\beta=0.2$

MHD Shocks in the ISM

D. F. Chernoff
Cornell University, Ithaca NY 14853, USA

D. J. Hollenbach
NASA Ames Research Center, Moffett Field, CA 94035, USA

C. F. McKee
University of California, Berkeley CA 94720, USA

We survey shock solutions of a partially ionized gas with a magnetic field. The gas is modeled by interacting neutral, ion, electron and charged grain components. We employ a small neutral-ion chemical network to follow the dissociation and ionization of the major species. Cooling by molecular hydrogen (rotational, vibrational and dissociation), grains and dipole molecules is included. There are three basic types of solutions (C, C*, and J) and some more complicated flows involving combinations of the basic types. The initial preshock conditions cover hydrogen nuclei densities of $1 < n < 10^{10} \text{ cm}^{-3}$ and shock velocities of $5 < v_s < 60 \text{ km/s}$. The magnetic field is varied over 5 decades and the sensitivity of the results to grain parameters, UV and cosmic ray fluxes is ascertained.

The parameter space is quite complicated, but there exist some simple divisions. When the initial ionization fraction is small ($x_i < 10^{-5}$), there is a sharp transition between fully C solutions at low velocity and strong J solutions at high velocity. When the initial ionization fraction is larger, C* and/or *very weak* J shocks are present at low velocities in addition to the C solutions. The flow again changes to strong J shocks at high velocities. When the ionization fraction is large and the flow is only slightly greater than the bulk Alfvén velocity, there is a complicated mixture of C, C* and J solutions.

1 INTRODUCTION

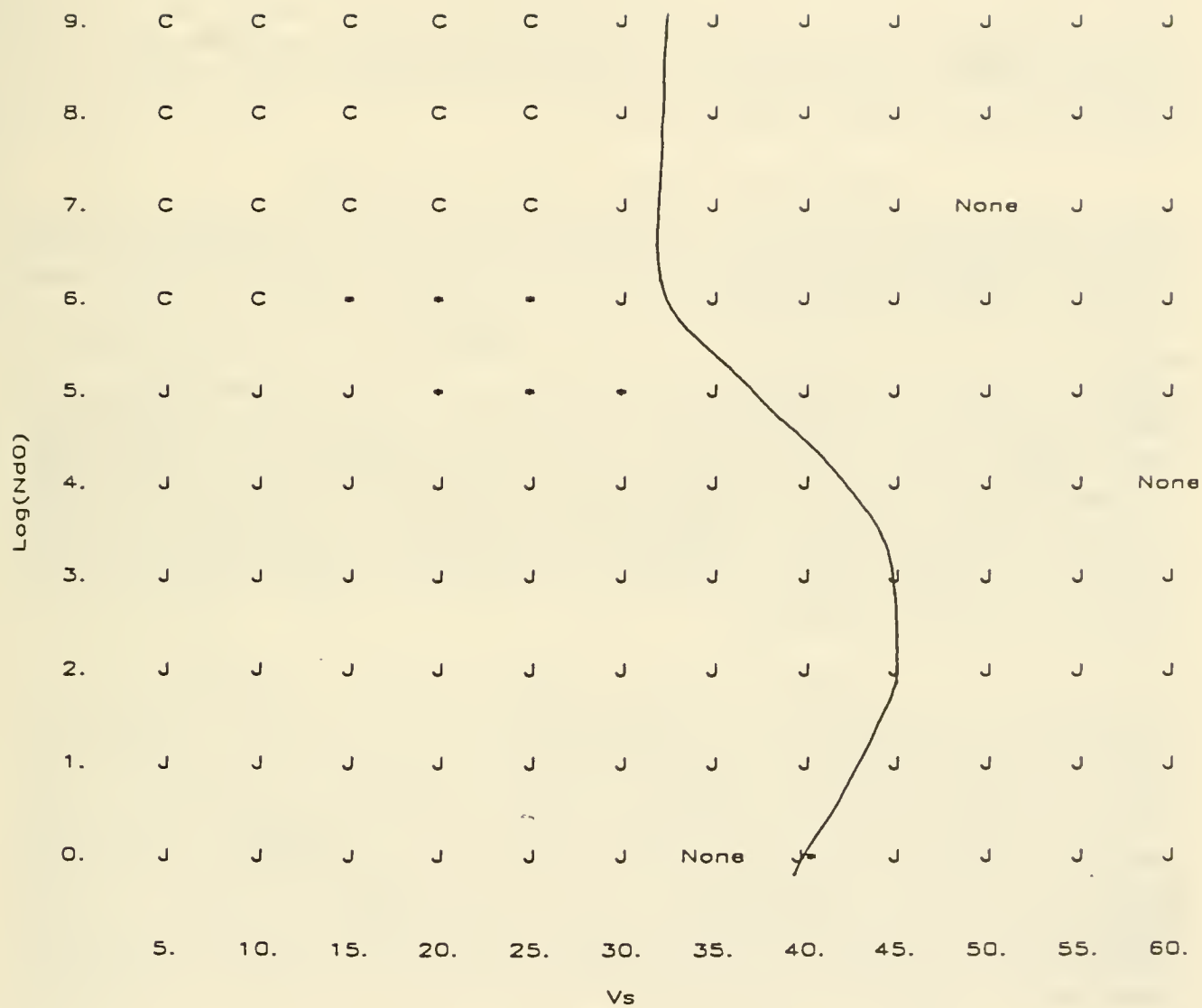
In the interstellar medium, shocked, partially ionized gas behaves as weakly coupled neutral and charged fluids (Mullan 1971, Draine 1980, Draine and Roberge 1982, Chernoff, Hollenbach and McKee 1982, Chernoff 1987, Chernoff and McKee 1988, Chernoff, Hollenbach and McKee 1989). Previously, detailed MHD calculations have been limited to a particular class of solutions (the “C” type, Chernoff, Hollenbach and McKee 1982, Draine and Roberge 1982) or have focused on a few illustrative special cases (Draine 1980). Here we report a survey of MHD multifluid models of interstellar shocks and sketch an overall picture of the gas’ behavior, sacrificing the detail necessary to produce accurate line ratios and line

intensities. Elsewhere, we focus on more accurate and detailed calculation of specific cases.

The general categorization of shock solution was discussed by Chernoff (1987). For simple cooling and ionization laws, there exist three basic sorts of solutions: C, C* and J. C solutions are completely continuous and the neutral gas is everywhere supersonic. J solutions have regions of subsonic neutral flow *with a viscous subshock*. The location of the subshock and its strength is determined by the condition that the flow be able to pass through a downstream critical point. C* solutions are completely continuous but the neutral gas heats up sufficiently (by ion-neutral friction) to become subsonic without a subshock. Solutions tend to be C when the ratio of radiative cooling to collisional heating is large and/or when the Alfvén Mach number of the neutral flow is low. Apparently, there is no guarantee that only a single time-independent solution exists for given preshock conditions. The present study includes some examples of multiple solutions and also of solutions more complicated than the three basic types. One of the virtues of the solution technique introduced by Chernoff (1987) is that all possible solutions may be found.

For the models discussed in this paper we assume that the ionization fraction is determined by balancing ionization (electron, ion and neutral collisional ionization rates plus cosmic ray rates) and recombination processes (atomic and molecular rates) at each point in the flow. We integrate the chemistry and follow the molecular versus atomic hydrogen composition of the gas. We have used realistic cooling functions for molecular hydrogen describing the rotational, vibrational (Hollenbach and McKee 1979) and dissociation processes (Hollenbach and McKee 1988). The neutral heating by ion collisions and drifting grains (using Draine's steady state solution for the grain motion, 1980) includes the most important heating effects. In addition, the temperatures of the ion and electron components are calculated using all the most important heating and cooling processes (collisional heating by the neutrals, radiative cooling by excitation of atomic and molecular transitions in the neutrals and heating by collisionless plasma instability).

Illustrative and *tentative* results are presented in the accompanying table (additional ones are included with the poster). The initial condition are the preshock hydrogen nuclei density (abscissa) and shock velocity (ordinate). The gas is completely molecular upstream. The magnetic field is given as $B = 10^{-6} n^{1/2} b$ G, for $b = 0.1$. (Other values of b are shown with the poster). The external ionization rate is $\zeta = 10^{-15}$ per nuclei per sec. A generic dipole coolant with abundance $x_d = 10^{-4}$ is present. The grains are 1% by mass, with density $\rho_{gr} = 2.5$ gm/cm³ and radius $a_{gr} = 10^{-5}$ cm. The solutions are labeled C, * (meaning C*) and J. 'None' means the algorithm failed to converge, but is not otherwise meaningful. The temperature contour of $T = 30000$ K is illustrated. To the right of that contour all solutions are strong J shocks. To the left, solutions are either C, C* or very weak J shocks. Detailed distinctions between solutions at low velocity (Alfvén Mach numbers of a few) are not represented because the 5 km/s intervals are not sufficiently fine to resolve such variations. Significant dissociation occurs to the right of the temperature contour and the viscous subshocks have compression ratios of close to 4.



What Sort of Standard Candle is Orion for Studying Molecular Hydrogen Line Emission in Galaxies?

Michael Burton^{1,2}, Phil Puxley³

¹ NASA Ames Research Center, ² University of California, Irvine

³ Institute for Astronomy, University of Hawaii

Abstract

The total shocked and fluorescent molecular hydrogen 1–0 S(1) line luminosities from Orion have been measured to be $\sim 2.5 L_{\odot}$ and $\sim 2.0 L_{\odot}$, respectively. The implications for using Orion to study the interstellar medium in galaxies is discussed.

Introduction : Orion as a Standard Candle

The star-forming complexes in galaxies are often likened to a conglomeration of Orion-like regions (perhaps 10^5 in a classical starburst). This comparison is invoked across much of the electromagnetic spectrum and, of relevance here, to H₂ near-IR line emission. There are, of course, several important questions which should first be asked : is Orion typical of H₂ line emitting sources in our galaxy, or is it in some special type of evolutionary phase? Do Orion-type regions dominate the H₂ line emission from galaxies, or do particularly exotic star-forming complexes such as DR 21 (Garden *et al.* 1986, 1989) or supernova remnants such as IC 443 (Burton *et al.* 1988, Burton 1988) or RCW 103 (Moorwood *et al.* 1988) dominate the global emission? Even if we assume that Orion-type regions are typical, how well do we understand its H₂ line emission? It is the purpose of this paper to discuss this last point. Estimates will be presented of the global H₂ line emission from Orion, with the contributions from shocks and fluorescence. The intention is to provide a calibration for the Orion standard candle, so that it may be better used to make comparisons with the line emission from galaxies.

H₂ line emission was first detected from Orion by Gautier *et al.* (1976), and mapped by Beckwith *et al.* (1978); the total luminosity in the 1–0 S(1) line, at $2.12 \mu\text{m}$, was measured to be $2.5 L_{\odot}$, not correcting for extinction. On the basis of vibrational line ratios, and also the evidence for high-velocity motions and broad line widths in the source (*e.g.*, Nadeau & Geballe 1979), it was concluded that the emission was shock-excited. There is a molecular hydrogen reflection nebula around the shocked region (Hough *et al.* 1986), resulting from the scattering of line radiation arising near the peak of the shocked region, and extending at least $80''$ from the peak. UV-radiation from the Trapezium star cluster has created a photodissociation region (*e.g.*, Tielens & Hollenbach 1985) lying on the front surface of the shocked region, and excites H₂ molecules by fluorescence (*e.g.*, Hayashi *et al.* 1985, Burton *et al.* 1989). Some of the fluorescent line emission may have the appearance of shocks since the gas density is high ($\geq 10^5 \text{ cm}^{-3}$) in much of the region, and collisional redistribution of radiatively-excited levels of the H₂ molecule can produce a thermal distribution for low-lying vibrational levels (*e.g.*, Burton, Hollenbach & Tielens 1989).

The H₂ line emission from external galaxies has been compared with that from Orion (*e.g.*, Fischer *et al.* 1983, Joseph *et al.* 1984, Kawara *et al.* 1987, Fischer *et al.* 1987). On the assumption that the Orion emission is shocked, and in the absence of measurements of additional transitions, the similarity of the observed $L_{\text{H}_2} / L_{\text{IR}}$ ratios is often invoked to associate the extragalactic 1–0 S(1) emission with shocks powered by vigorous star formation activity. The recent multi-transition study by Puxley *et al.* (1988, 1989), and their consequent suggestion that much of the extragalactic H₂ emission is fluorescent, casts doubt on this picture, though the low spectral resolution of

their data complicates the extraction of accurate line fluxes.

Observations and Analysis

The data upon which this analysis is based has been presented by Garden (1986). A map of the H_2 1-0 S(1) line, at $2.12\ \mu\text{m}$, in Orion was made with the UKIRT in January 1985 and obtained by frequency-switching a Fabry-Perot etalon (FP) with $\sim 130\ \text{km s}^{-1}$ resolution. The aperture size was $19''$ and the map made by raster scanning the telescope on a $15''$ spacing grid. An area of $\sim 7' \times 9'$, and containing ~ 1000 pixels centred on the Trapezium star cluster, was covered and is shown in Figure 1. Figure 2 is an enlargement of the shocked region around OMC-1. The outermost contour (labelled 1 unit) corresponds to the 1σ detection limit, which is $7 \times 10^{-21}\ \text{W cm}^{-2}$ per beam.

The total 1-0 S(1) line luminosity in the region mapped is $\sim 4.5\ L_\odot$. There are two basic components contributing to this luminosity; (a) a shocked component from the BN-KL region powered by an outflow from the source IRc2, and (b) a more extended, diffuse component from the Orion photodissociation region, powered by UV from the Trapezium star cluster. We now estimate the luminosity of each component.

From inspection of Figure 1, it can be seen that the level of the diffuse fluorescent component is about 8 units on the map, with a likely range from 6-10 units. If we subtract this background level from the shocked component (taken to cover a $3' \times 3'$ region centred on BN – see Fig. 2)), we obtain for the shocked 1-0 S(1) line luminosity (including emission from the molecular hydrogen reflection nebula) $2.5\ L_\odot$ ($2.3 - 2.6\ L_\odot$; the range reflecting the range in uncertainty in the level of the background). The extinction at $2.1\ \mu\text{m}$ to the shocked region is somewhat uncertain, but probably $\sim 1\ \text{mag}$. (Brand *et al.* 1988). The fraction of the total shocked H_2 line emission emitted through the 1-0 S(1) line is $\sim 1/15$ (Burton *et al.* 1988). Thus the total shocked H_2 line luminosity is estimated to be $94\ [88 - 99]\ L_\odot$.

The remaining S(1) line emission is fluorescently-excited. We estimate its luminosity to be $2.0\ [1.9 - 2.2]\ L_\odot$. This is a lower limit, but any additional contribution will likely be small; if we assumed a flux equal to the lowest contour on the map was emitted from a region extending 1 arcmin further in all directions, then the extra contribution will be about 10%. In a pure fluorescent source, the 1-0 S(1) line contributes $\sim 1.8\%$ of the total H_2 line emission (Black & van Dishoeck 1987). Thus, adopting one magnitude of extinction as before (although the extinction will likely be less since it lies in front of the shocked region), we estimate that the total fluorescent H_2 line luminosity of Orion is $\sim 290\ [270 - 310]\ L_\odot$. This is greater than the total shocked emission from the source.

This fluorescent luminosity can be compared to models for the Orion photodissociation region (*e.g.*, Tielens & Hollenbach 1985). The total luminosity of the ionizing stars in the HII region is $\sim 10^5\ L_\odot$. Thus the efficiency, $L_{\text{S(1)}} / L_{\text{Tot}}$, is $\sim 2 \times 10^{-5} \times 4\pi/\Omega$, where Ω is the solid angle subtended by the molecular cloud from the ionizing stars. For an UV-radiation field 10^5 times the ambient interstellar value (appropriate to the Orion PDR) and a gas density of $10^6\ \text{cm}^{-3}$, this efficiency is calculated to be $\sim 4 \times 10^{-5}$ (Burton, Hollenbach & Tielens, 1989), while for a density $10^5\ \text{cm}^{-3}$, the efficiency is $\sim 3 \times 10^{-6}$. Thus the fluorescent S(1) line luminosity is consistent with model predictions for high density photodissociation regions.

Conclusions

The H_2 1-0 S(1) line luminosity from the shocked and fluorescent emitting regions of Orion have been estimated to be 2.5 and 2.0 L_\odot , respectively. Thus, although the peak line flux from the shock is 100 times the diffuse component, the integrated fluorescent emission is comparable to the shocked component. The total fluorescent emission through all lines is estimated to be $\sim 300 L_\odot$, roughly three times the total shocked emission. Therefore when using Orion as a standard candle to study the ISM of galaxies, it is important to consider both the fluorescent and the shocked contributions to the emission.

References

- Beckwith et al. 1978, *Ap. J.*, **223**, 464.
 Brand et al. 1988, *Ap. J. (Letters)*, **334**, L103.
 Burton, 1988, *IAU Coll. 101 SNRs & ISM*, p399.
 Burton, Hollenbach & Tielens, 1989, *22nd ESLAB Symp.* (ESA SP-290) in press, & *Ap. J.*, to be submitted.
 Fischer et al. 1983, *Ap. J. (Letters)*, **273**, L27.
 Garden et al. 1986, *M.N.R.A.S.*, **220**, 203.
 Garden et al. 1989 *Ap. J. Suppl.*, in press.
 Hayashi et al. 1985, *M.N.R.A.S.*, **215**, 311.
 Joseph, Wright & Wade, 1984, *Nature*, **311**, 132
 Moorwood et al. 1988, *IAU Coll. 101 SNRs & ISM*, p391.
 Puxley et al. 1988, *M.N.R.A.S.*, **234**, 29P.
 Puxley et al. 1989, *22nd ESLAB Symp.* (ESA SP-290) in press, & *Ap. J.*, to be submitted.
 Black & van Dishesoeck, 1987, *Ap. J.*, **322**, 412.
 Burton et al. 1988, *M.N.R.A.S.*, **231**, 617.
 Burton et al. 1989, *Ap. J.*, submitted.
 Fischer et al. 1987, *Ap. J.*, **320**, 667.
 Garden, 1986, PhD Diss., Univ. Edinburgh.
 Gautier et al. 1976, *Ap. J. (Letters)*, **207**, L129.
 Hough et al. 1986, *M.N.R.A.S.*, **222**, 629.
 Kawara et al. 1987, *Ap. J. (Letters)*, **321**, L35.
 Nadeau & Geballe, 1979, *Ap. J.*, **230**, L169.
 Tielens & Hollenbach, 1985, *Ap. J.*, **291**, 747.

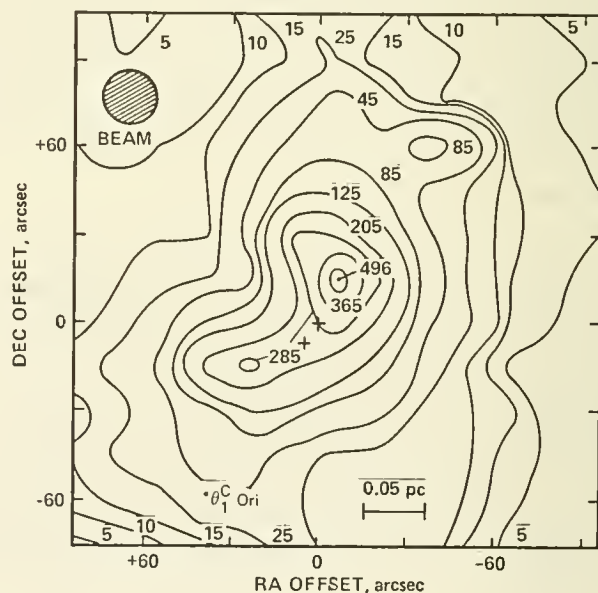
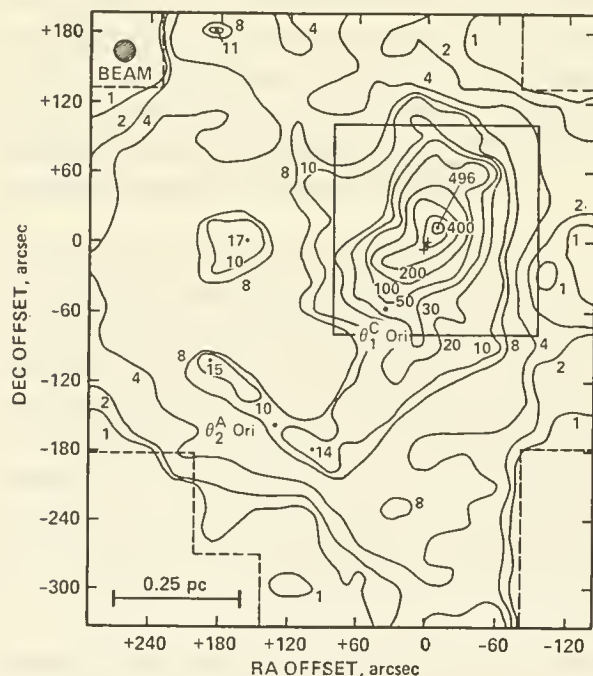


Figure 1. (left) Contour map of the H_2 1-0 S(1) line emission from Orion. The map is centred on the BN source. Contour levels are in multiples of the lowest contour, which corresponds to a line flux of $7 \times 10^{-21} \text{ W cm}^{-2}$ through a $19''$ aperture. The crosses denote the IR sources BN (upper right) and IRC2 (lower left). The optical stars θ_1^C Ori and θ_2^A Ori are denoted by the *. The dashed line defines the region observed.

Figure 2. (right) Enlargement of the region included in the box of Figure 1, showing the shocked emission region around OMC-1.

T. R. Geballe
Joint Astronomy Centre
Hilo, Hawaii

1. Introduction

Line emission from vibrationally excited molecular hydrogen has been detected in a considerable number of active galactic nuclei (AGNs), including those generally believed to contain compact and luminous central engines (e.g., Seyfert nuclei) and those in which the luminosity is believed to arise from massive bursts of star formation (starburst nuclei). In most of these AGNs, only the bright 1-0 S(1) line (rest wavelength 2.12 μ m) has been searched for and detected to date.

Line-emitting H₂ can be excited directly either by energetic collisions created by shock waves or by absorption of UV radiation. Each of these excitation mechanisms has been clearly identified in galactic and extragalactic regions. In active galactic nuclei strong sources of UV and (in some case) X-rays are present. If the nuclear molecular matter is quiescent (i.e., isolated from the active nucleus and not set into motion by episodes of star formation) the H₂ line emission will be dominated by fluorescence, or possibly by thermal emission due to heating by X-rays (Krolik, this conference). However, it is expected or indeed observed that a significant fraction of the interstellar medium in and near these nuclei is undergoing rapid motions; either generated by the central engine or by a nuclear starburst, which are capable of producing strong shock phenomena in nearby molecular gas. Thus, a priori it is not obvious which mechanism is responsible for the H₂ line emission from the nucleus of an active galaxy.

2. Observations

The standard way of discriminating between thermal and non-thermal H₂ line emission is by measuring the relative intensities of H₂ lines whose ratios are sensitive to the excitation mechanism. Three lines are commonly chosen for this comparison, the above mentioned 1-0 S(1) line and the 1-0 S(0) and 2-1 S(1) lines, whose intensities are enhanced relative to 1-0 S(1) in the case of fluorescence compared to their intensities in collisionally heated gas.

In March 1989 these three lines were observed at UKIRT in the nuclei of three Seyfert galaxies, NGC 4051, NGC 3227, and Mkn 273, in which different admixtures of star-forming activity are superposed on the activities of central

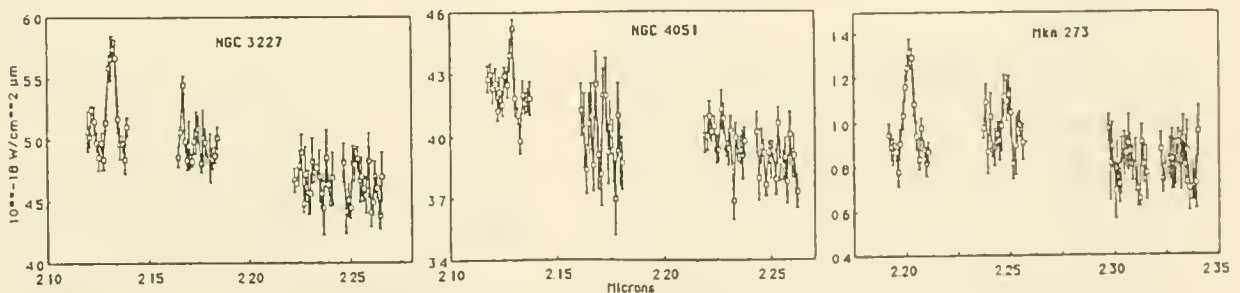


Fig. 1 Spectra of three Seyfert galaxies at the wavelengths of H₂ and H I lines. In wavelength order, the four spectral intervals are centered on H₂ 1-0 S(1), H I Br γ , H₂ 1-0 S(0) and H₂ 2-1 S(1).

engines (Mkn 273 has the most dominant starburst and the highest luminosity in H_2 lines, NGC 4051 the least in both respects). The spectra were obtained using the facility seven-channel cooled grating spectrometer (5" beam), which recently was outfitted with a low noise integrating amplifier. The resolution was $\sim 0.0034 \mu m$ (~ 450 km/s) and the spectra were sampled every 1/3 resolution element. The H I 7-4 (Br γ) line was observed along with the three H_2 lines.

3. Results

The spectra are shown in Figure 1; line intensities are given in Table 1. In all three cases a prominent 1-0 S(1) line is present, and the 1-0 S(0) and 2-1 S(1) lines are either weak or absent. In shocked gas the relative intensities of these lines are roughly 1.0 : 0.3 : 0.1; when purely fluorescent (no collisional relaxation) the relative values are 1.0 : 0.64 : 0.52. The observed values are consistent only with the former set of values. However, if UV excitation of H_2 occurs in dense ($> 10^5 \text{ cm}^{-2}$) molecular gas, the relative intensities approximate the former values (Sternberg and Dalgarno 1989). The densities of molecular clouds in Seyfert nuclei are uncertain, and hence on the basis of these H_2 line intensities alone, one cannot determine at present if the excited H_2 in each of these AGN is collisionally or radiatively excited.

The weakness of Br γ relative to 1-0 S(1) in all three AGNs may be a more effective discriminant, however. Fischer et al. (1987) have demonstrated that in Seyfert nuclei producing a power law ultraviolet spectrum a criterion that fluorescence can be a major contributor to the H_2 line emission is $[\text{Br } \gamma]/[1-0 \text{ S}(1)] > 5$. This limit is more than an order of magnitude higher than the values reported here. In a starburst the above threshold value depends on the nature and present state of the starburst; a limited theoretical study yields lower limits ranging roughly from 1 to 2.5 (Puxley et al. 1988). Indeed, in the seven starburst galaxies found by Puxley et al. to have fluorescent H_2 line emission, $[\text{Br } \gamma]/[1-0 \text{ S}(1)]$ ranges from 1 to 4.

Therefore, it may be concluded that the excited H_2 in NGC 3227, NGC 4051, and Mkn 273 is not fluorescent and that it is not in gas that is heated by absorption of UV photons.

Further details of this research will be given by Wilson et al. (1989).

Table 1

Line	Observed Flux (10^{-22} W/cm^2)		
	Mkn 273	NGC 4051	NGC 3227
1-0 S(1)	22.3 \pm 1.5	8.3 \pm 2.0	34 \pm 4
Br gamma	7.6 \pm 2.5	< 4.	< 7
1-0 S(0)	3.3 \pm 2.0	< 3.	< 7
2-1 S(1)	< 2.0	< 3.	< 7

REFERENCES

- Fischer, J., Geballe, T.R., Smith, H.A., Simon, M., and Storey, J.W.V. 1987, Ap. J., 320, 667.
Puxley, P.J., Hawarden, T.G., and Mountain, C.M. 1988, M.N.R.A.S., 234, 29P.
Sternberg, A. and Dalgarno, A. 1989, Ap. J., 338, 197.
Wilson, A.S., Heckman, T.M., Ward, M. J., and Geballe, T.R. 1989, in preparation.

LYMAN ALPHA RADIATION IN EXTERNAL GALAXIES

David A. Neufeld and Christopher F. McKee

*Departments of Physics and of Astronomy
University of California at Berkeley*

I. Introduction

The Ly α line of atomic hydrogen is often a luminous component of the radiation emitted by distant galaxies. Except for those galaxies which have a substantial central source of non-stellar ionizing radiation, most of the Ly α radiation emitted by galaxies is generated within regions of the interstellar medium which are photoionized by starlight. Conversely, much of the energy radiated by photoionized regions is carried by the Ly α line. Only hot, massive stars are capable of ionizing hydrogen in the interstellar medium which surrounds them, and because such stars are necessarily short-lived, Ly α emission traces regions of active star formation.

Observations of Ly α radiation - including indirect observations of the effects of such radiation upon the gas in which it is generated - may provide a valuable probe of the interstellar medium in star-forming regions of external galaxies; in the case of very distant galaxies Ly α observations may be almost the *only* such probe. Careful theoretical analysis is required to interpret these observations, because the transport of H Ly α photons is profoundly affected by the fact that in traversing an astrophysical medium such photons may suffer frequent absorption and resonant re-emission by hydrogen atoms in the ground state. Indeed, in escaping a neutral interstellar cloud of typical dimensions, H Ly α photons may suffer millions of resonant scatterings. The transfer of Ly α radiation in a highly opaque medium is thus a random walk process in which photons diffuse both in space and - by virtue of the velocity dispersion of the scattering H atoms - in frequency. Diffusion in frequency results in a broadening of the line profile: in traversing a medium of atomic column density $N(H^0)$, Ly α photons acquire a linewidth of $227 (10^{-20} \text{ cm}^2 N(H^0))^{1/3} \Delta v_5^{1/3} \text{ km s}^{-1}$ FWHM, where $\Delta v_5 \text{ km s}^{-1}$ is the velocity dispersion of the scattering H atoms.

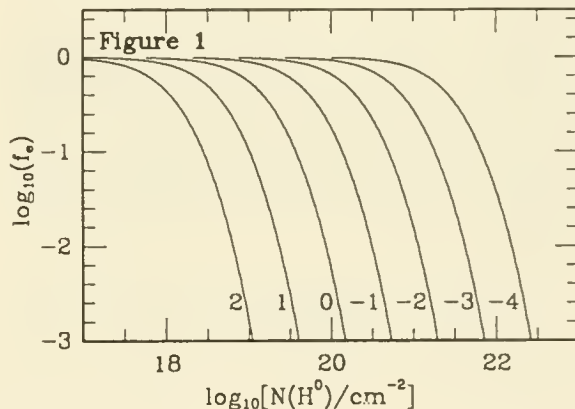
We argue that the *strength* of the Ly α emission observed from external galaxies may be used to estimate quantitatively the dust content of the emitting region, while the Ly α line *profile* is sensitive to the presence of shock waves. Interstellar dust particles and shock waves are intimately associated with the process of star formation in two senses. First, both dust particles and shock waves owe their existence to stellar activity; second, they may both serve as agents which facilitate the formation of stars, shocks by triggering gravitational instabilities in the interstellar gas that they compress, and dust by shielding star-forming molecular clouds from the ionizing and dissociative effects of external UV radiation. By using Ly α observations as a probe of the dust content in diffuse gas at high redshift, we might hope to learn about the earliest epochs of star formation.

Furthermore, the effects of Ly α radiation in selectively pumping warm H₂ molecules may be inferred from the in-

frared spectrum of at least one external galaxy; such effects may serve as signpost of interstellar gas which has been heated and partially dissociated and ionized by X-rays.

II. Ly α as a probe of interstellar dust

In addition to being scattered, Ly α photons may be destroyed by dust absorption, a process which dominates the heating of dust in HII regions. Indeed, because of the extra path length that they must travel, Ly α photons are particularly vulnerable to attenuation by interstellar dust. The effects of such attenuation have been described quantitatively by numerical solution of the transfer equation (Hummer and Kunasz 1980), and recently (Neufeld 1989) by an extension of an analytic method due to Harrington (1973) in which the essential features of the radiative transfer process are described by a Poisson equation. Figure 1 shows the fraction of Ly α photons, f_e , which can escape from the center of a dusty interstellar slab.

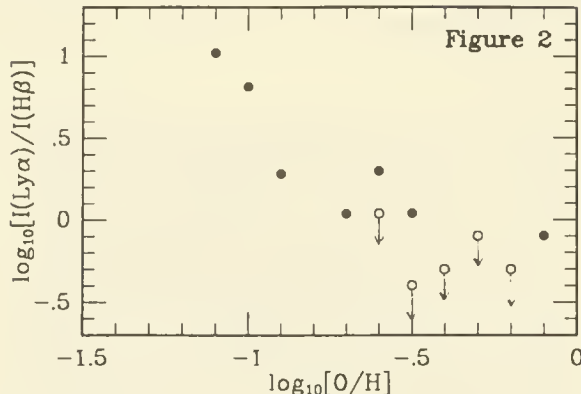


The horizontal axis gives the atomic column density $N(H^0)$ from the center of the cloud to its surface, and the different curves are labelled with the quantity $\log_{10}[\xi_d \Delta v_5^{-2/3} x(H^0)^{-1}]$, where $x(H^0)$ is the neutral atomic fraction, and ξ_d is the dust opacity per hydrogen nucleus, normalized relative to the standard Galactic value of Draine and Lee (1984).

In using observations of Ly α line strengths to estimate the dust content in an external galaxy, we require an estimate of the intrinsic, unattenuated luminosity. If the intrinsic equivalent width is known (from modelling of the stellar population), such an estimate may be derived from continuum measurements close to the Ly α wavelength. Alternatively, observations of Balmer or Brackett lines, or of free-free radio emission, might be used to determine the emission measure of the ionized gas. The distribution of ionized gas and of Ly α emission is also crucial.

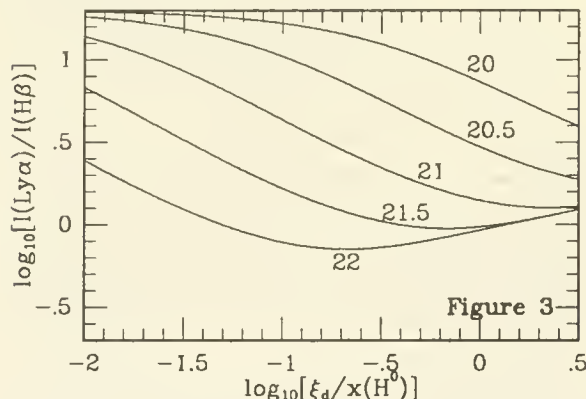
Hartmann *et al.* (1988) have recently presented measurements of the Ly α /H β ratio in several Markarian galaxies

of redshift $z < 0.1$. The results are plotted in Figure 2 as a function of the estimated $[O]/[H]$ ratio.



Without attenuation, the $Ly\alpha/H\beta$ ratio is expected from the theory of radiative recombination to lie around 20; the observed values range from about 1 (the detection limit in this data set) to about 10, presumably reflecting the fact that the resonantly scattered $Ly\alpha$ photons are far more vulnerable to dust absorption than the $H\beta$ photons. Furthermore, the ratio tends to be larger in galaxies of low metallicity in which the dust content might be expected to be smaller.

We have computed the expected $Ly\alpha/H\beta$ ratio for the idealized case of a plane-parallel slab in which the neutral fraction, dust content, and recombination line emissivity are constant. The results are shown in Figure 3 for slabs of various surface-to-center column densities $N(H^0)$. The scattering H atoms are assumed to have a velocity dispersion of 10 km s^{-1} , and each curve is labelled with the value of $\log_{10}(N(H^0)/\text{cm}^{-2})$.



The ratio decreases with increasing $N(H^0)$ until the slab becomes optically thick for absorption both of $Ly\alpha$ photons and of $H\beta$ photons. Further work is needed to treat the case where recombination line photons are generated within regions of low neutral fraction (HII regions) that are embedded in a medium of large neutral fraction (an interstellar cloud).

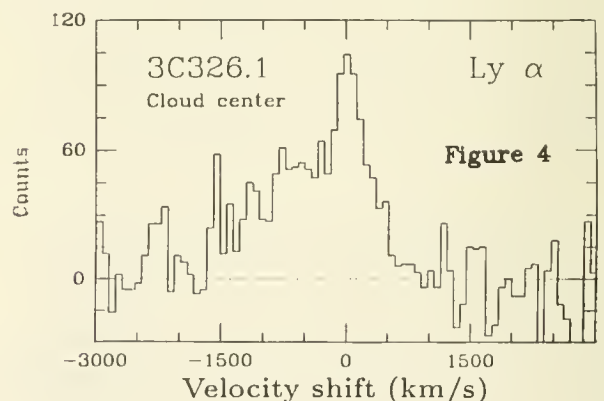
Measurements of the $Ly\alpha$ line width might in principle provide a further constraint upon the dust content of an emitting galaxy, since the line width yields an upper limit on the atomic column density through which a typical $Ly\alpha$ pho-

ton has travelled. For example, Hunstead and Pettini (1989) have recently reported the detection of a narrow emission line from the hydrogen cloud which gives rise to the $z=2.465$ damped $Ly\alpha$ line in the spectrum of the QSO 0836+113. The narrowness of the line ($\leq 50 \text{ km s}^{-1}$ FWHM) implies that the detected $Ly\alpha$ radiation has travelled through at most an atomic column of $(1 \times 10^{18}/\Delta v_5) \text{ cm}^{-2}$. However, the total column density through the cloud is known (from the absorption line it produces) to be $4.2 \times 10^{20} \text{ cm}^{-2}$. Thus the $Ly\alpha$ emission is either generated close to the near surface of the cloud and nowhere else, or we are prevented from seeing embedded sources of radiation due to the effects of dust attenuation. A detailed quantitative analysis needs still to be carried out.

III. $Ly\alpha$ as a probe of interstellar shocks

In considering the transfer of resonance-line radiation in a shocked interstellar cloud, we have found (Neufeld and McKee 1988) that the repeated scattering of $Ly\alpha$ radiation across a shock front results in a systematic blueshift which may greatly exceed the shock velocity. The blueshifting process is a first-order Fermi process analogous to that invoked to explain the acceleration of cosmic rays. When $Ly\alpha$ radiation is generated within a shocked cloud of neutral material the emergent line profile is given by: $\phi(v_b) \propto v_b^2 \exp(-0.034 v_b^3 / v_{s,7} N_{20})$, where $v_b = 100 v_{b,7} \text{ km s}^{-1}$ is blueshift relative to line center, $100 v_{s,7} \text{ km s}^{-1}$ is the shock velocity, and $N = 10^{20} N_{20} \text{ cm}^{-2}$ is the column density of hydrogen atoms on either side of the shock front. The spectrum peaks at a blueshift $270(N_{20} v_{s,7})^{1/3} \text{ km s}^{-1}$.

Fermi acceleration may be responsible for the blue asymmetric line profiles that have been observed in high redshift $Ly\alpha$ galaxies. The $Ly\alpha$ line profile in 3C326.1, measured by Djorgovski (1988), is shown in Figure 4.



The observed spectrum may be accounted for quantitatively by a model in which shocks, driven into a population of interstellar clouds by a radio lobe, trigger the formation of ionizing stars and Fermi accelerate the $Ly\alpha$ radiation emitted by HII regions surrounding those stars. To match the observed line profile, which shows a blue wing extending to 2000 km s^{-1} from line center, the required pressure behind the shocks is $6 \times 10^{-10} \text{ dyn cm}^{-2}$, consistent with a lower

limit on the pressure in the radio lobe that is set by the observed synchrotron emissivity. The shock velocity must lie between 10 and 400 km s⁻¹ and the pre-shock density between 0.16 and 260 cm⁻³. The virial temperature of the clouds is $\gtrsim 2 \times 10^4$ K, implying a line-of-sight velocity dispersion of at least 17 km s⁻¹ for thermal or turbulent support. To allow the escape of Ly α radiation, the dust opacity per hydrogen atom must lie at least a factor 60 below the standard Galactic value. The absolute strength of the observed Ly α emission requires that the shocks trigger star formation with an efficiency greater than 0.5%.

A further consequence of the Fermi acceleration mechanism is that galaxy mergers, particularly between galaxies with low dust content, should produce Ly α lines with strong blue wings.

IV. H₂ pumping and the spectrum of NGC 6240

In warm gas containing H₂ in vibrationally-excited states, H Ly α radiation may pump coincident lines of the H₂ Lyman bands (Shull 1978, Black and van Dishoeck 1987), thereby being converted into ultraviolet fluorescent photons with a characteristic spectrum that has been observed both in sunspots (Jordan *et al.* 1977) and in Herbig-Haro objects (Brown *et al.* 1981; Schwartz 1983). There are two H₂ Lyman band transitions that lie close to the Ly α rest frequency: the B-X 1-2 R(6) transition (at a redshift of 15 km s⁻¹ from line center) and the B-X 1-2 P(5) transition (at a redshift of 99 km s⁻¹). The relative pumping rates in the two transitions may serve, in principle, as a probe of the Ly α line profile in the region of the warm H₂.

The pumping process may be treated *analytically* by methods described by Neufeld (1989). Figure 5 shows the fraction of Ly α photons, $(1 - f_e)$, which are converted into fluorescent photons of the Lyman bands before escaping from the center of a slab with a molecular fraction relative to H atoms of $x(H_2) \equiv n(H_2)/n(H^0)$. Each curve is labelled with the quantity $-\log_{10} x(H_2)$.

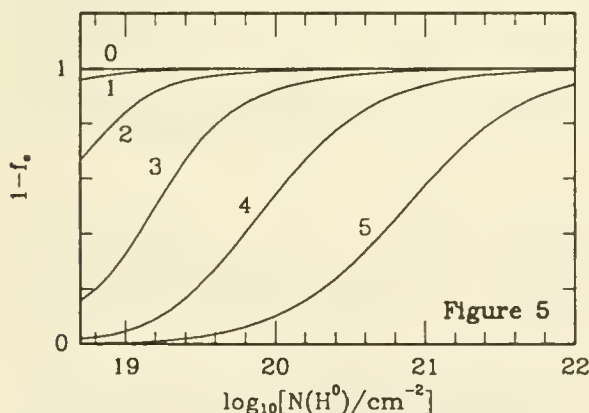


Figure 5

The results apply to a dust-free gas cloud at 4000 K in which the H₂ energy levels are thermally populated and the H atoms and H₂ molecules have a thermal velocity dispersion. Comparing Figures 1 and 5, we find that under these conditions, H₂ absorption dominates dust absorption when the molecular fraction exceeds about 10⁻⁴. Figure 6 compares the total rate of pumping in the two transitions. The vertical axis shows the number of pumps in the B-X 1-2 P(5)

transition divided by the number in the B-X 1-2 R(6) transition.

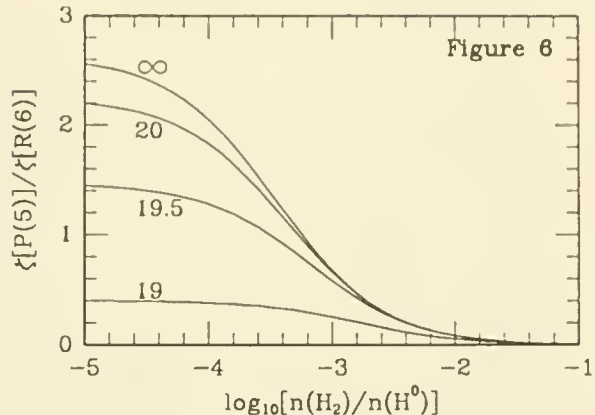


Figure 6

In addition to generating UV fluorescence, the pumping process may also modify the infrared emission spectrum of the warm, pumped H₂. For example, we expect the ($v=2, J=5$) and ($v=2, J=6$) states of H₂ to be selectively depopulated in regions of high Ly α flux. Such depopulation is the probable explanation of the anomalously small $v=2-1$ S(3) line intensity reported recently by Lester, Carr and Harvey (1988) for the starburst galaxy NGC 6240. (We might expect $v=2-1$ S(4) to be similarly diminished.) The required spatial coincidence of warm H₂ and Ly α emission may argue in favor of the model of Draine and Woods (1989), in which the copious H₂ rovibrational emission observed in NGC 6240 is produced in molecular clouds which are warmed, and partially ionized and dissociated by X-rays generated in a population of embedded supernova remnants. The expected diminution in the $v=2-1$ S(3) and $v=2-1$ S(4) line strengths is currently being investigated quantitatively by Neufeld, Draine and Woods.

The work of C.F.M. was supported in part by NSF grant AST-86-15177, and that of D.A.N. was conducted under the auspices of a special NASA astrophysics theory program which supports the Center for Star Formation Studies.

REFERENCES

- Black, J. H., and van Dishoeck, E. F. 1987, *Ap. J.*, 322, 412.
- Brown, A., Jordan, C., Millar, T. J., Gondhalekar, P., and Wilson, R. 1981, *Nature*, 290, 34.
- Djorgovski, S. 1988, in *Towards Understanding Galaxies at Large Redshifts*, ed. A. Renzini and R. Kron (Dordrecht: Reidel).
- Draine, B. T., and Lee, H. M. 1984, *Ap. J.*, 285, 89.
- Draine, B. T., and Woods, D. T. 1989, in *22nd ESLAB Symposium, Infrared Spectroscopy in Astronomy*, ed. M. Kessler (Noordwijk: ESA-STPB), in press.
- Hartmann, L. W., Huchra, J. P., Geller, M. J., O'Brien, P., and Wilson, R. 1988, *Ap. J.*, 326, 101.
- Harrington, J. P. 1973, *M.N.R.A.S.*, 162, 43.
- Hummer, D. G., and Kunasz, P. B. 1980, *Ap. J.*, 236, 609.
- Hunstead, R. W., and Pettini, M. 1989, in *The Epoch of Galaxy Formation*, ed. C. S. Frenk, R. S. Ellis, T. Shanks, A. F. Heavens, and J. A. Peacock (Dordrecht: Kluwer), p. 115.
- Jordan, C., Brueckner, G. E., Bartoe, J.-D., Sandlin, G. D., and van Hooser, M. E. 1977, *Nature*, 270, 326.
- Lester, D. F., Harvey, P. M., and Carr, J. 1988, *Ap. J.*, 329, 641.
- Neufeld, D. A., and McKee, C. F., *Ap. J. (Letters)*, 331, L90.
- Neufeld, D. A. 1989, *Ap. J.*, submitted.
- Schwartz, R. D. 1983, *Ap. J. (Letters)*, 268, L37.
- Shull, J. M. 1978, *Ap. J.*, 224, 841.

Observations of extended and counterrotating disks of ionized gas in S0 galaxies*

Ralf-Jürgen Dettmar[§],
Marlies Jullien-Dettmar,
Lowell Observatory, Flagstaff, Arizona
and

Andreas Barteldrees
Max-Planck-Institut für Radioastronomie, Bonn, FRG

Introduction

While many E/S0 galaxies have been found to show emission line spectra in their nuclear regions the question of the presence and nature of extended disks of ionized gas in these galaxies has been addressed only in recent years. Typically the ionized gas is detected in the inner region on a scale of ~ 1 kpc (e.g. Phillips *et al.* 1986, Caldwell 1984).

Here we present evidence that the disks of ionized gas of at least some S0 galaxies are much more extended than previously believed. In addition, with the detection of the counterrotation of gas and stars in NGC 7007 we strengthen the basis for arguments that the source of gas in S0 galaxies is external.

Object selection and observations

Our original objective was to find high rotational velocities in bulge-dominated, early type disk galaxies. For that purpose we selected objects, that show morphological similarities to NGC 4594 or NGC 7814, by visually inspecting the ESO/SRC-J film copies and by using the remarks in Corwin *et al.* (1985). Some of these objects are also in a sample of E/S0 galaxies studied by Phillips *et al.* (1986) and classified by Lauberts (1982) to be S0's. All of these originally selected galaxies show extended H α and [NII] emission. However, as a comparison with the type parameter for these objects given by Corwin *et al.* shows, the classification of these objects is very uncertain. Therefore we have selected two additional groups: (1) galaxies with an S0 classification confirmed by Corwin *et al.* that were also observed by Phillips *et al.*, (2) a comparison group consisting of confirmed S0's which are not in the Phillips *et al.* sample.

The observations were obtained with the B&C Cassegrain spectrograph at the 2.2m telescope on La Silla during bright time between June 8 and June 18, 1987. The dispersion was 1.74Å/pixel. The ESO #5 RCA CCD was used and the integration time was 40 minutes for each spectrum. We have used position angles from Lauberts (1982) to align the slit with the major axis. After standard reduction the frames were rebinned to constant $\Delta\lambda$, and the night sky and the galaxy continuum were subtracted. Rotation curves were measured by fitting Gaussian profiles to the H α [NII] emission lines.

The extent of the ionized gaseous disks

In Table 1 we summarize the characteristics of the observed S0 galaxies. Morphological types are given in columns (2) and (3). The diameter of the ionized gas d is given in arcsec in column (4) and in kpc in column (5), assuming $H_0=75$ km sec $^{-1}$ Mpc $^{-1}$. The three different groups of objects discussed above are separated by horizontal lines.

For most of the objects in Table 1 with detected emission lines, the extent of the gas is typically of the order of 10 kpc. This is significantly larger than most other known examples like NGC 4636 (~ 1 kpc), and NGC 5846 (~ 1.7 kpc) (Demoulin-Ulrich *et al.* 1984), NGC 5266 and NGC 3109

* Based on observations collected during MPI time at the ESO/MPI 2.2m telescope, La Silla/Chile

§ on leave from: Radioastronomisches Institut der Universität Bonn, Bonn, FRG

(~ 2 kpc; Caldwell, 1984). Only the gaseous disk of the SB0 galaxy NGC 1546, where the gas is counterrotating, is extended over 8 kpc (Galletta, 1987).

This scalelength of ~ 10 kpc should be compared with the scalelength for the radio continuum emission in E/S0 galaxies which was recently determined to be of the same order of magnitude for eight galaxies studied by Wrobel and Heeschen (1988). The presence of radio continuum radiation is strong evidence for star formation processes in these galaxies. Recent star formation also could explain the ionization of the gaseous disks. However, for most of the galaxies in Table 1 the emission lines of the gaseous disks are more LINER like, with [NII] stronger than H α for the whole range of distances from the nuclei. In four galaxies the ratio [NII]/H α changes from >1 for the nuclear region to <1 for the extended disk. This might indicate that also the dominant excitation process changes from nuclear activity to processes related to star formation.

The high detection rate of extended gaseous disks in our sample is perhaps biased by object selection as we favoured galaxies with dust lanes. Therefore the relation between the presence of dust, star formation, and the properties of the ionized ISM can not be addressed.

Table 1: Summary of observations

Object (1)	$T_{Lauberts}$ (2)	T_{Corwin} (3)	$d('')$ (4)	$d(\text{kpc})$ (5)	Remarks (6)
NGC 3573	-2	0	>89	>13	dust, [NII]/H α changes*
NGC 5220	-2	1	101	27	dust, [NII]/H α changes
NGC 5237	-2	0	50	0.3	dust, III spectrum, no rotation
NGC 6848	-2	0.5	75	20	dust, [NII]/H α changes
NGC 7123	-2	1	78	19	dust, small vel. gradient
ESO 13-G12	-2	-0.3	82	26	dust, small vel. gradient
IC 4704	-2	-3			dust, no detection
NGC 6771	-2	-2	71	19	dust
IC 4906	-2	-2.7	21	5	dust, [NII]/H α changes
ESO 235-G42	-2	-1	15	5	dust
NGC 7007	-2	-2	30	6	dust, counterrotation
NGC 7014	-2	-3.0			dust, no detection
NGC 7049	-2	-3.7	47	7	dust
NGC 7070A	-2	-2	48	7	dust, [NII]/H α changes
NGC 3203	-2	S0 ₂ §			no detection
ESO 506-G33	-2	-2	35	3	small vel. gradient
ESO 575-G59	-2	-0.7	28	8	dust

Notes: § from RSA, * the [NII]/H α changes from >1 for the the nuclear region to <1 in the disk

The counterrotating disk of ionized gas in NGC 7007

While most of the galaxies in Table 1 show a rotating gaseous disk, in some cases the velocity gradient is so small, that we can not from just one spectrum establish that this is due to rotation. These cases are indicated in column (6) of Table 1. The case of NGC 7007 is especially remarkable. The continuum-subtracted spectrum of NGC 7007 (Figure 1) shows counterrotating gaseous and stellar components. This is the third S0 galaxy known to show counterrotation of gas and stars

(Bertola *et al.* 1988). The relatively large percentage of S0 galaxies with peculiar gas motions (polar rings or counterrotation) is indicative of an external origin of the gas.

Acknowledgments. RJD and AB are grateful to the director of the MPI für Astronomie for the generous allocation of observing time. This work has been partly supported by the Deutsche Forschungsgemeinschaft under De 385/1-1 and De 385/2-1 and the Lowell Observatory Research Fund.

References

- Bertola, F., Buson, L.M., Zeilinger, W.W. 1988, *Nature*, **335**, 705.
 Caldwell, N. 1984, *PASP*, **96**, 287.
 Corwin, H. G., de Vaucouleurs, A., de Vaucouleurs, G. 1985, Southern Galaxy Catalogue, The University of Texas Monographs in Astronomy No. 4.
 Demoulin-Ulrich, M.-H., Butcher, H.R., Boksenberg, A. 1984, *Ap.J.*, **285**, 527.
 Galetta, G. 1987, *Ap.J.*, **318**, 531.
 Lauberts, A. 1982, The ESO/Uppsala Survey of the ESO(B) Atlas, ESO.
 Phillips, M.M., Jenkins, C.R., Dopita, M.A., Sadler, E.M., Binette, L. 1986, *A.J.*, **91**, 1062.
 Wrobel, J.M., Heeschen, D.S. 1988, *Ap.J.*, **335**, 677.

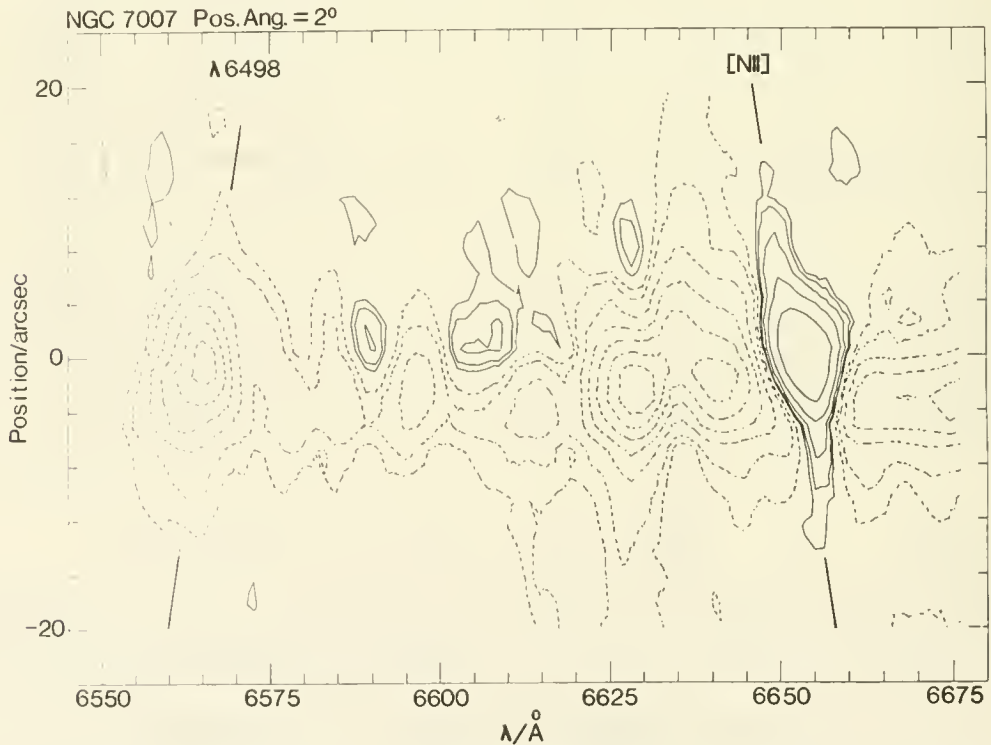


Fig. 1: The contour plot of the continuum-subtracted spectrogram of NGC 7007 shows the counterrotation of the ionized gas and the stellar component if, for example, the $\lambda 6583$ [NII] line is compared with the metal blend at $\lambda 6498$ or the underlying $H\alpha$ absorption. Emission is indicated by continuous lines, absorption by dashed contours.

THE GRAVITATIONAL WAKEFIELD OF A MOLECULAR CLOUD IN A DISK GALAXY

M. TAGGER¹
R. PELLAT²
J.F. SYGNET³

¹ Service d'Astrophysique, CEN Saclay

² Centre de Physique Théorique, Ecole Polytechnique

³ Institut d'Astrophysique de Paris

A molecular cloud (considered as a point macroparticle) represents a clump of increased mass density moving in the disk of a galaxy. Its presence generates a gravitational polarisation of the disk, somewhat analogous to the polarisation of a dielectric medium by a test charged particle. This means that the cloud travels along with a wakefield (a region of increased mass density) which is the collective response of the stars and gas to the perturbing mass. It can represent many times the mass of the cloud, and emits spiral density waves which propagate away.

In terms of statistical mechanics, this wakefield will appear as an increased two-particle correlation function which is the equivalent of the Debye sphere in a plasma — despite the absence here of negative charges. At short distances clouds will thus interact through their own gravitational field amplified by their wakefields, which might thus strongly affect their collisionality.

We present a calculation of this wakefield and discuss its importance in the collisional dynamics of molecular clouds.

THE EFFECT OF SUSPENDED PARTICLES ON JEANS' CRITERION FOR GRAVITATIONAL INSTABILITY

DAVID J. WOLLKIND

Department of Pure and Applied Mathematics

Washington State University

Pullman, WA 99164

and

KEMBLE R. YATES

Department of Mathematics

Southern Oregon State College

Ashland, OR 97520

SUMMARY

The effect that the proper inclusion of suspended particles has on Jeans' criterion for the self-gravitational instability of an unbounded nonrotating adiabatic gas cloud is examined by formulating the appropriate model system, introducing particular physically plausible equations of state and constitutive relations, performing a linear stability analysis of a uniformly expanding exact solution to these governing equations, and exploiting the fact that there exists a natural small material parameter for this problem given by N_1/n_1 , the ratio of the initial *number* density for the particles to that for the gas. The main result of this investigation is the derivation of an altered criterion

$$\lambda > \lambda_c^{(3)} \equiv c_1 \left(\frac{\pi}{G_0} \right)^{1/2} \left(\frac{m_1}{m_1^2 n_1 + m_g^2 N_1} \right)^{1/2} \quad (1)$$

which can substantially reduce Jeans' original critical wavelength for instability

$$\lambda_c \equiv c_1 \left(\frac{\pi}{G_0 \rho_1} \right)^{1/2}. \quad (2)$$

Here λ is the characteristic wavelength of the density fluctuations, G_0 is the universal gravitational constant, and c_1 is the speed of sound in a clean gas of *mass* density $\rho_1 = m_1 n_1$ while m_g is the mass of an individual suspended particle/dust grain. It is then shown that the existing discrepancy between Jeans' theoretical prediction using (2) and actual observational data relevant to the Andromeda nebula M31 can be accounted for by this new criterion of (1) assuming suspended particles of a reasonable grain size and distribution to be present.

Virial Theorem Analysis of the Structure and Stability of Magnetized Clouds

Ellen G. Zweibel, University of Colorado at Boulder

I have used the tensor virial equations to develop models of magnetized, self-gravitating, isothermal clouds confined by an external medium. These models are characterized by five parameters; the mass M and isothermal speed C_s of the cloud, the pressure P_e of the ambient medium, the strength of the magnetic field at infinity B_∞ , and the magnetic flux Φ which threads the cloud. The cloud is spheroidal, with semi major axis a and eccentricity e to be calculated from the two nontrivial components of the tensor virial equations with M , C_s , P_e , B_∞ , and Φ as input parameters. This work is a logical extension of Strittmatter's (1966). A sketch of a cloud model is shown in Figure 1.

I calculate "critical states," which represent extremal solutions in the sense that if the external pressure is increased while keeping the other parameters fixed, no equilibrium exists and the system presumably collapses. These critical solutions are compared with the exact magnetostatic models of Mouschovias (1976; from Mouschovias and Spitzer 1976) and Tomisaka et al. (1988) in Figure 2. These latter models represent states which have contracted from uniformly magnetized spheres with frozen in magnetic flux. The virial theorem models are parameterized by q , the ratio of B_∞ to the fieldstrength B_0 in the cloud. The points at fixed q and increasing η_c have increasing values of e . The slope of the line through the $q = 0.85$ solution agrees with the magnetostatic models; the difference in intercept is due to the effects of central concentration, which the virial theorem models ignore.

I have also used the virial equation to study the stability of these models to small perturbations. A sufficiently strong, uniform field can completely stabilize a cloud while a field which is much stronger than the external field can destabilize it.

This work was supported by NSF Grant R11-8722796 to the University of Chicago and by NSF Grant ATM 2506632 and NASA Grant NAGW 91 to the University of Colorado. A more detailed account will be published in the *Astrophysical Journal*.

References

- Mouschovias, T. Ch. 1976, Ap.J. **207**, 141
- Mouschovias, T. Ch. and Spitzer, L. 1976, Ap.J. **329**, 392
- Strittmatter, P.A. 1966, Mon. Not. Roy. Ast. Soc. **132**, 359
- Tomisaka, K., Ikeuchi, S. and Nakamura, T. 1988, Ap.J. **335**, 239

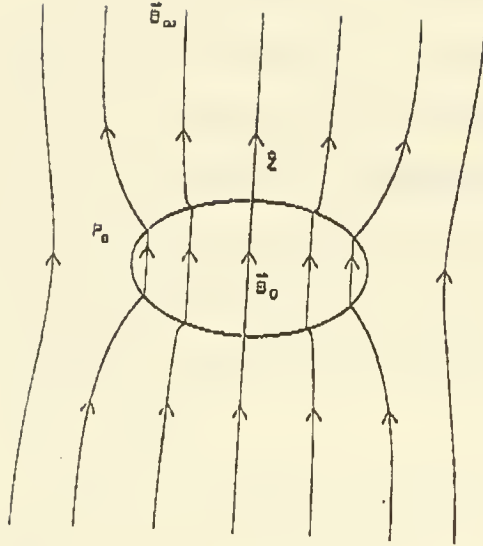


Figure 1

Figure 1: Sketch of a spheroidal,
magnetically supported cloud.

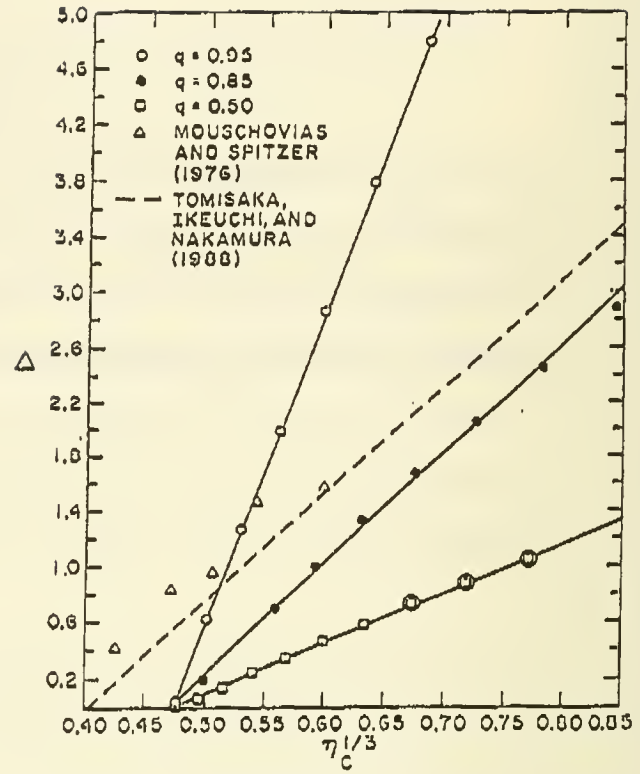


Figure 2

Figure 2: The variation of magnetic flux
parameter $\Delta_c = \frac{5\Phi^2}{6\pi^2 GM^2}$ with

critical pressure parameter
 $\eta_c^{1/3} = \frac{GM^{2/3}}{5 C_s^{8/3}} \left(\frac{4\pi P_e}{3} \right)^{1/3}$; q is

constant on each line while e
increases in the direction of
increasing η_c . The triangles are the
models of Mouschovias and the
dashed line is proposed by
Tomisaka et al.

EVOLUTION OF MAGNETIZED, ROTATING, ISOTHERMAL CLOUDS

KOJI TOMISAKA

Faculty of Education, Niigata University
Niigata 950-21, Japan

1. Introduction

Molecular cloud cores, in which star formation process now proceeds, are often found with elongated shape. This suggests that the core collapsed preferentially along the direction parallel to the global magnetic field and/or parallel to the cloud's initial angular momentum. Actually the magnetic field strength in the cloud has been measured recently with the Zeeman splitting (Goodman *et al.* 1989). The authors indicate the magnetic field of 10 – 30 μG exists in the cloud. Further, the observation of polarization in the near IR from background stars shows that the magnetic field runs perpendicularly to the major axis of the cloud (Tamura *et al.* 1987). As for the angular momentum, the rotation rate of 0.2 – 6 $\text{km s}^{-1} \text{pc}^{-1}$ is reported (Goldsmith and Arquilla 1985) in 16 dark cloud regions. If the cloud collapses from the diffuse cloud with density $n \sim 1\text{cm}^{-3}$ with strictly conserving the angular momentum which was shared from the galactic rotation, the rotation rate of the cloud will be $\Omega_{J=\text{const}} \sim 3(n/1000\text{cm}^{-3})^{2/3}\text{km s}^{-1}\text{pc}^{-1}$ (Mouschovias 1987). In a present paper, I will study the evolution of the rotating magnetized cloud.

2. Equilibrium Solutions and Critical Mass

First, I will see the equilibrium structure in which the self-gravity is counterbalanced by thermal pressure, magnetic force, and centrifugal force. This will enable us to estimate the critical mass of the cloud M_{cr} , which divides the clouds into subcritical clouds $M < M_{\text{cr}}$ and supercritical clouds $M > M_{\text{cr}}$.

The equilibrium solution is characterized by four parameters: the mass M_{cl} (or the central density ρ_c), plasma beta of the ambient medium $\beta_0 \equiv p_{\text{ext}}/(B_0^2/8\pi)$, magnetic flux threading the cloud $\Phi_B \equiv \pi R_{\text{cl}}^2 B_0$, and specific angular momentum $j \equiv 2/5 R_{\text{cl}}^2 \Omega_{\text{cl}}$. Numerical method is described in other paper (Tomisaka *et al.* 1988*a*). Figure 1 represents the M_{cl} vs. ρ_c relation for fixed R_{cl} . This shows that the maximum mass, which is shown by tick mark, increases according to the increase of magnetic field (decrease of β_0). Angular momentum has a similar effect: with increase of j , the critical mass increases for fixed β_0 . From these, I obtained an approximate formula for the critical mass of the cloud with *both* magnetic field and rotation as

$$M_{\text{cr}} \simeq \left\{ M_{\text{mag}}^2 + \left(\frac{4.8c_s j}{G} \right)^2 \right\}^{1/2} \quad (1)$$

M_{mag} means the critical mass of the nonrotating cloud as

$$M_{\text{mag}} \simeq 62 \left\{ 1 - \left[\frac{0.17}{G^{1/2} |dm/d\Phi_B|_c} \right]^2 \right\}^{-3/2} \frac{c_s^4}{p_{\text{ext}}^{1/2} (4\pi G)^{3/2}}, \quad (2)$$

where $G^{1/2} |dm/d\Phi_B|_c$ and c_s represent the mass-to-magnetic flux ratio at the center and isothermal sound speed (see Tomisaka *et al.* 1988*b* and 1989).

3. Quasistatic Evolution Driven by Plasma Drift and Magnetic Braking

Here, the evolution of *subcritical* cloud is studied, because the supercritical cloud will collapse in a short dynamical time scale. Subcritical clouds evolve driven by the plasma drift (ambipolar diffusion) and magnetic braking. Since the evolution time scales driven these two processes are ordinarily much longer than the dynamical time scale of the cloud (free-fall time at the center), the cloud evolves in a quasi-static fashion. Due to the plasma drift, mass and angular momentum is transferred across the magnetic field inwardly. As for the magnetic braking, because the torsional Alfvén wave propagating in the ambient medium (ρ_a) transfers the angular momentum, angular momentum flux flowing through a flux tube is estimated as $\sim 2V_A\rho_a Rv_\phi \times$ (area of the magnetic tube).

Figure 2 shows the evolution of a model cloud. (a) corresponds to the initial state ($t = 0$). The cloud rotates almost rigidly. At $t = 2 \times 10^6$ yr (b) the central density increases from $n_c = 1.6 \times 10^4 \text{ cm}^{-3}$ ($t = 0$) to $n_c = 3.3 \times 10^4 \text{ cm}^{-3}$ due to the increase of the mass-to-flux ratio by the plasma drift. Beyond $t = 4.3 \times 10^6$ yr (c), no quasistatic solutions exist and this indicates that the cloud enters the dynamical contraction phase after that. About 80 % of the initial angular momentum is lost in $t = 4.3 \times 10^6$ yr. While the central density increases by a factor 100 during the quasistatic evolution, the mass-to-flux ratio at the center increases only by a factor 2.

The time scales of the plasma drift and angular momentum loss are expressed, respectively, as $\tau_P \simeq 15(G\rho_c)^{-1/2} \sim 3 \times 10^6 \text{ yr}(n_c/10^5 \text{ cm}^{-3})^{-1/2}$ (Mouschovias 1987) and $\tau_{\parallel} \simeq 2.4 \times 10^6 \text{ yr} (M_{cl}/10.7 M_\odot)(R_{cl}/0.26 \text{ pc})^{-2} (B_0/30 \mu G)^{-1} (\rho_a/3.8 \times 10^{-23} \text{ cm}^{-3})^{-1/2}$ (Shu *et al.* 1987). The evolution is determined by these two time scales *and* available time left to the cloud (or how close the mass of the cloud is to the critical mass).

(1) the cloud mainly supported magnetic field. (a) the cloud with mass much less than the critical mass (Fig. 2): the cloud is long lived $\sim (4 - 7) \times 10^6 \text{ yr}$ and loses almost all the angular momentum (80%) in the quasistatic evolution phase. (b) the cloud with mass close to the critical mass: since the plasma drift works effectively in such a cloud, the cloud enters the dynamical contraction phase fast ($\sim 10^6 \text{ yr}$). A fairly large part of the angular momentum (60%) remains in the cloud at the final phase of the quasistatic evolution.

(2) the cloud in which rotation also plays an important role: since the decrease of angular momentum reduces the critical mass, magnetic braking makes the quasistatic evolution end in $\sim 6 \times 10^6 \text{ yr}$. In either cases (1) or (2), clouds enter the dynamical contraction phase in several 10^6 yr .

REFERENCES

- | | |
|--|--|
| <p>Goodman, A. A., Crutcher, R. M., Heiles, C., Myers, P. C., and Troland, T. H. 1989, <i>Ap. J.</i> in press.</p> <p>Goldsmith, P. F., and Arquilla, R. 1985, in <i>Protostars and Planets II</i>, ed. D. C. Black and M. S. Matthews (Tucson: University Arizona Press), p.137.</p> <p>Mouschovias, T. Ch. 1987, <i>Physical Processes in Interstellar Clouds</i>, ed. G. E. Morfill and M. Scholer (Dordrecht: Reidel), p. 453.</p> | <p>Tamura, M. <i>et al.</i> 1987, in <i>IAU Symposium 115, Star Forming Regions</i>, ed. M. Peimbert and J. Jugaku (Dordrecht: Reidel), p. 48.</p> <p>Shu, F. H., Adams, F. C., and Lizano, S. 1987, <i>Ann. Rev. Astr. Ap.</i>, 25, 23.</p> <p>Tomisaka, K., Ikenchi, S., and Nakamura, T. 1988a, <i>Ap. J.</i>, 326, 208.</p> <p>———. 1988b, <i>Ap. J.</i>, 335, 239.</p> <p>———. 1989, <i>Ap. J.</i>, 341, 000.</p> |
|--|--|

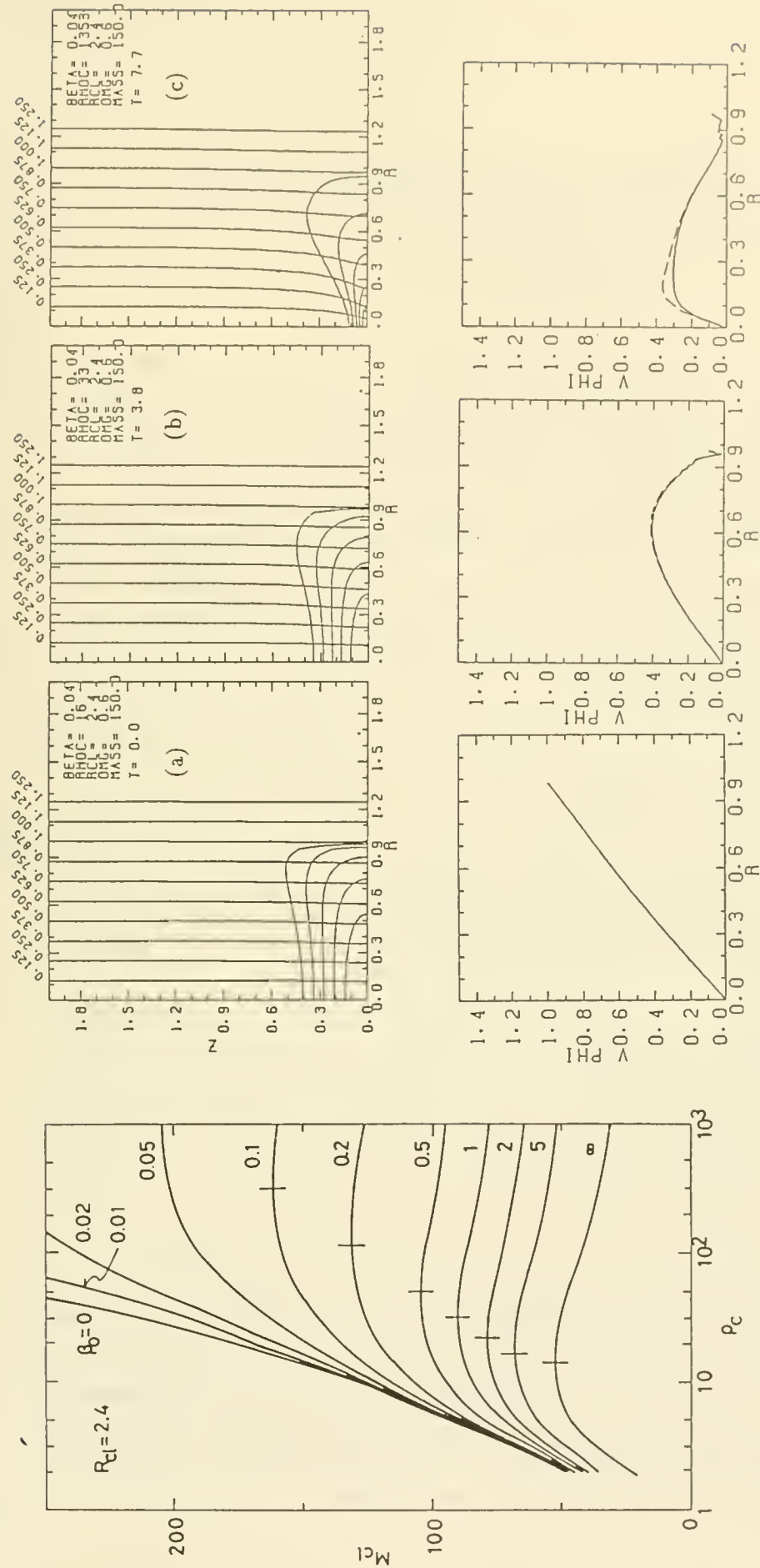


FIG 1.—Mass of the cloud, M_{cl} , vs. central density, ρ_c , for various values of β_0 . Except for $\beta_0 = 0$, M_{cl} takes a maximum value, which increases with increasing strength of the magnetic field B_0 . The critical density, at which the mass reaches the maximum, also increases with increasing strength of the magnetic field.

FIG 2.—The evolution of magnetized rotating clouds with $T = 10\text{K}$, $M_{cl} = 10.7M_\odot$, $B_0 = 30\mu\text{G}$, $\Omega_{cl} = 1\text{km s}^{-1}\text{pc}^{-1}$, $R_{cl} = 0.26\text{pc}$, $p_{ext}/k = 10^4\text{K cm}^{-3}$ and $\rho_a = 10\text{cm}^{-3}$ at (a) $t = 0$, (b) $t = 2 \times 10^6\text{ yr}$, and (c) $t = 4.3 \times 10^6\text{ yr}$. In the upper panel, the magnetic field line, which runs almost vertically, and the density contour are plotted. The contour level of the density is taken as $\log \rho = [(\log \rho_c)/5]n$, for $n = 0 - 4$. The horizontal and vertical axis mean, respectively, the normalized distance as r/R_{cl} and z/R_{cl} . In the lower panel, the normalized rotation velocity $v_\phi/(R_{cl}\Omega_{cl})$ is plotted against the normalized radial distance r/R_{cl} .

Infrared Polarimetry and the Magnetic Field in External Galaxies

Terry Jay Jones

University of Minnesota

Jones (1989) finds that interstellar polarization at 2.2 μ m is well correlated with the line of sight extinction to reddened stars in the Milky Way. This is true primarily for lines of sight that cross interstellar magnetic field lines. The correlation does not, however, have a slope of unity. Jones interpreted this result by modeling the net interstellar polarization as due to grains aligned by an interstellar magnetic field made up of equal contributions of a uniform component and a random component.

Recently, Jones and Klebe (1989) present infrared polarimetric measurements of six infrared luminous galaxies. Three of the galaxies (Arp 220, NGC 6240 and Mrk 273) show polarization consistent with purely interstellar polarization. Compared to the Milky Way, the strength of the polarization is low for the extinction inferred from the near infrared colors of the central portions of these galaxies. Jones and Klebe interpret these results to indicate that the projected magnetic field in front of the central bulges of these galaxies is more disordered than in the Milky Way, perhaps as a consequence of a recent merger, as suggested in images of these galaxies.

Here we report for the first time infrared polarimetry of the normal edge on spiral NGC 4565 and the interacting pair NGC 3690/IC 694 (Arp 299). These observations, as well as previous observations, were made with the Minnesota Infrared Polarimeter on the IRTF during the past year. Our goal is to explore the magnetic field geometry in these galaxies and to determine the extent to which the field is ordered and uniform.

Figure 1 shows the results of polarimetry for stars in the Milky Way taken from the literature plotted and as small dots. The dashed line is the model from Jones (1989). The three infrared luminous galaxies showing only interstellar polarization are plotted as open triangles. The polarization of the bulge of NGC 4565 seen through its dust lane is plotted as an open square. Note that for NGC 4565 the polarization per unit optical depth in the disk is as high as in the Milky Way. This indicates that the trend seen in the Milky Way is probably typical for normal undisturbed spiral galaxies.

The polarimetry of the two nuclei of Arp 299 (sources A and B) are plotted as open circles. Note that as with the infrared luminous galaxies, the polarization of Arp 299 is well below the relation for normal spiral galaxies. This suggests that the projected magnetic field in front of the nuclei of all of these galaxies contains a greater random component than is the case in normal spiral galaxies. In order to lower the polarization by a factor of two to three compared to the Milky Way a considerable disruption of the magnetic field along the line of sight is required. This suggests that the process of interaction between galaxies or the onset of a massive starburst significantly disrupts the magnetic field geometry. In NGC 6240 for example, all memory of the original net magnetic field direction has been lost.

Jones, T. J. and Klebe, D. I., 1989, Ap. J., 340, in press.

Jones, T. J., 1989, Ap. J., in press.

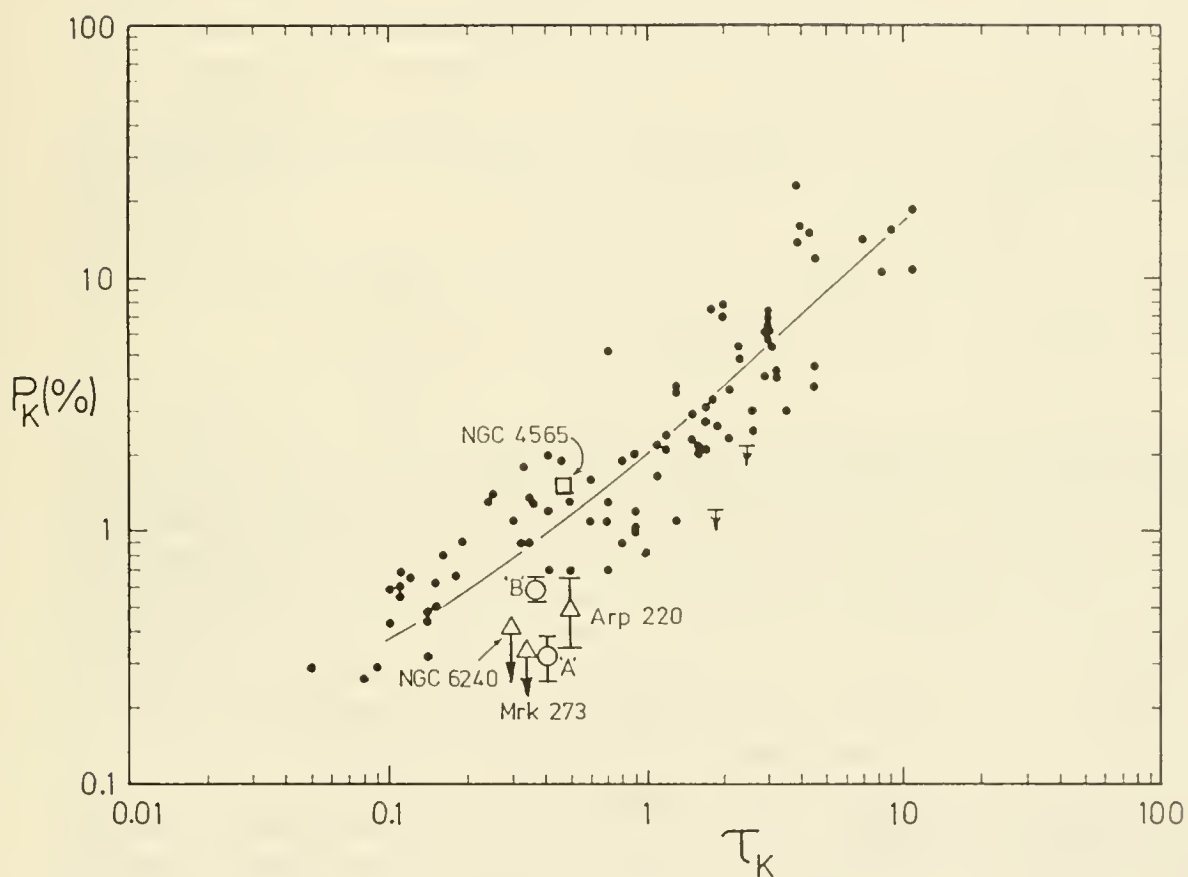


Figure 1. The relationship between interstellar polarization at 2.2um and extinction. The dots are individual stars in the Milky Way. The solid line is the model for the Milky Way from Jones (1989). The normal spiral galaxy NGC 4565 compares well with the Milky Way, but the infrared luminous galaxies and interacting galaxies are systematically weaker.

POLARIZATION IN THE LAGOON NEBULA

Marshall L. McCall and Michael G. Richer

York University
Toronto, Ontario, Canada

and

N. Visvanathan
Mt. Stromlo and Siding Spring Observatories
Canberra, A.C.T., Australia

Summary

A V-band polarimetric survey of stars associated with the Lagoon nebula has been conducted. The data have been combined with existing photometric and spectroscopic observations in order to investigate the alignment of magnetic field lines with identifiable symmetry axes and to evaluate the nature of dust in the immediate vicinity. Although stars are not in general highly polarized, electric vectors align with the minor axis of the Lagoon nebula, perpendicular to the major axis of the spatial distribution of massive stars. The observations indicate that the collapse of the molecular cloud progenitor was inhibited along directions perpendicular to magnetic field lines. Considering the low polarization efficiency and the high ratio of total to selective extinction, smaller grains of intranebular dust appear to have been destroyed.

Background

Theoretical efforts to interpret the spectra of photo-ionized gases are hampered by uncertainty about the quantity and nature of embedded dust. Internal dust affects the transfer of radiation through the nebula, thereby modifying the ionization and thermal balance everywhere. Studies of the polarization of stars in local HII regions help to determine the nature of surviving dust grains. For example, multi-colour polarimetric observations of stars embedded in the Orion nebula show that the wavelengths of peak polarization are systematically shifted redward with respect to stars outside the nebula. (McCall, M. L. 1981, *M.N.R.A.S.*, **194**, 485). Considering the constraints imposed by gas-phase metal abundances, the shift of the mean grain size may arise from preferential evaporation of the smaller grains embedded in the gas (McCall 1981).

Besides information about grains, polarimetry of stars associated with HII regions may provide some insights into the route to massive star formation. It has long been suspected that the collapse of molecular clouds is inhibited perpendicular to magnetic field lines due to the effects of magnetic pressure. Whether or not this is true might be gleaned from the degree of alignment of polarization vectors with observable symmetry axes.

For both problems, a good candidate for study is the Lagoon Nebula (M8). The nebula is especially well suited for a polarimetric study because of its association with a cluster of bright stars (NGC 6530). At least six O stars contribute to the ionization of the region. The flattened appearance of both the nebula and the zone of massive star formation suggests that the collapse of the molecular cloud progenitor was not symmetrical.

The authors have undertaken a study of the polarization of stars in the Lagoon nebula in order to study the orientation of the magnetic field lines with respect to the axis of massive star formation and to assess the effects of the environment on embedded dust. In this paper, the results of the initial V-band survey are presented.

Observations

Polarimetry of stars brighter than $V \sim 12$ in the vicinity of the Lagoon nebula was carried out over four nights using a two-channel polarimeter attached to the Australian National University 0.6 m telescope at Siding Spring Observatory. With this device it was possible to observe a source and a nearby background field simultaneously, and thereby accurately correct measurements for polarized background emission. Each night, four unpolarized standards were measured to correct for instrumental polarization, and several highly polarized standards were measured to determine the zero-point of position angles and to assess the degree of depolarization.

Observations of two K giants just in the foreground of the nebula were used to estimate the level of the foreground extinction and polarization. Both were found to be non-negligible, with $E(B - V) = 0.19$ and $P = 0.8\%$ at position angle $\theta = 79^\circ$.

Results

The polarization introduced by foreground dust is nearly perpendicular to the preferred plane of polarization for the most highly polarized stars. Once the correction is applied, the polarizations of stars in the Lagoon nebula are systematically shifted to higher values and electric vectors show a high degree of alignment (see Figure 1). Of those stars which are polarized at the three-sigma level, the electric vectors are oriented close to the minor axis of the nebular boundary (as delineated by [S II] emission) and essentially perpendicular to the major axis of the distribution of massive stars. The alignment appears to be related to local phenomena, because the the position angle of the galactic plane differs from the preferred direction by 40° . The observations suggest that the collapse of the molecular cloud progenitor was inhibited along directions perpendicular to magnetic field lines.

Applying the cluster method to classified stars in the survey sample, the ratio of total to selective extinction for dust in the immediate environment of the Lagoon nebula is 4.5. The large value confirms that the grains are on average larger in the Lagoon nebula than in the general interstellar medium. Considering that stars are not efficiently polarized even though electric vectors are highly organized, the shift in the grain size distribution may arise from preferential evaporation of the smallest particles.

The sample stars cluster around two distance moduli separated by 0.79 mag, suggesting that many stars are multiple. Neither the distance moduli nor the polarizations of Be stars differ systematically from the values for normal B stars, indicating that many of the Be classifications are in error, perhaps due to contamination by nebular emission.

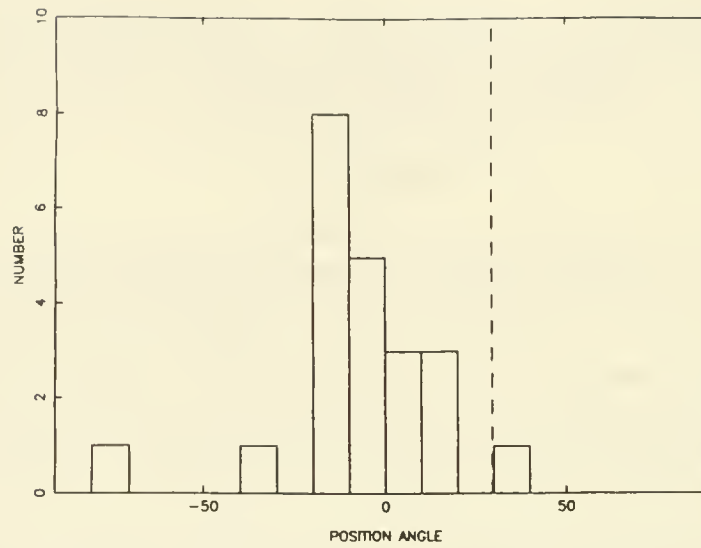


Figure 1. Histogram of position angles (in degrees east of north) for stars in the Lagoon nebula with $P/\delta P \geq 3.0$. All observations have been corrected for foreground dust. The dashed line shows the position angle of the galactic plane. The position angle of the minor axis of singly ionized sulphur emission is about 0° .

Granularity in the Magnetic Field Structure of M83

R. J. Allen^{1,2,3} and S. Sukumar²

¹Space Telescope Science Institute, Baltimore

²Department of Astronomy, University of Illinois, Urbana

³National Center for Supercomputing Applications, University of Illinois

Introduction

We have recently reported VLA 20 cm continuum polarization observations of the bright, nearly face-on southern spiral galaxy M83 (NGC 5236) at a spatial resolution of 2 kpc (Sukumar and Allen 1989). The strongest linearly-polarized emission is found in two giant arcs, with typical lengths of about 30 kpc, which are situated roughly opposite each other in the dark outer regions of the galaxy at a radius of 12 kpc from the center. These regions of high polarized intensity (and hence highly-uniform magnetic field) do not coincide with any prominent spiral-arm tracers, in contrast to the expectations of simple models for the large-scale compression of magnetic field in density-wave shock fronts. From a comparison of our data with previous results at 6 cm, we concluded that the low polarization in the central regions of the galaxy is a result of disorder in the interstellar magnetic field. The most likely cause of this disorder is the greater star formation activity observed in the inner parts of the galaxy.

The intrinsic direction of the magnetic field in the outer parts of the galaxy has also recently been determined on a length scale of 6.5 kpc from a comparison of the VLA 20 cm results with 6.3 cm observations obtained earlier with the Effelsberg telescope (Sukumar *et al.* 1989). There is very little Faraday rotation in the regions of the highly-polarized arcs of emission. The magnetic field in these polarized arcs is parallel to the general spiral arm structure seen in the usual optical tracers (dust, HII regions) in the bright inner parts of the galaxy disk. The maximum observed polarization at 2 kpc resolution is about 50%.

Higher-Resolution Observations

The VLA "D" configuration observations described in Sukumar and Allen (1989) have been supplemented with additional "B" and "C" configuration data. A total of 17.8 hours of observations were made between 1987 September and 1988 August in two 25 MHz frequency bands centered around 1452 and 1502 MHz. The combined spatial frequency coverage of the observations provided a high resolution of up to 10'' as well as remaining sensitive to structures as large as 30'.

A detailed comparison of the individual interferometer visibilities as a function of time revealed numerous differences between the signals recorded at the two adjacent frequency bands. These differences were traced to low-level intermittent correlator defects which, while they usually have little effect on the total intensity, are a serious limitation to the accurate determination of polarization. We found it necessary to reject about 20% of the data which showed inconsistencies between the two adjacent frequency bands. About 25 hours of cpu time on an Alliant FX-8 were required for this part of the data processing, which included plotting and flagging the visibility data, and initial map construction and self-calibration of the observations from each configuration separately. The NRAO AIPS software system was used for this work on the Alliant.

The final visibility data was constructed into images of the total and linearly-polarized radio emission at several different angular resolutions using the WERONG software package available on the CRAY X-MP/48 computer at the National Center for Supercomputing Applications in Illinois. Approximately one million visibility points were included in the constructions, which took a total of 2.5 cpu hours on the CRAY for further self-calibration and CLEANing to faint levels. Figure 1 shows the results of one of these constructions; maps of the 20-cm continuum intensity (Figure 1a) and linear polarisation (Figure 1b) of M83 with $10'' \times 10''$ resolution (FWHM) and $3'' \times 3''$ pixels. These two images have been extracted from larger fields of sizes 1024×1024 which were the final products of the construction. As an example, the total intensity map in Figure 1a required 2.5 million CLEAN iterations. The noise limit on the total intensity map in Figure 1a is $60 \mu Jy beam^{-1}$, and on the polarisation map in Figure 1b it is $25 \mu Jy beam^{-1}$. These maps are shown as contour diagrams with levels increasing by factors of $2^{(N/2)}$. In Figure 1b we have also shown the direction of maximum polarized intensity (the E field orientation) as vectors whose lengths are proportional to the intensity of the polarised emission. Assuming a distance of 8.9 Mpc to M83, the linear resolution in Figure 1 is 430 pc.

Discussion

Figure 1b shows that the smooth arcs of polarised emission found by Sukumar and Allen at lower resolution break up into stringy lumps or “granules” which are often still not entirely resolved. These concentrations exhibit only a weak correlation with discrete features on the periphery of the total intensity map in Figure 1a. With the increase in linear resolution from 2 kpc to 0.43 kpc, the maximum degree of linear polarization observed in the arc regions has grown from 50% to 75%; this is close to the expected theoretical maximum in the limit of a completely-aligned magnetic field.

We conclude that Figure 1b is showing us the basic structure of the ordered component of the magnetic field in M83. *This ordered component of the magnetic field is intrinsically granular*, with regions of typically a few hundred parsec in size exhibiting essentially perfectly-ordered field, separated by regions of roughly the same size (or somewhat larger) where the degree of field alignment is not high. Another remarkable feature of Figure 1b is that *the magnetic field direction is similar in neighboring granules*, in spite of the existence of disordered field between them.

Conclusions

A detailed discussion of these results is beyond the scope of this poster paper. However, while the large scale field morphology (cf. Sukumar and Allen 1989) may be adequately described by current models of galactic dynamos (e.g. Ruzmaikin *et al.* 1988), an explanation of the granular structure we have reported here will most likely require a discussion of the temporal and spatial behavior of instabilities in a multi-component magnetized interstellar medium. For further input to such models, the following features of the observations should be noted: The *direction* of the magnetic field is clearly tied to the mechanism responsible for the spiral structure in the galaxy, and; the *degree of order* of the magnetic field appears to be closely related to the turbulence in the interstellar gas.

Further analysis of these observations is in progress. We are particularly interested in the detailed correlation of the polarised emission with a number of other components, such as the total radio continuum emission, small-scale optically-visible features in the galaxy such as dust concentrations and small H II regions, and the distribution and degree of turbulence in H I, H α , and CO.

Acknowledgements

The VLA is a facility of the National Radio Astronomy Observatory, which is operated by Associated Universities, Inc. under agreement with the National Science Foundation. The image reconstructions were carried out using the facilities of the National Center for Supercomputing Applications at the University of Illinois; we thank R. Sault, M. Norman and Radha Nandakumar for their considerable help with the data processing and display of the images. SS thanks the College of Liberal Arts and Sciences of the University of Illinois for financial support. Research on the structure of galaxies at the University of Illinois is supported in part by the National Science Foundation under grant AST 87-15905.

References

- Ruzmaikin, A., Sokoloff, D., and Shukurov, S. 1988, *Nature*, **336**, 341.
 Sukumar, S. and Allen, R. J. 1989, *Nature*, **in press**, August 1989.
 Sukumar, S., Allen, R. J., and Klein, U. 1989, *Astr. Ap.*, submitted.

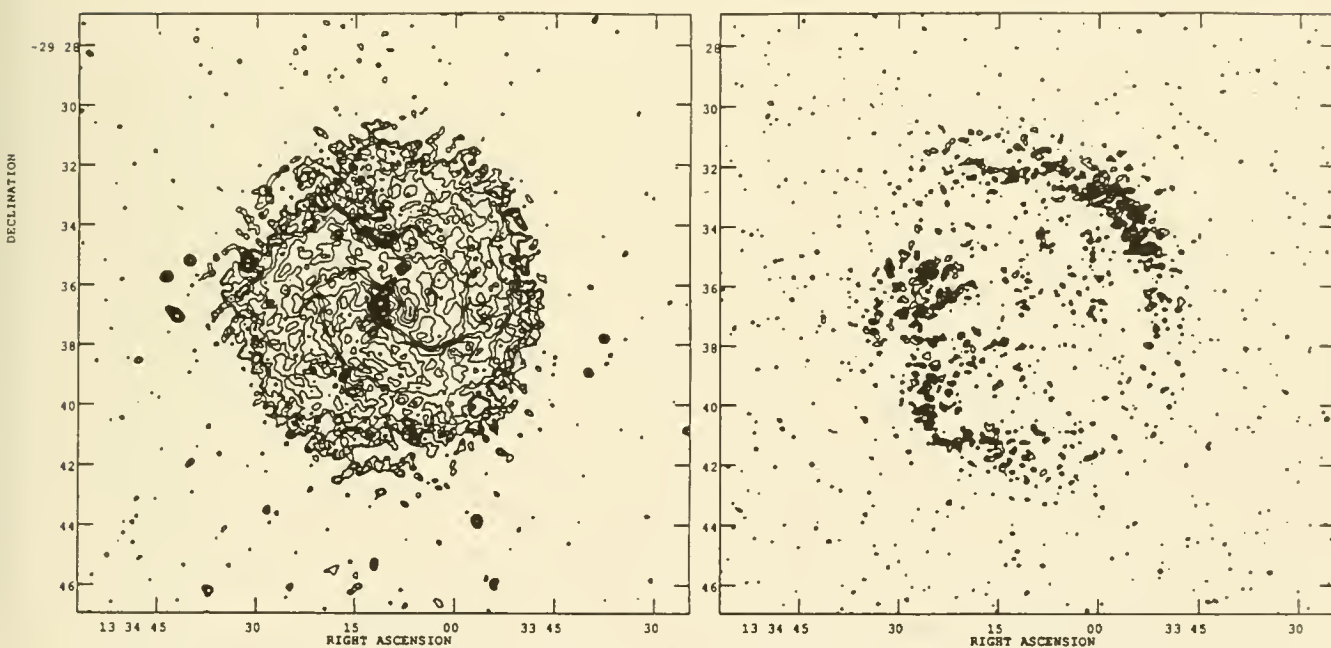


Figure 1a (left panel) Contour representation of the total radio continuum surface brightness of M83, observed with the VLA at 20 cm wavelength. Contours start at $150 \mu\text{Jy beam}^{-1}$ and increase thereafter by a factor $\sqrt{2}$. The restoring beam width is $10'' \times 10''$, and the rms noise is $60 \mu\text{Jy beam}^{-1}$.

Figure 1b (right panel) Polarized brightness of M83. The parameters are as in Figure 1a, except that the contours start at $80 \mu\text{Jy beam}^{-1}$ and the rms noise is $25 \mu\text{Jy beam}^{-1}$.

III - GAS DYNAMICS, HEATING, INTERACTIONS

B - HEATING OF THE ISM

Thermal Instabilities in Protogalactic Clouds

S. D. Murray and D. N. C. Lin (U.C. Santa Cruz)

The means by which a protogalaxy can fragment to form the first generation of stars and globular clusters remains an important problem in astrophysics. Gravitational instabilities grow on timescales too long to drive fragmentation before the background density grows by many orders of magnitude (see Murray and Lin 1989a, and references therein). Thermal instability provides a much more likely mechanism. After its initial collapse, a protogalactic cloud is expected to be shock heated to its virial temperature $\sim 10^6$ K. Cooling by H and He^+ below 10^6 K has a negative slope, so that the cloud is subject to strong thermal instabilities. Density enhancements may then grow rapidly, fragmenting the protogalaxy as it cools to lower temperatures.

Two possible outcomes exist for the final masses of the fragments resulting from thermal instability. Which will occur depends upon the importance of cooling by H_2 . Previous studies which assumed equilibrium cooling (e.g. Fall and Rees 1985) have concluded that perturbations will grow until their temperatures reach 10^4 K, at which point atomic cooling stabilizes, while the H_2 abundance is still small. This halts cooling and the growth of perturbations. The resulting temperatures and densities lead to Jeans masses in the appropriate range for proto-globular clusters.

Cooling is so efficient above 10^4 K, however, that the cooling time scale drops below the recombination time scale. Ionization fractions will therefore be significantly higher than in equilibrium, leading to much more efficient cooling. Studies which account for non-equilibrium ionization fractions (Palla and Zinnecker 1987; and Shapiro and Kang 1987) find that atomic cooling can proceed to temperatures ≈ 6000 K. The lower temperatures and higher ionization fractions increase the formation rate of H_2 above its equilibrium value. Molecular cooling can then lead to temperatures ~ 100 K. The end result may be to form a generation of primordial (Population III) stars, rather than protoclusters.

The studies above do not, however, consider the role of dynamical effects upon the growth of perturbations. This is done in the current study. The method used is similar to that used in Murray and Lin (1989a; see also the *Erratum* to appear September 15), which examined the growth of thermal instabilities with a one-dimensional Lagrangian hydrodynamics code, written for spherical symmetry. Perturbed regions therefore take the form of shells. The dynamical variables are integrated explicitly, while the temperature, ionization fraction, and molecular fraction are integrated implicitly, and account is taken for non-equilibrium values of these quantities.

Perturbations with non-negligible initial amplitudes develop large contrasts with the background protogalaxy with which they maintain pressure equilibrium. The resulting high densities enhance the formation of H_2 (assumed to form in the gas phase via H^-), which then leads to rapid cooling down to 100 K. The resulting Jeans mass is

well below the characteristic mass scales of globular clusters. These perturbations, therefore, would lead to the formation of Population III stars, not clusters.

The evolution is different only for perturbations with very small ($\lesssim 0.5\%$) initial amplitudes. They do not undergo a strong thermal instability, and so do not cool significantly ahead of the protogalaxy. They do not, therefore, develop large density contrasts with the background, leading to long formation timescales for H_2 , so that the cooling efficiency remains small. These perturbations, therefore, remain near 10^4 K, becoming density-enhanced regions in a protogalaxy of the same temperature. Their subsequent evolution depends upon whether the perturbed regions encompass more or less than a Jeans mass ($\sim 10^7 M_\odot$). In the former case, the condensation will continue to contract, while it will re-expand in the latter case. Either motion will occur on a dynamical timescale for the perturbed region, $\sim 10^{15}$ s. This timescale is sufficiently long that the protoclusters resulting from this evolution will be subject to contamination by a first generation of massive stars, after which they will evolve to form stars as discussed by Murray and Lin (1989a,b). The large Jeans mass would lead to difficulty forming bound stellar clusters. Cooling by contaminating metals may, however, reduce the Jeans mass significantly.

As discussed by Fall and Rees (1985), photodissociation of H_2 , or photoionization of H^- by hard photons from the background gas, hot stars, or an active galactic nucleus can also act to prevent cooling below 10^4 K, and therefore enhancing the formation of protoclusters relative to stars. Which process will dominate, and the necessary luminosity, depends upon the spectrum of hard photons. A broad spectrum, where much of the energy is at lower energies, near the maximum of the H^- cross section, will lead to photoionization of H^- being the dominant process. The critical luminosity for this process to reduce the H_2 abundance below that necessary for further cooling is $\sim 10^{43}$ ergs s^{-1} . If the spectrum is concentrated at higher energies, photodissociation will dominate, and the critical luminosity is $\sim 10^{45}$ ergs s^{-1} . The role of high energy photons may form an explanation for the observed variation of the specific frequency of globulars with galactic environment, being higher for galaxies in rich clusters, where x-ray heating at early times would be expected to be more important.

References

- Fall, S. M., and Rees, M. J. 1985, *Ap. J.*, **298**, 18.
Murray, S. D., and Lin, D. N. C. 1989, *Ap. J.*, **339**, 933.
Murray, S. D., and Lin, D. N. C. 1989, *Ap. J.*, in press.
Palla, F., and Zinnecker, H. 1987, in *Starbursts and Galaxy Evolution*, ed. T. X. Thuan, T. Montmerle, and J. T. Thanh Van (Gif Sur Yvette: Editions Frontières), p. 533.
Shapiro, P. R., and Kang, H. 1987, *Ap. J.*, **318**, 32.

High Brightness Neutral Hydrogen in M31: A New Probe of Interstellar Pressure ?

Robert Braun, NRAO, Socorro and NFRA, Dwingeloo

Rene Walterbos, University of California, Berkeley

An observational parameter of our own Galaxy, the peak brightness temperature of neutral hydrogen in emission, was determined almost twenty years ago (Burton 1970). This quantity, although possessing a degree of local variations, has a remarkably consistent peak value of 125 K towards spiral arm segments with a few isolated peaks extending to 135 K, once sufficient spatial and velocity resolution are used (≤ 70 pc, ≤ 5 km/s) to resolve the emission peaks. The higher spatial and velocity resolution of more recent surveys has not led to the detection of higher brightnesses. For many years this remarkable observational result has received little attention, primarily because similar data for other galaxies, which would allow a meaningful comparison and analysis, did not exist. Recently this situation has changed. A Westerbork survey of M33 (Deul and Van der Hulst 1987, and private comm.) with 40 pc x 8 km/s resolution has revealed consistent peak values of only 95 ± 5 K (although there is still some question of whether the velocity resolution was sufficient in this case), while a VLA survey of M31 (Braun 1989a) with 35 pc x 5 km/s resolution has shown consistent peak values but at a temperature of 155–165 K. It has become clear that although peak HI brightness seems to be a well-defined quantity within individual galaxies (with a degree of local variation) there are very significant differences in this quantity amongst different galaxies.

A complex interplay of processes is thought responsible for determining the kinetic temperature of HI (e.g. Draine, 1978; Kulkarni and Heiles, 1988) with the dominant cooling due to collisional excitation of heavy elements by H atoms and heating due to photoelectric emission from dust grains. Steady-state temperature calculations, as depicted in Figure 7 of Draine (1978), illustrate the stable ISM phases (where the curves have slope < 1) at about 10^4 K and between some 10's and 100's K depending on p/ζ , the ratio of gas pressure to effective primary ionization rate. These calculations show that the steady-state gas temperature depends upon the metallicity, grain depletion, ionization rate and gas pressure. Somewhat counter-intuitively, gas temperatures are expected to be lower for higher pressures and/or lower ionization rates such as might be expected in evolved star-forming complexes where the most luminous stars have already become supernovae, adding pressure but diminishing (after the first $\sim 10^4$ years) the ionizing photon flux. While there appear to be a large number of variables and time-dependant phenomena may also play an important role, all of these quantities are in fact related to each other by the current and previous rates of massive star formation. Such a parameterization may simplify the dependancies illustrated Draine's Figure 7. For the purposes of illustration the three data points noted above can be plotted on the "average depletion" curve in this figure (even though the dust properties of M33 are likely to be rather different than for M31 or the Galaxy). The galactic value corresponds to a value of $\log p/\zeta = 2.82$ in reasonable agreement with the best available estimates of about 2.7 (e.g. Kulkarni and Heiles 1988). The values for M33 and M31 correspond to $\log p/\zeta = 3.26$ and 2.68 respectively. This ranking in $\log p/\zeta$ reflects the relative star formation rates in the three galaxies. Although some improved calculations of dust heating of gas have now been done (e.g. Lepp and Dalgarno, 1988), a complete analysis incorporating the developments of the last ten years is still lacking. The relationship between HI kinetic temperature and observed brightness temperature in emission is also nontrivial in general, since it depends on the distribution of opacity and temperature occurring along the line of sight. However, the observed galactic values of peak HI emission are consistent with the upper envelope of optically thick kinetic temperatures (cf. Payne, Salpeter and Terzian 1983) so that it may be possible to relate these quantities in regions where column densities are sufficiently high.

A number of important points are illustrated in Figure 1 presenting small portions of the extensive database that has been assembled by our team to study M31 (VLA HI: Braun 1989a; VLA 20cm continuum: Braun 1989b; KPNO H_α , [SII], B and R: Walterbos and Braun 1989; INT TAURUS H_α : Brinks, Unger and Braun 1989). A region about 2 kpc on a side with major and minor axis coordinates (X,Y) as indicated is shown in [SII] (6716+6731), H_α , and 20 cm continuum on the left and in integrated HI and peak HI brightness on the right. All images are shown at an identical resolution of 10 arcsec. Optically this field is dominated by the giant (about 300 by 250 pc) HII region

complex at $X = 40.8$, $Y = -6.8$ which is a part of region 775 in the list of Pellet et.al (1978) with observed luminosities of 1.51 ± 0.07 and $0.49 \pm 0.02 \times 10^{38}$ erg s⁻¹ in H α and [SII] respectively. The contour levels and grey-scale of the [SII] image were chosen to be exactly half those used in H α so that regions which appear similar in the images have the ratio 0.5. Compact HII regions and condensations can be seen to have a ratio in the range 0.1 to 0.3, while the region of diffuse ionized gas between $42' < X < 44'$, and $-10' < Y < -3'$ has a very consistent ratio of 0.5 (see also Walterbos and Braun, these proceedings). A newly discovered supernova remnant (SNR) with ratio > 1 can be seen at $X = 45.4$, $Y = -5.2$. The radio continuum image shows discrete counterparts for some of the HII regions and SNR in the high resolution contours. However, the underlying low resolution (60 arcsec) grey-scale highlights the diffuse (primarily) non-thermal radio emission. The diffuse radio surface brightness in this region corresponds to minimum energy magnetic fields of a few μ G. This component is very well correlated with the diffuse ionized gas seen in H α and [SII] with the same suggestion of a diagonal edge running from $(X,Y) = (42,-10)$ to $(X,Y) = (44,-6)$. Integrated HI in this region shown at top right shows values in the range 1500 to 5500 K km s⁻¹ but relatively little structure that reflects the vigorous star formation activity. The peak HI brightness shown at center right on the other hand has values between 60 and 140 K and shows a clear anti-correlation with the ionized gas. In particular, the diagonal edge noted above is well-defined and forms one edge of the low-peak-temperature "cavity" in which the entire ionized/synchrotron complex is embedded. The anti-correlation of peak HI brightness with H α emission is very general, both on scales of 100's of pc and of kpc's. The highest observed HI brightnesses of 140–180 K are concentrated near $(X,Y) = (50,2)$ a gas-rich local minimum in current star formation activity within the so-called 10 kpc ring.

These tantalizing results have prompted us to embark on an observational program directed at a sample of 11 nearby galaxies: NGC 55, 247, 7793, 3031, 2366, 2403, 4236, 4826, 4736, 4244, and 5457. We hope to determine the gas properties and phases as a function of both galaxy type and position within the galaxies utilizing high resolution HI observations and optical narrow band imagery and spectroscopy which are now underway.

Braun, R. 1989a, Ap.J.Suppl. submitted

Braun, R. 1989b, Ap.J.Suppl. submitted

Brinks, E., Unger, S. and Braun, R. 1989, Ap.J.Suppl. in prep.

Burton, W.B. 1970, Astr.Ap.Suppl. **2**, 261.

Deul, E.R. and Van der Hulst, J.M. 1987, Astr.Ap.Suppl. **67**, 509.

Draine, B.T., 1978 Ap.J.Suppl. **36**, 595.

Kulkarni, S.R. and Heiles, C. 1988 in *Galactic and Extragalactic Radio Astronomy*, ed. Kellerman and Verschuur, Springer-Verlag, New York.

Lepp, S. and Dalgarno, A. 1988, Ap.J. **335**, 769.

Payne, H.E., Salpeter, E.E. and Terzian, Y. 1983, Ap.J. **272**, 540.

Pellet, A., Astier, N., Viale, A., Courtes, G., Maucherat, A., Monnet, G. and Simien, F. 1978, Astr.Ap.Suppl. **31**, 439.

Walterbos, R.A.M. and Braun, R., 1989, Ap.J.Suppl. in prep.

Fig. 1a-e.—Phases of the ISM in a 2 kpc square region of M31. Coordinates are major and minor axis coordinates (but labeled galactic latitude and longitude), with north-east to the right, in units of arcminutes. **a.** Contours of [SII] surface brightness (smoothed to 10") at (-1, 1, 2, 4, 8, 16, 32 and 64) times 1.66×10^{-17} erg cm⁻² s⁻¹ arcsec⁻² on a linear grey-scale from 0 to 8.3×10^{-17} erg cm⁻² s⁻¹ arcsec⁻². The sampled region is enclosed in dashed lines. **b.** Contours of H α surface brightness (smoothed to 10") at (-1, 1, 2, 4, 8, 16, 32 and 64) times 3.32×10^{-17} erg cm⁻² s⁻¹ arcsec⁻² on a linear grey-scale from 0 to 16.6×10^{-17} erg cm⁻² s⁻¹ arcsec⁻². The sampled region is enclosed in dashed lines. **c.** Contours of λ 20 cm continuum emission (smoothed to 10") at (-1, 1, 2, 4, 8 and 16) $\times 150 \mu$ Jy/10" beam on a linear grey-scale (smoothed to 60") from 0 to 2 mJy/60" beam. **d.** Contours of integrated HI at 3000 and 4000 K km s⁻¹ on a linear grey-scale from 1650 to 3950 K km s⁻¹. **e.** Contours of the peak HI brightness (10" \times 5 km/s resolution) at 60–140 K in steps of about 20 K on a linear grey-scale from 50 to 100 K.

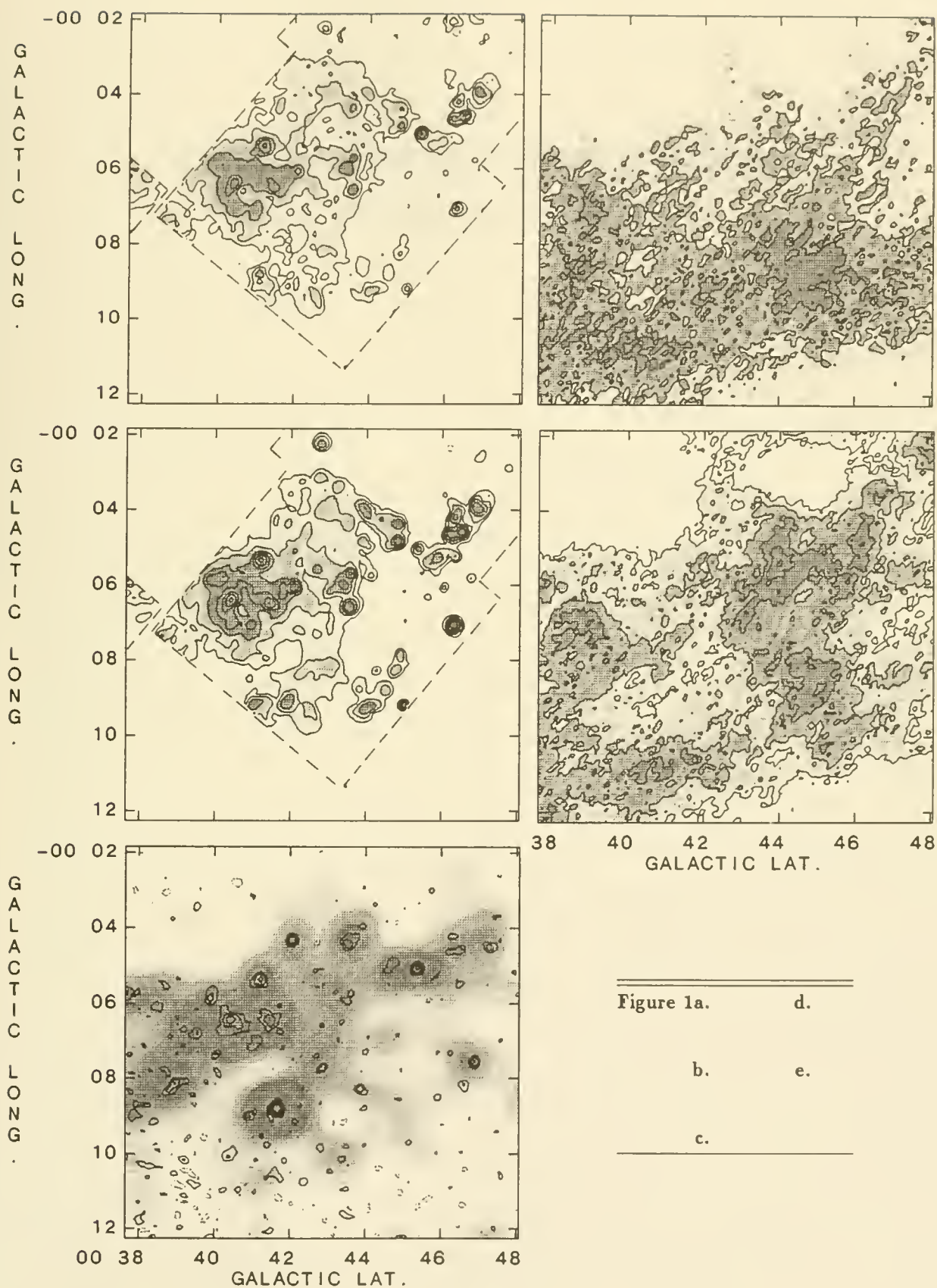


Figure 1a. d.

b. e.

c.

III - GAS DYNAMICS, HEATING, INTERACTIONS

C - INTERACTING GALAXIES

CO observations of southern mergers

F. Casoli, C. Dupraz, F. Combes

Radioastronomie, Ecole normale supérieure

24, rue Lhomond, F-75231 Paris Cedex 05, France

1. Introduction

There are good reasons to believe that the formation of some elliptical galaxies result from the merging of two disk galaxies, as Toomre and Toomre first suggested (1972, *Ap. J.* **178**, 623). Such a process strongly enhances the star-formation activity of the system, thus consuming its molecular gas. This might account for the low cold-gas content of elliptical galaxies compared to that of spirals. We present here CO(1-0) and CO(2-1) observations of a sequence of three objects, NGC 1614, NGC 3256, and NGC 7252, that present characteristic features of merger remnants: single body and extended tidal tails. NGC 3256 and 7252 even exhibit the $r^{1/4}$ radial light distribution that is the signature of elliptical galaxies, which indicates that their stellar bodies are in late stages of relaxation.

Both NGC 1614 and NGC 3256 undergo extended bursts of star formation revealed by their large far-infrared luminosities, and by the presence in the near-infrared spectrum of the $3.28\ \mu\text{m}$ feature (Morwood: 1986, *A. A.* **166**, 4) attributed to polycyclic aromatic hydrocarbons. On the other hand, NGC 7252 has a milder activity of star formation, as suggested by a lower infrared luminosity, and thus seems to have gone past the starburst phase.

2. Observations

The CO data were collected with the Swedish-ESO 15 m Submillimeter Telescope (SEST) (beamsize = $43''$ at 115 GHz, $23''$ at 230 GHz). For NGC 7252, we have only observed the central position in $^{12}\text{CO}(1-0)$. The spectrum is displayed on Figure 1 together with an HI spectrum obtained with the Nancay radiotelescope. We have mapped NGC 1614 and NGC 3256 in $^{12}\text{CO}(1-0)$ and $^{12}\text{CO}(2-1)$, and also observed the nucleus of NGC 3256 in $^{13}\text{CO}(1-0)$. The various CO spectra obtained towards the nuclei of both galaxies are presented in Figure 3. Characteristics of the galaxies are gathered below, with luminosities and masses in solar units and temperatures in Kelvins.

Name	L_{IR}	L_{B}	$M(\text{H}_2)$	$L_{\text{IR}}/L_{\text{B}}$	$L_{\text{IR}}/M(\text{H}_2)$	$T_{60/100}$
NGC 1614	$2.7\ 10^{11}$	$2.5\ 10^{10}$	$6.7\ 10^9$	11	40	52
NGC 3256	$2.4\ 10^{11}$	$4.5\ 10^{10}$	$16.2\ 10^{10}$	5	19	45
NGC 7252	$3.9\ 10^{10}$	$4.7\ 10^{10}$	$4.2\ 10^9$	0.8	9	38

3. Results and discussion

- The CO(1-0) emission of NGC 1614 and NGC 3256 is barely resolved by the 43" beam. In both objects, its full width at half maximum is about 7 kpc, after deconvolution of the beam. In NGC 7252, the CO emission is likely diluted in the beam (Dupraz *et al.*: 1989, submitted to A. A.).
- Using a conversion factor of $2.3 \cdot 10^{20} \text{ cm}^{-2} (\text{K km s}^{-1})^{-1}$ from $^{12}\text{CO}(1-0)$ emissivities to $\text{N}(\text{H}_2)$ column densities, we derive molecular masses of $M(\text{H}_2) = 6.7 \cdot 10^9$, $1.6 \cdot 10^{10}$ and $3.6 \cdot 10^9 M_\odot$ for NGC 1614, 3256 and 7252 respectively [NGC 7252 also contains $3.4 \cdot 10^9 M_\odot$ of atomic gas].
- In NGC 1614 and NGC 3256, the ratio of CO(2-1) to CO(1-0) integrated emissivities is about 1.2, in the main-beam temperature scale. This indicates that the molecular gas is not predominantly optically thin. In NGC 3256, the $^{13}\text{CO}(1-0)$ line is about 30 times weaker than the $^{12}\text{CO}(1-0)$ line, which suggests that the CO emission is not very optically thick either. Although definite conclusions cannot be drawn from such large scale observations, this situation appears intermediate between that of most spirals, where the $^{12}\text{CO}(1-0)$ optical depth is large, and that of starburst nuclei like M82's where it is smaller than one. Accordingly, the molecular masses derived above, by use of the standard conversion factor, may be somewhat overestimated.
- NGC 1614 and NGC 3256 are very actively star-forming mergers. Such objects are known to possess large amounts of molecular material. NGC 7252 is a more intriguing object, for this rather old merger remnant no longer experiences a starburst, and yet is still gas-rich. This shows that, at least in some cases, the star burst is unable to exhaust all of the molecular gas of the system, and that long-term processes, such as an activity of star formation typical of spiral galaxies, are required if the merger remnant is to become a normal elliptical galaxy, nearly devoid of cold gas.

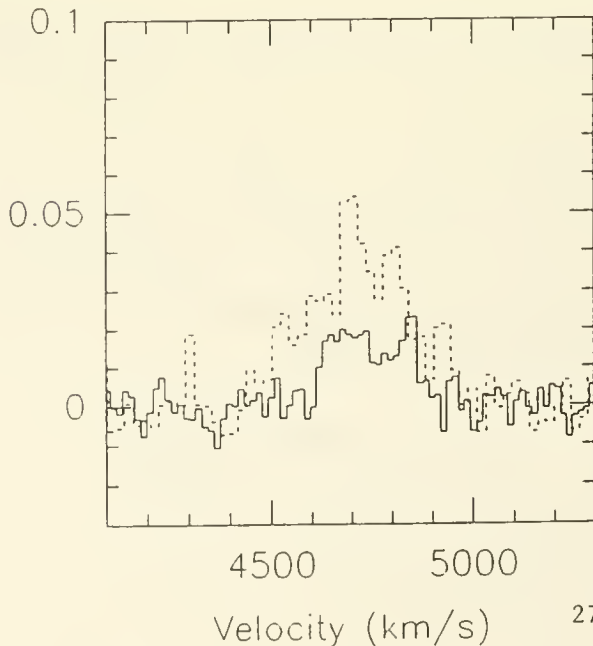


Figure 1: $^{12}\text{CO}(1-0)$ and HI spectra of NGC 7252; temperature scale is T_R^* .

Figure 2: left: isocontours of $^{12}\text{CO}(1-0)$ integrated emissivity for NGC 1614, levels are 1.5 (1.5) 7.5 K km s^{-1} ; right: same for NGC 3256, levels are 2.5 (5) 47.5 K km s^{-1} .

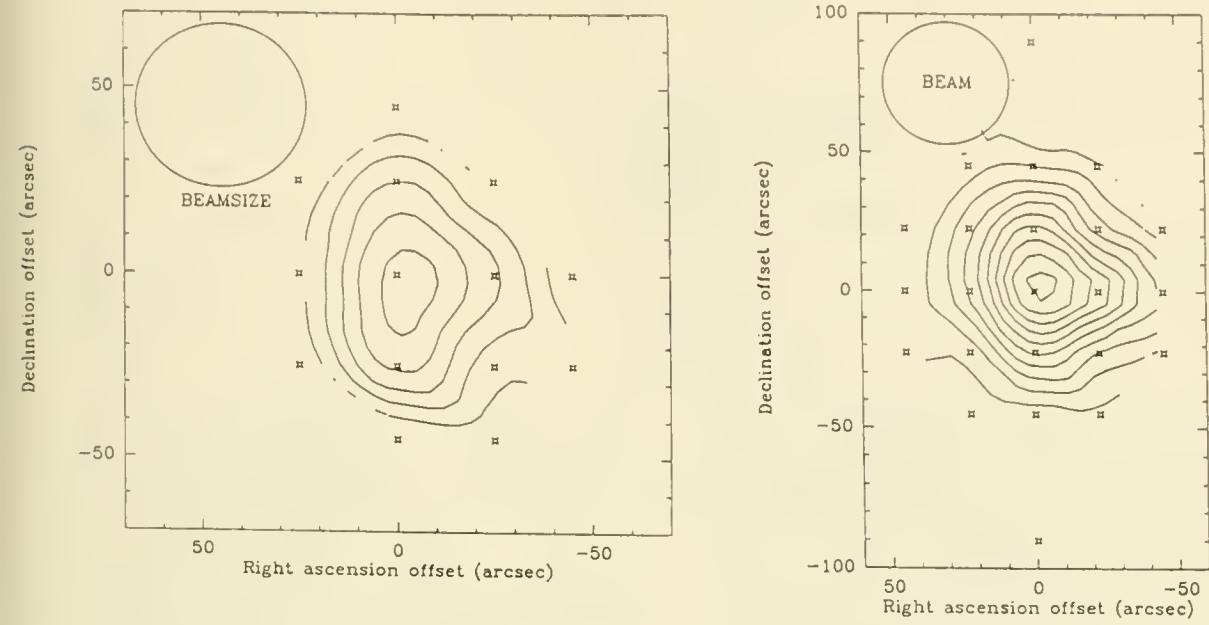
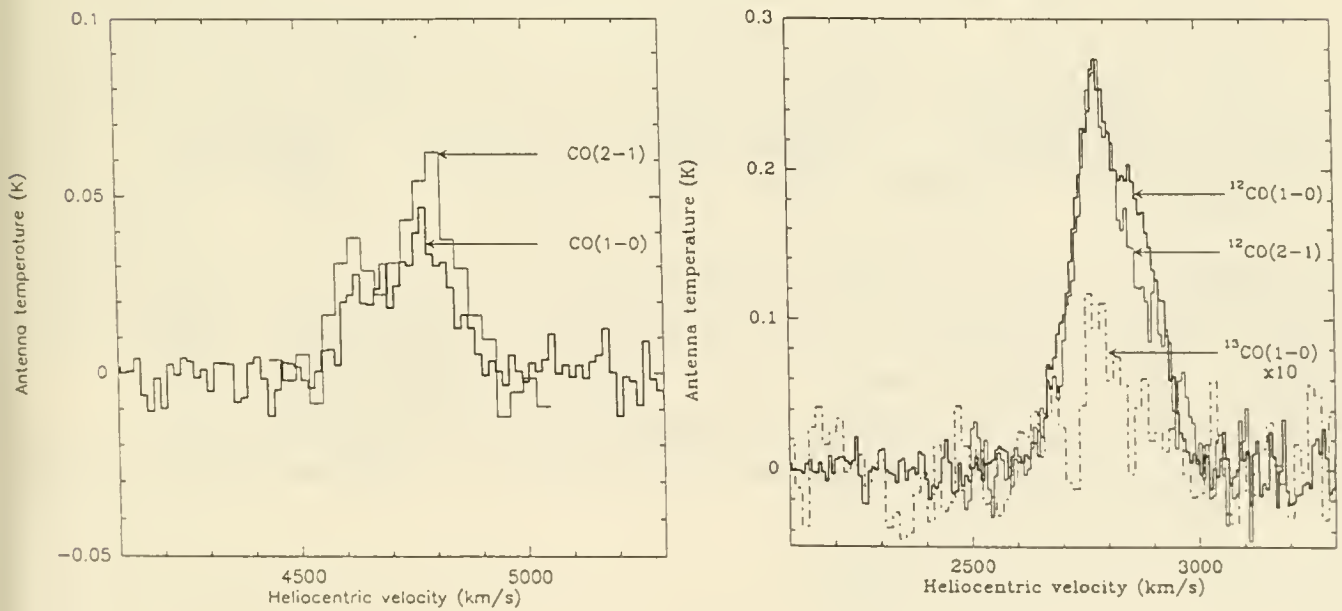


Figure 3: left: central $^{12}\text{CO}(1-0)$ and $^{12}\text{CO}(2-1)$ spectra of NGC 1614; right: same for NGC 3256, together with the $^{13}\text{CO}(1-0)$ spectrum multiplied by 10.



STAR FORMATION ON THE LEADING EDGE OF A RING-LIKE DENSITY WAVE IN

ARP 143.

P.N.Appleton ,
Astronomy Program,
Dept. of Physics,
Iowa State University,
Ames, IA 50011 .

INTRODUCTION

NGC2445 is a member of the pair of interacting galaxies Arp143 (=VV117) and has been classified as an irregular ring galaxy by de Vaucouleurs et al.(1976). Although not obviously a classical ring galaxy from its optical appearance, it nevertheless shows many of the symptoms of a collisional off-centre ring galaxy in the early stages of development. Optically the galaxy shows a rough ring of super-giant HII regions distributed asymmetrically with respect to the nucleus with most of the emission concentrated on the western side of the galaxy. We have mapped the HI emission in this system (with F.Ghigo and J. van Gorkom ; NRAO) and the observations show that the disk of NGC2445 is characterised by a large-scale banana-shaped HI wave with its peak to the west of the nucleus (See Fig.1a,b). Near-IR imaging (with E.I.Robson and A.J. Adamson; Lancs. Polytechnic, U.K.) demonstrates that, like the HI, the underlying population of old stars is very asymmetrically distributed with the bulk of the stars concentrated to the western side of the galaxy.

DISCUSSION

The multi-waveband approach to the study of this fascinating galaxy pair has revealed some surprising results. On the large scale, the HI observation have shown the presence of a gigantic HI plume extending from Arp 143 some 150 kpc to the north. CCD observations of Arp 143 (with J. Schombert; U.Michigan) have shown that the HI plume has a faint optical counterpart near its base. The plume may be the result of a head-on collision between a gas-rich dwarf disk system and NGC2445, resulting in scattered HI/stars to the north and a ring-like wave in the disk of NGC2445 (See Appleton et al 1987 and in prep.).

Hydrodynamic models of the gas response to such a collision show the development of a banana-shaped wave within the disk of the perturbed galaxy which expands with time to become an irregular ring (See Appleton and Struck-Marcell 1987, hereafter ASM; Struck-Marcell and Appleton 1987, hereafter SMA). The HI emission associated with the disk of NGC2445 shows precisely the distribution one would expect for the early development of an off-centre ring galaxy. The fact that the HI is seen in a rough banana-shaped rather than a complete ring

suggests that the ring is just developing. Indeed the regions of intense starformation are found on the LEADING EDGE of the banana-shaped wave where the HI contours change the most rapidly. These supergiant HII regions do not form a complete ring-like structure but appear as a set of clumps of intense emission. Radio-continuum emission is also concentrated on the western side of the galaxy where the optical HII regions dominate.

If the HI distribution is indeed the result of an off-centre collision which has induced a wave in the disk, then it should also be observable as a stellar wave. However the optical appearance of the disk is dominated by the young stellar population. We therefore observed the disk of the galaxy at J(1.25 m) H(1.65 m) and K(2.2 m) in the near-IR using the IRCAM array on UKIRT. K-band is well suited to the study of the morphology of the underlying evolved stellar population. The image (Fig 2) shows strong emission from the HII regions (probably from the supergiant population associated with recent starformation) in addition to much more extended emission from the underlying disk. In particular, a fainter ring-like component is observed which is spatially coincident with the brighter HI emission and we associate this with the density wave. The K-band surface brightness in this faint feature has a 2:1 over-density with respect to the unperturbed disk. This is consistent with the overdensity seen in the HI wave of $> 1.5:1$, the limit being due to the lower spatial resolution of the HI observations.

Numerical models of star formation in ring galaxies (ASM; SMA) have predicted both the shape of the HI and faint K-band wave as well as the rarefaction behind the wave which is best seen in the HI surface density map (Fig.1). Unlike conventional density wave models of star formation, the above models produce star formation by cloud-cloud collisions. These collisions are found to be intense on the OUTER edge of the expanding density wave. The normally stable equations governing the star formation properties of the ISM in the galaxy are driven out of equilibrium in the expanding wave. If the assumption is made that star formation is a threshold effect, dependant upon principally the mean mass of clouds in the wave, then strong "starbursts" can occur as the wave drives collisions in the LEADING edge of the wave. It would appear that in Arp 143, star formation occurs on the leading-edge of the wave where the collisions between clouds would be expected to be the most intense, rather than on the down-stream side of the density wave. The latter would be expected on the conventional density wave picture where star formation is caused by gas shocking as it falls into the potential well of the wave. Perhaps the clumpy nature of the HII regions in Arp143 is a result of slight irregularities in the original disk which have led these parts to cross the "starburst" threshold earlier than the rest of the wave-front. If so, then Arp 143 will soon turn-on along the whole wave-front, as more of the wave crosses the density threshold, causing it to become a true ring galaxy.

References

- Appleton, P.N., Ghigo, F.D., van Gorkom, J.H., Schombert, J.M. 1987., *Nature*, 330, 140. (& 330, 500).

de Vaucouleurs, G., de Vaucouleurs, A., & Corwin, H.G., 1976. Second Reference Catalogue of Bright Galaxies. Austin, Texas.
 Appleton, P.N. & Struck-Marcell, C., 1987. Ap.J., 318, 103. (ASM)
 Struck-Marcell, C. & Appleton, P.N., 1987. Ap.J., 323, 480. (SMA)

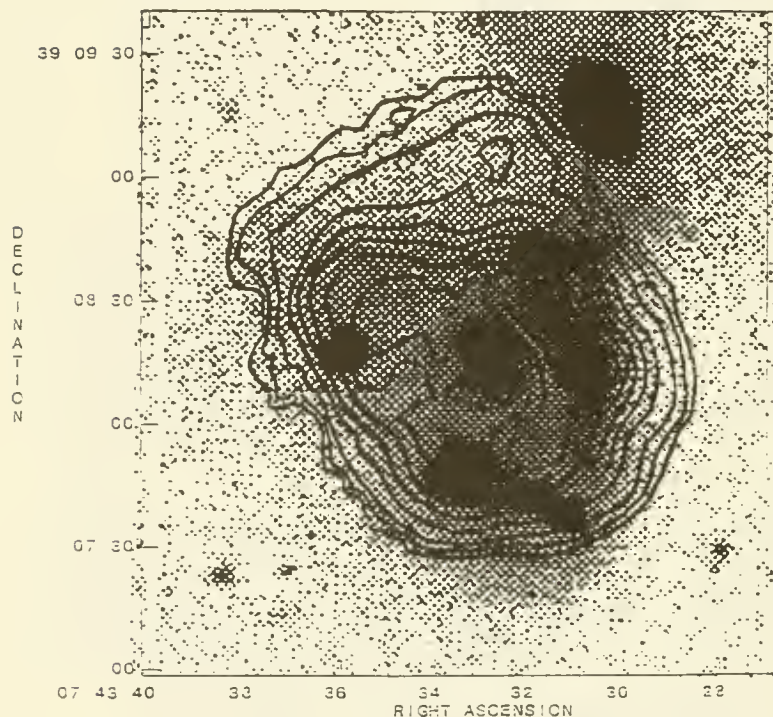


Figure 1a

CONTOURS OF HI SURFACE DENSITY SUPERIMPOSED ON THE B-BAND CCD IMAGE OF ARP 143. HI contours are 3.8, 7.6, 15 $\times 10^{19}$ at/cm², and thereafter in intervals of 1.5 $\times 10^{20}$ at/cm². Major starformation occurs in regions where the HI column densities are in excess of 5 $\times 10^{20}$ at/cm².

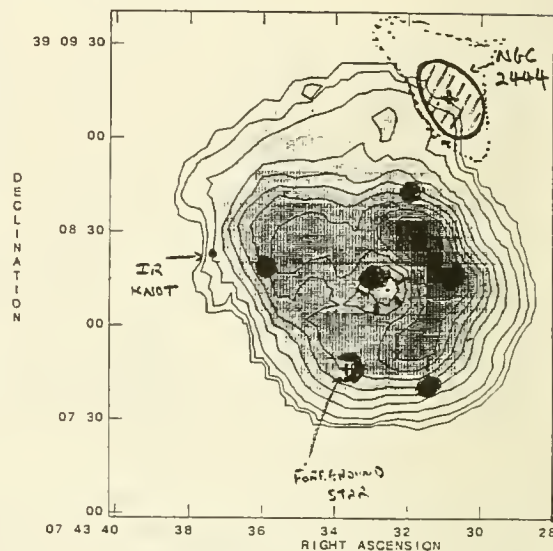


Figure 1b (Showing centres of the optical knots).



Fig.2 Near-IR K-band image of Arp 143

A Multi-Wavelength Study of the Peculiar Galaxy NGC 2976

L. J. Tacconi (NFRA/Dwingeloo)

J.M. van der Hulst, and P.R. Wesselius (Univ. of Groningen)

NGC 2976, a companion galaxy of M81, is a nearly edge-on system with no obvious spiral structure. In a spectrophotometric study of this system Carozzi-Meysonnier (1980) found that NGC 2976 has a small mass of $2 \times 10^9 M_{\odot}$ and low luminosity of $4.2 \times 10^8 L_{\odot}$, which places it among the latest types of disk systems. Low resolution ($12''$) HI observations (Appleton, Davies, and Stephenson 1981) indicate the presence of an HI tail connecting this galaxy with M81.

It has been suggested that interactions which occur among galaxies trigger bursts of star formation (*e.g.* Toomre and Toomre 1972, Larson and Tinsley 1978). Indeed, enhanced star formation has been observed in interacting systems by Hummel (1981) who found a correlation between the presence of tidal interaction and radio continuum flux, by Soifer *et al.* (1984), who found a similar correlation with high far-infrared flux, and by Kennicutt *et al.* (1987) who found enhanced star formation rates in a complete sample of interacting galaxies using H α and IRAS data. In addition, molecular clouds are the potential sites for future star formation, and many galaxies which exhibit strong CO emission, such as M82, M51, IC342, and NGC 4321, are members of groups or clusters of galaxies.

We are currently studying NGC 2976 at many wavelengths to investigate the extent to which an interaction with M81 may have affected the star formation history of this galaxy. Here, we present observations of NGC 2976 made at 50μ with the high resolution CPC instrument onboard IRAS, at 21-cm (both HI line and radio continuum) with the WSRT, and in the H α line (kindly taken for us at the KPNO 36" by J. Young, L. Allen, and S. Kleinmann). The far infrared emission is not centrally peaked as in other spirals (*e.g.* Wainscoat *et al.* 1987), but has obvious intensity peaks near the ends of the disk. The ionized gas as inferred from the H α observations, is largely confined to two large, symmetrically placed emission regions near the ends of the disk. Finally, the HI and 21-cm radio continuum emission also exhibit this strongly, double peaked structure. At all of the above wavelengths the emission peaks are roughly coincident and lie $\sim 1.2''$ to the NW and $\sim 1.1''$ to the SE of the optical center of this galaxy.

Figure 1 shows the FIR, HI, radio continuum, and H α maps of NGC 2976. The bi-modal distribution of the recent massive star formation and of the neutral interstellar medium is in contrast with that seen in blue and red images of NGC 2976 (Carrozzzi-Meyssonier 1980, and present investigators) which are not dominated by large concentrations at these positions, but show a smooth distribution, with HII regions scattered throughout the disk. The symmetric location of the peaks with respect to the nucleus of NGC 2976 suggests that they have a dynamical origin. A possible explanation is that these peaks are hot spots located at the ends of a bar. However, a velocity field, derived from the HI data, shows no signature of the presence of such a bar.

In each of the two large emission regions of NGC 2976, peak column densities of 1.6×10^{21} atoms cm^{-2} are observed in HI. Each region contains more than $3.5 \times 10^7 M_{\odot}$ of atomic gas over a $\sim 1 \times 1$ kpc region. Combined, these two regions contain more than half of the HI which we have observed in this galaxy. More than 20% of the total H α flux of the galaxy comes from the northwest complex, with an integrated flux of $\sim 1.8 \times 10^{-12}$ erg cm^{-2} s^{-1} . The southeast complex is somewhat fainter, with an integrated flux of 1.0×10^{-12} erg cm^{-2} s^{-1} . Although the large HII complexes dominate the H α emission from NGC 2976 and are unusual for a low mass galaxy, they are not unlike giant HII regions found in nearby luminous spiral galaxies such as M51 (van der Hulst *et al.* 1988).

REFERENCES

- Appleton, P.N., Davies, R.D., and Stephenson, R.J. 1981, *Astron. Astrophys.*, **92**, 189.
Carozzi-Meysonnier, N. 1980, *Astron. Astrophys.*, **92**, 189.

Hummel, E. 1981, *Astron. Astrophys.*, **96**, 111.

Kennicutt, R.C. Jr., Keel, W.C., van der Hulst, J.M., Hummel, E., and Roettiger, K.A. 1987, *A.J.*, **93**, 1011.

Larson, R.B. and Tinsley, B.M. 1978, *Ap.J.*, **219**, 46.

Soifer, B.T., Rowan-Robinson, M., Houck, J.R., de Jong, T., Neugebauer, G., Aumann, H.H., Beichman, C.A., Boggess, N., Clegg, P.E., Emerson, J.P., Gillett, F.C., Habing, H.J., Hauser, M.G., Low, F.J., Miley, G., and Young, E. 1984, *Ap.J. (Lett.)*, **278**, L71.

Toomre, A. and Toomre, J. 1972, *Ap.J.*, **178**, 623.

van der Hulst, J.M., Kennicutt, R.C., Crane, P.C., and Rots, A.H. 1988, *Astron. Astrophys.*, **195**, 38.

Wainscoat, R.J., de Jong, T., and Wesselius, P.R. 1987, *Astron. Astrophys.*, **181**, 225.

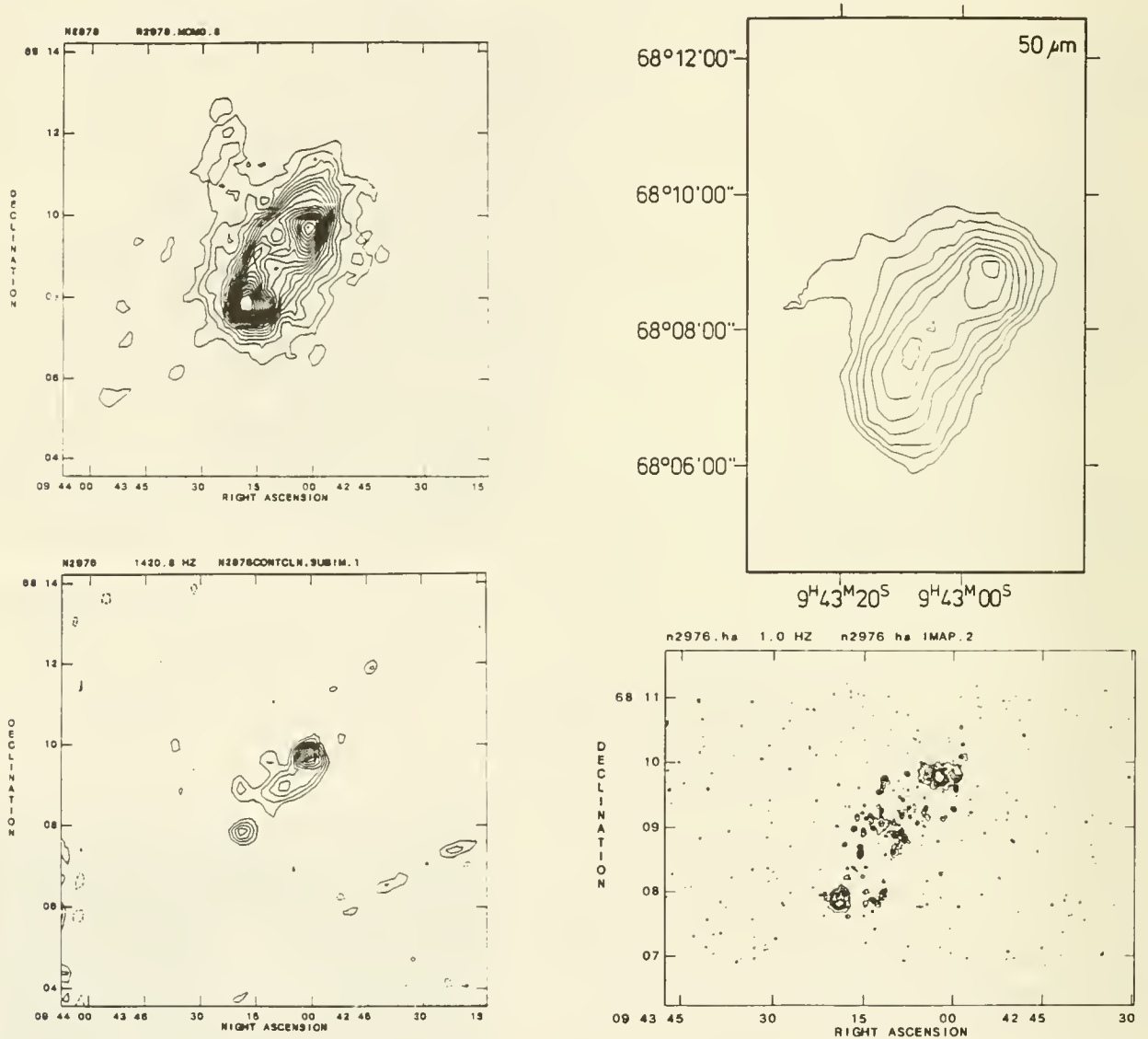


Figure 1: Contour maps of the HI (upper left), 50 μ (upper right), 21-cm radio continuum (lower left), and H α (lower right) images of NGC 2976. In each case, the lowest contour level is 3σ , with levels increasing in 1σ steps. The resolution of the HI and 21-cm continuum data is $22''$, and that of the 50 μ image is $\sim 80''$.

THE MORPHOLOGY-DENSITY RELATION FOR DWARF GALAXIES

H. C. Ferguson¹ and A. Sandage^{1,2}

¹The Johns Hopkins University, ²The Observatories of the Carnegie Institution of Washington

ABSTRACT

The morphology-density relation is examined for dwarf galaxies with absolute magnitudes $-18 \leq M_{B_T} \leq -12.5$, based on a deep photographic survey of nearby groups and clusters of galaxies. The following results are presented: 1) Compared to dwarf ellipticals, dwarf irregulars form a more extended population in nearby clusters, and may in fact be entirely absent from the cluster cores. 2) The spatial distribution of dwarf ellipticals in clusters depends on luminosity and the presence or absence of nucleation. Nucleated dE's and non-nucleated dE's fainter than $M_{B_T} \sim -13.5$ are concentrated toward the centers of clusters like the giant E and S0 galaxies. In contrast, non-nucleated dE's brighter than $M_{B_T} \sim -14.5$ are distributed like the spirals and irregulars. 3) The intrinsic shapes of the bright non-nucleated dE's are similar to those of the dwarf irregulars, suggesting a possible evolutionary connection between these two classes of galaxies.

INTRODUCTION

It is well known that elliptical and S0 galaxies dominate the central high-density regions of galaxy clusters, while spirals are preferentially found in low-density regions (Hubble and Humason 1931; Dressler 1980). Theoretical mechanisms that have been proposed to explain this include tidal stripping of gas from galaxies during close encounters and mergers, ram pressure sweeping of HI due to galaxy motion through the intra-cluster medium, gas evaporation, and conditions at the time of galaxy formation. Because these processes depend in different ways on galaxy mass and cluster properties, observations of dwarf galaxies in a range of environments offer us the opportunity to test which processes are most important.

As an extension of the Virgo Cluster Survey (Binggeli, Sandage and Tammann 1985; hereafter BST85), six additional groups of galaxies have been surveyed from Las Campanas Observatory using the 2.5 m du Pont telescope, nearly doubling the sample of galaxies and probing a different set of environmental conditions.

THE MORPHOLOGY-DENSITY RELATION

Fig 1. shows the morphology-density relation down to different limiting magnitudes for our entire sample. Nucleated dE's are the most strongly clustered toward dense environments, while irregulars are the least. Dwarf ellipticals without nuclei are, in general, less concentrated toward dense environments than nucleated dE's, but the degree of concentration depends on the luminosity cutoff. To examine the different spatial distributions in more detail, in Figs. 2 and 3 we plot the projected densities of various types of galaxies as a function of radius in the Fornax and Virgo Clusters. Exponentials have been fit to the radial profiles with results shown in Table 1. The radial profiles of the E+S0's, nucleated dE's and *faint non-nucleated* dE's are all the same to within the uncertainties. Similarly, the radial profiles of the spirals, irregulars, and *bright non-nucleated* dE's are indistinguishable.

THE dE-Im CONNECTION

There are several possible explanations for the more extended radial distribution of the bright non-nucleated dE's. First, the sample could be contaminated by foreground galaxies, a possibility that appears unlikely based on the luminosity function of dwarfs in groups of varying distances in our survey. Second, the bright non-nucleated dE's could be the dormant phase of dwarf irregular galaxies between bursts of star formation, as predicted in "Stochastic Self Propagating Star Formation" (SSPSF) models (Gerola, Seiden, and Shulman 1980; Tyson and Scalo 1988). Third, they could be the stripped remnants of dwarf irregulars that have passed through the cluster cores on radial orbits. The last two possibilities suggest that bright dE's should be flattened systems, like the dwarf

Table 1. Type-dependent density profiles in the Virgo and Fornax Clusters

Sample	M_{B_T} range	N	Exponential profiles for Virgo				
			Best fit $1/\alpha$ (deg.)	70% confidence min.	70% confidence max.	99% confidence min.	99% confidence max.
E+S0		62	1.61*	1.4*	2.0*	1.1*	2.8*
Sa+Sb+Sc		78	3.08	2.4	4.2	1.9	9.1
Sd-Im	≤ -14.2	74	3.77	2.9	5.6	2.1	22.2
faint dE(no N)	≥ -13.3	256	1.72	1.6	1.9	1.4	2.2
bright dE(no N)	≤ -14.2	112	3.90	3.1	5.6	2.3	12.5
dE,N	≤ -14.2	151	1.61	1.5	1.8	1.3	2.2

Sample	M_{B_T} range	N	Exponential profiles for Fornax				
			Best fit $1/\alpha$ (deg.)	70% confidence min.	70% confidence max.	99% confidence min.	99% confidence max.
E+S0		31	0.87	0.7	1.1	0.6	1.4
Sa+Sb+Sc		18	2.46	1.6	5.3	1.0	>50.0
Sd-Im	≤ -14.2	27	4.08	2.4	14.3	1.5	>50.0
faint dE(no N)	≥ -13.3	66	0.67	0.6	0.7	0.5	0.9
bright dE(no N)	≤ -14.2	34	2.69	1.9	4.6	1.3	>50.0
dE,N	≤ -14.2	57	0.87	.8	1.0	.6	1.3

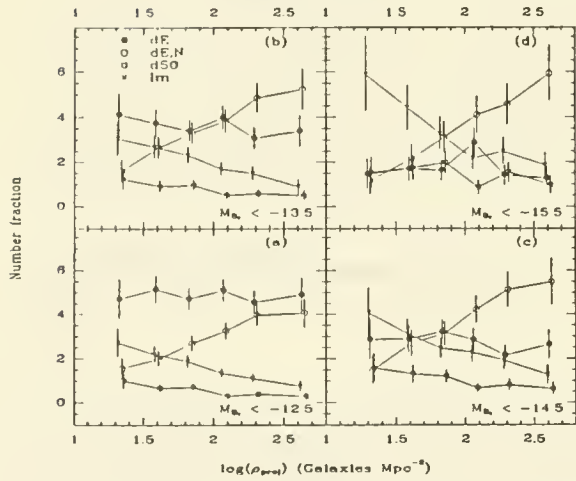


Fig. 1 – Morphology-density relation for dwarf galaxies. Late-type galaxies (Sd, Sdm, Sm and Im galaxies) are shown as crosses, dS0's as open squares, non-nucleated dE's as filled circles, and nucleated dE's as open circles. Projected densities are computed by counting the ten nearest neighbors brighter than $M_{B_T} = -12.5$.

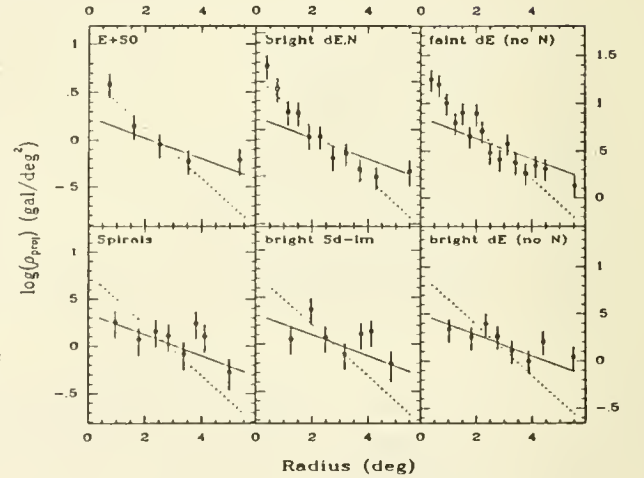


Fig. 2 – The projected density of galaxies as a function of radius in the Virgo Cluster. The solid line shows the best-fit exponential to the bright non-nucleated dE distribution; the dotted line shows the best fit to the faint non-nucleated dE distribution. Both fits are normalized to the number of galaxies in each sample. The fits were performed on the unbinned distributions using a maximum likelihood technique. Galaxies south of 9° declination and in the M and W clouds have been excluded. The bright samples contain galaxies down to $M_{B_T} = -14.2$ ($B_T = 17.5$). The faint dE sample contains galaxies fainter than $M_{B_T} = -13.1$.

irregulars. In Fig. 4., we compare the flattening distributions of the nucleated and non-nucleated dwarf ellipticals and the dwarf irregulars in the same luminosity range. The similarity of the distributions for the non-nucleated dE's and the irregulars supports the picture that the two classes are related.

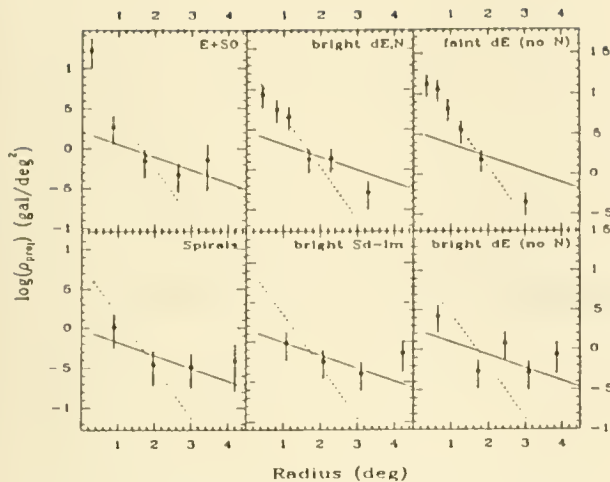


Fig. 3 – The projected density of galaxies as a function of radius in the Fornax Cluster. The solid line shows the best-fit exponential to the bright non-nucleated dE distribution; the dotted line shows the best fit to the faint non-nucleated dE distribution.

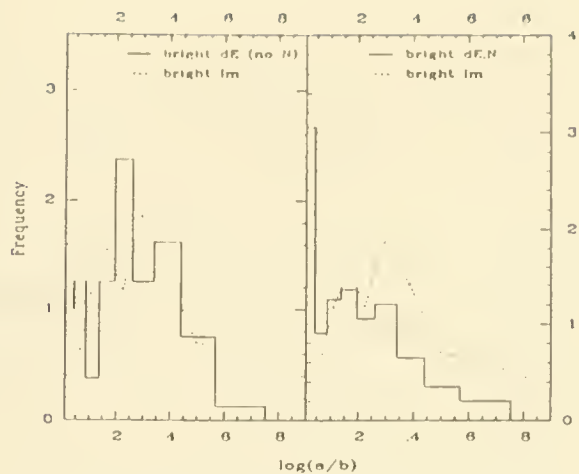


Fig. 4 – The distribution of axial ratios for bright nucleated and non-nucleated dE galaxies, and dwarf irregulars. The samples include galaxies brighter than $M_{BT} = -14.7$ from the Leo, Dorado, and NGC1400 groups and the Fornax and Virgo Clusters. The Im sample includes 129 Sd, Sdm, Sm, and Im galaxies. The dE,N sample includes 200 galaxies, and the non-nucleated dE sample includes 83 galaxies. The bins in axial ratio are those used by Sandage, Freeman, and Stokes (1970).

TESTS OF THE EVOLUTIONARY STATE OF dE's

HI observations of a sample of bright non-nucleated dE's are necessary to test the SSPSF models. Dwarf irregulars between bursts of star formation should be rich in HI. Only about 5 non-nucleated dE's brighter than $M_{BT} = -14.5$ have been observed to date with Arecibo (Bothun *et al.* 1986; Impey *et al.* 1988). None have been detected. Nonetheless, it would be useful to have a larger sample to make the test more conclusive.

Finally, we propose two tests of the hypothesis that the bright non-nucleated dE's are stripped irregulars. First, the similarity of the spatial distributions can be understood if the dwarf irregulars are on predominantly radial orbits. The dwarf irregulars have a higher velocity dispersion than the early-type cluster members (Hoffman *et al.* 1987), consistent with this picture, but the orbit distribution has not yet been examined in detail. Second, if the non-nucleated dE's are stripped Im's, then their metal abundances should be similar. The dE's as a whole are more metal rich than irregulars, but the comparison must now be carried out separately for the nucleated and non-nucleated dE's.

REFERENCES

- Binggeli, B., Sandage, A., and Tammann, G. A. (1985). *A.J.* **90**, 1681.
 Bothun, G. D., Mould, J. R., Caldwell, N., and MacGillivray, H. T. (1986). *A.J.* **92**, 1007.
 Dressler, A. (1980). *Ap. J.* **236**, 361.
 Gerola, H., Seiden, P. E., and Schulman, L. E. (1980). *Ap. J.* **242**, 517.
 Hoffman, G. L. *et al.* (1987). *Ap. J. Supp.* **63**, 247.
 Hubble, E. and Humason, M. L. (1931). *Ap. J.* **74** 43.
 Impey, C., Bothun, G., and Malin, D. (1988). *Ap. J.* **330**, 634.
 Sandage, A., Freeman, K. C., and Stokes, N. R. (1970). *Ap. J.* **160**, 831.
 Tyson, N. D. (1988). *Ap. J.* **329**, 618.

IV - M33 AND M51

Unbound Molecular Complexes in M33

Christine D. Wilson

California Institute of Technology

The HI content of the nearby spiral galaxy M33 ($d \sim 0.8$ Mpc) has been the subject of many detailed studies (most recently Deul and van der Hulst 1987), but similar data on the molecular gas component has been lacking. This galaxy is currently undergoing vigorous high-mass star formation, as evidenced by the many OB associations and HII regions, and so is expected to possess at least some molecular gas. Interferometric studies at OVRO have detected molecular clouds similar to Galactic Giant Molecular Clouds (GMCs) (Boulanger *et al.* 1988; Wilson *et al.* 1988). We have recently mapped the nuclear region of M33 in the CO J=1-0 line with the NRAO 12 m telescope (half power beam width $55'' \sim 210$ pc) out to a radius of $3.5'$ in order to trace the detailed distribution of the molecular gas.

The resulting map (Figure 1) reveals six large complexes with diameters of 200-400 pc, fully contained within our map. Interferometer observations of these regions have resolved them into individual molecular clouds similar to Galactic GMCs (Wilson *et al.* 1988). The complexes in Figure 1 are much larger than individual Galactic GMCs (Sanders, Scoville, and Solomon 1985), but are somewhat smaller on average than the large associations seen in the grand-design spiral galaxy M51 (Rand and Kulkarni 1989). If we extend the velocity-diameter relation observed for Galactic GMCs to these larger structures, the predicted velocity widths are a factor of 1.5-3 times greater than the observed full-width half-maximum velocities ($13\text{-}29$ km s $^{-1}$). The peak brightness temperatures are ~ 0.2 K, at least a factor of 10 lower than what is observed for Galactic GMCs. If these large structures are made up of objects similar to Galactic GMCs, the area filling factor of the small clouds is roughly 10%. These results suggest that these complexes are not very large GMCs, but rather are associations of many individual GMCs or GMCs embedded in a diffuse gas component.

We have calculated both virial and molecular masses for the complexes, adopting the Galactic value $\alpha = 3 \times 10^{20}$ cm $^{-2}$ (K km s $^{-1}$) $^{-1}$ for the ratio of H $_2$ column density to integrated CO flux. The value of α in M33 is unlikely to be much different from the Galactic value, since this nuclear region has roughly solar metallicity (Pagel 1985) and for the individual clouds resolved by the interferometer observations the CO flux-based mass is in rough agreement with the virial mass (Wilson *et al.* 1988). For all but one of these complexes the virial mass is a factor of 5-8 larger than the molecular mass, implying that they are not virially bound. The uncertainties of $\pm 40\%$ in these mass estimates are insufficient to resolve this discrepancy. Since the complexes lie within 1.3 kpc of the nucleus of M33, it is important to consider the effects of tidal forces. We have estimated the minimum mass required for tidal stability and find that the molecular masses all fail by factors of 3-8 to bind the complexes against tidal disruption. Thus both the discrepancy between the virial and molecular masses and the tidal stability analysis imply that these molecular complexes are not themselves gravitationally bound, but instead are transient associations of individual bound objects.

We can calculate the lifetimes of the complexes, assuming them to be made up of roughly 20 individual GMCs with a Galactic mass distribution. If the complexes are unbound, the individual clouds will escape from the complex in roughly the crossing time, $t_{cross} = R/v$, where R is the radius of the complex and v is the 3-dimensional velocity dispersion, $v = 1.36V_{FWHM}$. The crossing times are $1-2 \times 10^7$ yr, comparable to the lifetime of a $15 M_{\odot}$ star and roughly 10-20% of the time required to complete one orbit around M33. If we model the disruption of a complex as a simple expansion in radius to twice the initial radius over one crossing time, the resulting collision timescale indicates that roughly 10% of the clouds in the complex will suffer a collision during this time. Thus we might expect to see enhanced star formation efficiencies in these large complexes if the collisions of individual clouds promote high-mass star formation.

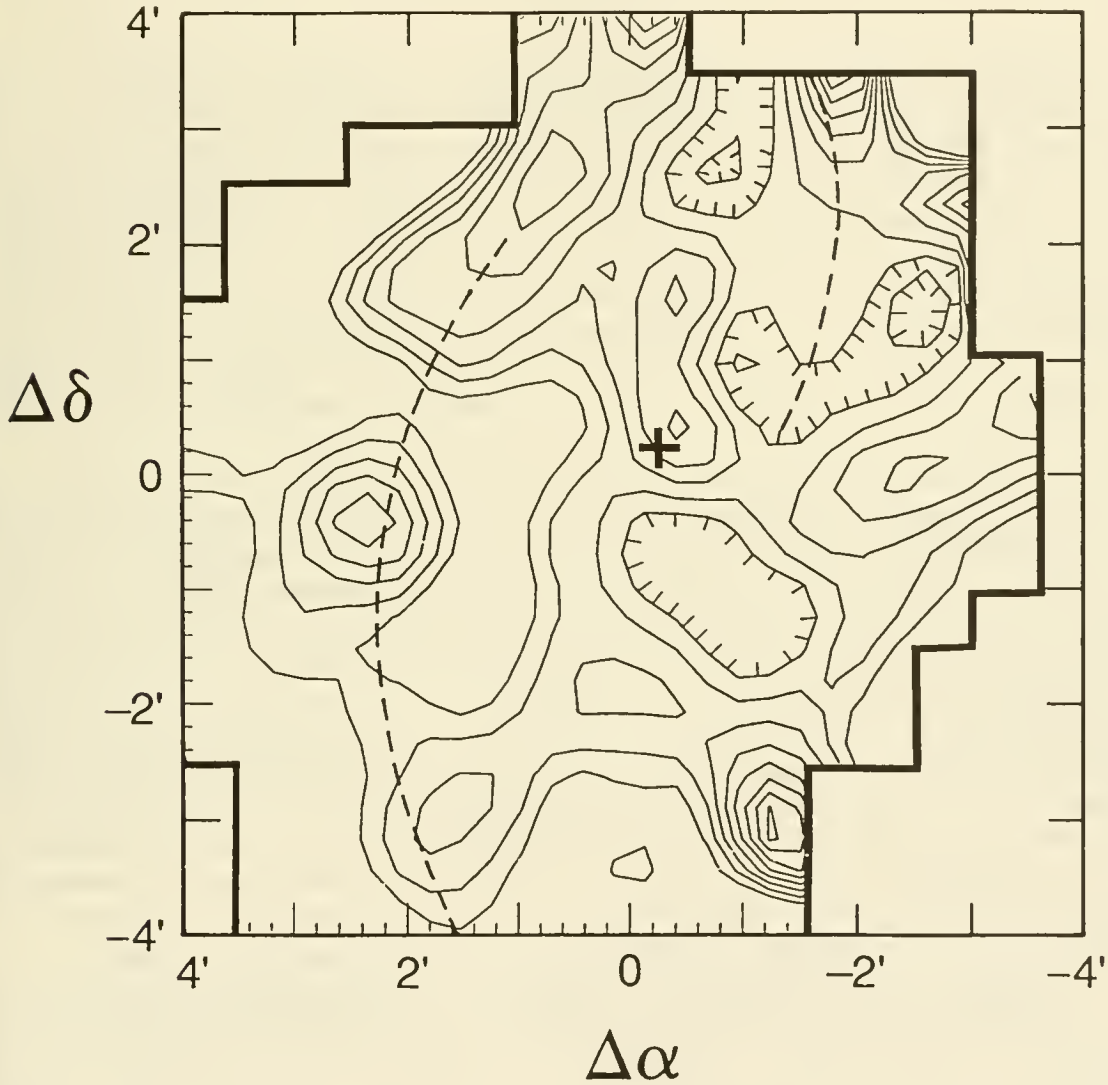
Deconvolved IRAS maps show considerable structure within this region, with a mean dust temperature derived from the $60/100 \mu\text{m}$ flux ratio of 33 K. The total mass of molecular gas derived from the $100 \mu\text{m}$ flux (cf. Thronson and Telesco 1986) is in reasonable agreement with the mass derived from the integrated CO flux, suggesting that we are unlikely to be significantly underestimating the molecular hydrogen mass by using the Galactic value of α . The ratio of the far-infrared luminosity to the molecular hydrogen mass is $3.8 L_{\odot}/M_{\odot}$, typical for regions with low levels of star-forming activity.

The total H_{α} flux is proportional to the high-mass star formation rate and the ratio of the H_{α} flux to the molecular gas mass traces the high-mass star formation efficiency. Both the high-mass star formation rates and efficiencies in the different complexes vary by a factor of 7. The average star formation efficiency does not appear to be enhanced in regions with large amounts of molecular gas, while the star formation rate per unit area is three times higher in regions with high molecular gas densities. These preliminary results suggest that, at least in M33, regions with high star formation rates are primarily due to an overabundance of molecular gas, not to a higher than average star formation efficiency.

References

- Boulanger, F., Vogel, S. N., Viallefond, and F., Ball, R. 1988, in *Molecular Clouds in the Milky Way and External Galaxies*, eds. R. Dickman, R. Snell, and J. Young, (Springer-Verlag: New York), 401.
- Deul, E. R. and van der Hulst, J. M. 1987, *Astr. Ap. Suppl.* **67**, 509.
- Pagel, B. E. P. 1985, in *Production and Distribution of C, N, O Elements* (ESO workshop), eds. I. J. Danziger, F. Matteucci, and K. Kj  r, 155.
- Rand, R. J. and Kulkarni, S. R. 1989, these proceedings.
- Sanders, D. B., Scoville, N. Z., and Solomon, P. M. 1985, *Ap. J.* **289**, 373.
- Thronson, H. A. and Telesco, C. M. 1986, *Ap. J.* **311**, 98.
- Wilson, C. D., Scoville, N. Z., Freedman, W. L., Madore, B. F., and Sanders, D. B. 1988, *Ap. J.* **333**, 611.

Fig. 1 – The map of the integrated CO emission is shown for the inner region of M33. The lowest contour is at 1.1 K km s^{-1} and the contours increase by 0.4 K km s^{-1} . The (0,0) position corresponds to $\alpha(1950) = 01^{\text{h}}31^{\text{m}}03.0^{\text{s}}$, $\delta(1950) = +30^{\circ}23'54''$ and the optical nucleus is indicated by the cross at $(\Delta\alpha = -0.3, \Delta\delta = 0.35)$. The two inner spiral arms are indicated by the dashed lines.



DEEP NARROW BAND IMAGERY OF THE DIFFUSE ISM IN M 33

J. Jeff Hester
Infrared Processing and Analysis Center
California Institute of Technology

and

Shrinivas R. Kulkarni
Department of Astronomy
California Institute of Technology

Very deep narrow band images have been obtained for several fields in the local group spiral galaxy M 33 using the "Wide Field PFUEP" reimaging CCD camera on the 1.5-m telescope at Palomar Observatory. The reimaging system uses a 306 mm collimator and a 58 mm camera lens to put a $16' \times 16'$ field onto a Texas Instruments 800×800 pixel CCD at a resolution of 1.2 arcseconds pixel⁻¹. The overall system is $f/1.65$. Images have been obtained in the light of H α , [S II] $\lambda\lambda 6717, 6731$, [O III] $\lambda 5007$, and line-free continuum bands 100 Å wide, centered at 6450 Å and 5100 Å. Assuming a distance of 600 kpc to M 33 (Humphreys 1980, *Ap. J.*, **241**, 587), this corresponds to a linear scale of 3.5 pc pixel⁻¹, and a field size of 2.8 kpc \times 2.8 kpc. In the present abstract we discuss our H α imagery of a field centered $\approx 8'$ NE of the nucleus, including the supergiant H II region complex NGC 604.

Two 2000 second H α images and two 300 second red continuum images were obtained of two slightly offset fields. The fields were offset to allow for discrimination between real emission and possible artifacts in the images. All images were resampled to align them with one of the H α frames. The continuum images were normalized to the line images using the results of aperture photometry on a grid of stars in the field, then the rescaled continuum data were directly subtracted from the line data. Figure 1 shows the resulting continuum subtracted H α image with a logarithmic stretch. The data were calibrated by comparison with published H α fluxes of H II regions in M 33 (Viallefond and Goss 1986, *Astron. Astrophys.*, **154**, 357; Searle 1971, *Ap. J.*, **168**, 327). The measured surface brightness sensitivity in the continuum subtracted image is $S_{H\alpha} = 5.2 \times 10^{-7}$ ergs cm⁻² s⁻¹ sr⁻¹ (3σ in a $3''.6 \times 3''.6$ region), which corresponds to an emission measure of 6 cm⁻⁶ pc assuming $T = 10^4$ K. There is a zero point uncertainty in the sky subtraction because the galaxy more than fills the field. A sky value was taken from the lowest surface brightness region in the field, located in an interarm region north of the nucleus.

H α emission structure can be seen throughout the galaxy ranging continuously from supergiant H II regions such as NGC 604 to faint features at the limits of detectability. The ubiquitous H α background (*i.e.*, the emission not associated with well defined H II regions) is significantly brighter in the spiral arms than in the interarm regions. Morphologically, this emission consists of filaments embedded in a very low surface brightness diffuse component. In an arm region ~ 800 pc west of NGC 604 the brightest filaments have

$S_{\text{H}\alpha} \approx 150 - 200 \text{ cm}^{-6} \text{ pc}$, while the surrounding nonfilamentary emission has $S_{\text{H}\alpha} \approx 20 \text{ cm}^{-6} \text{ pc}$. An average $\text{H}\alpha$ emission measure for the region, excluding bright H II regions, is $\sim 40 \text{ cm}^{-6} \text{ pc}$. Assuming a disk thickness of $\sim 300 \text{ pc}$ and $\langle n_e^2 \rangle \approx 1 \text{ cm}^{-6} \text{ pc}$, this gives a local filling factor of $\sim 13\%$ for the warm ionized material. Assuming photoionization accounts for most of the $\text{H}\alpha$ emission, this average brightness requires a conversion of $\sim 2.6 \times 10^{44}$ ionizing photons $\text{pc}^{-2} \text{ s}^{-1}$, or the total output of 1 O5 V star per $1.8 \times 10^5 \text{ pc}^2$. The average surface brightness of the diffuse background emission within $\sim 450 \text{ pc}$ of the nucleus is about a factor of 2 higher than the values given above.

The morphology of the $\text{H}\alpha$ background emission indicates that the warm ionized material is distributed in large scale sheets or surfaces. Filaments are due to projection effects (*i.e.*, limb brightening) in these regions. This is especially apparent in numerous locations where multiple "filaments" merge into single structures which bound regions of nonfilamentary emission. This morphology may be important in explaining the excitation mechanism for the emission. Within our Galaxy, Reynolds has shown that while UV from O stars is the only mechanism energetically capable of explaining the excitation of the diffuse $\text{H}\alpha$ background, this emission is often far removed from such stars. A structure such as that seen in M 33 would allow the warm gas to fill a substantial fraction of the volume of the galaxy while still permitting UV escaping from the immediate surroundings of O stars to have a substantial mean free path. The two dimensional $\text{H}\alpha$ emitting structures could be either sheets within a low density matrix or illuminated surfaces of large denser structures, or both.

Numerous shells and partial shells are seen, including multiple shells around the outskirts of NGC 604. The largest complete shell in the field, located $\sim 1 \text{ kpc}$ south of NGC 604, is $\sim 300 \text{ pc}$ in diameter. These structures have been studied previously in M 33 and other galaxies in both ionized and neutral gas (see review by Tenorio-Tagle and Bodenheimer 1988, *Ann. Rev. Astron. Astrophys.*, **26**, 145). In the present images, most of the complete shells can be seen to be limb brightened, with diffuse emission filling their interiors. Hence most of these shells have not broken completely through the galactic disk, although many may have broken through on one side or the other. A possible exception is the large faint bubble south of NGC 604, which has a very low surface brightness in its interior.

There seems to be a continuum of structure ranging from well defined shells through partial shells through the sheets of emission that make up the ubiquitous background. This is especially apparent around NGC 604, where the bubbles around the periphery of the H II complex merge into the filamentary structure of the $\text{H}\alpha$ background. These data appear to support a view that much of the warm ionized material found in the diffuse ISM occurs in sheets that were once part of such large shell-like structures. While this idea is far from new, the structure of the very low surface brightness $\text{H}\alpha$ emission provides a compelling demonstration of the plausibility of this idea, at least for M 33.

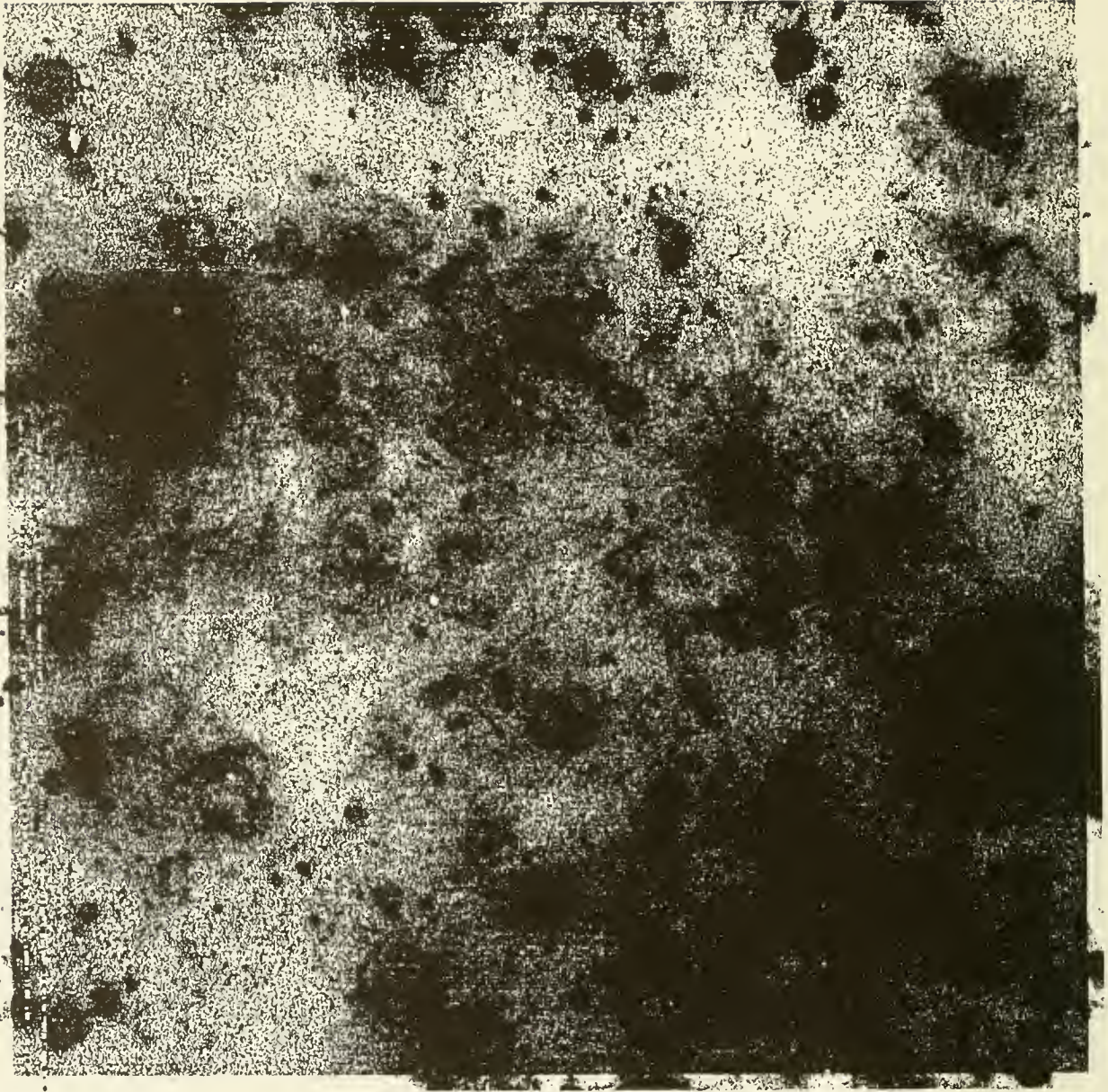


Figure 1. Continuum subtracted $H\alpha$ image of a field to the NE of the nucleus of M 33. The field is $16'$ on a side. The data were obtained with a reimaging camera on the 1.5-m telescope at Palomar Observatory. The surface brightness sensitivity of the image corresponds to an emission measure of $6 \text{ cm}^{-6} \text{ pc}$. The faintest structures discernable in this representation of the data have a surface brightness of ~ 3 times that level. The dot density increases logarithmically with the surface brightness.

A High Resolution CO Map of M51

D.S. Adler, K.Y. Lo, and R.J. Allen

Department of Astronomy, University of Illinois

Observations of the CO (1-0) emission in two fields of M 51 were taken with the Berkeley-Illinois-Maryland Array at Hat Creek, California from May 1988 to February 1989. When combined with two previously observed fields (Lo *et al.* 1988), a complete map of the central $5' \times 4'$ at a resolution of $7'' \times 10''$ was obtained. The project is part of an ongoing high-resolution survey of the molecular, atomic, and ionized gas distributions in nearby spiral galaxies.

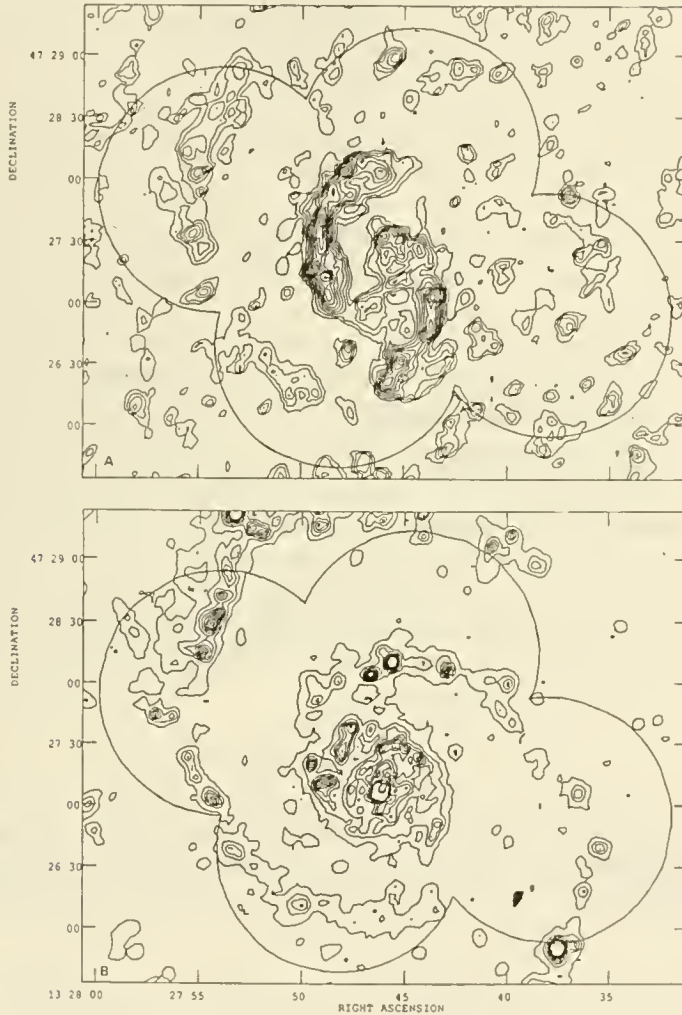


Figure 1. a.) Preliminary CO intensity map of M 51. The lowest contour corresponds to 10 Jy/beam km/sec, with successive contours at intervals of 10 Jy/beam km/sec. The half-power beam widths ($2'$) of the four fields are superposed. b.) The H α emission from the same region, from Tilanus *et al.* (1988). The HPBW from the four fields in figure 1a are drawn in for comparison.

Eleven different array configurations (three baselines each) were used on each of the two fields. Four long-spacing configurations and one compact configuration were added to the existing data from the previously observed fields. For each field, the spectrometer was set to an effective bandwidth of 290 MHz (750 km/sec) with a resolution of 3.25 km/sec, centered at $v_{LSR} = 470$ km/sec. The channel maps were averaged to 10.4 km/sec resolution before cleaning. The typical rms noise of a map was 0.2–0.3 Jy/beam, with a typical signal to noise of 4–6:1 for the two fields. The four cleaned fields were mosaiced using a routine described by Mundy *et al.* (1986).

Figure 1a presents a preliminary map of the integrated CO intensity distribution for the four fields. The lowest contour is 10 Jy/beam km/sec; successive contours are in 10 Jy/beam km/sec intervals. Figure 1a clearly shows that the CO emission displays spiral structure. Figure 1b displays the H α emission at a similar resolution (from Tilanus *et al.* 1987). On a global scale, the CO emission is seen to be fairly well correlated with the H α emission (as well as the 21 cm H I emission, radio continuum emission and dust lanes; Tilanus *et al.* 1987). On small scales, however, the CO is generally seen to be upstream (peaked on the dust lanes) of the H I and H α emission, consistent with previous results on M 51 (Lo *et al.* 1988; Vogel *et al.* 1988). While many of the peaks correlate (see figure 1), there are occasional anti-correlations in the distributions of the CO and H α emission.

The two recently observed fields (the northern and western fields in figure 1a) can be compared to the results of the interferometric study of Vogel *et al.* (1988 - hereafter VKS). Since the shortest spacing in the current survey is shorter than that of VKS, we expect to see more of the extended emission. This is evident when comparing the width of the spiral arms in each survey; ours are a bit broader. While some of the peaks in this region correspond to the peaks in VKS, several of them do not. These discrepancies are probably because of the low signal to noise inherent in observations of this nature.

Single-dish maps are currently being readied for inclusion with the interferometer data. These will help fill the short-spacing hole in the UV plane, and serve to recover the flux missing from the interferometer maps.

References

- Lo, K.Y., Tilanus, R., Allen, R.J., Wright, M.H., and Jackson, J. 1988, in the Proceedings of the UMASS Conference on Molecular Clouds in the Milky Way and External Galaxies, Dickman, R., Snell, R., and Young, J. eds., Springer Verlag, Berlin, page 439.
- Mundy, L.G., Scoville, N.Z., Baath, L.B., Masson, C.R., and Woody, D.P. 1986, *Astrophys. J. (Letters)*, 304, L51.
- Tilanus, R.P.J., Allen, R.J., van der Hulst, J.M., Crane, P.C., and Kennicutt, R.C. 1988, *Astrophys. J.*, 330, 667.
- Vogel, S.N., Kulkarni, S.R., and Scoville, N.Z. 1988, *Nature*, 334, 402. (VKS)

M51: Molecular Spiral Arms, GMAs and Superclouds

Richard J. Rand and S. R. Kulkarni
California Institute of Technology

Abstract. We present an aperture synthesis image of M51 in the CO $1 \rightarrow 0$ line at $9'' \times 7''$ resolution made with the Owens Valley Millimeter Interferometer. The image is a mosaic of 30 one-arcminute fields. The image shows narrow spiral arms which are coincident with the optical dust lanes and non-thermal radio emission, but are offset from the ridges of $H\alpha$ emission. Many dense concentrations of CO emission, termed Giant Molecular Associations (GMAs), are seen both along and between the arms. The typical GMA mass is about $3 \times 10^7 M_{\odot}$. Most of the on-arm GMAs appear to be gravitationally bound. These GMAs consist of several spectral components ("Molecular Superclouds") with typical mass $10^7 M_{\odot}$, which also appear to be bound. The observed streaming motions in the GMAs are consistent with density wave theory. The interarm GMAs are not gravitationally bound, and are likely to be due to a secondary compression of the density wave.

I. Introduction. While it is generally acknowledged that density waves are responsible for galactic spiral structure, their role in triggering coherent star formation remains obscure. Direct evidence for the existence of density waves has been provided by the detection of gas streaming motions in the grand-design spiral galaxies M51 (Tully 1974; Rydbeck *et al.* 1985) and M81 (Visser 1980). However, the global data on spirals seems to indicate that density waves have little to do with star formation (Elmegreen 1987a).

Because very little is understood about the relationship between density waves and star formation, we have undertaken a major program of radio synthesis mapping of M51 (NGC 5194) in the 2.6 mm CO $1 \rightarrow 0$ transition with the Owens Valley Millimeter Interferometer. Initial results for 8 one-arcminute fields revealed narrow molecular spiral arms and demonstrated the existence of spatially resolved velocity shifts across the arms in the NW quadrant of the galaxy (Vogel, Kulkarni, and Scoville 1988, hereafter VKS) in the sense predicted by density wave theory. The SFE was found to be higher in the arms than between the arms (VKS; Rand and Kulkarni 1989).

II. Results. The final product of our 3 year study is the mosaic of 30 one-arcminute fields shown in Figure 1. The resolution is $9'' \times 7''$, and the primary beam of each field is $65''$. Two arms of width $10'' - 20''$ can be traced for about 270° of azimuth. The emission breaks up into discrete features along these arms, while disconnected emission features delineate spiral arms further from the nucleus. Discrete features are also seen between the arms. We detect typically 25–35% of the flux contained within a single-dish beam at a given position (Lord 1987).

An overlay of the CO map with an $H\alpha$ CCD image (not shown) shows that the molecular arms are offset by $5'' - 10''$ to the inside of the $H\alpha$ ridge in the inner regions, implying a delay between the peak compression of the molecular gas and the peak of massive star formation of $\sim 10^7$ years. A similar offset is seen between the dust lanes and thermal radio emission (Tilanus and Allen 1989). An overlay of our map with a red-continuum CCD image (not shown) shows an excellent correspondence of the molecular arms and the dust lanes.

The molecular emission shows dense concentrations of gas, which we call GMAs, both on and between the arms. We derive masses of $10^7 - 6 \times 10^7 M_{\odot}$ for the on-arm GMAs and $10^7 - 4 \times 10^7 M_{\odot}$ for the interarm ones. Thus their masses are more than an order of magnitude greater than those of typical Galactic GMCs ($10^5 - 10^6 M_{\odot}$). We identify 28 GMAs in our map: 20 on the arms, and 8 between the arms.

a) On-arm GMAs. From a comparison of virial and flux-based masses, we find that most of the on-arm GMAs are gravitationally bound. A simple simulation shows that they cannot simply be explained as a chance superposition of a few large GMCs because the required on-arm surface density for this is much higher than observed. These GMAs are also probably tidally stable while on the arms, but may become unstable when they leave the arms. Spectra of the on-arm GMAs show that they are dominated by a few (1 to 4) velocity components, with typical mass $\sim 10^7 M_{\odot}$. A comparison of the virial and flux-based masses of these spectral components indicates that they are probably gravitationally bound.

The GMAs and their constituent Superclouds may be extreme cases of agglomeration through cloud-cloud collisions – a process which is expected to be more effective in assembling such high-mass clouds in M51 than in our Galaxy. Cloud-cloud collisions have been proposed as a mechanism for massive star formation in our Galaxy (Scoville *et al* 1986). In this scenario the massive star formation rate depends on the square of the local molecular cloud density. This process could therefore also explain the higher SFE seen on the arms in M51. Alternatively, such high mass clouds may form directly through gravitational instability, which is enhanced in the arms (Elmegreen 1987b).

b) Streaming motions in on-arm GMAs. In the narrow region of spiral phase where the gas is highly compressed, the density wave is predicted to disturb the basic circular rotation of the gas by causing a positive shift in the tangential velocity in the direction of rotation and a shift in radial velocity toward the nucleus. One of the most important results of VKS was the detection of such tangential and radial “streaming motions” in two GMAs near the major and minor axes, respectively, in the directions predicted by the models. With the now more complete data, streaming motions are detected in 4 additional complexes. In each case, the velocity shift is in the direction predicted by density wave theory.

c) Interarm GMAs. The interarm GMAs have a mean mass of $1.5 \times 10^7 M_{\odot}$ and show on average 3 or 4 distinct spectral components with a mean mass of $4 \times 10^6 M_{\odot}$. The virial masses of these GMAs are much greater than their flux-based masses. A simulation shows that they cannot all be explained as simple random superpositions of a few GMCs – the more massive ones must have a dynamical origin. A possible explanation is that they are formed by secondary compressions of the density wave. If this were the case, then we should expect to see streaming motions in these GMAs. The two interarm GMAs near the major and minor axes do indeed show tangential and radial velocity shifts in the sense predicted by density wave theory. In support of this interpretation is the fact that we see faint, narrow strings of HII regions giving the appearance of coherent spiral features in the NE and SW interarm regions near concentrations of interarm GMAs, indicating a large-scale, but relatively low-level, star forming event. All the evidence therefore indicates that these GMAs are indeed formed by secondary compressions of the density wave.

III. References

Elmegreen, B. G. 1987a in *I.A.U. Symposium No. 115, Star Forming Regions*, ed. M. Peimbert and J. Jugaku (Reidel, Dordrecht, 1987a), p 457-481.

Elmegreen, B. G. 1987b in *Galactic and Extragalactic Star Formation* ed. R. E. Pudritz and M. Fich (Kluwer), p 215-225.

Lord, S. Ph.D. thesis, Univ. Massachusetts (1987).

Rand, R. J. and Kulkarni, S. R 1989 in *Millimeter and Sub-millimeter Astronomy*, ed. A. Webster (Kluwer), in press.

Roberts, W. W. and Stewart, G. R. 1987, *Ap. J.*, **314**, 10.

Rydbeck, G., Hjalmarson, A. and Rydbeck, O. E. II. 1985, *Astr. Ap.*, **144**, 282.

Scoville, N.Z., Sanders, D.B. and Clemens, D.P. 1986, *Ap. J. Lett.*, **310**, L77.

Tilanus, R. P. J. and Allen, R. J. 1989, preprint.

Tully, R. B. 1974, *Ap. J. Suppl.*, **27**, 449.

Visser, H. C. D. 1980, *Astr. Ap.*, **88**, 159.

Vogel, S. N., Kulkarni, S. R. and Scoville, N. Z. 1988, *Nature*, **334**, 402-406 (VKS).

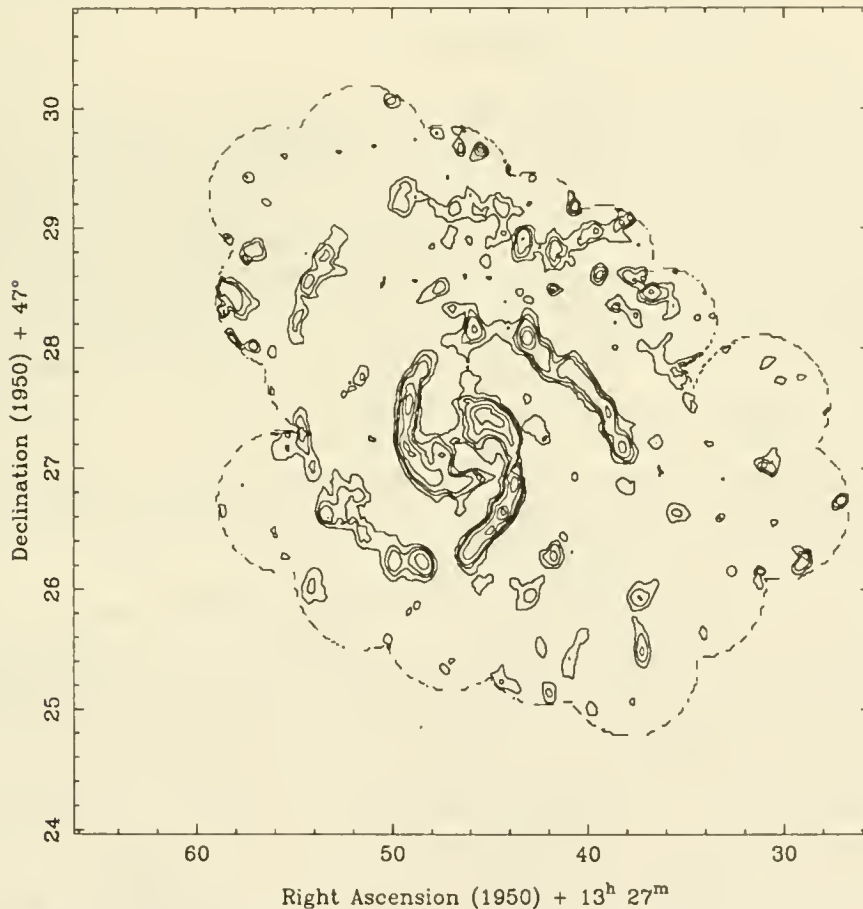


Fig. 1. Mosaic map of CO emission in M51. The mapped region is outlined by the dashed curve. No data from beyond the half-power point of the primary beam are included in the mosaic. Due to improvements in receiver sensitivity and atmospheric conditions over the three year span of the observations, there is a variation in rms noise of a factor of two over the mosaic. Sensitivity generally improves from NW to SE in the map, ranging from about $2 \text{ Jy km s}^{-1} \text{ beam}^{-1}$ to $4 \text{ Jy km s}^{-1} \text{ beam}^{-1}$. The lowest contour is $2.2 \text{ Jy km s}^{-1} \text{ beam}^{-1}$ and the interval is $4.5 \text{ Jy km s}^{-1} \text{ beam}^{-1}$.

DISSOCIATION AND IONIZATION OF MOLECULAR GAS IN THE SPIRAL ARMS OF M51

J.F. Lees

Princeton University
Observatory

K.Y. Lo

Department of Astronomy
University of Illinois

Abstract

We derive the star formation rate and efficiency in the arm and interarm regions of M51 from observations of the molecular (Lo *et al.* 1987) and ionized (van der Hulst *et al.* 1988) phases of the interstellar medium, and show that the HI observations of Tilanus and Allen (1989) are consistent with dissociation of molecular gas by these young, massive stars if $n_H \geq 200 \text{ cm}^{-2}$. However, these stars are not able to dissociate or ionize all the gas, and at least 60% must remain molecular in the interarm regions. The efficiency of star formation in M51 seems to be similar to that in the Galaxy, and does not appear to be enhanced in the spiral arms. Therefore, the effect of the strong density wave may be only to concentrate the gas, and hence the young stars, to the arm regions.

Introduction

The inner regions of the Whirlpool Galaxy, M51, ($r < 1' = 2.8 \text{ kpc}$, at a distance of 9.6 Mpc) have been mapped at high resolution in HI (Tilanus and Allen, 1989), CO emission (Lo *et al.* 1987), and H α and thermal radio emission (van der Hulst *et al.* 1988), with resolutions of 12, 7, and 8 arcseconds respectively. Van der Hulst *et al.* identified giant HII regions and derived their physical properties, such as the rms electron density, \bar{n}_e^2 , and excitation parameter, U . Assuming a volume filling factor for the ionized gas of $\delta = 1$, they then derived the total HII mass. Lo *et al.* (1987) calculated the column density of molecular gas using the Galactic conversion factor $N(\text{H}_2) = 3.6 \times 10^{20} I_{\text{CO}} \text{ cm}^{-2}$. They found the average column density in the arms to be $2 \times 10^{22} \text{ cm}^{-2}$, and the interarm column density to be in the range $(1.4\text{--}3.4) \times 10^{21} \text{ cm}^{-2}$. In this paper, we calculate the amount of molecular gas which could be dissociated by the young stars which are responsible for the H α and thermal radio emission, as a function of electron density in the ionized gas, and hydrogen density in the region immediately surrounding it. The HI column density so derived is then compared to the HI observations of Tilanus and Allen (1989), in order to determine the physical conditions of the interstellar medium in the spiral arms, such as volume density and filling factor.

Star Formation Rate and Radiation Field

Assuming an initial mass function (IMF) appropriate for the most massive stars ($dN/dM \propto M^{-2.5}$), we calculate the total number of stars of spectral type B2 or earlier, N_* , from the excitation parameter, $U \propto N_*^{1/3}$, for each HII region. In the inner spiral arms, there must be 1400 such stars per kiloparsec of arm length, but because the giant HII regions account for only 34% of the total disk thermal emission, this number could be increased by up to a factor of 3. Since the arms have a typical width of 500 pc, this implies a surface density of $(2.8\text{--}8.4) \times 10^{-3} \text{ OB stars pc}^{-2}$. Hence, the star formation rate (and radiation field, if the stars have the same scale height as in the Galaxy) in the spiral arms is 4–13 times that in the solar neighborhood. In the interarm regions, the upper limit to the surface density of young stars is $3.6 \times 10^{-4} \text{ pc}^{-2}$ (using the total H α flux given by Kennicutt and Kent (1983)), about half the density near the sun. So the arm contrast in young stars is at least 8. This can be compared to the CO arm contrast of between 3 and 15 (Lo *et al.* 1987).

If we assume the IMF used above extends to a lower mass limit of $0.4 M_\odot$, then we can calculate the total mass of newly-formed stars in the spiral arms, M_* , and compare this to the gas mass to derive a star formation efficiency, $\epsilon \equiv M_*/(M_* + M_{\text{gas}})$. We find $\epsilon \approx 0.15\text{--}0.4\%$ in the arms, and $\epsilon \leq 0.25\%$ between the arms. This is comparable to the efficiencies of 0.2–5% found for Galactic giant

molecular clouds (Wilking and Lada, 1985). Thus, star formation does not appear to be more efficient in M51 than in the Galaxy, and the efficiency is not necessarily enhanced in the spiral arms by the strong density wave.

Dissociation by Young Stars

Using the number of OB stars inferred above, we can find the total flux of dissociating photons. This should be fairly insensitive to the slope of the IMF. The mass of gas dissociated, however, depends not only on the volume density of the neutral gas, but also on the density within the HII region (since this affects the Strömgren radius), and the detailed geometry. Assuming the stars are in a single spherical OB association, completely embedded in molecular gas (so that no photons escape), we find that the mass of gas dissociated is $M(HI) = 2.9 \times 10^6 N_*^{7/6} n_e^{2/3} n_H^{-3/2} M_\odot$. If, instead, the stars are uniformly distributed in the arm, the HI mass is typically half this value, and if the stars are strung out along the arm ("cylindrical" geometry), the HI mass differs by $\pm 50\%$ for densities of interest. So the mean HI column density in the arms is typically $N(HI) \approx 7.3 \times 10^{20} N_*^{7/6} n_e^{2/3} n_H^{-3/2} \text{ cm}^{-2}$. The electron density given by van der Hulst *et al.* (1988) is $n_e = 1.57 \delta^{-1/2} \text{ cm}^{-3}$, where δ is the HII volume filling factor. Tilanus and Allen (1989) find that the mean HII column density in the arms is about $7 \times 10^{20} \text{ cm}^{-2}$. Therefore, if $\delta = 1$, we need $n_H \approx 200 \text{ cm}^{-3}$, and if $\delta = 0.1$, $n_H \approx 400 \text{ cm}^{-3}$. Typically, $n_H \approx 100 n_e$ is needed to explain the low HI column densities.

Alternatively, if the stars are not too deeply embedded within the molecular gas, then we can consider the molecular clouds to be immersed in an interstellar radiation field 4–13 times larger than in the solar neighborhood. Then, the atomic envelopes of molecular clouds will have a column density $N(HI)_{env} = 2.3 \times 10^{23} G^{1.5} n_H^{-1.5} \text{ cm}^{-2}$, where $G = 4\text{--}13$ (Federman *et al.* 1979). If each line of sight passes through one cloud, and if the density in the atomic gas is $n_H \approx 200\text{--}600 \text{ cm}^{-3}$, then the observed HI could be simply explained as the envelopes of molecular clouds along the line of sight, as proposed generally by Shaya and Federman (1987).

Finally, since the giant HII regions are so large ($d \approx 450 \text{ pc}$), they may burst through the molecular cloud layer, creating wormholes, and much of the dissociating radiation could escape into the halo. In this case, n_H could be much lower and still agree with the observations.

The Interstellar Medium in Interarm Regions

The observations referenced above also allow us to place limits on the fraction of the molecular gas in the arms which is ionized or dissociated by the young stars. The column density of H_2 in the arms is $2 \times 10^{22} \text{ cm}^{-2}$, whereas that of the HII and HI is only observed to be $\leq 7 \times 10^{21} \text{ cm}^{-2}$ and $7 \times 10^{20} \text{ cm}^{-2}$ respectively. In the interarm region, the molecular gas still dominates, with $N(H_2) = (1.4\text{--}3.4) \times 10^{21} \text{ cm}^{-2}$. $N(HI) \leq 6 \times 10^{20} \text{ cm}^{-2}$ and $N(e) \leq 10^{20} \text{ cm}^{-2}$. Therefore, the interstellar medium in the interarm regions must be at least 60% molecular. However, the molecular gas cannot be gathered into large complexes like those seen in the spiral arms, because the CO brightness temperature, averaged over 300 pc, is less than $0.6 K$ in the interarm regions (Lo *et al.* 1987).

The authors acknowledge support from NSF grant AST 87-15905.

References

- Federman, S.R., Glassgold, A.E., and Kwan, J. 1979. *Ap.J.*, **227**, 466
 Kennicutt, R.C., and Kent, S.M. 1983. *Astr.J.*, **88**, 1094
 Lo, K.Y., Ball, R., Masson, C.R., Phillips, T.G., Scott, S., and Woody, D.P. 1987. *Ap.J. Lett.*, **317**, L63
 Shaya, E.J., and Federman, S.R. 1987. *Ap.J.*, **319**, 76
 Tilanus, R., and Allen, R. 1989. *Ap.J. Lett.*, **339**, L57
 van der Hulst, J.M., Kennicutt, R.C., Crane, P.C. and Rots, A.H. 1988. *Astr.Ap.*, **195**, 38
 Wilking, B.A., and Lada, C.J. 1985. in *Protostars and Planets II*, p. 297

Spiral structure of M51:

Streaming motions across the spiral arms

R. P. J. Tilanus^{1,*}, R. J. Allen^{2,1}

¹Kapteyn Astronomical Institute, Postbus 800, 9700 AV Groningen, The Netherlands

²Space Telescope Science Institute, Science Computing Division

*Present address: Inst. for Astronomy, University of Hawaii

Streaming motions

The atomic hydrogen (HI) and the H α emission line in the grand-design spiral galaxy M51 have been observed with the Westerbork Synthesis Radio Telescope and the TAURUS Fabry-Perôt imaging spectrometer, respectively. Across the inner spiral arms significant tangential and radial velocity gradients are detected in the H α emission after subtraction of the axi-symmetric component of the velocity field (Figure 1).

The shift is positive on the inside and negative on the outside of the northern arm. Across the southern arm this situation is reversed. The direction of the shifts is such that the material is moving inward and faster compared to circular rotation in both arms, consistent with the velocity perturbations predicted by spiral density wave models^{2,3} for gas downstream of a spiral shock. The observed shifts amount to 20–30 km s⁻¹, corresponding to streaming motions of 60–90 km s⁻¹ in the plane of the disk (inclination angle 20°). Comparable velocity gradients have also been observed by Vogel *et al.*⁹ in the CO emission from the inner northern arm of M51. The streaming motions in M51 are about 2–3 times as large as the ones found in HI by Rots⁴ in M81, and successfully modelled by Visser^{7,8} with a self-consistent density wave model. We have not been able to detect conclusively streaming motions in the HI emission from the arms, perhaps due to the relatively poor angular resolution ($\sim 15''$) of the HI observations.

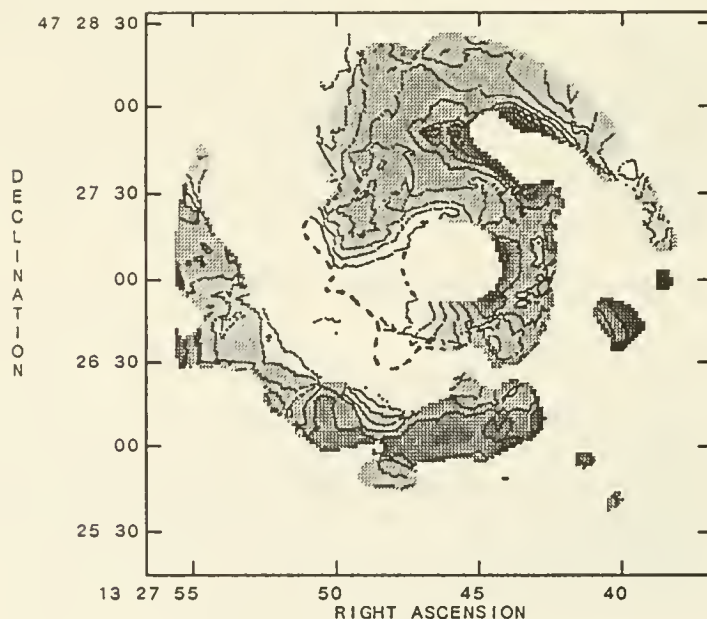


Figure 1. M51 (H α) streaming motions: the residual velocities across the ionized spiral arms, after subtraction of the axi-symmetric component of the velocity field. The axi-symmetric model used has been derived from a flat rotation curve. The gray levels correspond to observed residual velocities of -45 , ± 20 , ± 12.5 , ± 7.5 , and ± 2.5 km s⁻¹. The direction of the streaming motions is consistent with that the gas is flowing under the influence of a density wave perturbation.

The structure of the spiral arms

The location of various components of the ISM in the inner part of M51 is shown in Figure 2a-d. Figure 2 illustrates the main conclusions reached in Paper I⁵ and Paper II⁶:

i) The thermal radio continuum in M51 (Figure 2d) correlates closely with the optical H α emission from the giant H II complexes along the outside of the arms, and is in general well separated *spatially* from the nonthermal emission on the inside of the arms (Paper I).

ii) The ridges of maximum brightness of the nonthermal radio continuum emission in Figure 2b correlate closely with the dust lanes (Paper I). This observation is consistent with the nonthermal radio emission originating from shocked gas on the inside of the spiral arm, however...

iii) ...the detailed cross-sectional shape of the nonthermal radio arms (Figure 2b) disagrees with that expected from a simple one-component fluid model of the interstellar gas flowing under the influence of a density wave model. Opposite to the model arms^{7,8} the observed radio arms have their larger extent on the inner than on the outer side and terminate sharply just outside the dust lanes.

iv) The H I arms are displaced to a larger radius with respect to the nonthermal emission and the dust lanes (Figure 2a), and are found along the same ridges as the H II regions and the thermal radio continuum emission (Figures 2c,d) (Paper II). This is especially clear for the southern spiral arm which starts out just south of the nucleus and winds around to the left in Figure 2. Here, the H I arm is displaced from the dust lane and the nonthermal radio continuum by 450 pc. A more pronounced displacement has been found previously in M83 over a 7 kpc section of the inner eastern arm, where the H I arm is displaced downstream from the dust lane by 700 pc¹.

The model we have proposed^{1,6} to account for the separation of the H I arms with respect to the nonthermal continuum and/or dust lanes, as well as its coincidence with the ionized arm in both M51 and M83, explains the H I to arise from a partial photo-dissociation of a predominantly molecular ISM. This scenario was developed within the framework of the density wave theory of spiral structure², in particular with the description of the gas flow in a spiral potential first presented by Roberts³. The molecular material reaches its highest density at the position of the spiral shock on the inside of the arms as indicated by the nonthermal radio continuum ridges and the dust lanes in Figure 2b. Star formation is enhanced/triggered in this region, but the surrounding gas remains mostly molecular until the increasing star formation activity eventually results in giant H II complexes, and in a fraction of the H₂ becoming dissociated into H I. The process naturally leads to the H I clouds to appear downstream from the shock in the immediate neighborhood of the H II regions.

This picture of the constitution and distribution of the ISM in the spiral arms of galaxies is considerably strengthened by a recent high-resolution observation of the distribution of the CO emission in the inner northern spiral arm of M51 by Vogel *et al.*⁹. These authors find the 300 pc wide CO arm to be closely coincident with the dust lane well inside of the luminous H II regions. Using their observation we find that the H₂ column density in the arms is 10 times larger than can be expected from a compression of the interarm H I in the shock, confirming our initial assumption that the ISM is predominantly molecular in the inner region of M51. It also follows that on average about 10% of the molecular gas is dissociated into its atomic form by the star-formation process. Assuming that the number of dissociating photons is roughly equal to the number of ionizing photons, the dissociation process yields the observed column density of H I on a timescale of roughly a million years.

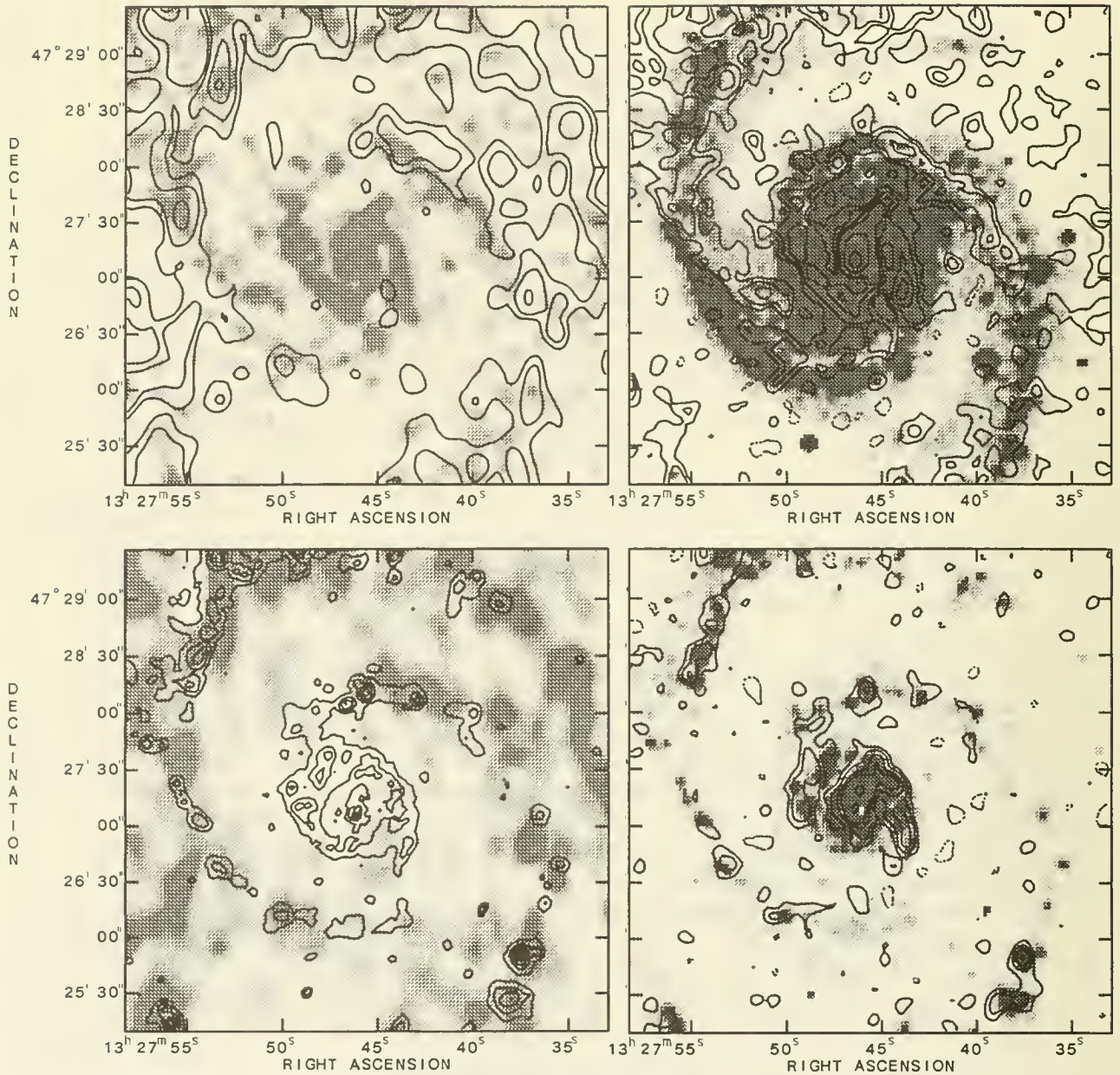


Figure 2. M51 central part: (a) *Top left panel:* the HI surface density distribution at a resolution of $12''.3 \times 17''.5$ (contours) and the nonthermal radio-continuum emission at $8''$ (gray scales). (b) *Top right panel:* the distribution of the nonthermal radio-continuum emission at $8''$ (contours) and the red optical continuum (gray scales) showing the dust lanes as white bands on the inside of the luminous arms. (c) *Bottom left panel:* the $H\alpha$ emission from the major H II regions (contours) and the HI distribution at full resolution (gray scales). (d) *Bottom right panel:* the thermal radio-continuum emission at $8''$ (contours) and the distribution of $H\alpha$ emission (gray scales).

References: ¹Allen, R.J., Atherton, P.D., and Tilanus, R.P.J. 1986, *Nature* **319**, 296. ²Lin, C.C., and Shu, F.H. 1964, *Astrophys. J.* **140**, 646. ³Roberts, W.W. 1969, *Astrophys. J.* **158**, 123. ⁴Rots, A.H. 1975, *Astron. Astrophys.* **45**, 43. ⁵Tilanus, R.P.J., Allen, R.J., van der Hulst, J.M., Crane, P.C., and Kennicutt, R.C. 1988, *Astrophys. J.* **330**, 667 (*Paper I*). ⁶Tilanus, R.P.J., and Allen, R.J. 1989, *Astrophys. J. Lett.* **339**, L70 (*Paper II*). ⁷Visser, H.C.D. 1980a, *Astron. Astrophys.* **88**, 149. ⁸Visser, H.C.D. 1980b, *Astron. Astrophys.* **88**, 159. ⁹Vogel, S.N., Kulkarni, S.R., and Scoville, N.Z. 1988, *Nature* **334**, 402 (see also 382).

HIGH SPATIAL-RESOLUTION IRAS IMAGES OF M 51.

R. Canterna^{1,2}, John A. Hackwell¹ and Gary L. Grasdalen²

Abstract

High spatial-resolution ($\approx 30''$) images of M51 in the four IRAS bands (12, 25, 60, and $100\ \mu\text{m}$) have been obtained. The spatial variation in flux in all four bands is coincident with the spiral features seen in $\text{H}\alpha$ and 6 cm with a few exceptions. In the nuclear region ($4'$) the position of the peak of maximum intensity shifts in relation to the visual nucleus: it is coincident with the nucleus at $12\ \mu\text{m}$, shifts approximately $45''$ to south-southwest, and is $45''$ northwest of the nucleus at 60 and $100\ \mu\text{m}$.

Introduction

High spatial resolution images of M51 have been obtained from the Calibrated Raw Detector Data (CRDD) obtained by IRAS in its Additional Observation (AO) program. A general technique to process unevenly-spaced IRAS data has been developed by Hackwell, Friesen, Canterna and Grasdalen (1988) using the maximum entropy image reconstruction algorithm of Gull and Skilling (1984). Convergence to the final images is determined by the following criterion, which is dependent on a proper estimation of the noise of the CRDD: maximization of the entropy of the image and satisfying the chi-squared constraint.

Results

Contour plots of our final resolution-enhanced images are displayed in Figure 1. Resolution of $\leq 30''$ was achieved. A comparison with UV, 6 cm radio, CO and $\text{H}\alpha$ maps shows that major features in the structure of M 51 are coincident along the major spiral arms. Most notably the major H II region complexes are quite prominent along the arms. The most important result is the change in the position of peak radiation within the nuclear region of M 51. In Figure 2 we present the 12, 25, and $60\ \mu\text{m}$ contours of the $5'$ region centered on the nucleus of M 51. For comparison, a contour plot of the $\text{H}\alpha$ radiation from Kennicutt (1988) degraded to $20''$ resolution. The $12\ \mu\text{m}$ peak is coincident with the visual and $\text{H}\alpha$ peak. The $25\ \mu\text{m}$ peak is positioned approximately $45''$ south-southeast from the $12\ \mu\text{m}$ and optical center. The 60 and $100\ \mu\text{m}$ peaks are offset approximately $45''$ north west from the visual nucleus. The offsets appear to be related to features seen in the CO and radio maps.

¹ The Space Sciences Laboratory, The Aerospace Corp.

² The Wyoming Infrared Observatory

References

Gull, S. F., and Skilling, J. 1984. Proc. I. E. E., 131, 646.

Hackwell, J. A., Friesen, L. M., Canterna, R., and Grasdalen, G.L., 1988. B.A.A.S. 20, 667.

Kennicutt, R. 1988. Private Communication.

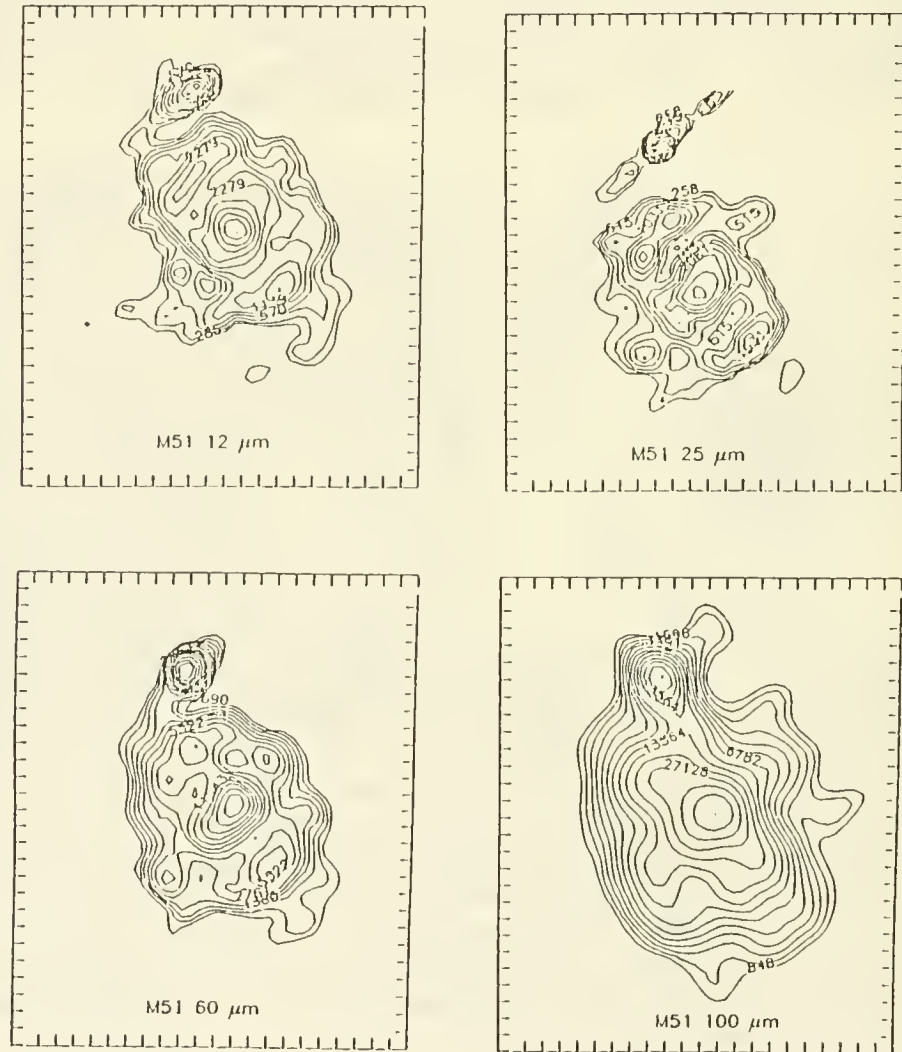
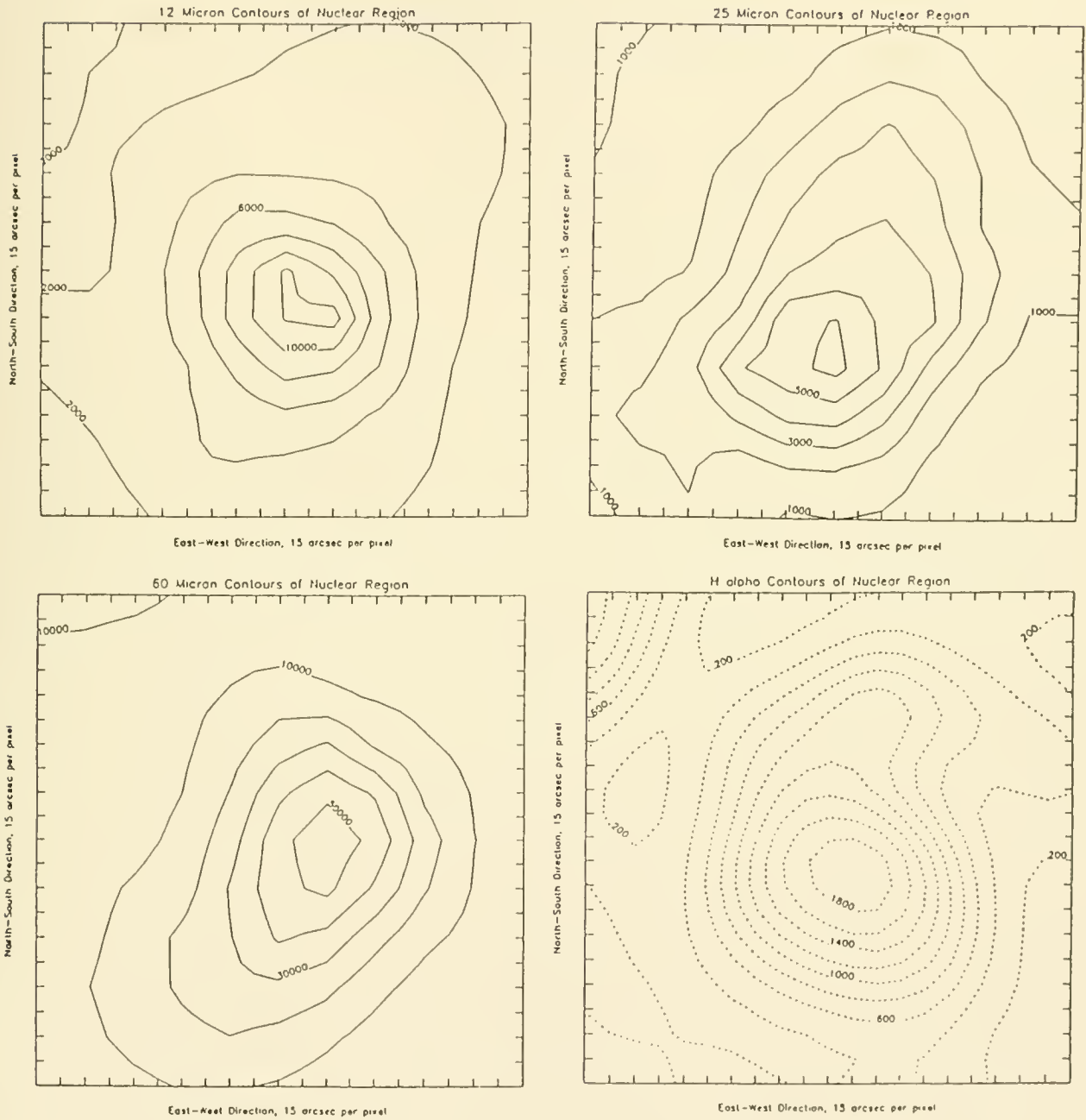


Figure 1. Contour plots of our high spatial-resolution images of M 51 from IRAS CRDD.

Figure 2. Contour plots of the nuclear region of M51 at 3 IRAS bands and H α (degraded to a resolution of 20").



V - STAR FORMATION IN GALAXIES

Are Bars Essential for Starbursts in Non-Interacting Galaxies?

Stephen M. Pompea and G.H. Rieke

Steward Observatory
The University of Arizona
Tucson, Arizona 85721

The presence of an optical bar in spirals is correlated with increased infrared luminosity. Hawarden et al. (1986) showed that the total infrared luminosity of barred galaxies in a sample of RC2 galaxies (which excluded liners) was about twice that ($4.3 \times 10^{10} L_{\odot}$) of the unbarred galaxies in the sample ($L = 1.7 \times 10^{10} L_{\odot}$). However, it is unclear whether bars or interaction are an absolute requirement to allow adequate quantities of gas to settle into the nuclear region for a moderate to high luminosity starburst. Optical searches for weak bars or oval distortions are hampered by large amounts of extinction, even in galaxies with low inclination. Observations in the Gunn *i* band to search for surface brightness distributions indicative of bars (Zaritsky and Lo 1986) represent a considerable improvement over visible measurements. Observations in the near infrared near two microns can further reduce the obscuration due to dust and delineate more clearly the underlying, old stellar population that dominates the gravitational potential. Thus using infrared imaging a range of galaxies with different inclinations and central obscurations can be studied.

This poster paper presents and analyzes our 1.6 and 2.2 μm images of a sample of galaxies that are classified as unbarred by the Revised Shapley-Ames Catalog. These galaxies have characteristic properties of nuclear starbursts and are examined through near infrared imaging in a search for hidden bars. We have selected a sample of 36 galaxies from the Revised Shapley-Ames Catalog that have far infrared luminosities $> 10^{10} L_{\odot}$ and hot IRAS colors between 60 and 100 μm , indicative of nuclear starbursts, but are not classified as Seyfert 1 or 2. Our determination of the presence of a bar relies primarily on an analysis of the 2 micron image using the "Galaxy Surface Photometry" (GASP) package (Cawson, 1983). The GASP analysis programs determine the galaxy surface brightness and ellipticity profiles as well as the position angle and the center coordinates of the ellipses. To test the way that GASP will characterize the surface brightness of barred galaxies, two galaxies with known bars, NGC 1068 and NGC 2523, were imaged with the 2 micron camera and analyzed with GASP.

Fifteen of the sample that are not clearly barred from optical data and are isolated were imaged at 1.6 and 2.2 μm ; 9 of these do not appear to have bars. Strong bars therefore do not appear to be an absolute requirement for high infrared luminosity in isolated galaxies.

Aspects of the Interstellar Medium in Starburst Galaxies

Michael N. Fanelli
Department of Astronomy
University of Virginia

We are engaged in a multifaceted program to investigate the stellar content and star formation history of actively star-forming galaxies. A large body of stellar spectra have been examined to identify spectral features characteristic of specific stellar types. These spectral diagnostics are then calibrated in terms of temperature (spectral type), gravity (luminosity class) and metallicity. The spectral data is compiled into a stellar library whose members represent specific locations in the HR diagram. Through the use of population synthesis techniques, both optimizing and evolutionary approaches, the stellar luminosity function in composite populations can be determined by analysis of their integrated light. We have concentrated on the ultraviolet wavelength region ($\lambda\lambda$ 1200–3200), utilizing the *IUE* archives supplemented by additional observations. In the optical, virtually all stars will contribute to the integrated light. In the ultraviolet however, cool stars will produce negligible flux due to their steep ultraviolet-to-visual continua, greatly simplifying the investigation of the hot component in a composite population.

Our initial stellar library has been applied to several blue compact galaxies, (BCGs), a class of starburst galaxy which is UV luminous. BCGs possess a complex interstellar medium which affects the emergent stellar continuum in several ways. This presents a challenge to the stellar analysis but affords insight into the properties of the gas and dust from which the massive OB stars have formed.

The optimizing synthesis method solves for the stellar luminosity function and extinction simultaneously. This therefore provides an independent measure of the extinction affecting the hot population component. Despite the rise of the reddening law towards the ultraviolet, BCGs are found to be brighter in the ultraviolet than expected. In general, measured extinctions are low, ($0.0 \leq E(B-V) \leq 0.35$), and found to be lower than values determined from Balmer line ratios or 6_{cm} thermal radio continuum fluxes. Use of the Balmer decrement to deredden galaxy continuum spectral energy distributions may be erroneous. The lack of heavy extinction implies a modest dust content in the star-forming regions. There is a trend for the more luminous starbursts to exhibit larger extinction. Haro 1, the most luminous object in our sample may be a link between ‘ordinary’ starbursts and the dusty systems observed by *IRAS*.

The 2200 Å interstellar extinction feature is not observed in most BCGs although a definitive analysis is hindered by the signal-to-noise characteristics of the long wavelength cameras on *IUE*. We have recently detected a strong 2200 Å bump in a starburst nucleus of unusually high ultraviolet surface brightness. Its depth is $\approx 60\%$ of the interpolated

continuum at the center and is believed to be the strongest 2200 Å feature observed in a composite extragalactic population.

Additionally, spectra of star-forming regions can be affected by interstellar absorption lines. Most of the observed features are found to arise in the stellar component but the interpretation is muddled in the case of resonance lines such as Mg II λ 2800 which are both very prominent in stellar spectra and commonly seen in absorption from the gas. Mg II λ 2800 is detected in most of our sample of BCGs.

An ionizing photon rate can be determined directly from the derived stellar population. Employing standard assumptions this rate can be used to predict observables such as $I(\text{H}\alpha)$ and $S_{6\text{cm}}$ in other bandpasses. Predicted values of the 6_{cm} flux are compared with observations. The ratios of predicted to observed flux are found to be in the range 0.36–0.72 for 5 objects with known 6_{cm} fluxes. Although no firm conclusions can be drawn with this limited sample the results imply that the ionizing population is accurately modeled. We believe that this ‘multiple constraint’ approach whereby predictions derived from data in one bandpass are compared to observations in other bandpasses promises to provide greatly improved accuracy to models of starburst systems.

Gravitational Star Formation Thresholds and Gas Density in Three Galaxies

M.S. Oey and R.C. Kennicutt, Jr.
Steward Observatory, University of Arizona
Tucson, AZ 85721

It has long been held that the star formation rate (SFR) may be described as a power law of the gas density, ρ^n , as given by Schmidt (1959). However, this relation has as yet remained poorly defined and is likewise poorly understood. In particular, most studies have been investigations of global gas and star formation properties of galaxies, due to lack of adequate high-resolution data for detailed studies of individual galaxies. The three spiral galaxies in this study have published maps of both H_2 (as traced by CO), and HI, thereby enabling us to investigate the relationship between total gas surface density and SFR.

Threshold gas densities below which massive star formation is suppressed in spiral galaxies were suggested early on by Quirk (1972), and evidence for such behavior has been presented by several recent authors. These preliminary reports lack detail, and consider only atomic HI gas. In addition, Kennicutt (1989) demonstrates strong evidence for thresholds in azimuthally-averaged, total ($H_2 + HI$) surface gas densities, based on the gravitational stability considerations suggested by Quirk. In Kennicutt's paper, Quirk's critical threshold gas density is given as a surface density by

$$\Sigma_c = \alpha \frac{\kappa c}{3.36G}$$

This expression was derived directly from the gravitational stability criterion for a thin disk of gas embedded in stars (Toomre 1964, Cowie 1981), where c is the gas velocity dispersion, and κ is the epicyclic frequency. In that study, Kennicutt empirically determined α , the dimensionless "stability parameter", to have a value near 0.7 for an assumed $c = 6 \text{ km s}^{-1}$.

The purpose of the present investigation is the comparison of spatially-resolved total surface gas density in three galaxies (NGC 6946, M51, and M83) to Σ_c as given by the above model. CO, HI, and $H\alpha$ data for NGC 6946 were taken from Tacconi-Garman (1988), and for M51 and M83 from Lord (1987). We used a CO- H_2 conversion of $N(H_2)/I_{CO} \cos i = 2.8 \times 10^{20} \text{ atoms cm}^{-2}/(\text{K km s}^{-1})$, and summed the H_2 and HI data for each galaxy to obtain the total hydrogen gas density. This total was then multiplied by a factor of 1.36 to include the contribution of helium to the total surface gas density. We assumed distances to NGC 6946, M51, and M83 to be 6.0, 9.6, and 8.9 Mpc respectively, with inclination angles of 30, 20, and 26°. $H\alpha$ flux was used as the measure of SFR for NGC 6946, and SFR for the remaining two galaxies was taken directly from Lord as computed from $H\alpha$ measurements.

Figure 1a-c shows the total density as a function of radius for each galaxy, with the threshold density Σ_c indicated by the broken line. Figure 2 shows the $H\alpha$ flux as a function of density for NGC 6946, with specific radii plotted with different symbols so that a single value for Σ_c applies to each data set, as indicated by the different lines. The remaining two galaxies show behavior similar to NGC 6946 in SFR vs. Σ . The results in Fig. 1 show a remarkable correlation between the total gas density and the threshold densities given by the gravitational stability criterion. In particular, the threshold density appears to define a lower limit to the gas densities. As a result, Fig. 2 does not indicate

the steep, nonlinear drop in SFR for densities below Σ_c which would be expected in the threshold model. Since none of the points in question are significantly below the threshold density beyond the range of errors, and considering that all the data lie well within the star-forming disks, it may not be surprising that all points exhibit star formation. It is also quite possible that the 45" mapping resolution of the hydrogen densities is not good enough to effectively isolate low-density regions below the threshold.

That the gas density should follow the threshold so closely would be logical in light of gas depletion by star formation. If star formation requires a threshold gas density, one would expect that after several characteristic star-forming time scales, the gas would be depleted to the level of the threshold. Thus the near coincidence of the gas density with the threshold in itself supports such a model. The noteworthy result here is the fact that the threshold marks a *lower* boundary to the gas, instead of an upper one, as would be expected from such a scenario. This observation may perhaps be understood in terms of gas infall models, or feedback mechanisms between the SFR and threshold density. It may also be that the observed Σ_c as a lower bound to the gas density is evidence of a threshold for molecular cloud formation, instead of star formation per se (Cowie 1981, Elmegreen 1979). There are several possibilities, and our result may prove to be a criterion in determining appropriate models for gas dynamics and star formation.

Likewise, we must bear in mind that the present study is preliminary in nature. There are many physical conditions for which gas density would follow a $1/R$ law, as does Σ_c (e.g. Struck-Marcell 1989, Wyse and Silk 1989). Also, if α in our study is in error by more than a factor of about 1.5, the threshold density will no longer neatly mark a lower boundary to the gas density. One should note however, that Kennicutt (1989) finds at most a 25% deviation in α for his sample. Hence we wish to emphasize that our result is fairly robust, and we are astonished to find that all three galaxies agree so well in the qualitative pattern.

The results of these full-disk studies thus show a remarkable correlation between the total gas density and the threshold densities given by the gravitational stability criterion. In particular, the threshold density appears to mark a lower boundary to the range of gas densities in these galaxies, which may have consequence in determining appropriate models for star formation and gas dynamics. More evidence is required to verify this result, and we are currently undertaking a high-resolution study of the nearby spiral M33 and other galaxies to further investigate this problem.

References

- Cowie, L.L. 1981, *Ap.J.* **245**, 66.
- Elmegreen, B.G. 1979, *Ap.J.* **231**, 372.
- Kennicutt, R.C. 1989, *Ap.J.*, in press.
- Lord, S.D. 1987, Ph.D. thesis, University of Massachusetts.
- Quirk, W.J. 1972, *Ap.J.Lett.* **176**, L9.
- Schmidt, M. 1959, *Ap.J.* **129**, 243.
- Struck-Marcell, C. 1989, this conference.
- Tacconi-Garman, L.J. 1988, Ph.D. thesis, University of Massachusetts.
- Toomre, A. 1964, *Ap.J.* **139**, 1217.
- Wyse, R.F.G. and Silk, J. 1989, *Ap.J.* **339**, 700.

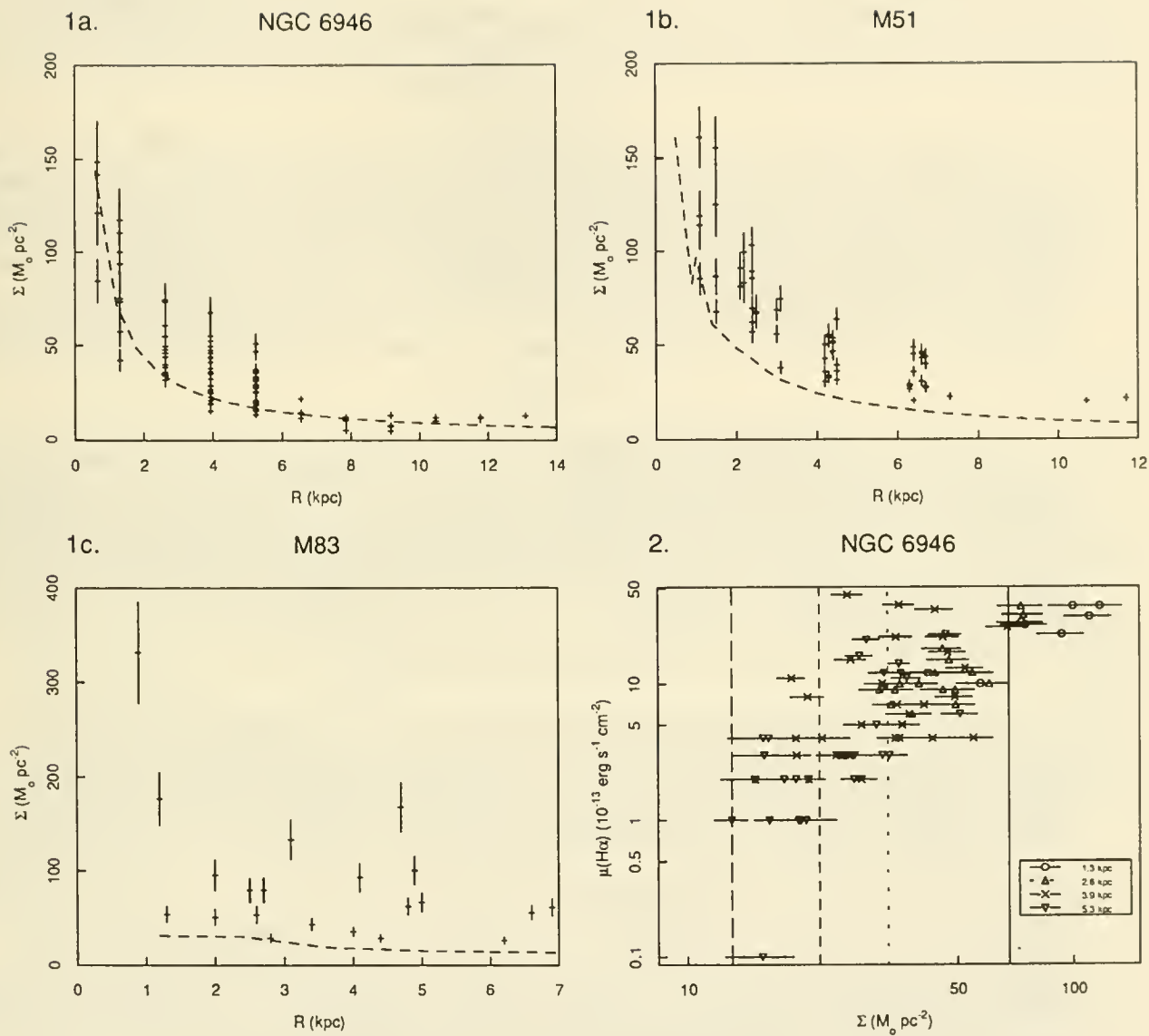


Fig. 1. Total surface density vs. radius for each galaxy. The threshold density Σ_c is indicated by the broken line.

Fig. 2. $\text{H}\alpha$ surface flux density per $45''$ beam vs. total surface density, for selected radii of NGC 6946. Different symbols indicate points at different radii, with corresponding thresholds as indicated by different line types in the legend. The point at $\mu(\text{H}\alpha)=0.1$ is actually a zero detection.

ONE-DIMENSIONAL CLOUD FLUID MODEL FOR PROPAGATING STAR FORMATION

Timothy N. Titus, University of Wyoming, and Curtis Struck-Marcell, Iowa State University

I. INTRODUCTION

The aim of this project was to study the propagation of star formation (SF) with a self-consistent deterministic model for the interstellar gas. The questions explored are: (1) Under what conditions does star formation propagate in this model?, and (2) What are the mechanisms of the propagation? In our study, we have used the deterministic Oort-type cloud fluid model of Scalo and Struck-Marcell (1984, also see the review of Struck-Marcell, Scalo and Appleton 1987). This cloud fluid approach includes simple models for the effects of cloud collisional coalescence or disruption, collisional energy dissipation, and cloud disruption and acceleration as the result of young star winds, HII regions and supernovae. An extensive one-zone parameter study is presented in Struck-Marcell and Scalo (1987).

II. RESULTS

To answer the questions above we carried out one-dimensional calculations for an annulus within a galactic disk, like the so-called solar neighborhood of the galactic chemical evolution. In the calculations the left-hand boundary is set equal to the right hand boundary. The calculation is obviously idealized, however, it is computationally convenient to study the first order effects of propagating star formation. The annulus was treated as if it were at rest, i.e., in the local rotating frame. This assumption may remove some interesting effects of a supersonic gas flow, but was necessary to maintain a numerical stability in the annulus.

A. When Does SFR Propagate?

Two initial perturbation types were studied: pure density or pure SFR perturbations in the 10 zones at the center of a 100 zone grid. (Note: in these calculations SFR is measured by the relative rate of cloud break-up due to star-formation activity as parametrized by Scalo and Struck-Marcell.) The initial density perturbation was an over-density of three times the equilibrium density. With low values of the time delay parameter (defined as the ratio of the mean cloud lifetime to the mean cloud collision time), the cloud fluid behaved much as one would expect. SFR propagated out with the shock wave or acoustical waves that formed from the initial perturbation. Starbursts did occur in the zones of the initial perturbation. The pressure from these bursts reinforces the outward propagating SFR wave while depleting the gas. With a small time delay, the SFR indicator is linearly dependent on the density in regions away from the initial density perturbation. With larger values of the time delay parameter the effective critical density for bursts is lowered, so that the initial conditions are nearly in the burst regime. As a result of feedback from bursts the SFR profile is no longer linearly dependent on the density profile in perturbed regions. In the small time delay case, the density amplitude is damped out with time. However, in the long time delay model, the bursting reinforces the outward propagating shock waves. The shock waves amplify the density perturbation, pushing these zones further into the bursting regime. The most intense star formation occurs in the shock regions, which are defined by abrupt velocity changes. This supports the idea that star formation propagates through pressure disturbances, in this Oort-type model.

If the disturbance consists of SFR enhancement in pressure equilibrium, will the SFR still propagate? In this case, the SFR perturbation is created by increasing the mean cloud mass, at a constant mass density. Two different strength SFR perturbations were used: one of moderate strength in which the cloud mass was increased by a factor of 1.26, and a relatively strong one with a cloud mass increase of 2.0. The weaker perturbation, with an initial SFR increase of 2.52, did not propagate. The second perturbation, with an SFR enhancement of 16.0, did propagate, but not as efficiently as a

density perturbation. The stronger SFR perturbation sets up shock waves and it is these shock waves that propagate the star formation.

To summarize, pressure waves, reinvigorated by bursts of SF seem to be the chief propagation mechanism in this cloud fluid model. Density enhancements play an important role, but a global density wave is not required to trigger propagating SFR.

B. SFR Interference

When two adjacent density perturbations are set-up some distance apart, the waves they generate initially propagate outward just like the waves from a single perturbation, until the waves encounter one another. Then the two opposing wave fronts cause a large density increase in the zones between them. These zones are pushed into the burst regime, setting up a new source for star formation. The SFR in the zones of interference becomes oscillatory, in the same manner as if we had placed an initial perturbation in these zones.

C. Random Noise

Our study of the effects of random noise consisted of using an initial density perturbation amplitude, as above, plus a random background noise of maximum amplitude 0.1. As expected, the random noise has a strong effect on the local SFR within the annulus if the density is initially near threshold. In zones that are near the burst regime, positive amplitude noise is able to induce bursting, and negative amplitude noise can effectively prevent bursting. Zones with densities that are far from the bursting regime are not strongly affected, and the SFR in these zones responds with a linear dependence density noise. While these results are not surprising, they are important to keep in mind in comparing simulations to galaxies with SFR 'noise' of indeterminate amplitude. It also raises the possibility that noise modulation of a hydrodynamical wave, could significantly complicate the observational recognition of that wave.

Skillman (1986) and Kennicutt (1989 and references therein) have recently presented observational evidence that the star-forming regions in disks are near the critical density for gravitational instability according to Toomre's Q parameter, and that SF falls off rapidly outside of such regions. These results and our simulation results suggest the possibility that the "normal" mode of SF in disks is a random burst mode, involving essentially the same physical processes as in density wave induced SF and nuclear starbursts.

III. CONCLUSIONS

We can summarize the results on the one-dimensional propagation of SF in the Oort cloud fluid model as follows. 1. SF is propagated by means of hydrodynamic waves, which can be generated by external forces or by the pressure generated by local bursts. SF is not effectively propagated via diffusion or variation in cloud interaction rates without corresponding density and velocity changes. 2. The propagation and long-range effects of SF depend on how close the gas density is to the critical threshold value, i.e. on the "susceptibility" of the medium.

This work supported in part by NASA grant NAGW 1009.

Kennicutt, R. C., Jr., preprint "The Star Formation Law in Galactic Disks" (1989).

Scalo, J. M. and Struck-Marcell, C., *Astrophys. J.*, 276, 60 (1984).

Skillman, E., in "Star Formation in Galaxies Proceedings" ed. C. J. Lonsdale (Washington: NASA) (1986).

Struck-Marcell, C. and Scalo, J. M., *Astrophys. J. Suppl.* 64, 39 (1987).

Struck-Marcell, C., Scalo, J. M., and Appleton, P. N., in "Star Formation in Galaxies Proceedings" ed. C.J. Lonsdale (Washington: NASA) (1986).

Titus, T. N., M.S. Thesis, Iowa State Univ. (1988).

Star Formation in Proto Dwarf Galaxies

A. Noriega-Crespo* *Canadian Institute for Theoretical Astrophysics*

P. Bodenheimer and D. N. C. Lin *Lick Observatory, University of California*

G. Tenorio-Tagle *Max-Planck-Institut für Astrophysik*

* Present address: *University of Washington, Seattle.*

Abstract

The effects of the onset of star formation on the residual gas in primordial low-mass Local-Group dwarf spheroidal galaxies is studied by a series of hydrodynamical simulations. The models have concentrated on the effect of photoionization. The results indicate that photoionization in the presence of a moderate gas density gradient can eject most of the residual gas on a time scale of a few 10^7 years. High central gas density combined with inefficient star formation, however, may prevent mass ejection. The effect of supernova explosions is discussed briefly.

Introduction:

The age spread observed in several dwarf stellar systems, based on the color and $[\text{Fe}/\text{H}]$ of individual stars within the system (see below), suggests that a large fraction of their primordial gas was retained, despite the energy release by their earliest generation of massive stars.

A significant variation in $[\text{Fe}/\text{H}]$ is found from the observed spectroscopic data of individual stars in the dwarf elliptical galaxies Draco and Ursa Minor (Zinn 1978; Kinman *et al.* 1981). The broad red giant branch photo-metrically observed in the dwarf galaxies Fornax (Buonanno *et al.* 1985), NGC 147 (Mould *et al.* 1983), NGC 205 (Mould *et al.* 1984), and Draco (Carney & Seitzer 1986) also indicates a spread in metallicity (see review by Aaronson 1986).

That some fraction of the gas remains inside the system is essential for the formation of the "next generation" of stars, and for the self-enrichment by the by-products of the first supernova (SN) explosions.

In this communication we present some numerical hydrodynamical simulations of the evolution of the residual gas for several dwarf models. We first consider just the effects of photoionization. This process seems to be an effective mechanism to remove gas from proto-globular clusters and to reduce, therefore, further self-enrichment (see *e.g.* Tenorio-Tagle *et al.* 1986). Some of these models have been recently published (see Noriega-Crespo *et al.* 1989). We present also some preliminary results of a more 'realistic' set of models, which include both the HII region and supernova phases (HII-SN), and the presence of an external medium.

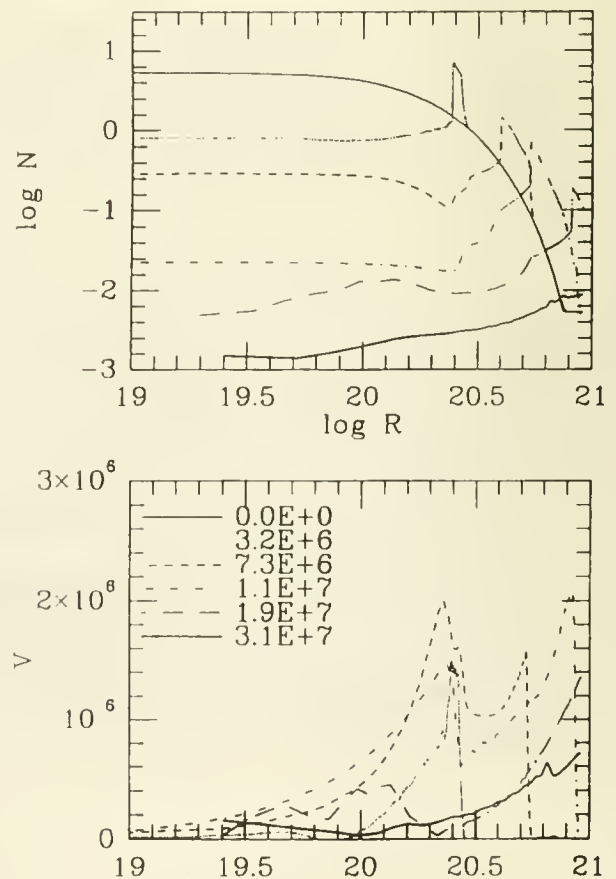
Photoionization:

The photoionization models considered galactic systems in the size range 0.3 to 1.0 kpc and in the mass range 10^5 to $10^7 M_\odot$ (see table). The HII-SN models have focused on the larger systems with a tidal radius of 1 kpc and a mass of $\gtrsim 10^7 M_\odot$. These models included the presence of a warm, neutral, low density external medium that extends from 1 to 3 kpc.

The main assumptions include: (i) a spherically symmetric gravitational potential (time independent) for the

galaxy, given by a King model (King 1966), (ii) a low metal abundance in most cases, (iii) an initial mass function similar to that in the solar neighborhood, (iv) an ionizing source located at the center of the galaxy (later on the supernova energy source), and (v) a mass in the gaseous component which is a substantial fraction of the total mass. The dynamics are examined for the relevant ranges of mass in gas, stars, matter and of galactic radius, metallicity, ionizing flux, and initial gas density distribution. The HII-SN models will examine also the supernova energy and the concentration of the gravitational potential.

Figure 1.



The results indicate that the effects of photoionization in the presence of a moderate gas density gradient can easily eject the gas on a time scale of a few times 10^7 years. However, with sufficiently high central gas density combined with inefficient star formation, the effect of the ionizing flux may be localized to prevent mass ejection.

Model Parameters										
(1)	(2)	(3)	(4)	(5)	(6)	(7)	(8)	(9)	(10)	(11)
Model	M_{gas}	c	R_t	M_\odot	ρ	Z	f	F_\odot	t_∞	Outcome
I.1	5.5	3	0.3	5.5	s	-2	0.019	49.0	1	E
I.3	5.5	3	0.3	8.5	s	-2	0.030	49.3	1	E
I.5	5.5	3	0.3	5.5	s	-2	0.140	50.0	1	E
I.6	5.5	3	0.3	5.5	u	-2	0.074	49.7	1	R
I.5	5.5	3	0.3	5.5	u	-2	0.140	50.0	1	R
I.6	5.5	3	0.3	5.5	u	-2	0.300	49.5	10	R
I.7	5.5	6	0.3	5.5	u	-2	0.140	50.0	1	R
II.1	6.0	3	0.3	6.0	s	-2	0.010	49.3	1	R
II.2	6.0	3	0.3	6.0	s	-2	0.050	50.0	1	M
II.3	6.0	3	0.3	6.0	s	-2	0.330	51.0	1	E
II.4	6.0	3	0.3	6.0	s	-3	0.000	50.0	10	E
II.5	6.0	6	0.3	6.0	s	-2	0.050	50.0	1	E
III.1	7.0	3	0.3	6.0	s	-2	0.010	50.0	1	R
III.2	7.0	3	0.3	6.0	s	-2	0.080	51.0	1	E
III.3	7.0	3	0.3	6.0	s	-2	0.050	50.0	10	E
III.4	7.0	3	0.3	5.5	s	-2	0.010	50.0	1	E
III.5	7.0	3	0.3	5.5	s	-2	0.001	49.0	1	R
IV.1	6.0	5	1.0	5.5	2.5	-2	0.150	50.3	1	E
IV.2	6.0	5	1.0	5.5	3.0	-2	0.130	50.3	1	M
IV.3	6.0	5	1.0	5.5	3.5	-2	0.130	50.3	1	R
V.1	7.0	5	1.0	6.5	3.6	-2	0.015	50.3	1	E
V.2	7.0	5	1.0	6.5	3.65	-2	0.015	50.3	1	R
V.3	7.0	5	1.0	6.5	3.95	-2	0.130	51.3	1	R
V.4	7.0	5	1.0	6.5	3.65	-3	0.130	50.3	10	E
V.5	7.0	5	1.0	6.5	3.90	0	0.015	50.3	1	R
V.6	7.0	5	1.6	6.5	3.90	0	0.130	51.3	1	R

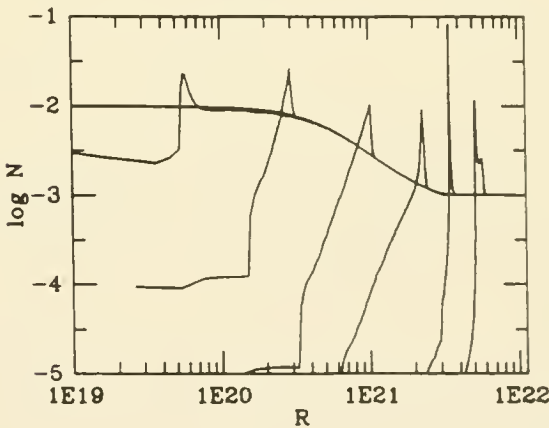
Column (1) lists the model number. Columns (2) and (5) list the logarithms of the stellar and gas mass, respectively, in units of M_\odot . Columns (3) and (4) indicate the concentration parameter c , and the tidal radius of the galaxy in kpc, respectively. In Column (6), the gas density distribution is indicated. The symbol s represents a gas distribution scaled to the stellar distribution. The symbol u represents uniform initial density. The numerical entries represent the logarithm of the equilibrium temperature in the isothermal cases. Column (7) gives the logarithm of the metal abundance, in solar units. Columns (8) and (9) represent the star formation efficiency, as defined by eqn. (1), and the logarithm of the ionizing flux in photons s^{-1} , respectively. Column (10) represents the characteristic lifetime for the ionizing flux, in units of 4×10^6 yr. Column (11) indicates the evolutionary outcome where the symbols R , M , and E represent gas retention, marginal mass loss, and total gas ejection, respectively.

Figure 1 shows, as an example, the evolution of the density and velocity distributions as a function of time for one of our photoionization low mass models (model I.1). The different lines correspond to different times. The model has a total mass $M_T = 3.3 \times 10^5 M_\odot$, and a similar mass in gas with a metallicity $Z=10^{-2} Z_\odot$. The model has a very low ionizing flux, 10^{49} photons s^{-1} , equivalent to one massive star ($\sim 20 M_\odot$). The system evolves into an ionization front preceded by a shock front (D-type), separated by a dense shell. In this case the photoionization provided with enough momentum to the gas that $\sim 90\%$ is removed in $\sim 3 \times 10^7$ years.

The effect of supernova explosions

For some models a flat density distribution seems to suppress gas mass loss driven by photoionization. In these cases (*e.g.* V.2 or V.6) the effect of SN explosions can eject all the gas. Figure 2. shows the time evolution of the gas density of a blast wave in a flat density distribution model. The parameters are those of model V.5 where there was no gas ejection by photoionization. The model includes the presence of an external medium that extends beyond the 1 kpc "optical" tidal radius up to 3 kpc.

Figure 2.



In this case the photoionization evolution was followed up to $\sim 3.2556 \times 10^6$ yrs. At this time the supernovae energy, 2×10^{52} ergs, is set at the inner boundary and the ionizing flux is turn off ($t = 0$). The different lines in Figure 2 correspond to different times. From left to right $0.0e+0$, $9.4e-4$, $5.4e+5$, $2.9e+6$, $9.2e+6$ and $3.4e+7$ years, respectively. The shock wave moves initially at several 10^8 cm s^{-1} , but by the last model, at 3.4×10^7 yrs, the gas is moving at $\sim 1.8 \times 10^6 \text{ cm s}^{-1}$. In this model all the gas inside the 1 kpc radius ($\sim 7\%$ of the total gas mass) is ejected at $\sim 7 \times 10^6$ yrs after the explosion.

The results suggest that, given a normal initial mass function, many protodwarf galaxies may have been dispersed by the onset of star formation.

ANC thanks Laurie Feinswog for exhilarating discussions

and her technical advice. ANC thanks the Connaught Fund of University of Toronto and the NSERC of Canada for their support to this project. He also thanks the Organizing Committee and the NSF under Grant AST 87-17867 for their support to participate in this meeting.

References

- Aaronson, M., 1986. In: *Star-Forming Dwarf Galaxies*, p. 125. eds Kunth, D., Thuan, T. X. & Tran Thanh Van, J., éditions Frontières, Gif sur Yvette, France.
- Buonanno, R., Corsi, C. E., Fusi Pecci, F., Hardy, E. & Zinn, R., 1985. *Astr. Astrophys.*, **152**, 65.
- Carney, B. W. & Seitzer, P., 1986. *Astr. J.*, **92**, 23.
- King, I. R., 1966. *Astr. J.*, **71**, 64.
- Kinman, T. D., Kraft, R. P. & Suntzeff, N. B., 1981. In: *Physical Processes in Red Giants*, p. 71. eds Iben, I. Jr. & Renzini, A., Reidel, Dordrecht, Holland
- Mould, J. R., Kristian, J. & DaCosta, G. S., 1983. *Astrophys. J.*, **270**, 471.
- Mould, J. R., Kristian, J. & DaCosta, G. S., 1984. *Astrophys. J.*, **278**, 575.
- Noriega-Crespo, A., Bodenheimer, P., Lin, D. N. C. & Tenorio-Tagle, G., 1989. *Mon. Not. R. astr. Soc.*, **237**, 461.
- Tenorio-Tagle, G., Bodenheimer, P., Lin, D. N. C. & Noriega-Crespo, A., 1986. *Mon. Not. R. astr. Soc.*, **221**, 635.
- Zinn, R., 1978. In: *Globular Clusters*, p. 191, eds Hanes, D. & Madore, B., Cambridge University Press.

Infrared Spectroscopy of the Dwarf Starburst Galaxy Henize 2-10

P.R. Blanco *Astronomy Department, University of Edinburgh.*

P.J. Puxley *Institute of Astronomy, University of Hawaii.*

We present 1.2–2.2 μm spectra of the nucleus of Henize 2-10, taken at UKIRT with CGS 2. This galaxy displays strong line emission from interstellar H^+ (1.282 & 2.166 μm) and $[\text{Fe}^+]$ (1.256 & 1.644 μm), in common with other star-forming galaxy nuclei. However the 1-0 S(1) line of molecular hydrogen at 2.122 μm is not detected – the upper limit of 0.15 (3σ) for the value of the flux ratio $I_{1-0\text{S}(1)}/I_{\text{Br}\gamma}$ is much lower than the typical values of 0.4–0.9 measured in a sample of 28 non-interacting starburst galaxies.

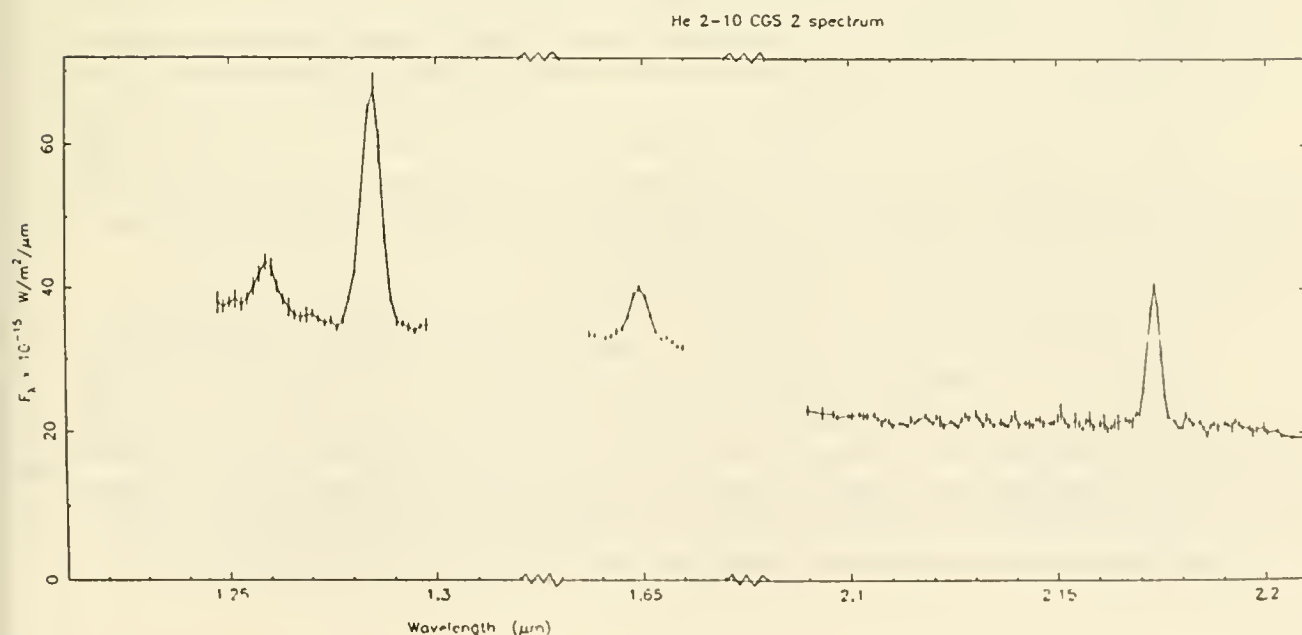
From the $\text{Pa}\beta/\text{Br}\gamma$ line ratio we derive a total extinction of $A_V \sim 4$ mag, greater than previous estimates based on the optical line spectrum (cf. Johansson 1987; $A_V \sim 1$ mag).

The de-reddened H^+ and $[\text{Fe}^+]$ line fluxes are used to estimate the total ionising luminosity and the average supernova rate in the central 150 pc of He 2-10. By comparison of these estimates with existing IRAS and radio continuum data we are able to set limits on the range of stellar masses present in this unevolved ($<10^7$ yr old) starburst nucleus.

Possible reasons for the low H_2/H^+ line ratios observed in young starburst systems (He 2-10, NGC 7714, IIZw40; eg. Moorwood & Oliva 1988) are briefly discussed.

Johansson (1987) *Astron. Astrophys.* 182, 179.

Moorwood & Oliva (1988) *Astron. Astrophys.* 203, 278.



SMALL-SCALE STAR FORMATION AT LOW METALLICITY

Marshall L. McCall
York University
Toronto, Ontario, Canada

and

Robert Hill and Jayanne English
University of Toronto
Toronto, Ontario, Canada

Summary

Massive star formation on small scales in a low metallicity environment is investigated by studying the morphology of HII regions in the Small Magellanic Cloud. A classification scheme based upon the symmetry of form in the light of $H\alpha$ is devised to make possible an examination of the properties of blister candidates with respect to nebulae embedded in a more uniform medium. As in the Milky Way, the asymmetrical surface brightness distribution of many HII regions demonstrates that massive stars often form at the edge of dense neutral clouds. However, the existence of many symmetrical nebulae with similar sizes, luminosities, and surface brightnesses shows that massive star formation often occurs well within clouds. Nevertheless, the statistics of the two different forms indicate that the rate of massive star formation declines less steeply with radius across host clouds than in the Milky Way, suggesting that triggering is predominated by a different mechanism.

Background

Much can be learned about massive star formation by studying HII regions ionized by so few stars that the energy input has not been sufficient to disrupt the connection between the ionized gas and the host molecular cloud. The morphology of such HII regions can yield valuable clues about the location of star formation sites in molecular clouds, and thereby can help to identify important triggering mechanisms. For example, asymmetrical Orion-like nebulae with diffuse emission falling away from a bright core or ridge arise from star formation at the edge of a molecular cloud, perhaps initiated by an external trigger such as a collision with another more diffuse cloud or an encounter with a supernova shock front. On the other hand, the existence of symmetrical Trifid-like HII regions shows that massive stars can form well within clouds, and suggests that an external trigger is not necessarily needed.

The Small Magellanic Cloud is an ideal laboratory for studying these important star formation issues at low metallicity. Considering the peculiarities of the molecular make-up of the interstellar medium and the consequences for heating and cooling, routes to star formation may be quite different than in the Milky Way. Certainly, with the reduced dust content, star formation occurring deep within molecular clouds is more readily observable. Most important, because of the advantages in resolution and detectability resulting from proximity, the SMC offers unique opportunities to gain insights into star formation in the early universe.

Observations

The authors have conducted an $H\alpha$ imaging survey of small HII regions in the Small Magellanic Cloud. Observations of HII regions smaller than about 2.0 arcmin (38 pc) were made with the CCD camera of the University of Toronto Southern Observatory at Cerro Las Campanas, Chile. Reductions and measurements were carried out using IRAF. A total of 15 fields were surveyed, containing a total of 26 distinct objects.

Following upon concepts developed for HII regions in the Milky Way, a two-stage classification system was designed to segregate objects on the basis of symmetry of form. From this system, it was possible to identify objects most likely to be Orion-like “blisters” (Type O) at the edge of molecular clouds and Trifid-like Stromgren spheres (Type T) located well within clouds. In addition to measuring total fluxes, the physical characteristics of the HII regions were evaluated by examining isophotes at a fixed percentage of the peak surface brightness. The diameter and surface brightness of such isophotes are directly related to parameters controlling the radius of a Stromgren sphere.

Results

While many SMC HII regions have the morphology of blisters, just as many show a degree of symmetry which precludes formation in a nonuniform medium. Examples of each type are shown in Figure 1. Neither the $H\alpha$ fluxes nor surface brightnesses of Type O HII regions differ systematically from those for Type T, demonstrating that covering factors, temperatures of ionizing stars, and extinction levels are probably comparable. Fluxes don't vary significantly with diameter, so variations in stellar temperatures can't be at the root of the diameter sequences. Since surface brightnesses decline with diameter, the sequences probably arise from variations in the gas density.

Whether or not massive star formation preferentially occurs at the edges of molecular clouds can be judged from the number of HII regions of Type O relative to Type T. For this purpose, it is useful to approximate the sites of massive star formation as a collection of identical spherical molecular clouds of radius R and to represent the probability of star formation at a particular point in a cloud as a power law in radius, i.e.

$$P = P_0(r/r_c)^\beta$$

where r is the distance from the centre of the cloud and P_0 , r_c , and β are constants. If HII regions of Type O exclusively arise from star formation in a shell of width ΔR at the edge of the clouds and if HII regions of Type T come from star formation within radius $R - \Delta R$ from the centres, then integration of the probability function yields

$$-\beta = 3 + \log(1 + q)/\log(1 - \Delta R/R)$$

where $q = N(\text{Type O})/N(\text{Type T})$. Type O objects become common at sizes above 10 arcsec, suggesting that the ionizing stars formed within 5 arcsec (1.5 pc) of the cloud boundaries. The size of the biggest Type T HII regions suggests that cloud radii must be much larger than 20 arcsec (6 pc). Thus, $\Delta R/R < 0.25$. Of the HII regions with sizes

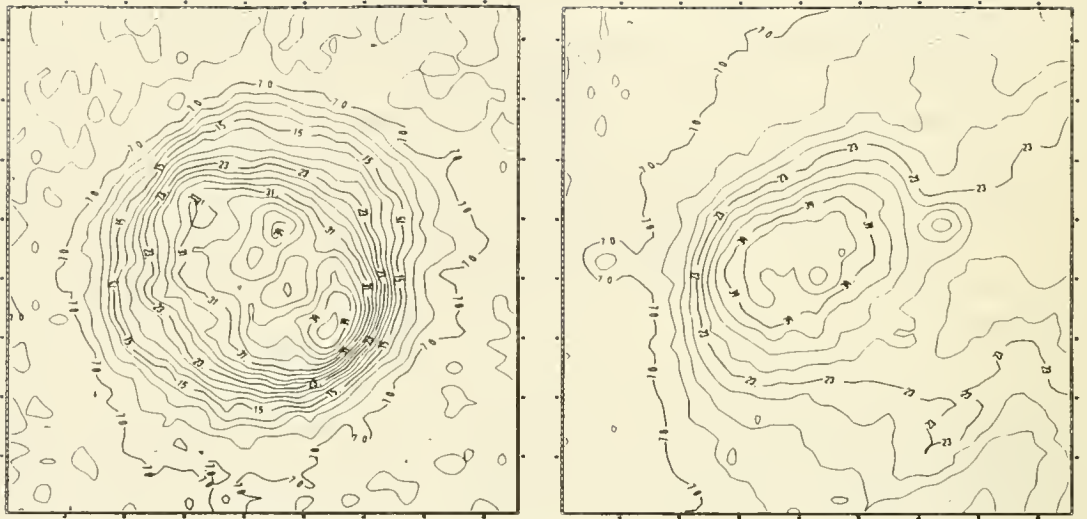


Figure 1. Examples of HII regions of Type T (left) and Type O (right) in the Small Magellanic Cloud, in the light of $H\alpha$. The sides of each box are 44 arcsec in length.

between 10 and 40 arcsec, eight are of Type O and nine are of Type T, so $q = 0.89$. Therefore, $\beta > -0.8$, compared with -1 to -2 in the Milky Way (Waller, W. H., Clemens, D. P., Sanders, D. B., and Scoville, N. Z. 1987, *Ap. J.*, **314**, 397).

The number of Type T objects is too great to accommodate a theory restricting massive star formation to the boundaries of molecular clouds. However, the observations suggest that the gradient in the star formation rate with radius through molecular clouds is shallower, and may even be inverted, with respect to that observed across clouds in the Milky Way. Thus, in the SMC, external triggers may play a larger role in initiating star formation.

Global and Radial Variations in the Efficiency of Massive Star Formation Among Galaxies

Lori E. Allen and Judith S. Young

*Five College Radio Astronomy Observatory
University of Massachusetts*

I. Introduction

It is now well established that interacting galaxies and merged systems have among the highest infrared luminosities observed (*cf.* Joseph and Wright 1985). It has also been shown (Young *et al.* 1986; Solomon and Sage 1988) that the global ratio of the far-infrared luminosity to the molecular gas mass is ~ 7 times higher in interacting galaxies than in isolated galaxies. If the FIR luminosity is produced by the heating of dust by young, massive stars, then these results imply that the perturbations due to galaxy-galaxy interactions result in more efficient production of massive stars in these systems than in their isolated counterparts. Because of the low spatial resolution of the IRAS detectors, the FIR luminosity derived from the 60 μm and 100 μm fluxes represents the *global* FIR emission only; it does not contain information on the *distribution* of star formation within a galaxy.

In order to determine the regions within galaxies which give rise to the most *efficient* star formation and to test the hypothesis that galaxies with high infrared luminosities per unit molecular mass are efficiently producing high mass stars, we have undertaken an $\text{H}\alpha$ imaging survey in galaxies whose CO distributions have been measured as part of the FCRAO Extragalactic CO Survey. From these images we have derived global $\text{H}\alpha$ fluxes and distributions for comparison with FIR fluxes and CO fluxes and distributions. Here we present our results on the global massive star formation efficiency ($\text{SFE} = L_{\text{H}\alpha}/M(\text{H}_2)$) as a function of morphological type and environment, and on the radial distribution of the SFE within both peculiar and isolated galaxies.

II. Observations and Analysis

Measurements of the $\text{H}\alpha$ flux were made using the KPNO No.1-0.9m telescope, with either the RCA or TI CCD direct imaging system, on photometric nights. The $\text{H}\alpha$ + [N II] emission line fluxes were obtained by observing each galaxy through two filters: a narrow ($\Delta\lambda 75 \text{ \AA}$) interference filter centered on $\text{H}\alpha$ at the velocity of the target galaxy, and either a broad R band filter ($\lambda 6470$, $\Delta\lambda 1110$), or a narrow R filter ($\lambda 7024$, $\Delta\lambda 380$). The continuum images were registered and scaled relative to the interference filter images using three to five unsaturated foreground stars. The continuum-subtracted images were flux-calibrated using observations from the same night of CCD photometric standard stars from the KPNO IRS Standard Star Manual.

Some of the $\text{H}\alpha$ fluxes have been corrected for extinction within the target galaxy, using near IR imaging of [S III] $\lambda 9532$, which suffers less extinction than does $\text{H}\alpha$ (Young *et al.* 1988).

We have derived massive star formation rates from $\text{H}\alpha$ luminosities, using an "extended" Miller-Scalo IMF and following the analysis of Kennicutt (1983), in which

$$\text{SFR}(> 2 M_{\odot}) = 3.54 \times 10^{-42} L_{\text{H}\alpha}.$$

The CO observations were made using the FCRAO 14-m telescope in the $J=1 \rightarrow 0$ transition at 2.6 mm. The CO integrated intensities ($\int T_{\text{R}}^* dv \text{ K km s}^{-1}$) were converted to H_2 surface densities using a constant $N(\text{H}_2)/I_{\text{CO}}$ conversion factor of $2.8 \times 10^{20} \text{ H}_2 \text{ cm}^{-2} / [\text{K}(\text{T}_{\text{R}}) \text{ km s}^{-1}]$ (Bloemen *et al.* 1986).

Radial distributions in both $\text{H}\alpha$ and CO have been obtained by azimuthally averaging the measurements made along the major axis of each galaxy. The $\text{H}\alpha$ images have been convolved with a $45''$ gaussian beam in order to make point-by-point comparisons of the molecular and ionized gas at similar resolution.

III. Results and Discussion

We find the mean global ratios $L_{\text{H}\alpha}/M(\text{H}_2)$ and $L_{\text{IR}}/M(\text{H}_2)$ show little variation as a function of morphological type from Sa-Scd, for the galaxies in this sample. Thus, we conclude that disk galaxies have similar *global* star formation efficiencies independent of the galaxy mass and mass distribution. From a comparison of $L_{\text{H}\alpha}/M(\text{H}_2)$ in isolated galaxies versus interacting/merging systems, we find a factor of ~ 7 enhancement of this ratio in interacting systems. Although the $\text{H}\alpha$ emission will suffer extinction and thereby provide a lower limit to the high mass star formation rate, we confirm the result that the high-mass star formation efficiency is enhanced in environmentally disturbed systems (Young *et al.* 1986; Sanders *et al.* 1986; Solomon and Sage 1988). Thus, the property which appears to have the strongest effect on the global efficiency of high mass star formation in galaxies is environment.

Within a small sample of peculiar and interacting galaxies, the radial distribution of star formation efficiency shows steep gradients with radius. In particular, M 82 and NGC 660 show star formation efficiencies which decrease by a factor of 10 to 100 with increasing radius. This is in sharp contrast with the relatively constant star formation efficiency found as a function of radius in the isolated galaxy NGC 6946 (Tacconi and Young 1986).

IV. Conclusions

1. On the basis of comparison of the global $L_{\text{H}\alpha}/M(\text{H}_2)$ and $L_{\text{FIR}}/M(\text{H}_2)$ for 111 galaxies we conclude that *environment* rather than morphological type has the strongest effect on the global efficiency of massive star formation.

2. Based on our study of a small sample, we find that the largest radial gradients are observed in the interacting/peculiar galaxies, indicating that environment affects the star formation efficiency *within* galaxies as well.

References

- Bloemen, J.B.G.L., *et al.*, 1986, *A.A.*, **154**, 25.
 Joseph, R.D., and Wright, G.S. 1985, *M.N.R.A.S.*, **219**, 87.
 Kennicutt, R.C. 1983, *Ap. J.*, **272**, 54.
 Sanders, D.B., *et al.*, 1986, *Ap. J.*, **305**, L45.
 Solomon, P.M., and Sage, L. 1988 *Ap. J.*, **334**, 613.
 Tacconi, L.J., and Young, J.S. 1986 *Ap. J.*, **308**, 600.
 Young, J.S., Kleinmann, S.G., and Allen, L.E. 1988, *Ap. J.*, **334**, L63.
 Young, J.S., *et al.*, 1986, *Ap. J.*, **311**, L17.

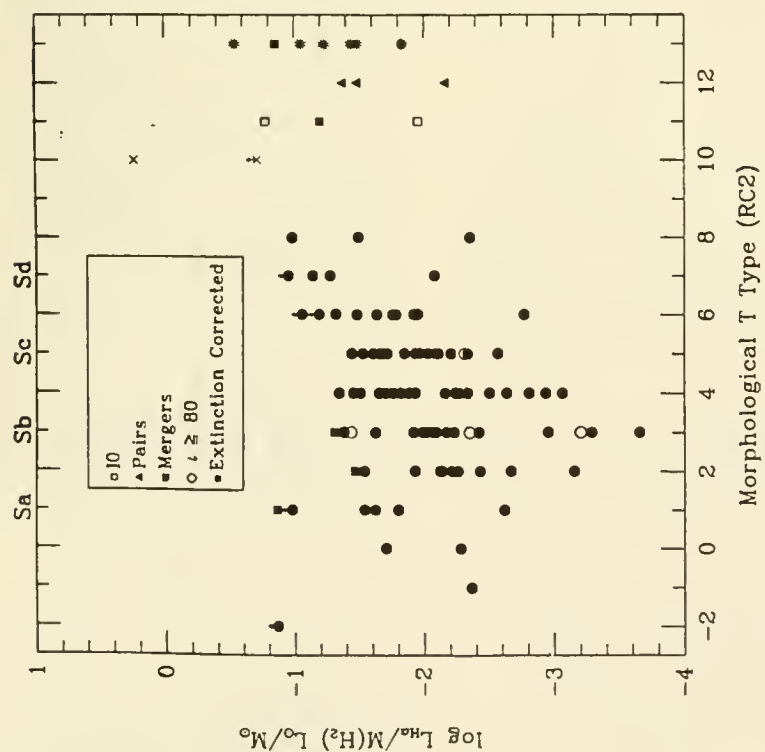
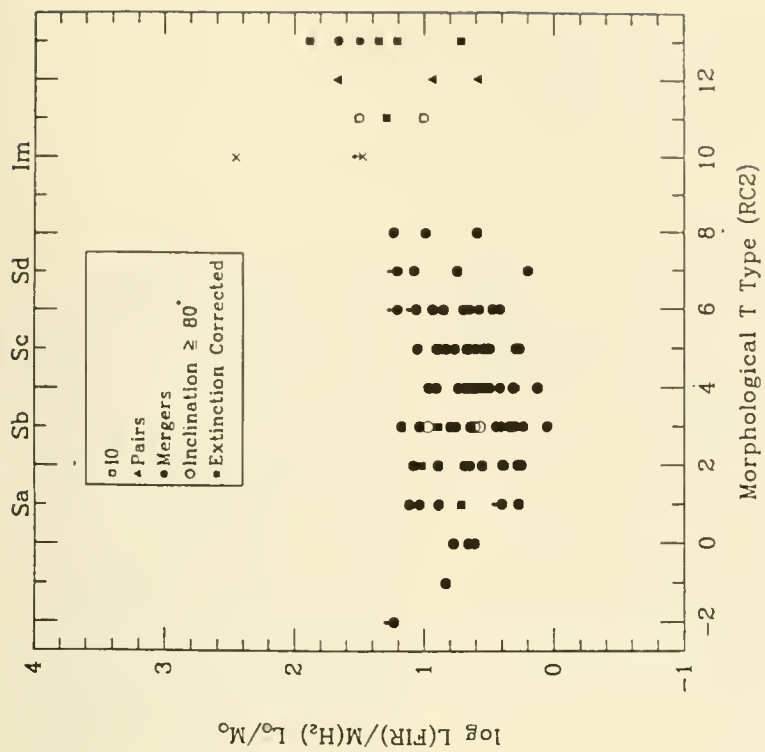


Figure 1. $L_{H\alpha}/M(H_2)$ and $L_{FIR}/M(H_2)$ as a function of morphological type for 111 galaxies. For spirals (types -1 through 8; S0/a through Sdm), the scatter within each type is much greater than the difference in the means between types, indicating that the global efficiency of massive star formation is not strongly dependent on galaxy morphology. The irregular/interacting/peculiar galaxies (types 10-13) have a mean global massive star formation efficiency ~ 7 times higher than that in spiral galaxies, as measured by both $L_{FIR}/M(H_2)$ and $L_{H\alpha}/M(H_2)$.

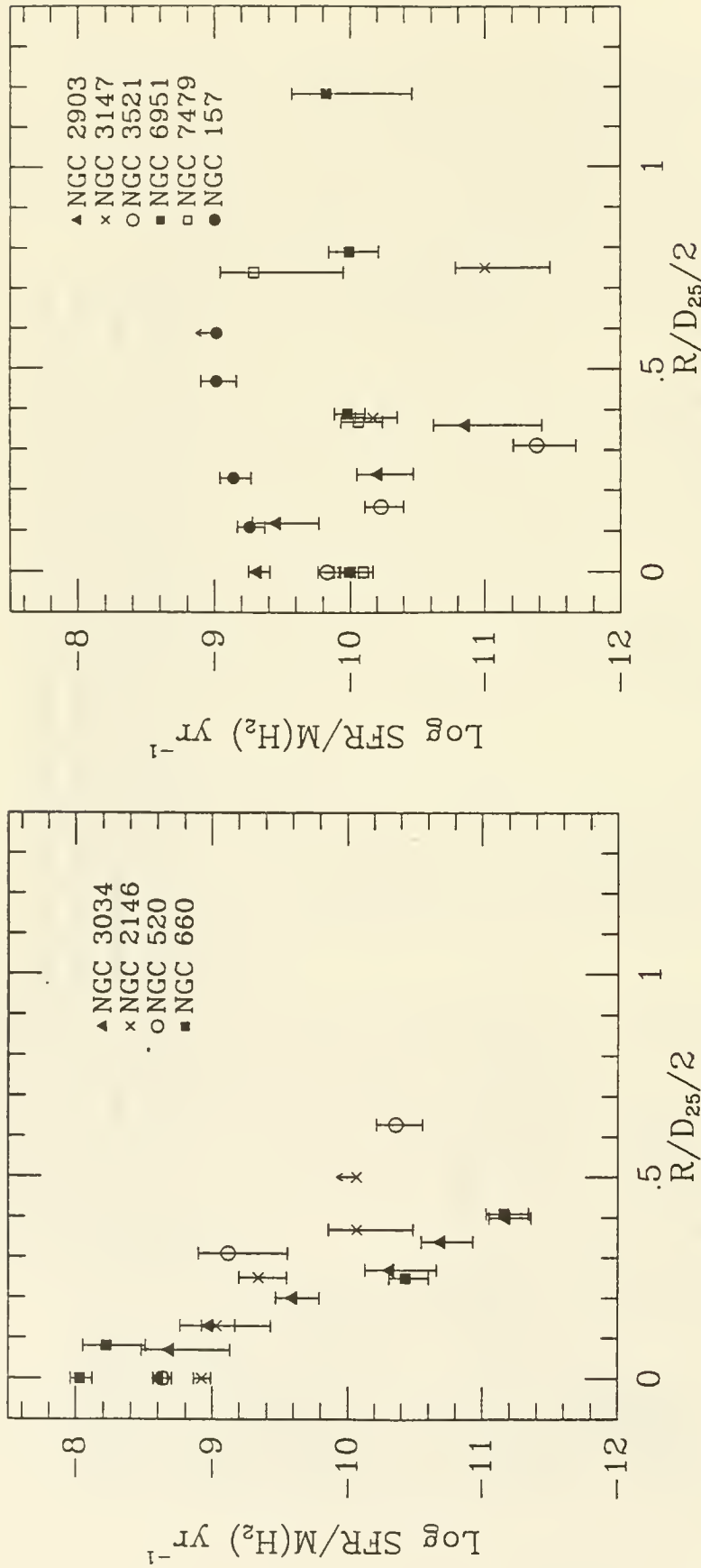


Figure 2. The efficiency of massive star formation as a function of galaxy radius, where the radius has been normalized by $D_{25}/2$ for a) interacting/peculiar galaxies and b) isolated galaxies. Of the interacting/peculiar galaxies, M82 and NGC 660 show the steepest gradients in the radial distribution of the massive star formation efficiency. In M82 the star formation efficiency decreases by a factor of 400 across the galaxy, when the extinction correction has been applied. Without the extinction correction, the radial gradient is still a significant factor of 100. In NGC 660, the extinction corrected data show a gradient in the star formation efficiency of about 10 when no correction for extinction in $1/\alpha$ is applied. NGC 520 and NGC 2146 show significant radial gradients in the SFE after correcting for extinction, but a nearly constant distribution when no correction is made. Of the galaxies in the isolated sample, NGC 7479, NGC 6951, and NGC 157 show roughly constant radial distributions in the SFE. NGC 3147, NGC 3521, and NGC 2903 show radial gradients of $\sim 10 - 40$.

Molecular Gas and Star Formation in the Centers of Virgo Spirals

BLAISE CANZIAN

MOTIVATION

The CO and H α flux distributions for a sample of Virgo spirals have been mapped out in an attempt to understand the coupling between gas dynamics and star formation in spiral galaxies. A broad range of morphological types were observed (types Sab through Scd) under the hypothesis that the gas dynamics is most influential in determining the overall appearance of a spiral galaxy. Only non-barred spirals were considered so that the well-studied but complicated properties of bars and their role in inducing star formation would not be a factor. All galaxies were chosen from the Virgo cluster to eliminate uncertainties due to distance errors. Since the dynamical seat of a spiral is at its center, it was expected that the dynamics of the central region would influence global properties of the rest of the disk. This could happen through the existence or absence of an inner Lindblad resonance (according to the degree of central concentration of mass) to modulate swing amplification of spiral waves, or the persistence of an oval distortion to initiate an instability which leads to spiral structure.

OBSERVATIONS

Observations at the Owens Valley mm-wave interferometer mapped out the CO $J = 1 \rightarrow 0$ emission at the centers of the eight spirals NGC 4254, 4303, 4321, 4501, 4535, 4536, 4569, and 4654. The resolution of the images is about $5'' \times 7''$, or $350 \text{ pc} \times 500 \text{ pc}$, assuming a distance of 14.6 Mpc. The $65''$ field of view encompasses the central 4.6 kpc of these galaxies. Velocity field information was obtained at 13 km sec^{-1} resolution over a 415 km sec^{-1} range. Observations took place over a period of three years, so the image quality improved with increasing system sensitivity over that time. These images are shown in Figure 1. Each contour level is a factor of 1.5 times the one outside it, and all images are produced from a subset of the same levels to permit easy comparison. All maps are at the same scale and have boundaries at the primary beam size. Units are $\text{Jy km sec}^{-1} \text{ beam}^{-1}$.

Maps of H α emission were made from CCD photometry using the Palomar 60-inch telescope with re-imaging optics. The H α maps were processed from two or three frames taken through narrowband ($\approx 80 \text{ \AA}$) filters encompassing H α emission in the rest frame of the galaxy and the surrounding continuum. The frames were scaled and the continuum was subtracted. Absolute flux calibration was accomplished using images of G2V stars and assuming their spectral energy distribution is similar to that of the sun. Flux-calibrated maps of H α emission are shown in Figure 2. The maps are at the same scale and show the same area as those in fig. 1, so the figures may be overlayed for comparison. As in fig. 1, each contour level is a factor of 1.5 greater than the one outside it. The units are $10^{-15} \text{ ergs sec}^{-1} \text{ arcsec}^{-2}$ at the surface of the earth.

DISCUSSION

One striking aspect of the CO distributions is the gratifying variety of forms displayed. Obvious molecular gas bars are present in NGC 4303 and NGC 4654, though neither galaxy shows an optical bar. The molecular gas distribution of NGC 4536 is elongated and is possibly a bar seen in projection in this rather inclined galaxy. The center of NGC 4254 has patchy CO emission with no obvious center. In contrast is NGC 4321, with the suggestion of spiral structure in the molecular gas to the very center and what possibly may be the start of two spiral arms. Other galaxies show rather featureless central gas concentrations with outlying wisps (NGC 4535 and NGC 4569) and without any other emission (NGC 4501).

Comparison with the $H\alpha$ emission maps reveals the tendency of the $H\alpha$ to follow the CO morphology. This tendency is perhaps most notable in the cases of NGC 4535 and NGC 4536. The center of NGC 4254 also has patchy $H\alpha$ emission, though the correlation with CO peaks is not entirely evident. Both maps of NGC 4501 are similarly stark and featureless. The three concentrations of CO emission along a diagonal line across the center of NGC 4321 match with those in the $H\alpha$ map, while the CO concentrations above and below are perhaps the elbows of interior spiral arms which begin to poke from the $H\alpha$ map. The $H\alpha$ emission distribution actually resembles a fan with four blades. This peculiar morphology may be evidence for an interesting dynamical state involving resonances at the center of NGC 4321. One notable exception to the tendency toward common morphology is NGC 4303, whose CO bar is completely absent from the featureless $H\alpha$ concentration. It is, of course, expected at this resolution that young stars be seen where there is molecular gas, but the similarity in form and scale of the two components is still remarkable.

Half of the galaxies show evidence for a bar or oval distortion in their central CO distributions despite the selection against bars. It is possible that many spirals house small bars which are not optically evident. Gas could be collected and sequestered by the resulting flow pattern (examples could be NGC 4321 and NGC 4536) or lose angular momentum and sink to the center (as in NGC 4303, perhaps), fueling much star formation in either case. Such distortions could be the source of a dynamical instability which drives spiral arm formation. Galaxies of earlier morphological type seem to have the more concentrated, featureless CO and $H\alpha$ distributions (NGC 4501, NGC 4569). Coherent spiral arm formation may be hindered in these galaxies by the lack of a central dynamical instability, so the mechanism for collecting so much gas at the centers of these galaxies could be dynamical relaxation.

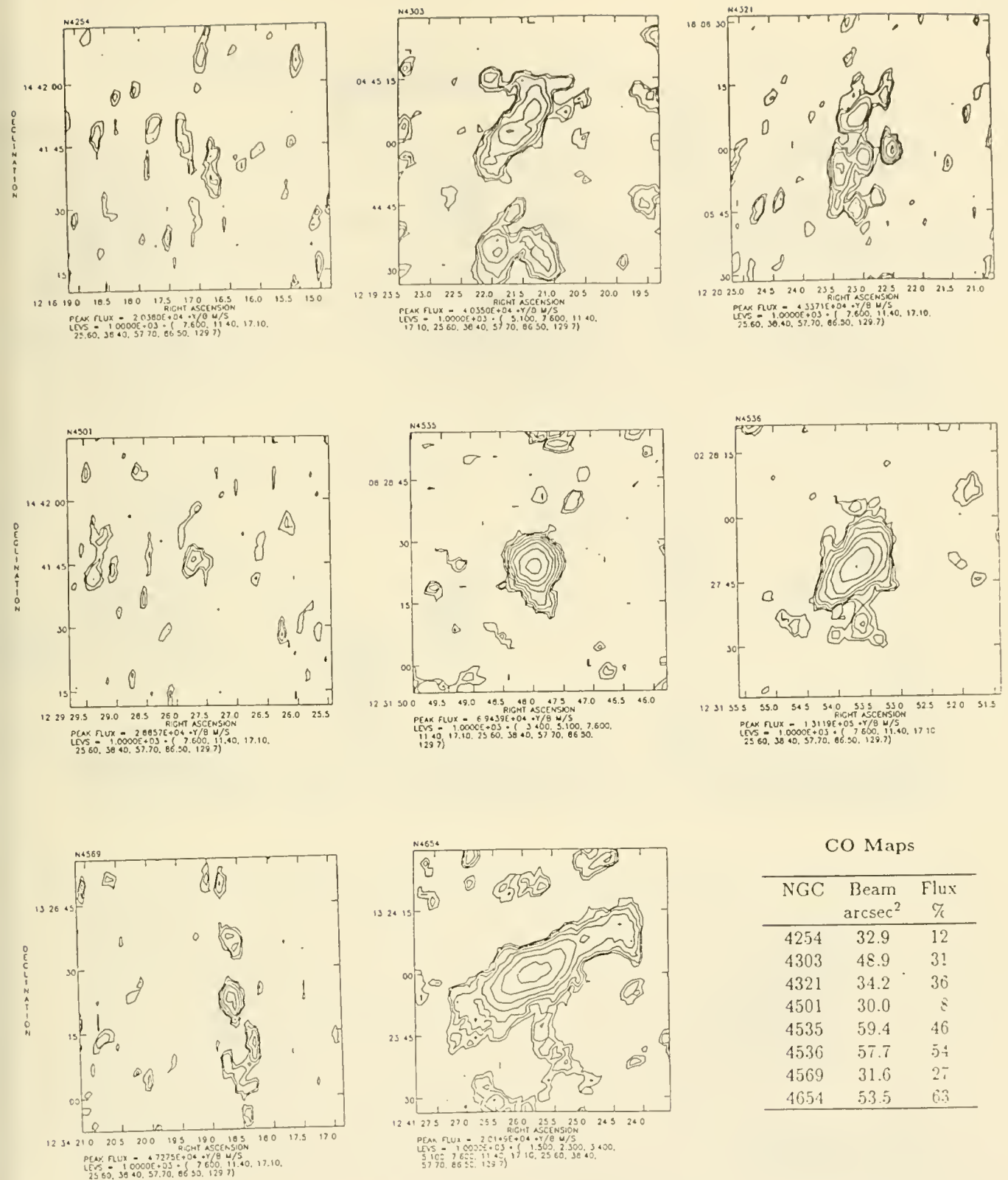


Figure 1. CO $J = 1 \rightarrow 0$ integrated emission from Virgo spirals (left to right, top to bottom) NGC 4254, 4303, 4321, 4501, 4535, 4536, 4569, and 4654. Contours are a subset of 1.5, 2.3, 3.4, 5.1, 7.6, 11.4, 17.1, 25.6, 38.4, 57.7, 86.5, and 129.7 Jy km sec⁻¹ beam⁻¹. Beam areas in arcsec² are shown in the small table. The estimated fraction of the total CO emission recovered in these interferometric images, also shown in the table, is based on single-dish observations at FCRAO by Jeff Kenney.

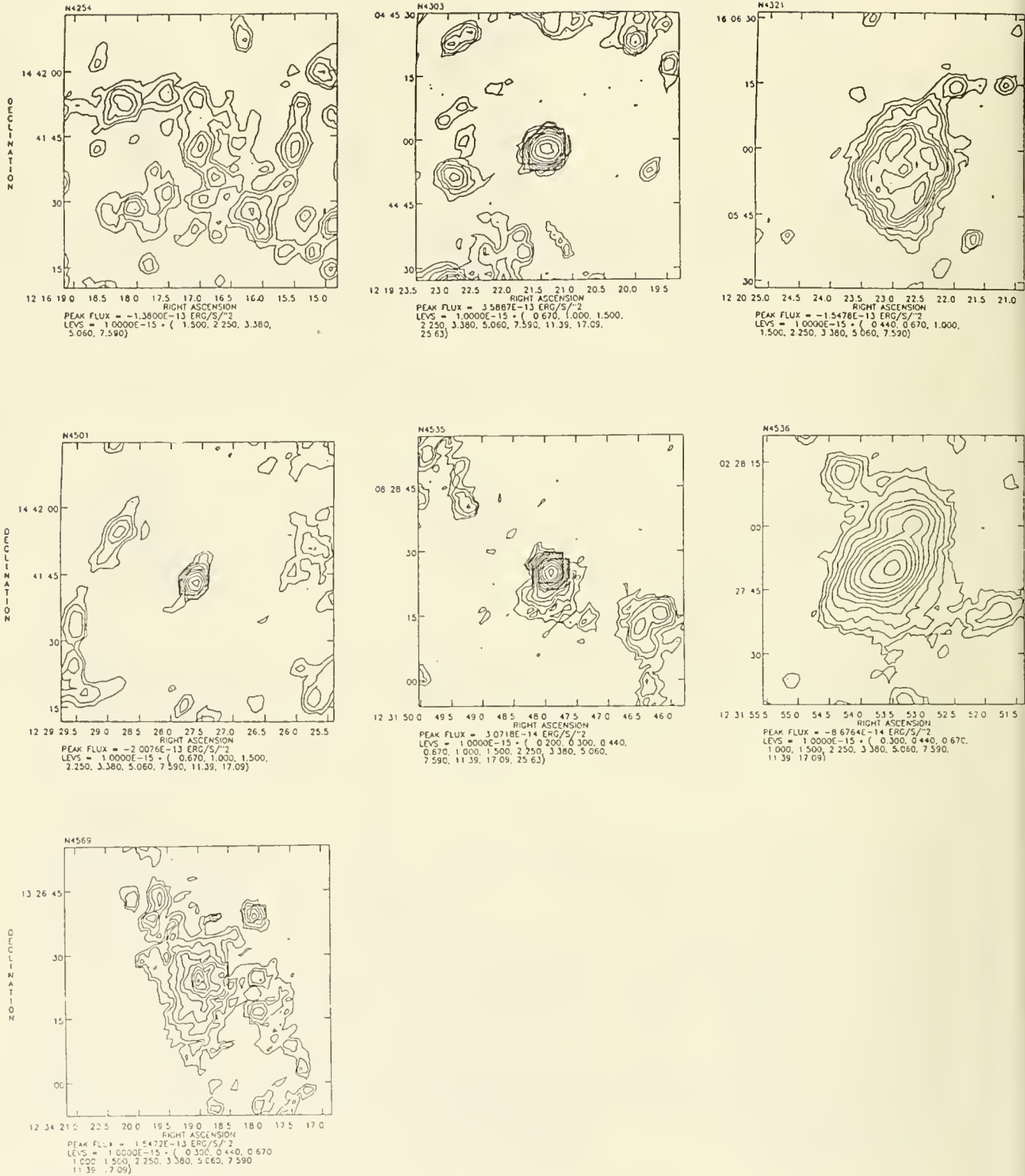


Figure 2. H α emission from the same Virgo spirals as in fig. 1 (except NGC 4654, the last, is omitted). Contours are a subset of 0.2, 0.3, 0.44, 0.67, 1, 1.5, 2.25, 3.38, 5.06, 7.59, 11.39, 17.09, and 25.63×10^{-15} ergs sec $^{-1}$ arcsec $^{-2}$ at earth. The scale is the same as in fig. 1.

Near-Infrared Mapping of Spiral Barred Galaxies

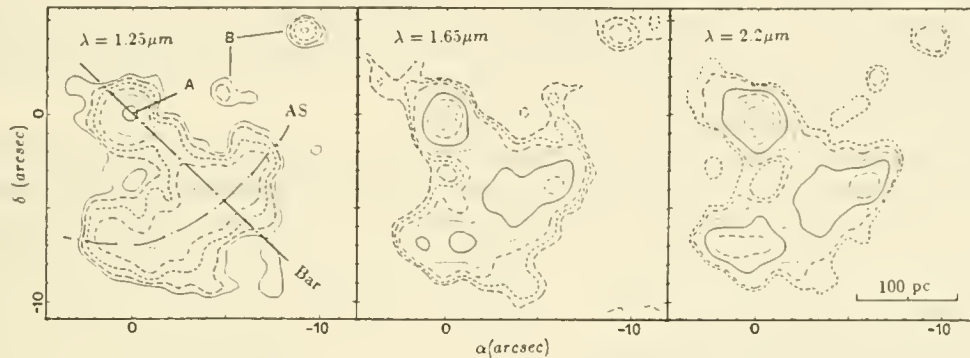
P. GALLAIS, D. ROUAN, F. LACOMBE

DESPA, Observatoire de Meudon, 92195 Meudon, FRANCE

In external galaxies, near-infrared emission originates from stellar populations, hot dust, free-free emission from H^+ regions, gaseous emission, non-thermal nucleus if any. Because of the low extinction compared to the visible, infrared wavelengths are useful to probe regions obscured by dust such as central parts where *starburst* phenomena can occur because of the large quantity of matter.

The results presented below were obtained with a 32×32 InSb CID array cooled at 4K, at the f/36 cassegrain focus of the 3m60 Canada-France-Hawaii telescope with a spatial resolution of $0.5''$ per pixel^{1,2}.

The objects presented below are spiral barred galaxies mapped at J($1.25\mu m$), H($1.65\mu m$) and K($2.2\mu m$). The non-axisymmetric potential due to the presence of a bar induces dynamical processes leading to the confinement of matter and peculiar morphologies. Infrared imaging is used to study the link between various components. Correlations with other wavelengths ranges and 2-colors diagrams ([J-H],[H-K]) lead to the identification of star forming regions, nucleus. Maps show structures connected to the central core; are they flowing away or toward the nucleus ?



Isophotes maps of NGC 5236 at J, H and K. Region A (nucleus), B ($6cm/10\mu m$ peaks) and AS (arc-like structure) are quoted on the J map; direction of the bar is also drawn. Contours are separated by 0.5 mag/arcsec^2 , lowest contours are $16.5 \text{ mag/arcsec}^2$.

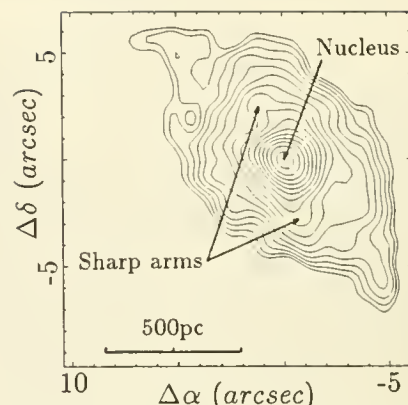
M83 is the nearest barred spiral located at a distance of 3.75 Mpc. It features an "amorphous" nuclei at visible wavelengths^{3,4} while infrared maps show a rather complex structure.

- A point-like source, which has typical color indices of a normal stellar nucleus, reddening by $A_v = 2$ and mixed with gaseous content.
- An arc-like structure, at 120 pc of the nucleus, showing a patchy distribution and extending from south-east to north. Southern color indices are characteristic of a giant and/or supergiant population while northern ones reveal the presence of gas.
- At north, a point-like source correlated with a low flux level source to radio and $10\mu m$ peaks^{5,6} characterizes a starburst region.

From these observations, several conclusions result:

- The star forming region, detected in the visible and the infrared cannot be very compact and must extend to the edge of the matter concentration.
- The general shape of the near-infrared emission and the location of radio and $10\mu m$ peaks suggest the confinement of matter between the inner Linblad resonances localized from CO measurements about 100 and 400 pc.
- The distribution of color indices in the arc from southern part to the star forming region suggests an increasing amount of gas and a time evolution eventually triggered by super nova explosions.
- Close to the direction of the bar, a bridge-like structure connects the arc to the nucleus with peculiar color indices. Perhaps, this structure can be linked to a high velocity component seen in UV⁷ and we can attribute it to a "jet"⁸ and/or a matter flow along the bar toward the nucleus, fuelling it⁹.

Isophotes map of NGC 1068 at J. Contours are separated by $0.25 \text{ mag/arcsec}^2$, the lowest contour is $16.5 \text{ mag/arcsec}^2$.

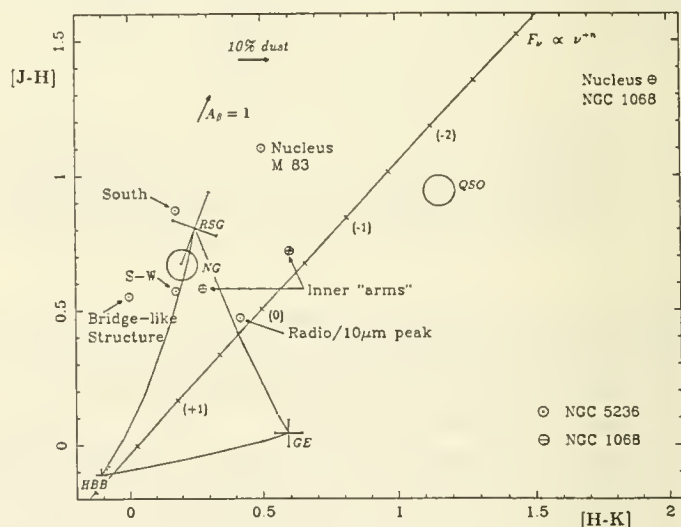


NGC 1068 is the nearest Seyfert 2 galaxy. It has been subject of many studies at all wavelengths. This object was mapped at J, H, K, L and M, and in polaro-imagery:

- No infrared counterpart to the radio jet, however a small structure is present at the north of the nucleus.
- Color indices of the nucleus are typical of quasar, if we assume that a hot dust component contributes to the emission. This agrees with the assumption of an obscured Seyfert 1 nucleus.
- A strong stellar bar oriented north-east/south-west.
- Two sharp arms linked to the nucleus, starting from north to north-east and south to south-west oriented in the direction of the bar. Color indices are those of a stellar component with contribution of ionized gas.

Two-colors diagram (J-H)/(H-K).

⊙ and ⊕ refer respectively to NGC 5236 and NGC 1068. The colors of three possible infrared contributors, red super giants (RG), gaseous emission (GE) and a 42500K blackbody (HBB) are plotted joined by mixed lines (from Campbell and Terlevich, 1984¹⁰). Straight line represents colors of a power-law with various spectral indices and filled circles represent the area populated by "normal" galaxies (NG) and quasars (QSO).



References

1. Tiphène, D., Rouan, D. and Lacombe, F., 1987, *Infrared Astronomy with Arrays*, Eds C.G. Wynn-Williams and E.E. Becklin, Hilo, Hawaii, march 24-26 1987.
2. Lacombe, F., Tiphène, D., Rouan, D., Léna, P. and Combes, M., 1989, *Astron. Astrophys.*, **215**, 211.
3. Pastoriza, M.G., 1975, *Astrophys. Spa. Sci.*, **33**, 173.
4. Wood, R. and Andrews, P.F., 1974, *Mon. Not. R. astron. Soc.*, **167**, 13.
5. Telesco, C.M., Decher, R. and Ramsey, D., 1986, in *Star Formation in Galaxies*, C.J. Lonsdale Persson (Editor), NASA Conference Publication 2466, p.497.
6. Telesco, C.M., 1988, *Ann. Rev. Astron. Astrophys.*, **26**, 343.
7. Bohlin, R.C., Cornett, R.H., Hill, J.K., Smith, A.M. and Stecher, T.P., 1983, *Astrophys. J. Letters*, **274**, L53.
8. Keel, C.W., 1987, in *Observational Evidence of Activity in Galaxies*, IAU Symposium n°121, Kachikian et al. (eds), p.25255.
9. Shlosman, I., Frank, J. and Begelman, M.C., 1989, *Nature*, **338**, 45.
10. Campbell, A.W. and Terlevich, R., 1984, *Mon. Not. R. astron. Soc.*, **211**, 15.

High-Mass Star Formation in Southern Disk Galaxies

Michael A. Dopita¹, J.R. Forster² and Lilia Ferrario¹

¹Mount Stromlo and Siding Spring Observatories,
Australian National University.

²Australia Telescope National Facility, Narrabri
CSIRO - Paul Wild Observatory

I. Introduction

Accurately calibrated images in the light of H α provide a reliable measure of the star formation rate in galaxies. This is because the H α flux effectively counts the total number of Lyman continuum photons produced by young, massive stars. The absolute flux in the continuum adjacent to H α may be used to measure the mass of intermediate and low mass stars. The gas content in the galaxy is most accurately obtained from radio observations in the 21 cm line of neutral hydrogen. Radio continuum observations also provide a measure of the star formation rate, since the radio flux density can be related to the number of Lyman continuum photons. Radio continuum data can be used to correct the optical observations for extinction.

Using high-resolution optical and radio images of external galaxies, the rate and distribution of star formation in the disk and nuclear regions can be derived. The distributions can be used to provide fundamental data on star formation processes in galaxies, and to test existing theories. For example, Dopita (1985) has shown that a general law of star formation in disk galaxies can be derived on the assumption that energetic processes, themselves associated with star formation, pressurize the interstellar medium and maintain the z-velocity dispersion of the gas. These ideas have since been developed, (Dopita, this conference) and this has led to a model in which star formation rates can be predicted as a function of gas content, metallicity and past star formation history. If σ_g , σ_* , and σ_t are the surface densities of gas, stars and of the matter, respectively, and if z_g and z_* are the scale heights of the gas and stars, respectively, then the rate of star formation of massive stars per unit area is given by a relation of the form:

$$\text{SFR} = \text{const.} [z_*/(z_* + z_g)]^{1/3} \cdot \sigma_t^{1/3} \cdot \sigma_g^{4/3}$$

This relationship agrees well with the observational data gathered by Kennicutt (1989) in other disk galaxies.

As part of a major study of the physical processes of star formation and the evolution of galactic discs, the detailed distribution of high-mass star formation within southern late-type spirals and Magellanic-type galaxies is being measured by means of narrow-band imaging in H α and the continuum, spectroscopic studies of prominent HII regions identified in the H α images, and by radio mapping in neutral hydrogen and the continuum. The radio mapping will be undertaken with the southern hemisphere's first large, multi-frequency synthesis array, the Australia Telescope. Some optical imaging and spectroscopic data has already been acquired; the optical data and some preliminary results are described below.

II. Observations

Optical images in H α and the adjacent continuum at $\lambda 6626\text{\AA}$ have been obtained for six galaxies using the 3.9 m Anglo-Australian Telescope (AAT) located at Siding Spring, NSW, Australia, and for four nearby galaxies using the 2.3 m new-technology telescope of the Mount Stromlo and Siding Spring Observatories. The filters used for the H α work are 16\AA wide (FWHM), and so exclude contamination from the nearby [NII] lines. After

calibration to absolute flux using the Magellanic Cloud PN as flux standards, these data can be used to derive the radial distributions of the massive young stars, and of the older stellar population.

Spectra of prominent HII regions are taken with AAT in the $\lambda\lambda 3600-7500 \text{ \AA}$ region. These will be used to provide data on variations in chemical abundance using the methodology developed by Evans and Dopita.

III. Results

Radial distributions of the $\lambda 6626 \text{ \AA}$ continuum (proportional to the number of older disk stars) and the H α flux (proportional to the number of young, massive stars) are shown in Fig. 1 for four galaxies mapped with the AAT. In these and all other galaxies studied so far, the scale length for star formation is greater, and in some cases much greater, than the scale length of the underlying exponential disk of stars already formed. If a relation of the form given above applies to the star forming disk, then the implication of these observations is that the radial distribution of the gas is flatter than that of the stars. We hope to confirm this supposition, and to define the exact form of the star formation law, using AT observations in both the HI and in the CO lines.

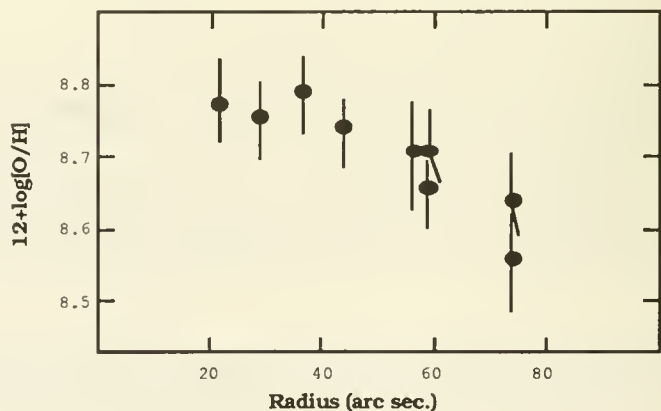
The star-forming activity as defined by the H α distribution shows a fairly sharp outer cut-off at a particular radial distance. This in agreement with the results of Kennicutt (1989), who suggests that this is caused by the onset of global instabilities in the gaseous layer (Quirk, 1972).

The radial distribution of the oxygen/hydrogen abundance ratio derived from spectroscopic observations of HII regions in NGC 3423 is shown below. The oxygen abundance gradient has a scale length which is two times greater than the star formation gradient, and four times greater than the scale length of the stellar disk. Since the O/H ratio is set directly by the total amount of star forming activity that has occurred in the disk gas, data of this type will put very strong limits on the history of star formation, and quantify the importance of infall or radial flows.

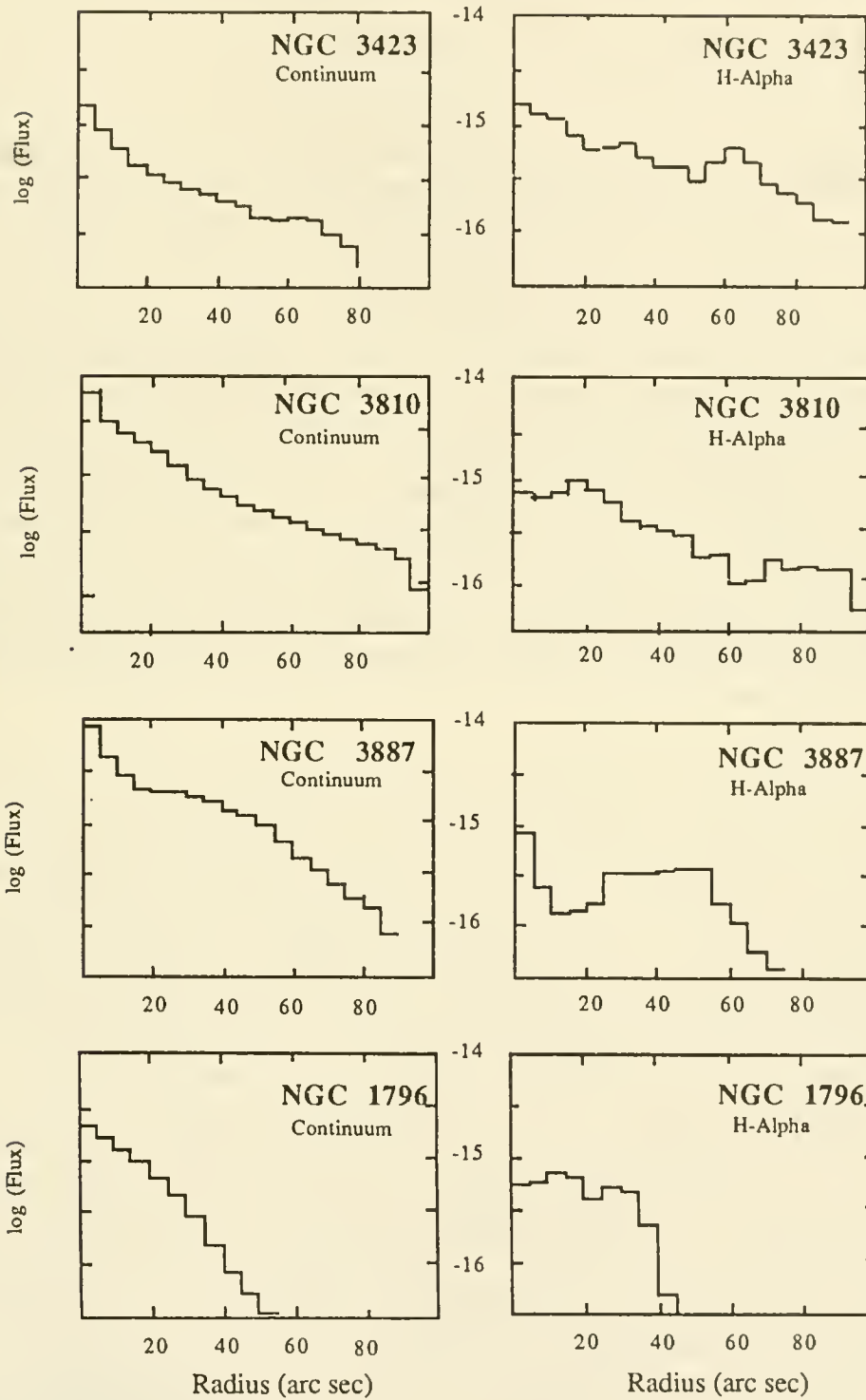
References

- Dopita, M.A. 1985 *Ap.J. (Lett.)*, **295**, L5.
Dopita, M.A., 1989 Proceedings of this Conference.
Kennicutt, R. 1989, *Ap. J.* (in press). See also proceedings of this conference.
Quirk, W.J., 1982, *Ap. J.*, **176**, L9.

Figure 2: The radial abundance gradient in NGC 3423. The scale length for the abundance gradient is about twice that of the star formation rate gradient, and four times that of the stars already formed.



Continuum and H-alpha Radial Variation



STARBURST OUTFLOWS FROM NEARBY GALAXIES

William H. Waller, University of Washington

1. NGC 5461: The Sc I galaxy, M101, is renowned for the kpc-size “superassociations” of star clusters and HII regions that dominate its spiral arms. NGC 5461 is one of the brightest of these superassociations, rivaling the Large Magellanic Cloud in $H\alpha$ luminosity. Figure 1 shows this region in the light of $H\alpha$, as observed with the McGraw-Hill 1.3 m telescope (Waller 1989). Unlike its complicated neighbor, NGC 5462, the NGC 5461 superassociation is dominated by a single unresolved HII region of outstanding luminosity (~ 1000 Orion nebulae). Figure 1 also shows 3 plume-like features of diffuse ionized gas diverging from the brilliant core toward the South, Southeast, and East. Detailed examination of corresponding continuum images indicates that only the southern plume has any sort of stellar counterpart. The other plumes are clearly diffuse with no underlying hot stars. Seen in projection, the plumes extend for roughly 650 pc (for an adopted distance to M101 of 4.8 Mpc). An HI map with a resolution of $30''$ (700 pc) reveals a pronounced bulging on the southeast (“plume”) side of NGC 5461 (Viallefond *et al.* 1981). Higher resolution mapping of the HI emission (using the VLA) as well as sensitive radial-velocity mapping of the diffuse $H\alpha$ emission (using Fabry-Perot interferometry or dense-pack multifiber spectroscopy) would greatly aid in the correct interpretation of this outflow candidate.

2. NGC 1569: Figure 2 shows this “posteruptive” Irr I galaxy in the light of $H\alpha$, as observed with the #1 0.9 m telescope at Kitt Peak (Waller 1989). Besides showing the peculiar “arm” noted by Zwicky (1971) and the filamentary extensions to the North and South (as noted by Hodge 1974), this image also reveals two arc-like features of diffuse ionized gas to the South. Both “arcs” are concentric with the bright center of the galaxy – where the super star clusters, A and B, are located. The inner arc (“Arc 1”) appears to follow the same curve as the SW “arm” thus suggesting that the two features represent limb-brightened fragments of a vast superbubble that was blown out by a central starburst sometime in the past. The displacements of the “arcs” from the center of the galaxy are estimated to be 1.2 and 1.5 kpc respectively (assuming a distance of 2.2 Mpc and an orientation along the minor axis which is inclined 27° to the plane of the sky). The $H\alpha$ velocity field of de Vaucouleurs (1981) shows a strong gradient along the minor axis which, if due to outflowing motions along the minor axis, would imply outflow velocities of up to 90 km s^{-1} . The resulting kinematic ages for the “arcs” would be 13 and 16 Myr respectively. These crude estimates for the age of the nuclear starburst are well-matched with the age that Israel and de Bruyn (1988) estimate based on the last major injection of energetic electrons into the ISM. The mechanical energy required to create the superbubble is estimated to be $\sim 10^{54}$ ergs, or the equivalent of $\sim 10^3 - 10^5$ supernovae – depending on the coupling efficiency between the supernova energy and mechanical motions of the gas. A coherent ($\Delta t \leq 1 \text{ Myr}$) salvo of this many supernovae could have detonated in the nucleus without exceeding the supernova rate that Israel and de Bruyn (1988) estimate from their radio continuum measurements.

3. M82: As the classic “starburst galaxy,” M82 displays all the luminous hallmarks of intense high-mass star formation and outflow activity (*cf.* Telesco 1988; Sofue 1988). The diffuse H α and x-ray emitting gas along the minor axis provides especially good evidence for a bipolar outflow of hot (10^7 K) gas which is shock heating the swept-up ISM to temperatures of $\sim 10^4$ K (Watson *et al.* 1984; Bland and Tully 1988). Figure 3a shows the H α emission within the disk and along the minor axis. Figure 3b shows the same field in the light of near-infrared [SIII]($\lambda 9532$). Both figures are based on CCD images taken with the McGraw-Hill 1.3 m telescope (Waller 1989). The longer wavelength emission clearly shows a more extended morphology along the major axis. The morphological discrepancy is most likely due to the greater obscuration by dust suffered by the H α photons. Figure 3c shows the map of visual extinction that I derive from a pixel-by-pixel comparison of the [SIII] and H α fluxes. The greatest extinctions are evident along an arc that includes two especially obscured regions on opposite sides of the bursting nucleus. The arclike morphology of the obscuration as well as the strong peripheral extinction can be attributed to a circumnuclear ring of dust that is highly inclined to the line of sight. This is akin to the “dusty chimney” picture that Nakai *et al.* (1987) proposed to explain the “spur-like structures” evident in their CO map. Alternatively, the arc could be tracing the remnant of a superbubble which burst towards the South. A recent high-resolution mapping of the HI in M82 (Yun, Ho, and Lo 1989) seems to corroborate the shell remnant scenario, in that the greatest concentrations of circumnuclear HI are to the Northeast and Northwest of the central starburst just beyond the obscuring arc. Although these comparisons do not lead to a well-defined morphology, they reinforce the picture of a circumnuclear pile-up of dust and gas ($M \sim 4 \times 10^8 M_{\odot}$) that has been shaped by the starburst and is now collimating the subsequent eruptions ($E \sim 10^{56}$ ergs).

References:

- Bland, J. and Tully, R. B. 1988. *Nature*, **334**, 43.
- Hodge, P. W. 1974. *Ap. J. (letters)*, **191**, L21.
- Israel, F. and de Bruyn, A. G. 1988. *Astr. Ap.*, **198**, 109.
- de Vaucouleurs, G. 1981. *Sky & Telescope*, **62**, 406.
- Nakai, N., Hayashi, M., Handa, T., Sofue, Y., Hasagawa, T., Sasaki, M. 1987. *Publ. Astr. Soc. Japan*, **39**, 685.
- Sofue, Y. 1988. in *Galactic and Extragalactic Star Formation*, eds. R. Pudritz and M. Fich (Dordrecht: Kluwer Academic Publ.).
- Telesco, C. M. 1988. *Ann. Rev. Astr. Ap.*, **26**, 343.
- Viallefond, F., Allen, R. J., and Goss, W. M. 1981. *Astr. Ap.*, **104**, 127.
- Waller, W. H. 1989. *Recent Starbirth and Starburst Activity in Nearby Galaxies*, Ph.D. Thesis, University of Massachusetts.
- Watson, M. G., Stanger, V., and Griffiths, R. E. 1984, *Ap. J.*, **286**, 144.
- Yun, M. S., Ho, P. T. P., and Lo, K. Y. 1988. *B. A. A. S.*, **20**, 1001.
- Zwicky, F. 1971. *Catalogue of Selected Compact Galaxies and Post-Eruptive Galaxies* (Zurich: Speich).

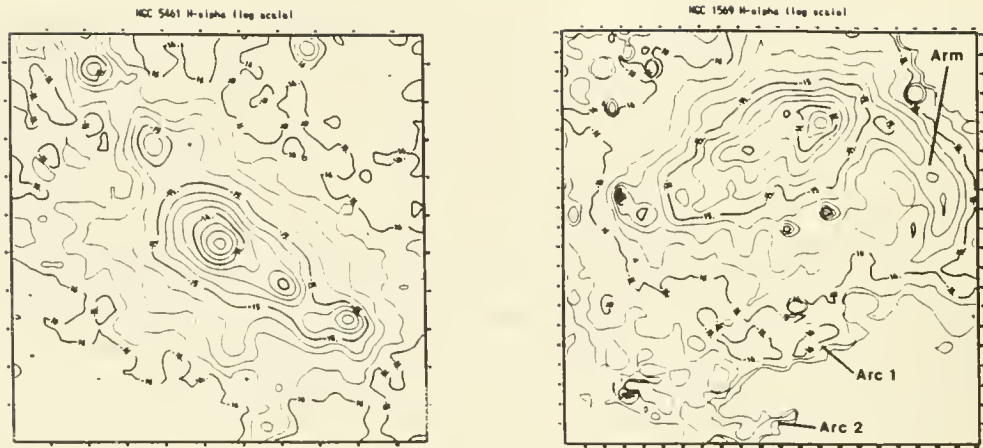


Figure 1. NGC 5461 in the light of H α . The field of view is $1.43' \times 1.43'$ (2 kpc \times 2 kpc at a distance of 4.8 Mpc). The surface brightness is contoured in logarithmic intervals of 0.25 starting at $10^{-16} \text{ erg s}^{-1} \text{ cm}^{-2} \text{ arcsec}^{-2}$. Low surface brightness "plumes" of ionized gas are evident, diverging from the brilliant core toward the South, Southeast, and East.

Figure 2. NGC 1569 in the light of H α . The field of view is $3' \times 3'$ (1.9 kpc \times 1.9 kpc at a distance of 2.2 Mpc). The surface brightness is contoured in logarithmic intervals of 0.25 starting at $3.2 \times 10^{-17} \text{ erg s}^{-1} \text{ cm}^{-2} \text{ arcsec}^{-2}$. The "arm" and "arcs" are diffuse features with no stellar counterparts.

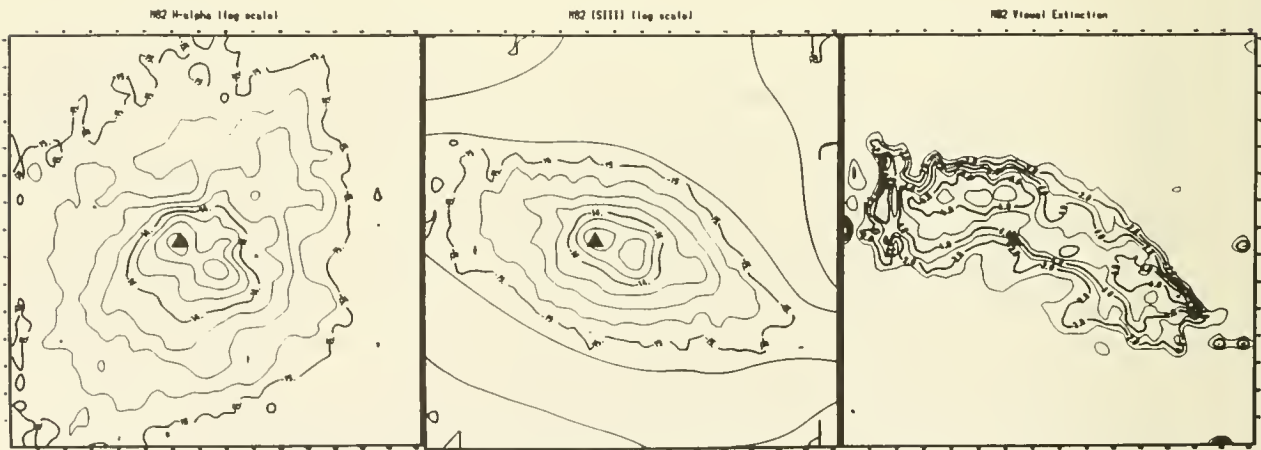


Figure 3. The H α emission from M82 (a); the corresponding [SIII] λ 9532 emission (b); and the visual extinction (c) as derived from the [SIII]/H α flux ratio. The field of view is $2' \times 2'$ (1.9 kpc \times 1.9 kpc at a distance of 3.25 Mpc). The surface brightness maps are contoured in logarithmic intervals of 0.25 starting at $10^{-15} \text{ erg s}^{-1} \text{ cm}^{-2} \text{ arcsec}^{-2}$ for the H α emission and $3.2 \times 10^{-16} \text{ erg s}^{-1} \text{ cm}^{-2} \text{ arcsec}^{-2}$ for the [SIII] emission. The map of visual extinctions is contoured from 1.0 to 7.0 mag. in intervals of 1.0 mag. The filled triangle designates the position of the 2.2 μ m stellar nucleus.

Dense Gas and HII regions in the Starburst Galaxy NGC 253

J.E. Carlstrom (U. C. Berkeley), J. Jackson (MPI), P.T.P. Ho (CfA),
and J.L. Turner (U.C.L.A.)

The energetic activity in the nuclear barred region of NGC 253 is attributable to a burst of star formation. NGC 253 is in many ways a twin of the 'prototypical' starburst galaxy M82; the strong non-thermal radio continuum, high far-infrared luminosity, and bright molecular emission of the central 1 Kpc parallel the morphology of the M82 starburst. Furthermore, the filamentary low ionization optical emission and extended X-ray emission along the minor axis in NGC 253 is similar to a scaled down version of the well developed galactic bipolar wind in M82. The infrared luminosity of NGC 253, $3 \times 10^{10} L_{\odot}$, is comparable to M82 but is emitted from a smaller region (Telesco and Harper 1980). This suggests that the NGC 253 starburst may be more intense and at an earlier evolutionary stage than M82. However, the presence of a non-stellar AGN in NGC 253 may complicate the comparison (Turner and Ho, 1985).

We used the Hat Creek millimeter interferometer to map emission from the $J = 1 \rightarrow 0$ transitions of HCN and HCO^+ , as well as 3 mm continuum emission, toward the nuclear region of NGC 253. The HCO^+ and continuum observations are sensitive to spatial scales from 6" to 45". The 2' field of view comfortably includes the entire starburst region ($\sim 40''$; 650 pc). Because the longer baseline HCN observations are not yet complete, they are only sensitive to spatial scales from 15"- 45".

The HCN and HCO^+ emission trace high density molecular gas ($n(\text{H}_2) > 10^4 \text{ cm}^{-3}$). Therefore the similar distributions of the HCO^+ emission (see figure 1), the HCN emission (not shown here), and the bright CO emission (see figure 1 in Canzian *et al.* 1988) suggests that the molecular gas associated with the starburst is dense. Although not resolved in the integrated emission map, the spectra (see figure 1) and the position velocity map in figure 2 reveal two components of dense gas. The two velocity components are separated by approximately 9" (~ 140 pc in projection). The emission centroid is coincident with the nucleus and the base of the X-ray emission (see figure 1). The two components are most easily explained as limb brightened emission from a torus of dense gas similar to the molecular circumnuclear ring inferred for M82. However, the molecular ring in NGC 253 is much smaller than the ring in M82 (140 pc vs. 400 pc).

The 3.3 mm continuum emission, resolved by the interferometer observations (see figure 3a), is confined to the heart of the starburst region. As in M82 (Carlstrom 1988), the 3.3 mm emission is distributed similar to emission at longer wavelengths which are dominated by nonthermal emission. The continuum emission in both galaxies peaks at the base of the optical filamentary emission and X-ray emission and appears to be 'bracketed' by dense molecular gas (see figure 3b). The 3.3 mm flux (0.35 ± 0.05 Jy) sets an upper limit to the thermal free-free emission from HII regions. Although thermal emission from dust is a small fraction of the 3.3 mm flux, the contribution from non-thermal emission is not presently known. The ratio of the infrared luminosity to Lyman continuum luminosity ($N_L = 4.7 \times 10^{53} \text{ s}^{-1}$ for $S_{ff} = 0.35$ Jy at 3.3 mm) for NGC 253 is twice the ratio measured for M82 (Carlstrom 1988). This suggests that the HII regions may be less evolved in NGC 253 with dust competing effectively for the ionizing photons. Alternatively, lower mass stars may be relatively important in NGC 253, supplying more non-ionizing luminosity.

The observations also support the evolutionary scenario of starbursts suggested by several authors and recently outlined by Rieke *et al.* (1988). In this scenario NGC 253 is at an earlier evolutionary stage than M82. Superbubbles of the thermalized ejecta of numerous supernovae have broken out of one of the poles of the galaxy disrupting the molecular clouds. Within the plane of the galaxy, a portion of the kinetic energy has compressed and pushed the molecular clouds out of the very center forming a dense molecular torus. Further evidence for this evolutionary scenario is given in Rieke *et al.* (1988).

Although a considerable number of observational investigations have focussed on the state of the interstellar medium of the starburst region in M82 and it is now fairly well understood, the relevance of this knowledge to other starburst galaxies has been debated. The high resolution observations of NGC 253 presented here demonstrate that M82 is not unique.

This work was supported by NSF grant AST87-14721.

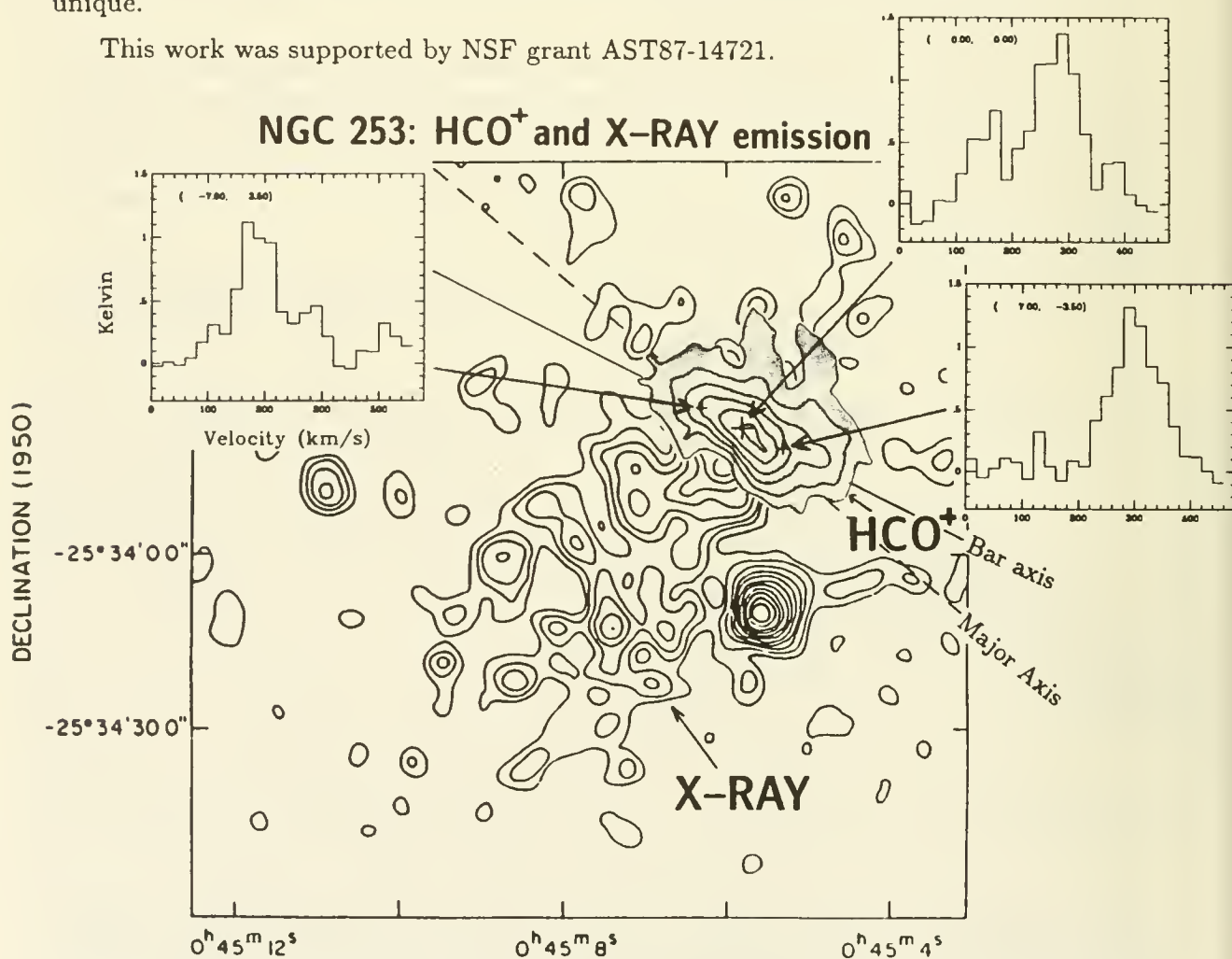


Figure 1. The HCO⁺ $J = 1 \rightarrow 0$ integrated emission plotted on the X ray map of Fabbiano and Trinchieri (1984). The HCO⁺ emission contours are multiples of $13.5 \text{ Jy} \cdot \text{km}^{-1}$ per beam. The synthesized beam is $10.8'' \times 7.0''$. The solid line marks the position angle of the major axis and the dotted line marks the position angle of the stellar bar (Scoville *et al.* 1985). Note that the dense molecular gas tends to 'bracket' the base of the X-ray emission.

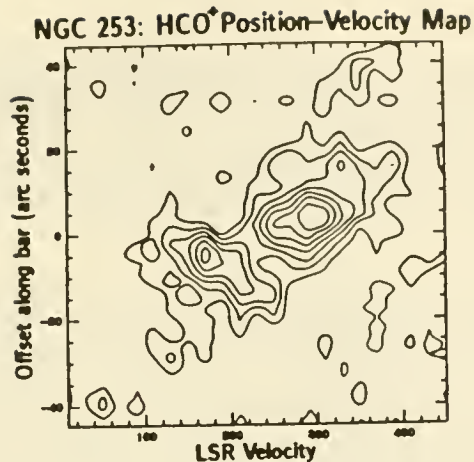


Figure 2. A position velocity map of the HCO^+ emission. The cut is along the major axis. The nucleus is at $0''$. Note that the HCO^+ emission is from two separate velocity components spatially separated by $\sim 9''$.

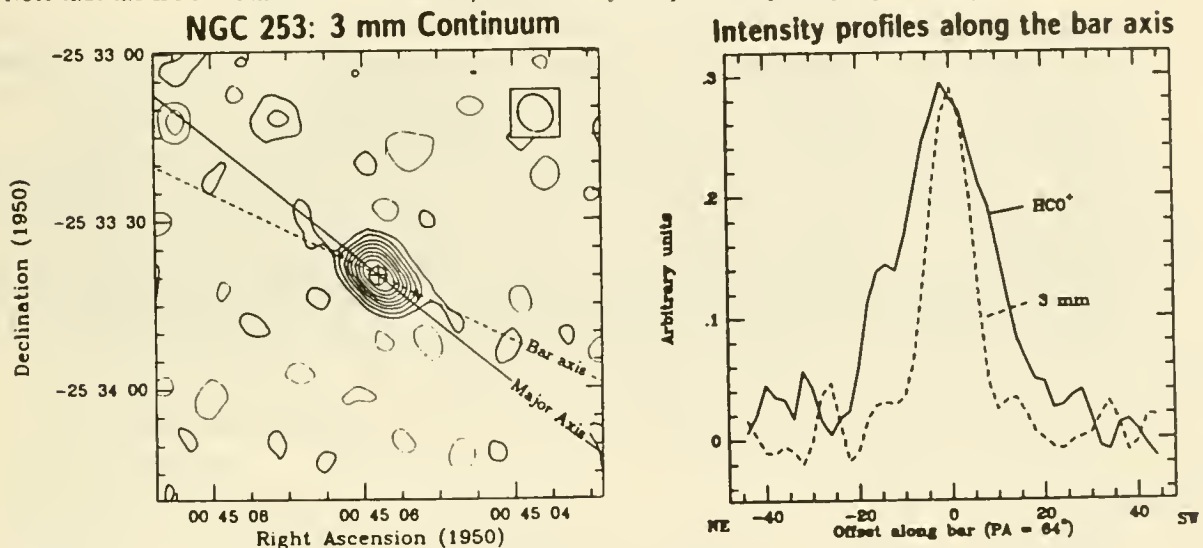


Figure 3. (a) The 3.3 mm continuum map. The contour interval is 18 mJy per beam. The beam, $7'' \times 6''$, is shown in the upper right corner. The cross marks the position of the nucleus. The total flux is 0.35 ± 0.05 Jy. (b) Comparison of the distribution along the major axis of the HCO^+ emission (solid line) and the 3.3 mm continuum emission (dashed line).

References:

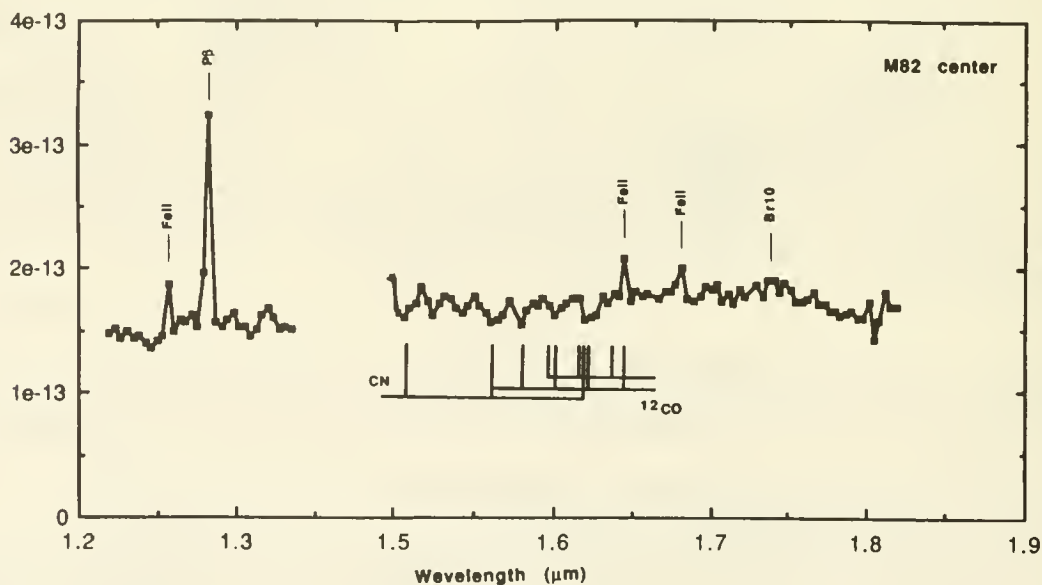
- Canzian, B., Mundy, L. G., Scoville, N. Z. 1988, *Ap. J.*, **333**, 157.
 Carlstrom, J. E. in "Galactic and Extragalactic Star Formation" ed. R. E. Pudritz and M. Fich, Dordrecht: Reidel, 1988.
 Carlstrom, J. E., 1988, Ph.D. Thesis, University of California, Berkeley
 Fabbiano, G., and Trinchieri, G. 1984, *Ap. J.*, **286**, 491.
 Rieke, G. H., Lebofsky, M. J., and Walker, C. E. 1988, *Ap. J.*, **325**, 679.
 Scoville, N. Z., Soifer, B. T., Neugebauer, G., Young, J. S., Matthews, K., and Yerka, J. 1985, *Ap. J.*, **289**, 129.
 Telesco, C. M. and Harper, D. A. 1980, *Ap. J.*, **235**, 392.
 Turner, J. T., and Ho, P. T. P. 1985, *Ap. J. (Letters)*, **299**, L77.

A NEAR INFRARED SPECTROSCOPIC STUDY OF THE INTERSTELLAR GAS IN THE STARBURST CORE OF M82

Dan Lester, Niall Gaffney (McDonald Observatory, U. Texas)
John Carr (U. Hawaii), Marshall Joy (NASA GSFC)

We have used the McDonald Observatory Infrared Grating Spectrometer, to complete a program of spatially resolved spectroscopy of M82. The inner 300pc of the starburst was observed with 4" (50pc) resolution. Complete J,H and K band spectra with resolution $0.0035\mu\text{m}$ ($\lambda\Delta\lambda=620$ at K) were measured at the near-infrared nucleus of the galaxy. Measurements of selected spectral features including lines of FeII, HII and H₂ were observed along the starburst ridge-line, so the relative distribution of the diagnostic features could be understood. This information has been used to better define the extinction towards the starburst region, the excitation conditions in the gas, and to characterize the stellar populations there. A complete discussion of these observations will appear shortly (Lester *et al.*, in press ApJ).

Figures 1 and 2 show the nuclear spectrum, which is rich in absorption and emission lines at this resolution. The CO absorption bands from the cool photospheres in the starburst dominates the infrared spectrum. Brackett γ , Paschen β and FeII are prominently in emission. Figure 3 shows the distribution of several diagnostic features across the starburst ridge-line. The near infrared continuum emission is strongly peaked at the center, while the Brackett γ emission is much more extended. Emission in the 1-0 S(1) line of H₂ is detected in the starburst region. Figure 3 shows that this line is not coextensive with either the continuum emission or the ionized gas, but extends well beyond them into the molecular 'ring' that surrounds the starburst. These three spectral diagnostics have been observed in a number of more distant starburst or interacting systems. The spatial inhomogeneity that we find among these diagnostics in M82 should caution us against using simple aggregate models for understanding the more distant, spatially unresolved galaxies.



Figures 1: J, H band spectra of the nucleus of M82

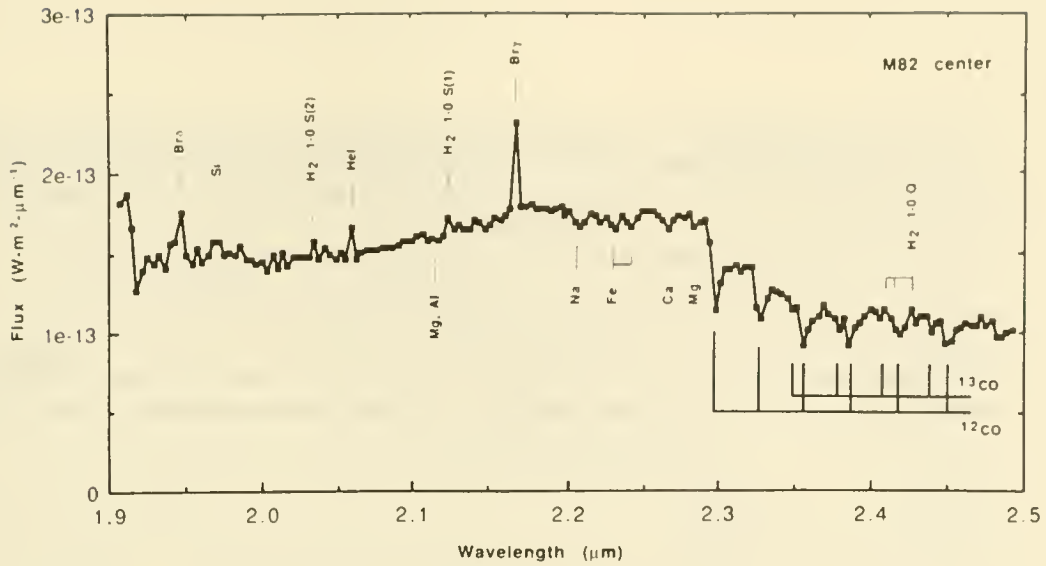


Figure 2: K band spectrum of the nucleus of M82

We find that the excitation of the H₂ emission in M82 is due to shocks. While the strong continuum at the nucleus makes it difficult to see other H₂ lines there (the stellar absorption features on which the lines are superimposed are more of a problem than is the small line-to-continuum ratio!) the very different spatial distribution of the H₂ and continuum allows us to see them elsewhere. Figure 4 shows a piece of spectrum taken 16'' away from the nucleus. At this position, the stellar continuum emission has fallen away substantially, leaving behind the 1-0 S(0) and 2-1 S(1) lines of H₂. The ratio of these lines indicates an excitation temperature of 1500-2000K, which is easily reconcilable with shocked regions in our own galaxy (*e.g.* Hollenbach and Shull 1977). A simple morphological interpretation of distribution of H₂ emission is that it surrounds the starburst. The H₂ emission can thus not be associated with individual star forming regions, but must be excited globally, on the scale of the starburst. The supernova driven wind that is known to be expelling material along the poles of the starburst disk may excite this emission.

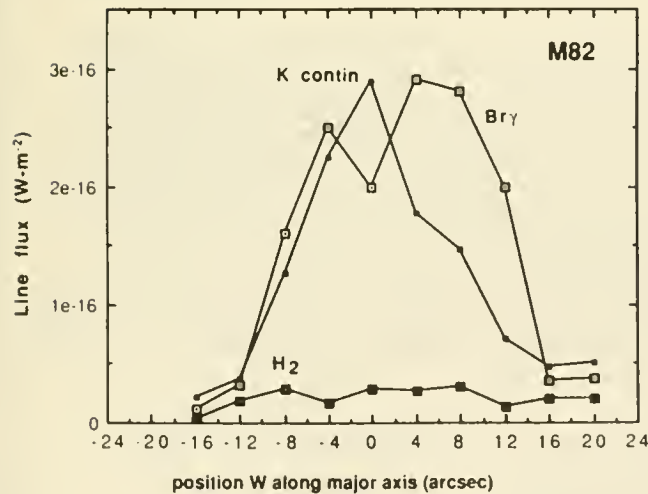


Figure 3: Distribution of 2μm continuum, Brackett γ, and H₂ along the starburst ridge.

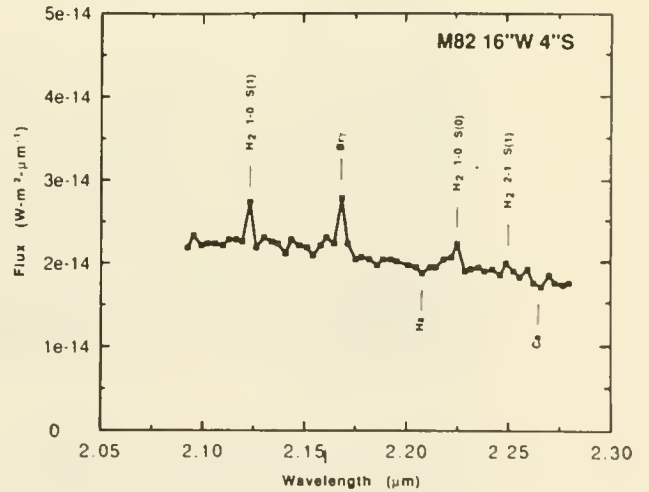


Figure 4: Spectrum of H₂ away from the continuum peak in M82

Emission in FeII 1.644 μ m is distributed more similarly to that of the ionized gas than anything else in our spectra. This line has been found to be especially strong in supernova remnants in our galaxy, where iron abundances have been increased by wholesale destruction of grains. (Graham *et al.* 1986). It is thus not surprising that the distribution of this line in M82 is similar, in general, to the distribution of the massive stellar progenitors of these supernovae. There is some evidence (in the lack of a 'hole' at the center, and enhanced emission over Brackett γ on the eastern edge of the starburst core) that FeII is distributed somewhat more like the nonthermal radio emission, however (see Figure 5). This distinction makes the origin of the the FeII in supernova remnants even more attractive. The lack of perfect correspondence between SNRs and massive stars can be understood in terms of non-coeval formation of individual massive stellar clusters in the galaxy.

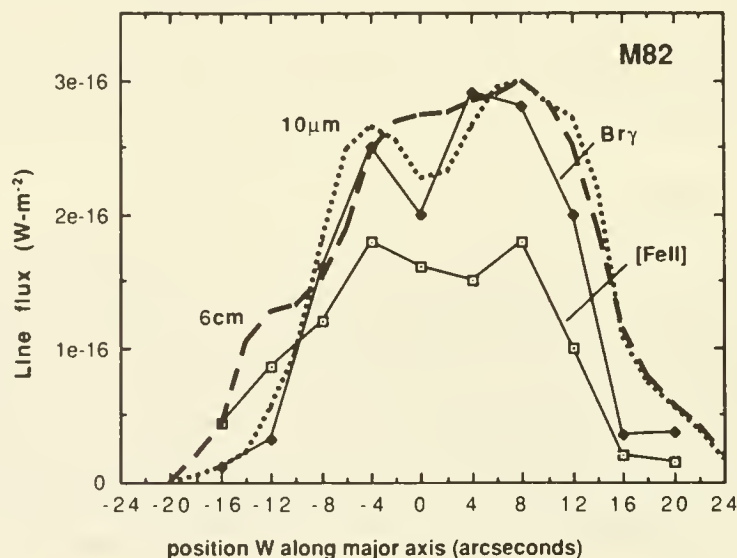


Figure 5: Distribution of radio and 10 μ m thermal emission is compared with that of Brackett γ and FeII along the starburst ridge line.

Four hydrogen recombination lines in the 1-2.2 μ m part of the spectrum give an extinction corresponding to $A_V=5.4$ at the nucleus. This extinction curve predicts an H α flux that agrees precisely with that which is observed (O'Connell and Magnano 1977), and is consistent with estimates of the thermal component of the radio emission. Larger extinction estimates based on Brackett α need to be reexamined in light of the internal consistency of these measurements. The larger extinction that is derived from the 9.7 μ m 'silicate' feature probably corresponds to those denser regions that produce most of the 10 μ m continuum emission. Application of this small extinction to the starlight from the nucleus of M82 yields a K band luminosity that can be reconciled with the dynamical mass in the nucleus with a normal IMF. The amount by which the 2 μ m starlight should be corrected for extinction is probably the single most important issue facing our understanding of stellar populations in the starburst region (Rieke *et al.* 1980).

Graham, J.R., Meilke, W.P.S., Allen, D.A., Longmore, A.J., and Williams, P.M. 1986 *M.N.R.A.S.* **218**, 93.

O'Connell, R.W. and Magnano, J.J. 1977 *Ap.J.* **221**, 62.

Hollenbach, D.J., and Shull, J.M. 1977 *Ap.J.* **216**, 419.

Rieke, G.H., Lebofsky, M.J., Thompson, R.I., Low, F.J., and Tokunaga, A.T. 1980 *Ap.J.* **238**, 24.

CLUES TO GALAXY ACTIVITY FROM RICH CLUSTER SIMULATIONS

August E. Evrard

Astronomy Department, University of California, Berkeley, CA 94720

ABSTRACT. New simulations of rich cluster evolution are used to evaluate the “first infall” hypothesis of Gunn and Dressler — the idea that the enhanced fraction of active galaxies seen in high redshift clusters is due to a one-time burst of star formation triggered by the rapid rise in external pressure as a galaxy plows into the hot intracluster medium (ICM). Using three-dimensional simulations which contain both baryonic gas and collisionless dark material, local static pressure histories for test orbits of galaxies are generated and a simple trigger threshold based on $dP/dt|_{P_{ISM}}$ is applied to define an “active” fraction of the population. The results lend qualitative and quantitative support to the first infall interpretation.

1. Motivation

Spectroscopic observations of galaxies in clusters at high redshift by Dressler and Gunn (1982; 1983; Dressler 1987; Gunn 1989) have revealed that the fraction of active galaxies in rich clusters increases with look-back time from values $\lesssim 5\%$ at the present to $\sim 30\%$ at $z \sim 0.5-0.8$. The active population includes Type I Seyferts, high excitation narrow-line emission systems and “post-starburst” galaxies designated E+A because their spectra are consistent with that expected from a superposition of an old stellar population with main sequence A stars formed during a significant burst occurring $\sim 10^9$ yr earlier (Dressler and Gunn 1983). The active galaxies are concentrated within the inner ~ 500 kpc of the cluster but appear somewhat less centrally concentrated than the passive population. The line-of-sight velocity dispersion of the active galaxies is typically $\sim 70\%$ larger than that of the passive population.

Gunn and Dressler suggest an infall model for these observations in which starbursts are triggered by gas-rich galaxies’ first infall into the highly pressurized cluster ICM. A pressure sensitive trigger is assumed to initiate the burst. As the galaxy falls into the cluster, the tenuous, hot phase of its interstellar medium (ISM) will be ram-pressure stripped while higher density, cold clouds remain bound within the galactic potential. Since pressures 30 – 300 times the conventional pressure in the cool phase of the Milky Way $P_{ISM} \simeq 10^{3.5}$ K cm $^{-3}$ are typical at the centers of rich clusters, the remaining gas in the infalling galaxy will be compressed as it climbs the rising pressure profile toward the center of the cluster. If the compression is rapid and the galaxy sufficiently gas-rich, then a significant starburst may be produced.

Recent numerical simulations (Evrard 1989) which follow the evolution of a gravitationally coupled system of collisionless particles and collisional gas allow gross details of this scenario to be examined experimentally. The simulations follow the dynamics within a $50 h_{50}^{-1}$ Mpc periodic cube whose initial density field is constrained to produce a rich cluster in a Hubble time (Bertschinger 1987). One Coma-richness cluster will be examined here. A cold dark matter initial spectrum with $\Omega=1$, $H_0=50 h_{50}$ km s $^{-1}$ Mpc $^{-1}$, $\Omega_{ICM}=0.1$ and a spectrum normalization $\sigma(16 h_{50}^{-1} \text{ Mpc}) \equiv b^{-1}=0.6$ is assumed. Two sets of 4096 particles are used to represent the dynamically distinct components. Gravity is calculated using the P3M technique and the 3-D gas dynamics is followed with Smoothed Particle Hydrodynamics (SPH) — the method is described in Evrard (1988). The evolution is followed from $z=7$ to the present and the simulations can

resolve structure down to $\sim 200 h_{50}^{-1}$ kpc. The origin of the ICM is assumed primordial — mass and energy input from galaxies is ignored. The thermal history of the ICM is thus determined by shock heating (and subsequent adiabatic evolution) of mildly supersonic, clumpy gas infalling into a hierarchically evolving potential well of dominant collisionless matter.

2. Results

The collisionless particles in the simulation are used to define test orbits for galaxies within the cluster potential. Local pressure histories $P(t)$ for a random selection of orbits are determined by interpolating the pressures of the nearby gas particle population. An “active” fraction is defined by those orbits which have undergone a rapid rise in pressure above the interstellar value $P_{ISM} = 10^{3.5}$ K cm $^{-3}$ in the last 10^9 yr. Specifically, the rise must be greater than a factor 5 in an interval less than $\Delta t = 0.36 \times 10^9$ yr (2 simulation output intervals). Only one burst per orbit is allowed.

Figure 1 shows the pressure histories of 30 orbits randomly drawn from within an Abell radius $R_A = 3 h_{50}^{-1}$ Mpc at both high ($z = 0.59$, $t_9 = 6.6$) and low ($z = 0.07$, $t_9 = 12.0$) redshifts. The cluster viewed at high z has a larger fraction of infalling orbits satisfying the active criteria. The fraction of active orbits using all (between 500 and 1000) collisionless orbits within an Abell radius at redshift z is shown in Figure 2. The fraction drops from roughly 20% at high z to $\lesssim 5\%$ for redshifts $z \lesssim 0.3$. A merger event creates the bump at $z = 0.1$.

Histograms of projected radii and velocities (relative to the known 3-D center-of-mass of the cluster) formed from a composite of 90 orbits compiled at high and low redshift are shown in Figures 3 and 4. The active orbits lie preferentially in the inner $1 h_{50}^{-1}$ Mpc at high z , extending out to $\sim 2 h_{50}^{-1}$ Mpc at low redshift. The histogram of line-of-sight velocities shows that the active fraction populates a high velocity subset of all orbits. The flatter and broader (by $\sim 70\%$) dispersion of the active sample agrees quantitatively with the observed redshift behavior of active galaxies in distant clusters (see Fig. 4 of Dressler 1987).

3. Summary

Numerical simulations of clusters including a gas dynamic ICM support the interpretation that the larger fraction of active galaxies seen in clusters at high redshift arises from galaxy-ICM interactions. A simple activity criterion based on a rapid static pressure increase was successful in reproducing several properties of the observed active cluster population : 1) a large drop in activity over the past ~ 5 billion years, 2) the central concentration of active galaxies and 3) their broader and flatter velocity distribution. It remains to be understood what is the “micro-physics” driving the starburst in this complex galaxy-ICM interaction.

References

- Bertschinger, E. 1987, *Ap. J. Lett.*, **323**, L103.
- Dressler, A. 1987, in *Nearly Normal Galaxies from the Planck Time to the Present*, ed. S.M. Faber, (Springer Verlag : New York), p. 265.
- Dressler, A. and Gunn, J.E. 1982, *Ap. J.*, **263**, 533.
- Dressler, A. and Gunn, J.E. 1983, *Ap. J.*, **270**, 7.
- Evrard, A.E. 1989, submitted to *Ap. J.*.
- Evrard, A.E. 1988, *M.N.R.A.S.*, **235**, 911.
- Gunn, J.E. 1989, in *The Epoch of Galaxy Formation*, eds. Ellis *et al.*, (Kluwer : Dordrecht).

Pressure Histories of Active and Passive Orbits

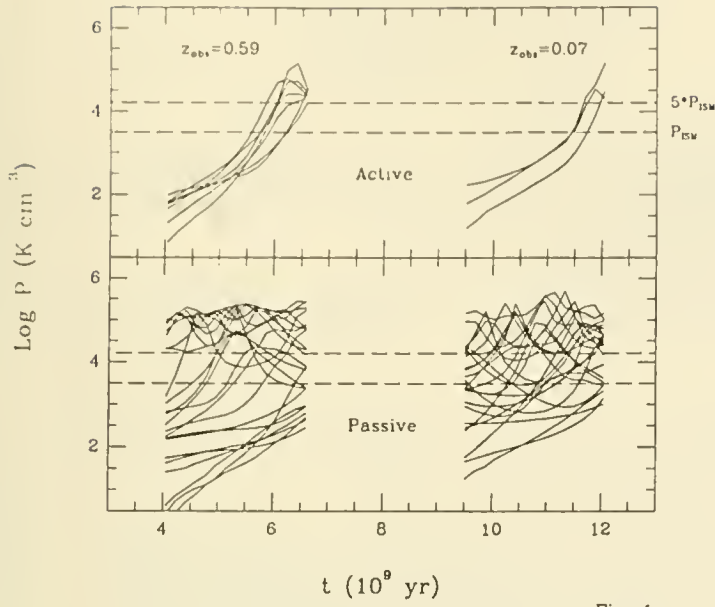


Fig. 1

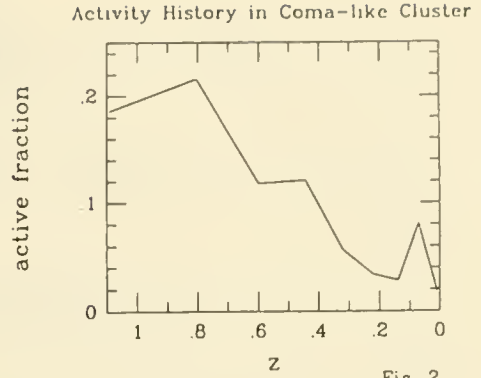


Fig. 2

Active/Passive Projected Radii at High and Low z

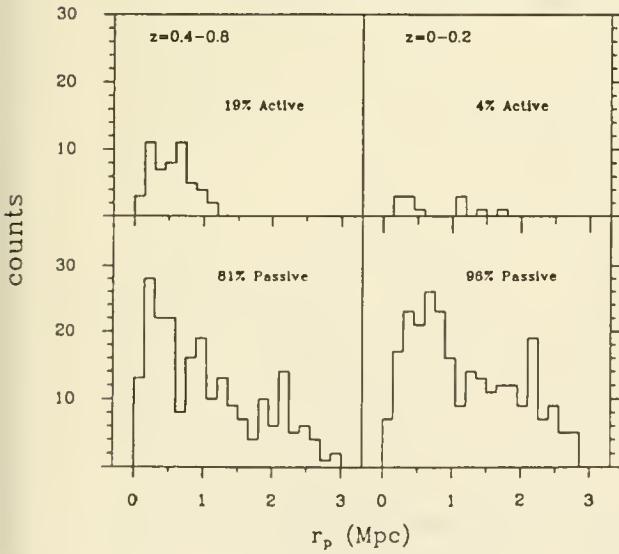


Fig. 3

Active/Passive Projected Velocities at High and Low z

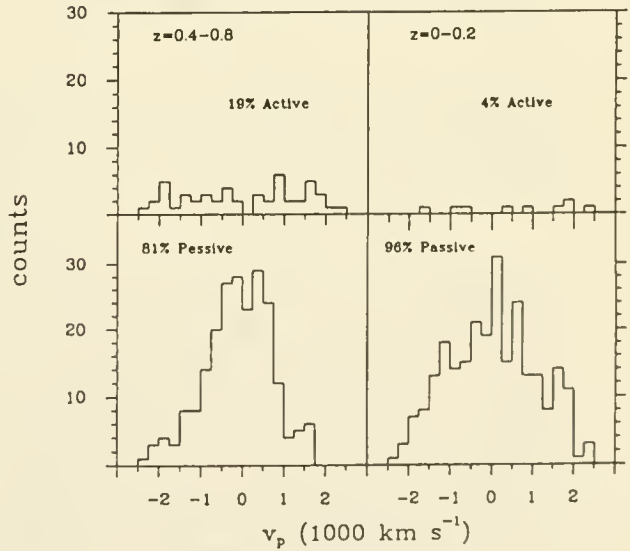


Fig. 4

CENTRAL STAR FORMATION IN 'SO' GALAXIES

L. L. Dressel (Vanderbilt University)
R. W. O'Connell (University of Virginia)
C. M. Telesco, R. Decher (NASA/MSFC)

As a class, SO galaxies are characterized by a lack of resolved bright stars in the disk. However, several lines of evidence support the hypothesis that a high rate of star formation is occurring at the centers of some SO galaxies:

- (1) Many of the warmest, most powerful far infrared sources in nearby bright galaxies occur in SO galaxies (Dressel 1988, Ap. J., 329, L69).
- (2) The ratios of radio continuum flux to far infrared flux for these SO galaxies are comparable to the ratios found for spiral galaxy disks and for star-burst galaxies.
- (3) VLA maps of some of these SO galaxies show that the radio continuum emission originates in the central few kiloparsecs. It is diffuse or clumpy, unlike the radio sources in "active" SO galaxies, which are either extremely compact or have jet-lobe structures. (See Figure 1.)
- (4) Imaging of some of these galaxies at 10.8 microns shows that the infrared emission is also centrally concentrated. (See Figure 2.)
- (5) Many of the infrared-powerful SO galaxies are Markarian galaxies. In only one case in this sample is the powerful ultraviolet emission known to be generated by a Seyfert nucleus.
- (6) Optical spectra of the central few kiloparsecs of these SO galaxies generally show deep Balmer absorption lines characteristic of A stars, and H β emission suggestive of gas heated by O stars. (See Figure 3.)

A key question to our understanding of these galaxies is whether they "really" are SO galaxies, or at least would have been recognized as SO galaxies before the episode of central star formation began. Some of Nilson's classifications (used here) have been confirmed by Sandage or de Vaucouleurs and collaborators from better plates; some of the galaxies may be misclassified Sa galaxies (the most frequent hosts of central star formation); some are apparently difficult to classify because of mixed characteristics, faint "non-SO" features, or peculiarities (due to the central star-formation process?). More optical imaging is needed to characterize the host galaxies and to study the evolution of their star-forming regions.

This research was supported by grant AST-8818606 from the National Science Foundation and by funds from NASA administered by the American Astronomical Society.

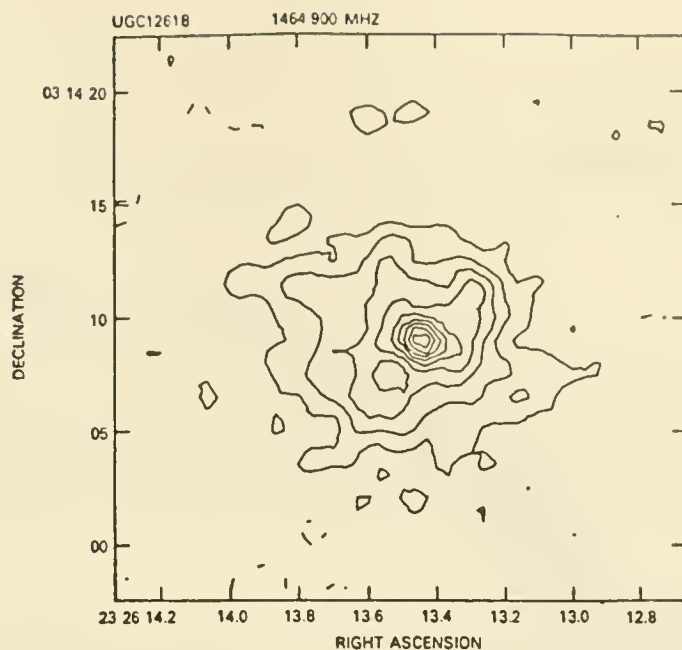


Figure 1: VLA map of UGC 12618 made at 1465 MHz in A array. Contours indicate linear increments in brightness. Beam FWHM is 1.3 arcsec.

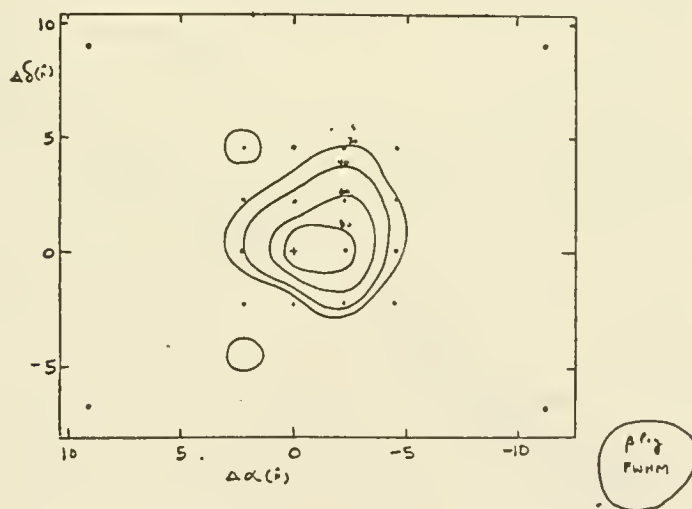


Figure 2: IRTF image of UGC 12618 at 10.8 microns. Contour intervals are 30, 40, 60, and 80 mJy/pixel; $\sigma = 15$ mJy/pixel. The cross indicates the optical center of the galaxy. Tick marks indicate distance from the galaxy center in 5 arcsec increments in right ascension and declination. (The scale is the same as in Figure 1.) FWHM for a point source is shown at the lower right. One pixel = 4.3" x 4.3".

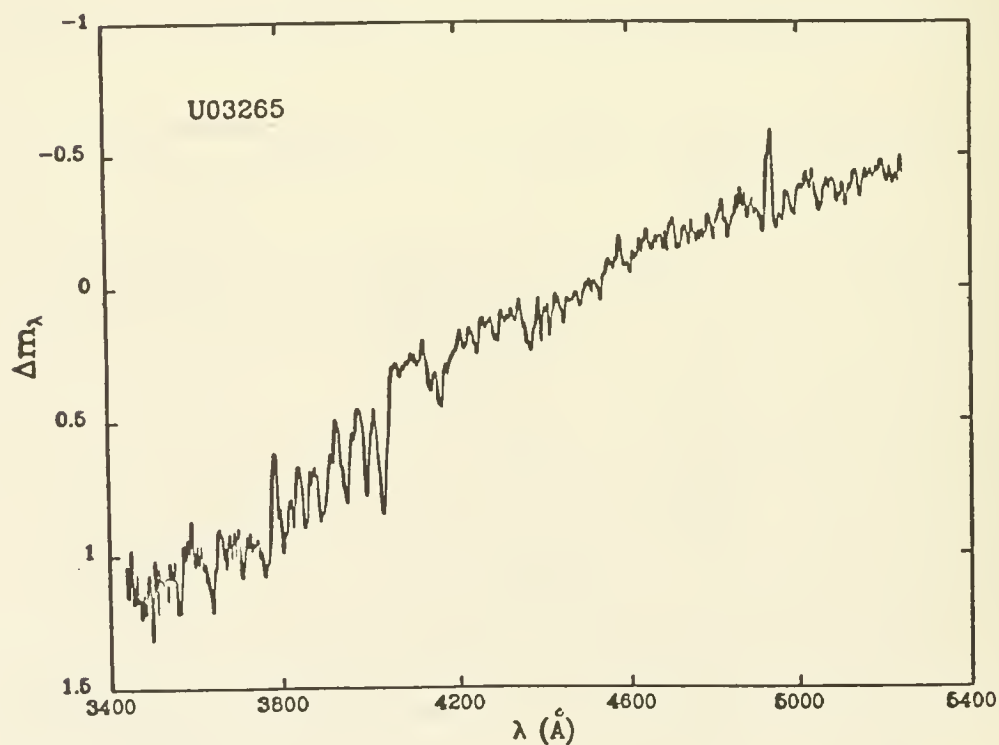
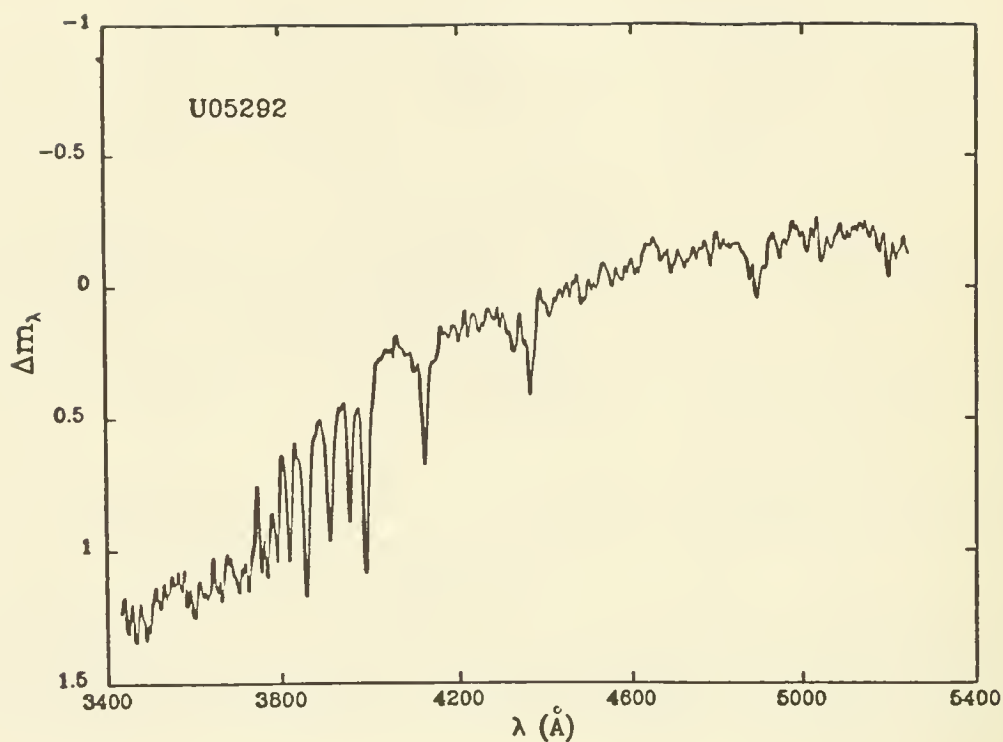


Figure 3. Optical spectra of UGC 05292 (S0) and UGC 03265 (SB0) in the rest frame of the observer. H β is seen in absorption in the former and in emission in the latter, and higher order Balmer lines are seen in absorption in both.

CURRENT STAR FORMATION IN S0 GALAXIES: NGC 4710

J.M. Wrobel

National Radio Astronomy Observatory

P.O. Box 0, Socorro, New Mexico 87801, USA

Elliptical (E) and lenticular (S0) galaxies lack the substantial interstellar medium found in the star-forming spiral galaxies. However, significant numbers of E and S0 galaxies are known to contain detectable amounts of interstellar matter (e.g., Jura 1988). Thus, it is worth investigating whether these galaxies are currently able to form stars from their ISM, or whether they should truly be consigned to the ‘dustbin of inert objects’ (Thronson and Bally 1987).

NGC 4710, an edge-on S0 in the Virgo Cluster, is a particularly promising candidate for study. It is known to be relatively dusty, as indicated by its Hubble subtype of S0₃ (Fig. 1; Sandage 1961) and its substantial far infrared power of 2×10^{36} W (Knapp *et al.* 1989) for an assumed distance of 20 Mpc. An elongated kiloparsec-scale radio continuum source resides in NGC 4710’s nucleus (Fig. 2; Wrobel and Heeschen 1988) and is aligned with the galaxy’s edge-on stellar disk. The radio source has a steep spectrum (Wrobel, Briggs, and Heeschen, in preparation). Steep radio spectra and radio-optical alignments are properties shared by the radio sources in flattened spiral galaxies thought to be undergoing rapid star formation (Condon *et al.* 1982). Supernova remnants produced at a rate of $\sim 0.3 \text{ yr}^{-1}$ could account for NGC 4710’s observed radio power. Furthermore, NGC 4710 conforms to the radio versus far infrared relation defined by star-forming galaxies (Wrobel and Heeschen 1988; Walsh *et al.* 1989).

The results cited above strongly imply that current star formation is responsible for NGC 4710’s far infrared and radio continuum properties. If this is indeed the case, then one expects this star formation to be fueled by molecular gas, which is presumably dominated by H₂ and can be traced by the ¹²CO J = 1 → 0 line. Both Kenney and Young (1988) and Sage and Wrobel (1989; see Fig. 3) have detected such an emission line from NGC 4710, and infer the presence of more than 10⁸ M_⊙ of H₂.

The origin of the molecular gas in NGC 4710 remains a mystery. The galaxy is very deficient in HI (Kenney and Young, in preparation), suggesting that it originally was a spiral galaxy from which the outer, mainly atomic, gas was stripped by the ram pressure of the Virgo Cluster’s intracluster medium, leaving only a central ISM rich in molecular gas. Alternatively, the CO may have originated via stellar mass loss with subsequent cooling, cooling flows, or capture from a gas-rich companion. Information on the morphology and kinematics of the CO can be compared with that of the galaxy’s other gases and stars to distinguish among these various possible origins for the molecular gas. Major axis CO mapping with single dishes indicate an unresolved source ($\text{FWHM} \leq 45 - 55'' \sim 5 \text{ kpc}$). Thus, the OVRO Millimeter Array is currently being used to image NGC 4710 in CO to provide the needed morphological and kinematical data (Wrobel and Kenney, in preparation).

In conclusion, studies of NGC 4710 provide compelling evidence that stars are currently forming in this S0's interstellar medium. Imaging of the molecular gas that fuels the current star formation should offer important insight into the origin of this newly discovered phase of the interstellar medium of S0 galaxies.

References

- Condon, J.J., Condon, M.A., Gisler, G., and Puschell, J.J. 1982, *Ap. J.*, 252, 102.
Dressel, L.L., and Condon, J.J. 1976, *Ap. J. Suppl.*, 31, 187.
Jura, M. 1988, in 'Multi Spectra Wavelength Astrophysics', p. 267.
Kenney, J., and Young, J.S. 1988, *Ap. J. Suppl.*, 66, 261.
Knapp, G.R., Guthathakurta, P., Kim, D.-W., and Jura, M. 1989, *Ap. J. Suppl.*, 70, 257.
Sandage, A. 1961, in 'The Hubble Atlas of Galaxies', plate 6.
Sage, L.J., and Wrobel, J.M. 1989, *Ap. J.*, 344, in press.
Thronson, H.A., and Bally, J. 1987, *Ap. J. (Letters)*, 319, L63.
Walsh, D.E.P., Knapp, G.R., Wrobel, J.M., and Kim, D.-W. 1989, *Ap. J.*, 337, 209.
Wrobel, J.M., and Heeschen, D.S. 1988, *Ap. J.*, 335, 677.

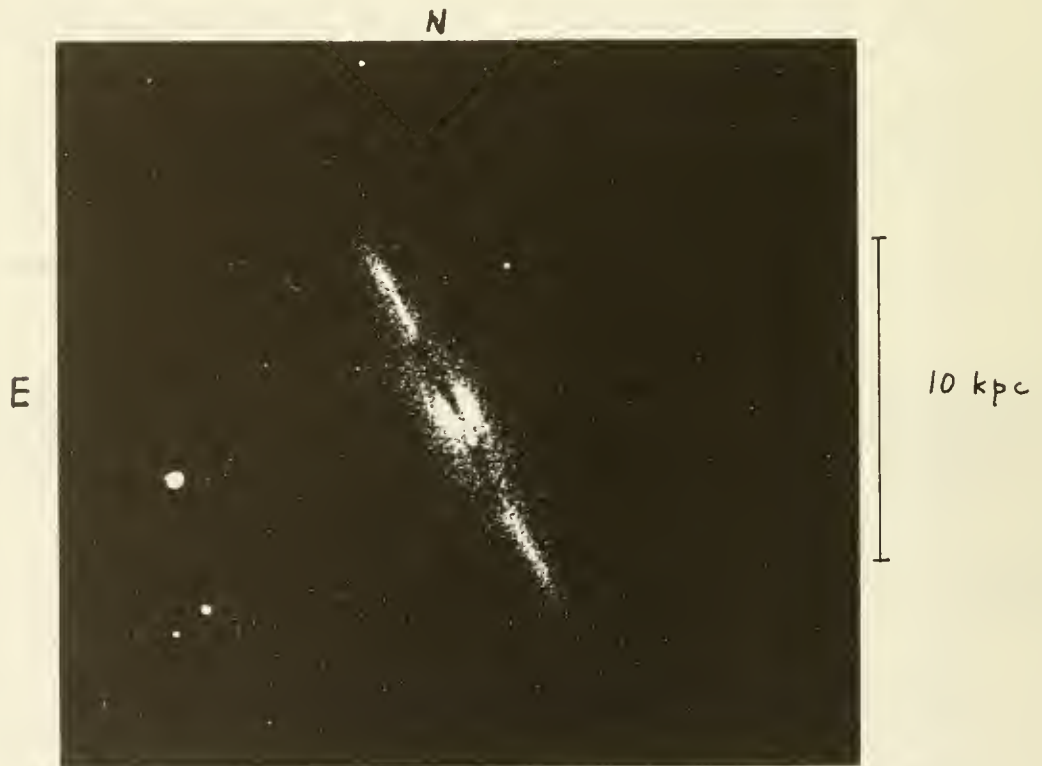


Fig. 1. – Reproduction of NGC 4710 from plate 6 of Sandage (1961).

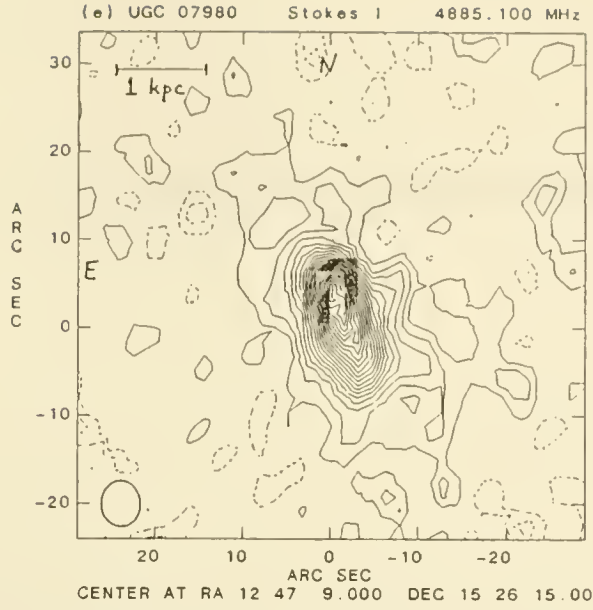


Fig. 2. - VLA 6-cm image of the inner regions of UGC 07980 = NGC 4710 (Wrobel and Heeschen 1988). Origin is at optical position (Dressel and Condon 1976; $\pm 4''$). Contour interval is $0.1 \text{ mJy beam}^{-1}$. Contours at integral levels between -4 and $+20$ are shown. Ellipse in south-east corner shows restoring beam orientation and size at FWIIM. Power at 6 cm is $4 \times 10^{20} \text{ W Hz}^{-1}$.

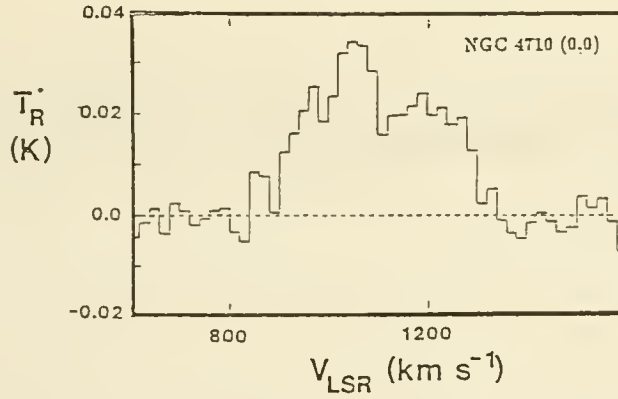


Fig. 3. - $^{12}\text{CO } J = 1 \rightarrow 0$ line from NGC 4710 (Sage and Wrobel 1989).

VI - ABSORPTION LINE SYSTEMS

Interpreting the Convergence of Lyman Series Absorption Lines

Edward B. Jenkins
Princeton University Observatory
Princeton, NJ

Abstract

A gas system at a redshift z with $N(\text{H}) \gtrsim 10^{17} \text{ cm}^{-2}$ in front of a quasar absorbs light over a broad wavelength band near and well below the system's Lyman limit, $\lambda \lesssim 912(1+z)\text{\AA}$. In the region where the Lyman series is converging, one can learn much about the velocity dispersion of some of the gas in the system by measuring how abruptly the intensity terminates with wavelength. For 21 such gas complexes appearing in a recent survey of quasar spectra (Sargent, Steidel and Boksenberg 1989), the median wavelength where half of the light is transmitted is about 918.5\AA in the respective rest frame of each system. This result implies that a typical Lyman limit system has either approximately 10^{17} cm^{-2} of hydrogen spread over $\Delta v \gtrsim 300 \text{ km s}^{-1}$ or considerably more than this amount of gas spread over half as large a velocity interval.

1. Introduction

Spectra of quasars at high z often show absorption at the Lyman limit from intervening gas systems at intermediate z having $N(\text{H}) \gtrsim 10^{17} \text{ cm}^{-2}$ (Tytler 1982, Bechtold, *et al.* 1984). In some circumstances, $N(\text{H})$ can be determined by measuring the strength of the Lyman limit absorption or the damping wings of Lyman- α . With a spectrum taken at low wavelength resolution, say, $\lambda/\Delta\lambda \sim 10^3$, it is usually not possible to distinguish individual Lyman series lines near the limit, yet one can still discern how rapidly the average intensity drops off as the limit is approached from the long wavelength side. The purpose of this discussion is to point out the information which is available from measurements of this series convergence.

2. Merging of Lines near the Series Limit

When the intervals between adjacent lines near the Lyman series limit are much less than the characteristic width of each absorption feature, the blended lines form a continuous absorption with an optical depth τ equal to that of the ionizing continuum just beyond the limit (Sugiura 1927). As the lines become well separated at longer wavelengths, there are large variations in τ even though the average of τ over wavelength remains constant. This transition from a smooth to fluctuating behavior can be easily registered in a high resolution spectrum. If the peaks and valleys from line to line vary substantially on either side of $\tau \sim 1$, a spectrum taken at a resolution which can not discern the features will still show a change, since the average, smoothed intensity of the spectrum will increase at progressively greater distances from the Lyman limit.

From the above discussion, it is clear that the dispersion of Doppler velocities is a fundamental parameter that governs the behavior of intensities of an atomic hydrogen spectrum seen in absorption near the series limit. At a relative wavelength displacement from the limit $\delta = \Delta z/(1+z)$, the equivalent velocity separation between adjacent lines in the series is given by

$$\Delta v = \frac{2c \delta^{3/2}}{(1-\delta)}. \quad (1)$$

A progression of strongly saturated absorption lines produced by gas whose velocity profile is a single, pure Gaussian should have an average intensity of 0.5 times the continuum level of the spectrum at a wavelength $\lambda_{1/2}$ where the intensity profile widths are half their separation, i.e., when $\tau = 1$ is found at a point $\Delta v/4$ from each profile's center. In this simple case one could derive the velocity dispersion parameter b (equal to $\sqrt{2}$ times the rms velocity) by measuring the spectrum's half-intensity point

$\delta_{1/2} = (\lambda_{1/2} - \lambda_{LL})/\lambda_{LL}$ and solving the equation

$$\exp(F^2/4) - AFN(H) = 0$$

with

$$F = \frac{c \delta_{1/2}^{3/2}}{b(1 - \delta_{1/2})} \quad (2)$$

and the constant $A = 7.3 \times 10^{-18} \text{ cm}^2$.

If the central optical depths of the lines are very large in the vicinity of $\delta_{1/2}$, it is probably inappropriate to invoke the traditional, practical assumption that the profile shape follows the wings of a Gaussian absorption, as with the classical Voigt profile. Rather, a small proportion of the gas may be in unrelated parcels at high velocities, as in the case where one may look through a galaxy and see fragments of halo gas with low column densities and high velocities supplementing a strong, narrow component from the galaxy's disk (see, e.g. Briggs, *et al.* 1985). In this context, at the wavelength where the transmission of light is about 0.5, the absorption by the high-velocity components strongly dominates that of the main component, as is illustrated in Figure 1. We can envision two regimes (or some intermediate combination thereof) which could apply near $\delta_{1/2}$: (a) a column density of hydrogen of about 10^{17} cm^{-2} is spread over a velocity at least Δv or (b) $N(H) \gg 10^{17} \text{ cm}^{-2}$ spans a velocity $\Delta v/2$.

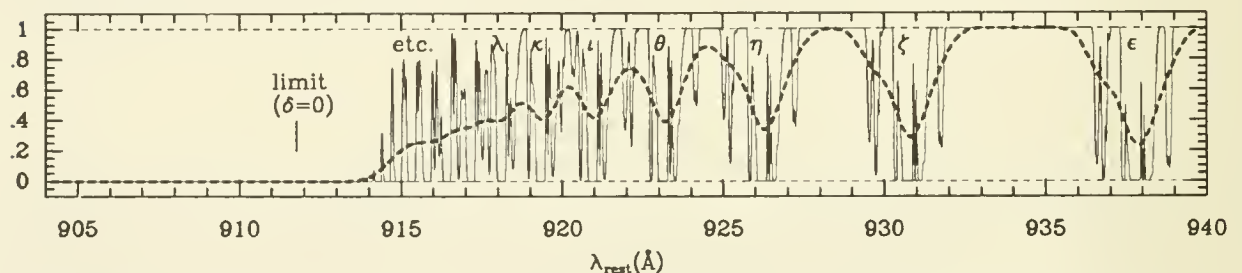


Fig. 1 -- Synthetic spectrum near the Lyman series limit of a gas complex containing 10^{19} hydrogen atoms cm^{-2} in a narrow velocity range accompanied by small clumps of material intercepting about half of the radiation within an interval $\pm 400 \text{ km s}^{-1}$. The dashed line shows a smoothed version of this spectrum. $\delta_{1/2} = 0.007$ (at 918 \AA).

3. Application

For an illustration on how to implement the above interpretation of the Lyman series convergence for real absorption systems, we can examine examples from the recent survey by Sargent, Steidel and Boksenberg (1989) of QSO spectra recorded at a resolution $\lambda/\Delta\lambda = 10^3$. In most cases, the position of the Lyman limit λ_{LL} can be inferred from the wavelengths of identified metal lines. For 21 of the Lyman limit systems seen in these spectra¹, the median $\delta_{1/2}$ was 0.0074 (see Fig. 2). A similar result was obtained by Tytler (1982).

For pure Gaussian profiles, the above result implies that a typical b would be 40 or 53 km s^{-1} for $N(H) = 10^{19}$ or 10^{18} cm^{-2} , respectively (eq. 2). Alternatively, most of the hydrogen which produces the Lyman limit absorption could be contained within a very narrow profile, and this gas might be accompanied by $N(H) \gtrsim \text{few} \times 10^{17} \text{ cm}^{-2}$ spanning $\pm 75 \text{ km s}^{-1}$. Neither of these choices seems too attractive,

¹Sargent, Steidel and Boksenberg (1989) identified metal-line redshifts for 25 of their Lyman limit systems. The author of this paper identified one more, making a total of 26. Out of this collection, 3 systems were too noisy to analyze and 2 had very gentle, strange looking drops in intensity that seemed to be inconsistent with the interpretation offered here. From the average number of systems with intermediate τ ($16.75 \lesssim \log N(H) \lesssim 17.5$) per unit z , in this sample one would expect about 1 system which, by chance, might confound the interpretation of another because it produced some intermediate absorption in the interval $0 < \delta < 0.05$. A coincidence of this sort could explain the strange looking cases.

because the spacing of Lyman lines at around $\delta \sim 0.01$ is sufficient that the strong contrasts in absorption could be resolved if the profiles were monolithic. Generally, a regular pattern of oscillating intensities near $\delta = 0.01$ is not evident in the data. Thus, one would favor an interpretation closer to case (a) discussed in the above paragraph, namely, that there is approximately 10^{17} cm^{-2} of hydrogen scattered over at least $\pm 150 \text{ km s}^{-1}$.

4. Conclusions

The Lyman series of atomic hydrogen offers a coherent replication template for absorption lines, with a smoothly varying interval between adjacent members. We can use this property to investigate the velocity spread of the absorbing gas, even as we examine a spectrum which was recorded at nowhere near the resolution needed to explicitly resolve even the broadest structures of each profile. The change in transmission created by the transition from a smooth absorption to well separated features occurs gradually. This property helps us to overcome the confusion created by noise in the spectrum or other, randomly placed absorption lines, such as those associated with the Lyman- α forest.

By measuring Lyman limit systems in a collection of low resolution quasar spectra, we have learned that the objects which are responsible for the absorption may contain material moving at velocities well over 100 km s^{-1} . Indeed, we have witnessed a similar phenomenon in a more familiar context: any line of sight through our own galaxy has a good chance of intercepting an isolated, high velocity cloud in the halo (Oort 1966) or a coherent stream of gas, such as the Magellanic Stream (Mathewson, Cleary and Murray 1974). Also, we know that some distant, highly ionized systems which show C IV and Si IV absorption lines in quasar spectra likewise show multiple components distributed over a span of many hundred km s^{-1} (e.g. Pettini, *et al.* 1983).

This research was supported by NASA grant NAG5-616 to Princeton.

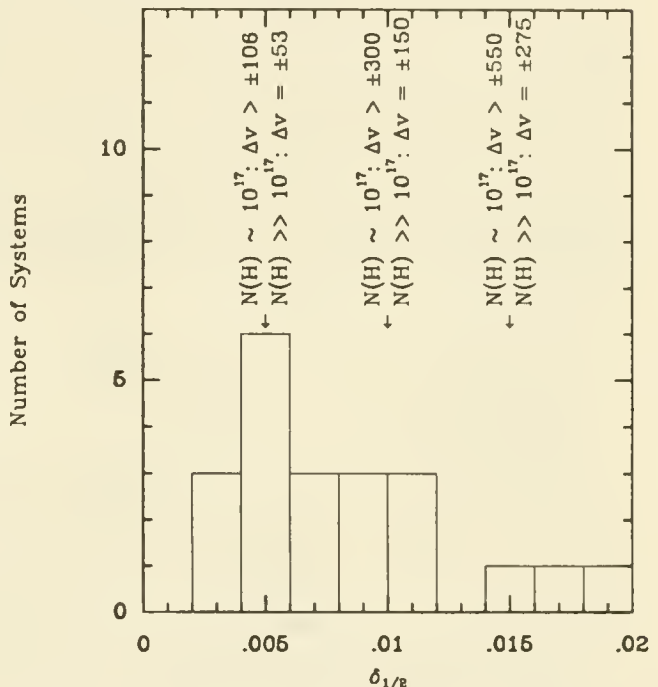


Fig. 2 — A histogram showing the frequency of measured half-intensity displacements $\delta_{1/2} = (\lambda_{1/2} - \lambda_{LL})/\lambda_{LL}$ in the survey of QSO spectra recorded by Sargent, Steidel and Boksenberg (1989).

References

- Bechtold, J., Green, R. F., Weymann, R. J., Schmidt, M., Estabrook, F. B., Sherman, R. D., Wahlquist, H. D., and Heckman, T. M. 1984, *Ap. J.*, **281**, 76.
- Briggs, F. H., Turnshek, D. A., Schaeffer, J. and Wolfe, A. M. 1985, *Ap. J.*, **293**, 387.
- Mathewson, D. S., Cleary, M. N., and Murray, J. D. 1974, *Ap. J.*, **190**, 291.
- Oort, J. H. 1966, *Bull. Astr. Inst. Netherlands*, **18**, 421.
- Pettini, M., Hunstead, R. W., Murdoch, H. S., and Blades, J. C. 1983, *Ap. J.*, **273**, 436.
- Sargent, W. L. W., Steidel, C. C., and Boksenberg, A. 1989, *Ap. J. (Suppl.)*, **69**, 703.
- Sugiura, M. Y. 1927, *Jour. de Physique*, **8**, 113.
- Tytler, D. 1982 *Nature*, **298**, 427.

Radio Continuum Observations of the Quasar-Galaxy Pair 3C 232-NGC 3067

Eric Haxthausen, Chris Carilli, and Jacqueline van Gorkom (NRAO¹).

The quasar-galaxy pair 3C 232-NGC 3067 is well known to show absorption by gas associated with the foreground galaxy against the background quasar (see Stocke *et al.* this volume). Observations by Carilli, van Gorkom, and Stocke (Nature 338, 134, 1989) found that the absorbing gas is located in a long tail of gas which extends from the galaxy toward the quasar and beyond (in projection). Though the HI observations of NGC 3067 indicate that the galaxy has been severely disturbed, there is no obvious candidate in the field which could cause such a disturbance, leading to the conclusion that the system has undergone a recent merger. Our radio continuum observations of this system were designed to study the nature of this highly disturbed galaxy.

We briefly review the VLA HI observations. Figure 1 shows the total HI column density associated with NGC 3067 and the optical field. Figure 2 is a position-velocity plot made along the galaxy axis. Note that the disk of the galaxy has an extended region of flat rotation in the east, with an extent of about 10 kpc and a peak rotation velocity of about 160 km sec⁻¹. In the west, the HI gas extends only to the point where the rotation curve should flatten (about 5 kpc), after which the disk truncates sharply. A cross in figure 1 indicates the position of the kinematic center of the galaxy, which is displaced by about 6" to the west of the optical centroid of the galaxy. Hence, we have strong evidence that this galaxy has been disturbed.

Further evidence that this galaxy has been disturbed is the long tail of HI extending towards and over the quasar. The tail has a length of 24 kpc and a width of 2.3 kpc. An analysis of the velocity dispersion for the emission from the tail shows a steady increase in velocity width from about 30 km sec⁻¹ near the galaxy, up to 200 km sec⁻¹ at the position of the cloud to the north of the quasar. Prior to our HI observations, this system had been considered one of the prime examples of absorption due to gas in the halo of a foreground galaxy. Our observations demonstrate that this conclusion is incorrect. In fact, our preliminary analysis of the quasar-galaxy pairs studied by Morton *et al.* (Ap.J. 302, 272, 1986) indicates that for every system with known Ca II absorbing gas outside the associated galaxy's optical radius, the galaxy shows evidence that it has been gravitationally disturbed. We conclude that the most likely origin for the low redshift absorption line systems is gas in interacting systems (unless, of course, our line of sight passes through the optical disk of a foreground galaxy), and not galactic halos or extended disks.

We observed this source with the VLA at both 20 and 3.6 cm. In figure 3 we show the 20 cm continuum image at 4" resolution, and the spectral index between 20 and 3.6 cm. In figure 4 we show the 20cm continuum and the HI column density. The quasar has a spectral index of -0.4 ± 0.1 between 20 and 3.6 cm, and appears to be resolved (by about 5% at 3.6cm, 0.7" resolution). NGC 3067 shows knotty continuum emission from the disk at about the 1 mJy level. The spectral index for the emission is -0.7 ± 0.1 ,

¹The National Radio Astronomy Observatory (NRAO) is operated by Associated Universities, Inc., under contract with the National Science Foundation.

which implies that the emission is synchrotron radiation from the disk (with minimum energy fields of about 1 to 5 μG , depending on assumptions). Notice the emission both to the north and south of the plane of NGC 3067. This may be emission from the disk seen in projection, or it may indicate high Z emission (distance from the plane of 1.6 kpc).

Crosses mark the position of the optical centroid of the galaxy (to the east), and the galaxy kinematic center (to the west). The highest surface brightness radio continuum emission from NGC 3067 is associated with the kinematic center of the galaxy (which also corresponds to the position of peak HI column density), which may be evidence for an active nucleus. The nucleus must be steep spectrum, since it is not seen at 3.6 cm to a 3σ level of 180 μJy (i.e. spectral index ≤ -1.2). The continuum emission extends about 3.9 kpc to the east of the kinematic center and 1.9 kpc to the west. Hence, the radio continuum displays a similar morphology as the HI gas: i.e. a truncated distribution in the west (albeit on a smaller scale). The truncation of the disk in the west is also evident in the optical line emitting gas, as determined from the long slit optical spectra of Rubin *et al.* (A.J. 87, 477, 1982). Notice that the radio continuum emission extends in radius only out to where the prominent dust lanes appear.

Our new continuum observations confirm our notion that NGC 3067 is a highly disturbed system, and, in particular, our notion that the western half of the galaxy extends only 1/2 as far in radius as the eastern half. This disturbance must have occurred recently, since the galactic rotation would smooth out the observed asymmetry in about 10^8 years. We are left with the problem that there are no obvious candidates which could have caused such a disturbance.

Figure 1: Total HI column density for gas associated with NGC 3067. Crosses mark the galaxy kinematic center (south) and the quasar (north). The lowest contour level is 2.9×10^{20} atoms cm^{-2} , while the peak is 32.4×10^{20} atoms cm^{-2} .

Figure 2: A position-velocity profile along the galaxy major axis.

Figure 3: The 20 cm continuum radio emission (contours) and the spectral index between 3.6 and 20 cm (grey scale). Typical values for the spectral index of the disk of the galaxy are -0.7. Crosses mark the location of the galaxy kinematic center (west) and the optical centroid (east).

Figure 4: The 20 cm continuum (grey scale) and the HI column density (contoured). 3C 232 has been blanked, and is represented by a cross to the north.

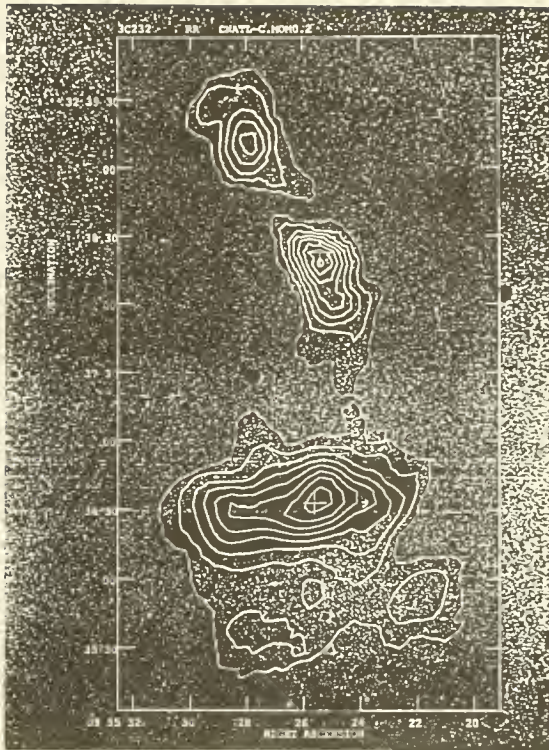


Fig. 1

← 3C
232

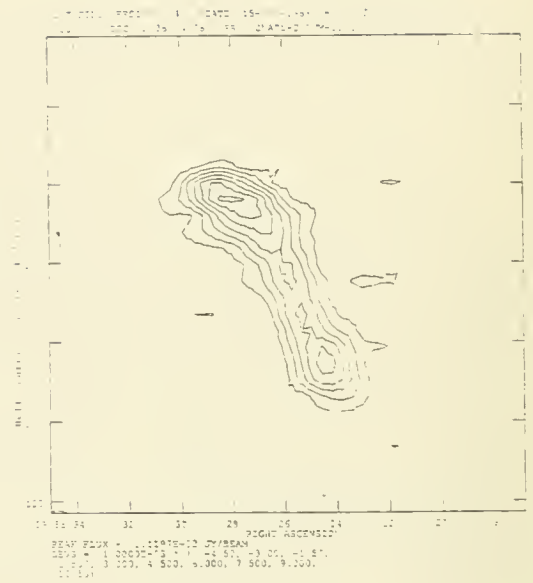


Fig. 2

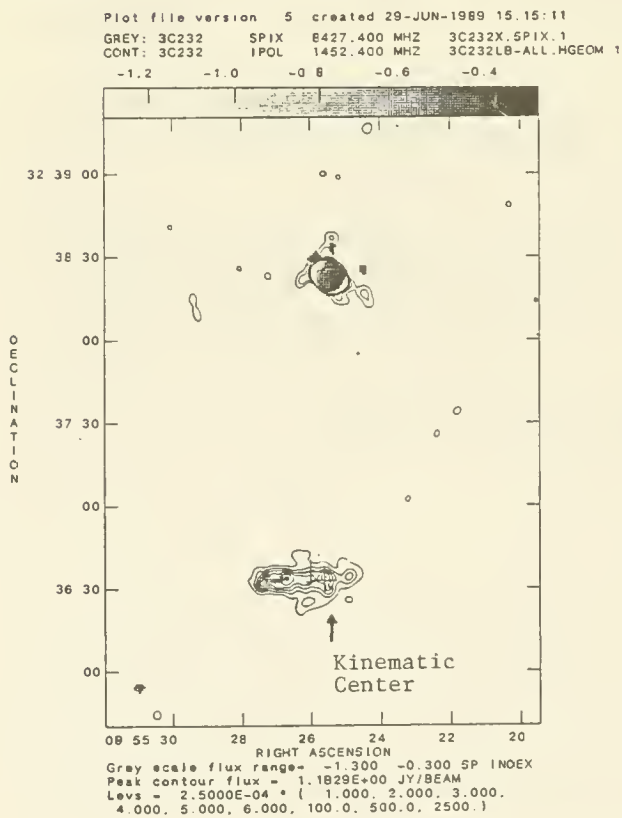


Fig. 3

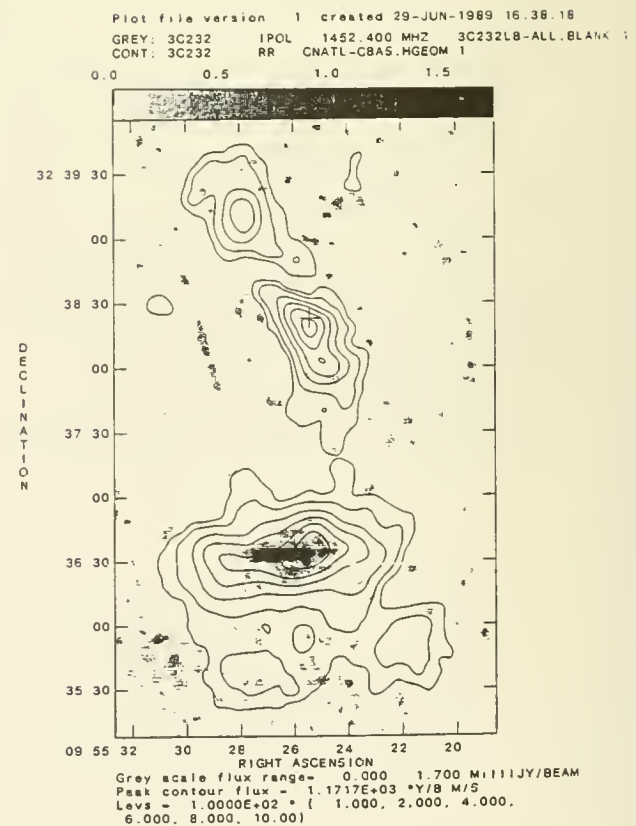


Fig. 4

PROBING THE INTERSTELLAR MEDIUM OF EXTERNAL GALAXIES

USING QUASAR ABSORPTION LINES:

THE 3C 232/ NGC 3067 SYSTEM

John T. Stocke, James Case, Megan Donahue,
J. Michael Shull and Theodore P. Snow

Center for Astrophysics and Space Astronomy
University of Colorado

Quasar absorption lines offer unique opportunities to probe the interstellar medium of external galaxies. We present new optical and UV absorption line spectroscopy of the quasar 3C232 ($z=0.55$) revealing new detail in the foreground absorption system due to the bright, spiral galaxy NGC 3067 ($cz=1420$ km/s). Specifically, our spectra show evidence for two and possibly three separate absorption components in CaII and Na I spanning ~ 150 km/s. The original HI detection of Haschick and Burke (1975) corresponds to the strongest of these metal systems which exhibits doublet ratios consistent with saturation in both CaII and Na I.

Due to the recent detection in HI emission of a tidal tail or "finger" of HI extending from the western edge of NGC 3067 through the position of 3C 232 (Carilli, van Gorkom and Stocke, 1989 and this conference), the morphology of the HI absorber is now known and is not either a "warped disk" nor a spherical halo as had been proposed. New deep continuum and H α imaging provides a sensitive upper limit on the ionizing continuum impinging upon this cloud (and thus a limit on the intensity of the extragalactic ionizing radiation field).

Together with the observed UV spectrum of 3C 232, the optical emission line ratios and the deep H α imaging set a minimum distance between the quasar and the HI cloud disregarding redshift information. This limit strains the "non-cosmological" redshift interpretation for 3C 232 -- and this quasar is one of the original 5 3C quasars found to be too close to NGC galaxies as if by chance (Burbidge, Burbidge, Solomon and Strittmatter, 1972).

Bowen, Pettini, Penston & Blades have concluded their survey to probe the outer halos of low redshift ($z < 2$) identified galaxies in CaII, using QSOs as probes. We have observed 11 QSO-galaxy pairs with sight-line separations of between 3 & $75h_{100}^{-1}$ kpc ($h_{100} = H_0/100$), down to 2σ equivalent width limits of less than $110\text{m}\text{\AA}$ for 10 of them. From previously published work we know that this limit would secure the detection of CaII column densities within our own galaxy, yet we find calcium in only one pair, an anonymous galaxy within 0.7 arcmins or $41h_{100}^{-1}$ kpc from the quasar 1543+489. The lines are weak and saturated ($\sim 65\text{m}\text{\AA}$), and the separation is the largest known for CaII absorption beyond the optical extent of a galaxy. What makes this all the more surprising is that observations of Supernovae SNWILD in NGC2268, and SN1987N in NGC7606, made with Max Pettini, continue to show strong absorption lines of both CaII and NaI, a result is typical of all high resolution spectroscopic observation of bright Supernovae.

One particular pair, that of MK205 & the face-on galaxy NGC4319, continues to be the focus of our attention, since the quasar's line-of-sight passes within $4h_{100}^{-1}$ kpc of the galaxy center and lies just adjacent to a spiral arm. Though expecting absorption by the disk and any extended halo, we are unable to detect CaII in this pair to a 2σ limit of $40\text{m}\text{\AA}$, meaning that the covering factor of the disk alone in CaII is less than unity at these equivalent width thresholds. Whether this is due to severe depletion of calcium along the spiral arm, or is perhaps some indication of the ionization conditions, remains to be seen. Some preliminary observations do suggest however that NaI is detected, and it is clearly of some importance to establish the conditions of the ISM in such a galaxy that led to this result.

We conclude that there still exists *no* evidence for extended CaII *halos* beyond a Holmberg radius, and we consider that the reported cases of large equivalent widths in the five QSO-galaxy pairs where CaII *has* been detected to be a consequence of either absorption within the disk (at about $1 R_H$), or absorption by disturbed or interacting galaxies. The most important example of this latter system is provided by Carilli, van Gorkom & Stocke (1), who detect a tail passing from NGC3067 across the line-of-sight of 3C232; up till now, this had provided the best case of halo absorption in CaII, with a strong equivalent width (2). *For whatever reasons*, the extent of CaII does not support the hypothesis that galaxies are responsible for QSO absorption lines, despite the fact that there now exists good evidence that the MgII absorption systems seen in QSO spectra are indeed due to the (extended) halos of intervening galaxies (3), and a preliminary attempt to understand the dynamics of these galaxies appears to be feasible.

References:

- (1): Carilli, van Gorkom & Stocke (1989), preprint
(2): Boksenberg & Sargent (1987), *Ap J.* **220**, 42
(3): Bergeron (1987), "The Post-Recombination Universe", Ed. Kaiser & Lasenby, P201.

<i>QSO - Galaxy Pairs Survey.</i>					
QSO	Galaxy	V_0	ρ	ρ	$W_\lambda(\text{CaII K})^b$
		(Kms^{-1})	(')	($h_{100}^{-1} \text{kpc}$)	($\text{m}\text{\AA}$)
0026 + 129	0026 + 1304	1590	5.7	26	< 62
0318 - 196	NGC1300	1555	9.6	27	< 108
0838 + 770	UGC4527	721	2.3	5	< 46
1048 - 090	anon 1	a	0.38	...	< 68
	anon 2	$z=0.1255$	0.43	39	< 68
1211 + 143	IC3061	2263	11.5	75	< 42
	Virgo Cluster	-180-2400	n/a	n/a	< 42
1219 + 047	NGC4303(\equiv M61)	1589	4.7	11	< 164
	Virgo Cluster	-180-2400	n/a	n/a	< 164
1219 + 755	NGC4319	1390	0.7	3	< 38
1341 + 258	1341 + 2555	5802	1.8	30	< 48
1411 + 442	ZWG219.061	? ^c	6.9	?	< 72
	UGC09105	? ^c	8.3	?	< 72
1543 + 489	anon 1	22700	0.7	41	65 ± 15
	anon 2	?	1.4	83	?
2308 + 098	anon	$z=0.1726$	0.15	18	< 84
NOTES: a. Stockton (1978) suggests $z \simeq 0.228, 0.346$ from poor quality data. b. Where lower limits are given, these are to 2σ . c. Awaiting redshift data.					

Detection of a $z=0.0515$, 0.0522 Absorption System in the QSO S4 0248+430 Due to an Intervening Galaxy

Donna S. Womble, Vesa T. Junkkarinen, Ross D. Cohen, E. Margaret Burbidge
Center for Astrophysics and Space Sciences, University of California, San Diego

I. INTRODUCTION

In some of the few cases where the line of sight to a QSO passes near a galaxy, the galaxy redshift is almost identical to an absorption redshift in the spectrum of the QSO. Although these relatively low redshift QSO-galaxy pairs may not be typical of the majority of the narrow heavy-element QSO absorption systems, they provide a direct measure of column densities in the outer parts of galaxies and some limits on the relative abundances of the gas.

Observations are presented here of the QSO S4 0248+430 and a nearby anonymous galaxy (Kuhr 1977). The $14''$ separation of the line of sight to the QSO ($z_e=1.316$) and the $z=0.052$ spiral galaxy, (a projected separation of 20 kpc ($H_o=50$, $q_o=0$)), makes this a particularly suitable pair for probing the extent and content of gas in the galaxy. Low resolution (6\AA FWHM), long slit CCD spectra show strong Ca II H & K lines in absorption at the redshift of the galaxy (Junkkarinen 1987). Higher resolution spectra showing both Ca II H & K and Na I D1 & D2 in absorption and direct images are reported here.

II. OBSERVATIONS AND ANALYSIS

The spectroscopic observations were taken on 4-6 October, 1988 with the UV Schmidt system and TI CCD detector on the Lick 3m telescope. The spectral regions covering Ca II ($\lambda\lambda 3700-4300$) and the predicted Na I ($\lambda\lambda 5700-6500$) absorptions were observed with long, $2''$ wide slits and spectral resolutions of 1.8 and 2.9\AA FWHM, respectively. The data were reduced using an optimal extraction routine included with the VISTA image and spectrum reduction package. Besides sky subtraction and optimal profile weighting, this routine also provides an accurate error array (Horne 1986). Standard flat-fielding, wavelength and flux calibration techniques were used.

As indicated in figures 1 and 2, at least two narrow absorption components occur in both Ca II and Na I, separated by $\Delta v \simeq 220 \text{ km s}^{-1}$. Because the resolutions obtained were not sufficient to resolve the individual lines, we assumed a 2-component system, consisting of two gaussian doublets, and used a maximum likelihood fitting technique to measure the equivalent widths in all four lines of both species. For each doublet, the free parameters were: redshift (z), amplitude of the stronger line (A) and half-width (σ) of the gaussian profile, and doublet-ratio (R) where $R=A_K/A_H$ for Ca II or $R=A_{D2}/A_{D1}$ for Na I. In each case, χ^2 was minimized by varying all eight parameters freely. Because of the relatively poor fit to the Na I lines ($\chi^2_\nu = 2.466$), the errors in these parameters were determined with a monte carlo simulation. For each of 1500 iterations, simulated data were produced (through introduction of gaussian deviates to the best fit data) and then refitted by minimization of χ^2 . The errors in the Ca II fit ($\chi^2_\nu = 0.785$) parameters were determined by varying one parameter while holding all others constant until χ^2 changed by 2.706 ($\Delta\chi^2$ for $\nu=1$, probability of 0.1). In both cases, the errors reported here are for a 90% confidence level. Plots of the best fits are indicated by the dashed lines in Figures 1 and 2.

The equivalent widths for each line with errors were determined from the fit parameters. Using the doublet ratio formalism of Strömberg (1948), and a calculated curve of growth accounting for both doppler broadening and natural damping, limits were obtained for the column densities in each system (see Table I). For a pure damping profile the doublet ratio equals $\sqrt{2}$. Only lower limits on the Ca II column densities could be determined because these

doublet ratios (including errors) span from below to above the limiting value of 1.414. Because the Na lines in both systems are highly saturated ($DR < 1.4$) both upper and lower limits could be obtained for this species.

Direct, broadband CCD images of the QSO-galaxy field were taken on 15 October, 1988 with the Lick 3m telescope. The data were flat-fielded only, no absolute flux calibrations were applied. The image of the galaxy shows a single spiral arm-like feature covering and extending past the position of the QSO by more than $15''$. A second, symmetric arm is not evident.

III. DISCUSSION

The column density ratio, $N(\text{Ca II})/N(\text{Na I})$ is sensitive to the depletion of Ca onto grains. Both large and small Ca II/Na I ratios are observed in the disk of our Galaxy; the small ratios probably come from regions where Ca has been depleted onto grains (Spitzer 1978). Cohen and Meloy (1975) have found that gas above the disk typically has a large Ca II/Na I ratio. Our "best fit" values give $N(\text{Ca II})/N(\text{Na I}) = 0.036$ and 0.013 for $z_1 = 0.0515$ and $z_2 = 0.0522$, respectively (assuming the lower column density solutions). If conditions are analogous to those in our Galaxy, the above Ca II/Na I ratios would imply a large Ca depletion and disk-type absorbing gas. However, within the formal 90% confidence intervals, larger Ca II/Na I are compatible with the data. A consequence of assuming very little depletion (say with $N(\text{Ca II})/N(\text{Na I}) \sim 10$), is that the observed lower limits on $N(\text{Na I})$ would imply $N(\text{Ca II}) \gtrsim 6 \times 10^{14} \text{ cm}^{-2}$ for the sum of the two components. This would result in $N(\text{Ca II})$ greater than 100 times that observed in other QSO-galaxy pair absorption systems (Blades 1988).

Of the six known absorption systems of this type, the Ca II and Na I lines measured in this object are amongst the strongest in total equivalent width (Blades 1988). Two others (0446–208, 1327–206) show large depletions of Ca – likewise implying disk absorption (Blades, *et al.* 1981, Baldwin, *et al.* 1985; Bergeron, *et al.* 1987). The column densities found here are considerably larger than in those intermediate redshift QSO absorption systems (with no apparent nearby galaxy) which have been observed at the predicted wavelength of Ca II (Blades 1988).

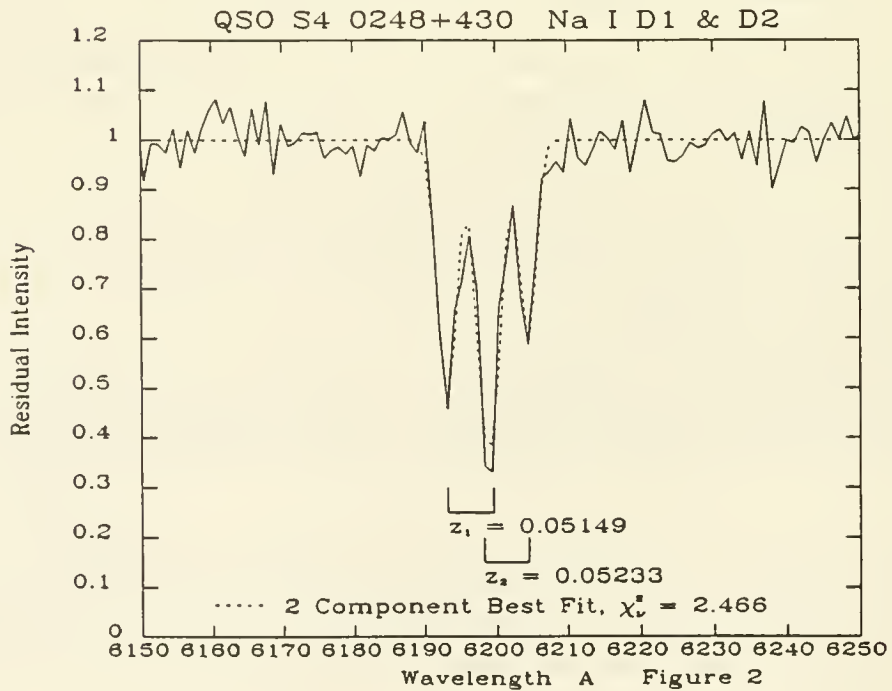
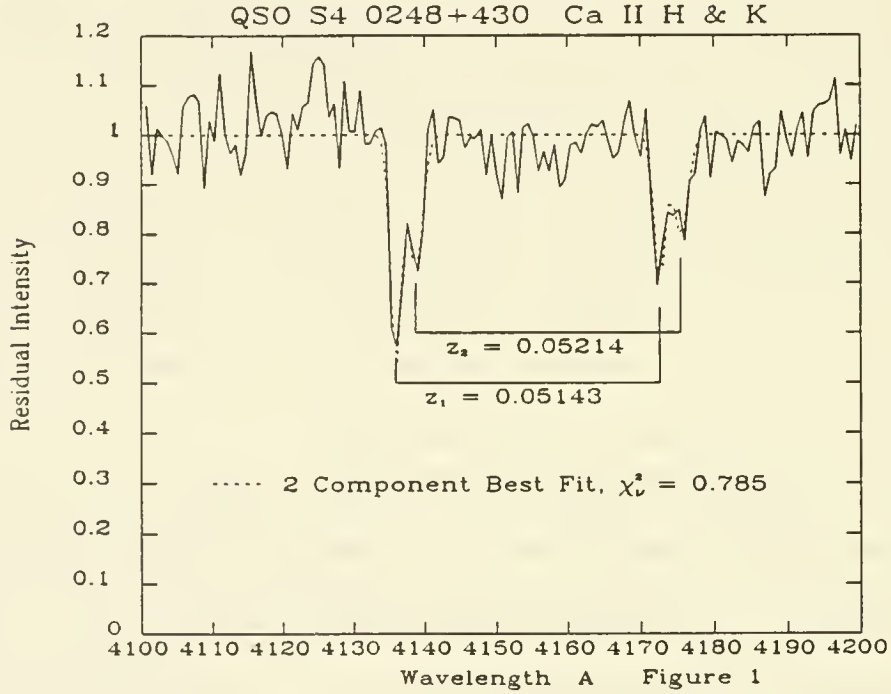
This work has been supported by NASA contract NAS 5–29293. DSW wishes to acknowledge Zonta International for their Amelia Earhart Fellowships.

References:

- Baldwin, J. A., Phillips, M. M., and Carswell, R. F. 1985, *M. N. R. A. S.*, **216**, 41P.
 Bergeron, J., D'Odorico, S. D., Kunth, D. 1987, *A. & A.*, **180**, 1.
 Blades, J. C. 1988, in *QSO Absorption Lines: Probing the Universe*, eds. J. Blades, D. Turnshek, C. Norman (Cambridge: Cambridge Univ. Press), p.147.
 Blades, J. C., Hunstead, R. W., and Murdoch, H. S. 1981, *M. N. R. A. S.*, **194**, 669.
 Cohen, J. G., and Meloy, D. A. 1975, *Ap. J.*, **198**, 545.
 Horne, K. 1986, *P. A. S. P.*, **98**, 609.
 Kuhr, H. 1977, *A. & A. Suppl.*, **29**, 139.
 Junkkarinen, V. T. 1987, *B. A. A. S.*, **10**, 953.
 Spitzer, L. 1978, *Physical Processes in the Interstellar Medium*, (New York: John Wiley & Sons).
 Strömberg, B. 1948, *Ap. J.*, **108**, 242.

TABLE I

	z_a	R	Equivalent Width (\AA)		Column Density ($\times 10^{13} \text{ cm}^{-2}$)
			(K or D2)	(H or D1)	
Ca II	0.05143	1.56 ± 0.40 0.27	0.90 ± 0.15	0.58 ± 0.18 0.14	$0.9 \leq N \leq 3.1$ or $N \geq 9.9 \times 10^3$
Na I	0.05149	1.07 ± 0.23 0.16	1.78 ± 0.23	1.66 ± 0.41 0.33	
Ca II	0.05214	1.33 ± 0.47 0.28	0.70 ± 0.18 0.16	0.52 ± 0.23 0.16	$N \geq 0.9$
Na I	0.05233	0.99 ± 0.25	1.19 ± 0.37 0.31	1.21 ± 0.23 0.19	$2.3 \leq N \leq 4.4 \times 10^3$



VII - RESULTS FROM NEW INSTRUMENTS AND TECHNIQUES

HIGH SPATIAL RESOLUTION STUDIES OF GALAXIES IN THE FAR IR: OBSERVATIONS WITH THE KAO, AND THE PROMISE OF SOFIA

D.F. Lester, P.M. Harvey University of Texas

Providing definitive measurements of the total luminous output of star forming regions, far-infrared continuum observations may be considered pivotal in our understanding of the way in which stars form, and the efficiency with which they do so on a galactic scale. The utility of such measurements for understanding the IR morphology of external galaxies is offset by the difficulty with which they must be made, involving stratospheric or space instruments. This imposes severe constraints on the available aperture size which, at these long wavelengths, implies corresponding constraints on spatial resolution. The largest far-infrared telescope is the 0.91m Kuiper Airborne Observatory (KAO), run by NASA Ames Research Center. At 100 μ m, this telescope is diffraction limited at 23" (FWHM of Airy disk). While the cryogenically cooled IRAS satellite gave high S/N measurements of the entire sky, it was diffraction limited at a spatial scale several times larger than that of the KAO.

The spatial resolution of the KAO at these wavelengths has only recently been fully exploited. At U.Texas, we have been pursuing a program of high spatial resolution observations from the KAO that, using special guiding and tracking methods to improve the pointing stability, and non-linear deconvolution algorithms to process the data, gives information at the diffraction 'limit'.

Much of our original work on the small scale far-infrared structure of galaxies was done using narrow slit apertures that we scanned back and forth across the sources. Our observations of M51 (NGC5194) (Lester, Harvey and Joy 1986) revealed that much of the far-IR luminosity of this galaxy came from the central 30" (700pc). The data suggested that this emission was coming from a region with a hole in the center — perhaps a ring of emission. Violent processes in the center of M51 may have cleared the core of ISM, and suppressed star formation there. Scans of the ultraluminous galaxy Arp220 showed that this luminosity arose from the central 3kpc (Joy *et al.* 1986). The starburst region in M82 was clearly resolved in our data (Joy *et al.* 1987), and the peak emission was found to be larger than the near-infrared nucleus. A study of the Seyfert/starburst nucleus of NGC1068 showed that half the far infrared emission came from the Seyfert nucleus, and half from the surrounding starburst. The extended spiral arms of the galaxy (outside the starburst) were measured as well (Lester *et al.* 1987). The far infrared emission from the radio galaxy NGC5128 (CenA) was resolved into emission from the active nucleus, and a starburst in the plane of the disk (Joy *et al.* 1988). The strong H₂O maser source at the center of the nearby spiral NGC4945 was found to account for nearly all the emission from this otherwise unremarkable galaxy. The surface brightness of the source implied that it is close to being optically thick at 100 μ m, suggesting several hundreds of magnitudes of visual extinction (Brock *et al.* 1988). Figure 1 is from a recent study by Joy *et al.* (1989) on the structure of

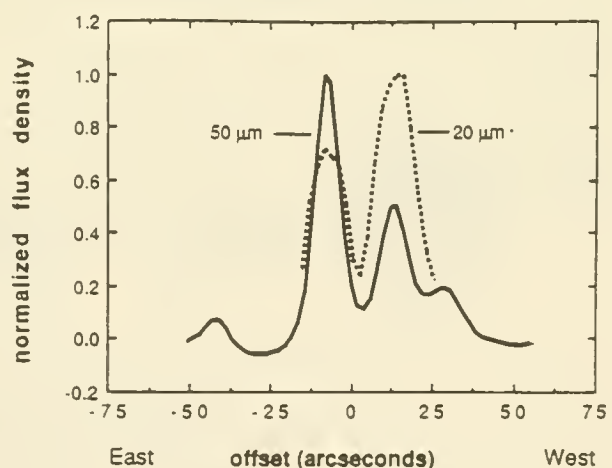


Figure 1: deconvolved 50 μ m KAO scan across Arp 299 compared with ground-based 20 μ m scan.

the interacting pair of galaxies in Arp299. Though much of the shocked gas is concentrated around NGC3690 (the westernmost component), and this component has the strongest emission from hot dust at 20 μ m, our data shows that it is the easternmost component (IC694) that supplies most of the far-IR luminosity.

A new generation instrument, with an array of ^3He cooled bolometers is now in use on the KAO. The detector sizes are $\lambda/2D \times \lambda/D$ allowing us to oversample the profile of a source in one direction. Work with that instrument on the structure of the starburst galaxy M83 is presented elsewhere in these proceedings (Smith *et al.*) With this array, and a new, precise and stable oscillating secondary mirror system for the KAO, observations with higher sensitivity and spatial dynamic range will be possible.

The importance of far infrared emission in tracing star formation in galaxies, and the need to trace out this star formation on spatial scales that can be compared with large scale characteristics of galaxies such as bulges, bars, and spiral arms, are strong drivers for a larger infrared telescope. Even a modest increase in spatial resolution would allow us to investigate the distribution of far IR emission across spiral arms in a number of nearby late-type spirals.

NASA, in collaboration with the West German Science Ministry (BMFT), plan a larger airborne telescope as a successor to the KAO that will achieve these goals. The Stratospheric Observatory for Infrared Astronomy (SOFIA) is entering the final stages of Phase B review with a targeted new start early in the next decade. SOFIA is a 2.7m diameter telescope that is carried in a Boeing 747SP. In addition to having 3 times the spatial resolution of the KAO, and 10 times the light gathering power, it will incorporate improvements over the KAO in lower optical emissivity and better telescope tracking stability. The thin primary mirror will equilibrate quickly to ambient temperature at altitude which, accompanied by airflow improvements across the telescope cavity will result in better image quality. The sensitivity of SOFIA will allow us to see a large number of typical bright galactic HII regions in local group galaxies. The spatial resolution of 8'' (FWHM Airy disk) at 100 μ m will allow these regions to be measured independently, if they are distributed similarly to those in our own galaxy. At this spatial resolution, the disks of normal galaxies will be easily resolved out to distances of several hundred Mpc. This portion of space includes many of the superluminous galaxies discovered by IRAS, and this spatial scale is relevant for studies of the morphology of regions of interaction among the majority of these galaxies that are members of colliding pairs. Figure 2 shows a schematic comparison of SOFIA with the existing KAO.

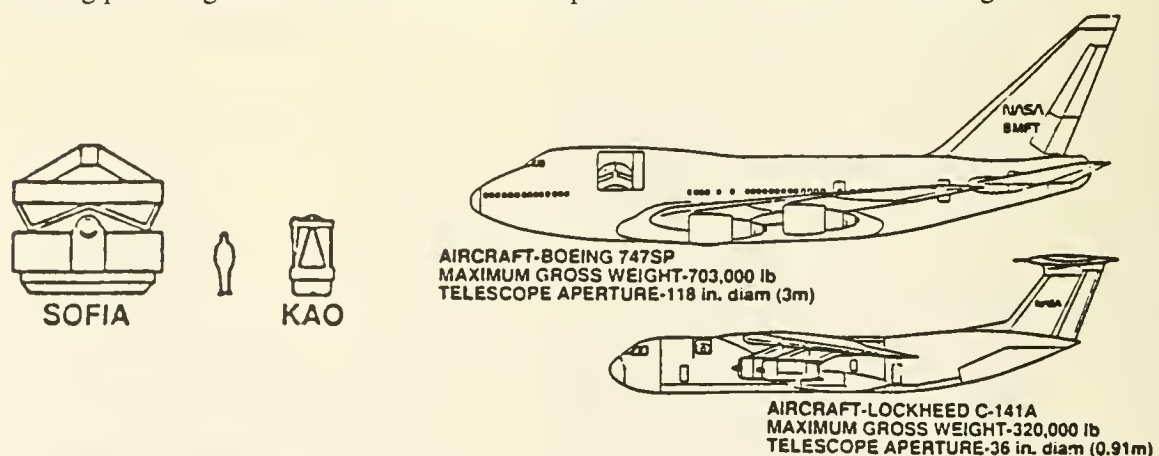


Figure 2: Comparison of 2.7m SOFIA and 747SP with existing 0.91m KAO and C-141

The design for SOFIA relies heavily on the successful technology of the KAO, which has demonstrated excellent stability for an open-port telescope operating at high altitude in a modern jet transport. Studies of telescope structure, mirror technology and support, aeroptics, and servo system design that have been carried out in the US and Germany over the past few years give us confidence that extrapolation of KAO technology to the larger size of SOFIA will be possible. One of the great successes of the KAO during the last 15 years has been the focal plane instrumentation that it has spawned. With instrumentation that is accessible from one flight to the next, and usually even during a flight, instruments become more sensitive and reliable with each flight series, and innovation is encouraged. This innovation has fed directly into the design of space infrared telescopes. Research on SOFIA will follow this tradition. Accessibility of focal plane instruments, and efficient instrument installation between flights are high priorities to the facility designers. The sketch below shows how the telescope will fit into the fuselage of the 747, and the light path from the telescope (at ambient temperature and pressure) through the air-bearing on which it is suspended, into the cabin.

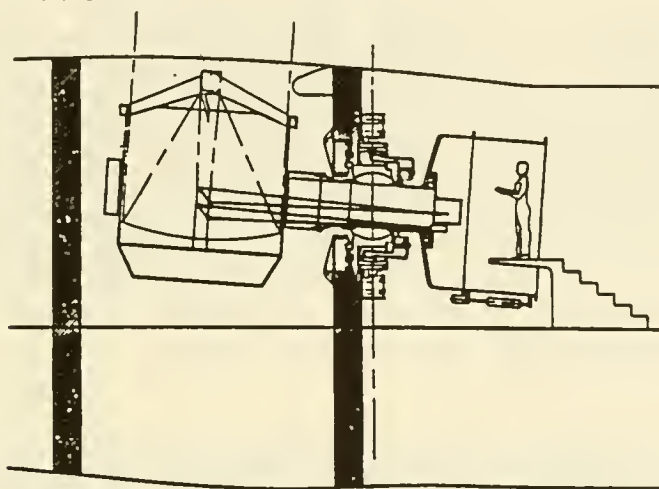


Figure 3: Cutaway view of the lightpath in SOFIA

Several technical challenges are being met by the SOFIA design team. In order to fit inside the fuselage of this airplane, an $f/1.2$ primary mirror must be fabricated, and in order that the thermal time constant and weight be minimized, the mirror must be very thin. Present plans call for a thin meniscus of low thermal expansion glass. Mirror thicknesses of the order of three inches or less, corresponding to thermal time constants of just two hours have been investigated. Clearly, the support system must be carefully designed, to fulfill the requirement that this mirror be diffraction limited at $\lambda > 30\mu\text{m}$. Though such a mirror has never been made, several manufacturers agree that it is possible. The large airbearing that supports the telescope requires special design considerations and innovative engineering but, like the mirror, is achievable with present technology.

- Brock, D., Joy, M., Harvey, P.M., and Ellis, H.B. Jr. 1988, Ap.J. 329, 208.
 Lester, D.F., Harvey, P.M., and Joy, M. 1986, Ap.J. 302, 280.
 Joy, M., Lester, P.M., Harvey, P.M., and Frueh, M. 1986, Ap.J. 307, 110.
 Joy, M., Lester, P.M., Harvey, P.M. 1987, Ap.J. 319, 314.
 Lester, D.F., Joy, M., Harvey, P.M., Ellis, H.B. Jr., and Parmar, P. 1987 Ap.J. 321, 755.
 Joy, M., Lester, D.F., Harvey, P.M., and Ellis, H.B. Jr. 1988 Ap.J. 326, 662.
 Joy, M., Lester, D.F., Harvey, P.M., Telesco, C., Decher, R., Rickard, L.J., and Bushouse, H. 1989 Ap.J. in press.

HIGH ANGULAR RESOLUTION MM- AND SUBMM-OBSERVATIONS OF DENSE MOLECULAR GAS IN M82

W. Wild¹, A. Eckart¹, R. Genzel¹, A.I. Harris¹, J.M. Jackson¹,
D.T. Jaffe², J.B. Lugten³ and J. Stutzki¹

¹ Max-Planck-Institut für extraterrestrische Physik, D-8046 Garching b.
München, West Germany

² University of Texas at Austin, Austin, Tx

³ Institute for Astronomy, Univ. of Hawaii, Honolulu, HI

We have observed CO(7-6) , CO(3-2) , HCN(3-2) and HCO⁺(3-2) line emission toward the starburst nucleus of M82 and have obtained an upper limit to H¹³CN(3-2). These are the first observations of the CO(7-6), HCN(3-2) and HCO⁺(3-2) lines in any extragalactic source. We took the CO(7-6) spectrum in January 1988 at the IRTF with the MPE/UCB 800 GHz Heterodyne Receiver (beam 30'' FWHM, Harris *et al.* 1987). In March 1989 we used the IRAM 30m telescope to observe the CO(3-2) line with the new MPE 350 GHz SIS receiver (beam 9'' FWHM, Harris *et al.* 1989) and the HCN(3-2) and HCO⁺(3-2) lines with the IRAM 230 GHz SIS receiver (beam 12'' FWHM, Blundell *et al.* 1988). The observational parameters are summarized in Table 1.

Line	Frequency	Resolution	Telescope	Receiver
CO(7-6)	806.65 GHz	30''	IRTF	MPE/UCB
CO(3-2)	354.79 GHz	9''	IRAM 30m	MPE SIS
HCN(3-2)	265.87 GHz	12''	IRAM 30m	IRAM SIS
HCO ⁺ (3-2)	267.56 GHz	12''	IRAM 30m	IRAM SIS

Table 1: Observational parameters

Fig. 1 shows spectra of the different lines for the offset position 10'' (160 pc) to the SW from the nucleus.

For this position, in the vicinity of the supernova remnant 41.9+58, each of the lines shows a strong, narrow feature at $V_{LSR} \sim 110 \text{ km s}^{-1}$. The CO(7-6) emission of the nuclear region of M82 consists only of this narrow feature and no emission of the bulk of the molecular gas is seen. The CO(3-2) and HCN(3-2) emission is strongest 10'' SW of the nucleus with the same feature clearly visible. It is also prominent in far-infrared emission lines (Lugten *et al.* 1986, Duffy *et al.* 1987).

Our preliminary results are summarized as follows:

We attribute the emission feature at $V_{LSR} \sim 110 \text{ km s}^{-1}$ to an unusually large star forming complex near the nucleus of M82 with dense gas and a large number

of young, massive stars ($L \sim 10^{10} L_{\odot}$). Estimates of the size and mass of this most active current star-forming region in M82 yield $5 \rightarrow 10''$ ($80 \rightarrow 160$ pc) and several $10^7 M_{\odot}$. The intrinsic strength of the CO(7-6) line then is a few 10 to 100 K. The excitation of this line as well as of HCN(3-2) and $\text{HCO}^+(3-2)$ requires densities $\geq 10^4 \text{ cm}^{-3}$. The close correlation between CO(7-6) emission and UV-radiation from young, massive stars in galactic sources suggests heating of the CO(7-6) emitting gas by UV-radiation or shocks. The character of this nuclear "hot spot" is not unlike that of the molecular mass concentration near the nucleus of our own galaxy. A more detailed discussion of the nuclear "hot spot" will be published elsewhere (Harris *et al.* 1989).

The HCN and HCO^+ data for other positions show that the central 1 kpc of M82 contains a large amount of dense gas ($n(\text{H}_2) \geq \text{several } 10^4 \text{ cm}^{-3}$). The $^{12}\text{CO}(3-2)$ line flux at all measured positions is weaker by at least a factor of 2 compared to the $^{12}\text{CO}(2-1)$ line. We find a similarly low ratio $I(^{12}\text{CO}(3-2))/I(^{12}\text{CO}(2-1)) \leq 0.5$ also in a number of galactic molecular cloud complexes. The low $^{12}\text{CO}(3-2)$ to (2-1) intensity ratio cannot be accounted for in simple one component models of the CO emission in molecular clouds. The low ratio may be due to a component of relatively low density ($n(\text{H}_2) \leq 10^3$) and low temperature (10 to 20 K) interclump gas where the $J=3$ level of ^{12}CO is subthermally populated, as in the model for the CO emission of the M17 interface (Stutzki *et al.* 1988). It is then likely that the large $^{12}\text{CO}(2-1)$ to (1-0) ratio is due to temperature gradients in predominantly externally heated clouds (see discussion in Young and Scoville 1984). A more detailed discussion will be presented in Wild *et al.* .

References

- Blundell, R., Carter, M., and Gundlach, K.H., 1988, *Internat. Journ. Infrared and Millimeter Waves* **9**, 361.
- Duffy, P.B., Erickson, E.F., and Haas, M.R., 1987, *Ap.J.* **315**, 68.
- Harris, A.I., Jaffe, D.T., Stutzki, J., and Genzel, R., 1987, *Internat. Journ. Infrared and Millimeter Waves* **8**, 857.
- Harris, A.I., Wild, W., Eckart, A., and Genzel, R., 1989, MPE-Report.
- Harris, A.I., Eckart, A., Genzel, R., Jackson, J.M., Jaffe, D.T., Lugten, J.B., Stutzki, J., and Wild, W., 1989, in prep.
- Lugten, J.B., Watson, D.M., Crawford, M.K., and Genzel, R., 1986, *Ap.J.(Letters)* **311**, L51.
- Stutzki, J., Stacey, G.J., Genzel, R., Harris, A.I., Jaffe, D.T., and Lugten, J.B., 1988, *Ap.J.* **332**, 379.
- Wild, W., Eckart, A., Genzel, R., Harris, A.I., Jackson, J.M., Jaffe, D.T., Lugten, J.B., and Stutzki, J., in prep.
- Young, J.S., and Scoville, N.Z., 1984, *Ap.J.* **287**, 153.

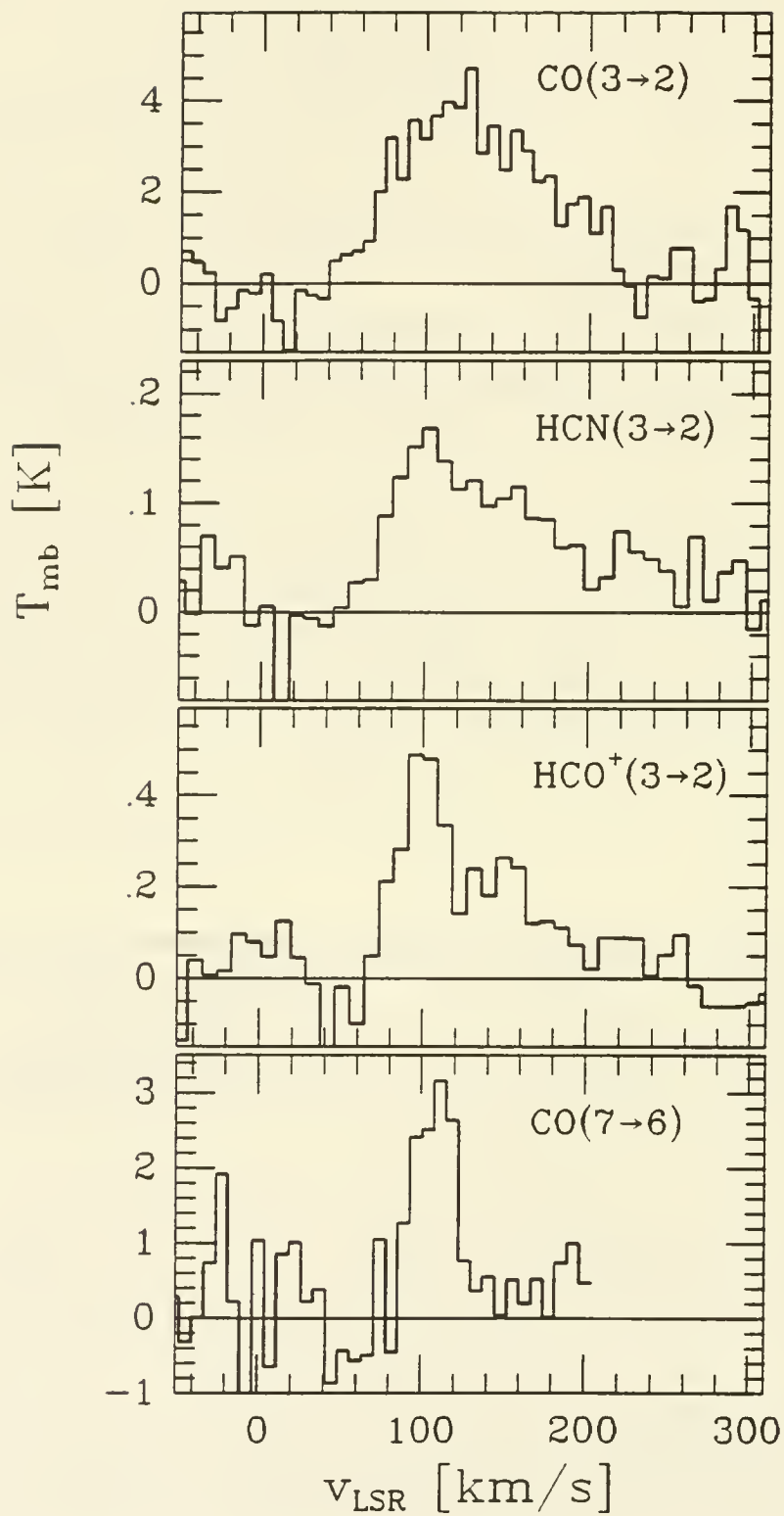


Fig. 1 Spectra of the nuclear "hot spot" of M82, 10" (160 pc) SW of the nucleus

The molecular spiral arms of NGC 6946

F. Casoli, F. Clausset, F. Viallefond, F. Combes and F. Boulanger

Radioastronomie, Ecole normale supérieure

24, rue Lhomond, F-75231 Paris Cedex 05, France

1. Introduction

High resolution observations of molecules in external galaxies are essential to understand the physical processes leading to the formation of stars. One question is that whether there is a spiral structure in the molecular gas, but it was not possible to resolve the spiral arms of external galaxies until the advent of large millimeter-wave telescopes.

With the IRAM 30 m telescope we are carrying through the mapping of NGC 6946 in the $^{12}\text{CO}(1-0)$ and $(2-1)$ lines. This galaxy is a large, gas-rich Scd spiral with a strong star formation activity. NGC 6946 is well studied at radio and optical wavelengths, so that it is possible to compare the location of the spiral arms tracers : HI ridge, HII regions and molecular clouds.

2. Observations

They were collected with the IRAM 30m telescope between November 1987 and April 1989. Mapping is still in progress ; we have already observed 309 positions in the $\text{CO}(1-0)$ line and 440 in the $\text{CO}(2-1)$ one. We used a position-switching procedure with signal in both the ON and OFF positions, but at different velocities. The average time spent on each positions is six minutes yielding an r.m.s. noise of about 70 mK in the $(\text{CO}1-0)$ line and 50 mK in the $\text{CO}(2-1)$. The map sampling is 10" (the HPBW is 23" at 115 GHz and 14" at 230 GHz).

Figure 1 shows the two $\text{CO}(2-1)$ maps that have been obtained simultaneously with this observing procedure in the inner regions of NGC 6946, at about 3.5 kpc from the nucleus. In $\text{CO}(1-0)$ we have mapped only the southern half of these regions, but we also have about 100 spectra of the nuclear region (see Weliachew, Casoli and Combes, 1988, A.A. **199**, 29).

3. Results and discussion

The disk CO emission is very contrasted (no lines for some positions, 1 K in $\text{CO}(1-0)$ for some others) and correlated with the optical spiral arms : this clearly shows up in figure 2 which presents superimposed contours of $\text{CO}(2-1)$ integrated emissivity and of $\text{H}\alpha$ line emission. The agreement is very good, and there is *no displacement across the arm* between the CO, HI and $\text{H}\alpha$ ridges of emission. The arms are barely resolved by the 23" beam and the molecular contrast averaged over the map is about 4. The $\text{CO}(2-1)$ maxima are closer to the position of the HII regions than those of $\text{CO}(1-0)$, which could be due to variations of excitation conditions.

The CO excitation in the disk of NGC 6946 is *low* : when all data are convolved to the same resolution of 23" the $\text{CO}(2-1)$ lines are about 0.45 times fainter than the $\text{CO}(1-0)$ ones, while in the nucleus they have roughly the same intensity. This suggests that in the disk of NGC 6946

most of the CO emission comes from cold optically thick gas located in cloud envelopes rather than from cloud cores.

The molecular and atomic component in the observed regions of NGC 6946 seems to be organized in *large gaseous complexes*. One such complex is centered at offsets (150, -20) (figure 1). It contains $2.4 \cdot 10^7 M_{\odot}$ of HI, $4.6 \cdot 10^7 M_{\odot}$ of H_2 [using $N(H_2) = 2.6 \cdot 10^{20} I(CO)$] and several HII regions. It has an elongated shape with a length of 1.8 kpc and is in approximate virial equilibrium. The molecular mass fraction in the regions we have observed is typically 0.5 and reaches 0.8 at some positions.

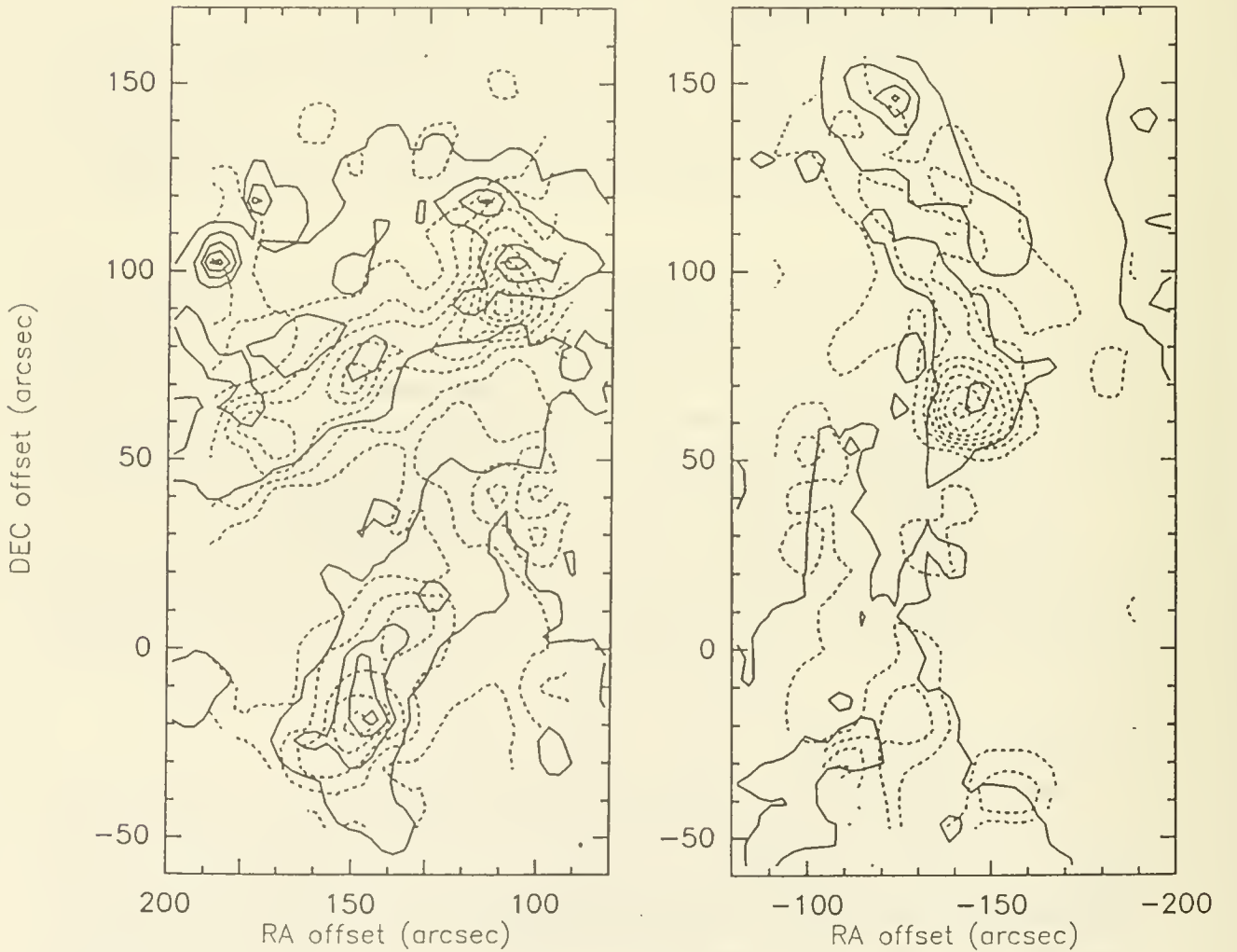


Figure 1 : superimposed H α [full line] and CO(2-1) [dashed] line emission in two fields of NGC 6946. Both fields have been mapped simultaneously. Levels : 1.5 to 15.5 K km s^{-1} by 2 for CO(2-1), 8 to 48 $10^{-26} \text{ erg s}^{-1} \text{ cm}^{-2} \text{ arcsec}^{-2}$ by 10 for H α . The sampling of the CO observations is 10" and the beamsize 14".

The Molecular Spiral Arms of NGC 6946

L. J. Tacconi (NFRA/Dwingeloo) and S. Xie (UMass)

A current interest in the study of star formation in galaxies has centered around the possible relationship between spiral density waves and the star formation efficiency. It is believed that in our galaxy most of the massive star formation occurs in spiral arms (Georgelin and Georgelin 1976). Recently, there has been a series of studies completed which suggest that the primary effect of a spiral density wave is to organize the ISM into a global spiral pattern (*e.g.* Scoville, Sanders, and Clemens (1986)), and that the observed spiral variations in the OB star formation efficiency on the spiral arms is due to orbit crowding in the spiral potential. In this picture the concentration of molecular gas is a purely kinematic concentration, and star formation in the arms results from cloud-cloud collisions (Scoville and Hersli (1979); Kwan and Valdes (1983)).

From $^{12}\text{CO}(J=1\rightarrow 0)$ observations at $45''$ resolution Tacconi and Young (1989) have found evidence for enhancements in both the CO emissivity and the massive star formation efficiency (MSFE) on optical spiral arms of the bright spiral galaxy NGC 6946. In the optically luminous and well-defined spiral arm in the NE quadrant, there are enhancements in both the H_2 surface density and MSFE relative to the interarm regions. In contrast, a poorly defined arm in the SW shows no arm-interarm contrast in the MSFE.

To further investigate the molecular gas content of these two spiral arms, we have made $^{12}\text{CO } J=2\rightarrow 1$ and $3\rightarrow 2$ observations with the James Clerk Maxwell Telescope. In the $J=2\rightarrow 1$ line, we have made observations of the NE and SW spiral arm and interarm regions in $4\times 9\ 10''$ spaced grids (36 points per grid). Because of decreased sensitivity in the $J=3\rightarrow 2$ line, we were limited to mapping the two arm regions in $2\times 3\ 10''$ spaced grids (6 points per grid). The centers of each of the grids lie $2.4'$ to the NE and $2.3'$ to the SW of the nucleus of NGC 6946.

With the CO $J=2\rightarrow 1$ data, we are able to fully resolve the two observed spiral arms in NGC 6946. In both cases the CO emission is largely confined to the optical spiral arm regions with the peak observed T_A^* being up to 4 times higher on the spiral arms than in the interarm regions. In Figure 1, sample $J=2\rightarrow 1$ spectra from both the arm and interarm regions of the northeast and southwest arms are shown. Typical $J=2\rightarrow 1$ integrated intensities ($\int T_A^* dv$) on the bright northeast spiral arm are $7\ \text{K km s}^{-1}$, dropping to $<1.5\ \text{K km s}^{-1}$ in the interarm regions. For the southwestern arm region, $J=2\rightarrow 1$ integrated intensities of 4.5 and $2.1\ \text{K km s}^{-1}$ are typical for positions which are on and off the spiral arm, respectively. Figure 2 shows spectra from both arms in the $J=3\rightarrow 2$ line. For this higher transition emission, peak antenna temperatures (T_A^*) observed on the northeast spiral arm are 2-3 times higher than those on the southwest arm.

We are currently estimating massive star formation efficiencies on and off the spiral arms through direct comparison of the CO maps with an $\text{H}\alpha$ image. We are also comparing the CO $J=2\rightarrow 1$ data with an HI map made at similar resolution. Thus, we will be able to determine structure in all components of the ISM on scales of $<20''$. The spatial resolution of the CO data coupled with the good velocity resolution will allow us to determine the effects of the spiral potential on the molecular gas kinematics. Observed kinematic differences between the NE and SW arms may provide clues to the reasons for the different MSFE's of these two regions.

The James Clerk Maxwell Telescope is operated by the Royal Observatory Edinburgh on behalf of the Science and Engineering Research Council of the United Kingdom, The Netherlands Organization for Scientific Research, and the National Research Council of Canada.

REFERENCES

- Georgelin, Y.M. and Georgelin, Y.P. 1976, *Astr. Ap.*, **49**, 57.
Kwan, J. and Valdes, F. 1983, *Ap.J.*, **271**, 604.
Scoville, N.Z. and Hersh, K. 1979, *Ap.J.*, **229**, 578.
Scoville, N.Z., Sanders, D.B., and Clemens, D.P. 1986, *Ap.J. (Lett.)*, **310**, L77.
Tacconi, L.J. and Young, J.S. 1989, *Ap.J.*. submitted

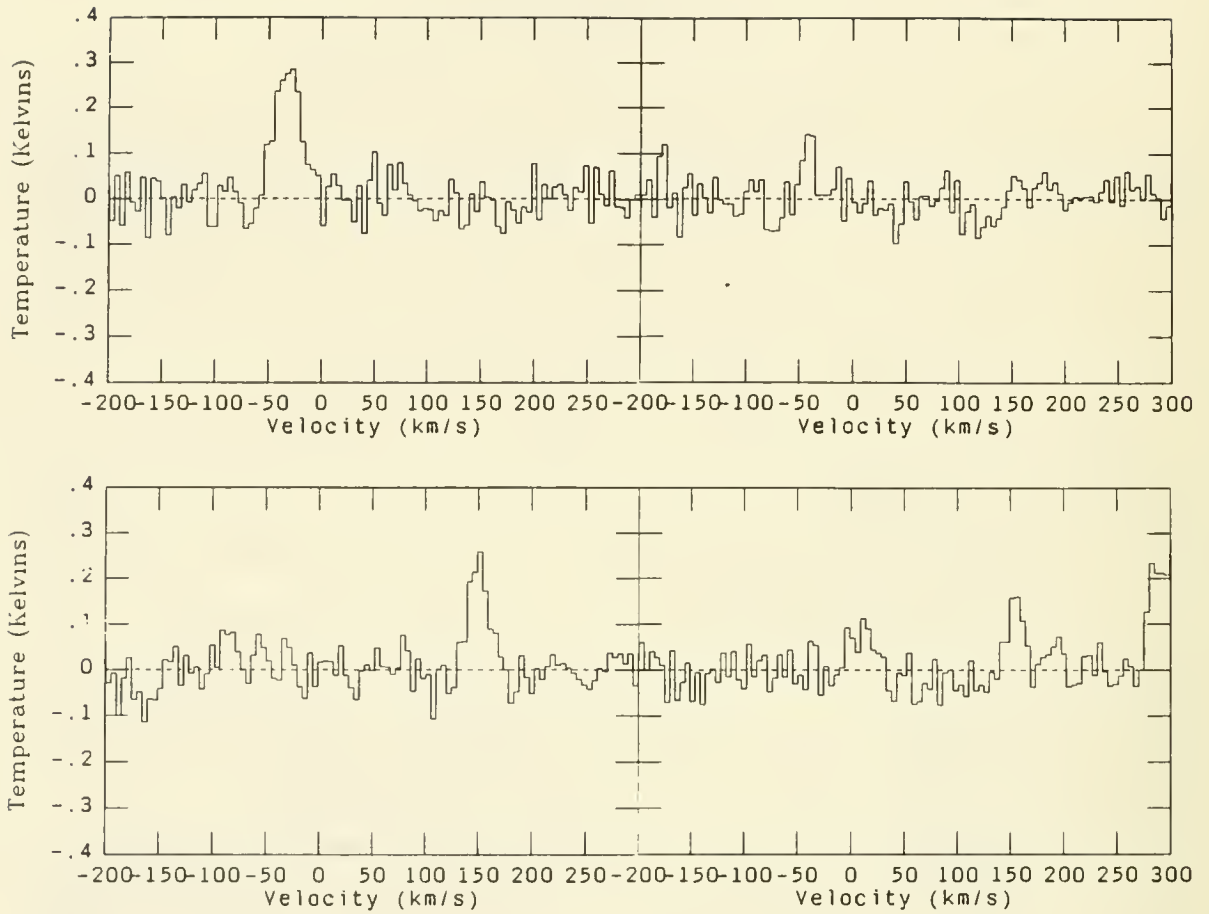


Figure 1: Sample $J=2 \rightarrow 1$ spectra from the spiral arm and interarm regions of NGC 6946. Spectra from the NE spiral arm are shown in the upper left (on arm spectrum) and right (off arm spectrum). Spectra from the SW are similarly shown in the lower left and right panels.

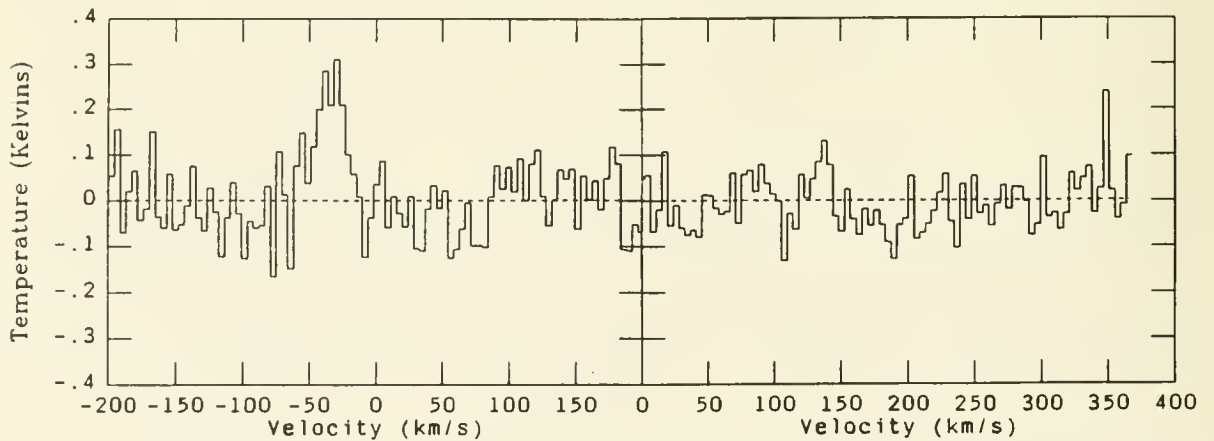


Figure 2: Sample $J=3 \rightarrow 2$ spectra from the two observed spiral arms in NGC 6946. A spectrum from the NE arm is shown on the left, while an example from the SW arm is presented in the right panel.

CO Mapping of the Nuclear Region of NGC6946 and IC342 with the Nobeyama Millimeter Array

SUMIO ISHIZUKI^{1,2}, RYOHEI KAWABE¹, SACHIKO K. OKUMURA¹, KOJI-ICHIRO MORITA¹,
AND MASATO ISHIGURO¹

¹ Nobeyama Radio Observatory, National Astronomical Observatory

² Department of Astronomy, University of Tokyo

INTRODUCTION

CO observations of nearby galaxies with nuclear active star forming regions (and starburst galaxies) with angular resolutions around $7''$ have revealed that molecular bars with a length of a few kiloparsecs have been formed in the central regions of the galaxies^{1–4}). The molecular bar is interpreted as part of shock waves induced by an oval or barred potential field. By shock dissipation or dissipative cloud-cloud collisions, the molecular gas gains an infall motion and the nuclear star formation activity is fueled. But the distribution and kinematics of the molecular gas in the nuclear regions, which are sites of active star formation, remain unknown. Higher angular resolutions are needed to investigate the gas in the nuclear regions. We have made aperture synthesis observations^{5,6}) of the nuclear region of the late-type spiral galaxies NGC6946 and IC342 with resolutions of $7''.6 \times 4''.2$ (P. A. = 147°) and $2''.4 \times 2''.3$ (P. A. = 149°), respectively. The distances to NGC6946 and IC342 are assumed to be 5.5 Mpc and 3.9 Mpc, respectively. We have found 100–300 pc nuclear gas disk and ring inside a few kpc molecular gas bars. We present the results of the observations and propose a possible mechanism of active star formation in the nuclear region.

OBSERVATIONS

The observations were made using the Nobeyama Millimeter Array (NMA), which consists of five antennas with a diameter of 10 meters. All antennas are equipped with SIS receivers with system noise temperatures (SSB) around 600 K at the zenith. A Fourier transform digital spectro-correlator FX was used. 10 baselines and 40 baselines are used for the mapping of NGC6946 and IC342, respectively. The field of view is $65''$ in diameter, which corresponds to 1.7 kpc and 1.2 kpc at the distance of NGC6946 and IC342, respectively.

RESULTS

NGC6946⁵): 300 pc Nuclear Molecular Gas Disk and Molecular Gas Bar

Figure 1a shows a map of CO integrated intensity. The galaxy has a strong nuclear concentration of molecular gas with a size of 300 pc and a diffuse feature with north–south extension of ~ 1.5 kpc. The diffuse feature is seen more clearly in a map of CO intensity integrated over a velocity range, $V_{LSR} = 21.4\text{--}99.5$ km s^{−1} (Fig. 1b). It shows a bar-like morphology generated at the reading sides. This bar-like structure is interpreted as part of shock waves or a density wave pattern in an oval potential field. A map of CO velocity field (Fig. 1c) indicates that the nuclear concentration is circularly rotating, i.e., a nuclear molecular disk, and that the gas in the bar-like structure has an infall motion. If we assume the conversion equation between molecular hydrogen mass and CO flux density,

$M(\text{H}_2) = 9000 \times (I_{\text{CO}}/\text{Jy km s}^{-1}) \times D_{\text{Mpc}}^2 M_{\odot}$, D_{Mpc} is the distance to the galaxy, the gas mass in the nuclear molecular disk is estimated to be $3 \times 10^8 M_{\odot}$. This means that about 10 % of the total molecular gas in the whole galaxy is concentrated to the central 300 pc region and 26 % of the dynamical mass inside a radius of 150 pc is in the form of H_2 molecule. The mass of molecular gas in the field of view ($\sim 1.7 \text{ kpc}$) is $4 \times 10^8 M_{\odot}$. A bright HII region with a size of 200 pc⁷⁾ and a radio continuum source⁸⁾ are found at the nuclear region. The nuclear molecular disk is a site of active star formation.

*Ic342*⁶⁾: 100 pc Nuclear Molecular Gas Ring and Molecular Gas Ridges

Figure 2a shows a map of CO integrated intensity. We have found a molecular ring with a diameter of 110 pc and two narrow ridges, each of which has a size of $\leq 80 \text{ pc} \times 500 \text{ pc}$. The map of CO velocity field (Fig. 2d) shows that the gas in the molecular ring is circularly rotating and that the gas in the ridges has an infall motion along the ridges. The mass of the molecular gas in the field of view is estimated to be $1.7 \times 10^8 M_{\odot}$. The molecular ring has a H_2 mass of $0.4 \times 10^8 M_{\odot}$. Figures 2b and 2c show VLA radio continuum maps at 2 cm and 6 cm⁸⁾, respectively. At 2 cm and 6 cm, about 100 % and 50 % of the emission is thermal origin, respectively. The flux density of radio continuum emission corresponds to the number flux density of UV photons from $3.5 \times 10^4 \text{ B3-O4 stars}$ ⁸⁾. The molecular gas ring just fits to the 6 cm continuum ring. This suggests that active star formation occurs in the nuclear molecular gas ring. The ridges are shifted to the leading side. They are also interpreted as molecular gas in shocks in the oval potential.

DISCUSSION

Here we propose a possible scenario of nuclear active star formation. An oval potential field with a few kpc scale produces shock waves which cause loss of angular momentum of gas and as a result the gas infalls toward the nuclear region. The infall motion of the gas slows down at the inner a few hundred pc region because the oval distortion of the gravitational potential becomes very small. Owing to the efficient gas supply in the oval potential and the slowing down of gas infall, a nuclear gas disk (or a ring) which has a few hundred pc size and a mass of a few $10^8 M_{\odot}$ is formed. In this massive nuclear disk, frequent cloud-cloud collisions probably occur and induce active, massive star formation.

REFERENCES

- 1) Lo, K. Y. *et al.* 1984, *Ap. J. (Letters)*, **282**, L59.
- 2) Ball, R. *et al.* 1985, *Ap. J. (Letters)*, **298**, L21.
- 3) Canzian, B., Mundy, L. G. and Scoville N. Z. 1988, *Ap. J.*, **333**, 157.
- 4) Ishiguro, M. *et al.* 1989, *Ap. J.*, in press.
- 5) Ishizuki, S. *et al.* 1989, submitted to *Ap. J.*
- 6) Ishizuki, S. *et al.* 1989, in preparation.
- 7) Bonnarel, F., Boulesteix, J. and Marcelin, M. 1984, *Astr. Ap. Suppl.*, **66**, 149.
- 8) Turner, J. L. and Ho. P. T. P. 1983, *Ap. J. (Letters)*, **268**, L79.

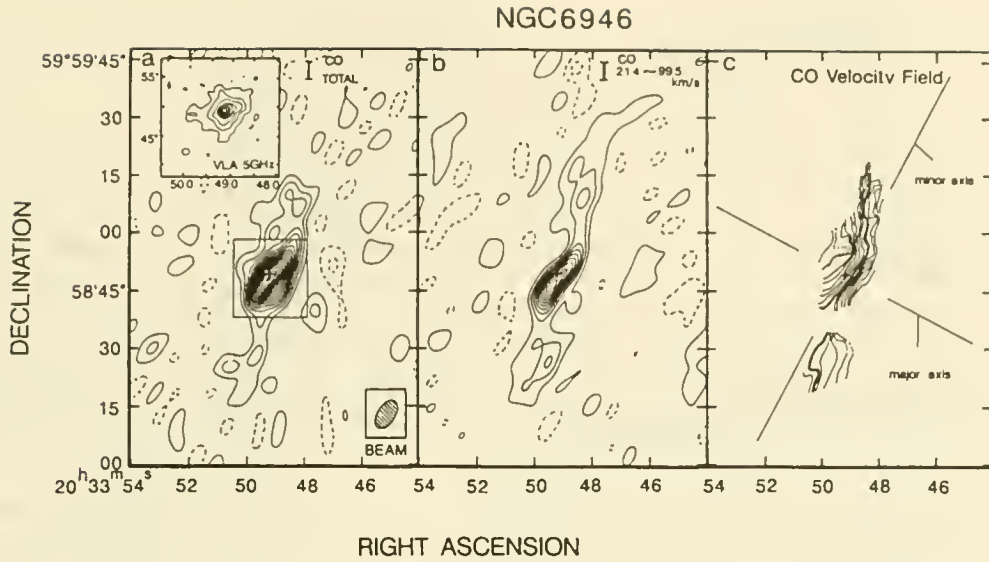


Figure 1 — NGC6946 — ($10''$ corresponds to 270 pc.) (a) A map of the total CO integrated intensity. An inset shows a map of the $\lambda\ 6\text{cm}$ radio continuum emission⁸⁾. A cross indicates its peak position. (b) A map of the integrated intensity in the velocity range $V_{LSR} = 21.4 - 99.5\text{ km s}^{-1}$. (c) A contour map of the CO weighted mean velocity. Dashed and solid curves indicate $V_{LSR} = -20, -10, 0, 10, \dots, 120\text{ km s}^{-1}$ from east to west. A thick solid curve indicates the systemic velocity, $V_{LSR} = 60\text{ km s}^{-1}$.

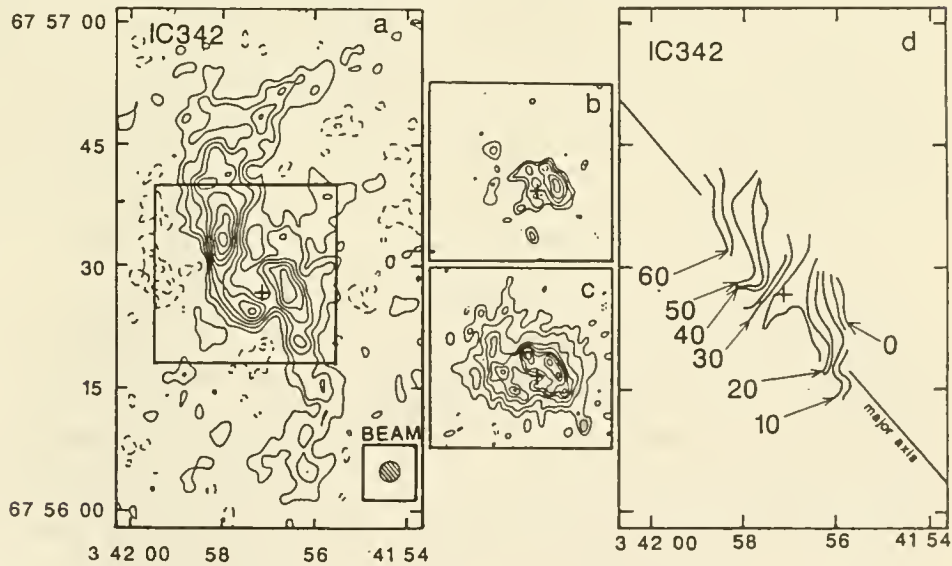


Figure 2 — IC342 — ($5''$ corresponds to 95 pc.) (a) A map of the total CO integrated intensity. A cross indicates the peak of $2.2\mu\text{m}$ emission. (b,c) Maps of the $\lambda\ 2\text{cm}$ and $\lambda\ 6\text{cm}$ radio continuum emissions⁸⁾, respectively. The size of the frames is the same as that of a box shown in Fig. 2a. (d) A contour map of the CO weighted mean velocity. The numbers indicates LSR velocities, V_{LSR} , in unit of km s^{-1} .

CO Excitation in Four IR Luminous Galaxies

Simon J. E. Radford,* P. M. Solomon,** and D. Downes*

The correlation between the CO and far infrared luminosities of spiral galaxies is well established.¹⁻³ The luminosity ratio, $L_{\text{FIR}}/L_{\text{CO}}$, in IR luminous active galaxies is, however, systematically five to ten times higher than in ordinary spirals and molecular clouds in our Galaxy.⁴ Furthermore, the masses of molecular hydrogen in luminous galaxies are large, $M(\text{H}_2) \approx 10^{10} M_{\odot}$, which indicates the observed luminosity ratios are due to an excess of infrared output, rather than a deficiency of molecular gas. These large amounts of molecular gas may fuel luminous galaxies through either star formation or nuclear activity. This interpretation rests on applying the $M(\text{H}_2)/L_{\text{CO}}$ ratio calibrated in our Galaxy to galaxies with strikingly different luminosity ratios. But are the physical conditions of the molecular gas different in galaxies with different luminosity ratios? And, if so, does the proportionality between CO and H_2 also vary among galaxies?

To investigate these questions, we observed CO($2 \rightarrow 1$) and ($1 \rightarrow 0$) emission from four luminous galaxies with the IRAM 30 m telescope. Three of the galaxies, Arp 193, Arp 220, and Mrk 231, have very high $L_{\text{FIR}}/L_{\text{CO}}$ ratios, and while VII Zw 31 has a moderate luminosity ratio it is one of the most gas rich galaxies yet detected, with $L_{\text{CO}} \approx 10^{10} \text{ K km s}^{-1}$. We mapped each galaxy in the ($2 \rightarrow 1$) line and obtained high quality ($1 \rightarrow 0$) spectra of the center positions. In figure 1 we show the spatial extent of the ($2 \rightarrow 1$) emission and the best fit gaussian distributions. For all of the sources, the FWHM sizes of the ($2 \rightarrow 1$) emission are either smaller than the $13''$ beam size or at the resolution limit. This confirms previous findings that molecular gas in active galaxies is concentrated in their nuclei.⁵ The CO morphology of these galaxies is quite distinct from equally gas rich galaxies with low luminosity ratios, such as NGC 1530 and NGC 3147, which we have also mapped, where the CO emission is extended on a scale of 10 kpc. These morphological differences are real, since the 30 m telescope would easily resolve the such extended emission at Arp 220's distance.

The spectra of both lines at the central positions are shown in figure 2. From these spectra we computed the intensity ratios, $I(2-1)/I(1-0)$, listed in the table, correcting for the different beam sizes with both a point source model that provides lower limits to the true ratios and the measured ($2 \rightarrow 1$) source sizes. The ratios are low, less than 0.9 for the three sources with high $L_{\text{FIR}}/L_{\text{CO}}$ ratios. Casoli *et al.*⁶ previously noted a low ratio in Arp 220, but this was fortuitous since their data lack adequate velocity coverage in the ($2 \rightarrow 1$) line and they failed to account for the difference between the beam sizes at the two wavelengths. Although the intensity ratio is a function of the molecular hydrogen density and the gas kinetic temperature, it depends primarily on the density for $I(2-1)/I(1-0) \leq 0.9$, since these low ratios result from subthermal excitation of optically thick gas. Using our observed ratios as constraints, we find for Arp 220 and Arp 193, with measured ratios of 0.6, the local densities⁷ of the emitting gas are in the range $150 \leq n(\text{H}_2) \leq 500 \text{ cm}^{-3}$ for gas kinetic temperatures between 20 and 60 K. For a kinetic temperature $T_k = 25 \text{ K}$ the intrinsic ($1 \rightarrow 0$) brightness temperature excitation $T_b = 8 \text{ K}$ corresponds to an excitation temperature of only $T_{\text{ex}} = 10.5 \text{ K}$, clearly subthermal. Here we note Maloney and Black⁸ dismissed the possibility of subthermal excitation in their calculation of intensity ratios. For a low kinetic

* Institut de Radio Astronomie Millimétrique, Grenoble

** Astronomy Program, State University of New York at Stony Brook

Quantity	Units	Arp 193	Arp 220	Mrk 231	VII Zw 31
cz	km s^{-1}	7000	5400	12650	16250
D_L	Mpc	94	72	170	220
$I_{\text{CO}}(1-0)$	$\text{K}_{\text{mb}} \text{ km s}^{-1}$	41	109	22	19
$L_{\text{CO}}(1-0)$	$10^9 \text{ K}_{\text{mb}} \text{ km s}^{-1} \text{ pc}^2$	3.1	4.9	5.5	7.8
$I_{\text{CO}}(2-1)$	$\text{K}_{\text{mb}} \text{ km s}^{-1}$	62	155	44	44
FWHM (2-1)	arcsec	14	15	16	18
Source size (2-1)	arcsec	5.2	7.5	9.3	12.4
$I(2-1)/I(1-0)$, if point source		0.55	0.52	0.73	0.85
$I(2-1)/I(1-0)$, with measured (2-1) size		0.61	0.62	0.93	1.22
$M(\text{H}_2)$	$10^{10} M_{\odot}$	1.3	2.1	2.4	3.1
Gas kinetic temperature, local H_2 density, and intrinsic (1-0) brightness temperature:					
$T_k = 10 \text{ K}: n(\text{H}_2)$	cm^{-3}	300-1000	300-1000
$T_b(1-0)$	K	6	6
$T_k = 25 \text{ K}: n(\text{H}_2)$	cm^{-3}	180-500	180-500	500-1300	...
$T_b(1-0)$	K	8	8	16	...
$T_k = 40 \text{ K}: n(\text{H}_2)$	cm^{-3}	140-400	140-400	400-800	3000
$T_b(1-0)$	K	9	9	19	30

Beam sizes: $(1 \rightarrow 0) = 21.5''$, $(2 \rightarrow 1) = 13''$; $H_0 = 75 \text{ km s}^{-1} \text{ Mpc}^{-1}$, and $q_0 = 0.5$.

temperature of 10 K, the density could be as large as 1000 cm^{-3} . We find higher ratios for Mrk 231 and VII Zw 31, but suspect telescope pointing difficulties may have exaggerated the measured source size of the latter. For these two the point source model gives ratios near 0.8, which imply $T_k > 20 \text{ K}$ and densities in the range of $500\text{--}2000 \text{ cm}^{-3}$.

We can directly estimate the galaxies' total molecular masses by combining our estimates of H_2 densities and intrinsic line brightness temperatures, $T_b(1-0)$, with the observed CO luminosity. If T_{mb} is the observed brightness temperature of the galaxy and A_b is the beam area, the fraction of the beam filled with N_c clouds radiating at the intrinsic brightness temperature is $T_{\text{mb}}(1-0)/T_b(1-0) = (N_c \pi r^2 / A_b) (\Delta v / \Delta V)$, where Δv is the velocity dispersion in an individual cloud of radius r and ΔV is the observed line width of the entire galaxy. If the clouds are near virial equilibrium, the dispersion is fixed by the density and radius, $\Delta v = (4\pi G m(\text{H}_2)/3)^{1/2} r n(\text{H}_2)^{1/2}$, and the sum of the individual cloud masses is

$$M(\text{H}_2) = \left(\frac{4m(\text{H}_2)}{3\pi G} \right)^{1/2} \frac{T_{\text{mb}}(1-0)}{T_b(1-0)} \Delta V A_b n(\text{H}_2)^{1/2}$$

This form of the CO mass-luminosity relation for virialized clouds shows the dependence on the observed CO luminosity, $L_{\text{CO}} = T_{\text{mb}} \Delta V A_b$, and on the quantities constrained by the intensity ratio, T_b and $N(\text{H}_2)$. The mass estimates in the table were computed from the $(1 \rightarrow 0)$ luminosity by these formulae.

We conclude most of the CO emission from these galaxies arises in regions with moderate ambient densities similar to the clouds in the Milky Way molecular ring. The emission is neither from dense ($n(\text{H}_2) = 10^4$ or 10^5 cm^{-3}) hot cloud cores nor from the cold low density gas ($n(\text{H}_2) = 100 \text{ cm}^{-3}$) characteristic of the envelopes of dark clouds.

References: (1) Sanders *et al.* 1986, *Ap. J.*, **305**, L45. (2) Young *et al.* 1986, *Ap. J.*, **304**, 443. (3) Solomon *et al.* 1986, 1987, 1988 *Ap. J.*, **334**, 613. (4) Mooney and Solomon 1988, *Ap. J. (Letters)*, **334**, L51. (5) Scoville *et al.* 1986, *Ap. J. (Letters)*, **311**, L47. (6) Casoli *et al.* 1988, *Astr. Ap.*, **192**, L17. (7) Goldsmith *et al.* 1983, *Ap. J. Suppl.*, **51**, 203. (8) Maloney and Black 1988, *Ap. J.*, **325**, 389.

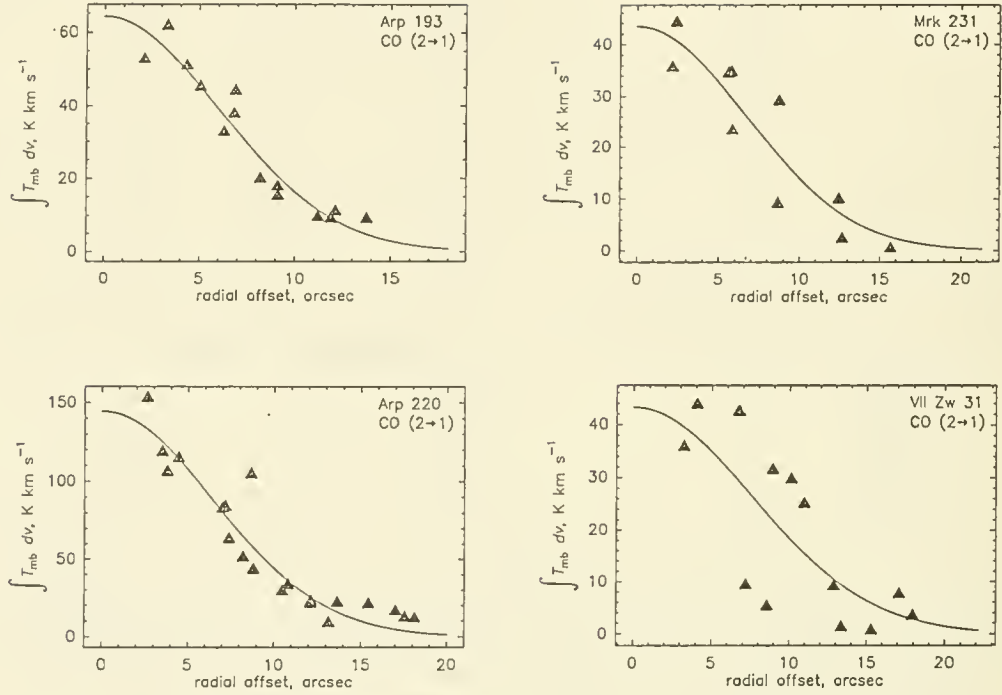


Figure 1. Radial distribution of integrated CO(2→1) emission.

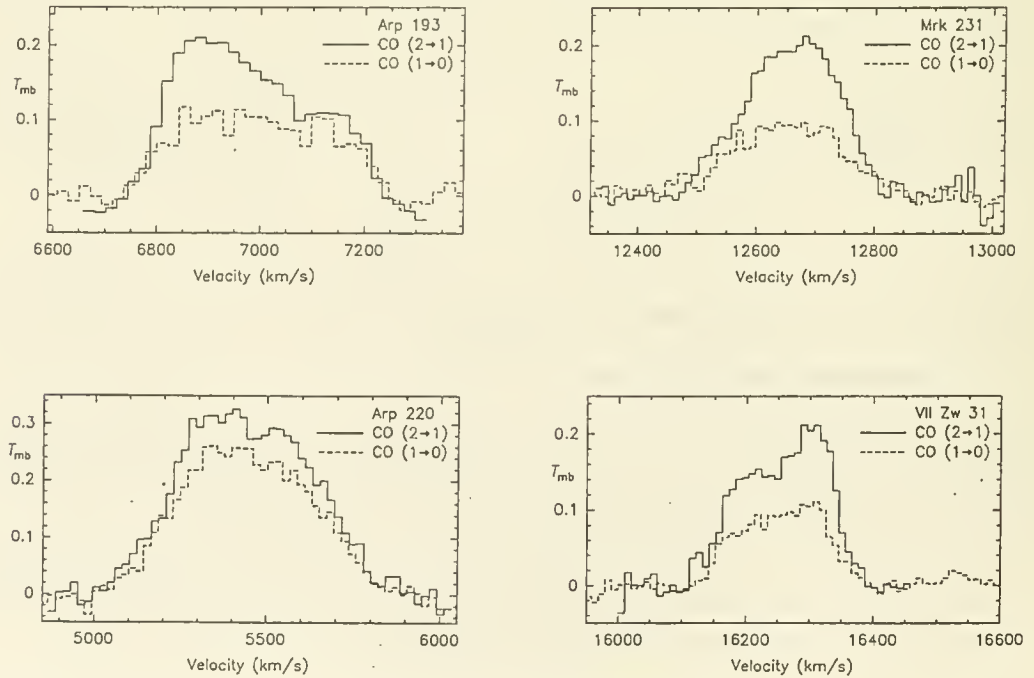


Figure 2. CO(2→1) and (1→0) spectra at central positions.

CS in nearby galaxies: distribution, kinematics and multilevel studies

R. Mauersberger^{1,2} and C. Henkel²

1. I.R.A.M., Avda. Divina Pastora, 7, N.C., E 18012 Granada, Spain

2. Max Planck Institut für Radioastronomie, Auf dem Hügel 69, D 5300 Bonn, F.R.G.

Recently, several high resolution studies of extragalactic CO and even of its rare isotopic substitutions have been published making use of advanced mm-wave interferometers and single-dish telescopes. From these studies, the morphology and kinematics of the molecular gas can be derived and compared to the distribution of stars and dust. On the other hand, the recent detection of many complex extragalactic molecules (see Henkel et al. 1987, 1988 and references therein) opens up the possibility to derive from observations of many transitions of the same molecule further important parameters, like kinetic temperature, gas density and excitation conditions. These are difficult to derive from CO alone, because of the low degree of excitation required to thermalize CO and because of severe beam dilution expected in these distant sources. While NH_3 is a good thermometer for extragalactic sources (Martin and Ho 1987), CS, which has been previously detected by Henkel and Bally (1985) toward the galaxies IC 342 and M 82, is a relatively abundant molecule, which is suitable as a probe to estimate H_2 densities (e.g. Linke and Goldsmith 1980).

As a result of observations at the IRAM 30-m telescope, maps of the distribution of the $J=2-1$ transition of CS toward the galaxies IC 342 and NGC 253 are presented. The distribution of the CS emission from NGC 253 is consistent with that the CO 1-0 line. The distribution of the CS emission from IC 342, however, resembles more that seen in the CO 3-2 line. For the first time, the detection of the isotopic substitution C^{34}S is reported toward an external galaxy: The C^{34}S 2-1 line has been detected toward NGC 253 and M 82 and the C^{34}S 3-2 line has been detected tentatively toward M 82. Also for the first time, extragalactic CS has been observed in the 3-2 (toward NGC 253, IC 342 and M 82) and 5-4 (NGC 253 and IC 342) transitions.

The results obtained from the observations of several transitions and isotopic substitutions of CS can be compared with model computations using a non-LTE statistical equilibrium program. Since CS requires densities an order of magnitude higher than CO to be excited, it may seen in a smaller volume than CO. Even in the optically thick case, the observed T_{MB} may be much smaller than the excitation temperature T_{ex} and, because of our lack of information on the beam-filling factor, only the ratios of different lines enter in our multi-level study. For this, we had to make some assumptions on geometry, since our beam size differs from transition to transition and time did not permit to map the CS 3-2 and 5-4 emission.

The values of $T_{MB}(\text{CO})$ measured toward IC 342, NGC 253 and M 82, 10K, 9 K and 15 K (Lo et al. 1984, Canzian et al. 1988, Lo et al. 1987), can only be considered as lower limits to T_{kin} . However, these relatively high values show that the beam filling factor of CO within a 7'' beam is probably $\geq 10\%$. From observations of lines from the CS and C^{34}S isotopes, one can directly estimate the optical depth of the CS lines without having to account for the unknown beam filling factor. For this, we assumed optically thin C^{34}S emission and a relative $^{32}\text{S}/^{34}\text{S}$ abundance of 23 (Wannier 1980).

For our multilevel analysis, we computed the expected intensities of the C^{34}S 2-1 line as well as of the CS 3-2 and 5-4 lines relative to the CS 2-1 transition. In order to determine the physical parameters, we first obtained for each source the ratio of the integrated intensities in the 2-1 transition of CS and C^{34}S , which could be measured with the same angular resolution. The such determined ratios are $9(\pm 2)$ for NGC 253 at the $(0'', 0'')$ offset, > 4.5 for IC 342 at $(-10'', 0'')$ and $16(\pm 5)$ for M 82 at $(-10'', 0'')$. Additionally, we determined line intensity ratios for transitions of the CS main isotope.

NGC 253 The H_2 density and the column density derived from the intensity ratio of the 2-1 transitions of CS and C^{34}S determined above and of the ratio of the line intensities of the 2-1 and 5-4 transition are, assuming $T_{kin}=60$ K, $n(\text{H}_2) = 10^{4.6}\text{cm}^{-3}$ and $N(\text{CS}) = 2(\pm 1) 10^{14}\text{cm}^{-2}\Delta v_{1/2}$. With $\Delta v_{1/2}=160$ km s^{-1} , $N(\text{CS}) = 3(\pm 1) 10^{16}\text{cm}^{-2}$. Here, $N(\text{CS})$ is the column density averaged over the CS emitting

region. All column densities are 'in the line of sight' and not reduced to 'face-on'. From a comparison of the line temperature expected from our model and the actually observed value reduced to an 11'' region, the 2—1 emitting gas has a clumping factor of ~ 0.17 . From this, the column density averaged over an 11'' region is $0.5 \cdot 10^{16} \text{cm}^{-2}$.

If we take the ratio from the 3—2 and 5—4 transitions, for which assumptions on geometry are not so important because of the more similar beam width, the density even becomes $n(\text{H}_2) = 10^{5.4} \text{cm}^{-3}$ for $T_{\text{kin}}=60 \text{ K}$ and $10^{5.2} \text{cm}^{-3}$ for $T_{\text{kin}}=90 \text{ K}$. These different H_2 densities derived from the various line ratios could be explained if the bulk of the CS gas is lower density gas (seen in the 2—1 transition) containing higher density condensations (traced out by the 5—4 line).

Canzian et al. (1988) derive for the NGC 253 bar an average H_2 column density of $1.5 \cdot 10^{23} \text{cm}^{-2}$. From this value, the relative CS abundance is $X(\text{CS})=3 \cdot 10^{-8}$.

IC 342 For IC 342, we have only a very crude upper limit on the optical depth, since we did not detect emission from C^{34}S . From observations of the 2—1, 3—2 and 5—4 lines, the maximum density compatible with our observations is, in the optically thin limit, $n(\text{H}_2) = 10^{5.0} \text{cm}^{-3}$. If the CS is optically thick, densities can become lower. These values are consistent with the upper limit derived from CH_3OH by Henkel et al. (1987). Using our model, we have calculated the column density of CS averaged over an 11'' region in the optically thin case, which is required to reproduce the observed value of T_{MB} . For $n(\text{H}_2) \sim 5 \cdot 10^4 \text{cm}^{-3}$, we require $N(\text{CS}) = 1.5(\pm 0.5) \cdot 10^{14} \text{cm}^{-2}$. Combining this value with the H_2 column density of $\sim 7 \cdot 10^{22} \text{cm}^{-2}$ derived from CO multi-isotope studies (Eckart et al. 1989), the relative CS abundance toward the center of IC 342 is $X(\text{CS}) \sim 2 \cdot 10^{-9}$.

M 82 From the ratios of the CO 2—1 and 1—0 lines, the kinetic temperature of the molecular gas near the nucleus of M 82 is probably $\sim 50 \text{ K}$ (Knapp et al 1980, Sutton et al. 1983). For M 82, the intensity of the C^{34}S emission at the $(-10'', 0'')$ offset shows that the CS lines are only moderately saturated. If we assume that this is also the case for the $(0'', 0'')$ position where the 3—2 line of CS was observed, from the 3—2 and 2—1 line intensities, the H_2 density of the CS emitting gas at $(0'', 0'')$ is $< 10^4 \text{cm}^{-3}$. From the ratio of the integrated intensity of the 2—1 and 3—2 transitions of C^{34}S , $n(\text{H}_2) \sim 10^4 \text{cm}^{-3}$ at the peak $(-10'', 0'')$. However, the highest density compatible with the error limits of our C^{34}S observations is 10^5cm^{-3} . H_2CO data indicate, however, that even higher densities may exist in this region, which could be confirmed by observations of the CS 5—4 line.

Toward the nucleus of M 82, Lo et al. (1987) find a mean H_2 column density of $2.6 \cdot 10^{22} \text{cm}^{-2}$. Assuming similar excitation conditions for the CS as in the case of IC 342, the CS column density is $\sim 7(\pm 3) \cdot 10^{14} \text{cm}^{-2}$ and the relative abundance of CS is $X(\text{CS}) = 1.5(\pm 1) \cdot 10^{-9}$.

Accounting for the uncertainties in the determination of the H_2 column densities, the values observed for all galaxies are compatible with those found in Galactic molecular clouds where relative CS abundances of $10^{-7.8} \dots 10^{-9.0}$ have been measured.

References

- Canzian, B., Mundy, L.G., Scoville, N.Z.: 1988, *Astrophys. J.*, **333**, 157
Eckart, A., Downes, D., Genzel, R., Harris, A.I., Jaffe, D.T., Wild, W.: 1989, *IRAM-preprint* 153
Henkel, C., Bally, J.: 1985, *Astron. Astrophys.*, **150**, L25
Henkel, C., Jacq, T., Mauersberger, R., Menten, K.M., Steppe, H.: 1987, *Astron. Astrophys.* **188**, L1
Henkel, C., Mauersberger, R., Schilke, P.: 1988, *Astron. Astrophys.* **201**, L23
Knapp, G.R., Phillips, T.G., Huggins, P.J., Leighton, R.B., Wannier, P.G.: 1980, *Astrophys. J.* **240**, 60
Linke, R.A., Goldsmith, P.F.: 1980, *Astrophys. J.* **235**, 437
Lo, K.Y., Berge, G.L., Claussen, M.J., Heiligman, G.M., Leighton, R.B., Masson, C.R., Moffet, A.T., Phillips, T.G., Sargent, A.I., Scott, S.L., Wannier, P.G., Woody, D.P.: 1984, *Astrophys. J.* **282**, L59
Lo, K.Y., Cheung, K.W., Masson, C.R., Phillips, T.G., Scott, S.L., Woody, D.P.: 1987, *Astrophys. J.* **312**, 574
Martin, R.N., Ho, P.T.P.: 1986 *Astrophys. J.* **308**, L7
Sutton, E.C., Masson, C.R., Phillips, T.G.: 1983 *Astrophys. J.* **275**, L49
Wannier, P.G.: 1980, *Ann. Rev. Astron. Astrophys.* **18**, 399

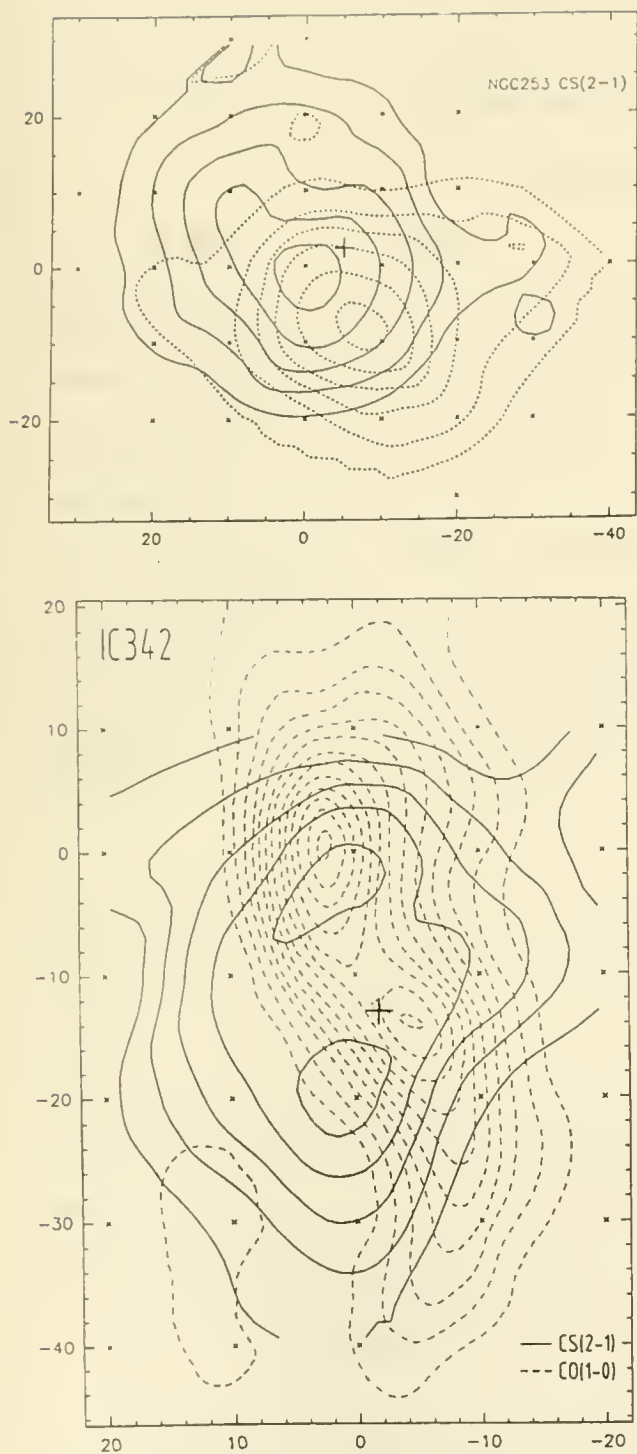


Figure 3. The integrated CS 2—1 emission toward IC 342 (reference position $\alpha(1950) = 3^h 41^m 57.5^s$, $\delta(1950) = 67^\circ 56' 40''$). The overlay shows the integrated CO 1—0 emission (Lo et al. 1984).

Figure 1. The distribution of the integrated CS 2—1 emission toward NGC 253. The reference position is $\alpha(1950) = 0^h 45^m 06.0^s$, $\delta(1950) = -25^\circ 33' 36''$. The solid contours are integrated from 50 to 250 km/s, the dashed contours from 250 to 450 km/s.

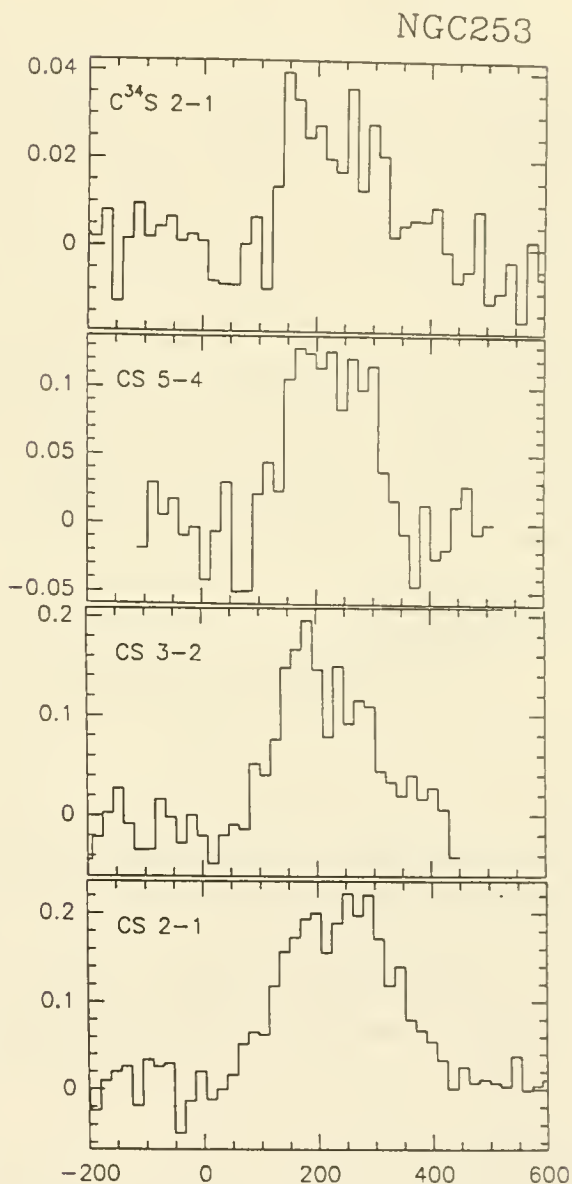


Figure 2. A compilation of the CS transitions measured toward NGC 253.

SPATIAL VARIATION OF THE PHYSICAL CONDITIONS OF MOLECULAR GAS IN GALAXIES

James M. Jackson, Andreas Eckart, Wolfgang Wild, Reinhard Genzel, Andrew I. Harris (MPE)
Dennis Downes (IRAM), D.T. Jaffe (Texas), and Paul T. P. Ho (CfA)

Introduction

Multi-line studies of ^{12}CO , ^{13}CO , C^{18}O , HCN , and HCO^+ at 3 mm, 1.3 mm, and 0.8 mm using the IRAM 30 m telescope, with the IRAM SIS receivers and the MPE 350 GHz SIS receiver, show that the densities and temperatures of molecular gas in external galaxies change significantly with position. ^{12}CO measures the densities and temperatures of diffuse interclump molecular gas, but not the bulk of the molecular gas. Simple one-component models, with or without external heating, cannot account for the weakness of the $^{12}\text{CO } J = 3 \rightarrow 2$ line relative to $J = 2 \rightarrow 1$ and $J = 1 \rightarrow 0$. ^{12}CO does not trace the bulk of the molecular gas, and optical depth effects obviate a straightforward interpretation of ^{12}CO data. Instead, we have turned to the optically thin CO isotopes and other molecular species. Isotopic CO lines measure the bulk of the molecular gas, and HCN and HCO^+ pick out denser regions. We find a warm ridge of gas in IC342 (Eckart et al. 1989), denser gas in the starburst nucleus of IC342, and a possible hot-spot in NGC2903. In IC342, NGC2146, and NGC6764, the $^{13}\text{CO } J = 2 \rightarrow 1$ line is subthermally populated, implying gas densities $\lesssim 10^4 \text{ cm}^{-3}$.

^{12}CO Studies

Recent IRAM 30 m observations of $^{12}\text{CO } J = 1 \rightarrow 0$, $J = 2 \rightarrow 1$, and $J = 3 \rightarrow 2$ toward M82 (see Wild et al., this volume) and IC342, as well as toward several Galactic high mass star-forming regions, show that simple models cannot account for the ^{12}CO data. In each of these regions, the $^{12}\text{CO } J = 2 \rightarrow 1$ line is as bright as or brighter than the $J = 1 \rightarrow 0$ line, but the $J = 3 \rightarrow 2$ line is weaker than $J = 2 \rightarrow 1$, typically by a factor of two. This cannot be explained by simple one-component models, nor by externally heated clouds. Furthermore, self-absorbed features are evident in the ^{12}CO spectra, often associated with peaks in the isotopic lines. It seems clear that ^{12}CO suffers in a complicated way from optical depth effects, and that one must turn to optically thin species to trace the bulk of the interstellar medium. Global properties such as mass or temperature derived from ^{12}CO must be treated with extreme caution.

CO Isotopic Studies

We have used the IRAM 30 m to observe $^{13}\text{CO } J = 1 \rightarrow 0$ (22'' beam) and $J = 2 \rightarrow 1$ (14'' beam) emission in IC342, NGC2146, and NGC6764. When both maps are convolved to the same angular resolution, in each case the ratio $T(2 \rightarrow 1)/T(1 \rightarrow 0)$ is ~ 1.0 . In the

nucleus of IC342, the corresponding C^{18}O ratio is ~ 1.8 . These ratios are much smaller than the value of 4.0 produced by warm, thermalized, optically thin gas. Since the large $\text{CO}/^{13}\text{CO}$ and $\text{CO}/\text{C}^{18}\text{O}$ brightness temperature ratios suggest optically thin emission in the isotopic lines, we conclude that the $J = 2 \rightarrow 1$ isotopic lines are subthermally excited. This constrains the densities to be near the CO critical density. If subthermal excitation occurs in all galaxies, then the ^{13}CO and $\text{C}^{18}\text{O } J = 1 \rightarrow 0$ lines trace total column density and may be used to estimate mass.

NGC2903

VLA 21 cm radio continuum, Lick $\text{H}\alpha$, and IRAM 30 m $J = 1 \rightarrow 0$ and $2 \rightarrow 1$ CO observations of the hot-spot galaxy NGC2903 show them all to be distributed nearly identically in a central bar. Thus synchrotron emission, H II regions, and molecular gas all accompany star formation. There is an unresolved “hot-spot” at the northern end of the bar that has a $^{12}\text{CO } T(2 \rightarrow 1)/T(1 \rightarrow 0)$ ratio ~ 1.0 , which may indicate substantially warmer or thinner CO emission. Otherwise, this ratio is typically ~ 0.7 , consistent with emission from molecular clouds with properties typical of those found in the Milky Way, that is, with large optical depths, excitation temperatures near 10 K, and sizes about 100 to 200 pc. Star formation extends throughout the bar, but the star formation rate per unit area is enhanced by an order of magnitude in the nucleus. A comparison with resolved IRAS ADDSCAN and CPC images shows that the far infrared to CO luminosity ratio, which is often interpreted as a measure of star formation efficiency, is typical of normal spirals and does not vary with position at 1.4 arcminute resolution. The nuclear starburst may then result from a large amount of molecular gas with normal star formation efficiency collected into a small nuclear region due to streaming motions induced by the bar.

IC342

Eckart *et al.* (1989, preprint) have mapped IC342 in the ^{12}CO and $^{13}\text{CO } J = 1 \rightarrow 0$ and $J = 2 \rightarrow 1$ lines and also obtained $J = 1 \rightarrow 0$ and $J = 2 \rightarrow 1$ C^{18}O spectra toward the nucleus. The $T(2 \rightarrow 1)/T(1 \rightarrow 0)$ ratio varies with position for both ^{12}CO and ^{13}CO . The CO isotopic $J = 2 \rightarrow 1$ lines are subthermally excited. Molecular gas temperatures and densities were derived using a radiative transfer code with a clumpy cloud model. The gas in the nucleus is substantially warmer (~ 30 K) than in the disk (~ 13 K). Further, a ridge to the east of the nucleus shows elevated temperatures. New $^{12}\text{CO } J = 3 \rightarrow 2$ observations at the IRAM 30 m with the MPE 350 GHz receiver show that this line is weaker than $J = 2 \rightarrow 1$ by about a factor of two. Simple one-component models, or externally heated cloud models, cannot account for the weak $J = 3 \rightarrow 2$ line. New HCN and $\text{HCO}^+ J = 3 \rightarrow 2$ data show that dense molecular gas ($n \gtrsim 10^5 \text{ cm}^{-3}$) is found only in the nuclear starburst region.

DETECTION OF CO EMISSION IN HYDRA I CLUSTER GALAXIES

W.K. Huchtmeier
Max-Planck-Institut für Radioastronomie
Auf dem Hügel 69
5300 Bonn 1 , W. Germany

Abstract

A survey of bright Hydra cluster spiral galaxies for the CO(1-0) transition at 115 GHz was performed with the 15m Swedish-ESO submillimeter telescope (SEST). Five out of 15 galaxies observed have been detected in the CO(1-0) line. The largest spiral galaxy in the cluster, NGC 3312, got more CO than any spiral of the Virgo cluster. This Sa-type galaxy is optically largely distorted and disrupted on one side. It is a good candidate for ram pressure stripping while passing through the cluster's central region. A comparison with global CO properties of Virgo cluster spirals shows a relatively good agreement with the detected Hydra cluster galaxies.

Observations

Observations were performed with the 15m Swedish-ESO submillimeter telescope (SEST) at La Silla in January 1989 under favorable meteorological conditions. At a frequency of 115 GHz the half power beamwidth (HPBW) of this telescope is 43 arcsec. The cooled Schottky heterodyne receiver had a typical receiver temperature of 350 K; the system temperature was typically 650 to 900 K depending on elevation and humidity. An acousto-optic spectrometer (Zensen 1984) with a bandwidth of 500 MHz yielded a channel width of 0.69 MHz or about 1.8 km/s. In order to improve the signal-to-noise ratio of the integrated profiles usually 5 to 10 frequency channels were averaged resulting in a resolution of 9 to 18 km/s. Observations were performed in the beam switching mode with a beam separation of 12 arcmin. An integration time of 2 minutes has been selected with a chopper wheel calibration every six minutes. The pointing of the telescope has been checked every few hours on well known SIO maser sources: VY CMA and W Hya.

For elevations greater than 80° the telescope could not follow the sources correctly. This daily interruption was used for pointing checks and for obtaining comparison spectra of known galaxies like NGC 4321 and NGC 4038. A comparison with data obtained at the 30m MRT (Pico Veleta) or the 14m FCRAO telescope were satisfying.

Bright spiral galaxies of the Hydra I cluster were selected for these CO observations because of the correlation between luminosity and CO content (e.g. Young et al. 1985) in spirals and the maximum of relative CO content near morphological type Sbc and Sc (e.g. Kenney and Young 1988). The Sa type galaxy NGC 3312 was included in the search list because it is by far the largest spiral galaxy in the Hydra cluster and of its peculiar appearance being distorted on one side (e.g. Gallagher 1978).

Five out of fifteen galaxies observed have been detected in the CO(1-0) line after integration times of two to three hours (see Fig. 1). Agreement in radial velocity with optical and radio (i.e. 21cm HI) measurements is good in general as is the case for the line widths in CO and HI. (HI data were taken from the HI-catalog; Huchtmeier and Richter 1989a).

Discussion

In Fig. 2 we plot the absolute magnitude (assuming a distance of 68 Mpc for Hydra I) against the corrected (inclination) 21cm HI line width of bright Hydra spirals. These measurements fit quite well to the full line which represents the Tully-Fisher relation for the Virgo cluster (Huchtmeier and Richter 1989b). We take this as a confirmation of the adopted distance. The Virgo and the Hydra cluster are of similar type and of similar mass; the velocity dispersion of both clusters is about equal. At the adopted distance the two brightest elliptical galaxies in both clusters have about the same luminosity.

Bright spiral galaxies in the Virgo cluster have been observed to a high degree of completeness and with a good signal to noise ratio (Stark et al. 1986, Kenney and Young 1988). We will take these data as a comparison sample for our observations assuming that we should expect similar conditions in two clusters of the same type and the same size. NGC 3314B and NGC 3312 have the strongest CO fluxes in our survey. Each of these galaxies got more CO than any Virgo cluster galaxy. In NGC 3312 we observed positions 20 arcsec north and south of the centre along the major axis of this galaxy. There is some indication of emission in these two off-center positions which is not present in the positions 20 arcsec off in right ascension. In the case of NGC 3314 (Fig. 1b) we see two galaxies along the line of sight the fainter being detected. The typically good baseline behaviour is seen in the profile for NGC 3314 A (upper limit).

In Fig. 3 the luminosity and the molecular hydrogen mass of Virgo cluster galaxies (Kenney and Young 1988) is presented for three different morphological types. The lower molecular content for early type spiral galaxies is evident. For a given morphological type luminosity and gas content correlate well. The Hydra observations are plotted into this diagram (open triangles). Two Hydra galaxies are outside the range described by the Virgo sample. NGC 3312 is on the bright end side of this sample and therefore rich in molecules. As an early type galaxy (Sa to Sab) it seems really rich in molecular content compared to the Virgo cluster. From this point of view we might call it peculiar, too. NGC 3314 does not fit to the range defined by the Virgo cluster. It is too rich in molecules or too faint in luminosity or both. We noted earlier that we see two galaxies along the line of sight in this case. It is at least complicated to derive the magnitude for two superimposed galaxies. A correction of one magnitude and a half is needed to move that object up to the expected luminosity.

In Fig. 4 we compare the HI mass and the H_2 mass for the Virgo sample and our Hydra sample. The range occupied by the Virgo sample defines a good correlation. The Hydra galaxies fit quite well into the Virgo range. NGC 3312 could be a bit HI deficient for its H_2 mass. NGC 3314 is within the range defined by the Virgo galaxies.

REFERENCES

- Gallagher, J. 1978 : *Astrophys.J.* 223, 386
- Huchtmeier, W.K., Richter, O.-G. 1989a : *A General Catalog of HI Observations of Galaxies*, Springer-Verlag/Publishers New York
- Huchtmeier, W.K., Richter, O.-G. 1989b : *Astron.Astrophys.* 210,1
- Kenney, J.D., Young, J.S. 1988 : *Astrophys.J.Suppl.Ser.* 66, 261
- Stark, A.A., Knapp, G.R., Bally, J., Wilson, R.W., Penzias, A.A., Rowe, H.E. 1986 : *Astrophys.J.* 310, 660
- Young, J.S., Scoville, N.Z., Brady, E. 1985 : *Astrophys.J.* 288,487
- Zensen, W. 1984 : Ph.D. Dissertation, Univ.Cologne

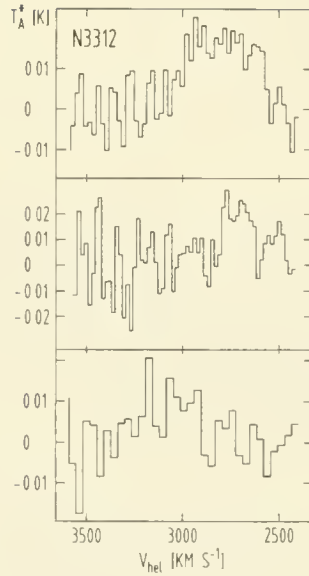


Fig.1 CO(1-0) profiles of Hydra cluster spiral galaxies.

a: NGC 3312 , center and two offset positions

b: NGC 3314 , A and B ; two galaxies along the line of sight

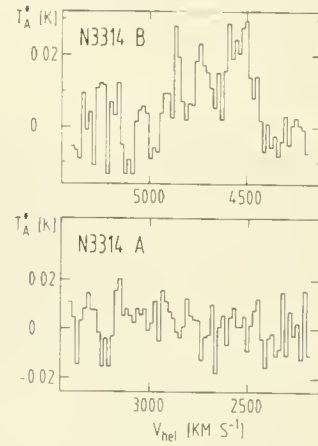


Fig. 2 Tully-Fisher relation of Hydra cluster spirals (full circles) and the Virgo cluster (full line).

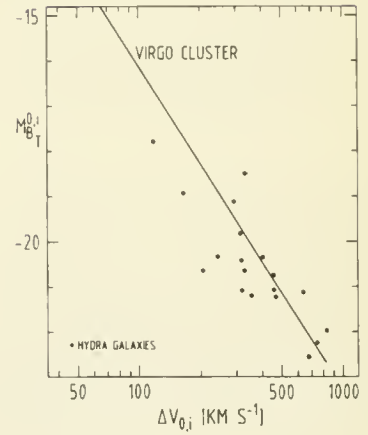
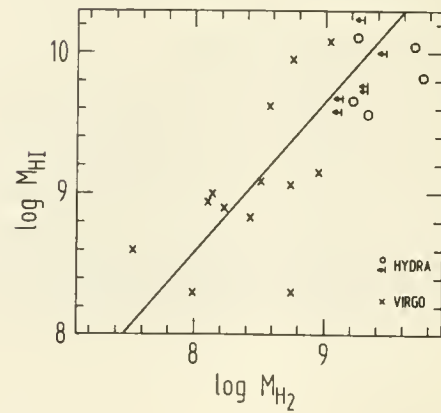
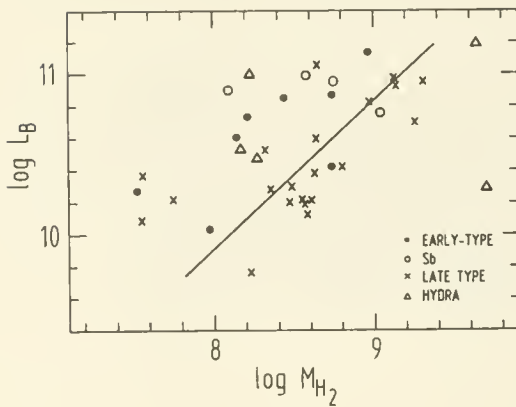


Fig. 3 Blue luminosity against molecular gas content (H_2) for the Virgo cluster and Hydra cluster galaxies (open triangles).

Fig. 4 Mass of neutral hydrogen against molecular gas content (H_2) for the Virgo cluster and Hydra cluster galaxies (open squares).



Non-stellar light from high-redshift radiogalaxies?

Steve Rawlings, MRAO, Cavendish Laboratory, Cambridge, UK.
S.A. Eales, STScI, Baltimore, USA.

Abstract

With the aid of a new IRCAM image of 3C356, we question the common assumption that radiosource-stimulated starbursts are responsible for the extended optical emission aligned with radio structures in high-redshift radiogalaxies. We propose an alternative model in which the radiation from a hidden luminous quasar is beamed along the radio axis and illuminates dense clumps of cool gas to produce both extended narrow emission line regions and, by Thomson scattering, extended optical continua. Simple observational tests of this model are possible and, in our view, necessary if we are to continue to accept that the colour, magnitude and shape evolution of radiogalaxies is controlled by the active evolution of stellar populations.

High-redshift ($z > 0.5$) radiogalaxies have different optical properties from their nearby counterparts: the rest-frame colours are far bluer^{1,2} and their optical structures are extended along the radio axes^{3,4}. These differences are commonly explained by models that invoke increased starburst activity at high z ¹; the alignment of optical and radio structures is then taken as evidence that the radiosource itself stimulates at least some of the star formation^{3,5}. This interpretation is not, however, without its problems and we here use recent observational results to suggest that the extended optical continua has a non-stellar origin.

There is growing evidence that radiogalaxies, which by definition lack *obvious* central quasars, do possess such objects hidden from us by obscuration. It is now clear from the polarisation of optical-line and -continuum⁶ and from the detection of both scattered and highly attenuated broad emission lines^{7,8} that Seyfert II galaxies contain obscured broad-line (Seyfert I) nuclei. A similar unification of quasars and radiogalaxies is suggested, but not proved, by the available data^{9,10}. However, there is additional indirect support for this unification: quasars clearly radiate their optical emission anisotropically¹¹ and differences in the radio properties of quasars and radiogalaxies are most reasonably interpreted by differing average orientations^{12,13,14}. Furthermore, there is a strong link between the bulk power developed in radio jets and the luminosity of the hidden quasar as inferred from the luminosities of the narrow emission lines¹⁵. This link leads us to suspect that known high- z radiogalaxies possess extremely luminous central quasars as, being drawn from bright flux-limited samples such as 3CR, they are of high radio luminosity.

Do we see any direct evidence for these hidden objects and can their presence explain any of the effects often attributed to starbursts? The answer is almost certainly yes: the extended emission line regions of high- z radiogalaxies have high effective ionisation parameters ($U_e \sim 10^{-2-3}$) and are most probably photoionized by the postulated hidden quasar¹⁶. How then might the associated extended optical continua produced? Although the 'standard' model of radiosource-stimulated starbursts is generally accepted, various alternatives have been proposed (although some perhaps rather more for their 'erotic fascination'¹⁷ than for their scientific validity): gravitational lensing¹⁸, the stimulation of radiosource activity by galaxy-galaxy interactions¹⁹, inverse-Compton scattering of microwave background photons by the radio lobes⁵, non-thermal emission associated with the radio jets, and finally scattering of either blazar or quasar light by either dust or thermal electrons^{20,21,22}.

For two high- z radiogalaxies, 3C356 and 3C368, images in the key infrared waveband have allowed us to compare the competing models²⁰. The off-nuclear infrared components (knots) identified in the 3C356²⁰ (Fig. 1) and 3C368⁵ have a number of common properties:

1. they are unresolved and on one side of the radio nucleus only (although aligned optical continua are seen on both sides of 3C368); there is no evidence for a smooth elongation in the infrared data.

2. they are red with spectral indices between B- and K-band of ~ 1.5 and ~ 2 respectively.
3. they are undetected in the radio at the 1 mJy level.
4. they are at similar distances from the radio core (≈ 50 and ≈ 30 kpc respectively) despite having radio structure differing in linear size by a factor of ~ 10 .

These properties constrain the emission mechanism for the infrared knots as follows: (2) eliminates dust scattering as this would produce a spectrum biased strongly to the blue; (1), and other arguments²⁰, eliminate inverse-Compton scattering by a lobe of relativistic electrons; (3) eliminates non-thermal jet emission, gravitational lensing and the electron-scattering of blazar light as each predicts coincident radio components. The galaxy interaction model is both physically implausible²⁰ and cannot explain aligned optical structures on *both* sides of the radio-core. Thus, if the infrared emission is starlight it must be from a young ($< 10^8$ yr) starburst stimulated by the radio source. To be consistent with such a model (2) indicates that the starburst must either be reddened by associated dust, which would be hard to produce in the short time available, or involve highly contrived stellar populations that seem, considering the differing ages of the proposed starbursts inferred from (4), unlikely to exist in both 3C356 and 3C368²⁰.

We now focus on our preferred infrared emission mechanism, Thomson-scattering of hidden quasar light by thermal electrons associated with the extended narrow-line region. This mechanism will naturally produce a power-law spectra similar to that of the hidden quasar and furthermore highly ionized ($U_e \sim 10^{-2}$) emission line gas, coincident with the knot, provides evidence for both a highly efficient scattering medium and for a hidden luminous quasar. The small solid angle subtended by the knot (< 0.1 sr) and its total narrow line luminosity ($\sim 5 \times 10^{37}$ W¹⁷) indicate that the hidden quasar must beam at least $\nu L_\nu \sim 5 \times 10^{39}$ $\Omega_c/4\pi$ W along cones of solid angle Ω_c . Although this inferred luminosity is higher than that of the brightest quasar in 3CR, this is not a serious cause for concern: *any* distribution in the values of Ω_c will cause a classification bias, those termed radiogalaxies will, on average, have narrower cones than those termed quasars making it misleading to compare *inferred* luminosities for these classes of object. We can use the [OII]3727 luminosity and size of the knot to put a lower limit to the electron number density n_e of $\sim 5 \times 10^6$ m⁻³ although the high U_e suggests that n_e is unlikely to orders of magnitude higher. At such densities the gas will scatter incident light with an efficiency approaching unity and, given the high luminosity inferred for the quasar, it is entirely feasible, on energetic grounds, that the infrared knot (with $\nu L_\nu \sim 10^{38}$ W) results from Thomson scattering by thermal electrons associated with the narrow-line clouds.

Finally we mention another possible problem for the standard starburst model, namely that there are reported correlations between radio properties, the blueness of the galaxy and emission line luminosity^{1,23}. At first sight these correlations appear to support our model because: (a) the bulk of the emission lines are photoionised directly by the active nucleus; and (b) radio luminosity is far more likely to be linked to non-stellar rather than stellar radiation¹⁵. However, using the available [OII] data at high z we find no more than marginal evidence for correlations between radio and optical properties (Fig. 2); moreover, using either the starburst or the scattering model, we have yet to find a convincing explanation for a link between optical properties and radio spectral index.

In conclusion, the Thomson scattering model discussed here provides an alternative, and in some ways more attractive, solution to the intriguing problem of why optical and radio structures are aligned in high- z radiogalaxies. The model can also be tested relatively simply by looking for polarisation and/or scattered broad lines in the extended optical continua.

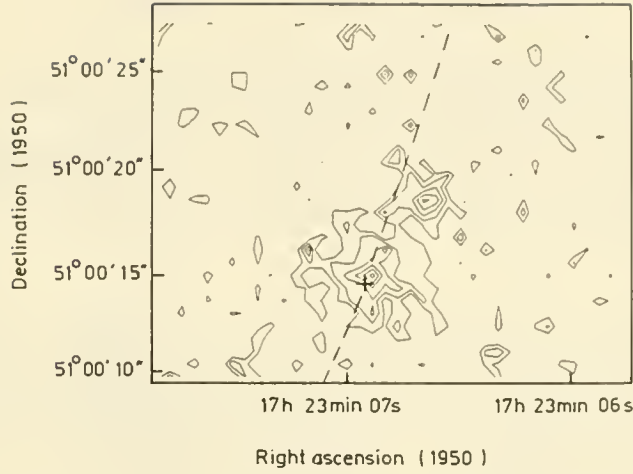


Fig. 1 K-band image of 3C356 ²⁰; the contour levels are $2 + n\sigma$; $n > 0$. The position of the radio-core and the direction of the radio structures (Laing, R.A., priv. comm.) are marked.

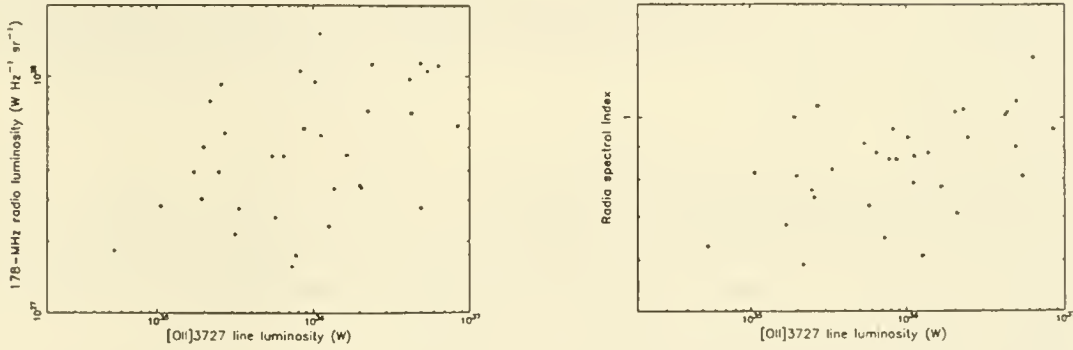


Fig. 2 The relations between [OII]3727 line luminosity, radio luminosity and radio spectral index. The objects plotted are those from the Laing *et al.* sample ²⁴ with $z > 0.5$ and with [OII]3727 data ¹⁶ (i.e. the sample is not necessarily unbiased).

References

- [1] Lilly S.J. & Longair M.S. MNRAS 211,833 (1984). [2] Spinrad H. PASP 98,269 (1986). [3] McCarthy P.J. *et al.* Ap.J. 321, L29 (1987). [4] Chambers K.C. *et al.* Nature 329,604 (1987). [5] Chambers K.C. *et al.* Ap.J., 329,L75 (1988). [6] Antonucci R.R.J. & Miller J.S. Ap.J. 297,621 (1985). [7] Miller J.S. & Goodrich R.F. BAAS 19, 695 (1987). [8] Ward M. *et al.*, in prep. [9] Antonucci R.R.J. Ap.J. 278, 499 (1984). [10] Fabbiano *et al.* Ap.J. 304, L37 (1986). [11] Jackson N. *et al.* Nature 338, 485 (1989). [12] Barthel P.D. Ap.J., 336,606 (1989). [13] Garrington S.T. *et al.* Nature 331, 147 (1988). [14] Pedelty J.A. *et al.*, preprint. [15] Rawlings S. & Saunders R. IAU 134, in press. [16] McCarthy P.J., PhD thesis, University of California at Berkeley(1989). [17] Thronson J.R. & Bally J. ApJ 319, L63 (1987). [18] Le Fèvre O. *et al.* Ap.J. 331,L73 (1988). [19] Djorgovski S. *et al.* AJ 93, 1307 (1987). [20] Eales S.A. & Rawlings, S., submitted. [21] Fabian A.C. MNRAS, in press. [22] Tadhunter C.N. *et al.*, preprint. [23] Lilly S.J., submitted. [24] Laing, R.A. *et al.* MNRAS 204, 151.

CO Distributions in Southern S0 Galaxies

Hugo van Woerden (Kapteyn Astronomical Institute)
and Linda Tacconi (Netherlands Foundation for Research in Astronomy)

Abstract. With the SEST, we have observed 7 S0 galaxies at 2.6 mm, and detected CO emission in five. Observing four offset positions per galaxy at $\geq 40''$ from the center, we find significantly extended CO emission in almost all cases. The (lower limits to) H_2 masses of several times $10^8 M_\odot$ amount to 0.2–0.3 times the HI mass in 4 or 5 galaxies.

1. Introduction

While most S0 galaxies appear to have used up their supply of gas, a minority contain sizable amounts of atomic hydrogen (Wardle and Knapp 1986). Van Driel (1987) and collaborators have mapped the distribution of HI in gas-rich early-type galaxies at Westerbork. The gas in S0's often lies in outer rings of radius $R \sim 2R_{25}$, sometimes also in an inner ring at $R \sim 0.5R_{25}$. The HI distribution in S0/a galaxies resembles the filled disks of spirals. Barred S0 and S0/a galaxies have outer rings of HI at 1.0–1.5 R_{25} and deep, central depressions (van Driel and van Woerden 1989).

Surveys of CO emission from S0 galaxies have been made by Thronson *et al.* (1989), Sage and Wrobel (1989), and Wiklund and Henkel (1989). In these single dish studies (beamwidths of 20–50''), generally one position per galaxy was measured. Maps of CO emission are required to provide the distributions of the molecular gas. Together with the HI distributions, they should inform us about the origin and evolution of the gas in S0 galaxies. We have therefore undertaken a study of CO *distributions* in southern S0 galaxies. We selected for observation galaxies with HI detections (Reif *et al.* 1982) and/or IRAS detections at 60 and 100 μm (Lonsdale *et al.* 1985).

2. Observations

We have used the 15-meter Swedish-ESO Submillimeter Telescope (SEST) at La Silla (Chile) for 74 hours in November 1988 to measure the ^{12}CO line emission at 2.6 mm in 7 galaxies (Table 1). The half-power beamwidth was 43'', with a main beam efficiency of 0.71. The spectrometer provided 722 channels in a bandwidth of 500 MHz = 1300 km s $^{-1}$. Our spectra were smoothed over 10 channels, giving a velocity resolution of 18 km s $^{-1}$. The single-sideband system temperature was 600–700 K, after correction to above the atmosphere. Integration times of typically 2 hours per position gave us an rms noise of ~ 5 mK in our 10 channel averages.

In the distant polar-ring galaxy, A0136-0801 (van Gorkom *et al.* 1987), we observed only the center, without detection. In the other 6 galaxies, we observed the center and 3 or 4 offset positions (Table 1) placed either along one axis (NGC 1291, 1326, and 2217), or at $\pm 40''$ on orthogonal axes (IC 1830, NGC 7233); in IC 5063, two offset positions lie on the dust lane (Danziger *et al.* 1981). Clearly, 4 offsets per galaxy do not yet provide a complete map of CO emission.

Observed antenna temperatures (T_A^*) were converted to flux densities per beam, S_{CO} , via

$$S_{CO}(\text{Jy}) = 28.3 T_A^*(\text{K})/f \quad (1)$$

which was derived from

$$S_{CO} = 2k\lambda^{-2} T_A^* \Omega_{mb}/(\eta_{mb}f)$$

where η_{mb} = main beam efficiency = 0.71, and Ω_{mb} = main beam solid angle = 4.9×10^{-8} sterad, and the quantity f , called the "correction factor for source-beam coupling" (Thronson *et al.* 1989) or "fraction of emission observed" (Kenney 1987), depends on the distribution relative to the beam. It is 1.00 for a point source at the beam center, and 0.72 for a flat distribution. We have used $f = 0.72$ for nondetections, giving upper limits to the CO flux, and $f = 1.00$ for detections, giving lower limits to the CO flux because of incomplete mapping.

3. Results

Table 1 summarizes our preliminary results. Column 3 gives the profile integrals for the central position and for the sum of all observed positions. Column 4 shows the distance, Δ , to the galaxy (as calculated from the HI velocity and $H_0 = 100$), and the HI mass from van Gorkom *et al.* (1987), Danziger *et al.* (1981), or Reif *et al.* (1982). Column 5 gives the H_2 mass and the $M(H_2)/M(HI)$ ratio. H_2 masses were calculated

Table 1 Preliminary Results						
Name D ₂₅ (arcmin)	Offsets $\Delta\alpha \cos \delta, \Delta\delta$ (arcmin)	$\int S_{CO} dV$: center (Jy km/s) "total"	Distance (Mpc) M(HI) ($10^8 M_\odot$)	M(H ₂) ($10^8 M_\odot$) M(H ₂)/M(HI)	(I ₁)/I ₀ R ₁ (kpc)	notes
A 0136-0801	centre only	≤ 100 (3σ)	55 8.3	≤ 33 (3σ) ≤ 4.0		
IC 1830 1.8 \pm 0.2	4: $\pm 0.67, 0.00$ 0.00, ± 0.67	$\geq 33 \pm 9$ $> 108 \pm 55$	12.7 11.4 \pm 1.8	$> 1.9 \pm 1.0$ $> 0.17 \pm 0.09$	0.6 \pm 0.5 2.5	
NGC 1291 10.5 \pm 0.8	3: $+1.00, 0.00$ $+2.00, 0.00$ $+4.00, 0.00$	$\geq 44 \pm 12$ $> 34 \pm 31$	6.9 8.1 \pm 0.7	$\geq 0.23 \pm 0.06$ $\geq 0.029 \pm 0.008$	(-0.2 ± 0.4) 2.0	
NGC 1326 4.0 \pm 0.6	4: $\pm 0.65, \pm 0.15$ $\pm 1.30, \pm 0.30$	$\geq 78 \pm 11$ $> 184 \pm 38$	12.2 14.0 \pm 1.6	$> 3.0 \pm 0.6$ $> 0.22 \pm 0.05$	0.6 \pm 0.2 2.4	a
NGC 2217 4.8 \pm 0.5	4: $\pm 1.00, 0.00$ $\pm 2.00, 0.00$	$\geq 44 \pm 14$ b $> 120 \pm 32$	13.8 11.9 \pm 0.9	$> 2.5 \pm 0.7$ $> 0.21 \pm 0.06$? 4.0	b
IC 5063 1.9 \pm 0.7	4: $\pm 0.63, \pm 0.14$ $\pm 0.27, \mp 0.58$	≤ 47 (3σ) $> 62 \pm 24$	33.0 25	$> 7.4 \pm 2.9$ $> 0.29 \pm 0.12$? 6.4	c
NGC 7233 2.2 \pm 0.5	4: $\pm 0.48, \mp 0.45$ $\pm 0.45, \pm 0.48$	$\geq 56 \pm 12$ $> 79 \pm 38$	18.9 $\leq 19.6 \pm 2.8$	$> 3.1 \pm 1.5$ $> 0.16 \pm 0.08$	0.1 \pm 0.2 3.7	d

Notes

a Detections (50 ± 12 and 39 ± 11 Jy km/s) at $40''$ in P.A. 77° and 257° .

b No detection at center; quoted detection is at $60''$ east.

c No detection. Two offset positions on dust lane.

d HI detection from group of galaxies.

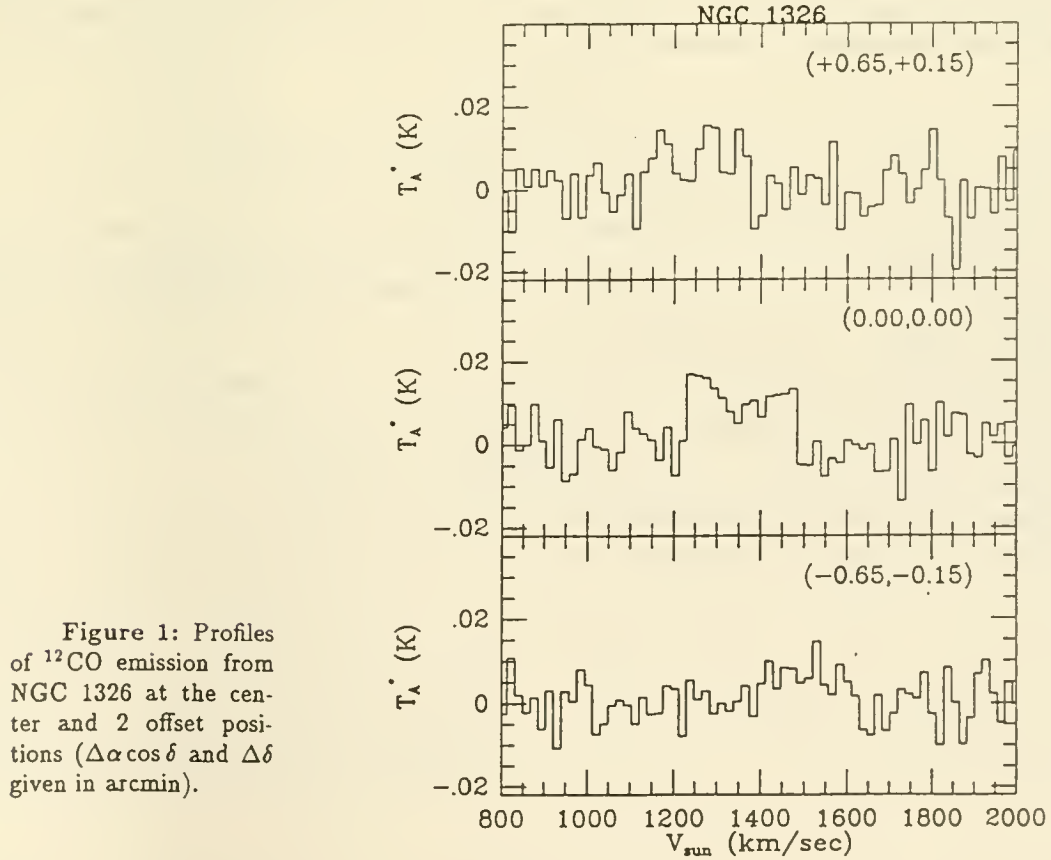


Figure 1: Profiles of ^{12}CO emission from NGC 1326 at the center and 2 offset positions ($\Delta\alpha \cos \delta$ and $\Delta\delta$ given in arcmin).

from the "total" profile integrals (sum of all observed positions) via

$$M(H_2)(M_\odot) = 1.1 \times 10^4 [\Delta(\text{Mpc})]^2 \int S_{CO} dV (\text{Jy km s}^{-1}) \quad (2)$$

Column 6 gives the ratio of the average profile integral $\langle I_1 \rangle$ at the first offsets to the central integral I_0 , and the offset distance, R_1 .

We have central detections above 3σ in four galaxies: NGC 1291, 1326, and 7233, and IC 1830, and a non-central 3σ detection in NGC 2217. The other two galaxies were not detected. The "total" profiles obtained by adding 3 or 4 offset positions to the central position have a much higher noise level, but also more signal; hence the CO distributions must generally be extended. Although the "total" profile integrals exceed 3σ only in NGC 1326 and NGC 2217, we consider these integrals in general a better approximation to the total CO emission than the central integral (except in NGC 1291). However, we emphasize that these "totals" are based on incomplete maps, and thus provide lower limits to the CO emission only.

The calculation of H_2 mass from CO emission, using the formula (2) as in Thronson *et al.*, assumes the same H_2/CO ratio as in our galaxy. The ratios of molecular to atomic hydrogen mass are of order 0.2–0.3 in most cases, which is lower than in many spiral galaxies (Young, this conference). In NGC 1291, the H_2/HI ratio may be an order of magnitude lower, but in this big galaxy the map is very incomplete.

In NGC 1326 the CO distribution is clearly extended, with the two offset positions at $\pm 40''$ from the center having well-detected CO emission. Preliminary calculations indicate that both central and offset profiles can be well fit by a model having the CO concentrated in a narrow ring at $20''$ ($=1.2$ kpc) radius and rotating at $225 \sin i \text{ km s}^{-1}$. In IC 1830 and NGC 7233, the average offset emission $\langle I_1 \rangle$ and its ratio to I_0 were estimated from the difference between total and central profiles, but here the ratios $\langle I_1 \rangle / I_0$ remain inconclusive.

Our present results represent only a first step towards our goal. A good determination of CO distributions requires more sensitive observations. In addition, for both the distributions and the total amount of molecular gas, more complete maps are required. There is an urgent need for feed arrays on millimeter telescopes.

ACKNOWLEDGEMENTS. We gratefully mention the help of the SEST staff at the telescope, and of Lowell Tacconi-Garman at the computer.

REFERENCES

- Danziger, I.J., Goss, W.M., and Wellington, K.J. 1981, *M.N.R.A.S.*, **196**, 845.
 Kenney, J.D. 1987. Ph.D Thesis, University of Massachusetts
 Lonsdale, C.J., Helou, G., Good, J.C., and Rice, W. 1985, *Catalogued Galaxies and Quasars Observed in the IRAS Survey*, JPL Preprint.
 Reif, K., Mebold, U., Goss, W.M., van Woerden, H., and Siegman, B. 1982, *Astron. Astrophys. Suppl.*, **50**, 451.
 Sage, L. and Wrobel, J. 1989, *Ap.J.*, **344**, in press
 Thronson, H., Tacconi, L., Kenney, J., Greenhouse, M.A., Margulis, M., Tacconi-Garman, L., and Young, J.S. 1989, *Ap.J.*, **344**, in press
 van Driel 1987. Ph.D. Thesis, University of Groningen
 van Driel, W. and van Woerden, H. 1989, *Astron. Astrophys.*, in preparation
 van Gorkom, J.H., Schechter, P.L., and Kristian, J. 1987, *Ap.J.*, **314**, 457.
 Wardle, M. and Knapp, G.R. 1986, *A.J.*, **91**, 23.
 Wiklund, T., and Henkel, C. 1989, *Astron. Astrophys.*, in press

The Hawaii Imaging Fabry-Perot Interferometer (HIFI)

Jonathan Bland

Rice University, Houston TX 77251-1892

Gerald Cecil

Institute for Advanced Study, Princeton NJ 08540

Brent Tully

Institute for Astronomy, Honolulu HI 96822

At Mauna Kea Observatory, we have conducted optical, imaging spectrophotometric studies of selected active galaxies using both the Canada-France-Hawaii 3.6m and University of Hawaii 2.2m telescopes (Tully, Bland & Cecil 1988). To maximize spatial resolution, we select galaxies independent of luminosity but known to possess interesting morphologies or high-velocity, extranuclear ionized gas (Walker 1968; Rubin & Ford 1968). We study both the large-scale patterns produced in IR-luminous, starburst systems (e.g. M82, NGC 253, NGC 6240) and those with compact, but spatially extended, circumnuclear, narrow line regions (e.g. M51, NGC 1068, NGC 4151). Current studies are restricted to the optical [SII], [NII] and [OIII] lines and the brightest Balmer recombination lines. These lines are, in principle, sufficient to constrain the dynamical structure and dominant excitation mechanism of the ionized component.

The HIFI system provides high kinematic resolution for a field-of-view as much as $10'$ at subarcsecond increments matched to the seeing above the site. Our approach differs from the TAURUS systems (Taylor & Atherton 1980) in the use of large free-spectral-range etalons ($\sim 100\text{\AA}$) with high finesse (60), and low read-out noise ($\sim 5e^-$) CCD detectors at the image plane. (For further details, see Bland & Tully 1989). Extranuclear emission line widths in NLRs can exceed 3000 km s^{-1} which necessitates an interorder separation in excess of 4000 km s^{-1} to avoid confusion. In a typical night, $\sim 10^2$ spectrophotometric images are obtained over a few emission lines. The large format detector arrays ($800 \times 800 \rightarrow 2048 \times 2048$) give rise to enormous data cuboids ($I(\alpha, \delta, \lambda) \sim 1\text{ Gbyte}$) that require sophisticated data handling capabilities. During the past four years, reduction packages have been developed for and are currently operating on SUN/3 and SUN/4 series workstations at Rice, Princeton and Hawaii. The data calibration and reduction steps are well defined (Bland & Tully 1989). However, the optimal method for visualizing these multidimensional data structures is largely unresolved.

Major results have already been presented for some well known systems: in particular, M51 (Cecil 1988), M82 (Bland & Tully 1988), NGC 1068 (Cecil, Bland & Tully 1989; Bland *et al.* 1989), NGC 4151 (Cecil, Bland & Tully 1987), NGC 4258 (Tully, Bland & Cecil 1988). At this conference, two papers are presented for NGC 1068 which adequately demonstrate the power and versatility of the HIFI system. Sokolowski, Bland & Cecil have studied the large-scale disk at the CFH 3.6m telescope across a region spanning $160''$ by $100''$ ($11.6\text{ kpc} \times 7.4\text{ kpc}$). The kinematics of the ionized gas display complex patterns which are well understood in terms of elliptic streaming motions (Bland *et al.* 1989). These motions, which we presume are driven by the stellar bar recently observed at 2μ (Scoville *et al.* 1988; Thronson *et al.* 1989), are presently being modelled by Athanassoula. This galaxy exhibits the clearest evidence to date for streaming induced by a bar-driven, density wave, which gains further support from the relationship of the dust lanes to the CO emission (Planesas,

Myers & Scoville, this conference), the 10μ emission (Telesco & Decher 1988), and the non-thermal radio emission (Wynn-Williams, Becklin & Scoville 1985). More interestingly, we find an unusually energetic phase of the ISM which permeates throughout the *entire* disk as indicated by $[\text{NII}]/\text{H}\alpha \approx 1 - 6$ with line widths $\text{FWHM} > 200 \text{ km s}^{-1}$ which is distinct from the population of HII regions with $[\text{NII}]/\text{H}\alpha < 0.5$ and line widths $< 100 \text{ km s}^{-1}$. We propose two possible origins for the extended, high excitation gas involving either the active nucleus or the IR-luminous, molecular ring, both of these having comparable bolometric luminosities ($\sim 1.5 \times 10^{11} L_{\odot}$), which we anticipate will be resolved after the launch of ROSAT. In a complementary, high resolution study at the UH 2.2m telescope, Cecil has decomposed the extended NLR into three major, dynamically distinct components: one of these is centred on the nucleus; another arises from gas near systemic velocity; and the remainder comprises the high velocity gas. The morphology and dynamics of the high velocity component is explained as the terminus of a radiatively excited, outflowing nuclear wind with a mechanical luminosity similar to the ionizing luminosity of the active nucleus (Cecil, Bland & Tully 1989).

This research is supported by NSF grant AST-88-18900 (Rice, Hawaii) and by NASA grant NAS 8-32902 (Princeton).

Bland, J. and Tully, R.B., 1988, *Nature*, 334, 43.

Bland, J. and Tully, R.B., 1989, *Astron. J.*, August issue.

Bland, J., Cecil, G. N., Tully, R. B. and Widemann, T. 1989, *Astrophys. J.*, submitted.

Cecil, G. N. 1988, *Astrophys. J.*, 329, 38.

Cecil, G. N., Bland, J. and Tully, R. B. 1987, *Active Galactic Nuclei*, ed. P. J. Wiita. Georgia State University, Atlanta.

Cecil, G. N., Bland, J. and Tully, R. B. 1989, *Astrophys. J.*, submitted.

Rubin, V. C. and Ford, W. K. 1968, *Astrophys. J.*, 154, 431.

Scoville, N. Z., Matthews, K., Carico, D. P. and Sanders, D. B. 1988, *Astrophys. J. Lett.*, 327, L61.

Taylor, K. and Atherton, P. D. 1980, *Mon. Not. R. astr. Soc.*, 191, 675.

Telesco, C. M. and Decher, R. 1988, *Astrophys. J.*, 334, 573.

Thronson, H. A., Hereld, M., Majewski, S., Greenhouse, M. A., et al. 1989, *Astrophys. J.*, 343, 158.

Tully, R. B., Bland, J. and Cecil, G. N. 1988, *IAU Symp.*, 134, 000. ed. D. E. Osterbrock and J. S. Miller, Santa Cruz.

Walker, M. F. 1968, *Astrophys. J.*, 151, 71.

Wynn-Williams, C. G., Becklin, E. E. and Scoville, N. Z., 1985, *Astrophys. J.*, 297, 607.

VIII - AUTHOR INDEX AND GALAXY INDEX

AUTHOR INDEX

Adamson, A.J.	89	Devereux, N.A.	47,92,103,127
Adler, D.S.	130,291	Dickey, J.M.	6,8
Allen, L.E.	321	Donahue, M.	196,359,
Allen, R.J.	130,263,291, 298	Dopita, M.A.	331
Applegate, D.N.	276,	Downs, D.	378,384
Balbus, S.A.	177	Dreher, J.	146
Ball, R.	95	Dressel, L.L.	346
Barteldrees, A.	246	Dupraz, C.	273
Bernard, J.P.	105	Dwek, E.	229
Bisht, R.S.	86	Eales, S.A.	103
Blanco, P.R.	317	Eckart, A.	71,368,384
Bland, J.	143,395	Elston, R.	169
Blitz, L.	59	Elfhag, T.	50
Bodenheimer, P.	314	Engargiola, G.	97,116
Borkowski, K.J.	177	English, J.	318
Bothun, G.	193	Erickson, E.F.	40
Boulanger, F.	371	Eskridge, D.B.	29
Bowen, D.	360	Evrard, A.E.	343
Brand, P.W.J.L.	81	Fabbiano, G.	33
Brown, R.	221,224,269	Fabian, A.C.	201
Bregman, J.N.	23,203	Fanelli, M.N.	307
Brinks, E.	221	Federman, S.	4
Bruhweiler, F.	175	Feigelson, E.D.	100
Burbidge, E.M.	362	Ferguson, H.C.	281
Burton, M.	238	Ferrario, L.	331
Buss, R.H.	113	Ferriere, K.M.	227
Cameron, M.	71	Forman, W.	185,198,201
Canterna, R.	301	Foster, J.R.	331
Canzian, B.	325	Fristrom, C.C.	177
Carilli, C.	146,356	Gaffney, N.	340
Carlstrom, J.E.	78,337	Gallagher, J.S.	149,172
Carr, J.	340	Gallais, P.	329
Case, J.	359	Geballe, T.	241
Casey, S.	116	Genzel, R.	368,384
Casoli, F.	273,371	Ghosh, S.K.	86
Cecil, G.	140,143,395	Gioia, I.	196
Cheng, K.P.	175	Grabelski, D.A.	206
Chernoff, D.F.	235	Grasdalen, G.L.	301
Claussen, M.	47	Guhathakurta, P.	26
Clausset, F.	371	Gullixson, C.A.	1623
Cohen, R.,D.	362	Haas, M.R.	40
Colgan, S.W.J.	40	Hackwell, J.A.	301
Combes, F.	273,371	Hanson, M.M.	6
Conner, S.	146	Harper, D.A.	97,116
Corbelli, E.	180	Harris, A.I.	368,384
David, L.	185,198	Harvey, P.M.	84,211,365
Desert, X.	105	Haxthausen, E.	356
Dettmar, R.-J.	68,172,246	Heiles, C.	108
Deustra, S.	193	Heithausen, A.	68
		Helou, G.	6
		Henkel, C.	75,381
		Hester, J.J.	182,288

Hibbard, J.E.	214	McKee, C.F.	235,243
Hill, J.M.	169,318	Meixner, M.	59
Ho, P.T.P.	337,384	Morita, K.-I.	375
Hodge, P.	160	Mountain, C.M.	81
Hogg, D.E.	23	Murray, S.D.	267
Hollenbach, D.J.	37,40,235	Myers, S.T.	62
Huang, Y.	47	Nakai, N.	56,81
Huchtmeier, W.K.	386	Neufeld, D.	243
Hunter, D.A.	116,149	Noriega-Crespo, A.	314
Hyland, A.R.	211	Norman, M.L.	232
Ishigaro, M.	375	O'Connell, R.W.	346
Ishizuki, S.	375	O'Dell, C.R.	166
Isobe, T.	100	Oey, M.S.	309
Israel, F.D.	8	Okumura, S.K.	375
Iyengar, K.V.K.	86,133	Olberg, M.	71
Jackson, J.	337	Pellat, R.	249
Jackson, J.M.	368,384	Perley, R.	146
Jaffe, D.T.	368,384	Planesas, P.	62
Jenkins, E.B.	353	Pogge, R.W.	29
Jones, C.	185,198,201	Pompea, S.M.	305
Jones, T.J.	258	Price, J.S.	163,123
Joseph, C.L.	45	Puchalsky, R.	59
Joy, M.	211,340	Puxley, P.J.	81,238,317
Jullien-Dettmar, M.	246	Radford, S.J.E.	378
Junkkarinen, V.T.	362	Rand, R.J.	182,293
Kamega, O.	56	Rawlings, S.	188,389
Kawabe, R.	375	Rengarajan, T.N.	86,133
Kenney, J.D.	47	Richer, M.G.	260
Kennicutt, R.C.	154,309	Rickard, L.J.	123
Keppel, J.	172	Rieke, G.H.	305
Kim, D.-W.	26,33	Roberts, M.S.	23,172
Knapp, G.R.	26,120	Rothermal, H.	71
Knezek, P.M.	47,53	Rouan, D.	329
Kulkarni, S.R.	182,293	Rubin, R.H.	40
Lacombe, F.	329	Rupen, M.P.	21
Lee, M.G.	157,160	Rydbeck, G.	71
Lee, J.F.	296	Salpeter, E.E.	180
Leisawitz, D.	111	Sancisi, R.	12
Lester, D.F.	84,340,365	Sandage, A.	281
Lin, D.N.C.	267,314	Sanders, D.B.	65
Lo, K.Y.	95,130,291,296	Sarazin, C.L.	203,204
Lord, S.D.	40	Sargent, A.I.	65
Loewenstein, M.	191	Schloerb, F.P.	47,72
Luan, L.	108	Scoville, N.Z.	62,65
Lugten, J.B.	368	Sellgren, K.	108
MacLow, M.-M.	227	Shull, J.M.	359
Maloney, P.	1	Skillman, E.D.	154
Martin, R.N.	78	Smith, B.J.	84
Mason, S.F.	163	Smith, P.A.	81
Mauersberger, R.	381	Snow, T.P.	359
McCall, M.L.	151,260,318	Soker, N.	203
McGregor, P.J.	211	Sokolowski, J.	143

Solomon, P.M.	378	White, R.E.	204
Stanford, S.A.	65	Whittet, D.C.B.	89
Stemwedel, S.W.	123	Wiklund, T.	71,75
Stern, C.	201	Wild, W.	71,368,384
Stevenson, C.	151	Wilson, C.D.	285
Stoeke, J.T.	196,359	Wolfire, M.G.	37
Stone, J.M.	232	Wollkind, D.J.	250
Strom, C.	4	Womble, D.S.	362
Struck-Marcell, C.	18,312	Wright, M.	59
Stutzki, J.	368	Wrobel, J.M.	349
Sukumar, S.	263	Xie, S.	47,72,373
Sugnet, J.F.	249	Yates, K.R.	250
Tacconi, L.J.	47,279,373,392	Young, J.S.	47,53,72,92,127, 321
Tacconi-Garman, L.	47	Zaritsky, D.	169
Tagger, M.	249	Zinnecker, H.	71
Tandon, S.N.	86	Zweibel, E.G.	227,252
Taniguchi, Y.	56,137		
Telesco, C.M.	346		
Tenorio-Tagle, G.	314		
Thronson, H.A.	116		
Tielens, A.G.G.M.	37		
Tilanus, R.P.J.	298		
Titus, T.N.	312		
Tollestrup, E.V.	211		
Tolstoy, E.	8		
Tomisaka, K.	255		
Tucker, W.	185		
Tully, R.B.	143,395		
Turner, J.L.	337		
Ulmer, M.P.	206		
Unger, S.W.	221		
Vander Hulst, J.M.	12,279		
van Driel, W.	32		
Van Gorkom, J.H.	26,214,356		
Van Woerden, H.	32,392		
Verma, R.P.	86		
Verter, F.	229		
Viallefond, F.	371		
Viscuso, P.	47		
Visvanathan, N.	260		
Voit, G.M.	126,196		
Walker, C.E.	78		
Walker, C.K.	78		
Walker, W.H.	334		
Walsh, D.	120		
Walterbos, R.	224,269		
Wang, Z.	15		
Welch, D.C.	151		
Welty, D.E.	42		
Werner, M.W.	108,113		
Wesselius, P.R.	279		
White, D.A.	201		

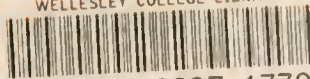
GALAXY INDEX

A 0136-0801	393	Mrk 1021	138
Arp 143	276	Mrk 1022	138
Arp 193	378	Mrk 1194	138
Arp 220	258,365,378	Mrk 7625	138
Arp 244	65	MS 0839+2938	197
Cen A (NGC5128)	71,211,365	NGC 55	68
Circinus	86	NGC 157	324
Cygnus A	146	NGC 253	131,337,381
GR 8	160	NGC 404	75
Henize 2-10	317	NGC 520	324
IC 10	160	NGC 591	57
IC 342	40,72,131,375, 382,384	NGC 628	20
IC 1613	160,163	NGC 660	324
IC 1830	392	NGC 891	21,182
IC 5063	393	NGC 925	20
LMC	149,157,229	NGC 1058	6
M 31	131,221,224,269	NGC 1068	62,140,143,330
M 33	169,285,288	NGC 1291	392
M 51	118,131,169,291 293,296,298, 301, 311	NGC 1326	392
M 51 (NGC5194)	365	NGC 1569	334
M 81	131	NGC 1614	273
M 82	37,78,81,324, 335,340,365, 368,382	NGC 1796	333
M 83	81,84,131,263 311,	NGC 2146	72,324,384
M 86	201	NGC 2217	392
M 101	12,131,169	NGC 2363	149
Maffei 2	81	NGC 2366	20,149
Mrk 52	57,58,138	NGC 2403	20,169
Mrk 190	58	NGC 2685	194
Mrk 201	58	NGC 2782	58
Mrk 231	378	NGC 2903	20,324,385
Mrk 273	241	NGC 2976	279
Mrk 293	258	NGC 2992	58
Mrk 307	138	NGC 2997	169
Mrk 326	138	NGC 3067	356,359
Mrk 353	138	NGC 3147	324
Mrk 439	58	NGC 3198	20
Mrk 489	138	NGC 3227	58,59,241
Mrk 538	138	NGC 3256	273
Mrk 545	138	NGC 3312	217,386
Mrk 602	138	NGC 3314	388
Mrk 603	138	NGC 3423	332
Mrk 1002	138	NGC 3489	194
Mrk 1012	138	NGC 3504	58
		NGC 3521	324
		NGC 3573	247
		NGC 3593	75
		NGC 3543	118
		NGC 3690/IC694 (Arp299)	40, 8,258,365
		NGC 3726	20
		NGC 3810	333
		NGC 3887	333

NGC 3998	194	NGC 7070A	247
NGC 4038/9	65	NGC 7123	247
NGC 4051	241	NGC 7233	392
NGC 4203	194	NGC 7252	273
NGC 4242	20	NGC 7469	58,59
NGC 4254	94	NGC 7479	324
NGC 4254	118,325	NGC 7625	58
NGC 4258	20	S 4 -248+430	362
NGC 4303	325	Sag Irr	160
NGC 4321	94,118,325	Sex A	160
NGC 4365	194	Sex B	160
NGC 4369	75	SMC	318
NGC 4395	20	UGC 03265	348
NGC 4438	214	UGC 05292	348
NGC 4449	149	UGC 12618	347
NGC 4472	194	I Zw 18	152,154
NGC 4473	194	VII Zw 31	378
NGC 4501	94,118,325	3C232	356,359
NGC 4535	325	3C326.1	244
NGC 4536	325	3C356	389
NGC 4550	194	3C368	389
NGC 4565	21,89,259,325		
NGC 4636	194		
NGC 4638	194		
NGC 4649	194		
NGC 4654	94,118,325		
NGC 4697	194		
NGC 4710	118,349		
NGC 4945	86,365		
NGC 5018	26		
NGC 5022	26		
NGC 5033	20,59		
NGC 5055	20		
NGC 5220	247		
NGC 5236 (M83)	329		
NGC 5237	247		
NGC 5371	20		
NGC 5461	334		
NGC 5866	118		
NGC 6240	245,258		
NGC 6503	20		
NGC 6764	384		
NGC 6771	247		
NGC 6814	58		
NGC 6822	160		
NGC 6848	247		
NGC 6946	12,40,97,118, 131,311,371, 373,375		
NGC 6951	324		
NGC 7007	247		
NGC 7049	247		

1. Report No. NASA CP-3084		2. Government Accession No.		3. Recipient's Catalog No.	
4. Title and Subtitle The Interstellar Medium in External Galaxies: Summaries of Contributed Papers				5. Report Date July 1990	
				6. Performing Organization Code	
7. Author(s) D. J. Hollenbach and H. A. Thronson, Jr.		DATE DUE		8. Performing Organization Report No. A-90075	
9. Performing Organization Name Ames Research Center Moffett Field, CA 94035				10. Work Unit No. 188-44-53	
				11. Contract or Grant No.	
12. Sponsoring Agency Name and Address National Aeronautics and Space Administration Washington, DC 20546				13. Type of Report and Period Covered Conference Publication July 3-7, 1989	
				14. Sponsoring Agency Code	
15. Supplementary Notes Point of Contact: D. J. Hollenbach Mc (415) 291-1300 D. J. Hollenbach: Ames Harley A. Thronson, Jr.					
16. Abstract The Second Wyoming Conference on "Galaxies" was held on July 3-7, 1989, to discuss the current understanding of the basic physical processes underlying interstellar phenomena. The topic was presented at the meeting and summaries of the contributed papers were presented. The papers covered a variety of topics in the field of galaxies and focused on such topics as the distribution and morphology of the atomic, molecular, and dust components; the dynamics of the gas and the role of the magnetic field in the dynamics; elemental abundances and gas depletions in the atomic and ionized components; cooling flows; star formation; the correlation of the nonthermal radio continuum with the cool component of the interstellar medium; the origin and effect of hot galactic halos; the absorption line systems seen in distant quasars; the effect of galactic collisions; and the potential that new instrumentation brings to the field. A number of papers characterized the interstellar medium of particular types of galaxies, such as elliptical, dwarf irregulars, Seyferts, and spirals. Some emphasis was given to the origin of starbursts, and the physical parameters in the interstellar medium which control starburst activity. Analysis of IRAS data formed an important contribution to the proceedings, and a number of papers considered the origin of the far-infrared continuum and the role of small dust grains and polycyclic aromatic hydrocarbons in the emission of the near- and mid-infrared continuum.					
17. Key Words (Suggested by Author(s)) Galaxies, Interstellar medium, Infrared astronomy, Radio astronomy, Submillimeter astronomy			18. Distribution Statement Unclassified-Unlimited Subject Category - 90		
19. Security Classif. (of this report) Unclassified		20. Security Classif. (of this page) Unclassified		21. No. of Pages 424	
				22. Price A18	

WELLESLEY COLLEGE LIBRARY



3 5002 03097 1779

Astro qQB 856 .W96 1989 supp

Wyoming Conference (2nd :
1989 :

The interstellar medium in
external galaxies 03097 1779

Astro qQB 856 .W96 1989 supp

Wyoming Conference (2nd :
1989 :

The interstellar medium in
external galaxies

National Aeronautics and
Space Administration
Code NTT-4

Washington, D.C.
20546-0001

Official Business
Penalty for Private Use, \$300

SPECIAL FOURTH-CLASS RATE
POSTAGE & FEES PAID
NASA
Permit No. G-27



POSTMASTER: If Undeliverable (Section 158
Postal Manual) Do Not Return
